GAS TURBINE COMBUSTOR WALL COOLING

by

ABRAHAM AWOLOLA ASERE, B.Sc.(Hons.),
Ass.M.Inst.E., M.Inst.Pet.

A thesis submitted for the degree of
Doctor of Philosophy at the University of Leeds
under the supervision of Dr. G.E. Andrews

Department of Fuel and Energy
Houldsworth School of Applied Science
The University of Leeds
Leeds LS2 9JT
England

February 1986

Dedicated to the memory of my mother,
Mrs. Adedẹwẹ Asere

ABSTRACT

The need for better methods of cooling gas turbine combustors and a review of current cooling techniques have been presented. Three cooling methods are investigated: (a) Full Coverage Discrete Hole Film Cooling (Effusion), (b) Impingement/Effusion Hybrid Cooling Systems, and (c) Transpiration Cooling.

The aim of these cooling techniques is to effectively and efficiently cool gas turbine combustors with a significant reduction in current cooling air requirements. The range of test conditions were coolant temperature, T_c, of $289 \leqslant T_c \leqslant 710$ K and combustion gases temperature, T_g, of $500 \leqslant T_g \leqslant 1900$ K. The discharge coefficients of the effusion and the impingement/effusion systems have also been studied.

A detailed analysis has been made of the heat transfer of the cooling systems, jet penetration into the cross-stream, prediction of the cooling jet temperatures at various stages in the cooling process and the cooling film heat transfer coefficient.

The results of the discharge coefficient (C_d) indicate a decreasing C_d with increasing wall thickness to diameter ratio, t/D, and a weak effect of cross-stream flow. The results of both the effusion and the impingement/effusion hybrid systems indicate a high cooling performance of similar magnitude to that of the transpiration system. Graphical design correlations for the cooling wall have been made. The optimum hole geometries for both cooling configurations have been developed. The influence of the coolant to hot gas density ratio has been studied over the range 1.4 - 3.4.

In the design of effusion and impingement/effusion cooling systems, wall thickness, hole density, hole diameter and wall design pressure loss are significant parameters for cooling performance maximisation.

ACKNOWLEDGEMENTS

I wish to thank my Supervisor, Dr. G. E. Andrews, for his moral support, advice, encouragement, unparalleled help, kindness and friendliness throughout the period of this work.

My sincere gratitude to Professor A. Williams and Dr. W. A. Gray for their help and advice.

My unqualified thanks to Miss Penelope Margaret Withers (B.A. Hons.).

I thank Mr. R. A. Boreham (technician), whose skills play a significant role in the completion of this work. To all the other technicians who help me in various capacities, I say thanks.

I thank the following also for their help and kindness: Mrs. Pauline A. Brown, Mrs. Sheilagh J. Gibbens (both secretaries in the Dept. of Fuel and Energy), Mrs. Helen Barker (my typist), Mr. C. A. Johnson, Mrs. P. Butcher (both - Russian Dept.), Mr. A. Smith and Jane Poyner (both - Inter-loans, Boyle Library).

Many thanks to Ms. Ruth Sawtell for her help and kindness.

My thanks to the G.E.C. - Ruston Gas Turbines Limited for the sponsorship.

I wish to thank my State Government for its help.

Finally, I wish to thank all my friends for their kindness and friendship.

PUBLICATIONS DURING THE COURSE OF THIS RESEARCH

1. Andrews, G.E., Asere, A., and Mkpadi, M.C., 'Transpiration and full coverage discrete hole film cooling', I.Chem.E., 11th Annual Research Meeting, pp. 86-91, 1984.

2. Andrews, G.E. and Asere, A.A., 'Transpiration cooling of gas turbine combustion chamber walls', 1st UK National Heat Transfer Conference, I.Chem.E. Symposium Series, No. 86, pp. 1047-1056, 1984.

3. Andrews, G.E., Asere, A.A., Gupta, M.L., and Mkpadi, M.C., 'Full coverage discrete hole film cooling: The influence of hole size', ASME - Paper No. 85-GT-47, 1985.

4. Andrews, G.E., Asere, A.A., Hussain, C.I., and Mkpadi, M.C., 'Full coverage impingement heat transfer: The variation in pitch to diameter ratio at a constant gap', AGARD Meeting 'Heat Transfer and Cooling in Gas Turbines', Paper 26, Bergen, Norway, May 1985.

5. Andrews, G.E., Asere, A.A., Hussain, C.I., and Mkpadi, M.C., 'Transpiration and impingement/effusion cooling of gas turbine combustion chambers', ISABE and AIAA, Paper ISABE 85-7095, 1985.

6. Andrews, G.E., Asere, A.A., Mkpadi, M.C., and Tirmahi, A., 'Transpiration cooling: Contribution of film cooling to the overall cooling effectiveness', Paper accepted for presentation at ASME International Gas Turbine Conference, Dusseldorf, Fed. Rep. Germany, June 8-12, 1986.

7. Andrews, G.E., Alikhanizadeh, M., Asere, A.A., Hussain, C.I., Azari, M.S., and Mkpadi, M.C., 'Small diameter film cooling holes: Wall convective heat transfer', Paper accepted for presentation - ASME International Gas Turbine Conference, Dusseldorf, Fed. Rep. Germany, June 8-12, 1986.

CONTENTS

page

CHAPTER 1

Nomenclature

η	=	Cycle efficiency
η_{conv}	=	Convection cooling effectiveness
η_{ad}	=	Adiabatic effectiveness
T_{ex}	=	Turbine exhaust temperature
T_{in}	=	Combustor outlet (or turbine inlet) temperature
$T_{1,2}$	=	Coolant air temperature
T_m	=	Flame tube temperature
T_a	=	Adiabatic wall temperature
T_∞	=	Mainstream temperature
Ni	=	Nickel
Cr	=	Chromium
Fe	=	Iron
Mn	=	Manganese
Cu	=	Copper
Si	=	Silicon
C	=	Carbon
S	=	Sulphur
Ti	=	Titanium
Re	=	Reynolds number
$C_{p1,2}$	=	Specific heat capacity
x	=	Distance from slot opening
M	=	Blowing rate
$\rho_{1,2}$	=	Density of mainstream and coolant respectively
$u_{1,2}$	=	Mainstream and coolant velocity respectively
s	=	Slot height
$\mu_{1,2}$	=	Mainstream and coolant dynamic viscosity
E	=	Parameter in adiabatic cooling effectiveness equation

B	=	Parameter in adiabatic cooling effectiveness equation
$W_{1,2}$	=	Molecular weights of mainstream and coolant respectively
α	=	Angle of coolant injection
Pr	=	Prandtl number

CHAPTER 1

INTRODUCTION

The need for extracting power from the combustion of fuel - solid, liquid or gas, led to the development of various types of engines. Gas turbines were developed for their high power to weight ratio, compactness and rapid start-up.

1.1 EARLY GAS TURBINES

Gas turbines have been known as a power house as long ago as 150 BC, when the rising flue gases above a fire were used to drive a turbine (1) in Alexandria by Hero. Around the same time the Chinese were operating windmills. In AD 1791, John Barber patented the forerunner of the gas turbine (2), proposing the cooling of the blades with water injection. Stolze, in 1872, designed a gas turbine with heat addition through a heat exchanger by external combustion. Between 1900 and 1904, Stolze's turbine was built and tested but was abandoned due to inefficiency. This was the first gas turbine to be built and tried (2). In 1905, a gas turbine designed by Armangaud Lemale, which used paraffin oil as fuel, was built by the Société des Turbo-Moteurs but its efficiency was zero. Messrs. Brown, Boveri, in 1928 built the Holzwarth gas turbine, which was a constant volume turbine as opposed to the constant pressure turbine of today. This turbine was used in a German steel plant. It was the cumulative experience gained in the building and testing of these turbine designs, most especially the constant pressure gas turbine for the Velox steam generator, that heralded the birth of the modern gas turbine.

1.2 MODERN GAS TURBINES

With the experience gained from early gas turbines, more constant pressure gas turbines were built for industrial use. The first industrial use of the gas turbine reported was its application in the Houdry Catalytic Process (3) for the production of high-grade gasoline from wide ranges of hydrocarbons, in 1937. By 1939 industrial gas turbines had been well established. A Hungarian engine called Jendrassik (4), using axial flow compressor and turbine, was reported around this time to have achieved an efficiency of 0.021. The SABAR process, in the making of nitric acid (HNO_3), employed a gas turbine.

In the oil and gas industry, the turbo-expander is used variously to separate carbon dioxide (CO_2), hydrogen sulphide (H_2S) and nitrogen (N_2) from natural gas. Gas turbines are now extensively used in pumping oil and gas through pipelines over long distances. Its use is preferred because it can work (1) without supervision for weeks.

In the electricity generating industry the gas turbine is available in power sets from 1 to 100 MW.

In surface transportation the gas turbine engine has also found applications, particularly for very heavy trucks and tanks. The application of gas turbines in the motor industry started in 1950, when it was used in Rover cars. Its use later became more widespread in trucks mostly made by Ford, and now nearly all motor manufacturers have gas turbine engines under development.

The Swiss were the first to employ gas turbine engines in a railway locomotive in 1941 (1), but its use for rail transport has not been widespread.

The use of the gas turbine for aircraft propulsion was not started until the late 1920's, when Stein and Griffith (4,5) separately put forward their proposals for a gas turbine. Whittle (5), working independently around the same time as Griffith, wrote a thesis on the future application of the gas turbine in aircraft. In 1930 Whittle applied for his first gas turbine patent and in 1937 a Whittle engine achieved its first run. It was not until 1941, however, that Whittle flew his W1 engine which employed ten reverse flow combustors. Earlier, in 1939, von Ohain (7) had flown an experimental turbo-jet engine, called Heinkel, in Germany. General Electric spearheaded the use of gas turbines for jet propulsion in the USA and its first engine, which flew in 1941, used Whittle's engine. It was Whittle that brought about the modern propulsion of aircraft employing gas turbines. The early gas turbine powered aircrafts were used for military purposes and it was not until 1953 that civil aircraft came into being. The civil aircraft, called Dart Turboprop, was built in the UK by Rolls Royce.

The birth of the modern gas turbine engine was laden with problems. The most important of these was the high temperature attained by burning fuel in the combustor and encountered by the turbine blades.

1.3 THE COMBUSTION CHAMBER

The combustion chamber design took a large proportion of experimentation by Whittle and his co-workers. The problem of stabilization and relight of the flame was the first to be encountered. On solving this, came the protection of the combustor wall from the high temperature environment created by combustion

products and flames. Many modes of combustor arrangements around the engine were tried and today three main forms are in existence.

1.3.1 Types of Gas Turbine Combustor

Three main types of combustion chambers are in use. These are:

A) the multiple can combustor,

B) the tubo-annular combustor, and

C) the annular combustor.

1.3.1A The multiple can combustor

This type of combustor is used on centrifugal and earlier types of axial flow compressor engines. An early version was developed by Joseph Lucas Limited of Britain (8). It is a modern version of the early Whittle engine combustor. It differs from Whittle's combustor by having straight-through chambers which reduce the large pressure loss that occurs in Whittle's combustor.

The combustors are deposed around the engine (9), each having an inner flame tube with an outer air casing which are supplied with compressor air. To allow the combustors to operate at the same pressure with equal combustion propagation, the chambers are all inter-connected. Figure 1.1 (9) depicts the multiple can combustor arrangement. An example of the German multiple combustor arrangement was that employed in powering Junker's Jumo 004 engine, called the Jumo 004 combustor (8).

1.3.1B The tubo-annular combustor

The tubo-annular combustor is an embodiment of both the multiple and annular combustor. It primarily consists of separate flame tubes (9) fitted inside a common air casing as depicted in fig. 1.2 (9). Its advantages include ease of overhaul and testing as well as cooling of the flame tube.

1.3.1C The annular combustor

This combustor consists of a single flame tube completely annular in form having an inner and outer casing (8,9). It is open at the front to the compressor and at the rear to the turbine nozzle guide vanes, leading to the turbine blades. It has a length approximately 75% of the other combustors for an engine of the same diameter. It has a series of fuel injectors but since it is a single combustor there is no need for interconnectors.

The advantages of the annular combustor, shown in fig. 1.3, include considerable savings in weight and production cost, improved combustion propagation, saving of about 15% in wall cooling air and high combustion efficiency.

As from the early days of the modern gas turbine, it has been recognized that increases in the combustor outlet temperature lead to increase in engine power as well as improved cycle efficiency. Increased combustor temperature however has serious penalties for the combustor wall material and hence it must be cooled.

1.4 COOLING OF THE COMBUSTOR WALL

The need to protect solid surfaces exposed to high temperature environments is an old one. In the case of the gas turbine combustor wall, the high temperature environment is gaseous and the last 30 years have witnessed the development of sophisticated cooling techniques.

The gas turbine cycle efficiency (η) depends, apart from pressure ratio, on temperature inlet to the turbine blades as shown by the equation below.

$$\eta = 1 - \frac{T_{ex}}{T_{in}}$$

where η = Cycle efficiency

T_{ex} = Turbine exhaust temperature

T_{in} = Combustor outlet (or turbine inlet) temperature

The effect on the combustor wall of increasing T_{in} is such that it leads to the heating of the wall beyond the critical temperature of the wall material. This leads to loss in strength of the material and where there is local heating, buckling of the combustor develops as well as cracks. In short, without adequate protection of the combustor wall, service failure of the flame tube results.

The first approach to the protection of the combustor wall from high temperature was the development of high temperature alloys. An alloy often used for combustor walls is Nimonic-75 (8,10). Inconel (8) is another material used. Typical analyses of these two alloys are given in table 1.1.

TABLE 1.1

	Ni%	Cr%	Fe%	Mn%	Cu%	Si%	C%	S%	Ti%
Nimonic-75	74.5	20.0	3.0	0.6	0.3	0.6	0.1	-	0.4
Inconel	78.5	14.0	6.5	0.25	0.2	0.25	0.08	0.015	-

Table 1.1: Analysis of the composition of combustor high temperature material

The temperature that Nimonic-75 can withstand is typically 973 K. In the work presented here, Nimonic-75 has been used.

The temperature in the primary zone of a gas turbine combustor is of the range 1800-2300 K. With this sort of temperature and the thermal limitation on material alloys, methods of cooling the combustor wall are called for. In the early days of both industrial and

aerospace gas turbines, large amounts of air were used to dilute the combustor mainstream gas temperature as well as cool the wall. However the inlet temperature (T_{in}) to the turbine blades has increased and continues to increase, as fig. 1.4 (1) shows. The trend, according to fig. 1.4, of temperature inlet to the turbine (T_{in}) is upwards. The advent of supersonic and high power engines such as the RB211 creates high loading and high compressor air delivery temperatures (11) which increases the difficulty of cooling the combustor wall to acceptable levels. Currently the combustor outlet temperature of around 1500 K is typical with a compressor delivery temperature at 600-850 K depending on the engine pressure ratio and load. At this combustor outlet temperature, 40-50% (12) of total air available for combustion may be used in cooling the combustor wall. Figure 1.5 (after Ref. 12) shows the achievement of cooling the combustor wall.

With the increasing use of alternative fuel as well as low calorific value fuels (13-15), a large proportion of the air available may be used to sustain combustion (16) with little left for cooling the combustor wall. Now low emission combustor design concepts also involve lean primary zones, leaving less air for dilution or cooling. The demand for greater efficiency in both industrial and aero-engines with emphasis on reliability, durability and more simplicity for inspection and maintenance and for the economy of fabrication of the combustor components means that a simple, efficient and effective method of combustor wall cooling must be achieved. Operation at higher T_{in} and with a leaner primary zone, produces a requirement for more efficient cooling using less air and this is the objective of the present work.

1.5 TYPES OF WALL COOLING TECHNIQUES

Whittle (6) pointed out during the development of his aero-engine that progress must be made in the development of cooling techniques if advancement in the gas turbine were to be realized. Ever since, many cooling techniques have come into being. These cooling techniques, which use air as the coolant, are:

1.5.1 Convection wall cooling;

1.5.2 Impingement wall cooling;

1.5.3 Slot film wall cooling;

1.5.4 Thermal-barrier coating wall cooling;

1.5.5 Transpiration wall cooling;

1.5.6 Effusion wall cooling, and

1.5.7 Impingement/effusion wall cooling.

1.5.1 Convection Wall Cooling

This cooling technique uses the process of heat transfer by convection at the back of the flame-tube to cool the combustor. As shown in fig. 1.6(a), the coolant air is made to flow in the annular passage between the flame tube and the outer combustor skin. Convection wall cooling of the combustor wall is widespread but its merit in simplicity of design is punctuated by large cooling air requirement and the extreme difficulties faced when used under high heat flux. Convection cooling alone is generally inadequate and is usually combined with film cooling (49), where it makes a significant contribution to the overall cooling. Work done in Ref. 17 has shown that the cooling effectiveness of a convection cooling method decreases with increasing Reynolds number as

$$\eta_{conv} \propto \frac{1}{Re^{0.2}}$$

where $\eta_{conv} = \frac{T_2 - T_1}{T_m - T_1}$ = cooling effectiveness

Re = Reynolds number based on coolant air flow

T_2 = Coolant air temperature in the annular passage

T_1 = Coolant air temperature before entry to the annular passage

T_m = Flame tube temperature on the coolant side

To optimize convection cooling technique, corrugated 'wiggle-strip', spot-welded to successive lengths of flame-tube, fig. 6.1 (g), has been employed (48). Other methods employ transverse ribs mounted circumferentially on the inner and outer cooling annulus walls with the coolant air passing over the ribs.

1.5.2 Impingement Wall Cooling

This is a cooling technique in which the cooling air exhausts as jets from perforated holes, fig. 1.6(b), impinging on the surface to be cooled, normally referred to as 'target'. The technique has been employed in various fields as a method of convectively cooling or heating surfaces. Examples include drying of paper (19) and textiles, annealing of metals, tempering of glass, cooling of electronic equipment and gas turbine blades (20,21). In its application to cooling of hot surfaces, the impinging jet is constrained to exhaust at one end. The surface heat transfer coefficients, using this technique, were found to be an order of magnitude higher than achievable using the convection method of cooling with air (22). Heat and mass transfer between impinging gas jets and solid surfaces has been reviewed by Martin (23). The technique, although extensively used in turbine blade cooling, has not been widely applied to combustor cooling.

1.5.3 Slot Film Wall Cooling

This is a cooling process whereby the cooling air is ejected into the mainstream through slots, fig. 1.6(c). The coolant air then forms a protective layer of cooling film or heat sink between the hostile hot gas and the flame tube. The cooling potential of the protective film deteriorates with increasing distance from the point of coolant ejection due to entrainment of mainstream which causes increased dilution of the coolant. At distances where the protective film effectiveness falls below a given level, new slots are located. Slot film cooling has been thoroughly investigated. In his investigation of de-icing problems on an aeroplane wing, Wieghardt (24) correlated his experimental results in terms of adiabatic wall effectiveness, η_{ad}, as

$$\eta_{ad} = \frac{T_a - T_\infty}{T_1 - T_\infty}$$

where T_a = Adiabatic wall temperature

T_1 = Coolant temperature upstream of injection

T_∞ = Mainstream gas temperature

Librizzi et al (25) worked on film cooling using variable slots' heights and correlated their cooling effectiveness η_{ad} as

$$\eta_{ad} = \frac{1}{1 + 0.329(C_{p_2}/C_{p_1})\{(x/Ms)[(\mu_2/\mu_1)Re_2]^{-0.25}\}^{0.8}}$$

where $C_{p1\,\&\,2}$ = Specific heat capacity of mainstream and coolant respectively

x = Distance from slot opening

M = Blowing rate = $(\rho_2 u_2)/(\rho_1 u_1)$

s = Slot height

$\mu_{1\,\&\,2}$ = Dynamic viscosity of mainstream and coolant respectively

Re_2 = Reynolds number of coolant based on slot height

Goldstein et al (26) presented their cooling effectiveness as

$$\eta_{ad} = \frac{1.9\,Pr^{\frac{2}{3}}}{1 + 0.329(C_{p_1}/C_{p_2})E^{0\cdot8}B}$$

where $E = (x/Ms)[(\mu_2/\mu_1)Re_2]^{-0\cdot25}$

$B = 1 + 1.5 \times 10^{-4}\, Re_2\, [(\mu_2\, W_1)(\mu_1 W_2)]\sin\alpha$

$W_{1\,\&\,2}$ = Molecular weights of mainstream and injected coolant respectively

α = Angle of coolant injection

Papell et al (27), Seban and Back (28) and Hartnett et al (29) investigated adiabatic wall effectiveness and heat transfer coefficients of slot film cooling. Multiple slots have been studied by Chin et al (30) and Sturgess (31) studied turbulence effect on slot film effectiveness. Sivasegaram and Whitelaw (50) investigated the importance of lip thickness and injection angle. Figure 1.6(h) shows the improved form of the slot cooling method used in Ref. 31. Machined rings (48) and Z-rings have also been employed - fig. 1.6(I).

This is the dominant technique for cooling combustor walls and uses up to 40% of total air available for combustion, and does not stand as a suitable proposition for future gas turbines of high compressor ratio and less air available for cooling.

1.5.4 Thermal-barrier Coating Wall Cooling

The need to protect gas turbine hot-section components, most especially the combustor flame side and the turbine blades, has led to investigation into the use of thermal-barrier coating.

The combustor flame side is coated with a thin layer of ceramic material. The surface formed is then smoothed with a special machine to make sure there is no contour that will affect the flow aerodynamics. The same treatment may be applied to turbine blades.

Winter (32), using a Rolls-Royce Derwent I combustor, investigated the effect of mainstream temperature on the flame tube metal with and without ceramic coating. He concluded that there was nothing to be gained by coating the flame tube with ceramic material, if the emissivity of the ceramic material was higher than that of the metal wall. Gladden et al (33), using variable thicknesses of Zirconia coating on turbine blades, investigated the cooling performance of the blades in comparison with uncoated ones. The work of Gladden et al shows a reduction in metal temperature with coating compared to without. A simulated coating loss resulted in high metal temperature. Mizutani et al (15) used ceramic fiber refractory to line their combustor flame surface in their investigation of low-calorific fuel combustion in industrial gas turbines.

The effect on the combustor metal wall in the event of loss or damage to the coating is to sharply increase the surface temperature. High thermal stresses leading to cracks also result from coating-loss locations. These effects do not make thermal barrier attractive, and more research in this field is called for. However, thermal barrier coatings are receiving widespread applications indicating that many of the problems have been overcome.

1.5.5 Transpiration Wall Cooling

With this technique, the surface to be cooled is usually a porous material. The coolant is forced through the porous wall and ejected into the mainstream, fig. 1.6(d). The secondary fluid,

coolant air, is deflected by the mainstream towards the porous wall to form a layer of cool gas between the wall and the mainstream.

In its simplest form, the porous wall is a woven wire. Other forms are sintered powder metals, fiber metals, foam metals and electro-formed sheets (34,35).

The protection of the hot section of the gas turbine components using this technique has been recognized for more than 30 years (36) as the most effective and efficient. However the materials used for this technique suffer from serious disadvantages such as:

(a) weak thermal strength;

(b) small pore size openings susceptible to clogging by fluid particles;

(c) thermal oxidation of material, and

(d) external pressure variation can cause non-optimum coolant flow distribution.

The above mechanical disadvantages preclude the wide-spread application of this technique but various cooling devices may be compared with it as it gives an indication of the optimum wall cooling performance that can be achieved (16). To overcome the above drawbacks of the transpiration system, complex transpiration walls, Transply (51) and Lamilloy (52) have been developed. The transpiration cooling technique is further considered in Chapter 4.

1.5.6 Effusion Wall Cooling

The surface to be cooled, with this method of cooling, consists of a series of holes, inline or staggered, drilled straight through or inclined at a known angle. The coolant is forced, under pressure, through the holes to the hotter side of the wall, where

it leaves as jets. The jets are then deflected by the mainstream, back towards the wall to form a blanket of heat sink over the wall surface. The technique has elements of the convection cooling and transpiration cooling techniques and its design simplicity make its application in gas turbine hot sections very attractive.

The effusion cooling technique has various forms and most of these have been extensively investigated. The single row and double rows of holes effusion cooling have been widely investigated by Refs. 37, 38, 39 and 40. The other form of effusion technique is the full coverage effusion cooling method, fig. 1.6(e). With this form of effusion cooling, the surface to be cooled is covered with perforated holes. Extensive work has not been carried out in this area and most information is for application to turbine blades (41,42). Mkpadi (43) worked on full coverage effusion cooling with application to the gas turbine combustor. Part of the present work, presented here, is for full coverage discrete hole film cooling with direct application to the combustion chamber and may also be adapted for use in turbine blades. The effusion cooling method is the subject of Chapters 5 and 6.

1.5.7 Impingement/Effusion Wall Cooling

Figure 1.6(f) depicts the impingement/effusion wall cooling technique. This technique is more properly described as the full coverage discrete holes impingement/effusion wall cooling system. It consists of two separately optimized full coverage effusion walls, combined with a gasket, representing the impingement gap z, between the two walls. The first or outer wall is called the impingement wall and the main pressure loss occurs here, and the inner or flame-side wall is called the effusion wall. Coolant is forced through

the impingement and effusion holes to the flame-side of the effusion wall where it leaves as jets. These jets are deflected by the mainstream towards the wall to interact and coalesce forming a cool layer of gas between the hot mainstream and the wall. This technique enhances the process of coolant heat removal (44) within the wall.

The technique of full coverage impingement/effusion cooling has received little previous study. Hollworth et al (45,46) have carried out related work which investigated the influence of effusion holes on impingement heat transfer. The present work is a continuation of that of Ref. 43. Full coverage impingement/effusion cooling is the subject of Chapters 7 and 8.

1.6 RESEARCH SCHEME

As the pressure ratio and cycle temperature of modern gas turbines rise, the problems associated with maintaining an adequate flame-tube wall temperature increase. For industrial gas turbines the surface area to be cooled is relatively larger than for an aero-gas turbine combustor due to the larger combustor volume used. These factors place a requirement for design using low coolant flow per unit surface area and this is the main aim of the present work.

1.6.1 Salient Reasons for Effective and Efficient Gas Turbine Combustor Wall Cooling Methods

The reasons for effective and efficient combustor wall cooling are:

(a) As pointed out in section 1.4, a typical current combustor outlet temperature is 1500 K with 40-45% of total air available for combustion being used for cooling. Future advanced gas turbine

combustor outlet temperatures of 1700-2000 K are envisaged. With the present methods of cooling, 60-70% (16) of the available combustion air may be needed for cooling the combustor wall. This is just not acceptable for efficient combustion as insufficient air will be left for a substoichiometric primary zone.

(b) The increasing tendency to burn low calorific value fuels of 2-18 MJ/m^3 means a large proportion of the combustion air, 70-80%, will be used for combustion sustainment. This leaves 20-30% air for cooling or dilution.

(c) With high turbine blades temperature inlet, there will be increased cooling air flow bypassing the combustor to cool the turbine stators and rotors. The net effect is a reduction in combustor cooling air.

(d) For low emission combustors, particularly for NO_x control, very lean primary zones are required. If this is coupled with the requirement for higher temperature operation, then very little air may remain for cooling and dilution purposes.

It is for the above reasons that research reported here was undertaken. The present investigation focuses on the combustor and looks at three main methods of cooling. These are:

(i) Full coverage discrete hole cooling system,

(ii) Full coverage discrete hole impingement/effusion combined system, and

(iii) Transpiration system.

1.6.2 Research Objectives

(1) To investigate the influence of coolant mass flow rate on the cooling effectiveness of new designs for the above three techniques.

(2) To study the effect of wall thickness on the cooling performance of full coverage designs.

(3) To investigate the dependency of cooling effectiveness on hole size and hole concentration.

(4) To predict the cooling effectiveness of a practical cylindrical combustor using the two full coverage cooling systems.

(5) To develop a heat transfer computer model for a cylindrical gas turbine combustor.

(6) To predict heat transfer coefficients for effusion flame side and also for impingement wall in double wall systems as well as the wall temperature.

(7) To look at jet penetration in the systems.

(8) To investigate the effects of coolant density on cooling effectiveness of the system.

(9) To look at the discharge coefficient of the holes with and without mainstream crossflow.

1.7 REFERENCES

1. Harman, R.T.C., 'Gas Turbine Engineering, Applications, Cycles and Characteristics', The MacMillan Press Ltd., London and Basingstoke, 1981.

2. Meyer, A., 'The combustion gas turbine, its history and development', Proc. Inst. Mech. Engrs., pp. 197-222, 1939.

3. Nelson, W.L., 'Petroleum Refinery Engineering', 2nd ed., McGraw-Hill, New York, 1941.

4. Smith, D.M., 'Discussion on the combustion gas turbine', Proc. Inst. Mech. Engrs., 1939.

5. Armstrong, F.W., 'The aero-engine and its progress fifty years after Griffith', Aeronautical Journal, pp. 499-520, Dec. 1976.

6. Whittle, F., 'The early history of the Whittle jet propulsion gas turbine', Proc. Inst. of Mech. Engrs., Vol. 152, pp. 419-435, 1945.

7. Hawthorne, W.R., 'General considerations', Design and Performance of Gas Turbine Power Plants - High Speed Aerodynamics and Jet Propulsion, Vol. XI, Oxford University Press, 1960.

8. Olson, W.T., 'Combustion chamber development', Design and Performance of Gas Turbine Power Plants - High Speed Aerodynamics and Jet Propulsion, Vol. XI, Oxford University Press, pp. 289-350, 1960.

9. The Jet Engine - Rolls-Royce Ltd., Revised Ed. 1973.

10. Harvey, D.W., 'The combustion system for the Olympus 593 Concorde Engine', Proc. Int. Propulsion Symposium held at the College of Aeronautics, Cranfield, April 1969.

11. Marsland, J., Odgers, J., and Winter, J., 'The effects of flame radiation on flame-tube metal temperatures', 12th Symposium (Int.) on Combustion, pp. 1265-1276, 1968.

12. Hennecke, D.K., 'Heat transfer problems in aero-engines', Heat and Mass Transfer in Rotating Machinery, Ed. D.E. Metzger and N.H. Afgan, Hemisphere Publ. Corp., London, pp. 353-379, 1984.

13. Bahr, D.W., 'Comparison effects of broadened property jet fuels on older and modern J79 combustors', ASME-83-GT-81.

14. Gleason, C.C., Oller, T.L., Shayeson, M.W., and Bahr, D.W., 'Evaluation of fuel character effects on J79 engine combustion system', Air Force Aero Propulsion Laboratory (AFAPL/SFF),1979.

15. Mizutani, Y., and Matsumoto, T., 'A study on a combustor burning low-calorific fuel gases', 83-Tokyo-IGTC-31.

16. Andrews, G.E., and Asere, A., 'Transpiration cooling of gas turbine combustion chamber walls', 1st UK National Heat Transf. Conference, I.Chem.Eng. Symp. Series No. 86, pp. 1047-1056, 1984.

17. Esgar, J.B., Colladay, R.S., and Kaufman, A., 'An analysis of the capabilities and limitations of turbine air cooling methods', NASA TN D-5992, 1970.

18. Colladay, R.S., 'Analysis and comparison of wall cooling schemes for advanced gas turbine applications', NASA TN D-6633, 1972.

19. Daane, R.A., and Han, S.T., 'An analysis of air-impingement drying', Tappi Vol. 44, No. 1, pp. 73-80, 1961.

20. Florschuetz, L.W., and Isoda, Y., 'Flow distributions and discharge coefficient effects for jet array impingement with initial crossflow', J. Eng. for Power, Vol. 105, pp. 296-304, 1983.

21. Sparrow, E.M., Goldstein, R.J., and Rouf, M.A., 'Effect of nozzle-surface separation distance on impingement heat transfer for a jet in a crossflow', Trans. ASME - J. Heat Transf., pp. 529-533, 1975.

22. Gordon, R., and Cobonpue, J., 'Heat transfer between a flat plate and jets of air impinging on it', Int. Heat Transfer Conference, Part II, pp. 454-460, 1961.

23. Martin, H., 'Heat and mass transfer between impinging gas jets and solid surfaces', Advances in Heat Transfer, Vol. 13, 1977.

24. Wieghardt, K., 'Hot-air discharge for de-icing', AAF Trans. No. F-TS-919-RE, Air Material Command, Dec. 1946.

25. Libbrizzi, J., and Cresci, R.J., 'Transpiration cooling of a turbulent boundary layer in an axisymmetric nozzle', AIAA, Vol. 2, pp. 617-624, 1964.

26. Goldstein, R.J., 'Film cooling', Advances in Heat Transfer, Ed. T.F. Irvine and P. Hartnett, Vol. 7, Academic Press London, 1971.

27. Papell, S.S., and Trout, A.M., 'Experimental investigation of air film cooling applied to an adiabatic wall by means of an axially discharging slot', NASA TN D-9, 1959.

28. Seban, R.A., and Back, L.H., 'Effectiveness and heat transfer for a turbulent boundary layer with tangential injection and variable free-stream velocity', ASME - J. Heat Transf., Vol. 84, pp. 235-244, 1962.

29. Hartnett, J.P., Birkebak, R.C., and Eckert, E.R.G., 'Velocity distribution, temperature distributions, effectiveness and heat transfer for air injected through a tangential slot into a turbulent boundary layer', ASME - J. Heat Transfer, Vol. 83, pp. 293-306, 1961.

30. Chin, J.H., Skirvin, S.C., Hayes, L.E., and Burggraf, F., 'Film cooling with multiple slots and louvers', ASME - J. Heat Transfer, Vol. 83, pp. 281-292, 1961.

31. Sturgess, G.J., 'Account of film turbulence for predicting film cooling effectiveness in gas turbine combustors', ASME - J. Eng. Power, Vol. 102, pp. 524-534, 1980.

32. Winter, E.F., 'Heat transfer conditions at the flame tube walls of an aero gas turbine combustion chamber', Fuel - Quart. J. Fuel Science, Vol. 34, pp. 409-428, 1955.

33. Gladden, H.J., and Liebert, C.H., 'Effects of a ceramic coating on metal temperatures of an air-cooled turbine vane', NASA TP-1598, Feb. 1980.

34. Wheeler, H.L., 'Transpiration cooling in the high temperature gas turbine', Bendix Filter Division, The Bendix Corporation, Michigan, March 1964.

35. Grootenhuis, P., 'The mechanism and application of effusion cooling', J. Royal Aero. Soc., Vol. 63, pp. 73-89, Feb. 1959.

36. Bayley, F.J., Cornforth, J.W., and Turner, A.B., 'Experiments on transpiration cooled combustion chambers', Proc. Instn. Mech. Engrs., Vol. 187 17/73, 1973.

37. Brown, A., and Saluja, C.L., 'Film cooling from a single hole and a row of holes of variable pitch to diameter ratio', Int. J. Heat Mass Transfer, Vol. 22, pp. 525-533, 1979.

38. Foster, N.W., and Lampard, D., 'The flow and film cooling effectiveness following injection through a row of holes', ASME - J. Eng. Power, Vol. 102, pp. 584-588, 1980.

39. Wilson, D.J., Goldstein, R.J., and Eriksen, V.L., 'Predicting heat transfer coefficients with film cooling from a row of holes', ASME - J. Heat Transfer, May 1974.

40. Jabbari, M.Y., and Goldstein, R.J., 'Adiabatic wall temperature and heat transfer through two rows of holes', J. Eng. Power, Vol. 100, pp. 303-307, 1978.

41. Kumada, M., Hirata, M., and Kasagi, N., 'Studies of full-coverage film cooling. Part 2: Measurement of local heat transfer coefficient', ASME - 81-GT-38.

42. Mayle, R.E., and Camarata, F.J., 'Multihole cooling film effectiveness and heat transfer', ASME - J. Heat Transfer, pp. 534-538, 1975.

43. Mkpadi, M.C., 'Full Coverage Effusion Cooling of Gas Turbine Combustion Chamber', Ph.D. Thesis, Dept. of Fuel and Energy, University of Leeds, Leeds, 1982.

44. Andrews, G.E., Asere, A.A., Gupta, M.L., and Mkpadi, M.C., 'Full coverage discrete hole film cooling: The influence of hole size', ASME paper No. 85-GT-47.

45. Hollworth, B.R., and Dagan, L., 'Arrays of impinging jets with spent fluid removal through vent holes on the target surface. Part 1: Average heat transfer', ASME - J. Eng. Power, Vol. 102, pp. 994-999, 1980.

46. Hollworth, B.R., Lehmann, G., and Rosiczkowski, J., 'Arrays of impinging jets with spent fluid removal through vent holes on the target surface. Part 2: Local heat transfer', ASME - J. Eng. Power, Vol. 105, pp. 393-402, 1983.

47. Wood, G.R., 'A 6 MW gas turbine for industrial application in the Ruston Tornado', GEC Journal of Science and Technology, Vol. 48, No. 1, pp. 3-10, 1982.

48. Cohen, H., Rogers, G.F.C., and Saravanamuttoo, H.I.H., 'Gas Turbine Theory', 2nd Ed., Longman Group Ltd., London, 1974.

49. Sjoblom, B., 'Combined film and convection cooling in a gas turbine combustor', Paper No. 34, Int. Joint Gas Turbine Congress and Exhibition, July 9-11, 1979.

50. Sivasegaram, S., and Whitelaw, J.H., 'Film cooling slots: The importance of lip thickness and injection angle', J. Mech. Eng. Science, Vol. 11, No. 1, pp. 22-27, 1969.

51. Wassel, A.B., and Bhangu, J.K., 'The development and application of improved combustor wall cooling techniques', ASME Paper No. 80 - GT - 66.

52. Nealy, D.A., and Reider, S.B., 'Evaluation of laminated porous wall materials for combustor liner cooling', ASME Paper No. 79-GT-100.

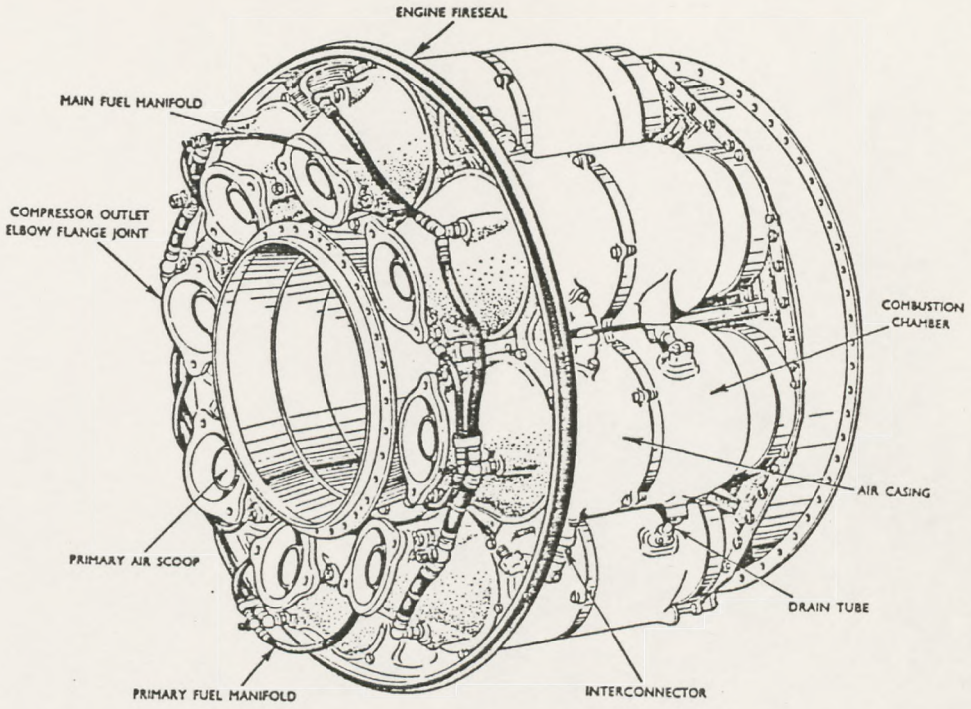

Fig. 1.1: The multiple can combustor

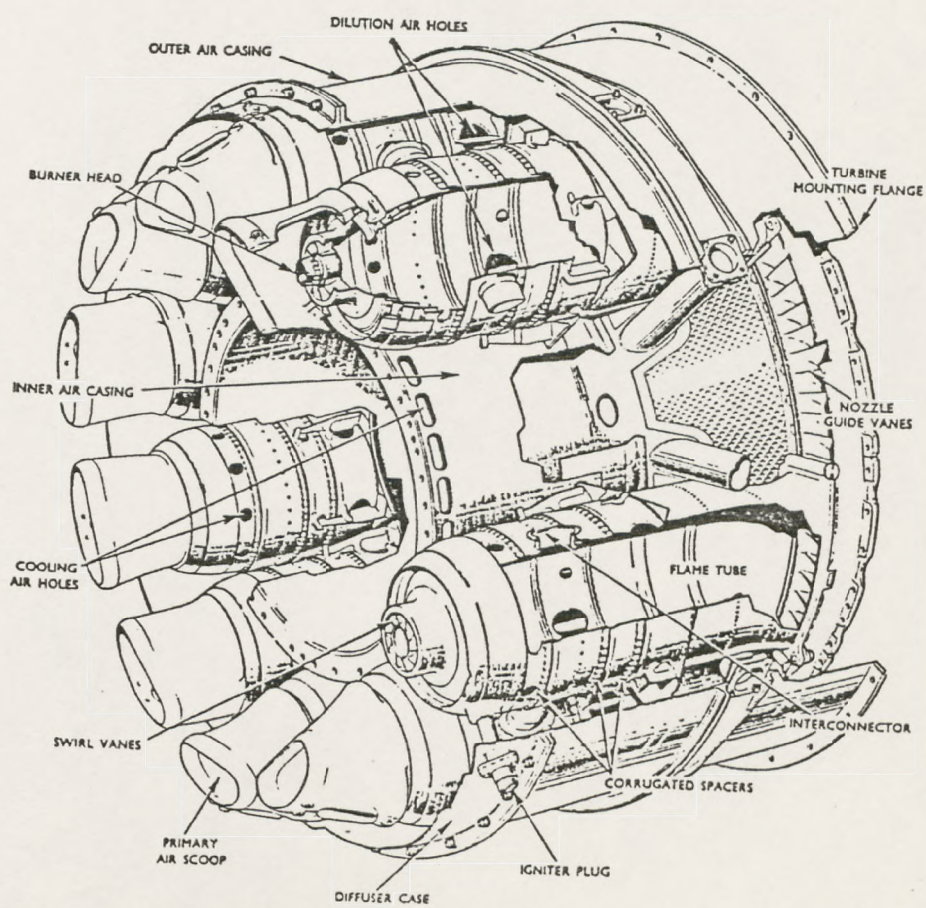

Fig. 1.2: The tubo-annular combustor

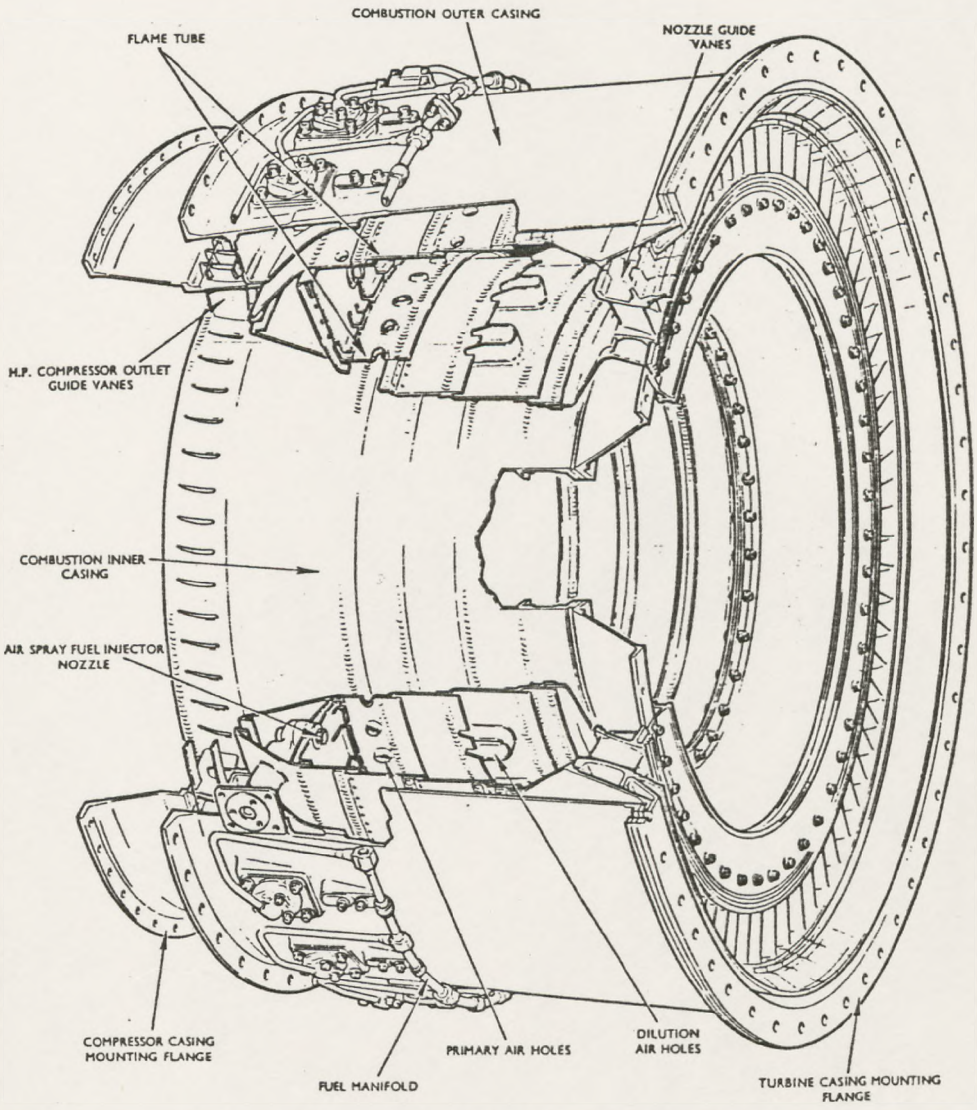

Fig. 1.3: The annular combustor

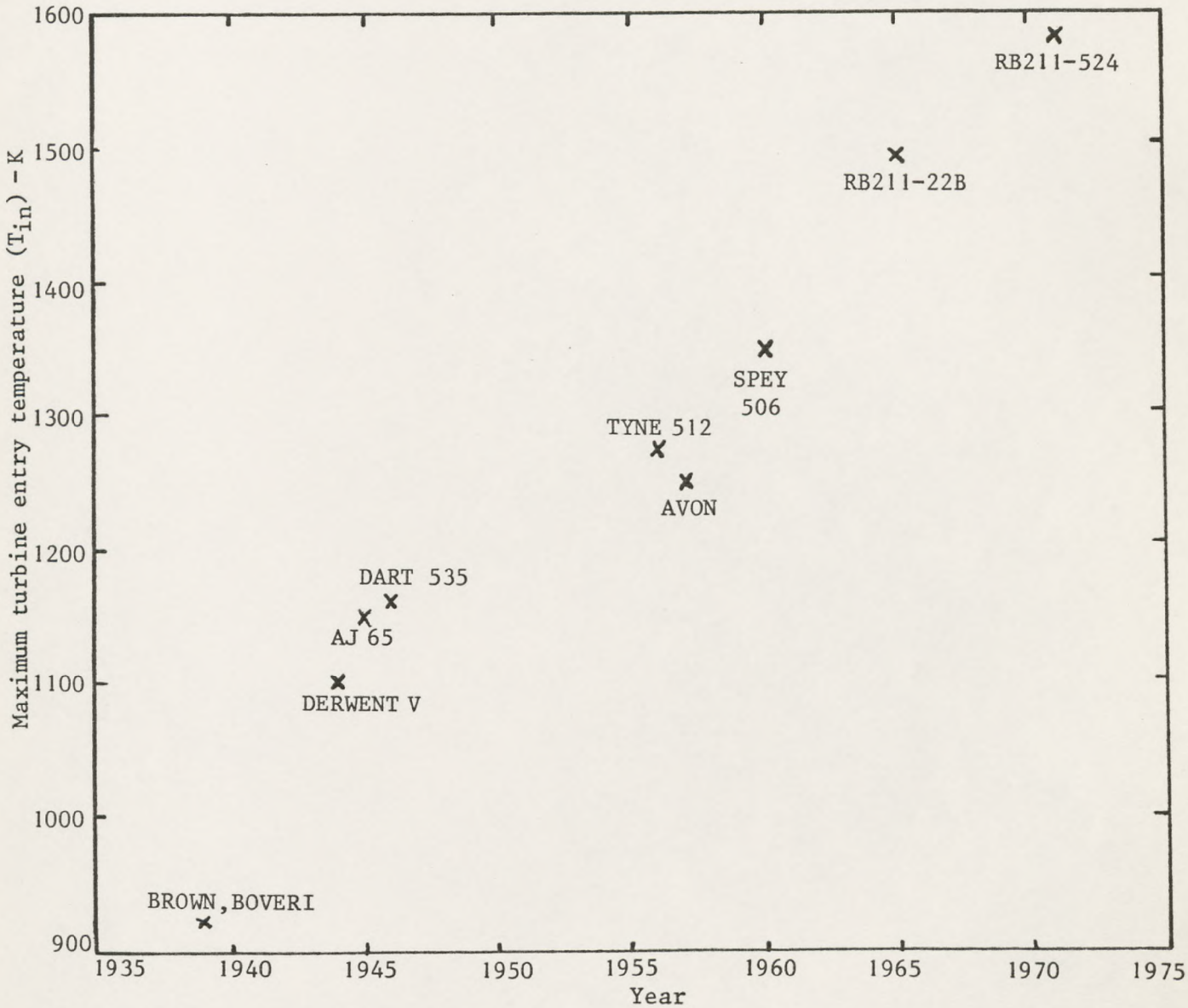

Fig. 1.4: Trend of turbine blade inlet temperature (- K) with engine design

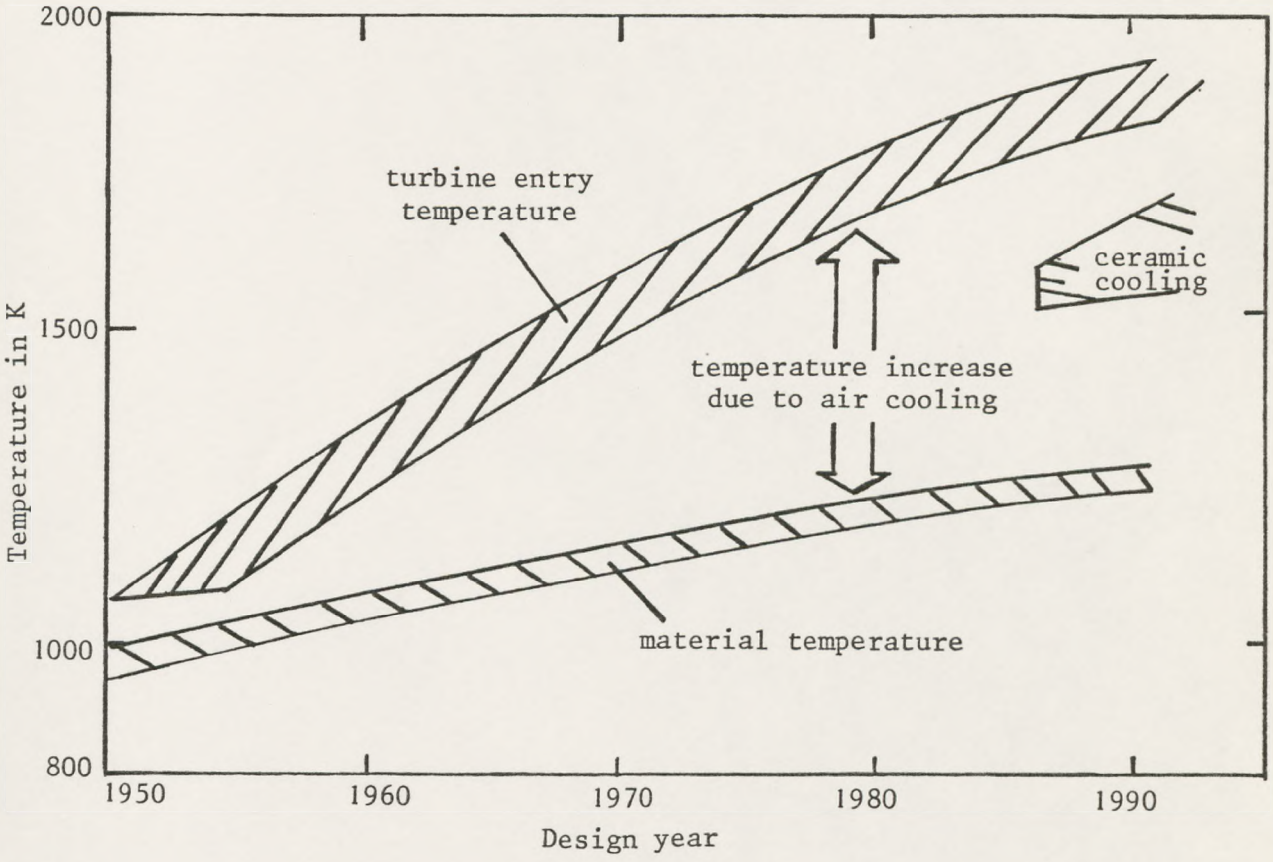

Fig. 1.5: Achievement in material wall cooling

Fig. 1.6: Various techniques of wall cooling

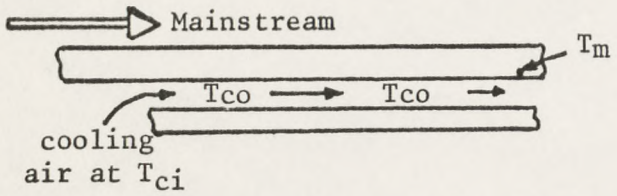

(a) Convection cooling

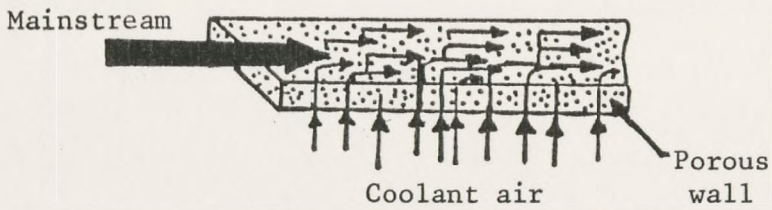

(d) Transpiration cooling (under investigation)

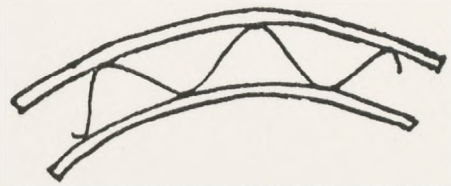

(g) Wriggle strip method

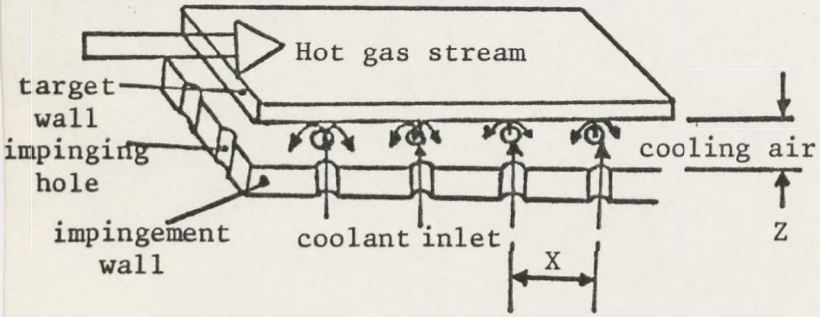

(b) Impingement cooling

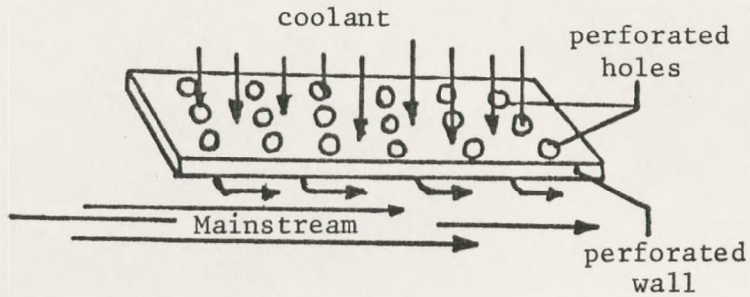

(e) Effusion cooling (under investigation)

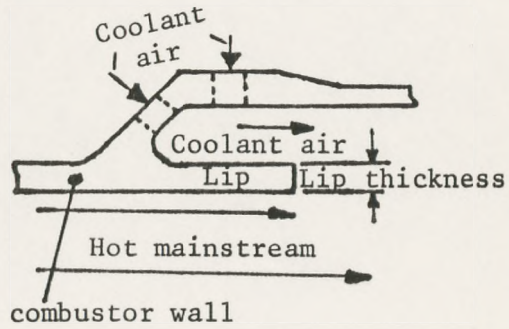

(h) Improved slot film cooling method

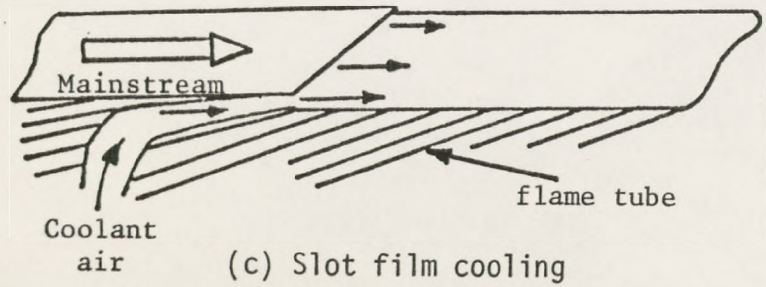

(c) Slot film cooling

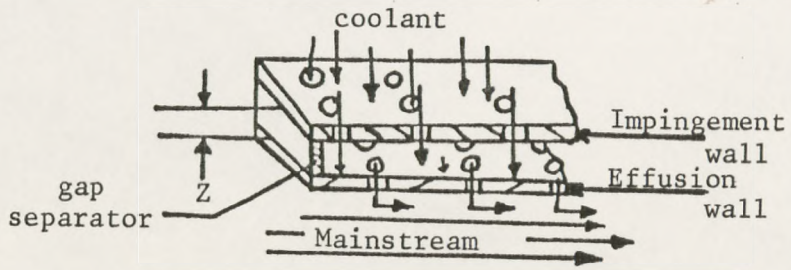

(f) Impingement/effusion wall cooling (under investigation)

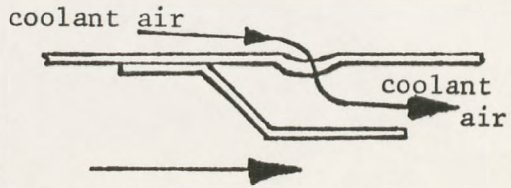

(i) Internal splash ring method

CHAPTER 2

Nomenclature

$\dot{M}$ = Air mass flow rate - kg/s

C_d = Discharge coefficient

E = Velocity of approach

Z = Correction factor

ε = Expansibility factor

A = Area - m^2

ρ = Density of air - kg/m^3

ΔP = Pressure loss

d,D = Diameter - m

m = Area ratio

K = A constant

T = Temperature - K

P = Pressure

G = Coolant mass flow rate - kg/sm^2

n = Number of holes - m^{-2}

X = Hole pitch - m

π = Pi = 3.141593

$\dot{V}$ = Volume flow rate - m^3/s

Subscripts:

V,D = Venturi upstream pipe

R = Reynolds number

a = standard

ac = corrected

CHAPTER 2

EXPERIMENTAL APPARATUS AND PROCEDURE

2.1 INTRODUCTION

The experimental apparatus consisted mainly of the plenum chamber, the combustor, fuel injectors or burners, fan air blowers, the venturi and the test plate (this test plate will subsequently be referred to as the test wall). Most of the apparatus has been used and discussed in Ref. 1 but modifications, for improved accuracy, have been made. Where the old apparatus was used without alteration, only a brief description will be given.

2.2 THE TEST RIG

The test rig is shown in fig. 2.1 and plate 2.1. Not included are the control panels, the fans and the fuel storage tanks.

2.2.1 The Plenum Chamber

The plenum chamber is shown in fig. 2.1 and plate 2.1, sitting on the combustor. The major dimensions are presented in fig. 2.1. The chamber was designed and built in the Department of Fuel and Energy. Apart from the last section of the wall on which the test plate rests, the chamber was made of mild steel. The last section, 152.4 mm from the test wall resting face, was made of stainless steel. The plenum consisted of an electric heater section, which preheated the coolant air from ambient to a temperature $\geqslant$ 700 K, equivalent to a typical compressor air delivery temperature. This was followed by the first main section of the chamber, before which there was a circular air distributor. The air distributor was made

of stainless steel, diameter 95 mm, with 112 drilled holes of mean diameter 1.59 mm and mean hole pitch of 8 mm. At a distance of 152.4 mm from the circular distributor, downstream of the preheater, was another stainless steel air distributor. This was a square section and had a total of 121 holes, on a square array, of mean diameter 1.02 mm, on a mean hole pitch of 12.5 mm. This distributor was 304.8 mm from the test wall. Internally, the plenum chamber was insulated with 'vicuclad'. Previous use of this material as insulator reported a gradual disintegration of the material (1) into dusty particles, resulting in blockage of the test wall holes; otherwise it was credited as a good insulator. To overcome this problem, the surface of the 'vicuclad' in contact with coolant air was given a smooth coating of high temperature 'auto-stick' cement (2). With this in place, there was no problem with the insulation throughout the tests carried out.

The plenum had a total of five thermocouples for monitoring the coolant temperature and another four for checking the heat loss through the insulator.

The coolant thermocouples were inserted horizontally into the chamber and hence perpendicular to the coolant flow. The first two of these thermocouples were located in the first stage of the chamber, after the preheater and circular distributor. The first thermocouple was 421 mm from the test wall and it measured the outlet temperature of the preheated air (coolant). The second thermocouple, 351 mm from the test wall, performed the same function as the first. The plenum chamber proper has three thermocouples. The first and second of the thermocouples were 235 and 55 mm respectively from the test wall while the last one, encased in an L-shaped metal pipe with its end tip sticking out, was approximately

5.5 mm from its tip to the test wall and measured the air temperature at the proximity of the test wall. All these thermocouples were Type K mineral insulated grounded junction thermocouples with a diameter of 1.6 mm. The four thermocouples for checking for heat loss were located at approximately 182 mm from the test wall, two on either side of the box-like plenum. One from each side was placed, through a drilled hole, to just touch the vicuclad metal side face, while the other two were brazed to the outer surface of the plenum metal wall.

At 228.5 mm from the test wall were located four static pressure tappings with holes of 1.5 mm inside diameter, with the end tips made flush with the auto-stick face of the plenum. The four pressure pipes were then connected with a ring pipe, plate 2.1, and connected to a 10-pair selector box (3) for a digital static pressure output. The previous plenum used in Ref. 1, had only one air distributor and one thermocouple and the new plenum was an improvement on it.

Finally, the plenum square end had 28 tap drilled equidistance holes for 2BA screws, for bolting the test wall.

2.2.2 The Combustor - Mk IV

The previous combustor, Mark III, has been described by Mkpadi (1). The Mk III combustor was designed to have an equal wall temperature, during testing, as that of the test wall. It was a parallel, air cooled, double wall combustor with the spent duct coolant, exhausted through holes into the main combustor at the trailing end.

The principle of the design of the Mk IV combustor was the same as that of the Mk III, an externally air cooled duct. However,

the Mk III design used 3.2 mm stainless steel and had a central slot to allow boundary layer traverses at any axial position along the test wall. During high temperature operation, thermal distortion was too severe to allow the cooling air to be throttled and the duct temperature increased to match the test wall temperature. With a lower temperature duct wall, the test wall will lose heat through radiative exchange to the duct walls. Hence the test wall will be radiatively cooled. The correction for this radiative cooling has been detailed in Chapter 5.

The Mk IV combustor is shown in fig. 2.1, while the schematic section of the combustor is shown in fig. 2.2. To achieve the same combustor wall temperature as the test wall, the combustor was designed as a counterflow air cooled duct, with the spent coolant fluid rejected to the test room, fig. 2.2. This temperature matching with the test wall was achieved by throttling the coolant air.

The versatility of the Mk IV has been discussed in Chapters 6 and 8. The thermal expansion of the combustor at both low and high testing temperature was constrained to one-dimensional, by the incorporation of two welded metal bridges, fig. 2.2 and plate 2.3. The magnitude of the expansion was reduced by using high temperature resistant 18/8 stainless steel, 6.35 mm thick, for both outer and inner skins. The combustor inner wall was not attached to the outer skin but could slide on the outer skin through two slots, either side of the rectangular combustor lagged with kao-wool to prevent cooling air from leaking. The exhaust connector was designed with a break in-between, to accommodate the combustor expansion during the test. The instrumentation of the combustor

took into account its high temperature expansion and no problem was encountered throughout the tests. Another improvement of this combustor over that of Mk III was the location of static pressure tappings, six in all, three on each side and on the same plane directly opposite each other. They all had a diameter of 1.5 mm. The middle two were on the central plane, plate 2.2, of the test wall, 38.1 mm below the wall. The combustor was 791.7 mm long, 152.4 mm wide and 76.2 mm high. It was a rectangular conduit with an open top, plate 2.3. The pressure tappings were 93.65, 460.35 and 698 mm respectively along the combustor wall central line, downstream of the Jet Mix (4) flame stabilizer.

The temperature of the combustor, inner skin, was measured by eight Type K mineral insulated grounded junction thermocouples arranged on each side of the wall in the same format as the pressure tappings. The second and third pairs of these thermocouples were located directly under the test wall's first and fifth thermocouples, downstream of the leading edge of the test wall. The third pairs were permanently monitored and the reading indicated was matched, by coolant throttling, with that of the test wall thermocouple. The boundary layer traversing thermocouples, as well as the permanent gas stream temperature monitoring thermocouples, entered through holes which could all be sealed with specially made blanking screws, if temperature monitoring was not required. Matching of the wall temperatures at high testing temperature is limited to the melting point of the duct material (5).

The exhaust connector was designed to serve as a link between the combustor trailing end and the main exhaust pipe. It was rectangular for its first section, immediately after the combustor, with its other section cone-shaped to match the existing exhaust

cylindrical pipe. Unlike the one used on the Mk III rig, it was water cooled and,with its segmented part lagged with kao-wool to prevent leakage, was able to take the thermal expansion of the combustor. The first rectangular section was attached, by bolting, to the combustor, plate 2.1, while the other half was bolted to the main exhaust pipe, fig. 2.1.

2.2.3 The Propane Burner

Vitiated air was produced by burning propane at this burner, 1540 mm from the jet mix stabilizer, fig. 2.1. The burner, enclosed in a long perforated cylindrical tube, was a multihole injector type and uses about 25% of the total combustion air to generate very high temperature combustion flue gases which were exhausted as jets, interacting and mixing with the rest of the mainstream, downstream of the burner. Final combustor air inlet temperature from 300 K to 950 K could be generated in this way, by either adjusting the main air mass flow rate or the mass flow rate of the propane. Further discussion of this burner may be found in Refs. 1 and 6. The only modification made to this burner was the replacement of the igniter with a cheaper 125 igniter. Operating conditions of the burner are detailed in Ref. 1, fig. 3.3.

2.2.4 The Venturi

The venturi, located upstream of the propane burner and downstream of the air fan, was designed and built in the Department. It has been described and used by Ref. 1. It was used to measure the mainstream air supplied mass flow rate. Though no alteration was made, the discharge coefficient of the throat was recomputed. The apparatus was brought down and measurements of the pipe and

throat diameters were taken. The throat inside diameter was found to have a mean value of 63.77 mm compared with 63 mm used by Ref. 1, while the upstream pipe mean diameter was found to be 150.55 mm instead of 152 mm used in Ref. 1. The cause of the above difference may be due to rust which was found along the inner surface of the venturi wall. Though the differences were not significant, a reprocessing of the calibrating data was carried out. The results are presented in the Appendix, table 2.1. The mass flow rate of fluid through the venturi is correlated as in equation 2.1.

$$\dot{M} = C_d E Z \varepsilon A (2\rho_v \Delta P)^{0.5} \qquad \ldots (2.1)$$

where $\dot{M}$ = Air mass flow rate

C_d = Discharge coefficient

E = Velocity of approach factor

$$E = \frac{1}{(1 - m^2)^{0.5}}$$

$$m = \frac{\text{cross-sectional area of Venturi throat}}{\text{cross-sectional area of upstream pipe}} = \left(\frac{d}{D}\right)^2$$

d = Throat's diameter = 63.77 mm

D = 150.55 mm

$\therefore$ m = 0.1794

and E = 1.0165

Z = Correction factor = $Z_R . Z_D$ (7) = 0.991

Z_R = Reynolds number correction factor

Z_D = Upstream pipe size correction factor

ε = Expansibility factor (7) = 0.995 (table 2.1)

A = Cross-sectional area of throat = $\frac{\pi d^2}{4}$ = 3.194×10^{-3} - m^2

ρ_v = Air density at upstream pipe temperature and absolute pressure

ΔP = Pressure loss between the upstream and the throat

The computation of C_d from the above equation from the calibrating data, table 2.1, yielded a mean C_d value of 0.929 ± 0.002. This value of C_d is lower than in BS 1042 due to the mild steel construction and the weld at the throat. The venturi was calibrated against a finely machined aluminium venturi to full BS 1042 specification. Equation 2.1 may be expressed as equation 2.2.

$$\dot{M} = C_d K(2\rho_v \Delta P)^{0.5} \quad \ldots (2.2)$$

where $K = E Z \varepsilon A$

substituting, $K = 3.2014 \times 10^{-3}$

Using the above value of C_d, the air mass flow rate to the combustor is given by equation 2.3.

$$\dot{M} = 2.9726 \times 10^{-3}(2\rho_v \Delta P)^{0.5} \quad \ldots (2.3)$$

The air density is corrected for from standard value of air density at 273 K (T_a) and 1.01333×10^5 Pa (P_a) which is $\rho_a = 1.293$ kg/m^3. Knowing the upstream venturi pipe air temperature (T_v) and absolute pressure (P_v), the air density (ρ_v) is given by the gas law as in equation 2.4.

$$\rho_v = \frac{\rho_a T_a P_v}{P_a T_v} \quad \ldots (2.4)$$

From equations 2.3 and 2.4, the mass flow rate of the combustor air was determined.

2.2.5 The Test Wall

The material used for the test walls was the high temperature alloy, Nimonic-75. The composition of this material has been presented in Chapter 1, section 1.5, table 1.1. The test area was

a 152.4 mm square with holes, which simulates a part of the wall of a combustor, Chap. 1, fig. 1.3.

2.2.5A Design requirements

The selection of suitable hole geometries applicable in full coverage gas turbine combustor wall cooling situations requires the knowledge of the coolant mass flow rate per unit surface area. To enhance the selection of realistic geometries, a survey of coolant flows per unit surface areas for a range of aero and industrial gas turbines was carried out (8-10). The results are presented in table 2.2; the data were obtained by dividing the engine mass flow by the operating pressure and the flame tube surface area. The latter parameter was approximately evaluated by taking combustion chambers as simple cylinders or annular rings; however the resultant values of the coolant mass flow per unit surface area, G, are reliable to ± 10% for design purposes. Table 2.2 indicates that a range of G values from 0.9 to 1.5 kg/sm^2 bar is representative of current cooling techniques. To reduce the proportion of the present cooling requirement from $\geqslant$40% to 10-20% of the total flow rate, a G value of $0.2 \leqslant G \leqslant 0.4$ is called for. The correlating equation for G, discharge coefficient of the hole and the pressure loss across the wall, has been presented in Chapter 3.

For the effusion and impingement/effusion cooling of the combustor, the maximum pressure loss of the wall is that of the combustor pressure loss (9,10). The design of the effusion or impingement plate is specified by the desired pressure loss, $\Delta P/P$, and the required G. The hole pitch, X, for a square array of holes (n - number of holes/m^2) is given by equation 2.5.

$$X = n^{-0.5} \qquad \ldots (2.5)$$

TABLE 2.2

G%	A	B	C	D	E	F	G	H
10	0.22	0.14	0.24	0.20	0.23	0.33	0.10	0.30
20	0.45	0.28	0.47	0.41	0.47	0.67	0.20	0.60
30	0.67	0.43	0.71	0.61	0.70	0.99	0.30	0.90
40	0.90	0.57	0.95	0.82	0.93	1.32	0.40	1.20
50	1.12	0.71	1.18	1.02	1.16	1.65	0.50	1.50

Table 2.2: Coolant air flow at 1 bar per unit surface area, G - kg/sm^2, for a range of gas turbines A-H

The holes' mean diameter is given as

$$D = \left(\frac{4}{\pi}\frac{A}{n}\right)^{0.5} \qquad \ldots (2.6)$$

Combining equations 2.5 and 2.6, X is shown to be related to the total coolant flow area per square metre of wall area, A, by equation 2.7.

$$\frac{X}{D} = \left(\frac{\pi}{4A}\right)^{0.5} \qquad \ldots (2.7)$$

From the definition of G and equation 2.6, it may be shown that the hole pitch to diameter ratio is related to the pressure loss as in equation 2.8.

$$\frac{X}{D} = \left(\frac{\pi}{4} C_d P\right)^{0.5} \left(\frac{2}{RT}\right)^{0.25} \frac{(\Delta P/P)^{0.25}}{G^{0.5}} \qquad \ldots (2.8)$$

For a hole G of 0.8, Chapter 3, and a pressure P of 1 bar, equation 2.8 reduces to equation 2.9.

$$\frac{X}{D} = 72.4\left(\frac{\Delta P/P}{T}\right)^{0.25} \frac{1}{G^{0.5}} \qquad \ldots (2.9)$$

The values of X/D for two practical values of $\Delta P/P$, at two coolant temperatures and a range of G from 10% to 100% of the combustion air flow, as summarised in table 2.2, is presented in table 2.3. Table 2.3 shows that for combustor wall cooling applications impingement heat transfer correlations for a range of X/D from 3 to 18 are required.

TABLE 2.3

$\frac{\Delta P}{P}$ %	T (K)	X/D									
		G ($kg\ s^{-1}m^{-2}$ at 10^5 Pa)									
		0.2	0.3	0.4	0.5	0.6	0.8	1.0	1.5	2.0	3.0
3	300.2	16.6	13.2	11.5	10.2	9.3	8.1	7.2	5.9	5.1	4.2
	700.2	13.1	10.7	9.3	8.3	7.6	6.6	5.9	4.8	4.1	3.4
5	300.2	18.4	15.0	13.0	11.6	10.6	9.2	8.2	6.7	5.8	4.8
	700.2	14.9	12.2	10.5	9.4	8.6	7.4	6.7	5.4	4.7	3.8

Table 2.3: Impingement geometries of combustor wall cooling

From the above correlations, test walls of holes' mean diameter, D, for a given $\Delta P/P$ and G value were designed.

2.2.5B Hole size manufacture and determination

All the test walls were manufactured by GEC Gas Turbines Limited. In the present work two methods of holes manufacture have been employed. One was by mechanical drilling, while the other was by laser drilling. The methods of manufacture were reflected in the holes discharge coefficient (Chapter 3).

To determine the hole diameters a special measuring gauge was used. This gauge was called the Kwik-Chek Hole Gage. It was manufactured in the USA (11). It has a high standard of accuracy and a setting standard supplied with it indicates a precise measurement up to 0.01 mm. Using this gauge, the holes' mean diameter was determined. For the very low pressure loss wall, Chapter 3, a small hole gauge set was used. The four gauges had ranges 10 - 12.7, 7.6 - 10, 5.1 - 10 and 3.18 - 5.1 mm respectively. The set (12) was used in conjunction with a micrometer which has an accuracy to 0.001 mm (12). The computation of the mean holes' diameter and the error involved has been discussed in Chapter 3. A typical test wall with wall thermocouple locations but without test holes is shown in fig. 2.4 while a real test wall is presented in plates 2.6 and 2.7.

For testing, the wall was bolted to the plenum wall using 2BA screws and 'auto-stick' cement, which serves as high temperature sealant preventing the coolant air from leaking. The 'auto-stick' cement is capable of withstanding a temperature of up to 1373 K without losing its sealing capability. The rig was then set up as indicated in fig. 2.1 and plates 2.1 - 2.2.

2.2.6 Combustor Accessories

The top of the combustor also houses other apparatus that cover up the top of the duct.

2.2.6A The stabilizer cover

The stabilizer cover was next to the stabilizer and protected the leading end of the combustor. It was designed and built as a counterflow double skin air-cooled unit. The cooling air was supplied by the same fan that supplied the combustor coolant but separate

from the combustor mainstream air fan. The spent coolant was made to discharge to the test room through 12 drilled holes of diameter 12 mm and hole pitch of 30 mm. It was 288 by 178 mm and had a height of 20 mm. The hollow space was 13 mm. It also had flanges with which it was bolted to the rig. The temperature of this unit flat face, in contact with the mainstream, was monitored by three thermocouples along the centre line of the wall, equidistant from each other.

2.2.6B The heat flux meter

The heat flux meter sits sandwiched between the stabilizer cover and the test wall, plate 2.3. It is the unit used in measuring the heat transfer coefficient of an unperforated flat plate. It is a box, 63.5 mm wide with a 254 mm span and 13 mm high with a horizontal perforated partition inside, 6.35 mm above the unperforated base plate. Both the temperature of the inlet and outlet coolant air, that cools the wall, as well as the base plate temperature were measured during testing with the Type K mineral insulated grounded junction thermocouples. It was used by Ref. 1, and detailed dimensions of the design may be found in that reference.

2.2.6C The combustor trailing end plate cover

This was a stainless steel box mainly used to cover this part of the combustor. It previously served as a gas sampling probe but in the present work no sampling work was undertaken.

2.2.6D The traversing mechanism and thermocouples

The traversing mechanism was a machine operated by a Miniangle Stepping Motor, Type 34PM-C006 (13) with accuracy better than 0.1 mm.

This mechanism is shown in plate 2.2 resting on its block. It has two sliding directional blocks, vertical and horizontal. The vertical block was used for thermal boundary layer traversing while the horizontal block was used to traverse thermocouple across the combustor to check the combustion gas temperature's uniformity, discussed in Chapters 6 and 8. The traverse stepping motors were controlled from a separate unit called 'Unislide'(14). The stepping motor was activated by the Unislide, which also governed the distance travelled in either the vertical or horizontal directions through a specification controller. The vertical traversing block was adapted to carry three thermocouples 50 mm apart (5) as shown in plate 2.2.

2.3 THE FLOW SYSTEM

Flow metering systems were required for the air coolant flow, combustion air, and fuel in the form of propane and kerosine.

2.3.1 Coolant Air

The coolant air was supplied by a departmental compressor, and to make sure the air was dry and clean, a metal filter and a carbon filter were fitted in the flow line before the rotameters. The coolant air temperature was measured upstream of the rotameters with a Type K thermocouple. The coolant gauge pressure was also measured upstream of the rotameters, plate 2.5, using for high pressure at high flow the Appleby and Ireland gauges also shown in plate 2.5; at low coolant flow and low pressure the Furness Control electronic micromanometer was used. The accuracy of the Appleby and Ireland gauges was better than 1%, and the electronic micromanometer better than 0.1%.

As discussed in Chapter 3, three rotameters were used in measuring the volume flow rate of the coolant air. The ranges of the rotameters are 15-150 l/min, 50-500 l/min and 200-2000 l/min. The coolant flow rates were controlled by valves shown in plate 2.5. The coolant flow route is shown in fig. 2.3.

The calibration of the rotameters in l/min by the manufacturer was done at a temperature of 288 K and at an absolute pressure of 101.33×10^3 Pa. At operating conditions different from the above, a correction for actual fluid flow is necessary. Flow through rotameters is governed by the general orifice plate flow equation as

$$\dot{V} = \text{Const.} \frac{h}{\rho^{0.5}} \qquad \ldots (2.10)$$

where $\dot{V}$ = Volume flow rate

h = Float height

ρ = Fluid density

For a given h, the actual volume flow rate, $\dot{V}_{ac}$, is related to the rotameter indicated volume flow rate, $\dot{V}$, by equation 2.11.

$$\dot{V}_{ac} = \dot{V}\left(\frac{\rho}{\rho_{ac}}\right)^{0.5} \qquad \ldots (2.11)$$

where $\dot{V}$ and ρ = rotameter's calibration condition

V_{ac} and ρ_{ac} = actual flow condition

The correct fluid mass flow rate through the rotameter is given by equation 2.12.

$$\dot{M} = \rho_{ac} \dot{V}_{ac} = \dot{V}(\rho\, \rho_{ac})^{0.5} \qquad \ldots (2.12)$$

2.3.2 The Combustion Air

The combustion air was supplied by a fan and the measurement of the air mass flow rate was as discussed above and the route it follows is shown in fig. 2.3.

2.3.3 The Propane Fuel

The propane fuel was burnt during low and high temperature tests, supplied from an external bank of cylinders, fig. 2.3, through a pipe. The flow rate was measured using a rotameter, plate 2.4, of flow range 15-125 l/min (15). The temperature and pressure gauge were also monitored. At the burner, it was ignited by the igniter discussed above. The igniter was activated by a 16 joule ignition unit, type HP/16/LIT, (16), which delivers charges of 200-250 volts on the pressing of a switch on the control panel, plate 2.4. The propane line also has a nitrogen purge line which automatically comes on when the fuel is shut off and purges the system.

2.3.4 The Kerosine Fuel Line

The kerosine fuel was only burnt during the high temperature test. It was contained in a tank, fig. 2.3, which has at its inlet and outlet, metal filters that remove any particles in the fuel. The fuel was pumped overhead by an HR Flow Inducer, Type MHRE-200, Vol-200-250 (17), to obtain a constant flow through the flow measuring rotameter on the control panel. The rotameter had a range of 0.14-0.9 l/min, and was a GEC-Elliott Series 1100 type (18). After the measuring rotameter, the fluid passed through three series of solenoid valves which controlled its flow to the three jet mix stabilizers. In case of an ignition failure these solenoids

were activated from the control panel and stopped the fuel flow to the injectors. The first use of this kerosine line in the present work reveals a flame bias caused by an uneven distribution of the fuel to the injectors. To eliminate uneven fuel feed to the injectors, three rotameters, Type B6HS, of ranges 20-280 cm^3/min each, were installed on the fuel line just before the injectors, fig. 2.3, but after the solenoids. During a test, it could be checked to see if there was equal flow of fuel to the injectors. If the rotameters did not indicate equal flow levels, it means one or two of the injector/injectors holes have been blocked and the test was terminated, the rig stripped down and the blockage cleared. Since the installation of these rotameters with the Mk IV combustor, the flame bias has ceased. The kerosine was ignited by an igniter located in the combustor, 20 mm downstream of the stabilizer through the same ignition unit as for the propane.

2.4 INSTRUMENTATION

All the thermocouples referred to in the preceding sections were Type K mineral insulated grounded junction type. Their readings were monitored, plate 2.5, using three digital output and six Way Type K selector units (there were about 70 thermocouples), all of Digitron Model 3750-K (19). The temperature of the combustion gases at 333.35 mm downstream of the stabilizer was measured by a permanently placed Pt/Pt 6% Rh thermocouple, plate 2.2. The digital output of this thermocouple was obtained using the Newport digital output, model 267B-BC1 (20). For high temperature tests, the traversing thermocouple was reduced to the middle one which was at the centre line of the test wall. The Type K

thermocouple was also replaced by a Pt/Pt 13% Rh thermocouple which was monitored by an 'Ancom' digital output and switch (21), Type DTR 1600. Both Pt/Rh thermocouples were mineral insulated.

All the pressure gauges of the rotameters were measured by the Appleby and Ireland pressure gauges, plate 2.4. At low coolant flow rates and for all other pressure measurements, the 10-pair selection box was used and the outputs of these were monitored on the Furness Control (22) digital micromanometer.

2.5 THE TESTING PROCEDURE

Three main testing formulations were carried out in the present investigation. These were discharge coefficient, low temperature test and high temperature test. At both low and high temperature tests, thermal boundary layer traverses were carried out. The procedures for these tests, apart from that for discharge coefficient which has been discussed in Chapter 3, are discussed in the following subsections.

2.5.1 Low Temperature Test

For the low temperature, the rig was prepared by bolting either the single test wall - effusion wall, or the impingement/effusion combined system (see Chapters 7 and 8), to the plenum using 2BA screws and auto-stick cement as sealant. The plenum was placed at its location on the combustor with all other combustor accessories installed. The fan and the cooling air were then turned on, including cooling water for the connector and the main exhaust pipe. The final and middle test wall thermocouples were linked to an X-Y plotter. This plotter indicated when the test wall temperature

reached stability by plotting the temperature profiles against time. The traversing machine was also switched on with the thermocouples half way of the combustor height. At this stage the igniter was started, followed by the switching on of the propane fuel, having previously turned on the cylinders. The combustor inlet air temperature was the only one on which close watch was made during this period. If the fuel was successfully ignited, the air inlet temperature would start rising rapidly but without ignition this temperature would remain at a constant level, few degrees above ambient. With successful ignition, the igniter was switched off and standard testing level of inlet temperature was set. The standard combustor air inlet temperature for the low temperature test was 773 ± 1 K. The combustor wall temperature on the same plane as the test wall final temperature (fifth thermocouple) was matched with its opposite number (final temperature) on the test wall. This was continually adjusted by coolant air throttling to the combustor wall until the final test wall temperature indicated stability on the plotter. The process normally took at least 30 minutes but may be more.

Having attained stability, the recordings of all the parameters discussed earlier, including the test wall temperature, were then made. If traversing at this test wall coolant flow rate was required, traversing was done, otherwise the adiabatic temperature of the wall was measured. This was done by traversing the triple thermocouples until they nearly touched the test wall. At this point the thermocouples were physically adjusted by hand until they touched the wall. The indicated readings were then recorded as the adiabatic temperature of the wall. After this, a new test wall

coolant flow rate was set on the rotameter and the process repeated. Throughout the test, the combustor air inlet temperature set at the beginning was maintained.

At the end of the test, the propane was the first to be turned off and, although the nitrogen purge comes on line automatically, the rest of the fluid lines were left on for a considerable length of time for cooling purposes. When the equipment indicates ambient temperature, the fluid lines were shut down.

2.5.2 High Temperature Test

The high temperature test procedure was the same as that of the low temperature test. However in addition to this was the preheating of the test wall coolant air and the firing of kerosine. Having set the test wall coolant air, the electric preheater in the coolant line was switched on from the mains and the plenum preheater coolant temperature was allowed to rise to $\leq$ 700 K and left at this level throughout the test. The kerosine pump was switched on. After the combustor air inlet temperature had achieved stability, the combustor igniter was switched on and kerosine was allowed to flow into the injectors, where it was injected as jets into and atomized by the mainstream. The trend of events in the test room was continuously monitored on an overhead television screen, plate 2.4, with a camera in the test room and the flame could be seen through an air cooled glass window, fig. 2.1 and plate 2.5. When there was ignition, a blue kerosine flame was easily seen through the window as well as the flame quality produced by each of the stabilizers. If the flame was distorted or one or two of the stabilizers showed unstable flames, the inlet rotameters at the base of the stabilizers would be checked to see which of the injectors was blocked. Sometimes

it was possible to unblock the injector by switching on the particular injector solenoid valve and increasing propane flow to produce higher inlet temperature. This process occasionally removes the blockage, otherwise the rig was shut down and the blockage cleared. With the absence of blockage problems, the data acquisition process was as for the low temperature test. The adiabatic temperature was measured in the same way but, as stated earlier, with one thermocouple, the Pt/Pt 13% Rh.

The problem of physical adjustment was difficult because of the intense heat and the bending of the thermocouple on contact with the test wall. This problem was overcome by observing the thermocouple through the window in the control room and telling when the thermocouple just touched the test wall.

2.5.3 Thermal Boundary Layer Traversing

At low temperature the thermal boundary layer on the test wall was traversed using the triple Type K thermocouples as stated earlier. At any given test wall coolant flow rate, the thermocouples were traversed until they nearly touched the test wall. The thermocouples were then physically adjusted by hand until they actually touched the test wall. This position of the thermocouple was recorded, as zero distance, and also the thermocouple readings at this point. The Unislide was then set to move the thermocouples 0.5 mm away from the wall in a vertical direction. This was followed by a series of other downward movements, first in steps of 1 mm at a time through a distance of 10 mm and then in steps of 2 mm through a distance of another 10 mm. This was finally followed by steps of 5 mm, until constant temperature was established for a series of further downward traverses. The temperature indicated by

the thermocouples at each traverse step was recorded against total distance travelled away from the test wall. The temperature at which readings remain constant for further downward traverse was taken as the temperature of the mainstream. The process was repeated for a range of test wall coolant flow rates.

The same process was repeated at the high temperature test, with the Pt/Pt 13% Rh thermocouple, for a range of test wall coolant flow rates.

2.6 DATA ACQUISITION FORMAT

The data acquisition format sheets for a single test are shown in the Appendix, table 4 (A-G). The reduction of the data has been discussed in Chapters 5 and 7.

2.7 REFERENCES

1. Mkpadi, M.C., 'Full Coverage Effusion Cooling of Gas Turbine Combustion Chamber', Ph.D. Thesis, Dept. of Fuel and Energy, University of Leeds, Leeds, 1982.

2. 'Auto-stick Cement' by Carlton Brown & Partners Limited, Elford Mill, Elford, Nr. Tamworth, Staffs., B79 9BL, England.

3. 10-pair Selection Box, Furness Control Ltd., Bexhill, England.

4. Andrews, G.E., Al-Dabbagh, N.A., and Abdul Aziz, M.M., 'Mixing and fuel atomization effects on premixed combustor performance', ASME Paper 83-GT-55, 1983.

5. Andrews, G.E., and Asere, A.A., 'Gas turbine combustor wall cooling XII', Report No. GEA/HT/21, Dept. of Fuel and Energy, University of Leeds, 7.2.85.

6. Andrews, G.E., Gupta, M.L., and Mkpadi, M.C., Report No. GEA/HT/4, Oct. 1980.

7. BS 1042 Part 1 : 1964 (Fluid measurement).

8. Andrews, G.E., and Mkpadi, M.C., 'Full coverage discrete hole wall cooling: Discharge coefficients', Trans. ASME, J. Eng. Power, Vol. 106, pp. 183-192, 1984.

9. Andrews, G.E., Asere, A.A., Hussain, C.I., and Mkpadi, M.C., 'Full coverage impingement heat transfer: The variation in pitch to diameter ratio at a constant gap', AGARD-CP-390, pp. 26, 1-13, Bergen, Norway, 6-10 May 1985.

10. Andrews, G.E., Asere, A.A., Hussain, C.I., and Mkpadi, M.C., 'Transpiration and impingement/effusion cooling of gas turbine combustion chambers', 7th Int. Symp. on Air Breathing Engines, Peking, 1985.

11. Kwik-Chek Gage Company, 1021 Commercial Ave., PO Box 41, East Petersburg, Pennsylvania 17520.

12. Draper of Japan.

13. Shinkoh Communications Industry Co. Ltd.

14. Time and Precision Ltd., Basingstoke, Hants., England.

15. GEC-Marconi Process Control Ltd., Flowmeter Division, Croydon, England.

16. AISH & Co. Ltd., Poole, Dorset, UK.

17. Watson-Marlow Ltd., Falmouth, Cornwall, England.

18. GEC-Elliott Process Instruments Ltd., England.

19. Digitron Instrumentation Ltd.

20. Newport Electronic Inco. Santa Ana, California, 92705.

21. Ancom S, Cheltenham, Glos., England.

22. Furness Controls Ltd., Bex Hill, England.

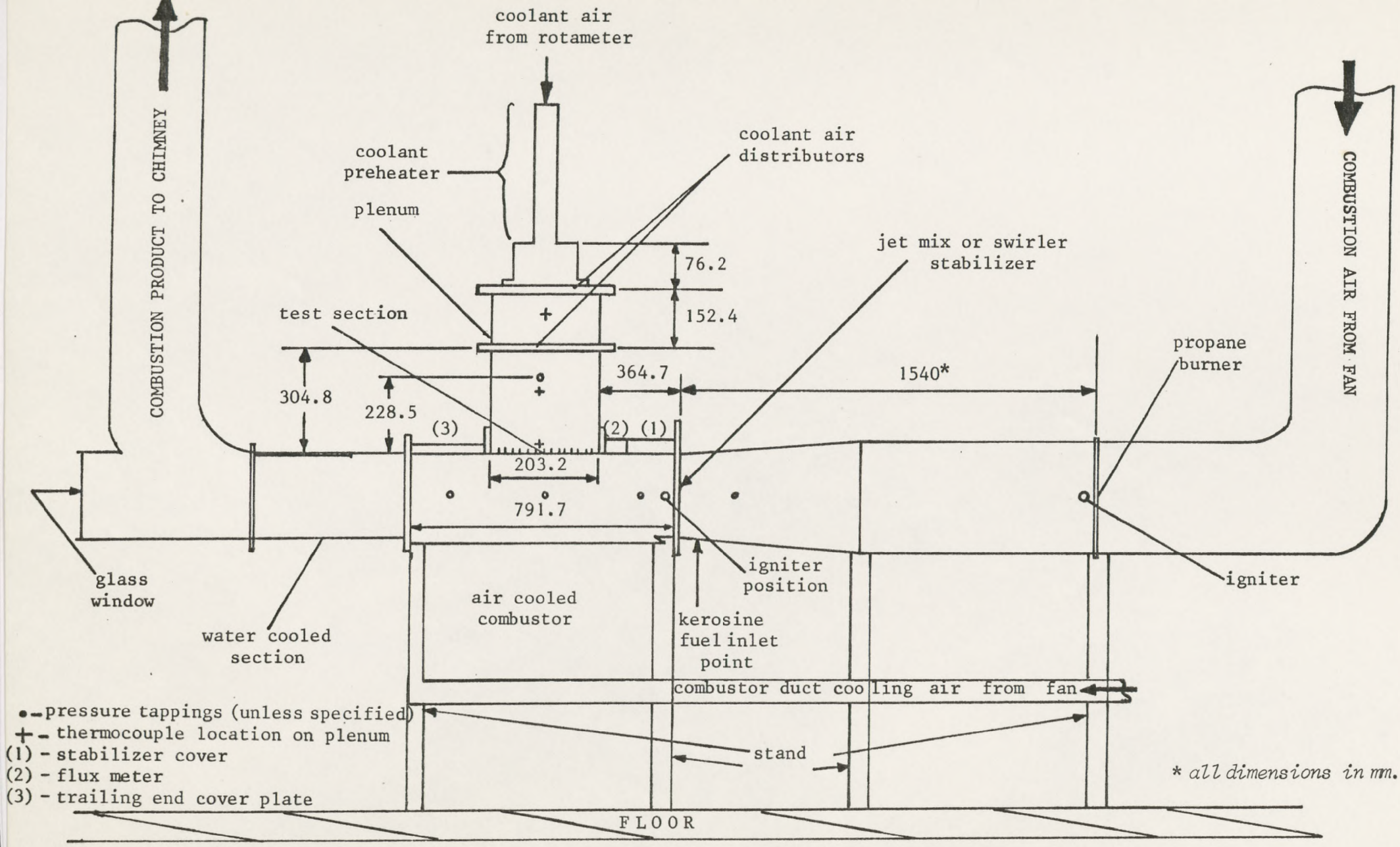

Fig. 2.1: Test rig

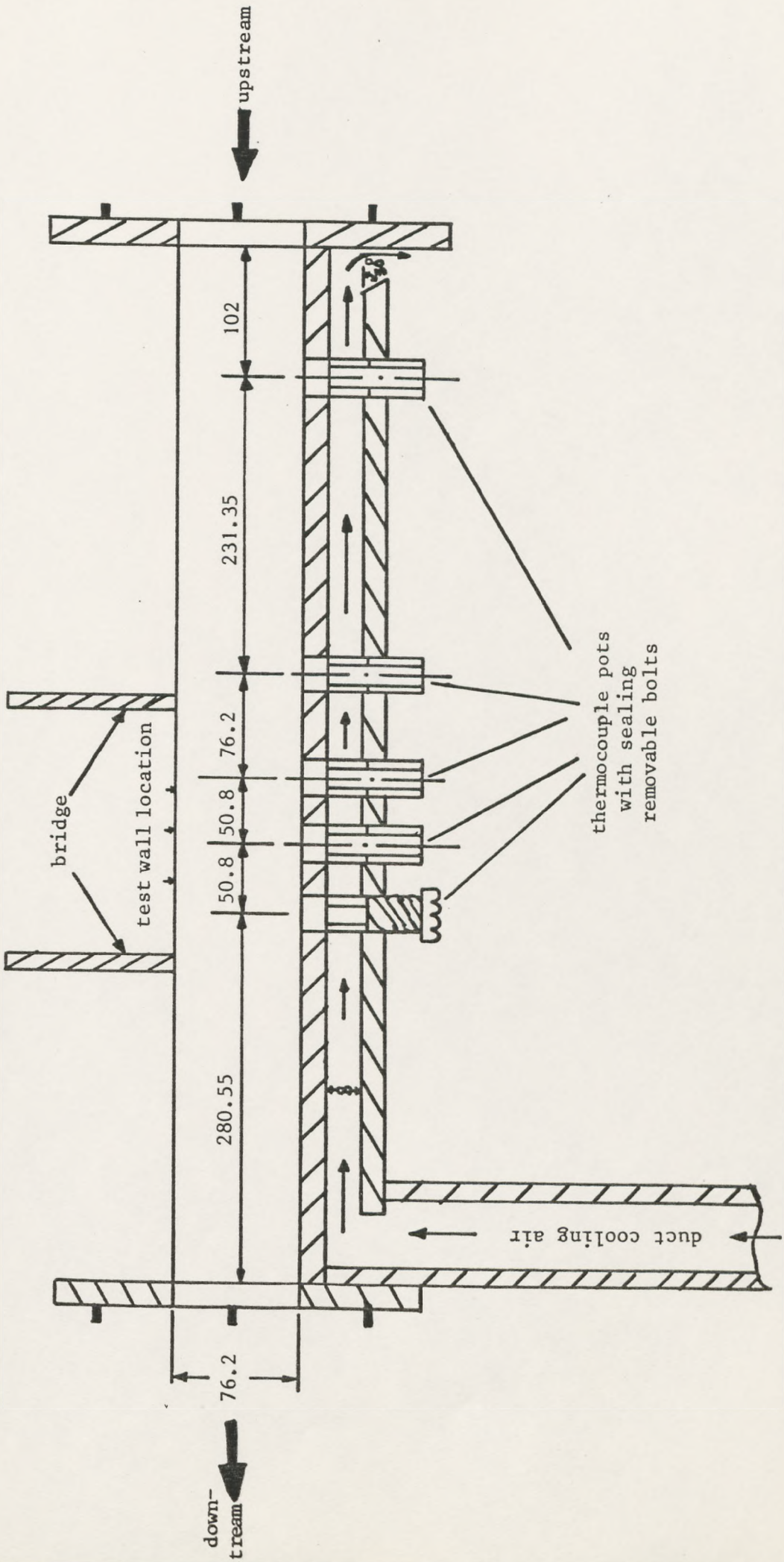

Fig. 2.2: Schematic section of the counterflow air cooled combustor

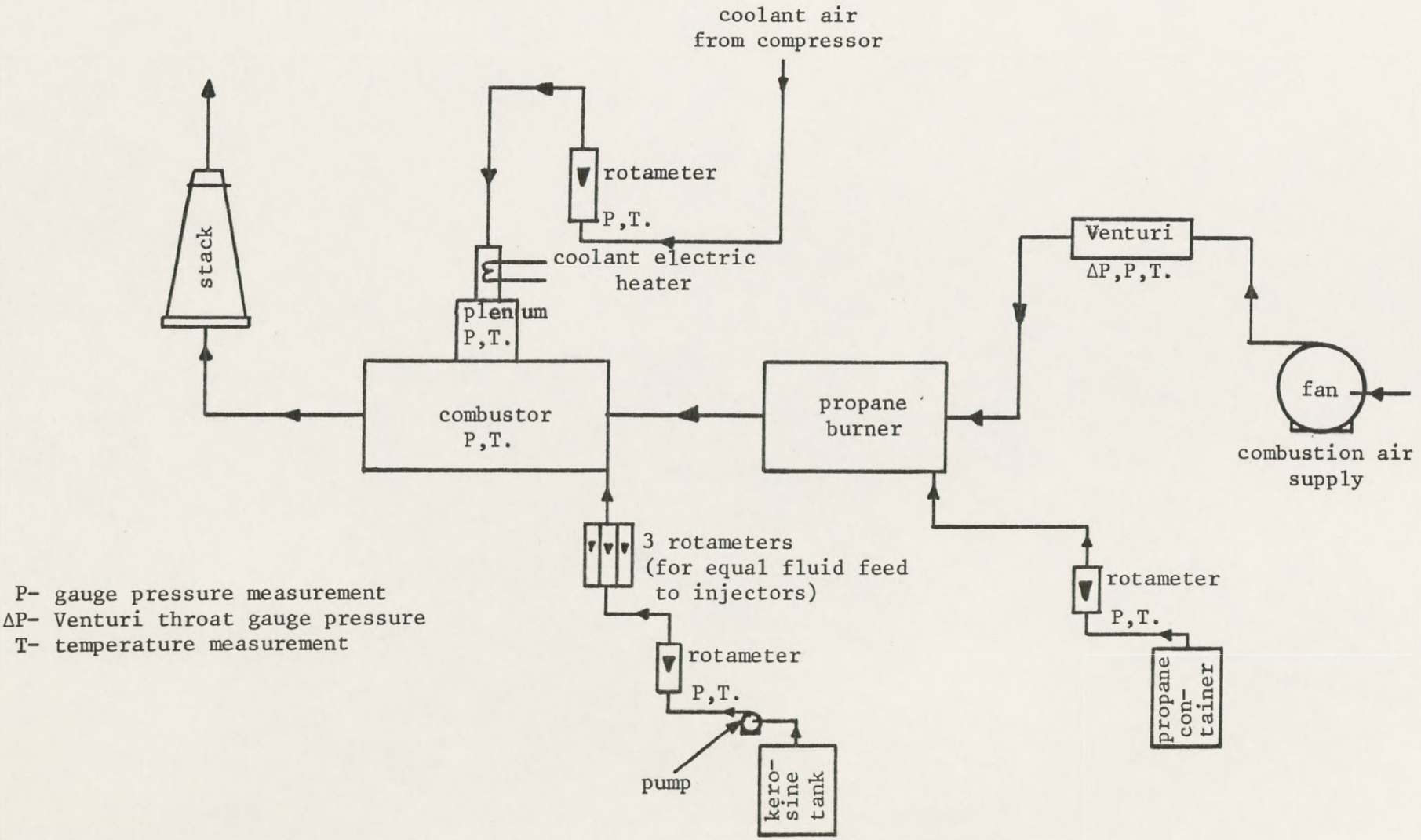

Fig. 2.3: The fluid flow diagram

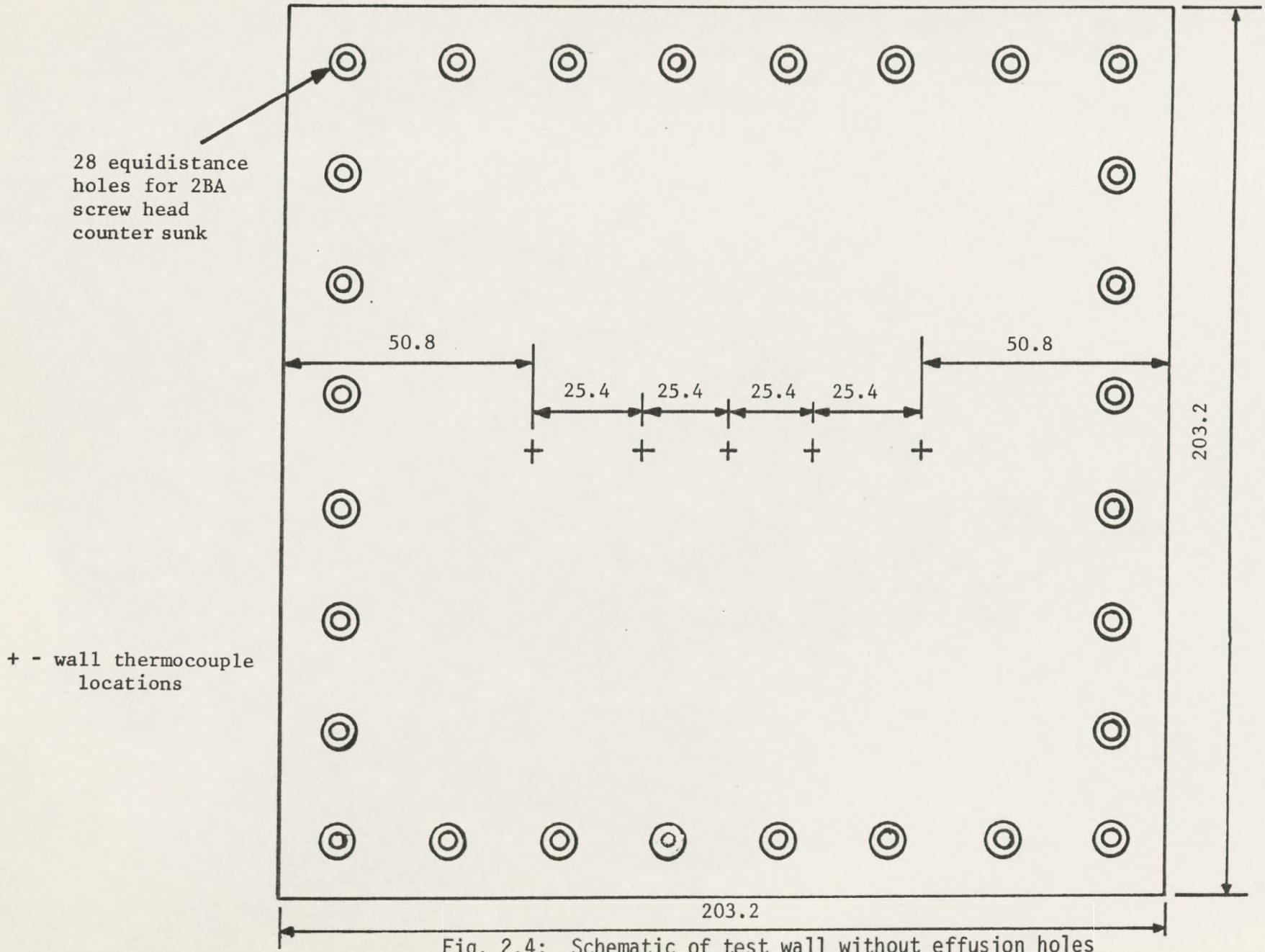

Fig. 2.4: Schematic of test wall without effusion holes

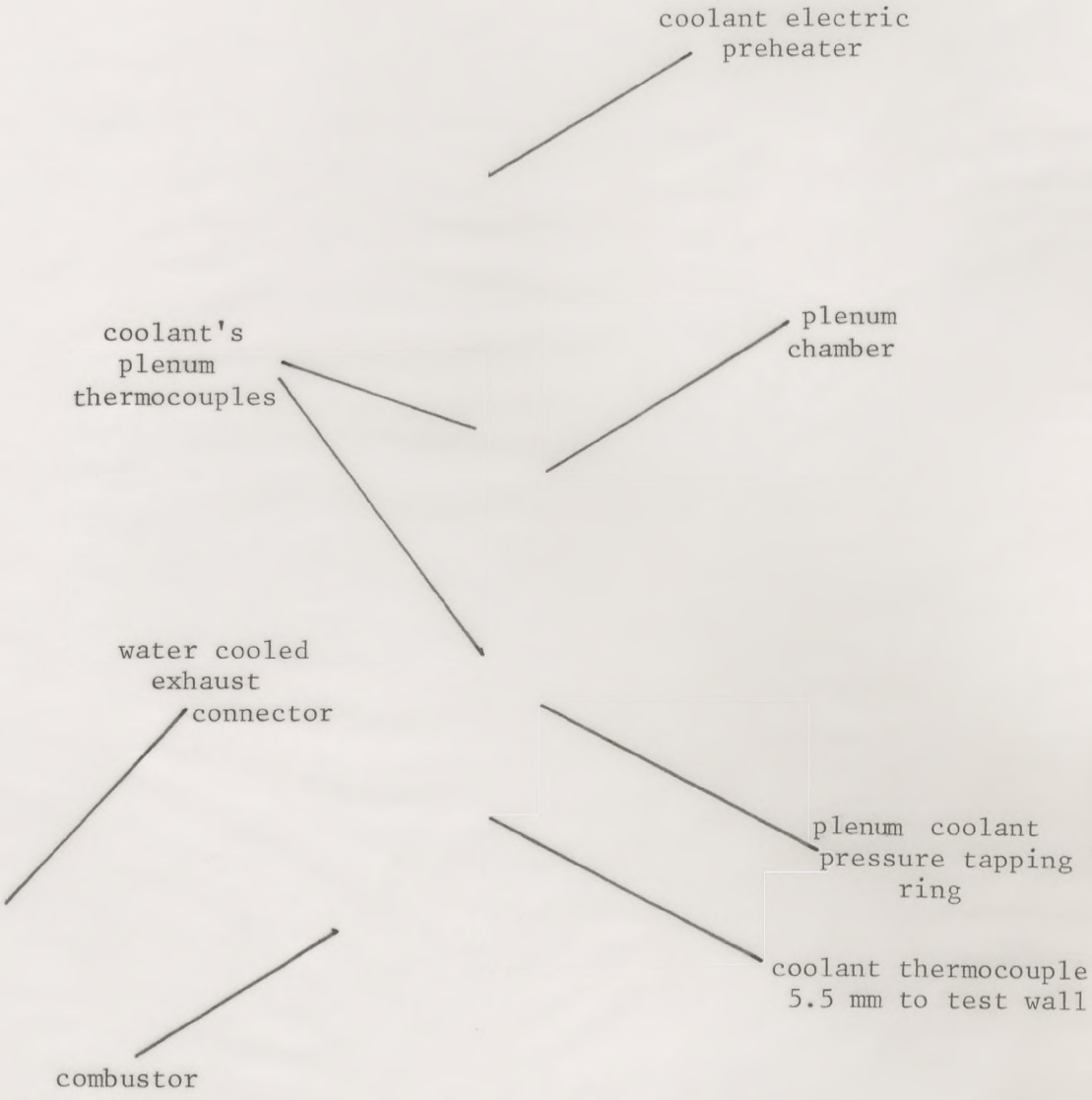

Plate (2.1): The rig assembly

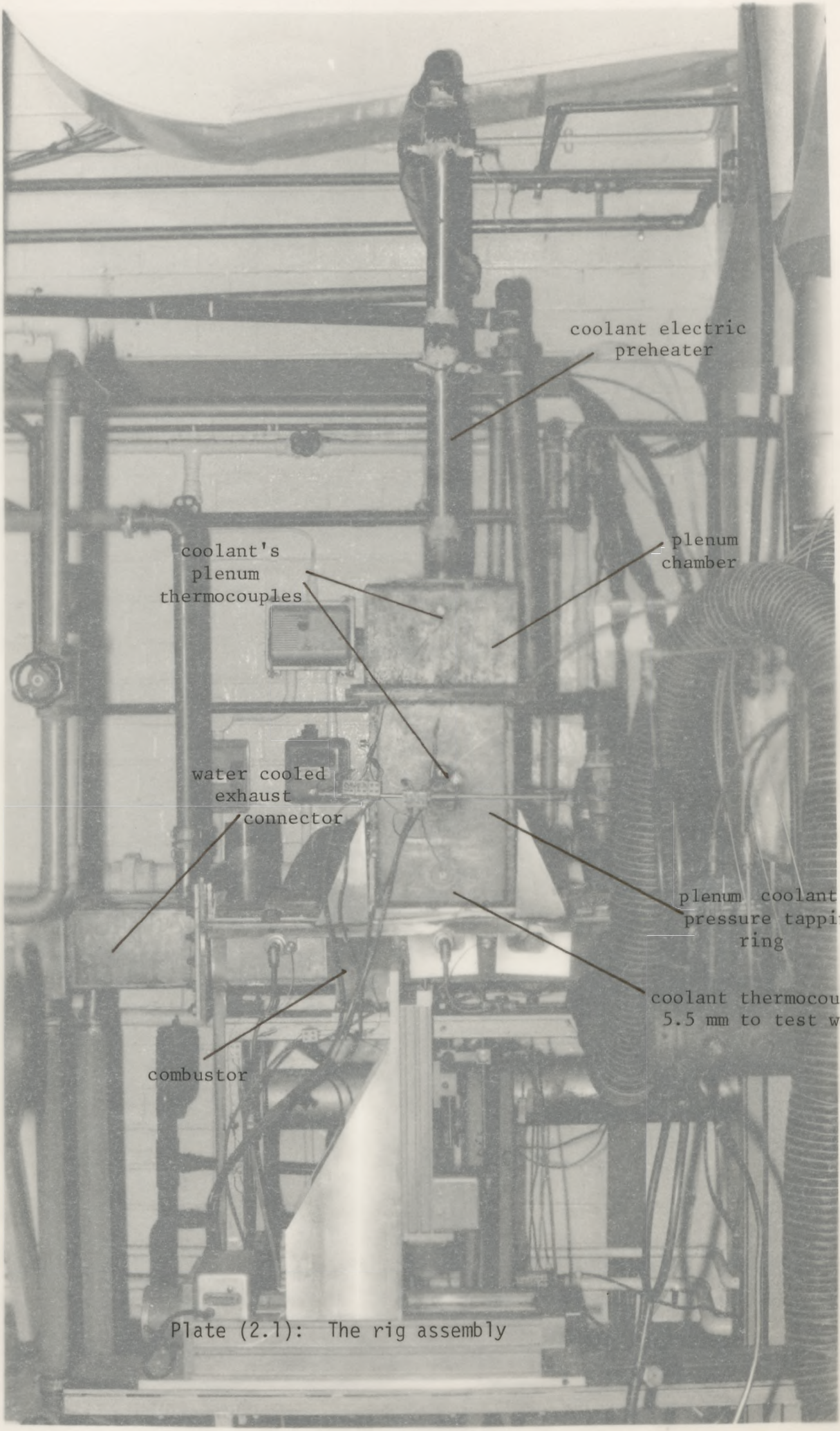

Plate (2.1): The rig assembly

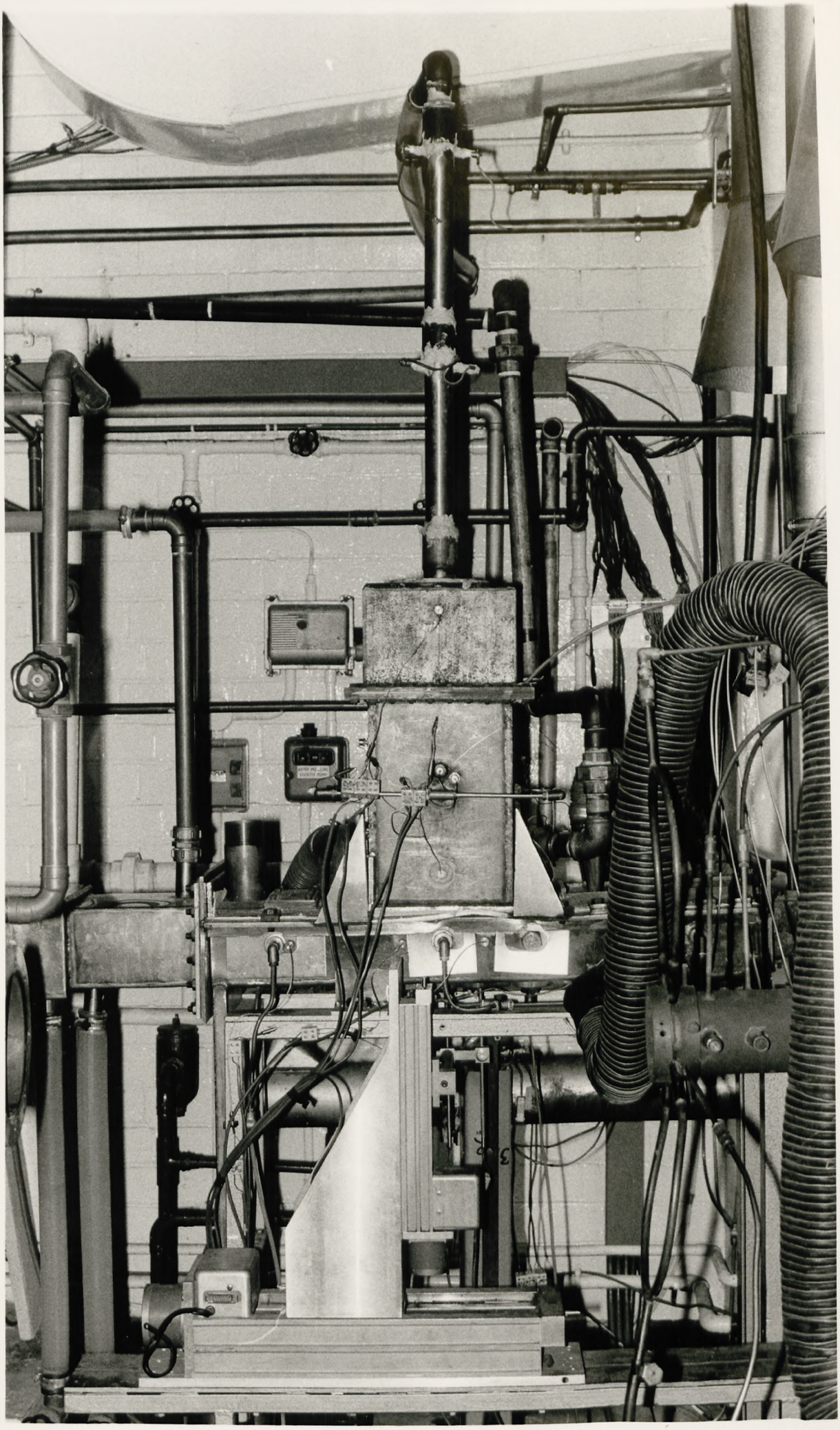

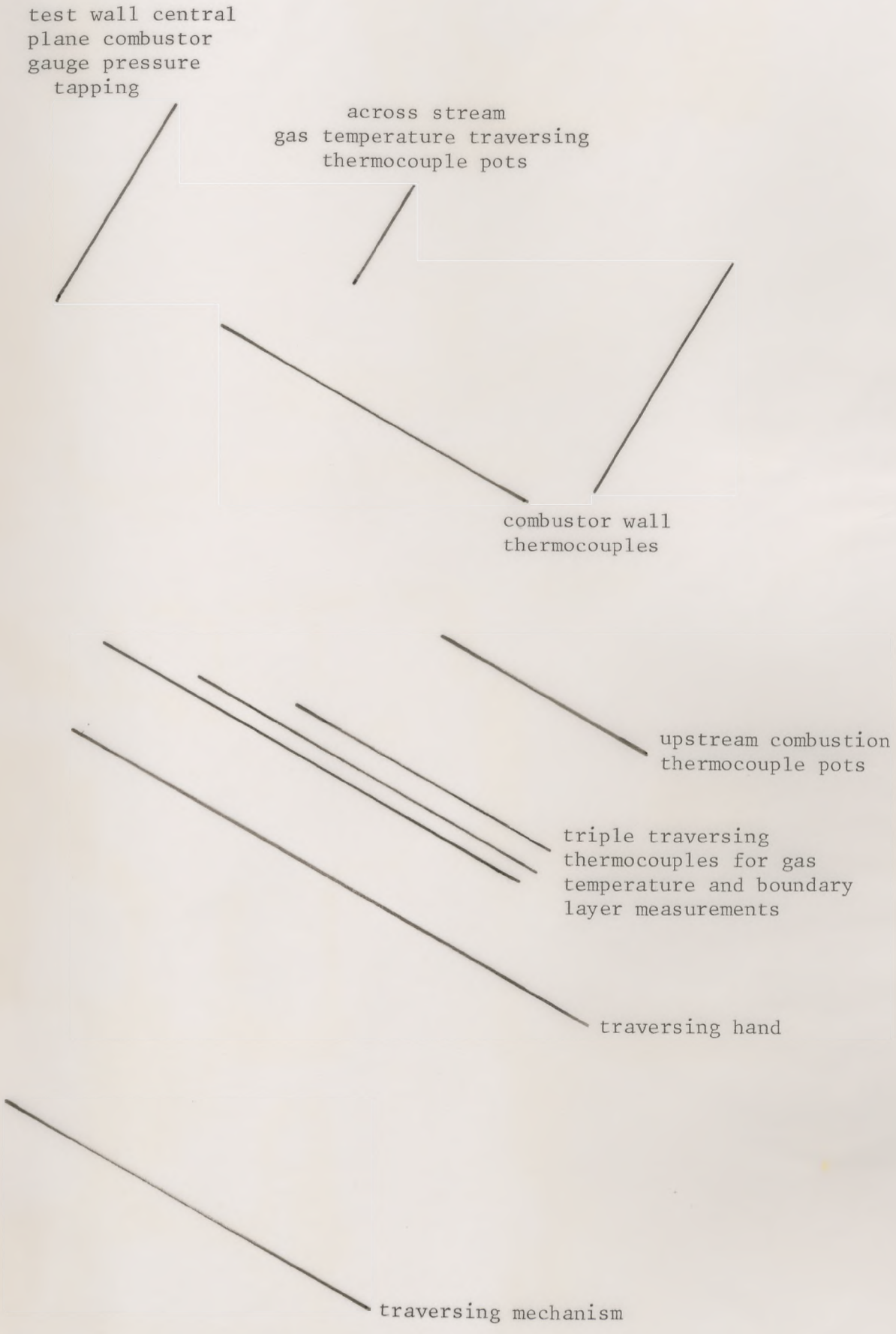

Plate (2.2): Experimental rig showing traverse thermocouples and thermocouple pots

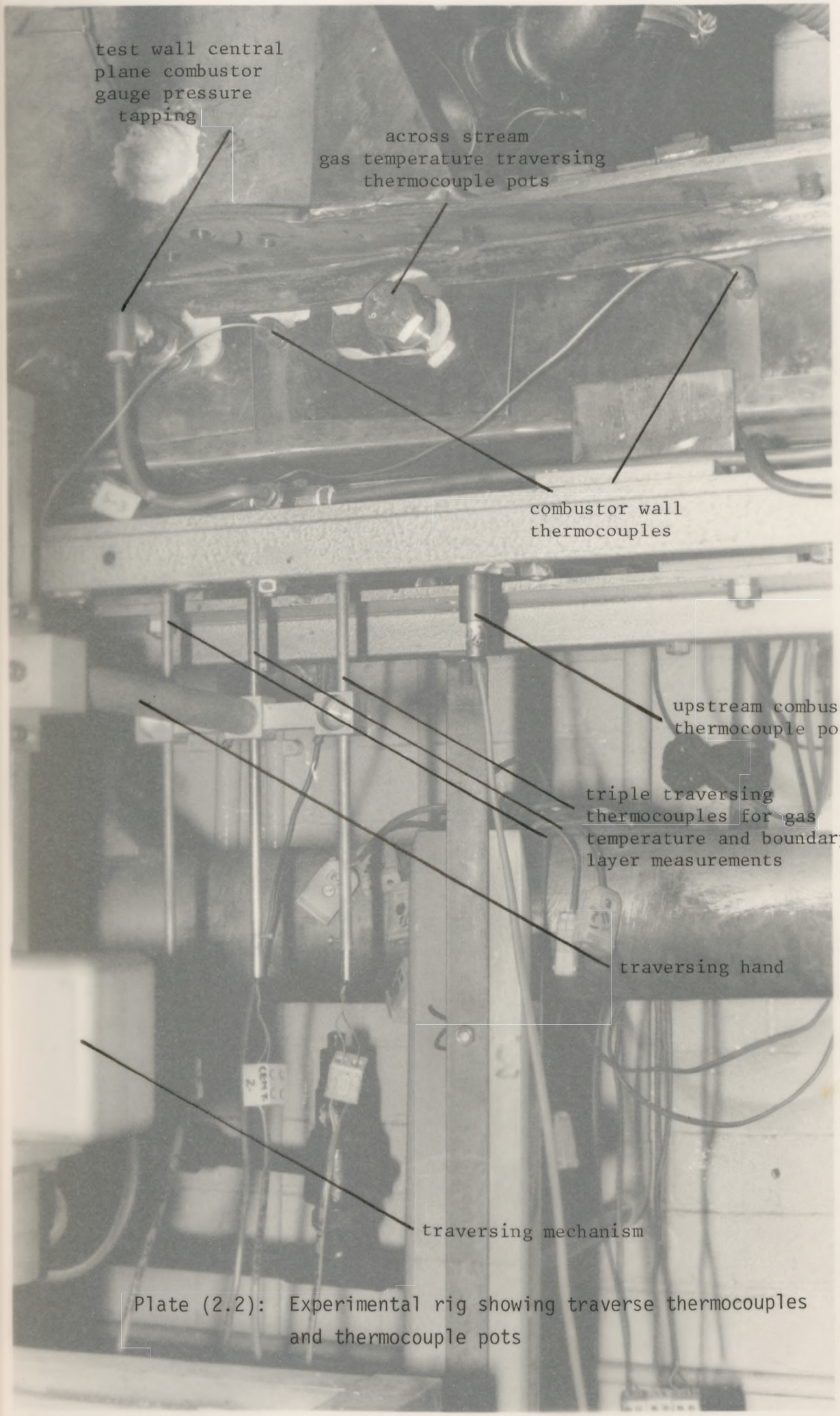

Plate (2.2): Experimental rig showing traverse thermocouples and thermocouple pots

CENT.
2.

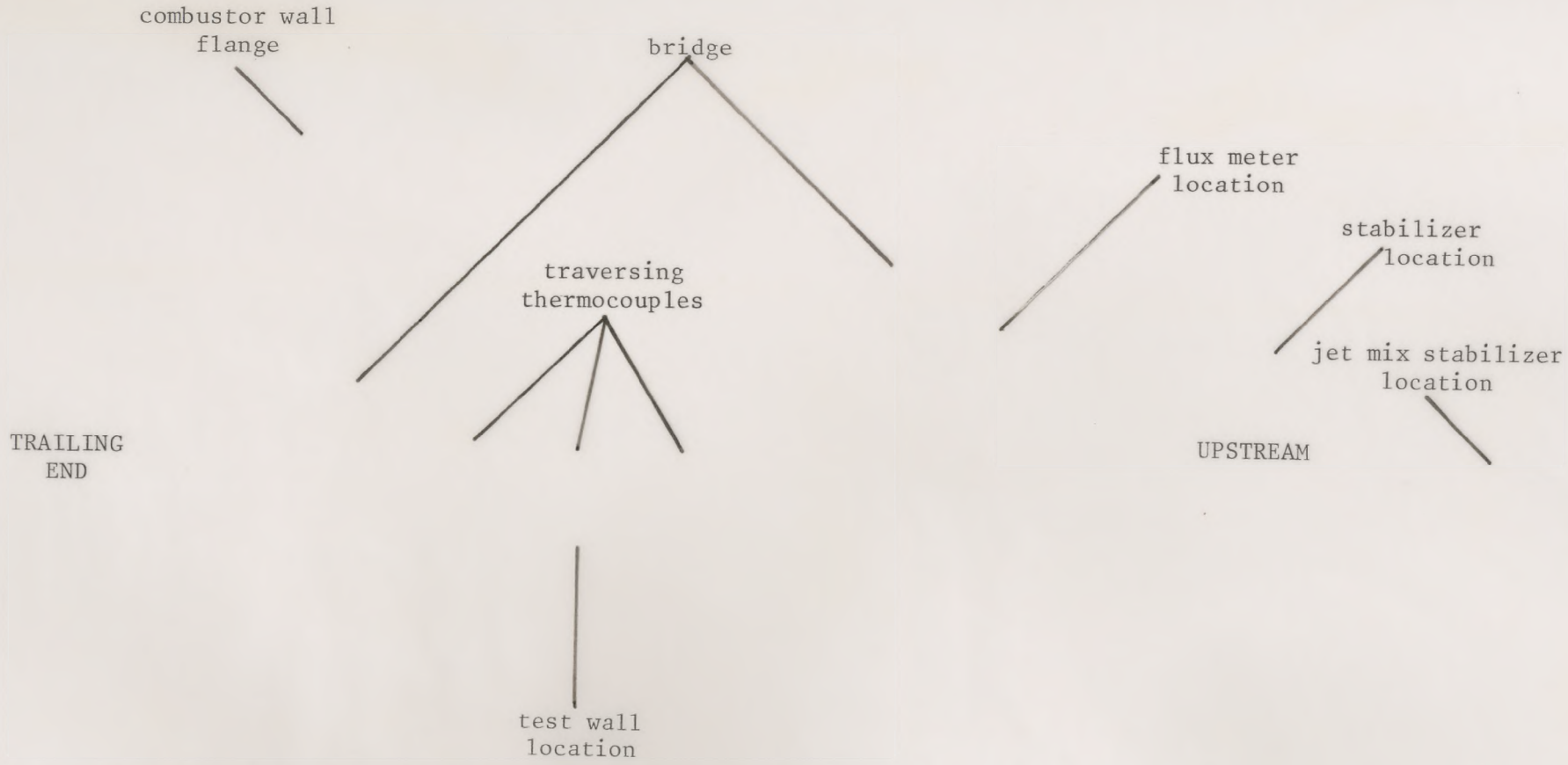

Plate (2.3): Top view of the combustor

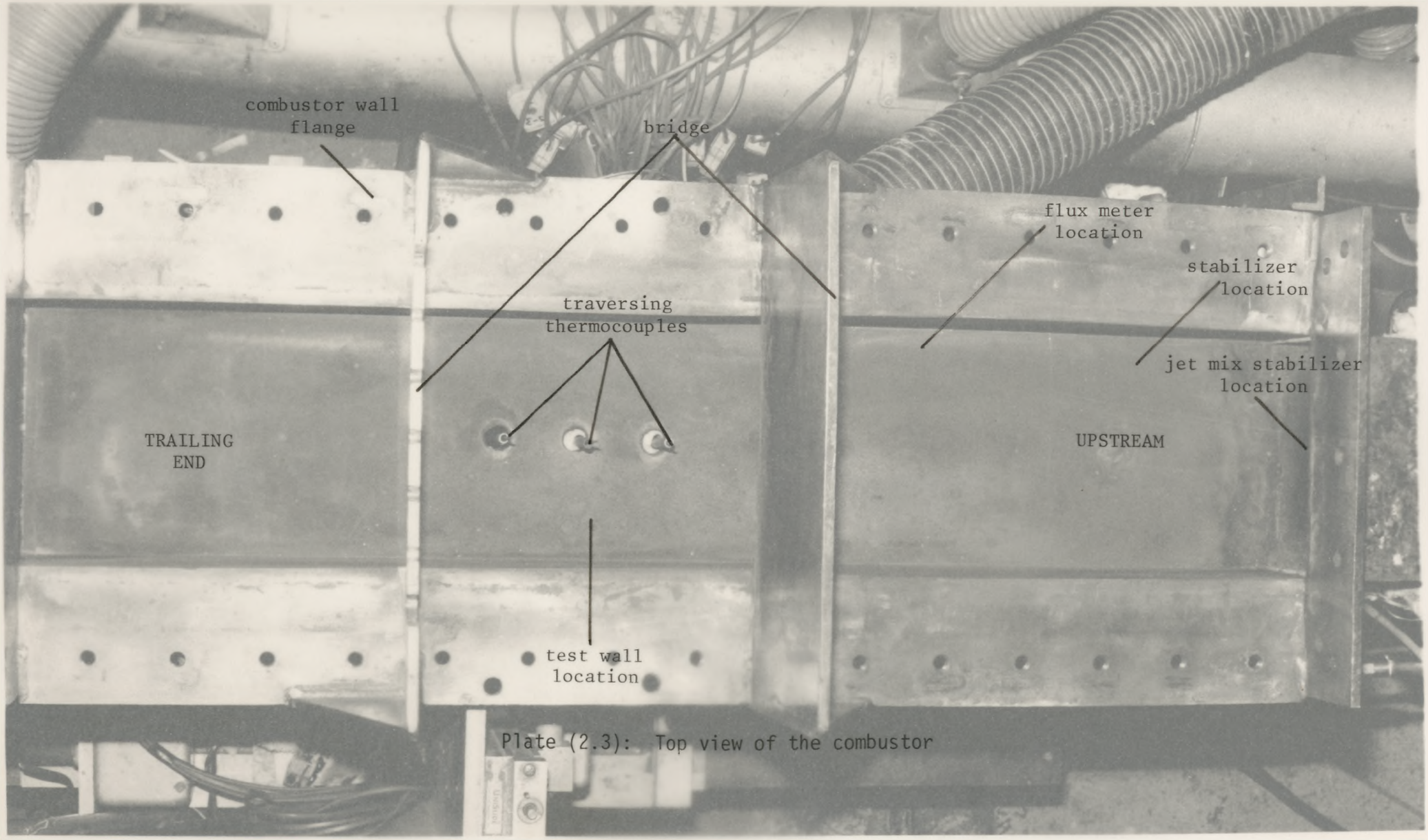

Plate (2.3): Top view of the combustor

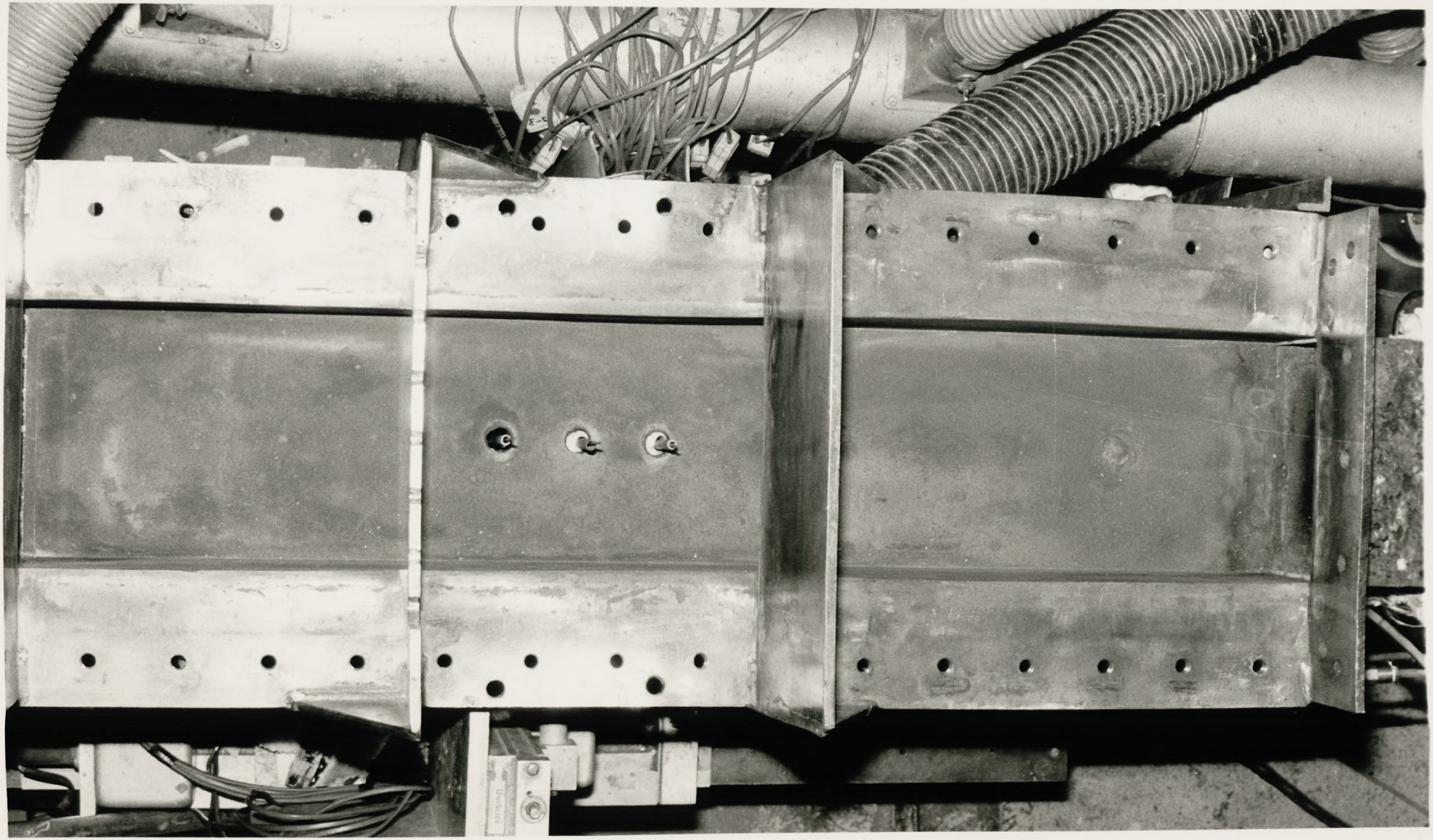

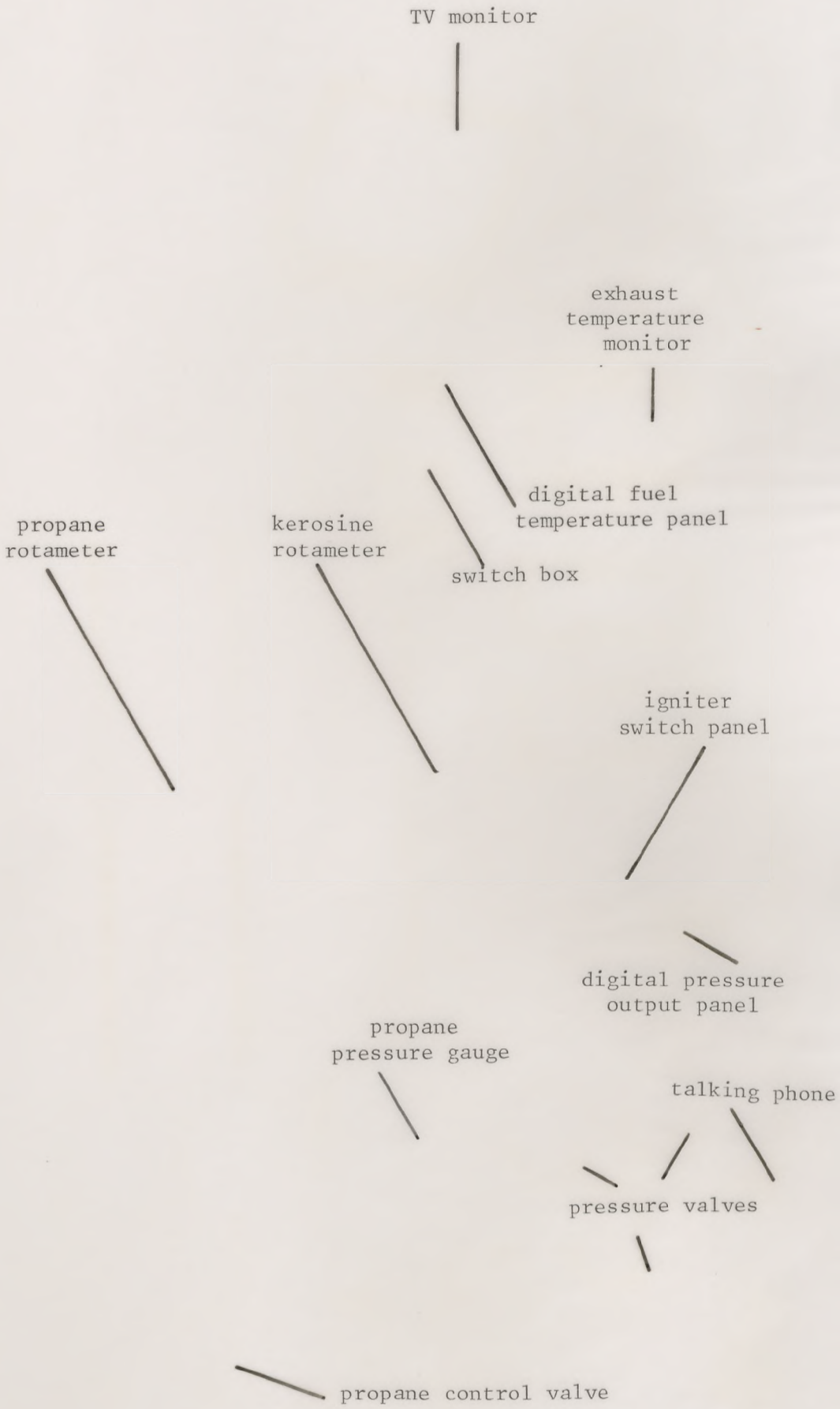

Plate (2.4): Control and monitoring panel

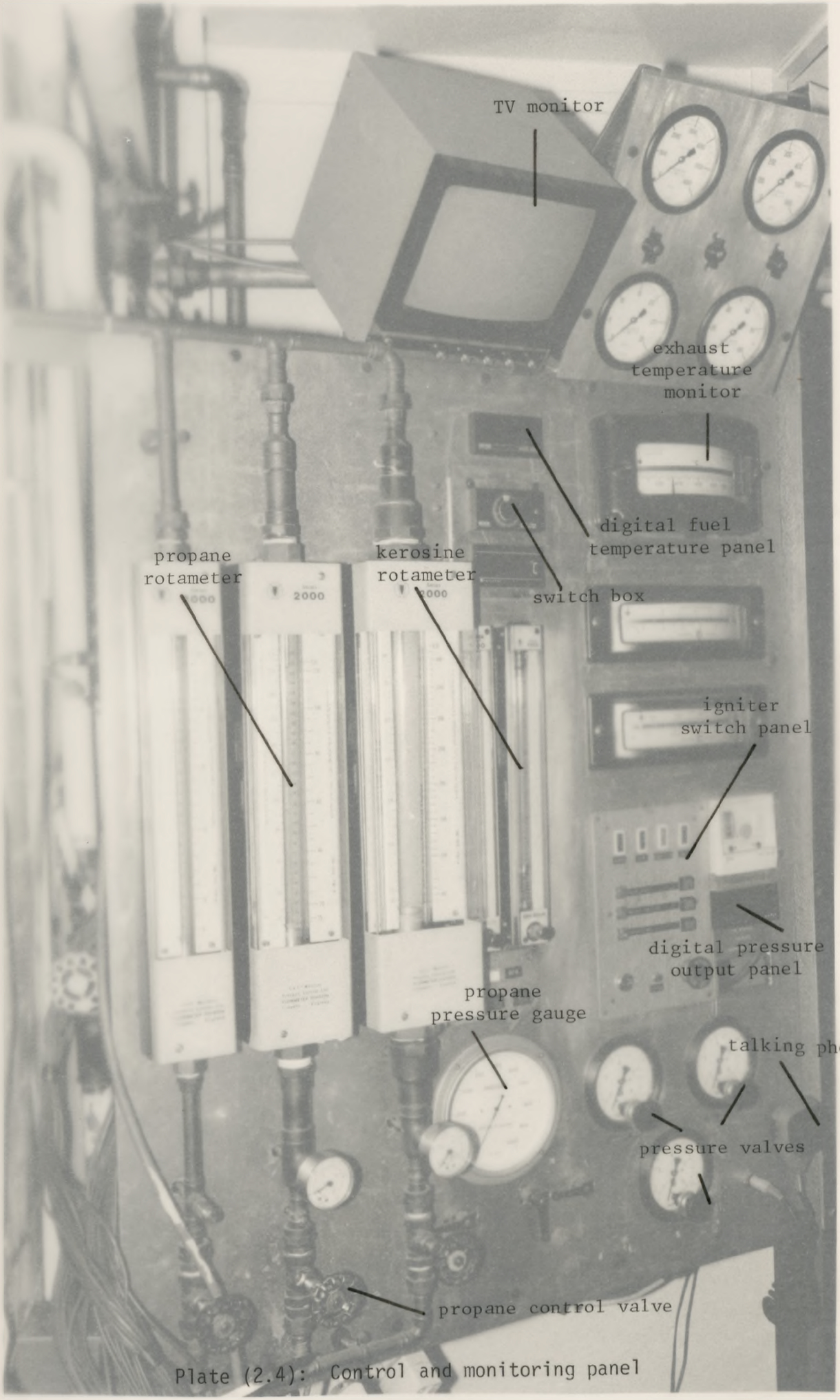

Plate (2.4): Control and monitoring panel

Series 2000
Series 2000
Series 2000
PRESSURE
PRESSURE

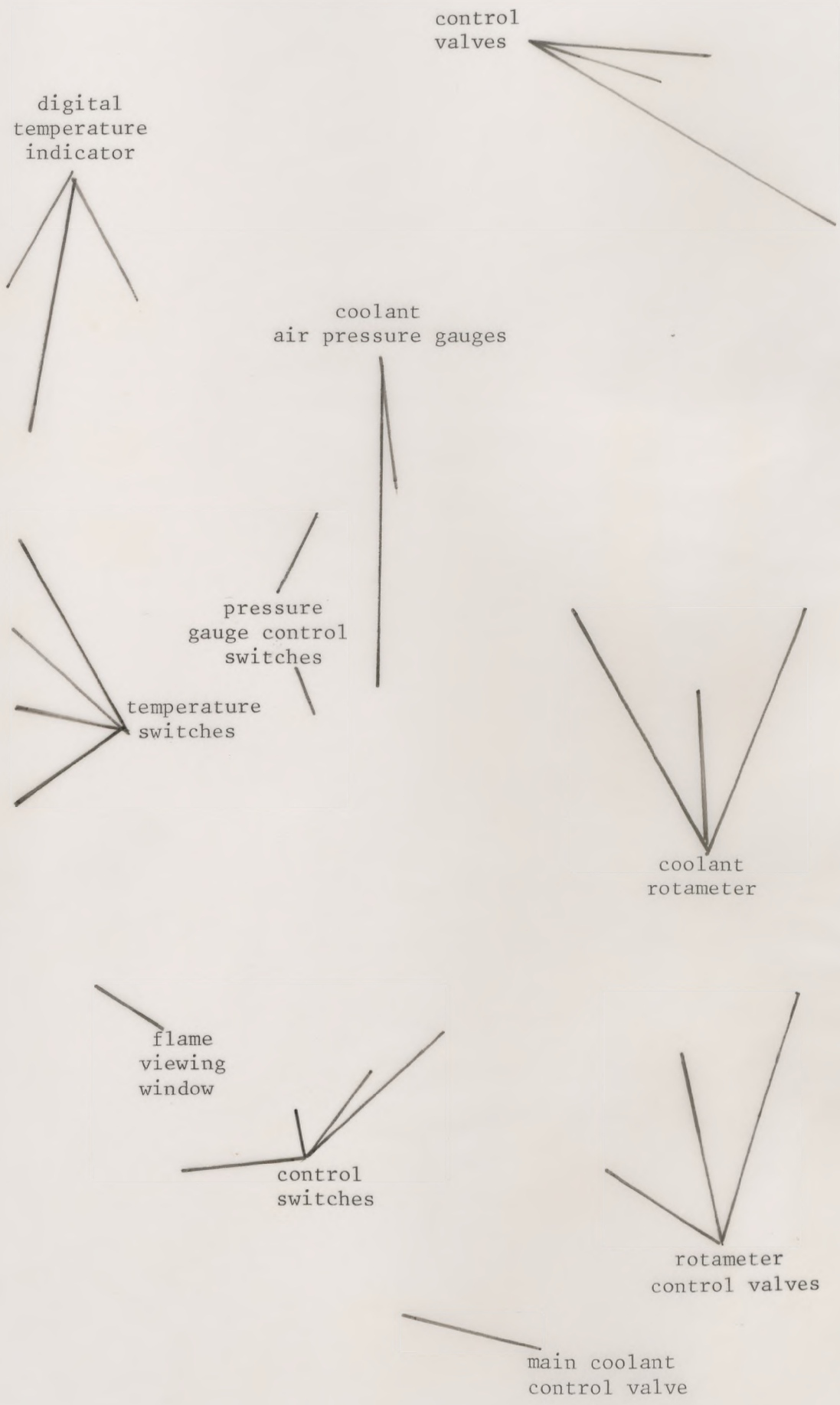

Plate (2.5): Temperature and coolant flow measurement panel

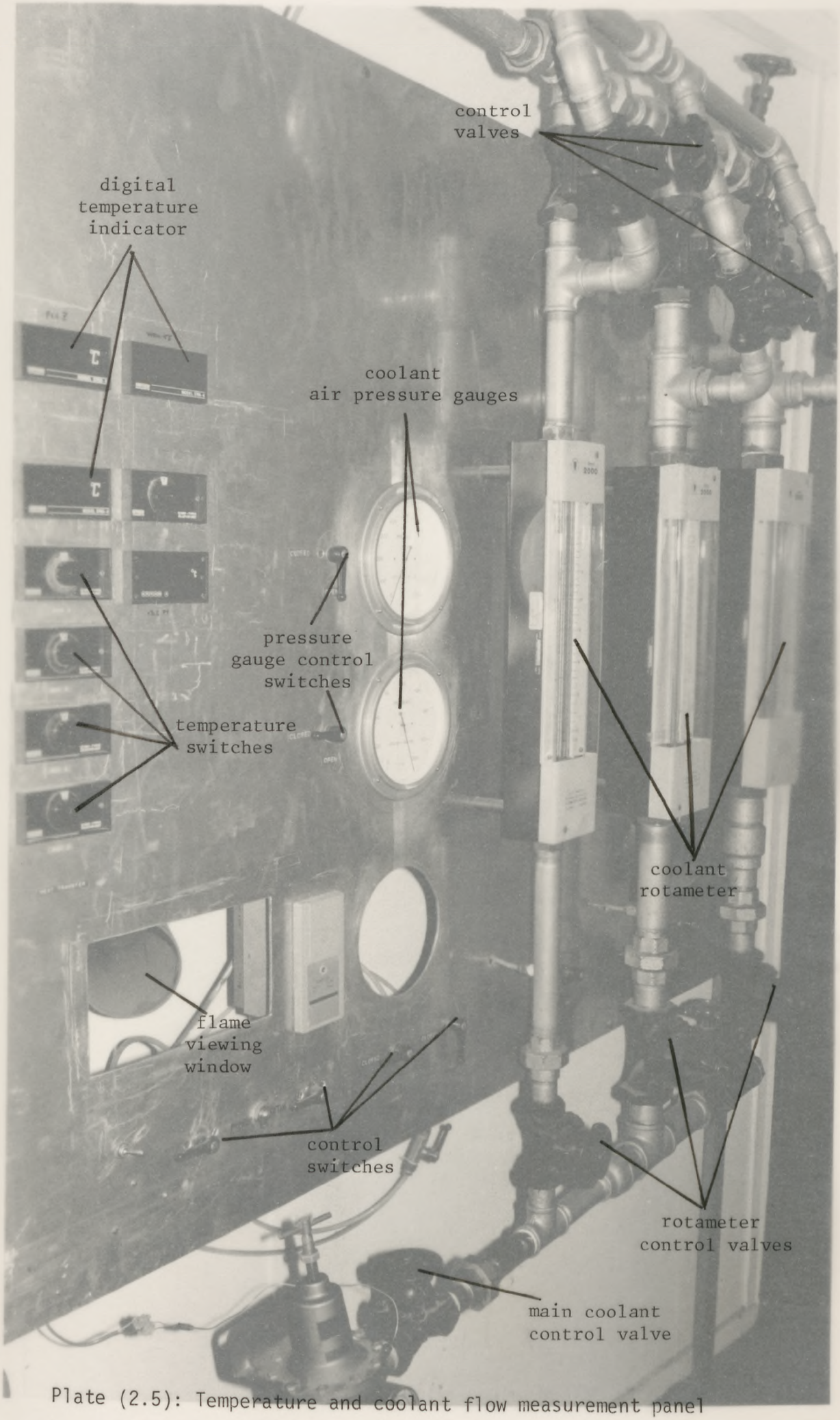

Plate (2.5): Temperature and coolant flow measurement panel

CLOSED
OPEN
CLOSED
OPEN
HEAT TRANSFER
CLOSED
CLOSED
OPEN

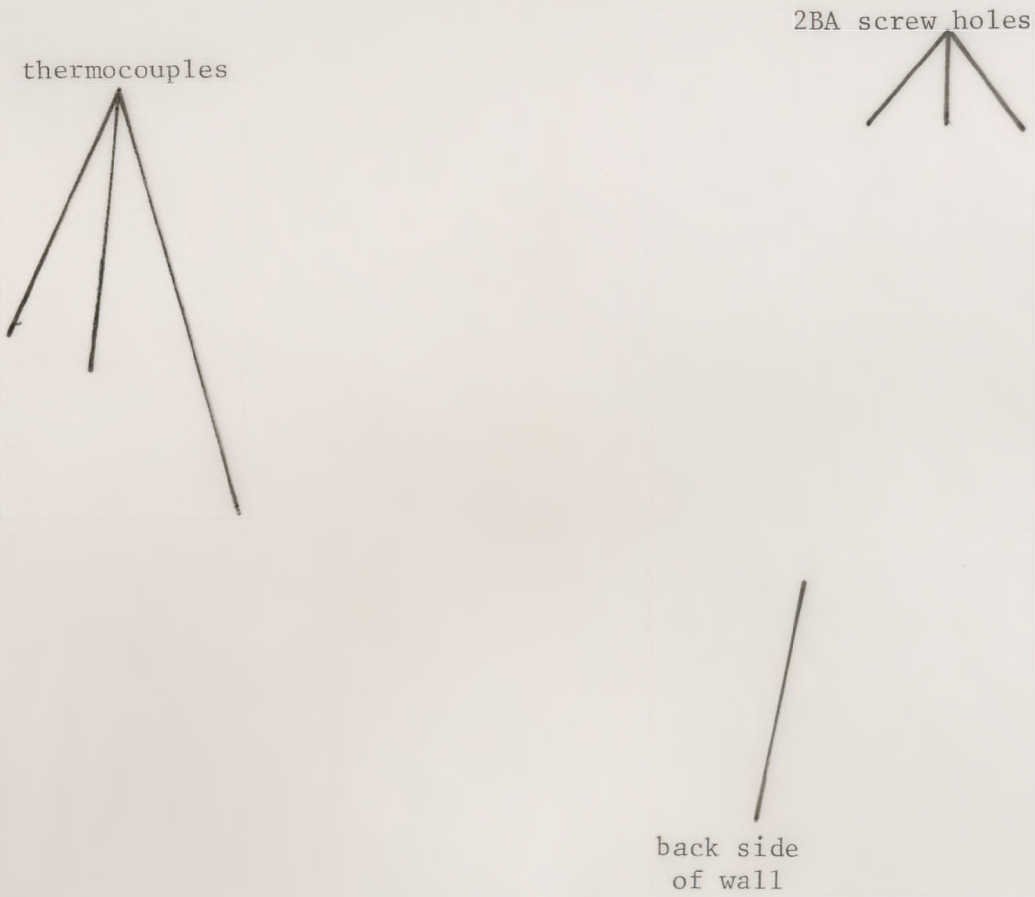

Plate (2.6): An effusion test wall (coolant face)

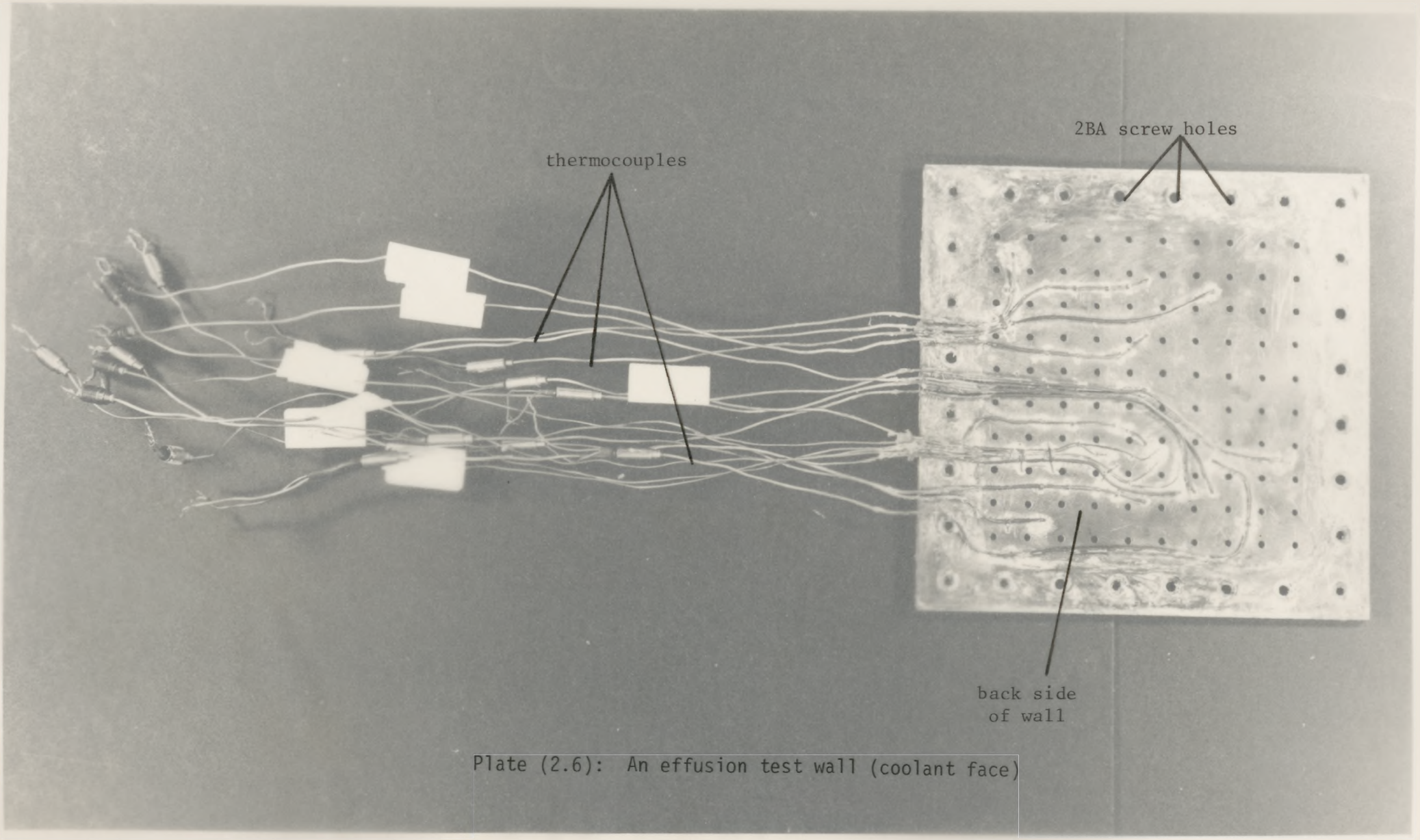

Plate (2.6): An effusion test wall (coolant face)

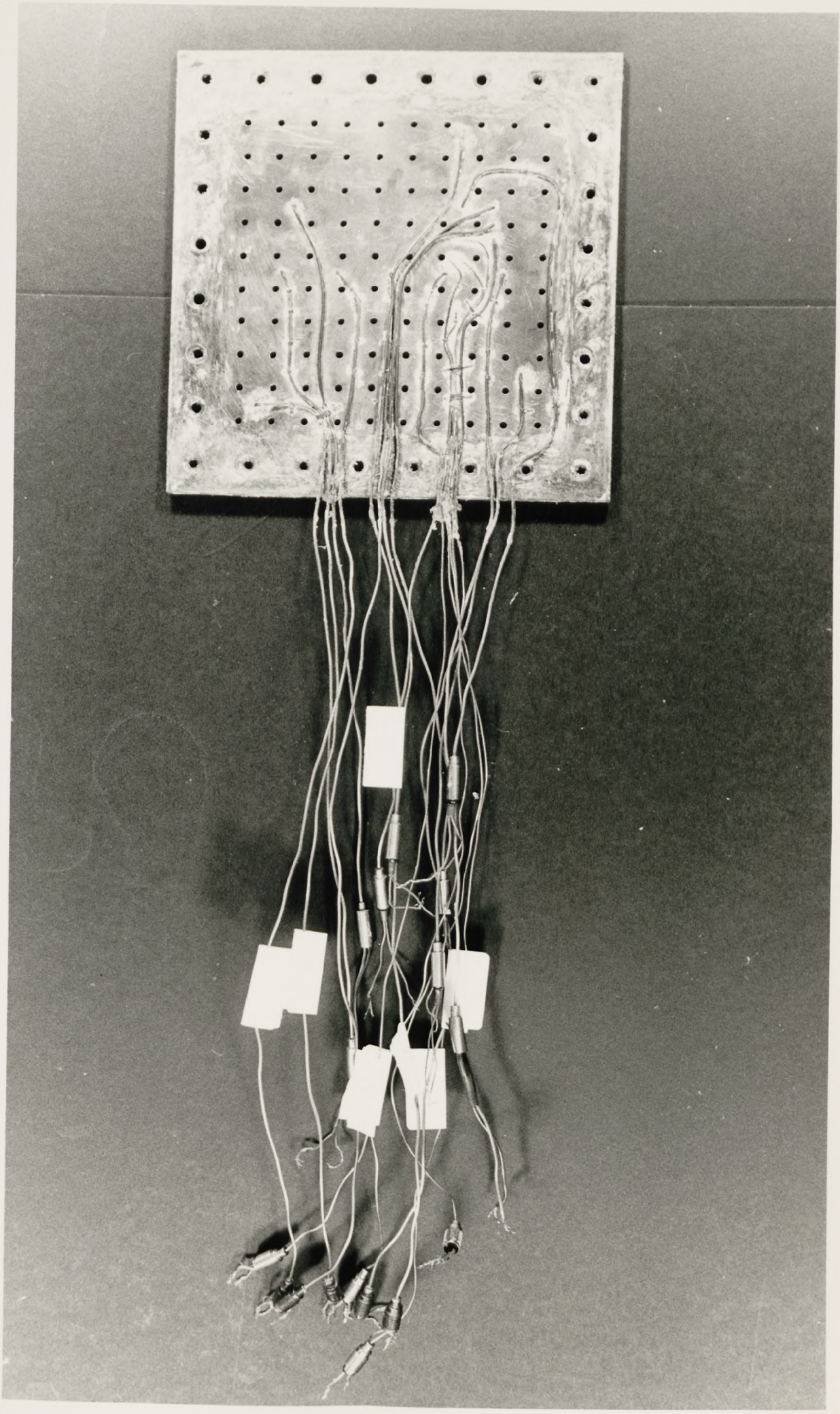

Plate (2.7): Effusion test wall showing the flame face

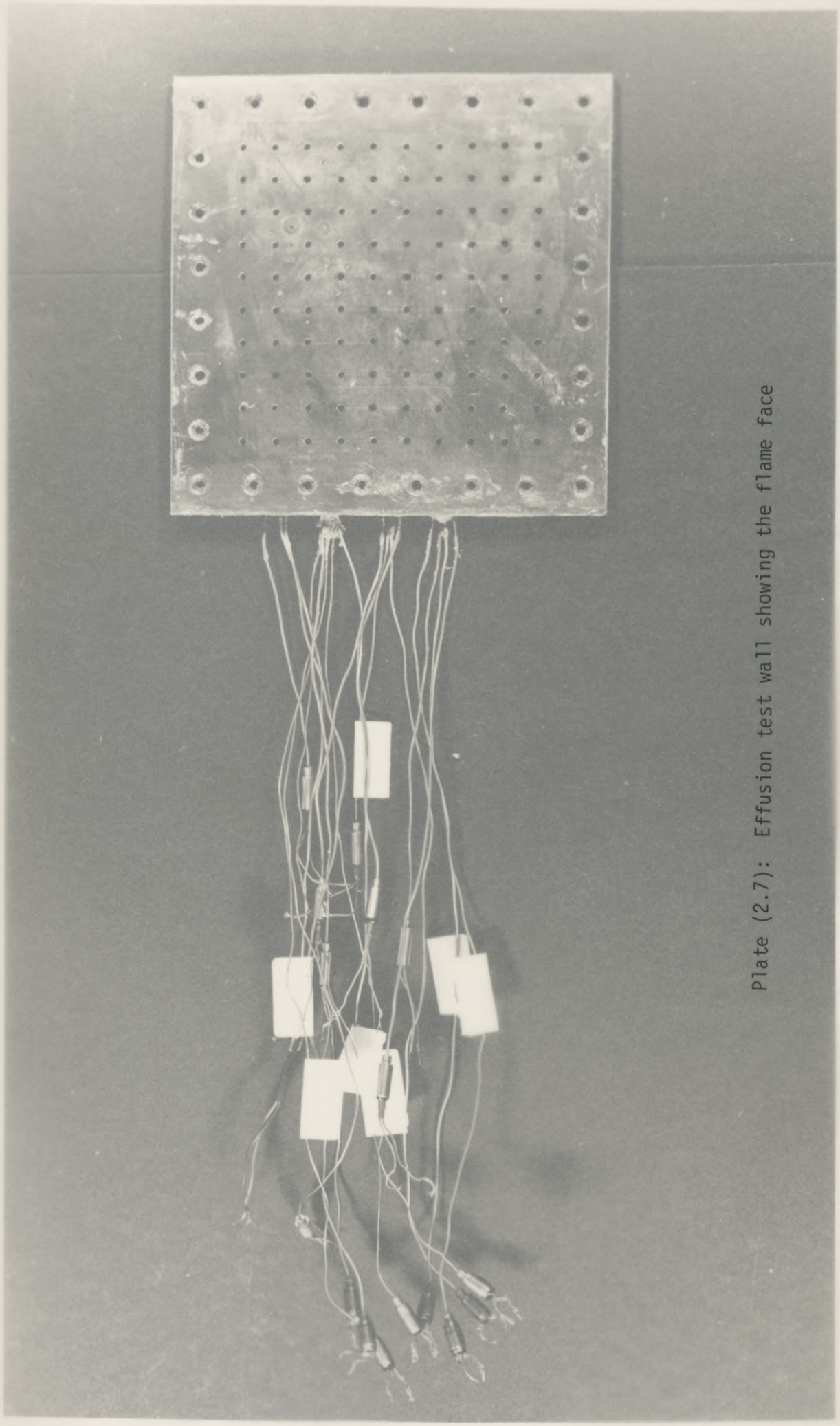

Plate (2.7): Effusion test wall showing the flame face

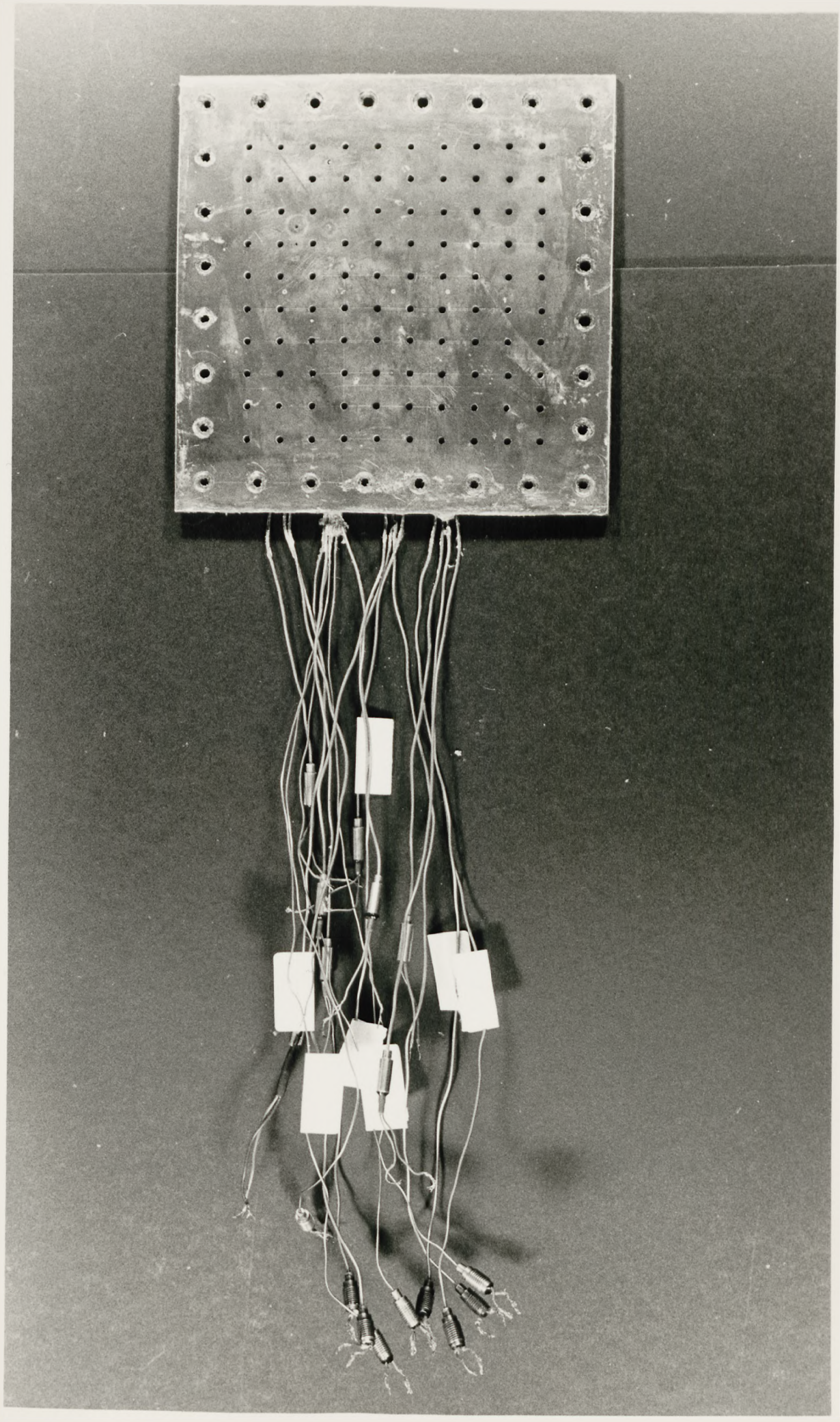

2.8 APPENDIX

TABLE 2.1

CALIBRATION OF MILD STEEL VENTURI USING THE ALUMINIUM VENTURI

EXPT. CONDITION-ATMOS. PRESS.=770MMHG, TEMP.=19C

ALUMINIUM VENTURI USED AS STANDARD--THROAT DIAMETER=35.2906MM
UPSTREAM PIPE DIAMETER=158.344MM, M&M1=PROVISIONAL FLOW RATE
Z=CORRECTION FACTOR(=ZR*ZD), E=EXPANSIBILITY FACTOR
D=AIR DENSITY AT UPSTREAM ABSOLUTE PRESSURE, P=PRESSURE LOSS AT THROAT
M2 & M3 =IMPROVED MASS FLOWRATE OF AIR, DISCHARGE COEFFICIENT=0.9866

M-KG/H	M1-KG/S	Z	E	D-KG/M3	P-MMH2O	M2-KG/H	M3-KG/S
333.048	0.0925	0.991	0.9770	1.0997	446.00	330.106	0.09170
367.635	0.1021	0.991	0.9720	1.1077	545.00	364.333	0.10120
402.360	0.1119	0.991	0.9665	1.1228	653.00	399.241	0.11090
439.114	0.1220	0.992	0.9599	1.1306	781.00	435.606	0.12100
471.345	0.1309	0.992	0.9537	1.1415	903.00	467.580	0.12988
499.640	0.1388	0.992	0.9477	1.1489	1021.00	495.748	0.13771
515.399	0.1432	0.992	0.9442	1.1546	1089.00	511.487	0.14209
539.952	0.1500	0.993	0.9381	1.1583	1207.00	535.937	0.14887
588.669	0.1635	0.994	0.9255	1.1734	1455.00	585.137	0.16254
589.514	0.1639	0.994	0.9255	1.1770	1454.68	585.977	0.16277
651.987	0.1811	0.994	0.9061	1.1905	1735.34	648.085	0.18002
750.609	0.2085	0.994	0.8686	1.2201	2583.07	746.105	0.20725

MILD STEEL VENTURI DISCHARGE COEFFICIENT DETERMINATION
MEAN UPSTREAM PIPE DIAMETER=150.549124MM, MEAN THROAT DIA.=63.76667MM
M2 & M3 =IMPROVED MASS FLOW RATE, D2=AIR DENSITY (AS ABOVE)
P=PRESSURE LOSS AT VENTURI THROAT-MMH2O, Z=CORRECTION FACTOR
E=EXPANSIBILITY FACTOR, C_d=DISCHARGE COEFFICIENT

M2-KG/H	M3-KG/S	D2-KG/M3	P-MMH2O	Z	E	CD
330.106	0.09170	1.2137	41.0	0.990	0.9978	0.91541
364.333	0.10120	1.2139	50.0	0.990	0.9973	0.91524
399.241	0.11090	1.2143	60.0	0.990	0.9968	0.91573
435.606	0.12100	1.2148	70.0	0.991	0.9963	0.92353
467.580	0.12988	1.2150	80.0	0.991	0.9957	0.92724
495.748	0.13771	1.2155	90.0	0.991	0.9952	0.92720
511.487	0.14208	1.2156	95.0	0.991	0.9949	0.93133
535.937	0.14887	1.2220	104.0	0.992	0.9944	0.93172
585.137	0.16254	1.2247	122.0	0.992	0.9935	0.93363
585.977	0.16277	1.2247	122.0	0.992	0.9935	0.93388
648.085	0.18002	1.2256	150.0	0.992	0.9920	0.93862
746.105	0.20725	1.2272	200.0	0.992	0.9893	0.93771

MEAN Z= 0.9911 MEAN C_d = 0.92853 ERROR RANGE =+-0.0015

OTHER PARAMETERS USED
RE & RE2 =REYNOLDS NO. OF ALUMINIUM & M.STEEL VENTURIS
ZR & ZR2 = REYNOLDS NO. CORRECTION FACTOR, AR&SR=PRESSURE RATIOS
ZD&ZD2=PIPE SIZE CORRECTION FACTORS FOR AL.&M.STEELVENTURI

RE	ZR	ZD	AR	RE2	ZR2	ZD2	SR
0.17E+06	0.997	0.994	0.9578	0.113E+06	0.996	0.994	0.9861
0.19E+06	0.997	0.994	0.9486	0.125E+06	0.996	0.994	0.9852
0.21E+06	0.997	0.994	0.9387	0.137E+06	0.996	0.994	0.9843
0.23E+06	0.998	0.994	0.9269	0.149E+06	0.997	0.994	0.9831
0.24E+06	0.998	0.994	0.9158	0.160E+06	0.997	0.994	0.9824
0.26E+06	0.998	0.994	0.9051	0.170E+06	0.997	0.994	0.9814
0.27E+06	0.998	0.994	0.8990	0.175E+06	0.997	0.994	0.9809
0.28E+06	0.998	0.994	0.8884	0.184E+06	0.998	0.994	0.9801
0.30E+06	1.000	0.994	0.8664	0.201E+06	0.998	0.994	0.9884
0.30E+06	1.000	0.994	0.8664	0.201E+06	0.998	0.994	0.9884
0.34E+06	1.000	0.994	0.8333	0.222E+06	0.998	0.994	0.9857
0.38E+06	1.000	0.994	0.7711	0.256E+06	0.998	0.994	0.9810

TABLE 2.4(A)

Plate (P) Temperature Test

Plate Combination: Impingement → No. Holes: ..... Holes Mean Diameter: ..... Hole Pitch: .....

Design Plate ΔP/P: ..... Plate Thickness: ..... Holes Layout Format: ..... Plate Material: .....

Effusion → No. Holes: ..... Holes Mean Diameter: ..... Hole Pitch: .....

Design Plate ΔP/P: ..... Plate Thickness: ..... Holes Layout Format: ..... Plate Material: .....

Separation Gap (Z): ..... Atmospheric Pressure: ..... At Temperature: ..... Exp. Date: ..... Exp. Duration: .....

Data Definitions:

Unit - I →

T_a - Ambient temperature T_v - Venturi upstream air temp. TOP_1 - Propane inlet temp. TOP_2 - Kerosine (or other fuel) inlet temp.
T_1 - Rotameter coolant air temp. T_2 - Propane burner air inlet temp. T_3 - Coolant temp. outlet of preheater (421 mm upst. of P).
T_4 - Coolant temp. - 351 mm upst. P T_5 - Coolant temp. 235 mm upstream of P. T_6 - Coolant temp. 55 mm upst. of P. T_7 - Cool. temp. 3.5 mm upst. of P.
T_8 - 1st inner plenum metal wall face (PMWF) Temp. (198 mm to P). T_9 - 2nd inner PMWF temp. (198 mm to P). T_{10} - 1st outer PMWF (182 mm to P).
T_{11} - 2nd outer PMWF Temp. (182 mm to P).

UNIT → 1															
T_a	T_v	TOP_1	TOP_2	T_1	T_2	T_3	T_4	Coolant vol.f.r.	T_5	T_6	T_7	T_8	T_9	T_{10}	T_{11}
°C	°C	°C	°C	°C	°C	°C	°C	L/min	°C	°C	°C	°C	°C	°C	°C

TABLE 2.4(B)

Plate (P) Temperature Test

Plate Combination: Impingement → No. Holes: ..... Holes Mean Diameter: ..... Holes Pitch: .....

Design Plate ΔP/P: ..... Plate Thickness: ..... Holes Layout Format: ..... Plate Material: .....

Effusion → No. Holes: ..... Holes Mean Diameter: ..... Holes Pitch: .....

Design Plate ΔP/P: ..... Plate Thickness: ..... Holes Layout Format: ..... Plate Material:

Separation Gap (Z): ..... Exp. Date: ..... Atmos. Pressure: ..... At Temp: ..... Exp. Duration: .....

Data Definitions:

Unit II →

Impingement Plate → T_1 - 1st thermo. plate temp; T_2 - 2nd thermo. plate temp; T_3 - 3rd thermo. plate temp; T_4 - 4th thermo. plate temp; T_5 - 5th thermo. plate temp;

Gap → T_6 - Coolant temp. between plates

Effusion Plate → T_7 - 1st thermo. plate temp; T_8 - 2nd thermo. plate temp; T_9 - 3rd thermo. plate temp; T_{10} - 4th thermo. plate temp; T_{11} - 5th thermo. plate temp.

Experimental Remark:

UNIT → II												
T_1	T_2	T_3	T_4	T_5	T_6		Coolant rotamtr flowrate		T_7	T_9	T_9	T_{10}	T_{11}
°C	°C	°C	°C	°C	°C		L/min		°C	°C	°C	°C	°C

TABLE 2.4(C)

Plate (P) Temperature Test

Plate Combination: Impingement → No. Holes: ..... Holes Mean Diameter: ..... Hole Pitch: .....

Design Plate ΔP/P: ..... Plate Thickness: ..... Holes Layout Format: ..... Plate Material: .....

Effusion → No. Holes: ..... Holes Mean Diameter: ..... Hole Pitch: .....

Design Plate ΔP/P: ..... Plate Thickness: ..... Holes Layout Format: ..... Plate Material: .....

Separation Gap (Z): ..... Exp.Date: ..... Atmos. Pressure: ..... At Temperature: ..... Exp. Duration: .....

Data Definitions: (Imp. = impingement; l.edge = leading edge; cool. = coolant; temp. = temperature; EFS = effusion plate; Z-D = Z-direction)

Unit III → T_1 - Imp.cool zone temp. (107.5 mm from l.edge, 100.9 mm in Z-D)
T_2 - " " " " (122 mm from l.edge, 106.5 mm in Z-D)
T_3 - " " " " (122 mm from l.edge, 99 mm in Z-D)
T_4 - " " " " (122 mm from l.edge, 91.5 mm in Z-D)
T_5 - Plate back temp. bet. 4 adj. EFS hole (106.5 mm from l.edge, 61 mm in Z-D)
T_6 - Plate back temp. midway of 2 adj. EFS hole (108 mm from l.edge, 83.5 mm in Z-D)
T_7 - Plate back temp. midway of 4 arrays EFS hole (108 mm from l.edge, 93.5 mm in Z-D)
T_8 - Plate back temp. at EFS holes entrance (101.2 mm from l.edge, 84 mm in Z-D)
T_9 - EFS temp. (16 mm from l.edge; 15 mm in Z-D)
T_{10} - EFS temp. (31 mm from l.edge; 107.9 mm in Z-D)
T_{11} - EFS temp. (108 mm from l.edge; 136.4 mm in Z-D)

Unit IV → T_1 - EFS temp. (137.0 mm from l.edge, 31.5 mm in Z-D)

UNIT III												UNIT IV
T_1	T_2	T_3	T_4	T_5	T_6	T_7	T_8	Coolant rotam.f.r.	T_9	T_{10}	T_{11}	T_1
°C	°C	°C	°C	°C	°C	°C	°C	L/min	°C	°C	°C	°C

TABLE 2.4(D)

Plate (P) Temperature Test

Plate Combination: Impingement → No. Holes: ..... Holes Mean Diameter: ..... Holes Pitch: .....

Design Plate ΔP/P: ..... Plate Thickness: ..... Holes Layout Format: ..... Plate Material: .....

Effusion → No. Holes: ..... Holes Mean Diameter: ..... Holes Pitch: .....

Design Plate ΔP/P: ..... Plate Thickness: ..... Holes Layout Format: ..... Plate Material: .....

Separation Gap (Z): ..... Exp. Date: ..... Atmos. Pressure: ..... At Temp: ..... Exp. Duration: .....

Data Definitions:

Unit IV → T_2 - Propane burner inlet air temp. T_3 - Combustor air inlet temp. T_4 - Stabilizer cover burner end temp.
T_5 - Stabilizer cover mid-way temp. T_6 - Stabilizer cover rear end temp. T_7 - Flux meter coolant inlet temp.
T_8 - Flux meter coolant outlet temp. T_9 - Flux meter (flame-side) plate temp. T_{10} - Combustor wall (182.35 mm from burner end) temp.
T_{11} - Combustor wall (182.35 mm from burner) temp.

Unit V → T_1 - Combustor wall CW (407.2 mm from burner) temp. T_2 - CW (407.2 mm from burner end) temp.

UNIT IV											UNIT V	
T_2	T_3	T_4	T_5	T_6	T_7	T_8	T_9	Coolant rotam. f.r.	T_{10}	T_{11}	T_1	T_2
°C	°C	°C	°C	°C	°C	°C	°C	L/min	°C	°C	°C	°C

TABLE 2.4(E)

Plate (P) Temperature Test

Plate Combination: Impingement→ No. Holes: ..... Holes Mean Diameter: ..... Holes Pitch: .....

Design Plate ΔP/P: ..... Plate Thickness: ..... Holes Layout Format: ..... Plate Material: .....

Effusion → No. Holes: ..... Holes Mean Diameter: ..... Holes Pitch: .....

Design Plate ΔP/P: ..... Plate Thickness: ..... Holes Layout Format: ..... Plate Material: .....

Separation Gap (Z): ..... Exp.Date: ..... Atmos. Pressure: ..... At. Temp: ..... Exp. Duration: .....

Data Definitions:

Unit V → T_3 - Combustor wall (562.2 mm from burner end) temp. T_4 - CW (526.2 mm from burner end) temp. T_5 - CW (686.55 mm from burner end) temp.
T_6 - CW (686.55 mm from burner end) temp.
T_7 - Combustor mainstream temp. (plate l.edge plane) T_8 - Combustor mainstr. temp. (P. Central plane) T_9 - CM temp. (P. trailing edge plane)
T_{10} - CM high temp. test thermocouple. T_{11} - Combustor mainstream temp., 25.4 mm upstream of test plate.

$TA_{(1,2,3)}$ - Plate adiabatic temp. at the leading edge, centre and trailing edge.

T_{RS} - Transverse transversing of CM.

U N I T V													
T_3	T_4	T_5	T_6	T_7	T_8	T_9	CRF	T_{10}	TA_1	TA_2	TA_3	T_{11}	TRS
°C	°C	°C	°C	°C	°C	°C	L/min	°C	°C	°C	°C	°C	°C

TABLE 2.4(F)

Plate (P) Temperature Test

Plate Combination: Impingement → No. Holes: ..... Holes Mean Diameter: ..... Holes Pitch: .....

Design Plate ΔP/P: ..... Plate Thickness: ..... Holes Layout Format: ..... Plate Material: .....

Effusion → No. Holes: ..... Holes Mean Diameter: ..... Holes Pitch: .....

Design Plate ΔP/P: ..... Plate Thickness: ..... Holes Layout Format: ..... Plate Material: .....

Separation Gap (Z): ..... Exp. Date: ..... Atmos. Pressure: ..... At. Temp: ..... Exp. Duration: .....

Data Definitions:

P_1 - Rotameter coolant static pressure
P_2 - Propane inlet (gauge) pressure
P_3 - Air pressure loss at Venturi throat
P_4 - Venturi upstream air static pressure
P_5 - Combustor air inlet static pressure
P_6 - Plenum coolant air pressure upstr.of plate
P_7 - Combustor mainstr.static pressure (100 mm from burner end)
P_8 - Comb. mainstr. stat.press. mid-plane of test plate (466.7 mm from b.end)
P_9 - Comb. mainstr. stat. press. (704.35 mm from burner end)
P_{10}- Flux meter coolant rotameter press.
CRF- Coolant rotameter volume flow rate
LKF- Liquid fuel (kerosine) vol.flow rate
PFF- Propane fuel volume flow rate
FMF- Flux meter coolant volume flow rate
PP- Coolant plenum static pressure - cross flow discharge coefficient test
TPC- Plate temp. cross flow discharge test

PRESSURE SEGMENT (ALL GAUGES)										FLUID FLOW SEGMENT				DISCHARGE DATA	
P_1	P_2	P_3	P_4	P_5	P_6	P_7	P_8	P_9	P_{10}	CRF	LKF	PFF	FMF	PP	TPC
										L/min					

TABLE 2.4(G)

Boundary Layer Temperature Monitoring

Transverse Location:

No. of Plate Holes: ..... Holes Mean Dia: ..... Hole Pitch: ..... Plate ΔP/P%:....

Holes Format: ..... Plate Material: ..... Plate Thick: ..... Exp.Date: .....

Transverse Thermocouple Recording Steps

Vertcl. step dist. trav. by thermo-couple mm	Cool. f.rate L/m / Reference temp. °C / Plate Transverse 'step' temp. / Trans-verse mach. setting mode					
		°C	°C	°C	°C	°C
0	0 ↔ 200					
0.5	200					
1.0	200 ↔ 400					
2.0	400					
3.0	400					
4.0	400					
5.0	400					
6.0	400					
7.0	400					
8.0	400					
9.0	400					
10.0	400 ↔ 800					
12.0	800					
14.0	800					
16.0	800					
18.0	800 ↔ 2000					
20.0	2000					
25.0	2000					
30.0	2000					
35.0	2000					
40.0	2000					
45.0	2000					

CHAPTER 3

Nomenclature

ΔP	=	Static pressure loss across the wall - Pa
G	=	Coolant (air) mass flow rate per unit test surface area - kg/sm^2
ρ	=	Air density - kg/m^3
A	=	Area - m^2
u	=	Mean coolant holes' velocity - m/s
D,d	=	Diameter of hole - mm (or m where specified)
μ	=	Air viscosity (see definition and correlation in Chapter 5) - kg/ms
n	=	Number of holes per unit surface area - m^{-2}
M	=	Mach number of hole
γ	=	Ratio of specific heats
R	=	Gas constant, 287.04 J/kgK
Re	=	Reynolds number
T	=	Coolant air temperature - K
P	=	Static pressure - 10^5 Pa
t	=	Wall thickness or length of hole - mm
ε	=	Expansibility factor
C_d	=	Discharge coefficient
$\Delta P/P\%$	=	Desing holes pressure loss
X	=	Hole's pitch
Z	=	Gap between impingement and effusion wall - mm
Z/D	=	Dimensionless gap
IMP	=	Impingement wall
EFF	=	Effusion wall
REF	=	Reference alphabets for wall combination (table 3.4)
X/D	=	Dimensionless hole pitch
$C_{d'}$	=	C_d error

K	=	Hole dynamic pressure - Pa
C_c	=	Contraction coefficient
e	=	Surface roughness - mm
F_c	=	Friction factor

Subscripts:

h	=	holes
2	=	effusion holes
i	=	inlet
a	=	total
f	=	friction

CHAPTER 3

DISCHARGE COEFFICIENT

3.1 INTRODUCTION

The design of cooling systems for hot sections of gas turbine components employing drilled effusion holes or impingement cooling requires an adequate knowledge of the pressure loss characteristics of the holes. An accurate knowledge of the pressure loss characteristics of full coverage discrete hole film cooling or impingement/effusion hybrid cooling systems, in gas turbine combustors, is important in the determination of the air split between the combustion and wall cooling requirements. In the case of a gas turbine combustor wall, the heating of the coolant as it passes through the wall holes acts as a throttle on the coolant air and will direct air from the wall cooling to the combustor, a phenomenon first recognized by Andrews et al (1,2). Accurate information on the discharge coefficients, C_d, of the holes involved in the cooling system geometries is the major design parameter of significance in the prediction of the mass flow.

Discharge coefficients of various nozzles and orifices have been extensively studied. Lichtarowicz et al (3) investigated the discharge coefficients for non-cavitating incompressible flow through orifices with length to orifice diameter ratios (t/d) of 0.5 to 10, over a range of Reynolds numbers of $1 \leqslant Re \gtrsim 10^5$. They found that at $t/d < 2$, the fluid through the orifices separates from the wall without reattaching, though this depends on the Reynolds number. Asihmin et al (4) investigated the discharge coefficient of orifices using a real fluid for $2 \leqslant t/d \leqslant 5$, at Reynolds number

of 1.5×10^5. Nakayama (5,6), Grace et al (7) and Spikes et al (8) investigated the discharge coefficient of small nozzles. Like Ref. 3, Ref. 5 found that C_d's of nozzles of $(t/d) < 1.3$ were unstable. Rohde et al (9) investigated the discharge coefficient of orifices in a thick plate at 90^o and 45^o, and found that increasing the temperature of air flowing through the orifices from ambient to 811 K, produced negligible effect on the C_d. This observation had also been noted by Andrews et al (1).

Extensive investigations of discharge coefficients of holes drilled in flat plates have also been carried out (10-16), but most of these use < 20 holes, apart from the work of Andrews et al (1,2). Where the investigations are related to wall cooling, they are mostly for turbine blade application but often use relatively low cross-flow velocities (15).

The work reported here is a continuation of the work carried out in Refs. 1, 2 and 17. Because of interest in the reduction in the number of holes of both single skin combustor effusion wall and large diameter holes, the discharge coefficients of 9688, 17222, 26910 and 4306 (large diameter) m^{-2} holes' walls were investigated. Also in the application of small impingement holes number, C_d's of 269, 1076, 4306 and 9688 m^{-2} impingement holes of the impingement/effusion cooling system were investigated.

3.1.1 Discharge Coefficient, C_d, Correlating Equations

Coolant mass flow per square metre of wall area, G, is related to the total coolant flow area per square metre of wall area and the combustor wall pressure loss, ΔP, by equation 3.1.

$$G = C_d A(2\rho\Delta P)^{0.5} \qquad \ldots (3.1)$$

where C_d = Discharge coefficient

A = $\frac{\text{Total cross-sectional area of hole}}{\text{Total test surface area of wall}}$

ρ = Coolant density

ΔP = Static pressure loss across the wall

G = Coolant mass flow rate per unit surface area

Rearranging, equation 3.1 becomes

$$C_d = \frac{G}{A(2\rho\Delta P)^{0.5}} \qquad \ldots (3.2)$$

The determination of C_d in equation 3.2 is not quite straightforward as the hole sizes in the present work for both effusion and impingement/effusion hybrid walls are small and metal thickness is significant. These small hole sizes result in hole's length (or metal thickness - 90° holes) to diameter ratio (t/d) of $0.4 \leqslant t/d \leqslant 10.0$.

For a given wall holes geometry, the coolant hole velocity, u, may be shown by equation 3.3.

$$u = \frac{G}{\rho A} \qquad \ldots (3.3)$$

Combining equation 3.3 with equation 3.1, holes' mean velocity, u, is given by

$$u = C_d\left(\frac{2\Delta P}{\rho}\right)^{0.5} \qquad \ldots (3.4)$$

Hole pressure loss and discharge coefficient, C_d, are strongly dependent on Reynolds number. References 2, 3 and 9 have shown that C_d is independent of the holes' Reynolds numbers, Re, for values $Re > 5 \times 10^3$. The holes' Reynolds number may be correlated as in equation 3.5,

$$Re = \frac{\rho u D}{\mu} \qquad \ldots (3.5)$$

where D = Mean diameter of the holes

μ = Coolant viscosity (see Chapter 5 for correlating equation)

The holes' mean diameter may be shown as in equation 3.6.

$$D = \left(\frac{4A_h}{\pi n}\right)^{0.5} \qquad \ldots (3.6)$$

where A_h = Holes' cross-sectional area

n = Total number of holes

The coolant mass velocity (ρu) may be expressed as in equation 3.5b

$$\rho u = \frac{\dot{M}}{A} = G \qquad \ldots (3.5b)$$

Combining equations 3.5, 3.6 and 3.5b, Re may be shown to be

$$Re = \left(\frac{4A_h}{\pi n}\right)^{0.5} \frac{G}{\mu} \qquad \ldots (3.7)$$

To establish C_d values at high Reynolds numbers where C_d becomes independent of Re, for use in engine designs (2), investigation at higher G values is required. At higher G values, there are high wall pressure losses, compressibility effects become important and a constant flow C_d is not obtained for the hole sizes employed in the present work. The Mach number, M, of the holes employed in this work (2) is given by equation 3.8.

$$M = \frac{u}{(\gamma RT)^{0.5}} = \frac{G}{PA}\left(\frac{RT}{\gamma}\right)^{0.5} = C_d\left(\frac{2\Delta P}{\gamma P}\right)^{0.5} \qquad \ldots (3.8)$$

Nakayama (6) and Andrews et al (2) working at high G values, as employed in the present work, corrected for compressibility effect using equation 3.9.

$$\varepsilon = 1 - 0.59\,\frac{\Delta P}{P} + 0.0107\,\frac{t.\Delta P}{d.P} \qquad \ldots (3.9)$$

for $1.5 < t/D < 10$

where ε = Expansibility factor equal to the ratio of the actual mass flow to the equivalent incompressible mass flow at the same pressure loss

ΔP = Static pressure loss across test wall

P = Static pressure upstream of wall

t = Holes' length

D = Holes' mean diameter

Using the above equation the corrected discharge coefficient is expressed as in equation 3.10.

$$C_d = \frac{G}{\varepsilon A(2\rho\,\Delta P)^{0.5}} \qquad \ldots (3.10)$$

The above equations are employed in the present work.

3.2 EXPERIMENTAL PROCEDURE

The diameter of the perforated test walls were determined using the Kwik-Chek measuring gauge described in Chapter 2. The large hole densities were measured one by one for five times to get an arithmetic mean. Both sides of the wall were measured in this way and the diameters were then fed into the computer to determine the mean values of the holes' diameter at hole inlet and outlet. The calculation involved in the determination of the mean hole diameter is shown in section 3.3.3 as well as the errors. The minimum hole area was used in the pressure loss computation.

The walls were bolted onto the end of the plenum using high temperature 'auto-stick' cement as a sealant to prevent air leakage from the edges. Two methods of testing were investigated. These were (a) free discharge coefficient measurement, and (b) cross-flow discharge coefficient measurement.

To measure the discharge coefficient of the holes for case (a), the plenum was placed on the combustor duct with the duct's flux meter, stabilizer cover and duct trailing end cover plate removed. The plenum was connected to the air lines. Compressed air was blown through the test wall and allowed to discharge freely into the test room. The result from this test is called the 'free' discharge coefficient. The air flow rate was measured using three air rotameters as discussed in Chapter 2 and Ref. 17. The maximum errors of the three rotameters are shown in table 3.1.

TABLE 3.1

Rotameter Range	Calibrated Maximum Error %
15-150 l/min	± 0.8
50-500 l/min	± 1.1
200-2000 l/min	± 1.52

Table 3.1: Rotameter maximum error

The temperature and pressure of the air were measured upstream of the rotameter using a 1.6 mm diameter mineral insulated grounded junction Type K thermocouple. These parameters were recorded to correct for the density of the air. The air temperature was again measured in the plenum at four locations using thermocouples of the type discussed above. The temperature readings were taken using digital thermocouple transducers. The static pressure of the coolant in the plenum was measured using four inter-connecting pressure tappings, 1.0 mm in diameter, through a pressure digital output transducer, which has an accuracy better than ±1%. The

pressure tappings were located 228.6 mm upstream of the test wall in the plenum. The plate temperature was taken as the output of the wall thermocouple at 76.2 mm from the wall leading edge.

The cross-flow discharge coefficient (b) was measured in the same way as that of the free discharge except at this stage the rig was set up ready for a low temperature test. In this instance, the stabilizer cover, flux meter and duct trailing end cover-plate were installed on the duct. Combustion air at the flow rate required for the combustion test was fed into the cross-flow duct. The mean velocity of the cross-stream was 22 m/s. The air flow through the test wall holes was then discharged onto the combustor cross-stream. The combustor wall had in place three jet mix stabilizers (18) at 410 mm upstream of the test wall. These were used for firing kerosine but in the case of low temperature and cross-flow discharge coefficient tests, they were not fuelled but served as practical condition turbulence generators at the plane of the test wall. The combustor had six pressure tapping holes, inter-connected in pairs, located three on either side of the duct walls. These paired pressure tappings were located at the test wall plane, 93.65, 460.35 and 698 mm downstream of the jet mix stablizers. These pressure tapping holes were 1.0 mm in diameter. In all the investigations the centre pair pressure tappings were monitored. The mainstream temperature was also taken at the central plane of the test wall.

Two rigs were used in this investigation, Mk III and Mk IV. These rigs are similar except that Mk III has only one pressure tapping. The description of Mk IV can be found in Chapter 2. The designed parameters of the investigated walls are shown in table 3.2.

TABLE 3.2

Wall Holes No. m^{-2}	Manufac. Method	$\Delta P/P$ %	Dia.(D) mm Inlet Outlet	Thick. or Holes Length (t) - mm	Hole Pitch (X) - mm	t/D	X/D	Holes Incln. Angle (α^o)
9688	Laser	3.0	0.837 1.038	6.35	10.16	7.59	12.14	90
9688	Laser	3.0	0.986 1.013	3.32	10.16	3.37	10.3	90
9688	Laser	0.1	2.195 2.275	6.51	10.16	2.96	4.63	90
9688	Laser	3.0	0.822 0.823	6.68	10.16	8.14	12.37	30 (150)
17222	Drilled	3.0	0.763 0.781	6.35	7.62	8.50	10.20	90
17222	Drilled	3.0	0.763 0.778	3.29	7.62	4.32	9.99	90
26910	Drilled	0.1	1.311 1.33	3.37	6.10	2.55	4.62	90
26910	Drilled	0.1	1.625 1.607	0.69	6.10	0.43	3.77	90
4306	Drilled	0.0027	8.217 8.228	6.35	15.24	0.77	1.85	90

Table 3.2: Design parameters for single effusion wall

For the impingement holes, the design parameters are shown in table 3.3 and table 3.4.

TABLE 3.3

Wall Holes No. m^{-2}	Manufac. Method	$\Delta P/P$ %	Dia.(D) mm Inlet Outlet	Thick. or Holes Length (t) - mm	Hole Pitch (X) - mm	t/D	X/D	Holes Incln. Angle (α^o)
269	Drilled	3.0	5.7 5.704	6.35	60.0	1.11	10.53	90
1076	Drilled	3.0	2.859 2.894	6.35	30.48	2.22	10.66	90
1076	Drilled	3.0	2.903 2.815	3.34	30.48	1.17	10.66	90
4306	Drilled	3.0	1.41	6.35	15.24	4.49	10.78	90
9688	Laser	3.0	0.986 1.013	3.32	10.16	3.37	10.3	90

3.3 RESULTS AND DISCUSSION

The results of the discharge coefficients are presented with the effective C_d being the average value of the C_d's at $Re \geq 4 \times 10^3$, but in the case of 26910 m^{-2} holes' wall, this is taken as at $Re \geq 2 \times 10^3$. A computer program has been used to analyse the results. Raw C_d results are the C_d results without correction for compressibility effect, eq. 3.2, and corrected C_d's are with this correction, eq. 3.10. Samples of computer output results are shown in table 3.6 (A-D) of the appendix.

3.3.1 Effusion Wall

Figures 3.1-3.19 show the results of both 'free' and 'cross' flow discharge coefficients of the walls investigated. The results indicate a high value of C_d for the laser drilled 9688 m^{-2} holes as shown in fig. 3.1. The holes were found to be tapered with a larger exit diameter than the inlet diameter used in the C_d evaluation. The main pressure loss occurs due to the one dynamic head loss at the exit and this will be a lower pressure loss than for a cylindrical hole. This is the reason for C_d being greater than unity.

The effect of cross-flow on C_d depends on the hole size and hence the pressure loss or hole velocity. For the 4306, 9688 and 26910 m^{-2} holes' walls, at 90°, the effect of cross flow is to reduce the C_d, with the magnitude of the reduction varying between 2.4% and 3.4%, and as high as 17% for the final C_d of the very large holes, 4306 m^{-2} wall, figs. 3.18-3.19. Cross-stream effects on the 17222 m^{-2} holes' walls, figs. 3.7-3.10, were very weak, with an overall average increase of 0.7%. The 9688 inclined wall placed at 30° and 150° positions, figs. 3.15-3.17 in the direction of the mainstream, showed an increase in C_d values in comparison with free-discharge. The magnitude of these increases is 1.3% and 5.6%

respectively for the two positions.

At low Reynolds values, Re $\leqslant 10^3$, the results indicate that compressibility effect is negligible or non-existent but at Re $\geqslant 10^3$, compressibility effect is indicated to be strong. In all cases, C_d increases with Re until Re $\geqslant 10^3$ is reached, when C_d gets to an equilibrium state.

3.3.1A Effect of number of holes on C_d

The effect of number of test wall holes on the discharge coefficient was investigated using the 3.0% design pressure loss, 9688 m^{-2} and 17222 m^{-2} holes effusion wall. The results are presented in figure 3.20. The results show that C_d of holes decreases as the number of holes increases, although difference in hole manufacturing technique also contributes. The C_d of 9688 m^{-2} holes, for t equal to 6.35 mm, is 28% higher than the C_d of 17222 m^{-2} holes at the same value of t. For t value of 3.3 mm, the magnitude of the difference in C_d, between the two walls, is less, 14%. The influence of the t/d ratio will be discussed later.

3.3.1B Effect of diameter (D) of hole on C_d

The effect of mean hole diameter on the discharge coefficient is shown in figure 3.21. This shows that at low design pressure loss, D is large and Reynolds number (Re) is mainly laminar. The results indicate a strong influence of Re on C_d in the laminar regime. There is evidence, presented later, that for a fixed t/d the C_d increases as the hole diameter increases. This may be evidence for a hole pitch/diameter, X/D, influence on C_d as the test refers to a constant pitch. For large holes there is also evidence that the final C_d is not reached until a higher Reynolds number

than for the small holes.

3.3.1C Effect of holes' inclination to cross-stream on C_d

The results of the discharge coefficient of holes at different holes angle to cross-flow are shown in fig. 3.22 for 9688 m^{-2} holes wall at 30, 90 and 150 degrees to the direction of the mainstream flow for a hole diameter of 0.82 mm with a comparison with a D of 2.2 mm at 90°. The results indicate a weak dependence of C_d on holes' inclination provided the holes' diameters are nearly the same. With widening difference in the holes' diameters, the results indicate that hole diameter or t/d has a much more important influence than hole inclination.

3.3A The prediction of C_d with inlet, outlet pressure loss

The aerodynamic features influencing pressure loss through a long hole are shown in fig. 3.23. The hole aerodynamics indicate a reattachment to the wall after an initial detachment, at about t/d of 0.8 (24). For all hole geometries in this investigation, flow reattachment will contribute to the pressure loss as shown in fig. 3.23.

As the holes discharge into a far larger area then, provided the velocity profile is uniform, the exit pressure will be one hole dynamic head. At the hole inlet, the fluid separates, contracts and expands to reattach to the wall. The expansion results in pressure loss. Wall friction losses are expected to be small compared with this inlet loss for small t/d. Employing momentum and energy equations, the inlet pressure loss, K_i, in terms of hole dynamic heads, is given by equation 3.11A.

$$K_i = \frac{\Delta P}{\frac{1}{2}\rho u^2} = \left(\frac{1}{C_c} - 1\right)^2 \qquad \ldots (3.11A)$$

where C_c = Contraction coefficient.

For a sharp edge orifice discharging into a large area, a value of 0.61 for C_c applies (25). Using this value of C_c, equation 3.11A gives K_i as 0.44. The empirical value of K_i has been given as 0.5 (26), while Benedict et al (26) have reported a value of 0.58.

The total pressure loss factor, K_a, may be shown to be related to the discharge coefficient by using the mass continuity equation and equation 3.1.

$$K_a = \frac{1}{C_d^2} \qquad \ldots (3.11B)$$

For a short cylindrical tube the total pressure loss, K_a, is the sum of the inlet and exit pressure loss

$$K_a = K_i + 1 \qquad \ldots (3.11C)$$

A prediction of C_d, which is dependent on K_i, provided the exit velocity profile is uniform, can be shown as equation 3.11D.

$$C_d = \left(\frac{1}{K_i + 1}\right)^{0.5} \qquad \ldots (3.11D)$$

Using the above values of K_i, equation 3.11D gives the predicted values of C_d as shown in table 3.3B.

TABLE 3.3B

K_i	Predicted C_d
0.44	0.833
0.50	0.816
0.58	0.796

Table 3.3B: Predicted values of C_d

The above analysis of C_d gives good agreement with the measured values of C_d shown in table 3.5 . The factors ignored in the simple theory of K_i are the influence of upstream hole inlet frictional effects and hole manufacturing method which cause the velocity distribution at the vena contraction to be non-uniform. The frictional effects may be accounted for by the use of a velocity coefficient, C_v. This results in a modified K_i as in equation 3.11E.

$$K_i = \left(\frac{1}{C_v C_c} - 1\right)^2 \qquad \ldots (3.11E)$$

where K_i = Inlet pressure loss

C_v = Ratio of the actual mean velocity to the ideal uniform velocity at the vena contraction

C_c = Contraction coefficient

The reasons for C_d higher than 0.84 in the present work were partly due to the larger outlet diameter as discussed previously in relation to the tapered laser drilled holes (section 3.3.1), and further due to a change in the contraction coefficient for large diameter small X/D holes. It must be noted that there is no correlation for the C_d of short tapered holes and the present equation is only for cylindrical orifices without tapering. From the simple theory of the inlet pressure loss above, and the definition of C_c, fig. 3.23, the high C_d results for the large diameter small X/D geometries may be explained by an increase in A_v and the contraction coefficient tending to unity, giving K_i tending to zero. This will result in a discharge coefficient that gives a value of closer to unity from equation 3.11D. For shaped edged orifice plates it is known that C_c increases as the area ratio increases, and the present results indicate a similar phenomenon with the hole X/D equivalent

to the pipe/orifice diameter ratio.

3.3B Wall friction effects

Wall friction effects have been correlated as in equation 3.11F by Andrews et al (2).

$$K_f = 4F_c \frac{t}{d} \qquad (3.11F)$$

where K_f = Frictional pressure loss

F_c = Frictional factor based on hole surface roughness to diameter ratio (e/d) and Reynolds number

The effect of wall friction is to cause pressure loss and to reduce the C_d. The non-inclusion of friction losses in the prediction of C_d indicates that for a t/d of 4.5 friction losses are negligible. For t/d > 4.5, the results indicate lower C_d and hence an influence of wall friction as in fig. 3.44.

3.3.2 Impingement Holes' Discharge Coefficient, C_d

The combinations of walls investigated are shown in table 3.4, and

TABLE 3.4

Holes Combination/m²		Mean Holes Diameter-mm		ΔP/P%		t/D		X/D		Gap		Wall
Imp.	Eff.	Imp.	Eff.	Imp.	Eff.	Imp.	Eff.	Imp.	Eff.	Z	Z/D	Ref.
269	4306	5.7	3.27	3.0	0.1	1.11	1.94	10.53	4.66	8	1.4	A
1076	4306	2.86	3.24	3.0	0.1	1.17	1.03	10.66	4.7	8	2.8	B
1076	4306	2.86	3.27	3.0	0.1	2.22	1.94	10.66	4.66	8	2.8	C
1076	4306	2.86	3.27	3.0	0.1	2.22	1.94	10.66	4.66	7	2.5	D
1076	4306	2.86	3.27	3.0	0.1	2.22	1.94	10.66	4.66	12	4.2	E
1076	4306	2.88	8.22	3.0	0.0027	2.21	0.77	10.6	1.85	8	2.8	F
4306	4306	1.41	8.22	3.0	0.0027	4.49	0.77	10.78	1.85	8	5.8	G
9688	9688	0.99	2.2	3.0	0.1	3.37	2.96	10.3	4.63	4.5	4.6	H
1076	26910	2.86	1.3	3.0	0.1	2.22	4.86	10.66	4.66	9.4	3.3	I

the results for both modes of test, "free discharge" and "cross-flow discharge" are presented in figs. 3.24-3.40. The effective C_d's are also shown along with the parameters of the wall investigated. As shown in table 3.4, the hybrid wall will be hereinafter referred to as wall A, B, C, etc. The results demonstrate the same trend of C_d dependence on Reynolds number as shown by the single walls. Compressibility effects are more distinct in these results than in the effusion wall results but this is due to the high Reynolds and Mach numbers involved with the impingement wall. All the results show that the effect of cross-flow was to reduce the impingement hole discharge coefficient. Chu et al (16) investigated the effect of cross-flow on impingement holes' discharge coefficient and concluded that the C_d was unaffected by the mainstream. The conclusion of these authors is confirmed in the present work with relatively small influence of cross-flow. The reduction involved in the value of free discharge C_d at cross-flow varies between 0.5 to 6% and is as high as 8% for wall C, figs. 3.28 and 3.29. The smallest reduction in C_d due to cross-flow is shown by walls F and G, figs. 3.34-3.37, which have large diameter effusion holes. Wall I, fig. 3.40, has only free-discharge C_d results.

3.3.2A Effect of impingement holes' number on C_d

Figure 3.41 shows the effect of the number of impingement holes on C_d for walls A, C and G. The effusion walls of these hybrid systems have design pressure losses of 0.1%, 0.002% and t/D_2 of 1.94 and 0.77 respectively. The concentrations of the impingement holes are of ratios 1:4:16 respectively. The results indicate that at low Reynolds number, $Re \leq 10^4$, the C_ds of the high density impingement holes were greater than those of the low density impingement holes. This was somewhat unexpected, in that the

impingement t/ds were greater for the high hole density and a smaller C_d would be expected. The C_d of the low density impingement holes, however, continues to increase to values greater than the high density holes. These results suggest that where an impingement hole air is split between several effusion holes, the 'suction' effect gives a Reynolds number dependence of the C_d.

Figure 3.42 shows the effect of the number of impingement holes on C_d for the large diameter effusion wall. The two walls are F and G in table 3.4. The table shows that the mean hole diameter of the effusion wall was 8.22 mm, t/D_2 = 0.77 and the impingement holes density in both hybrid walls is in a ratio of 1 to 4. The results indicate that the C_d of the higher density impingement holes, wall G, was again greater than that of the low density impingement holes of wall F at all Reynolds numbers investigated. These results are in contrast to the final results of fig. 3.41 in which the final C_d of low density impingement holes was 4% superior to high density holes. However, the very low impingement hole density at which this occurred in fig. 3.41 was not tested with the very large effusion holes.

3.3.2B Effusion holes' diameter effect on impingement holes' C_d in an impingement/effusion system

Two walls, C and F, table 3.4, have been investigated to determine the effect of effusion wall hole diameter on impingement holes' C_d. The concentration of holes for impingement walls and effusion walls in both hybrid systems were the same. The hole length in both cases as well as the impingement hole mean diameter were the same, but the mean diameter of the effusion wall of the hybrid wall, F, was a factor of 2.5 greater than that of the effusion wall of C.

Figure 3.43 shows the effect of effusion holes' mean diameter on impingement holes' discharge coefficient for a Z/D of 2.8. The results reveal that the C_d of the impingement holes for the large effusion holes' diameter was lower at all Reynolds numbers investigated. Thus, for a given impingement holes geometry, in an impingement/effusion system, the effect of large effusion holes diameter is to reduce the C_d of the impingement holes. It is clear that the overall C_d of an impingement/effusion system is not solely determined by the impingement wall. The change in the impingement aerodynamics due to the effusion holes' inlet influences the pressure loss, especially where there are a larger number of effusion holes.

3.3.3 Effective Incompressible Flow C_d

3.3.3A Error in effective C_d determination

The total error in effective C_d is shown by equation 3.2 to be a function of errors involved in the measurements (1,20-22) of all the parameters in the right-hand side of the equation. The accuracy in the flow measurements, using the rotameter, has been stated in section 3.2. The error involved in the determination of the parameter A is mainly in the determination of the holes' mean diameter. The Kwik-Chek small holes diameter gauge is highly accurate, with a resolution of 0.01 mm. A calibrating standard supplied with it has an exact hole diameter of 1.78 mm. Using this instrument, it has been found that an error in hole's cross-sectional area is less than 0.1%. This value has also been found by Ref. 17. Each mean holes' diameter is determined by measuring a single hole five times and finding the arithmetic mean. This is done for all the holes on both sides of the wall. The main uncertainty in the hole diameter is the hole's shape, such as 'roundness' and hole taper. The computer

calculation is as stated below:

Measured diameter, $d \rightarrow \Sigma d_n^2$; n = total number of holes

$$\text{Mean holes' } D = \left(\frac{\Sigma d_n^2}{n}\right)^{0.5} \quad \ldots (3.11)$$

$$\text{Standard deviation} = \frac{\Sigma(D - d)^2}{n} = s$$

$$\text{Standard error} = \frac{s}{n^{0.5}} = E$$

$$\text{Relative error} = \frac{2E}{D}$$

$$\text{Average mean hole diameter} = \frac{\text{Sum of mean of D at front \& back of wall}}{2}$$

Total cross-sectional area of the holes, A, is

$$A = \frac{\pi}{4} \Sigma d_n^2 \quad \ldots (3.12)$$

$$\text{Standard relative error in area} = \frac{E^2}{\Sigma d_n^2} = \frac{A'}{A} \quad \ldots (3.13)$$

The error involved in the determination of the air density is that of temperature and total pressure measurements. The error of the thermocouple has been shown to be less than 0.1% and that of the pressure measurements to be within 1%.

The overall error involved in the discharge coefficient determination is shown in equation 3.14 (20-23) as

$$\left(\frac{C_d'}{C_d}\right) = \left[\left(\frac{G'}{G}\right)^2 + \left(\frac{A'}{A}\right)^2 + \left(\frac{0.5\rho'}{\rho}\right)^2 + \left(\frac{0.5\Delta P'}{\Delta P}\right)^2\right]^{0.5} \quad \ldots (3.14)$$

The relative standard errors of the right-hand parameters have been estimated as:

$$\frac{G'}{G} = 2\%$$

$$\frac{A'}{A} = 0.7\%$$

$$\frac{\rho'}{\rho} = 0.1\%$$

$$\frac{\Delta P'}{\Delta P} = 1\%$$

Substituting into equation 3.14 gives

$$\frac{C_{d'}}{C_d} = 2.18\%$$

The above error value is the maximum that may be encountered in this work. For an effective C_d value of 0.7822, the error in the value is

$$C_{d'} = \frac{2.18}{100} \times 0.7822 = \pm 0.017$$

It is however realistic to accept that the error involved in the effective C_d values is ±0.02, at a fixed nominal flow rate. This is the accuracy of an individual data point in the figures. At high Reynolds number for some designs, C_d is relatively independent of Reynolds number, but the results show considerably more data scatter in this value than ±0.02. The major data scatter occurs at high Reynolds number for impingement/effusion cooling where there is evidence of a periodic variation as Reynolds number is increased, e.g. fig. 3.26. For effusion only and the final high Reynolds number, C_d is more uniform, e.g. fig. 3.5, but some designs do exhibit a periodic variation in C_d with Reynolds number and a final high Reynolds number C_d is difficult to determine for these designs, e.g. fig. 3.17. Consequently the accuracy of the final high Reynolds number C_d is much less than the accuracy of an individual data point. The reasons for this small but significant variation of corrected C_d with Reynolds number in the turbulent region are not known.

3.3.3B Values of free and cross-flow C_d

The values of both 'free' and 'cross' flow corrected effective C_d are presented in table 3.5 for the single effusion wall and the impingement holes of the impingement/effusion wall.

It should be noted that the temperature of air during the tests is at room temperature and varies between 289 K to 293 K.

TABLE 3.5

No. Holes m^{-2}	t/D	Effective Discharge Coefficient Free Flow	Cross-Flow
4306	0.77	1.12	0.93
9688	7.59	1.06	1.03
9688	3.37	0.86	0.85
9688	2.96	0.89	0.86
17222	8.5	0.75	0.76
17222	4.32	0.71	0.72
26910	2.55	0.78	0.76
26910	0.43	0.74	0.71
9688 (30°)	8.14	1.02	1.03
9688(150°)	8.14	1.02	1.08
(Wall - Table 3.4)	Impingement Wall		
A	1.11	0.88	0.83
B	1.17	0.82	0.81
C	2.22	0.87	0.80
D	2.22	0.82	0.81
E	2.22	0.84	0.82
F	2.21	0.69	0.68
G	4.49	0.85	0.84
H	3.37	0.89	0.88
I	2.22	0.78	-

Table 3.5: C_d for 'free' and 'cross' flow discharge with compressibility correction

From the table, the effect of the present magnitude of cross-flow is seen to be small and to be more significant for the impingement/effusion design.

3.3.4 Influence of Dimensionless Holes' Length (t/d) on the Mean High Reynolds Number (Re) Discharge Coefficient C_d

The influence of t/d on the mean high Reynolds number discharge coefficients for both 'free' and 'cross' flow is shown in fig. 3.44. The present results for the single wall are also compared with those of other workers, using orifices or nozzles. Although the present results are in reasonable agreement with previous work, there are certain significant differences. The abnormally high C_d for the larger drilled hole at t/d $\sim$ 7.5 has already been discussed. At low t/d, results for large hole diameter are significantly higher than those for a small thickness. This may be an influence of hole pitch to diameter ratio X/D. If this is small then the hole approach conditions may be influenced and the inlet contraction coefficient moved away from unity, thus reducing C_d.

Within the range of previous works, the upper limit of the present results compares well with those of Mkpadi (17) and Asihmin et al (4). The lower limit of the results are close to those of Ward-Smith (19), Nakayama (5) and Lichtarowicz et al (3). At large values of t/d the present work compares well with those of the others.

3.4 CONCLUSIONS

(1) For multiple holes of a single wall, the high Reynolds number discharge coefficient is not strongly affected by the cross stream, although the effect is significant for some designs.

(2) The C_d of single wall holes is strongly dependent on holes' mean diameter. The smaller the holes' diameter, the smaller the C_d for equal hole t/d.

(3) Inclination of holes, with the range of holes' diameters investigated, has a weak effect on the discharge coefficient.

(4) The C_d of impingement holes has a weak dependence on hole concentration but is more strongly affected by the effusion holes' diameter. The larger the effusion holes' diameter, the poorer the value of the impingement holes' C_d.

(5) For all geometries of holes investigated, apart from the 26910 m^{-2} holes, compressibility effect is significant at the region where C_d is independent of Reynolds number, i.e. $Re \geqslant 10^4$.

3.5 REFERENCES

1. Andrews, G.E., and Mkpadi, M.C., 'The measurement of the discharge coefficient of thick drilled plates: 100 1.41 mm diameter holes in a 6.35 mm thick plate', Report Number GEA/HT/1, Dept. of Fuel and Energy, University of Leeds, Leeds, 15.1.80.

2. Andrews, G.E., and Mkpadi, M.C., 'Full coverage discrete hole wall cooling - Discharge coefficients', ASME Paper 83-GT-79, and also ASME - J.Eng. Power, Vol. 106, pp. 183-192, 1984.

3. Lichtarowicz, A., Duggins, R.K., and Markland, E., 'Discharge coefficients for incompressible non-cavitating flow through long orifices', J.Mech.Eng.Sci., Vol. 7, No. 2, pp. 210-219, June 1965.

4. Asihmin, V.I., Geller, Z.I., and Skobel'Cyn, Yu A., 'Discharge of a real fluid from cylindrical orifices' (in Russian), Oil Ind., Moscow, Vol. 9, p. 55, 1961.

5. Nakayama, Y., 'Action of the fluid in the air micrometer: (1st Report, Characteristics of small-diameter nozzle and orifice, No. 1, In the case of compressibility being ignored)', Bull. J.S.M.E., Vol. 4, No. 15, pp. 507-515.

6. Nakayama, Y., 'Action of the fluid in the air micrometer (2nd Report, Characteristics of small-diameter nozzle and orifice, No. 2, In the case of compressibility being considered)', Bulletin of JSME, Vol. 4, No. 15, pp. 516-524, 1961.

7. Grace, H.P., and Lapple, C.E., 'Discharge coefficients of small diameter orifices and flow nozzles', Trans. ASME, Vol. 73, p. 639, 1951.

8. Spikes, R.H., and Pennington, G.A., 'Discharge coefficients of small submerged orifices', Trans. ASME, Vol. 173, p. 661, 1959.

9. Rohde, J.E., Richards, H.T., and Metger, G.W., 'Discharge coefficients for thick plate orifices with approach flow perpendicular and inclined to the orifice axis', NASA TN D-5467, Oct. 1969.

10. Kolodzie, P.A., Jr., and Van Winkle, M., 'Discharge coefficients through perforated plates', A.I.Ch.E. Journal, Vol. 3, No. 3, 305, 1957.

11. Smith, P.L., Jr., and Van Winkle, M., 'Discharge coefficients through perforated plates at Reynolds numbers of 400 to 300', A.I.Ch.E. Journal, Vol. 4, No. 3, 1958.

12. Dittrich, R.T., 'Discharge coefficients for combustor-liner air-entry holes 11-Flush Rectangular holes, step louvers and scoops', NACA, TN 3924, April 1958 (update - 1974).

13. Hay, N., Lampard, D., and Benmansour, S., 'Effect of cross flows on the discharge coefficient of film cooling holes', ASME - J.Eng. Power, Vol. 105, pp. 243-248, 1983.

14. Damerow, W.P., Murtaugh, J.C., and Burggraf, F., 'Experimental and analytical investigation of the coolant flow characteristics in cooled turbine aerofoils', NASA Report CR 120883, 1977.

15. Tillman, E.S., and Jen, H.F., 'Cooling air flow studies at the leading edge of a film cooled airfoil', ASME - Paper 83-GT-82.

16. Chu, T., Brown, A., and Garrett, S., 'Discharge coefficients of impingement and film cooling holes', ASME - Paper 85-GT-81.

17. Mkpadi, M.C., 'Full coverage effusion cooling of gas turbine combustor chamber', Ph.D. thesis, Dept. of Fuel and Energy, University of Leeds, Leeds, 1982.

18. Andrews, G.E., Abdul Aziz, M.M., and Al-Dabbagh, N.A., 'Mixing and fuel atomisation effects on premixed combustion performance', ASME Paper 83-GT-55, 1983.

19. Ward-Smith, A.J., 'Internal Fluid Flow: The Fluid Dynamics of Flow in Pipes and Ducts', Clarendon Press, Oxford, 1980.

20. Taylor, J.R., 'An Introduction to Error Analysis: The Study of Uncertainties in Physical Measurements', University Science Books, 1982.

21. Topping, J., 'Errors of Observation and Their Treatment', 3rd Edition, Chapman and Hall Limited, London, 1969.

22. Kline, S.J., and McClintock, F.A., 'Describing uncertainties in single-sample experiments', Mech. Eng., pp. 3-8, Jan. 1953.

23. Quenouille, M.H., 'Rapid Statical Calculations', 2nd Ed., Griffin, London, 1972.

24. Ward-Smith, A.J., 'Pressure Losses in Ducted Flows', Butterworths, 1971.

25. Rouse, H., and Abdul-Fetoug, A.H., 'Characteristics of irrational flow through axially symmetric orifices', Trans. ASME, Vol. 72, pp. 421-426, 1950.

26. Benedict, R.P., Carlucci, N.A., and Swetz, S.D., 'Flow losses in abrupt enlargements and contractions', J. Eng. Power, Vol. 88, pp. 23-81, 1966.

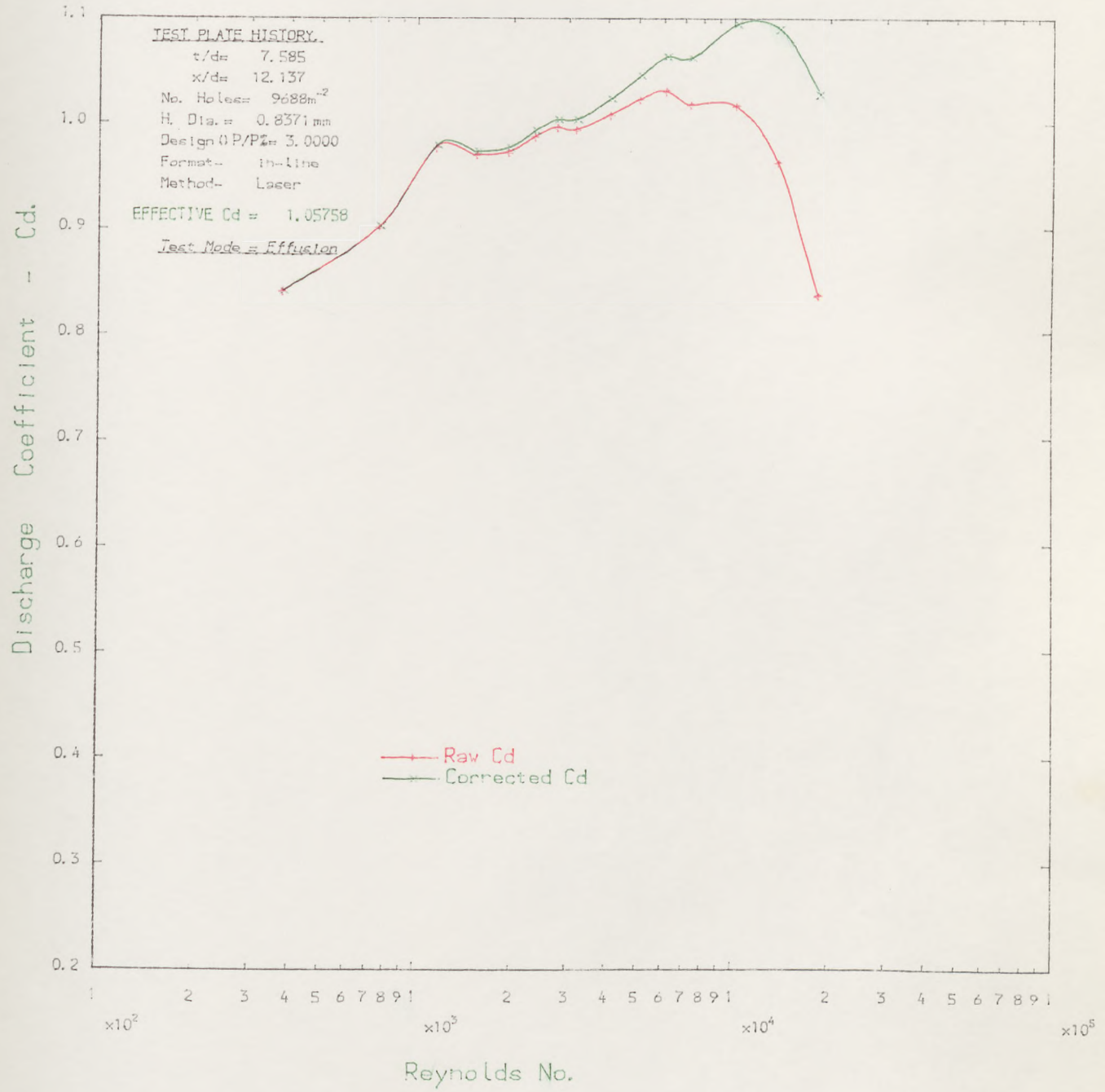

FIG. 3.1 : FREE-DISCHARGE Cd DEPENDENCE ON REYNOLDS NUMBER- (cold test).

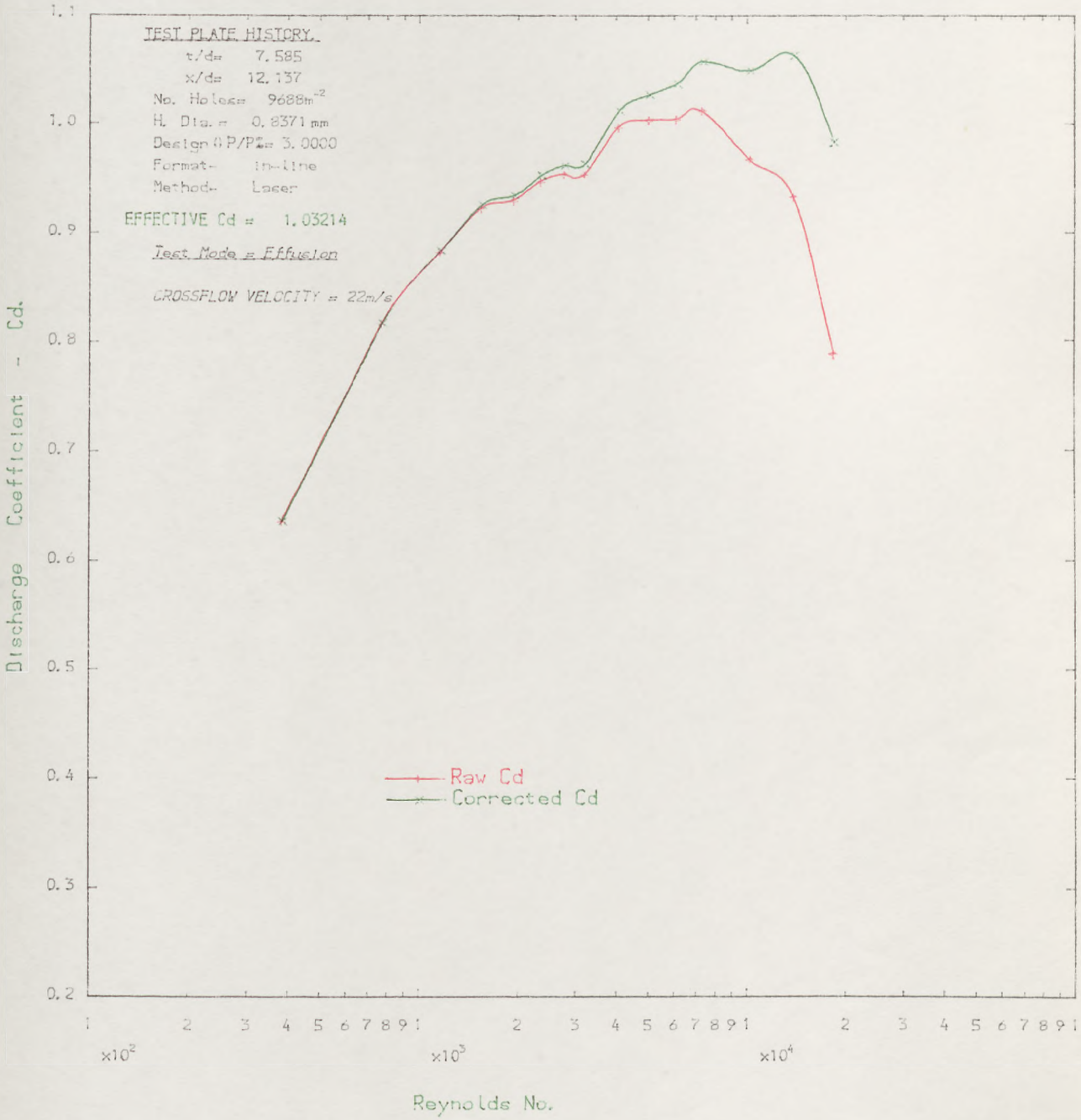

FIG. 3.2 : CROSS-FLOW Cd DEPENDENCE ON REYNOLDS NUMBER- (cold test).

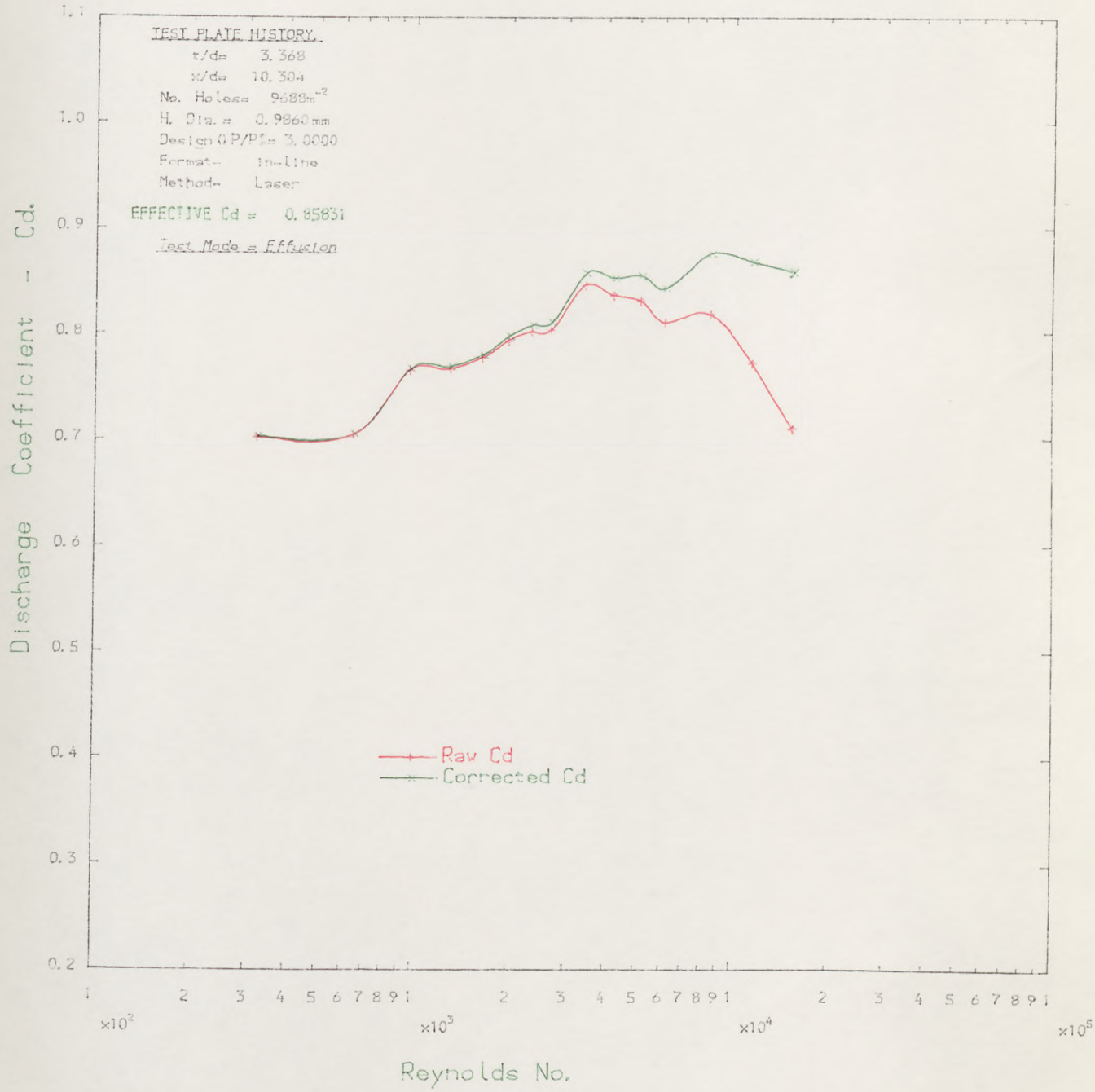

FIG. 3.3 : FREE-DISCHARGE Cd DEPENDENCE ON REYNOLDS NUMBER- (cold test).

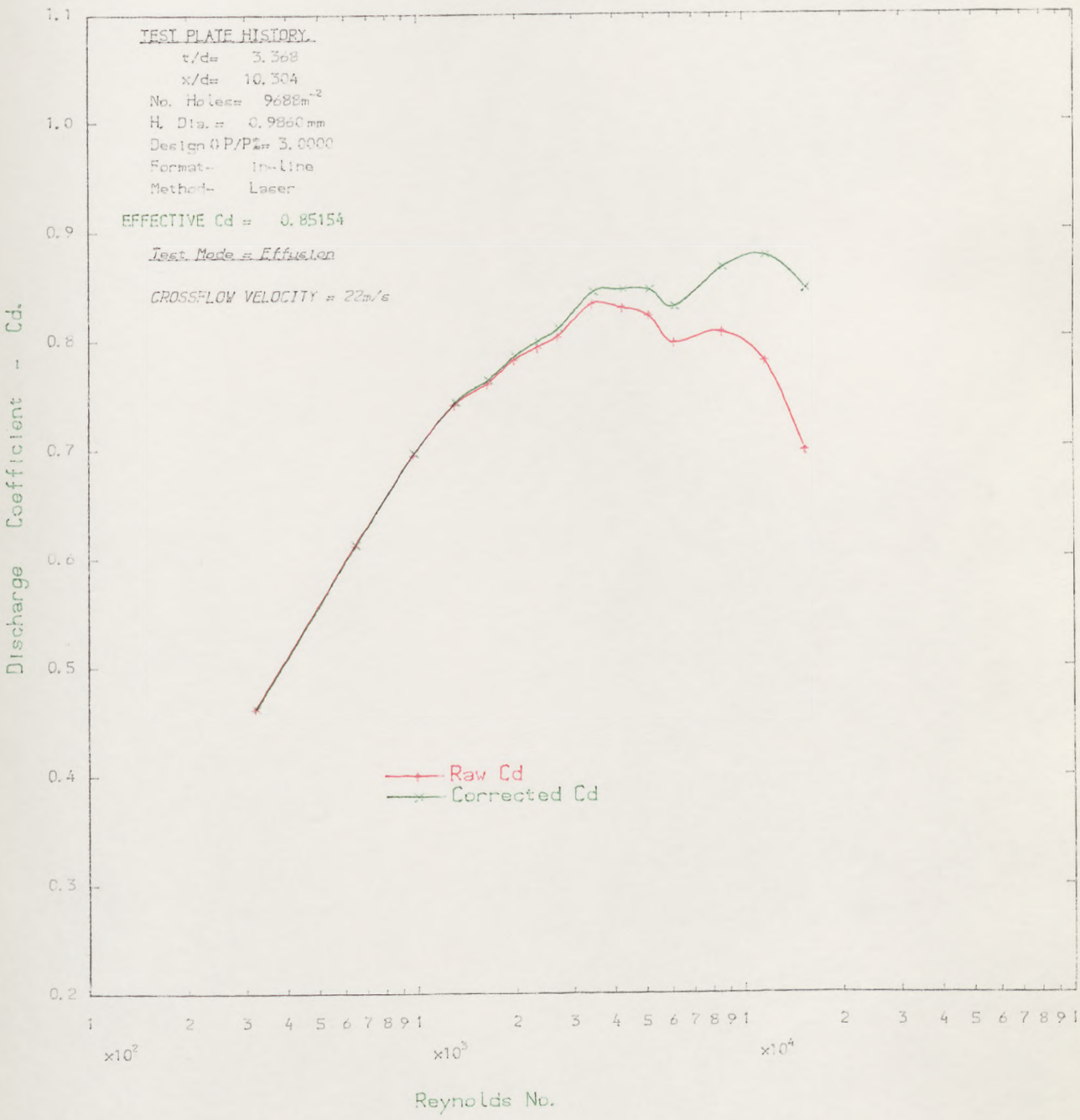

FIG. 3.4: CROSS-FLOW Cd DEPENDENCE ON REYNOLDS NUMBER- (cold test).

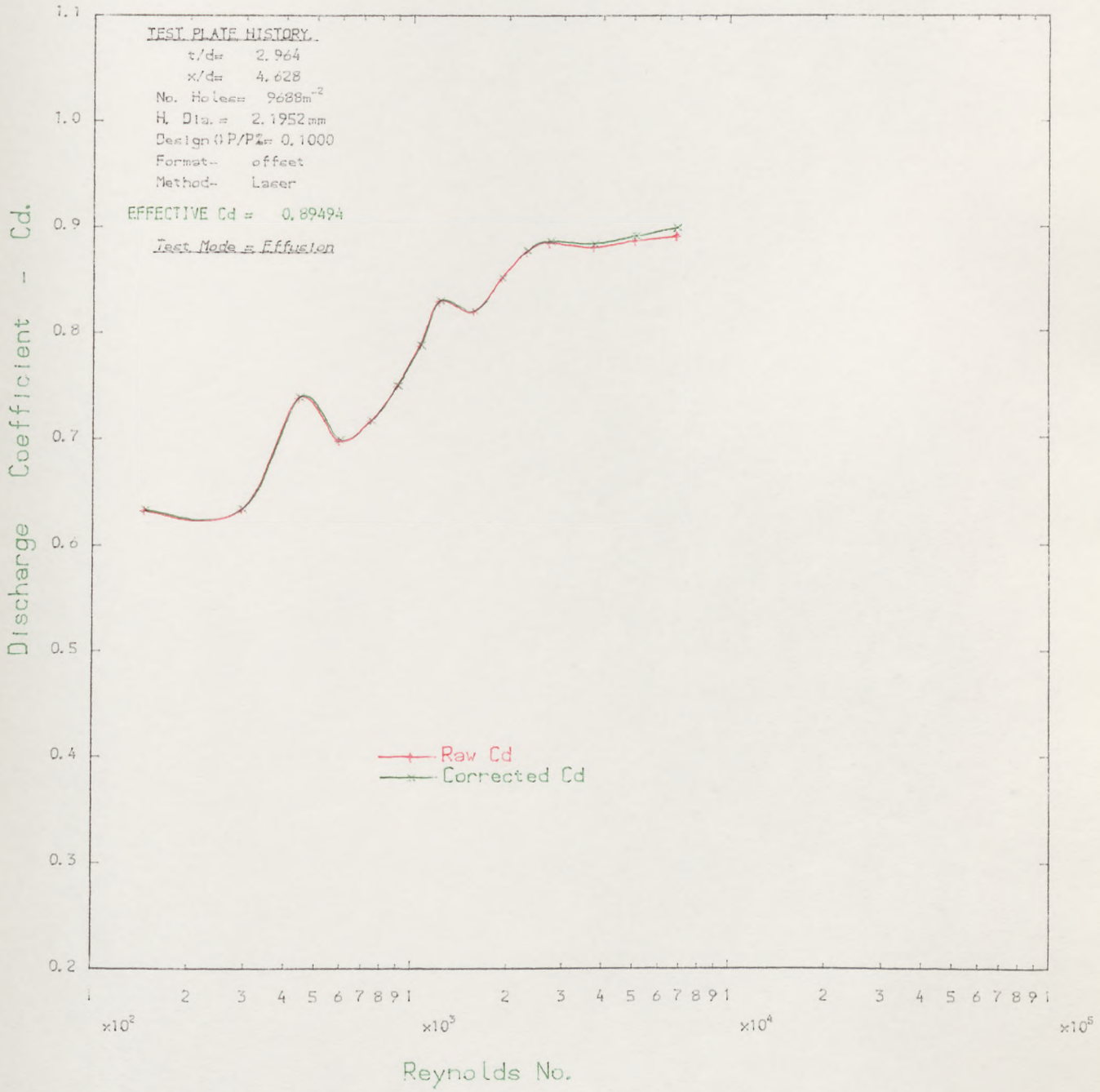

FIG. 3.5 : FREE-DISCHARGE Cd DEPENDENCE ON REYNOLDS NUMBER- (cold test).

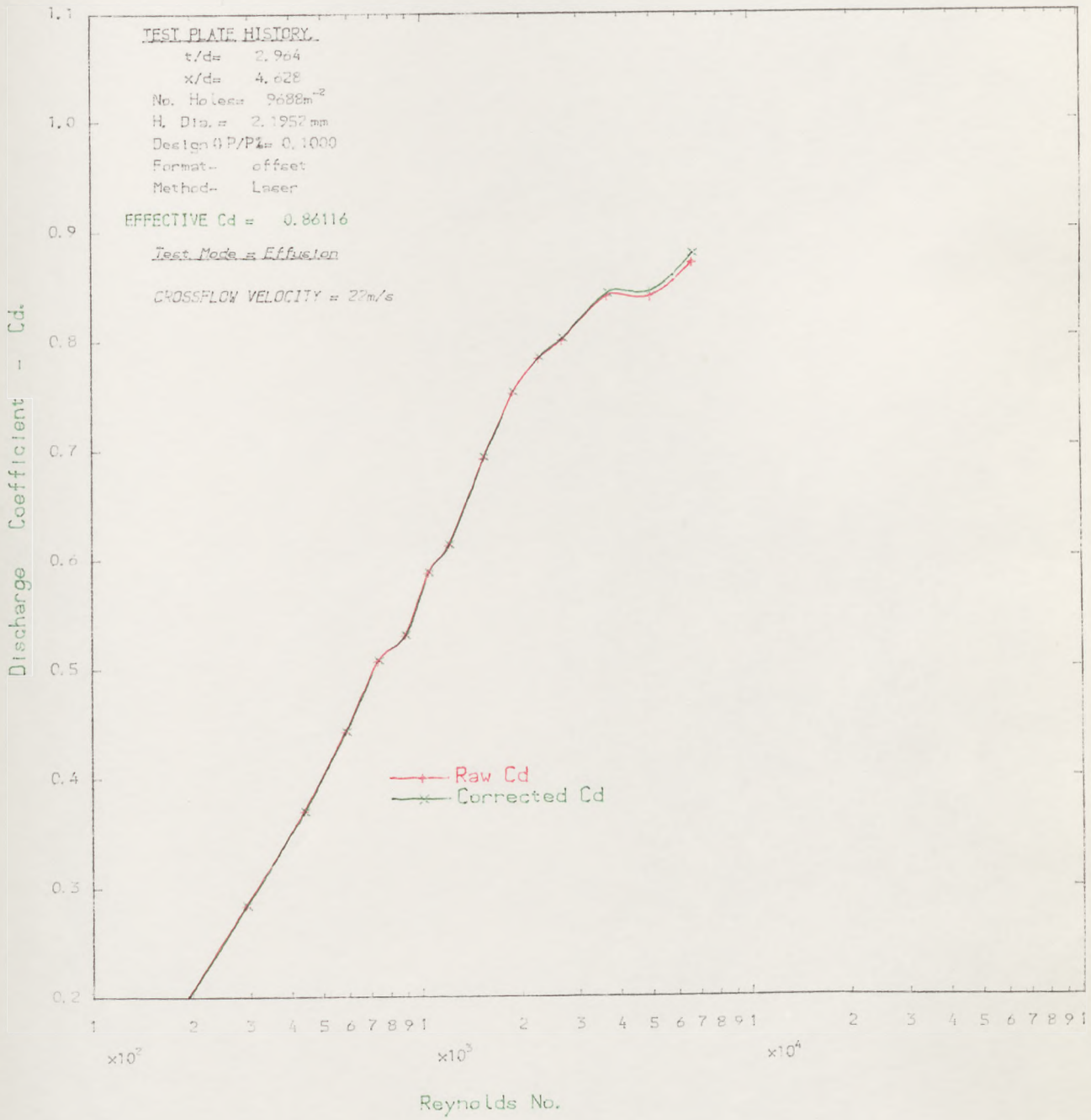

FIG.3.6 : CROSS-FLOW Cd DEPENDENCE ON REYNOLDS NUMBER- (cold test).

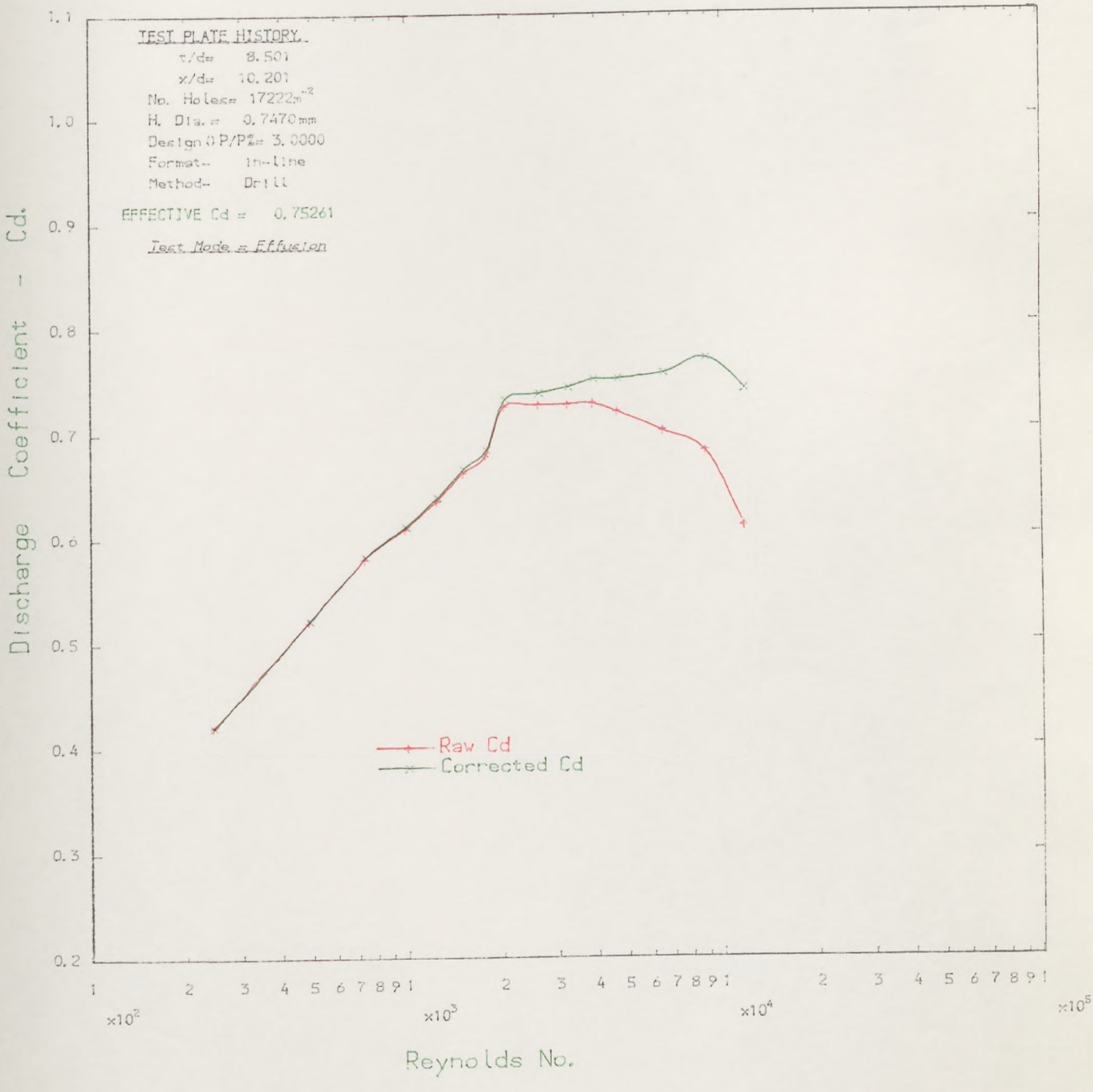

FIG. 3·7 : FREE-DISCHARGE Cd DEPENDENCE ON REYNOLDS NUMBER- (cold test).

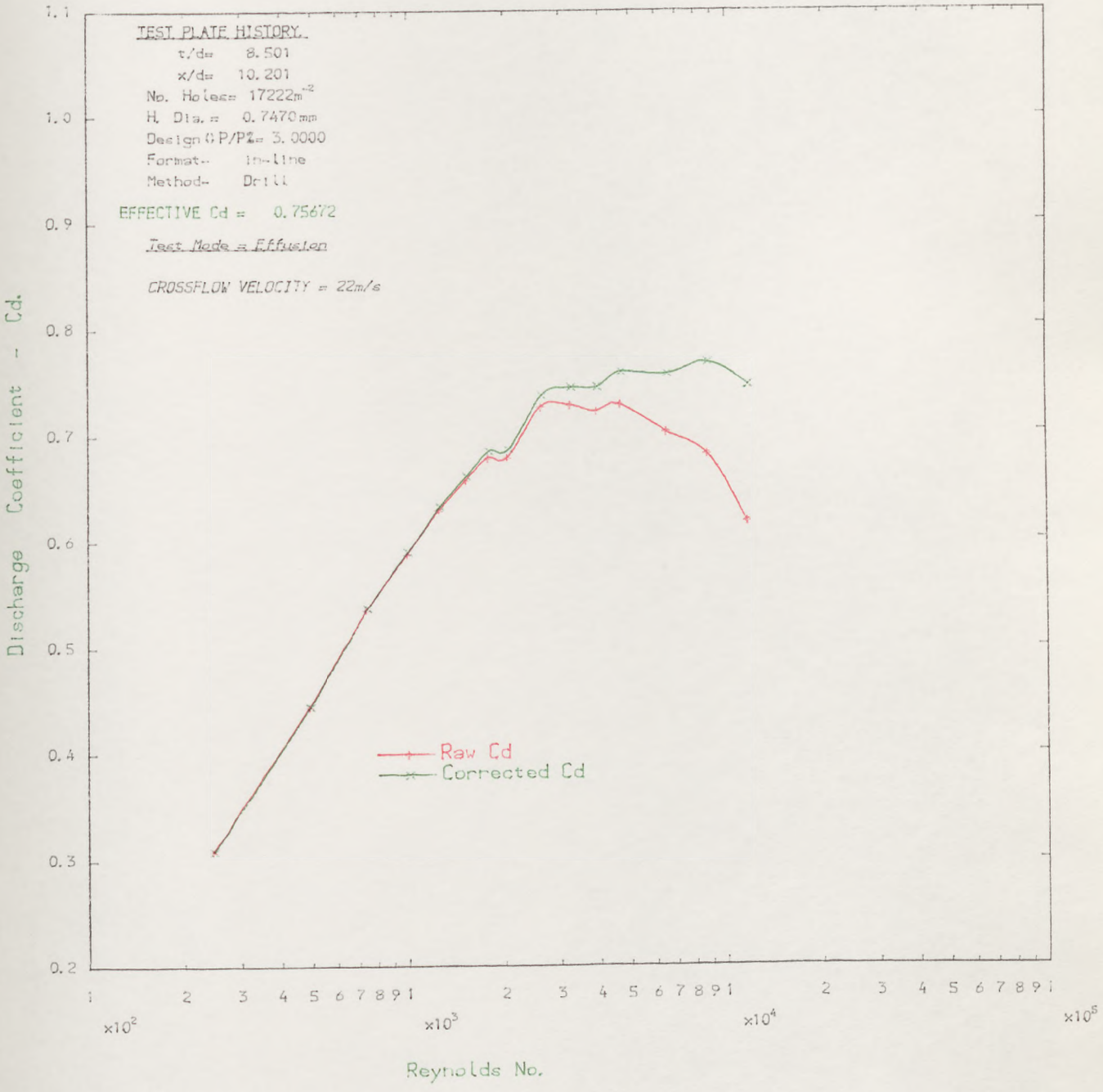

FIG.3·8 : CROSS-FLOW Cd DEPENDENCE ON REYNOLDS NUMBER-(cold test).

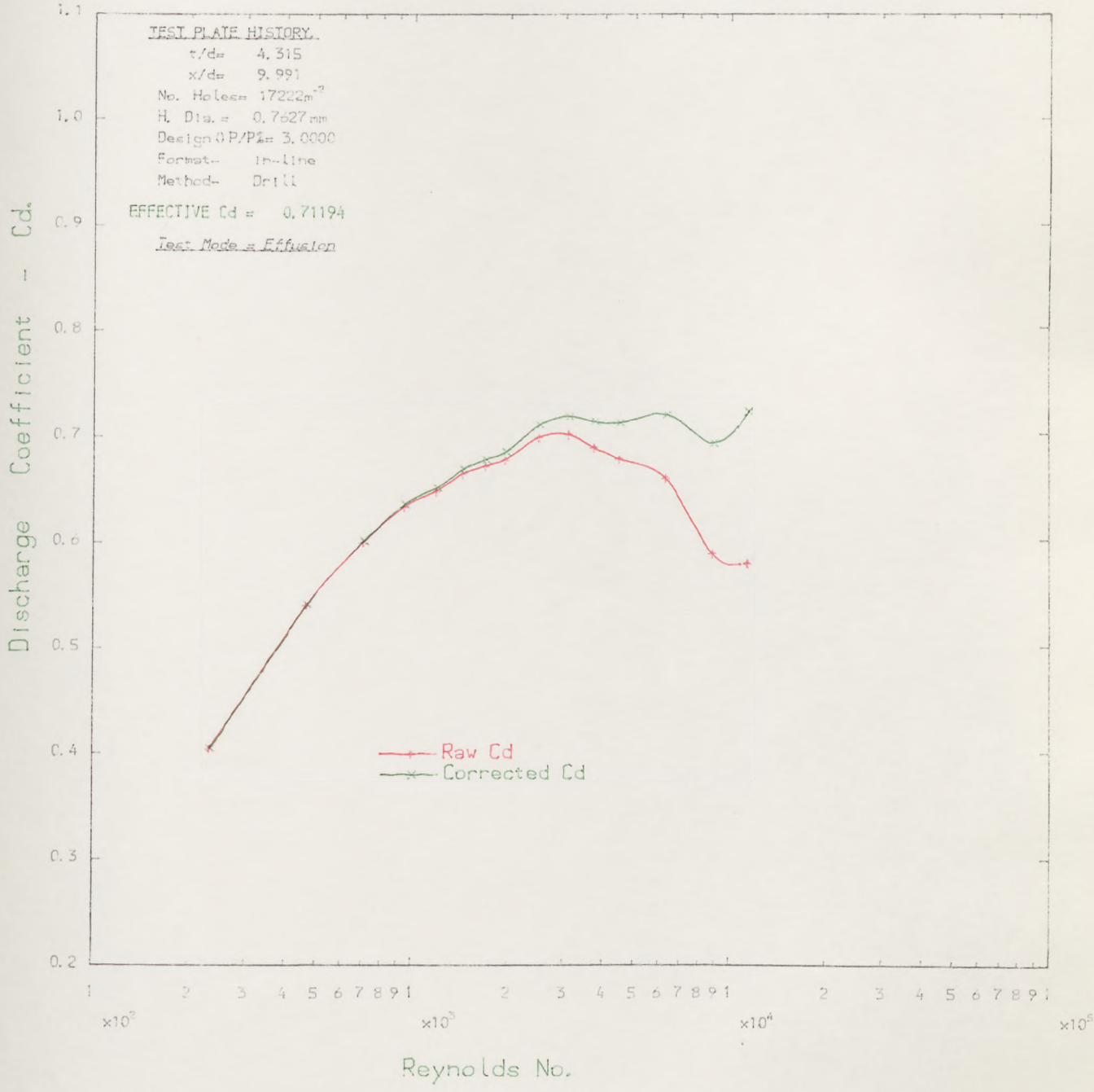

FIG.3·9. FREE-DISCHARGE Cd DEPENDENCE ON REYNOLDS NUMBER (cold test).

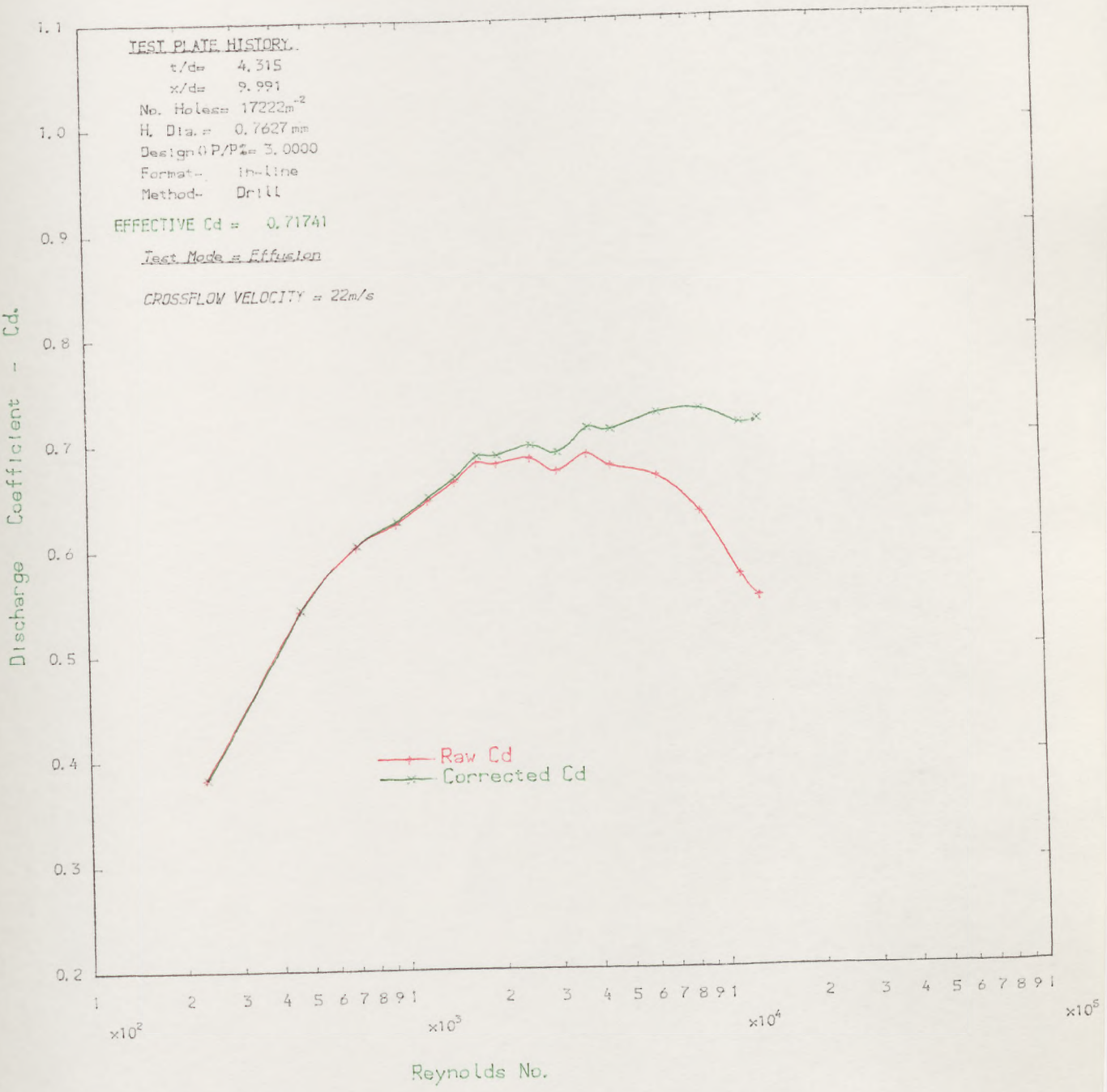

FIG. 3.10: CROSS-FLOW Cd DEPENDENCE ON REYNOLDS NUMBER- (cold test).

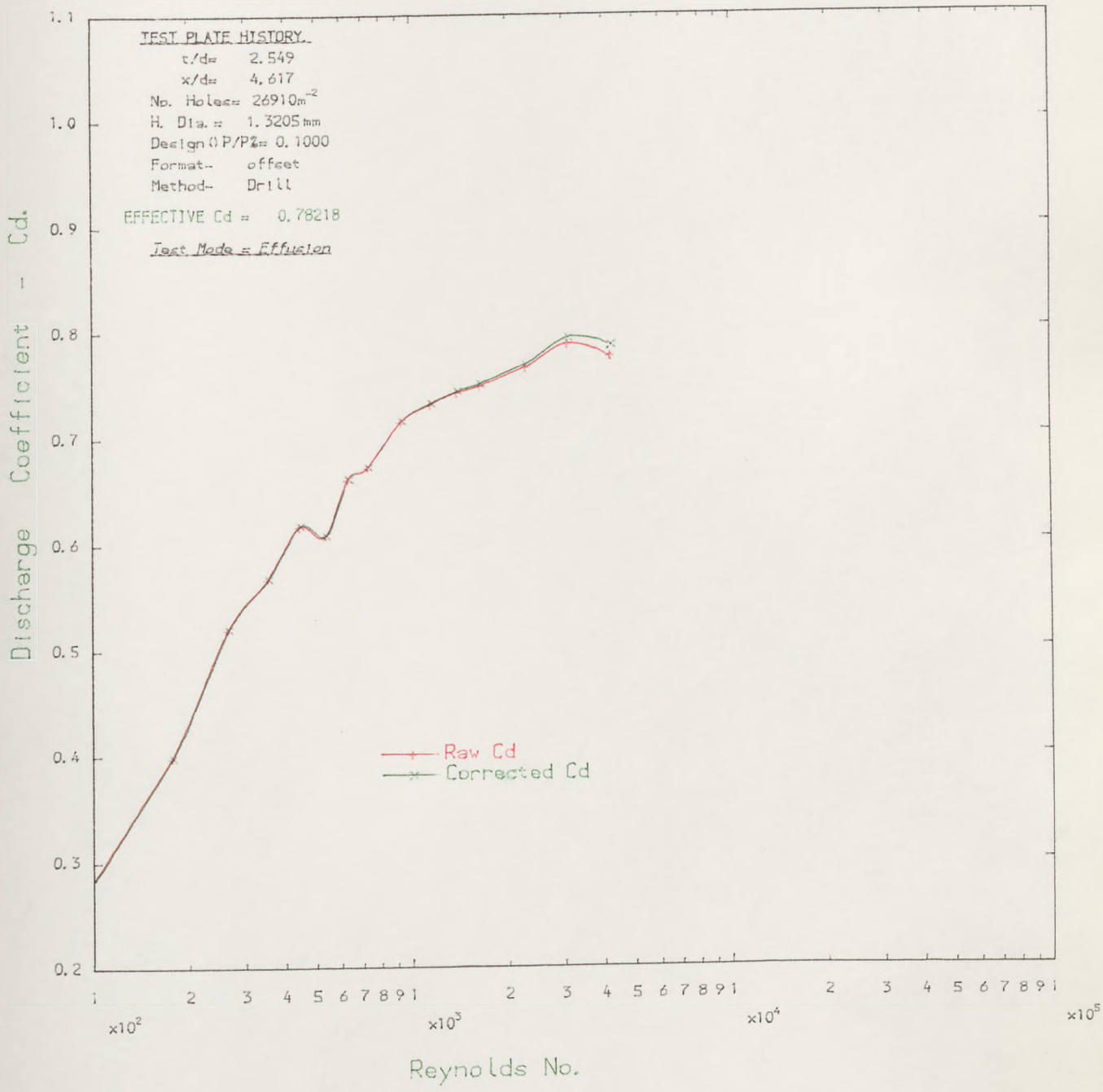

FIG.3.11 : FREE-DISCHARGE Cd DEPENDENCE ON REYNOLDS NUMBER- (cold test).

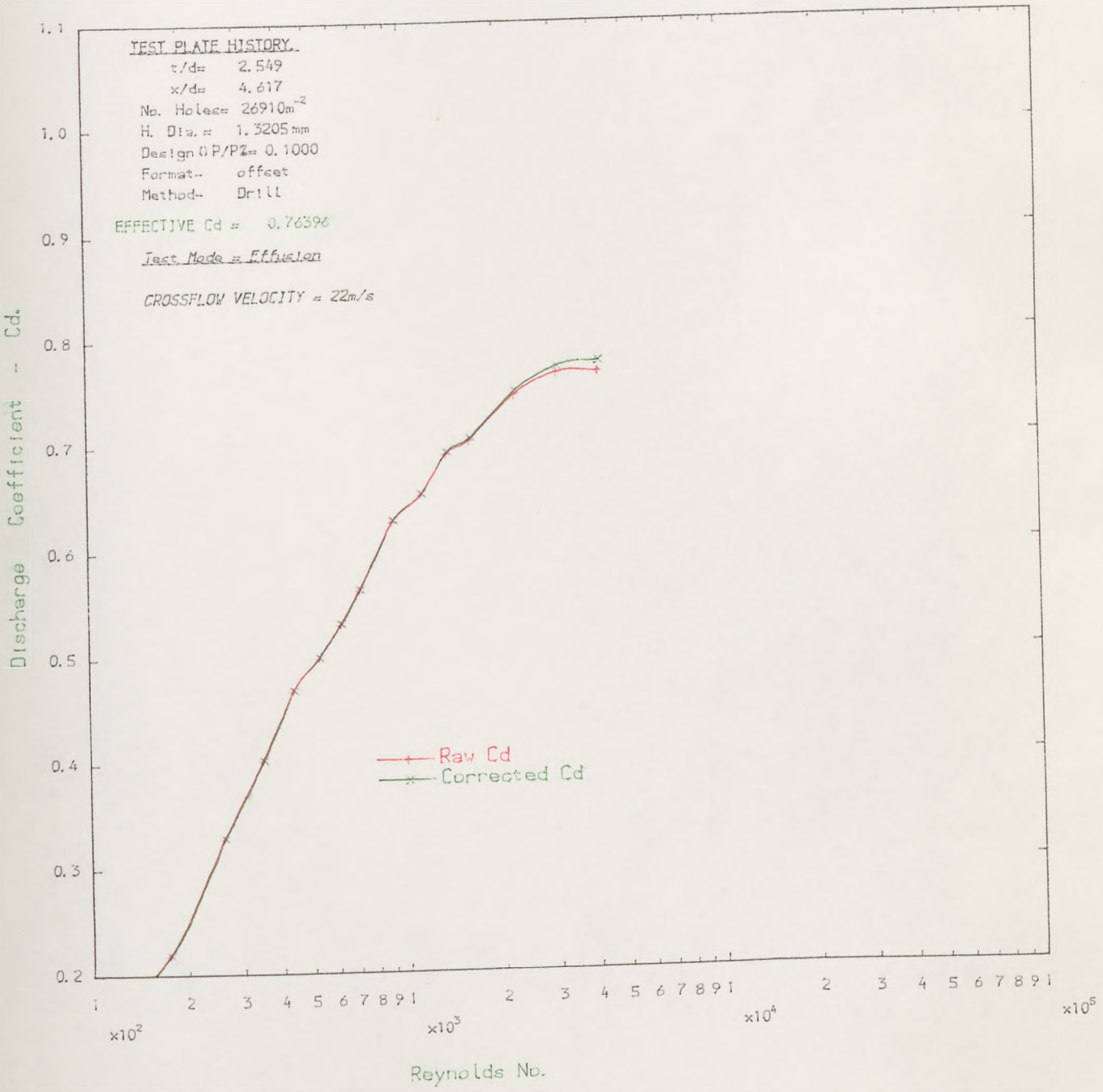

FIG. 3.12: CROSS-FLOW Cd DEPENDENCE ON REYNOLDS NUMBER - (cold test).

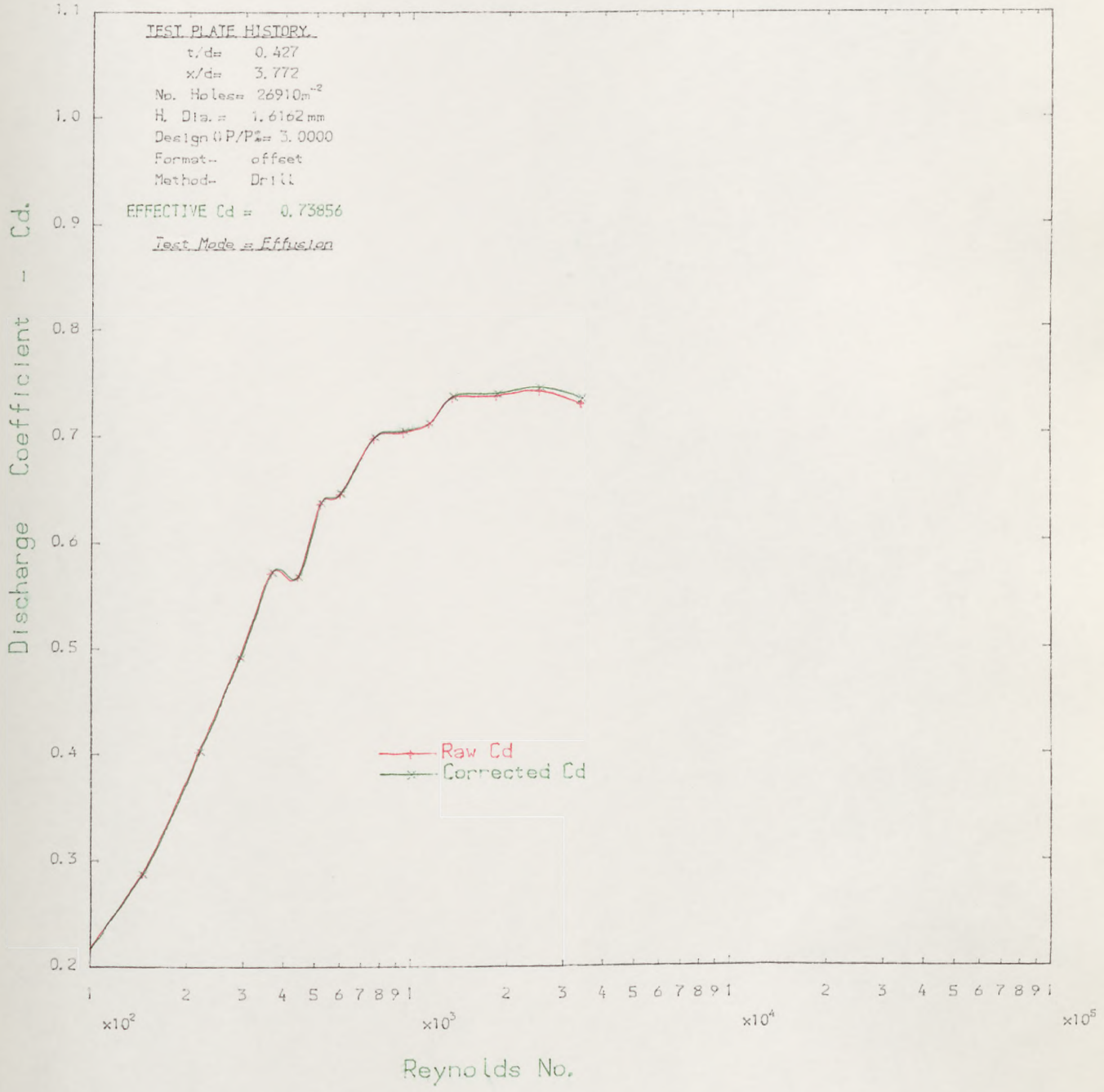

FIG.3.13. FREE-DISCHARGE Cd DEPENDENCE ON REYNOLDS NUMBER- (cold test).

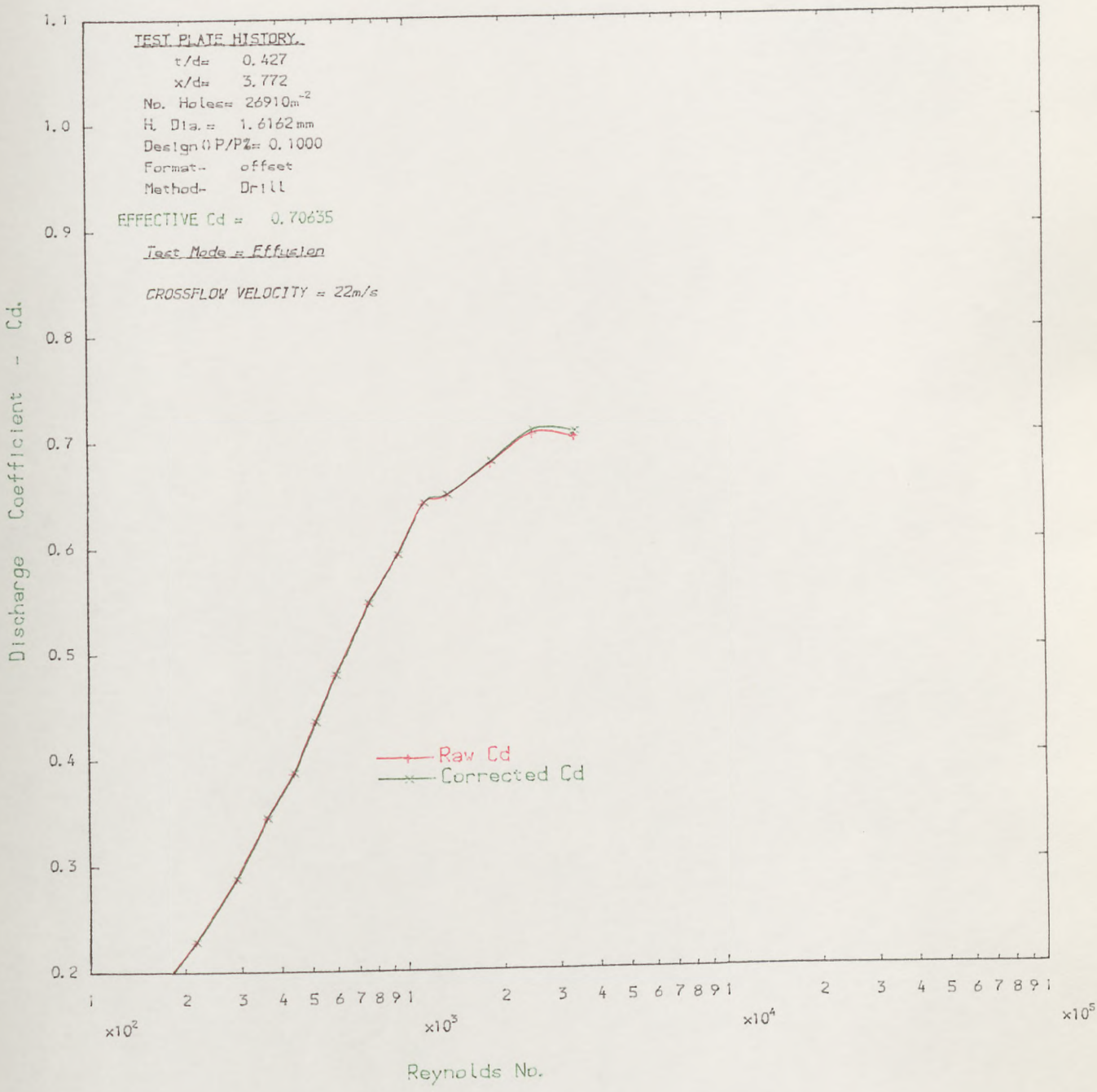

FIG.3.14: CROSS-FLOW Cd DEPENDENCE ON REYNOLDS NUMBER-(cold test).

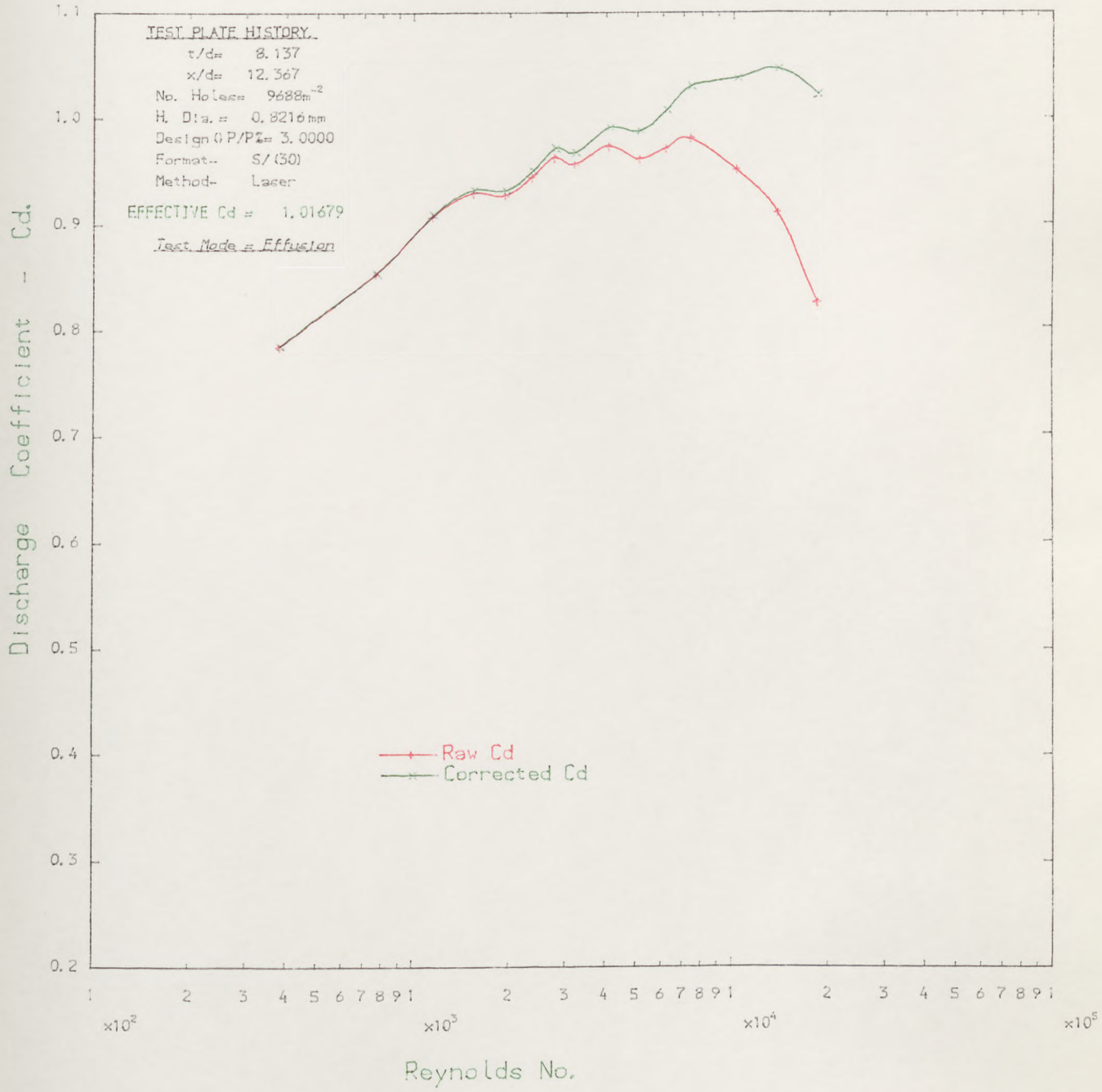

FIG. 3.15: FREE-DISCHARGE Cd DEPENDENCE ON REYNOLDS NUMBER (cold test).

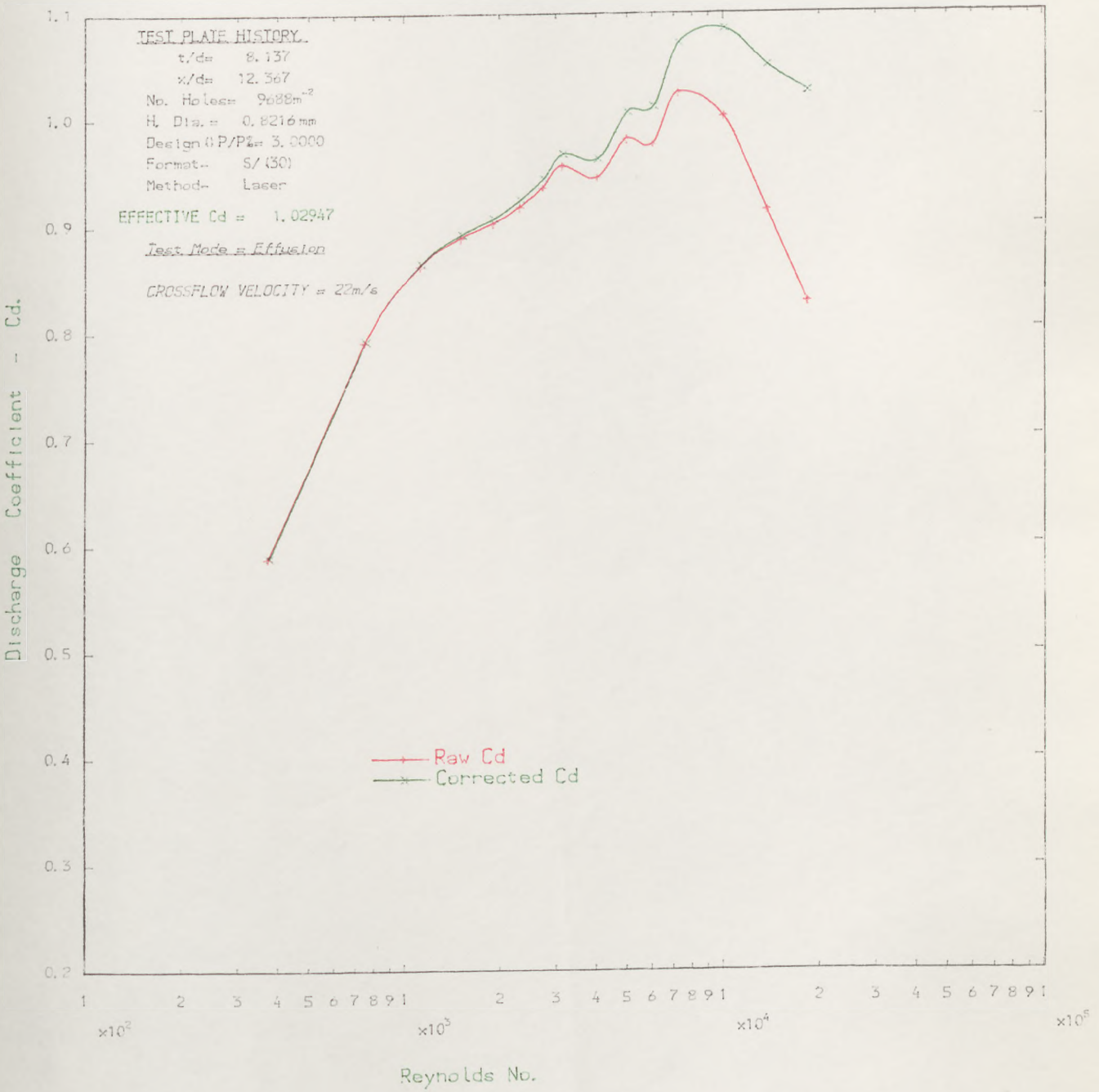

FIG. 3.16: CROSS-FLOW Cd DEPENDENCE ON REYNOLDS NUMBER- (cold test).

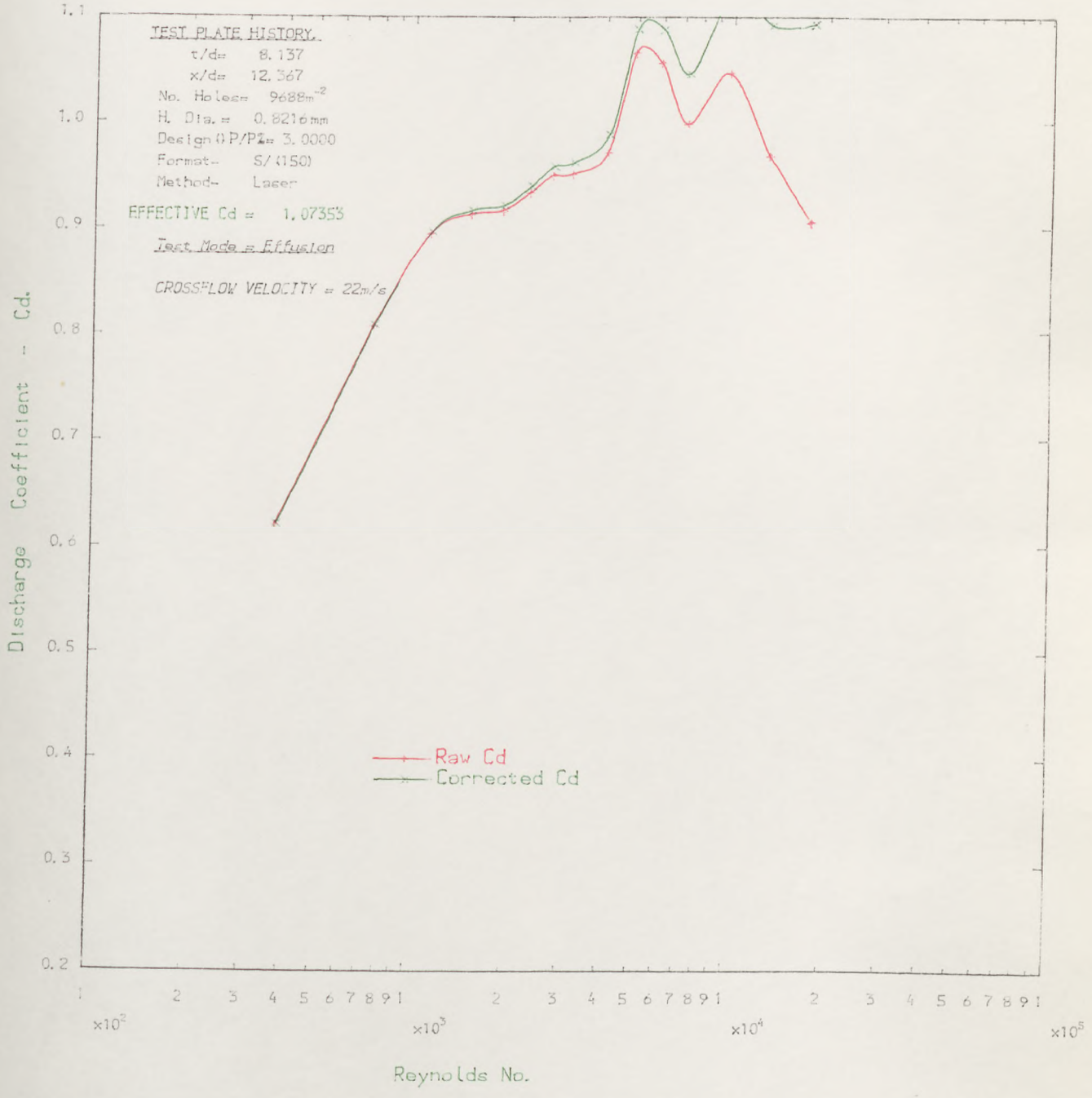

FIG.3.17: CROSS-FLOW Cd DEPENDENCE ON REYNOLDS NUMBER- (cold test).

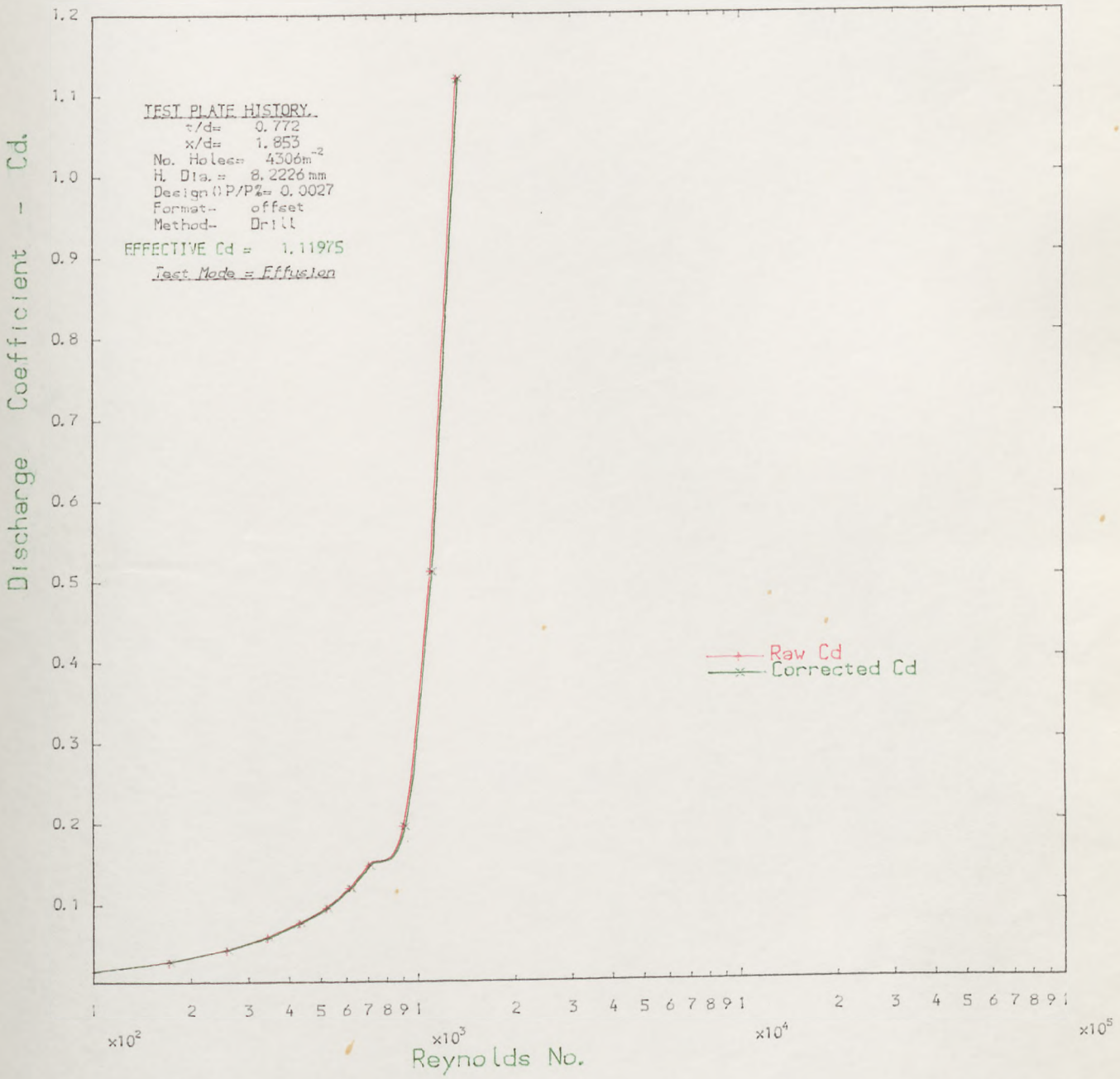

FIG.3.18: FREE-DISCHARGE Cd DEPENDENCE ON REYNOLDS NUMBER- (cold test).

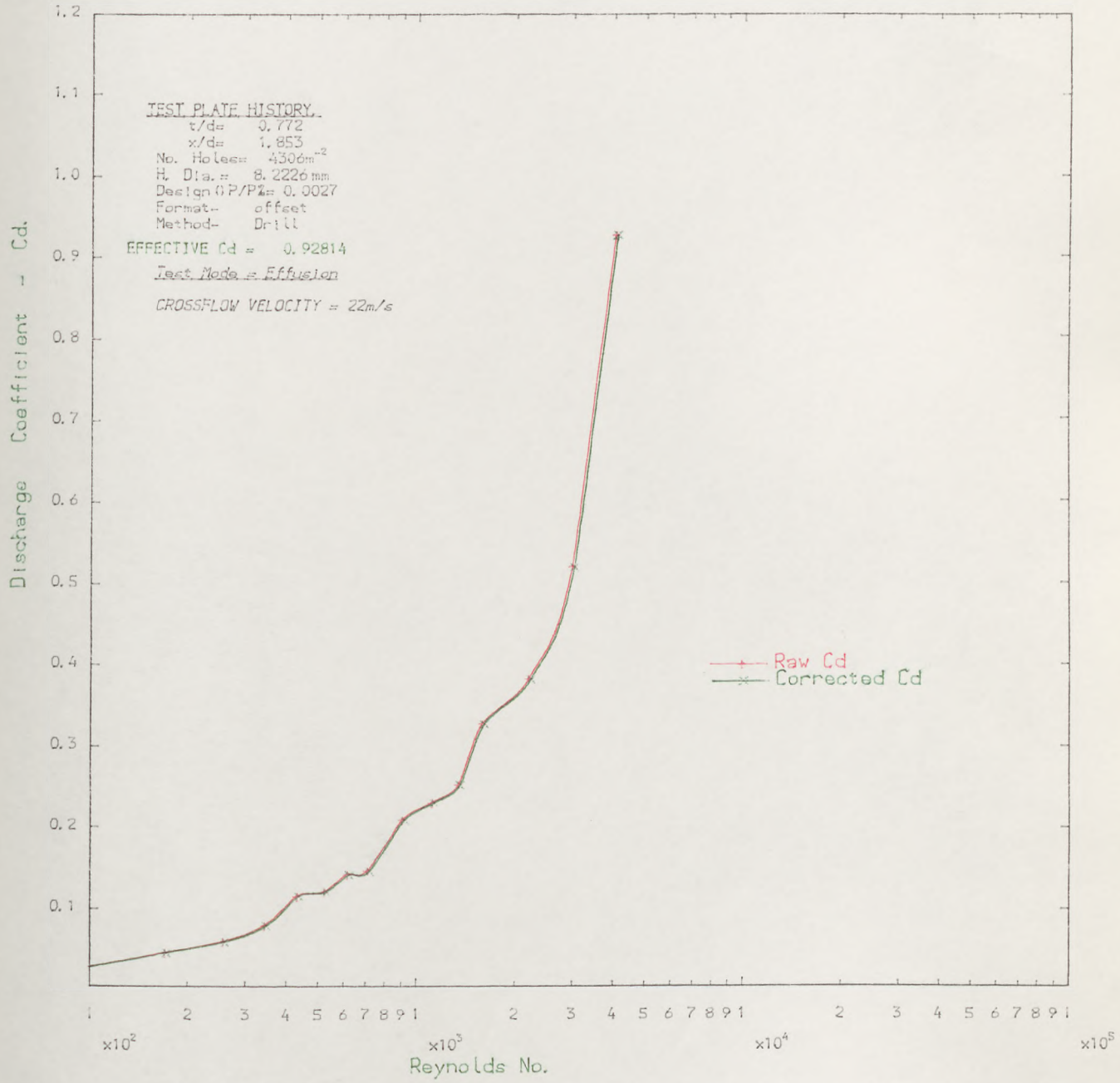

FIG.3.19. CROSS-FLOW Cd DEPENDENCE ON REYNOLDS NUMBER-(cold test).

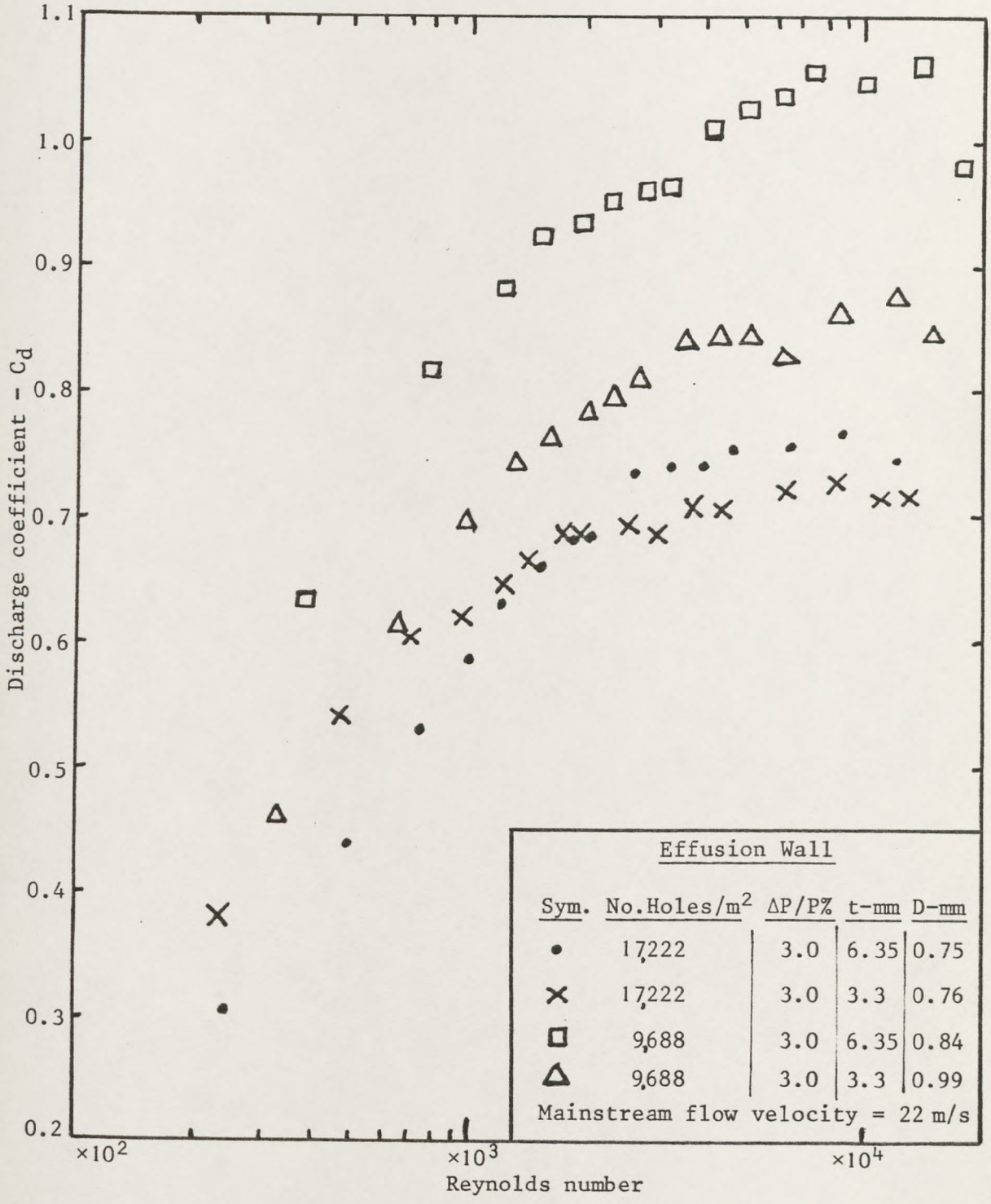

Fig. 3.20: C_d dependence on wall holes' number

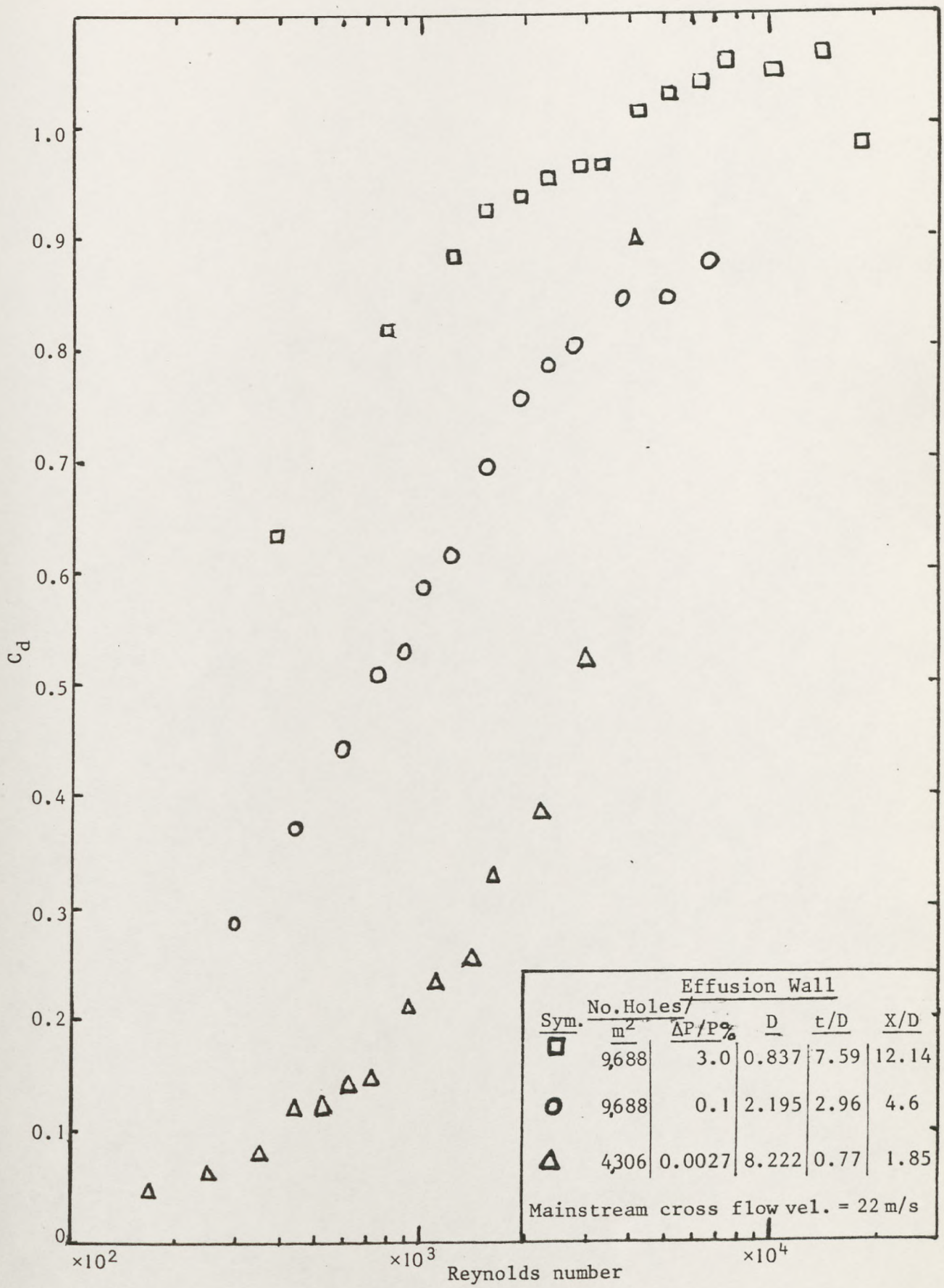

Fig. 3.21: Effect of holes' diameter on C_d

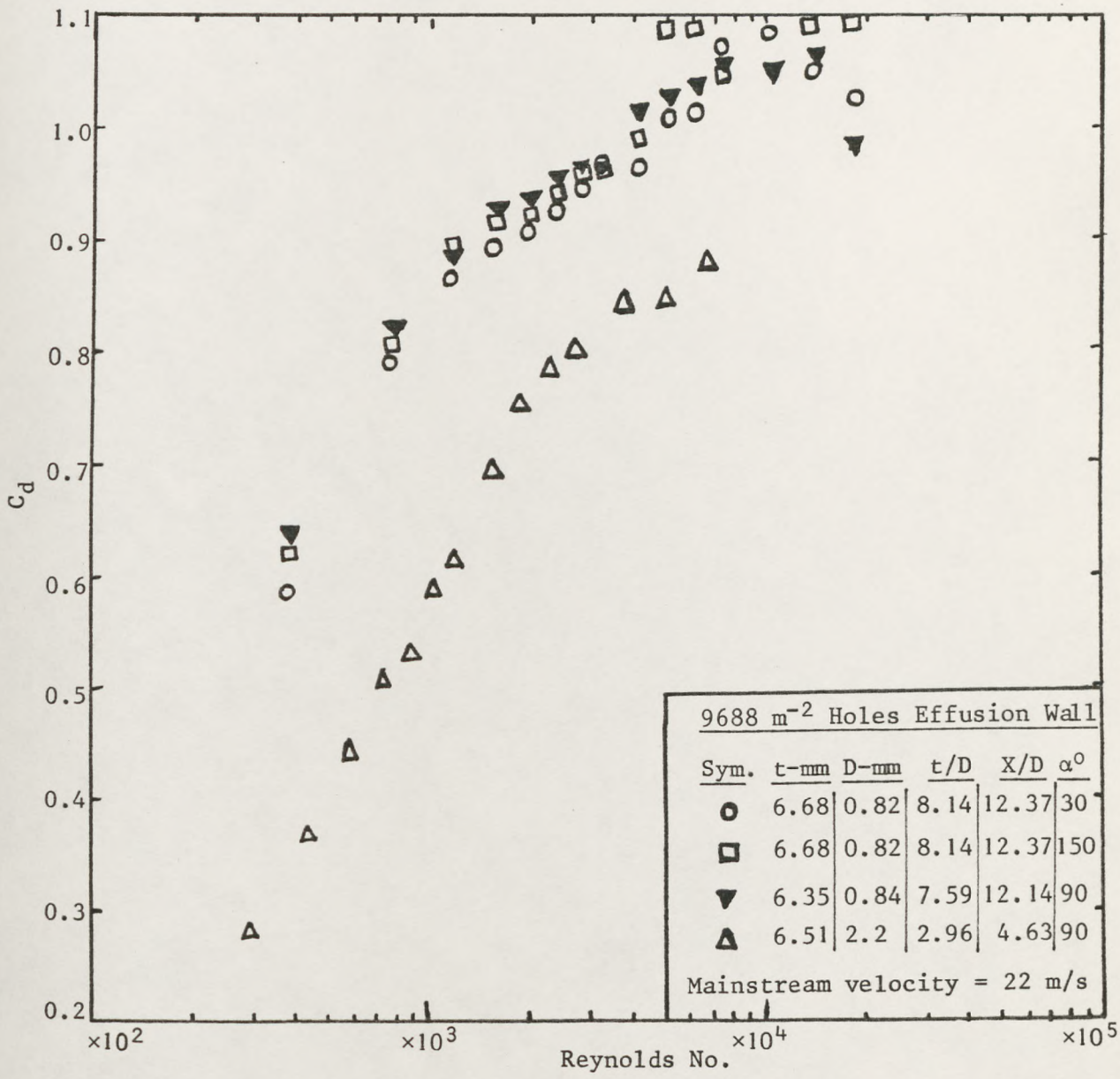

Fig. 3.22: Effect of holes inclination to cross-stream on C_d

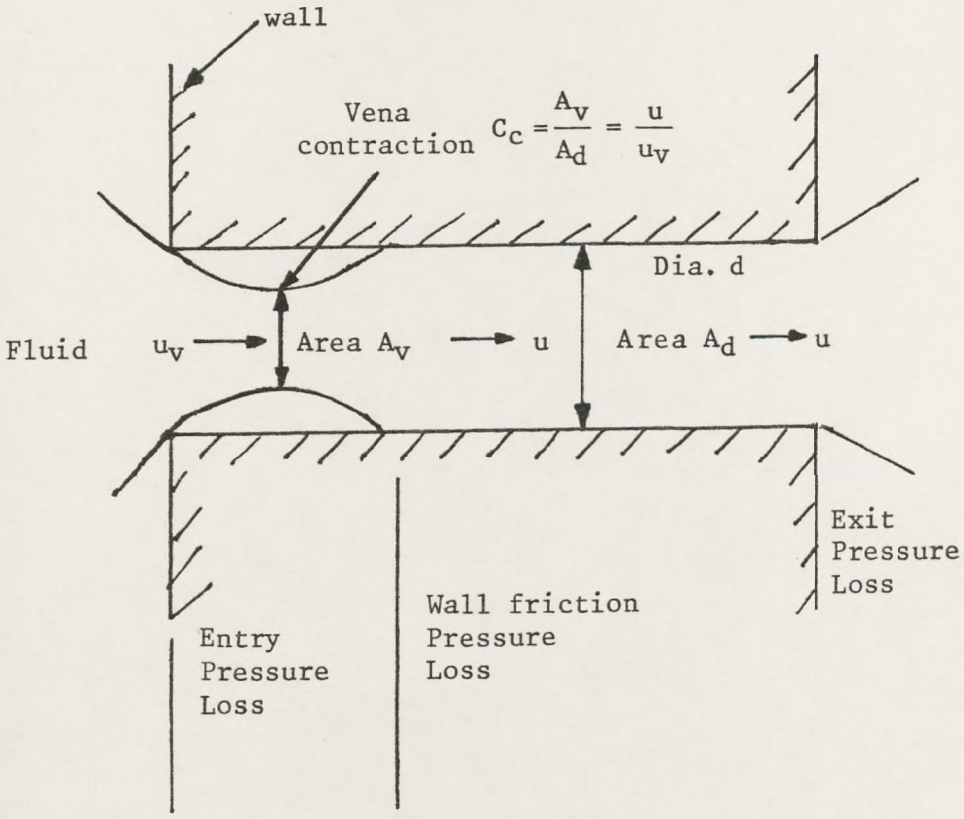

Fig. 3.23: Wall's hole aerodynamics

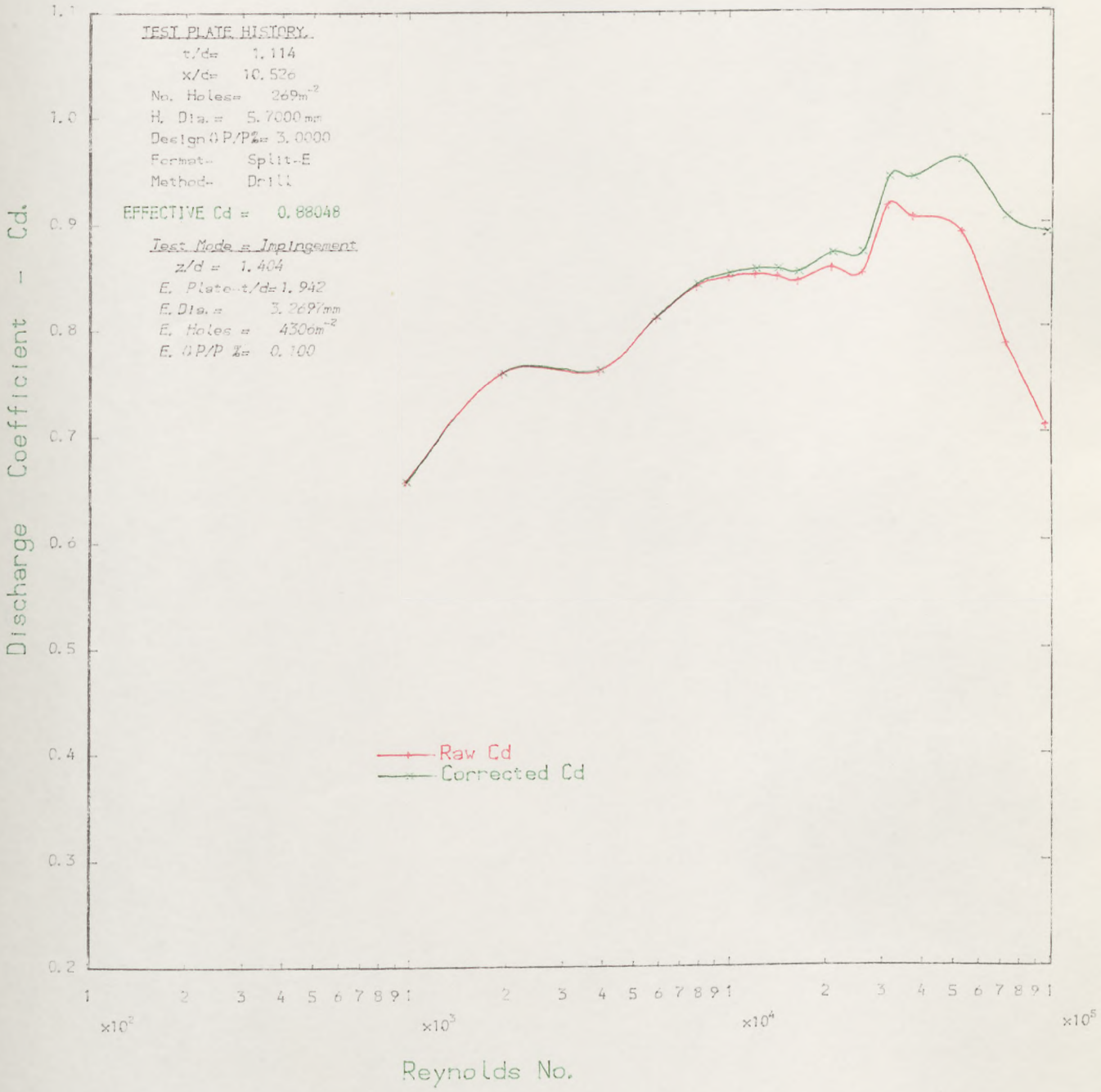

FIG.3.24. FREE-DISCHARGE Cd DEPENDENCE ON REYNOLDS NUMBER- (cold test).

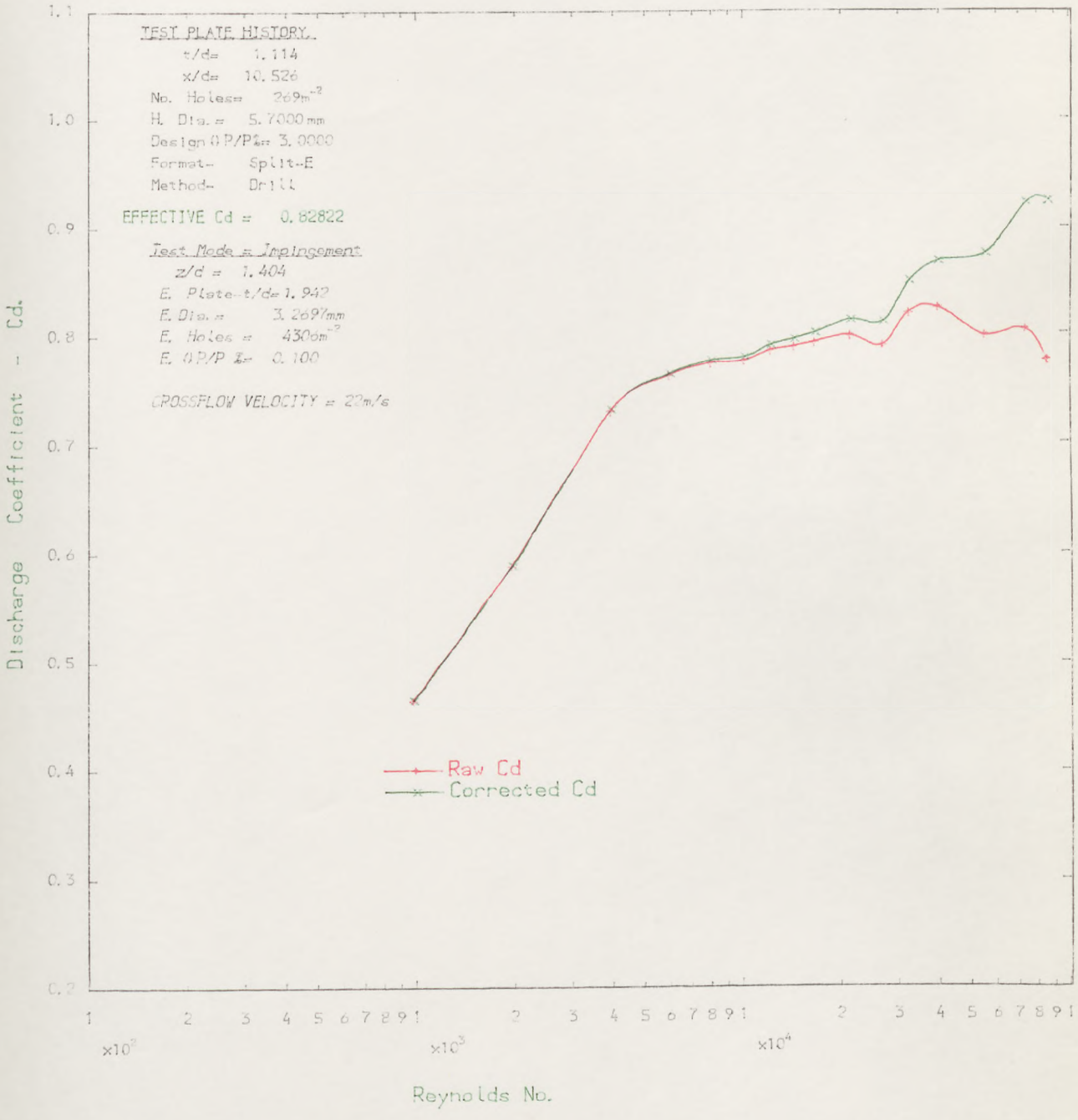

FIG.3.25. CROSS-FLOW Cd DEPENDENCE ON REYNOLDS NUMBER- (cold test).

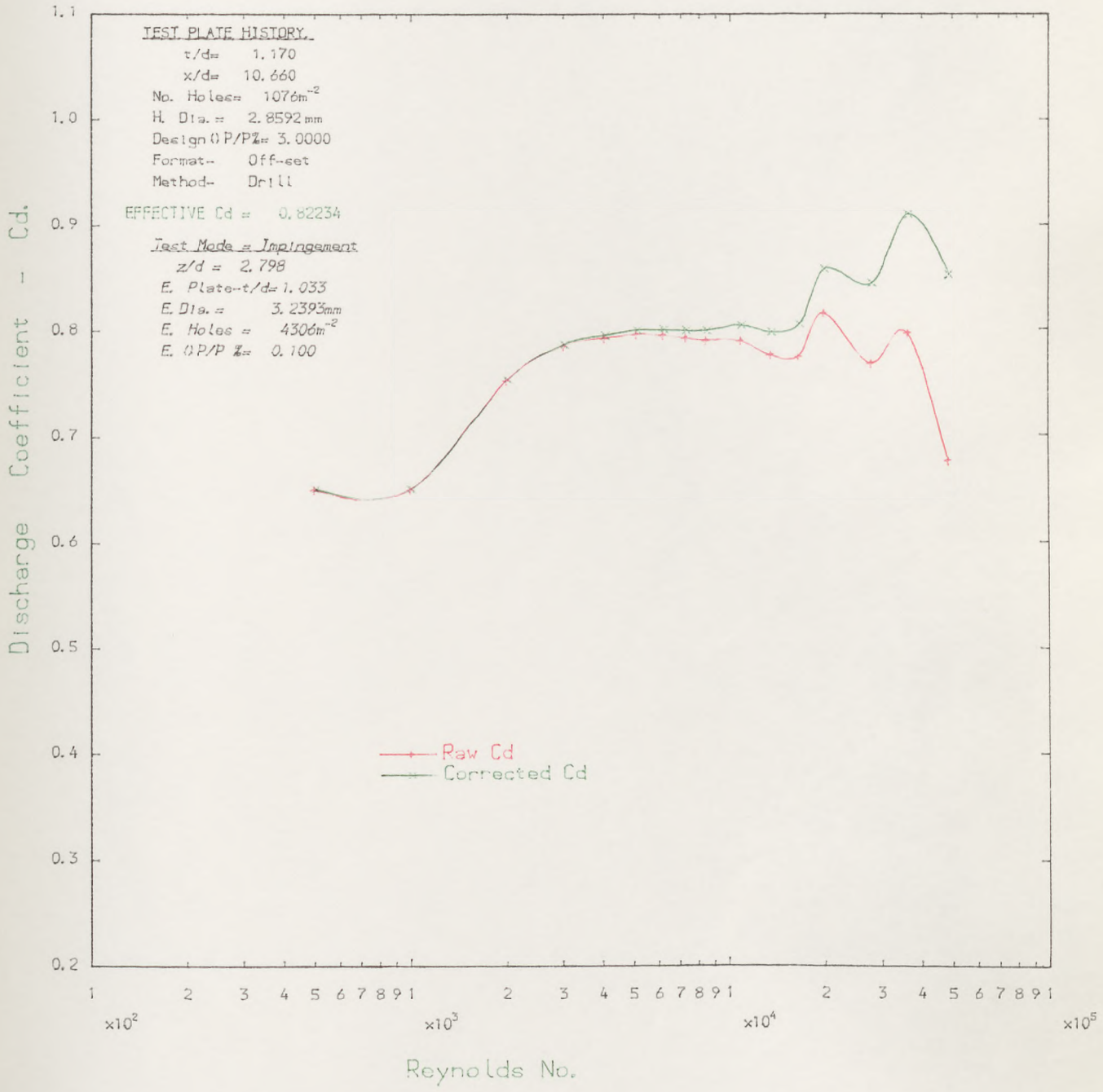

FIG.3.26. FREE-DISCHARGE Cd DEPENDENCE ON REYNOLDS NUMBER- (cold test).

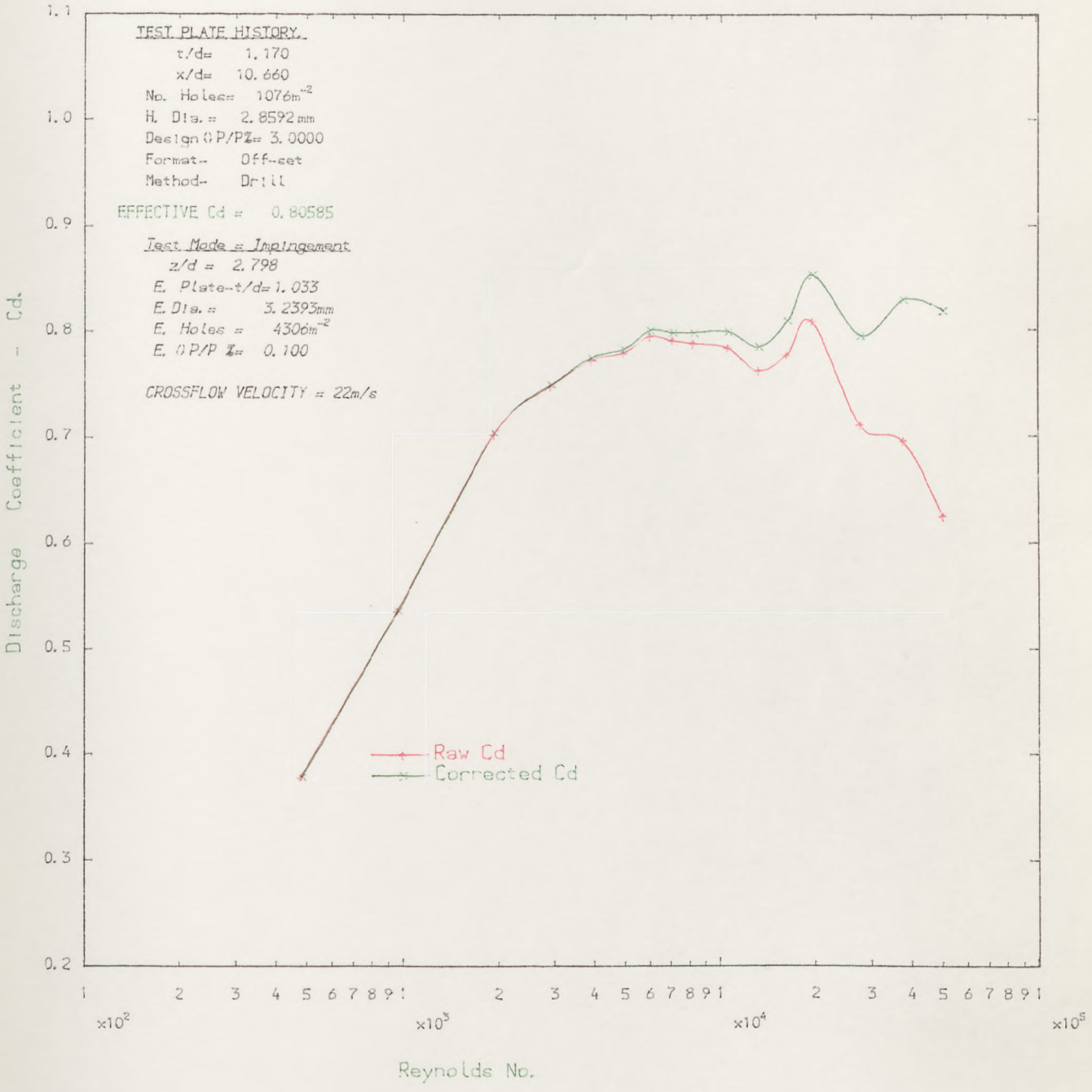

FIG.3.27. CROSS-FLOW Cd DEPENDENCE ON REYNOLDS NUMBER-(cold test).

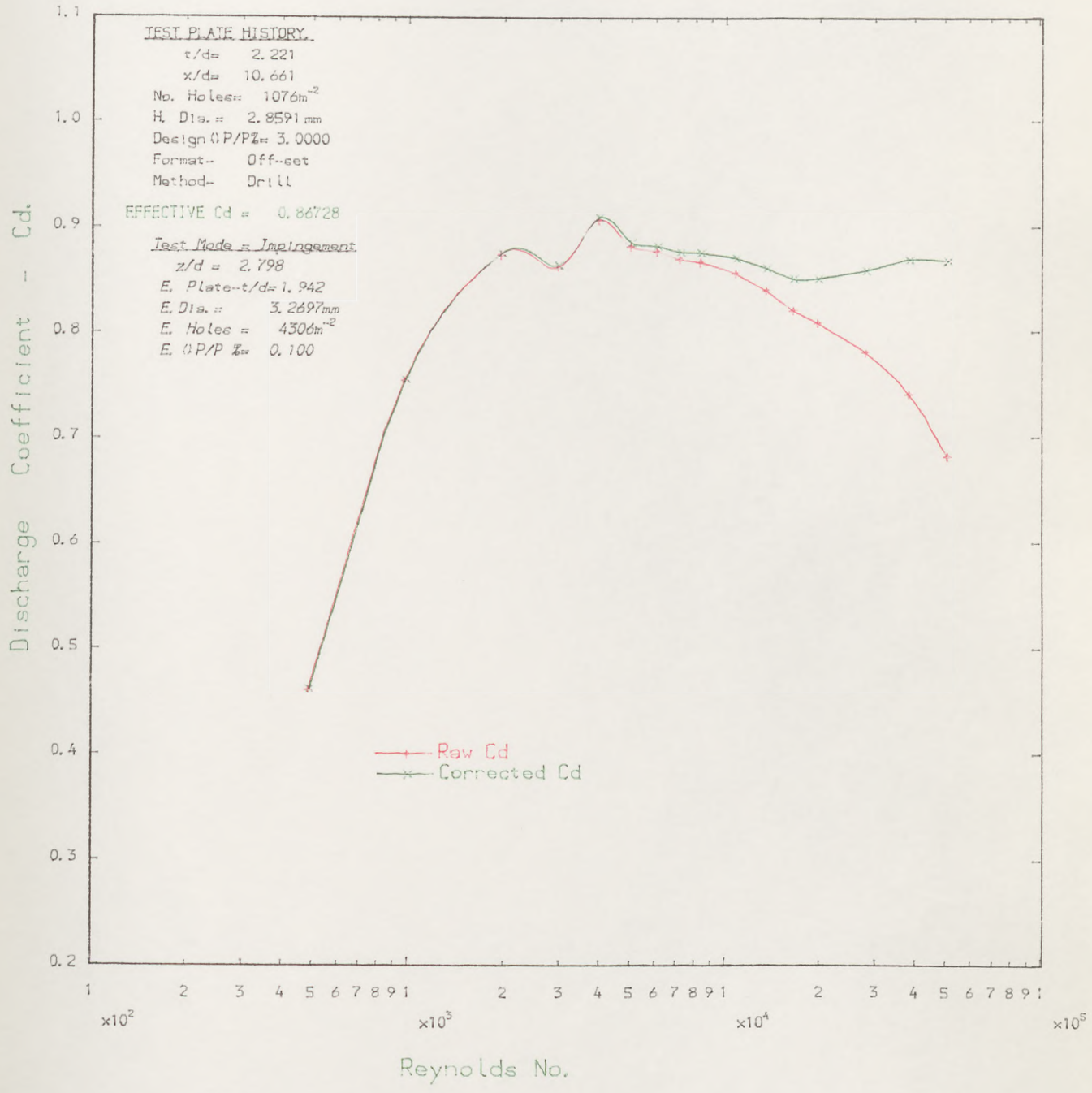

FIG.3.28: FREE-DISCHARGE Cd DEPENDENCE ON REYNOLDS NUMBER.-(cold test).

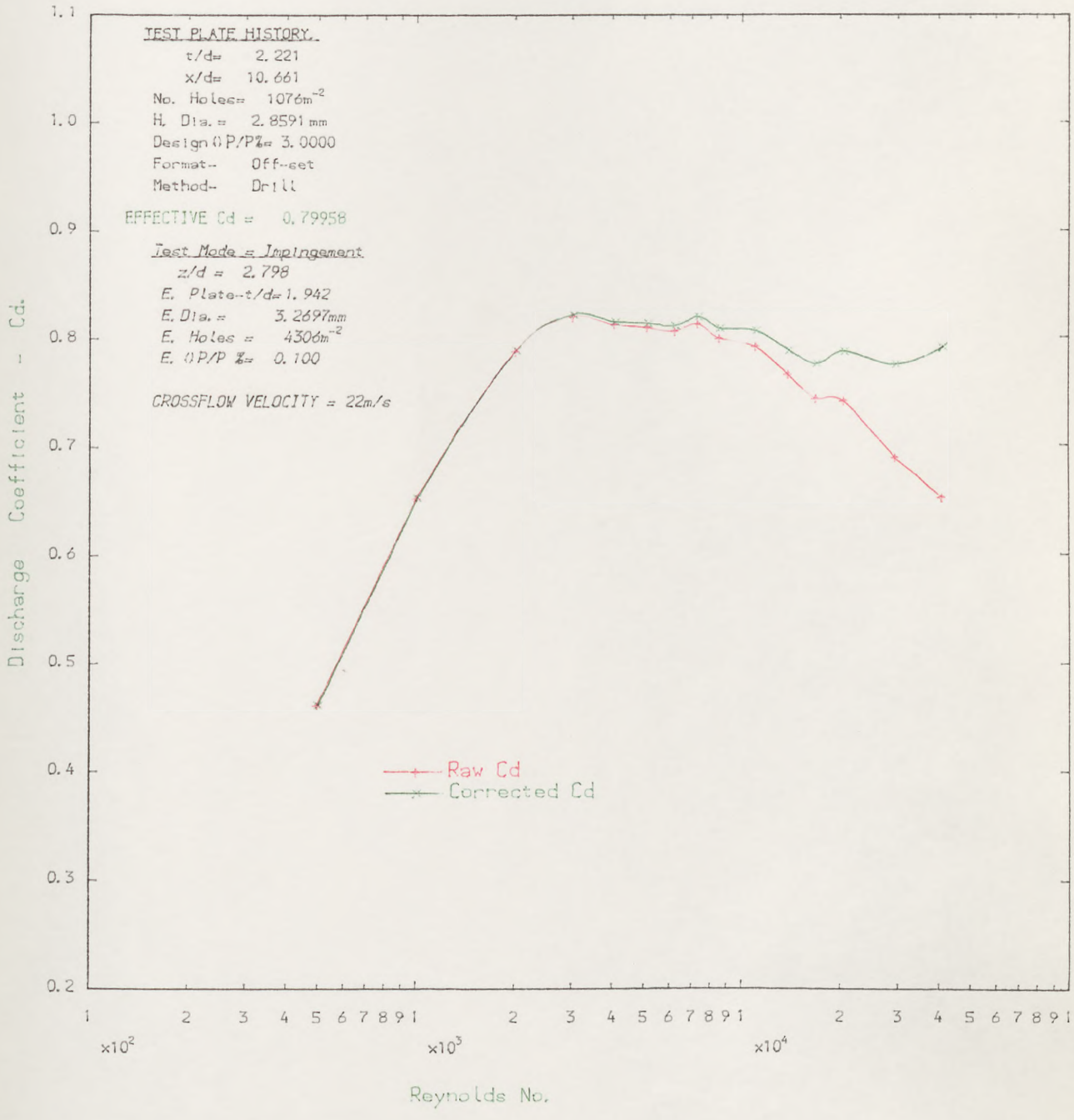

FIG.3.29. CROSS-FLOW Cd DEPENDENCE ON REYNOLDS NUMBER- (cold test).

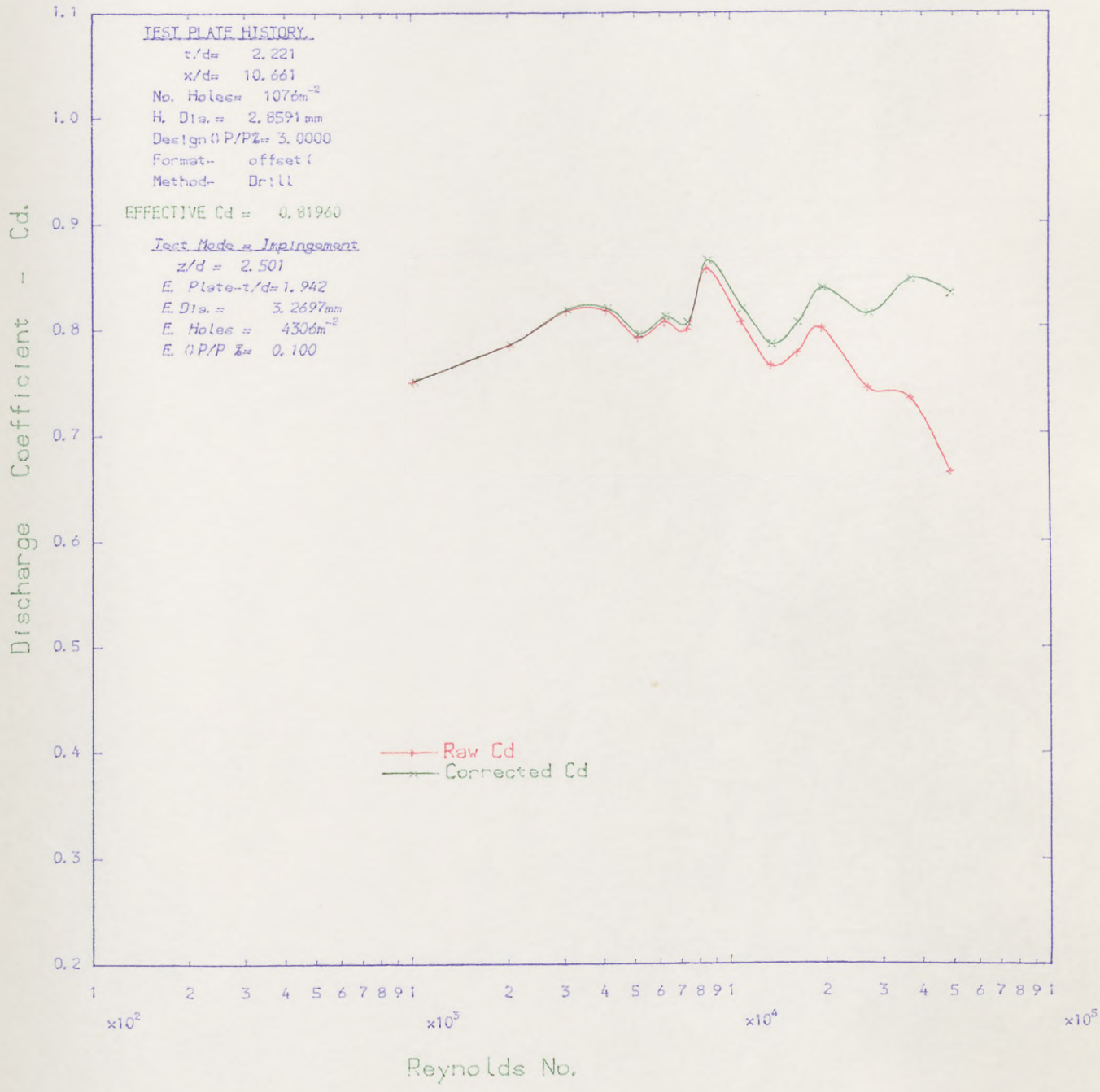

FIG.3.30: FREE-DISCHARGE Cd DEPENDENCE ON REYNOLDS NUMBER--(cold test).

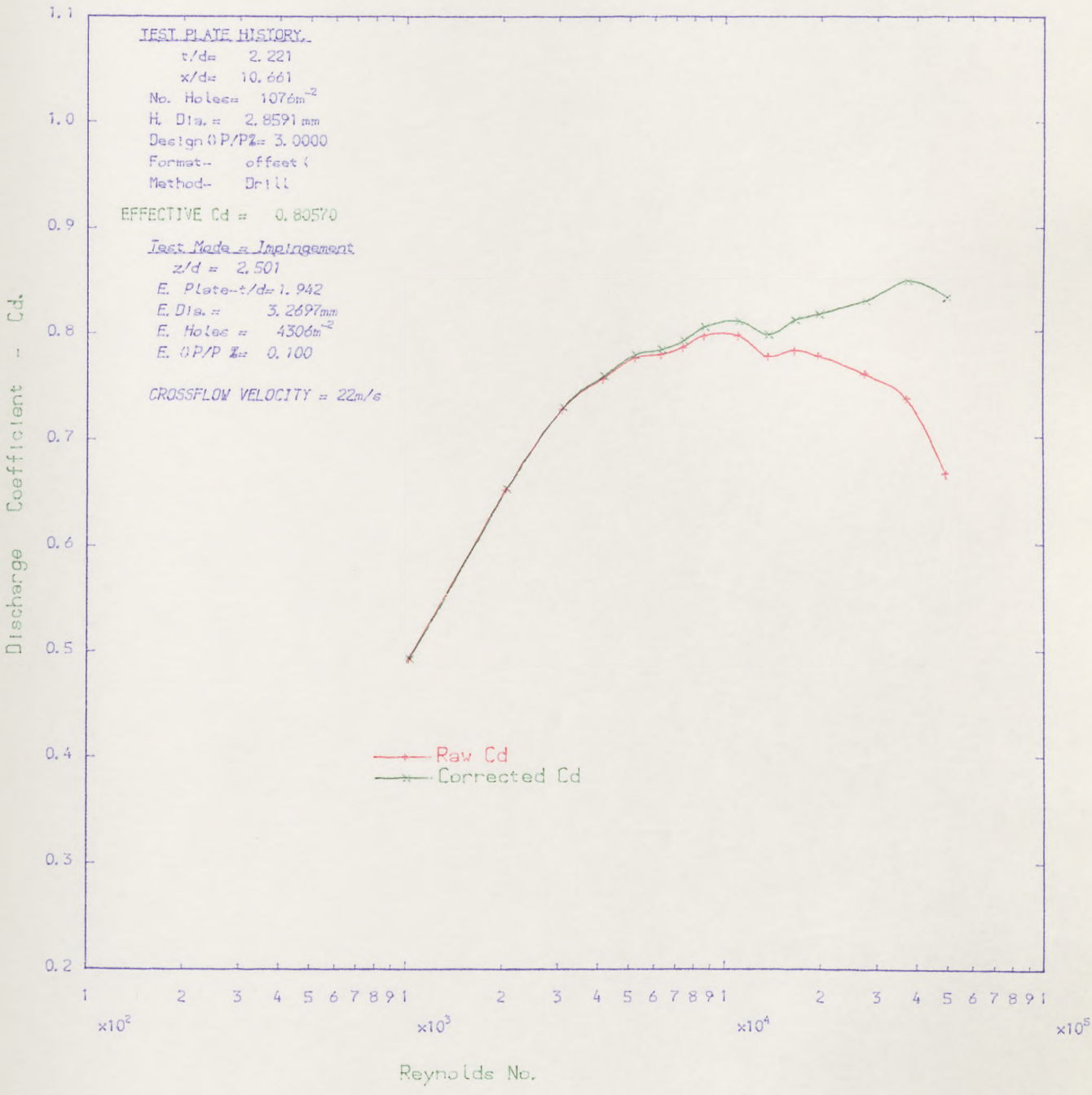

FIG.3.31. CROSS-FLOW Cd DEPENDENCE ON REYNOLDS NUMBER-(cold test).

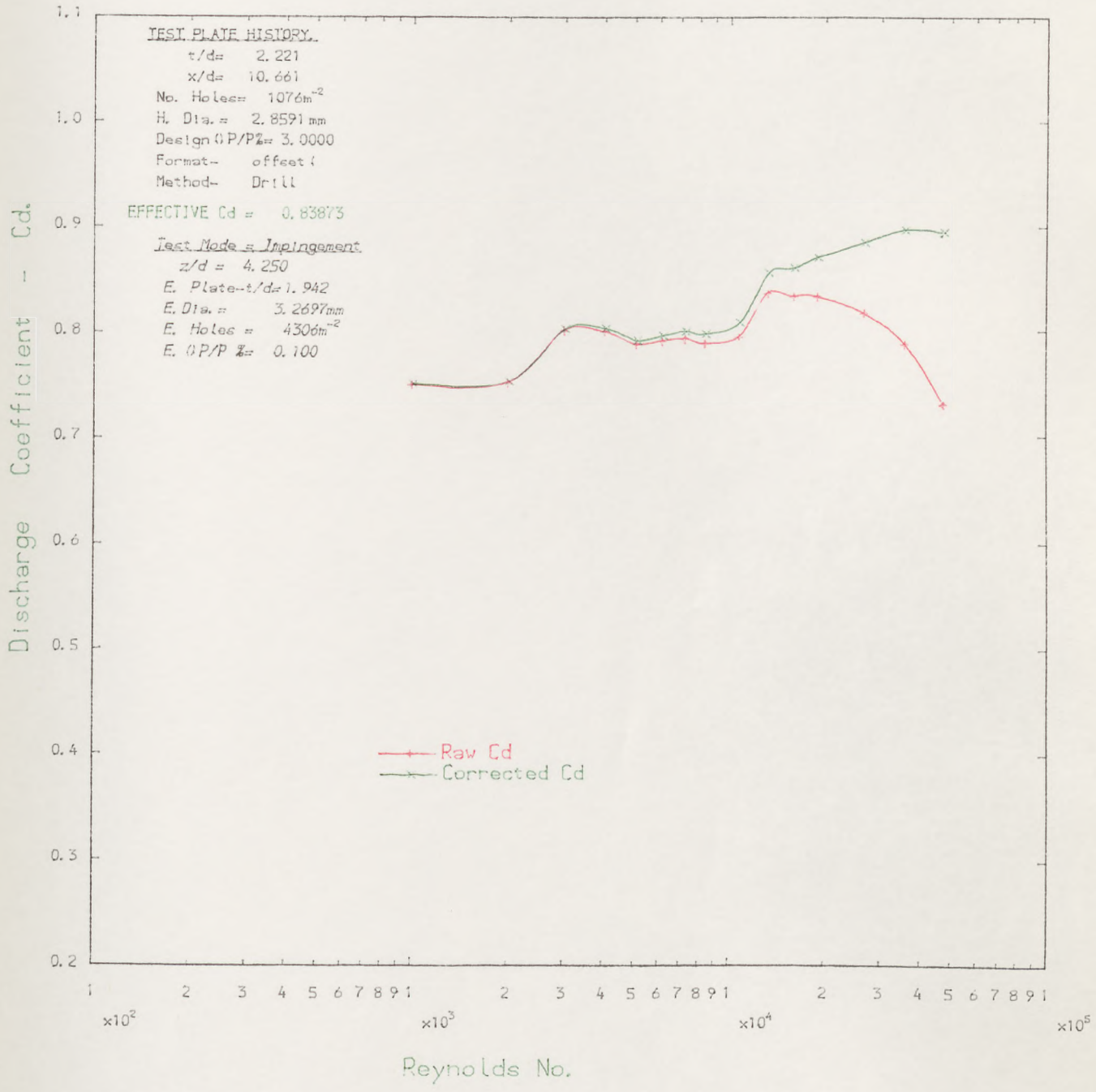

FIG.3.32: FREE-DISCHARGE Cd DEPENDENCE ON REYNOLDS NUMBER-(cold test).

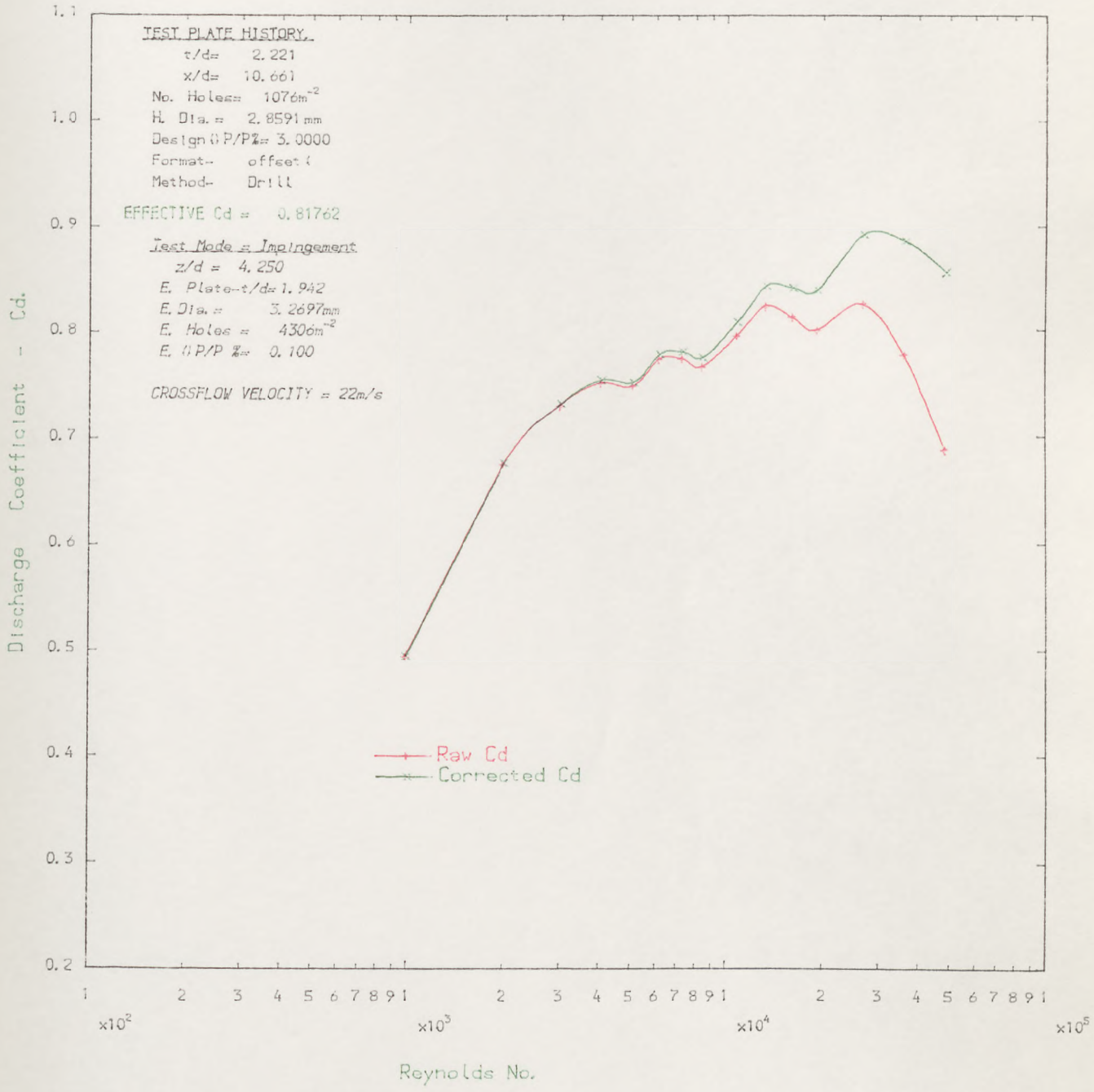

FIG.3.33. CROSS-FLOW Cd DEPENDENCE ON REYNOLDS NUMBER- (cold test).

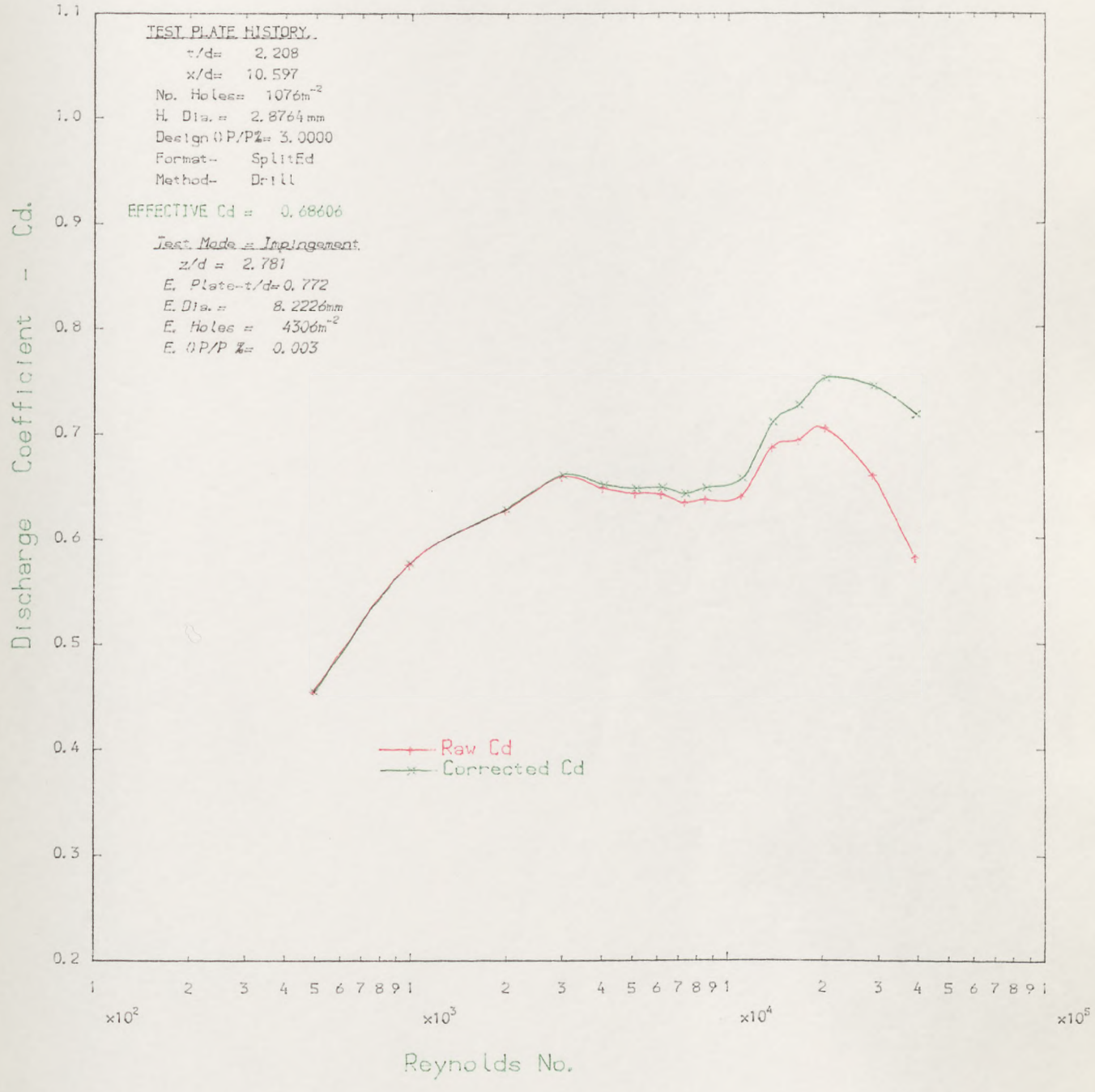

FIG.3.34. FREE-DISCHARGE Cd DEPENDENCE ON REYNOLDS NUMBER- (cold test).

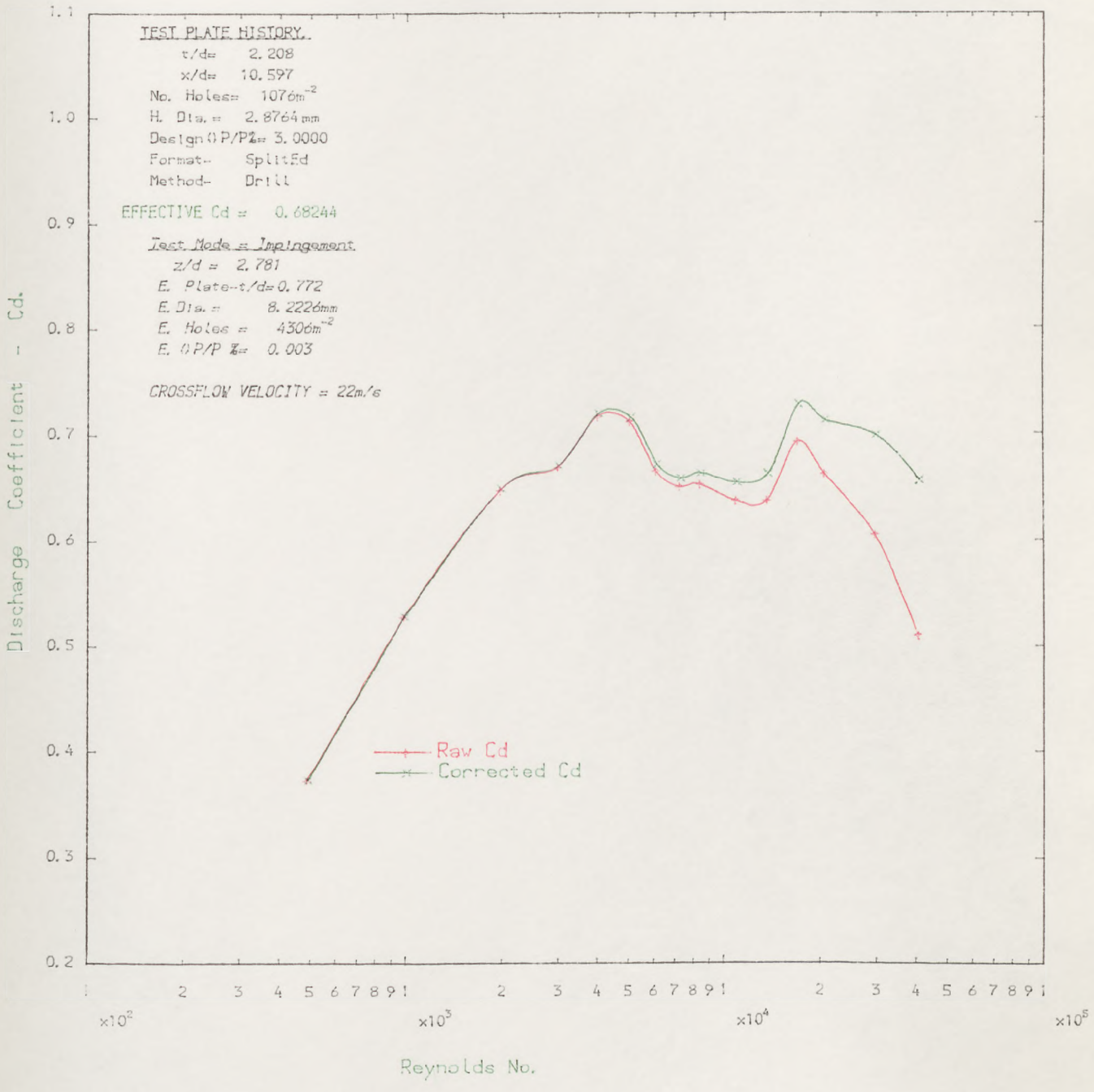

FIG.3.35: CROSS-FLOW Cd DEPENDENCE ON REYNOLDS NUMBER- (cold test).

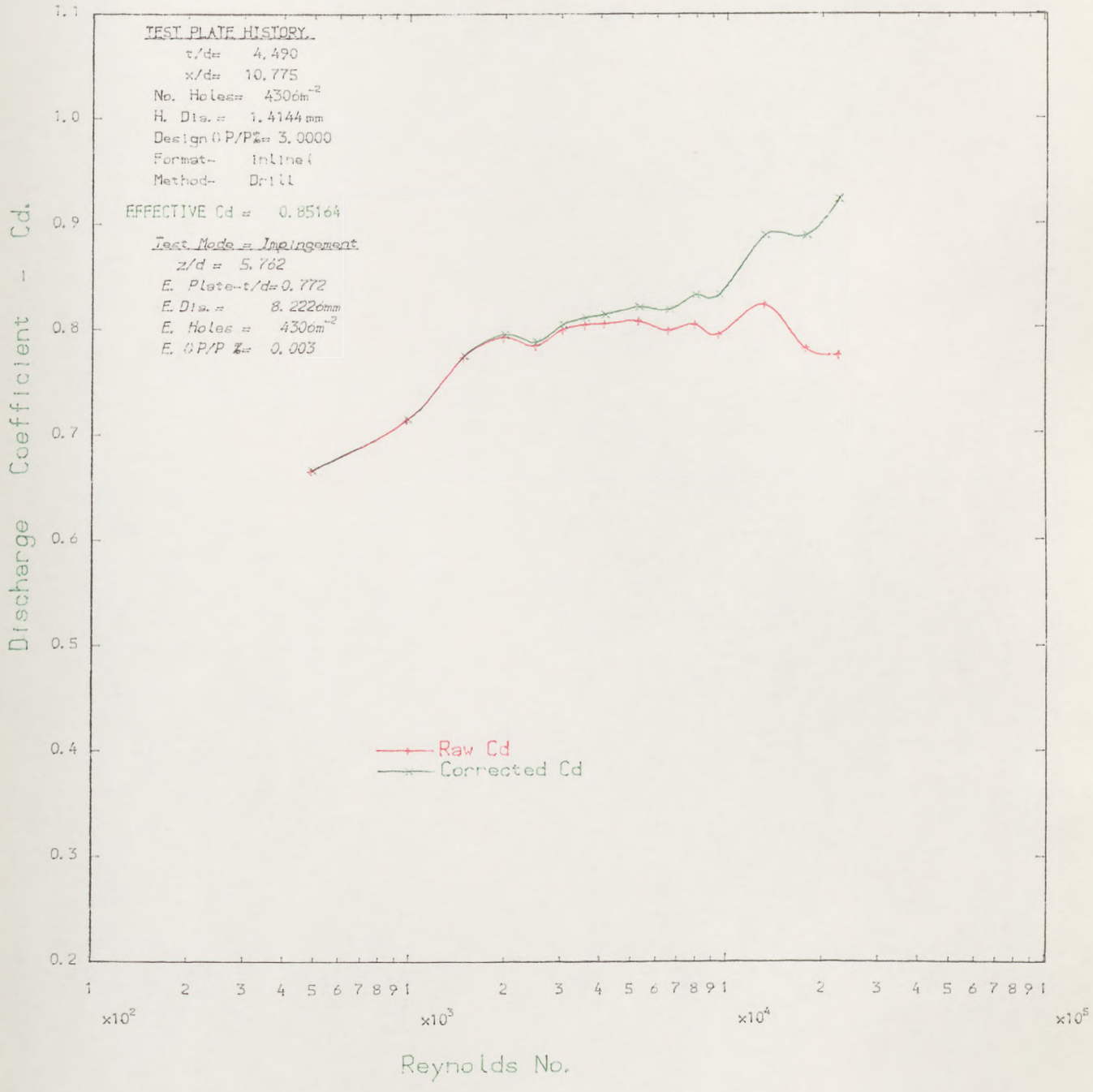

FIG.3.36: FREE-DISCHARGE Cd DEPENDENCE ON REYNOLDS NUMBER-(cold test).

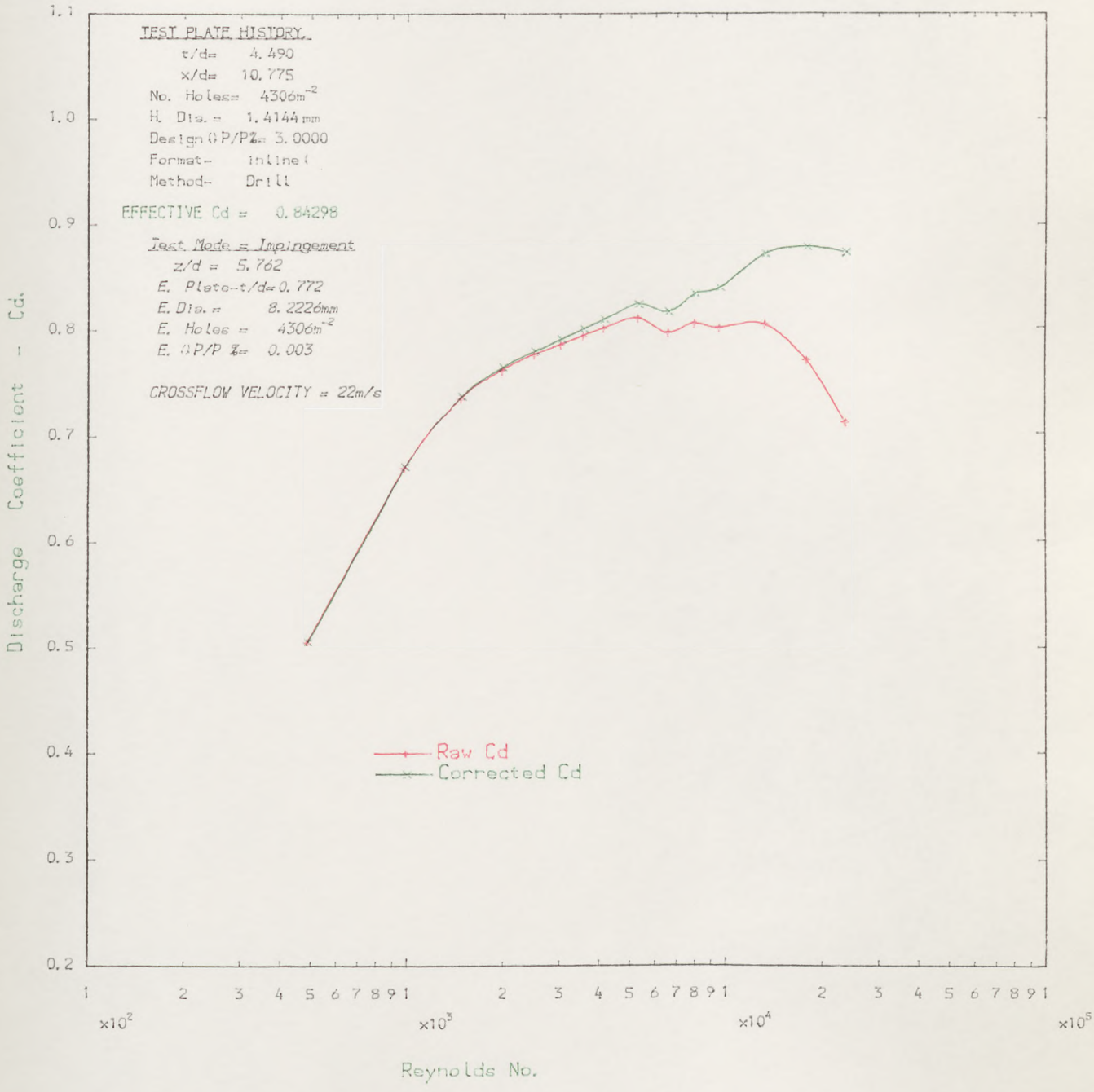

FIG.3.37. CROSS-FLOW Cd DEPENDENCE ON REYNOLDS NUMBER- (cold test).

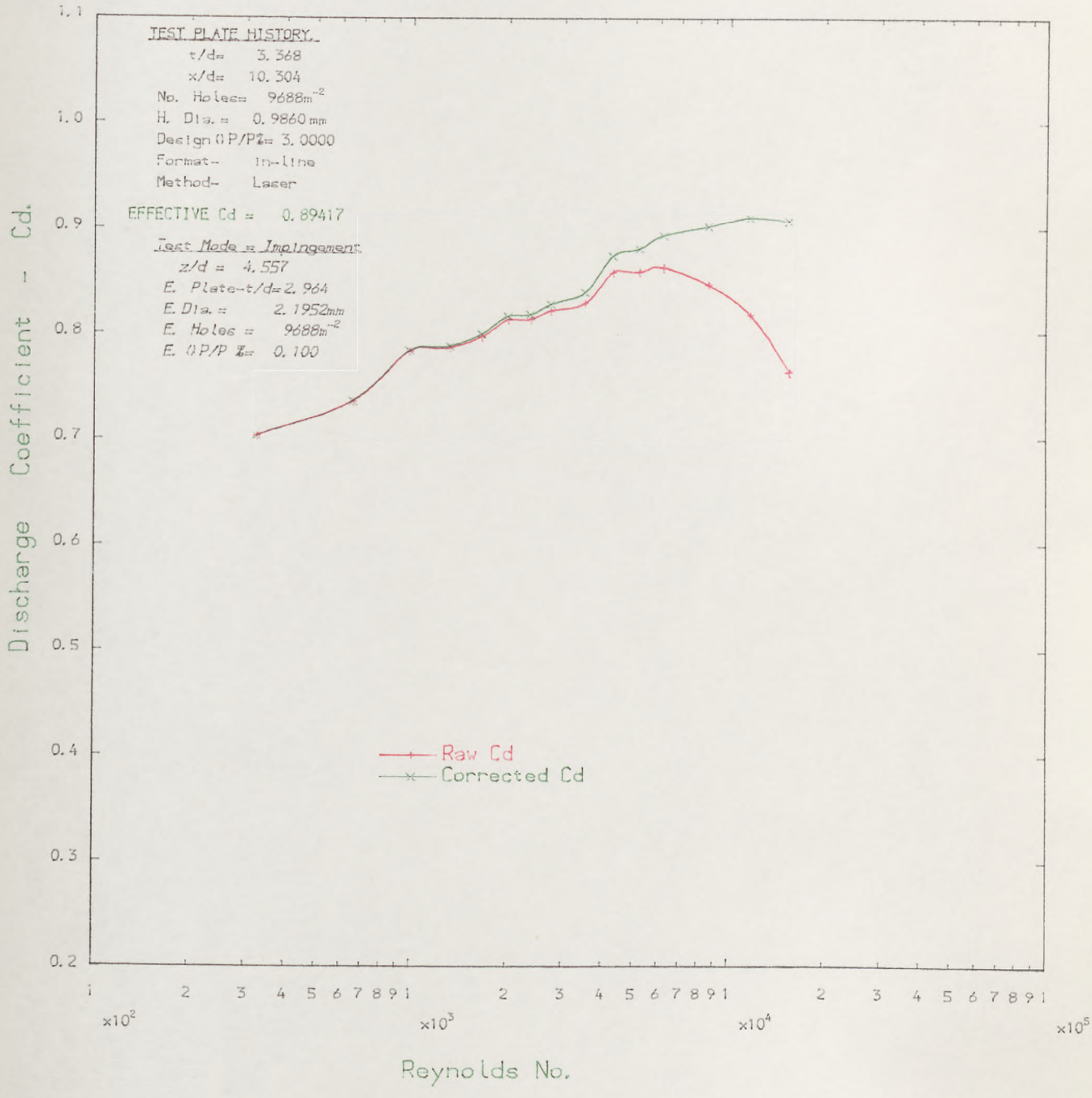

FIG.3.38: FREE-DISCHARGE Cd DEPENDENCE ON REYNOLDS NUMBER- (cold test).

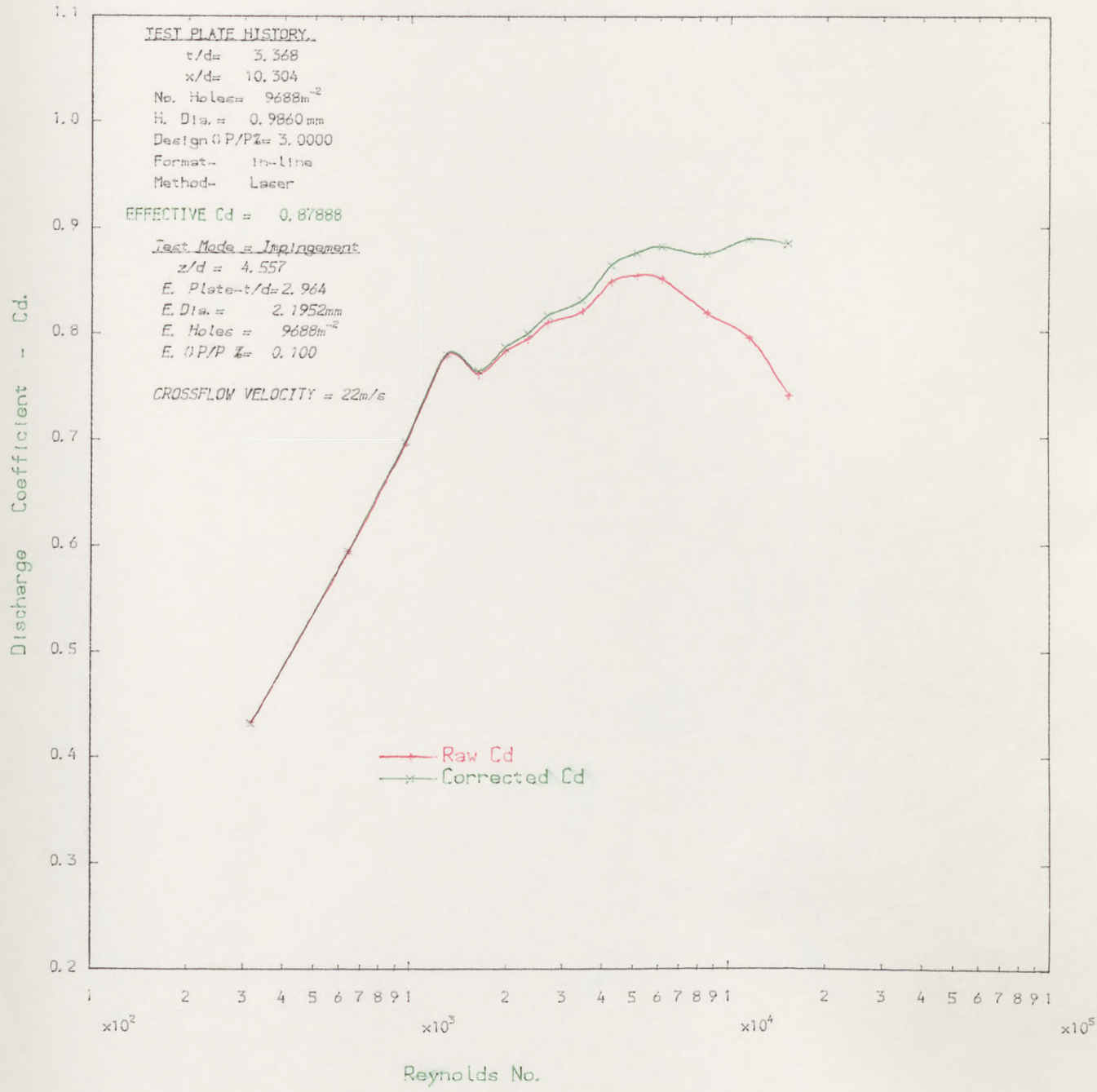

FIG.3.39. CROSS-FLOW Cd DEPENDENCE ON REYNOLDS NUMBER (cold test).

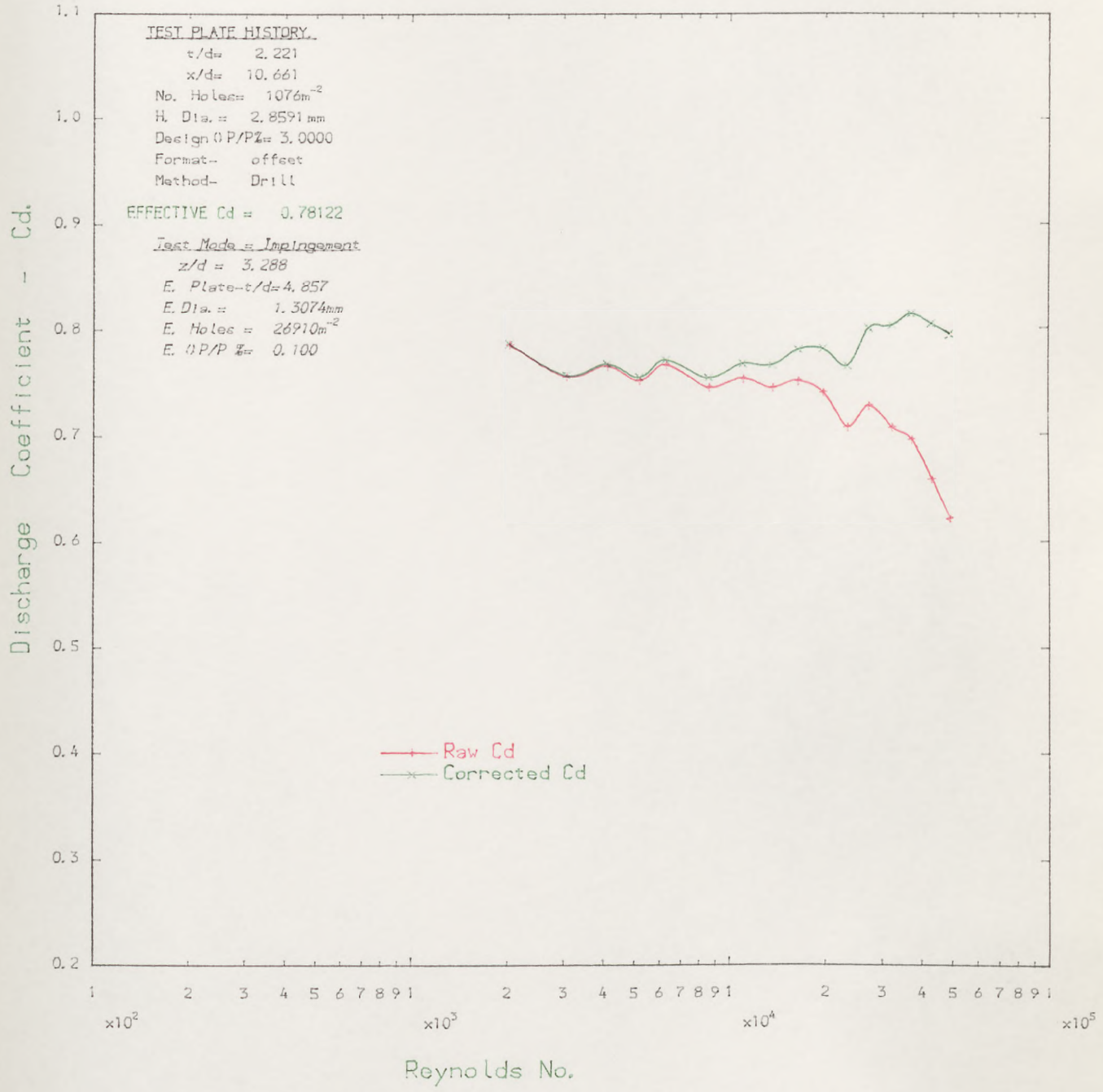

FIG.3.40: FREE-DISCHARGE Cd DEPENDENCE ON REYNOLDS NUMBER-(cold test).

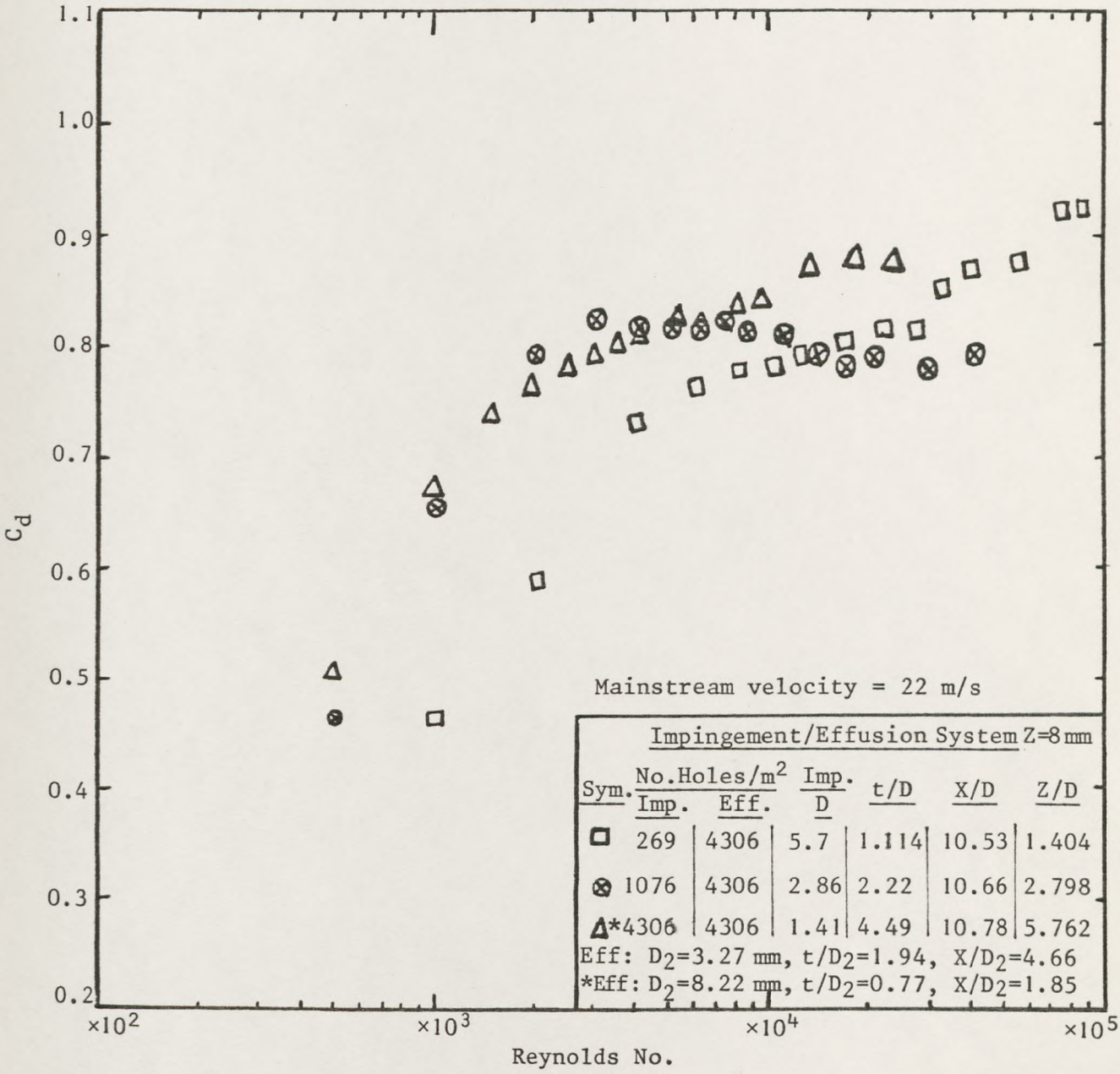

Fig. 3.41: Effect of impingement holes number on C_d

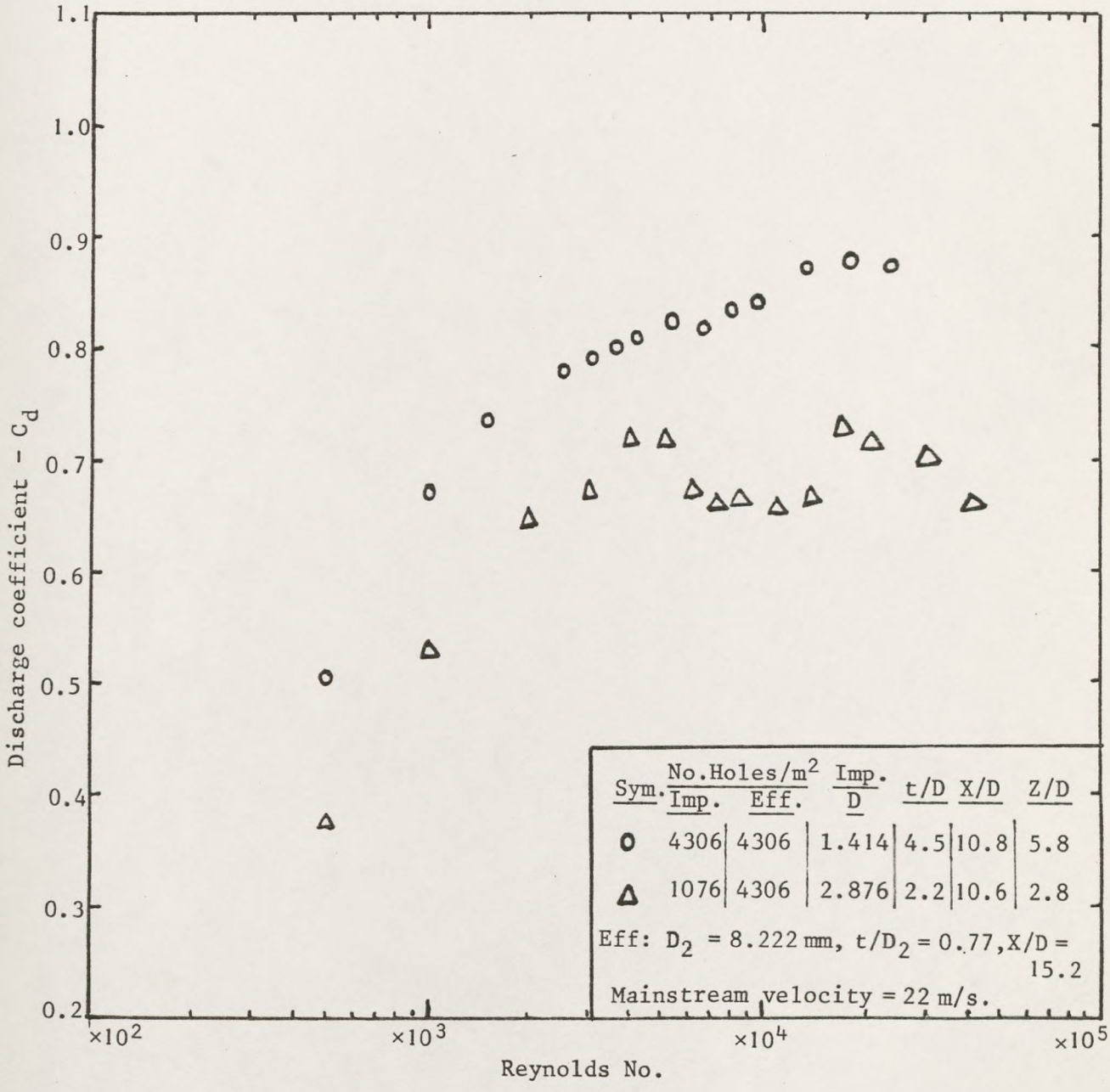

Fig. 3.42: Effect of impingement holes number on C_d

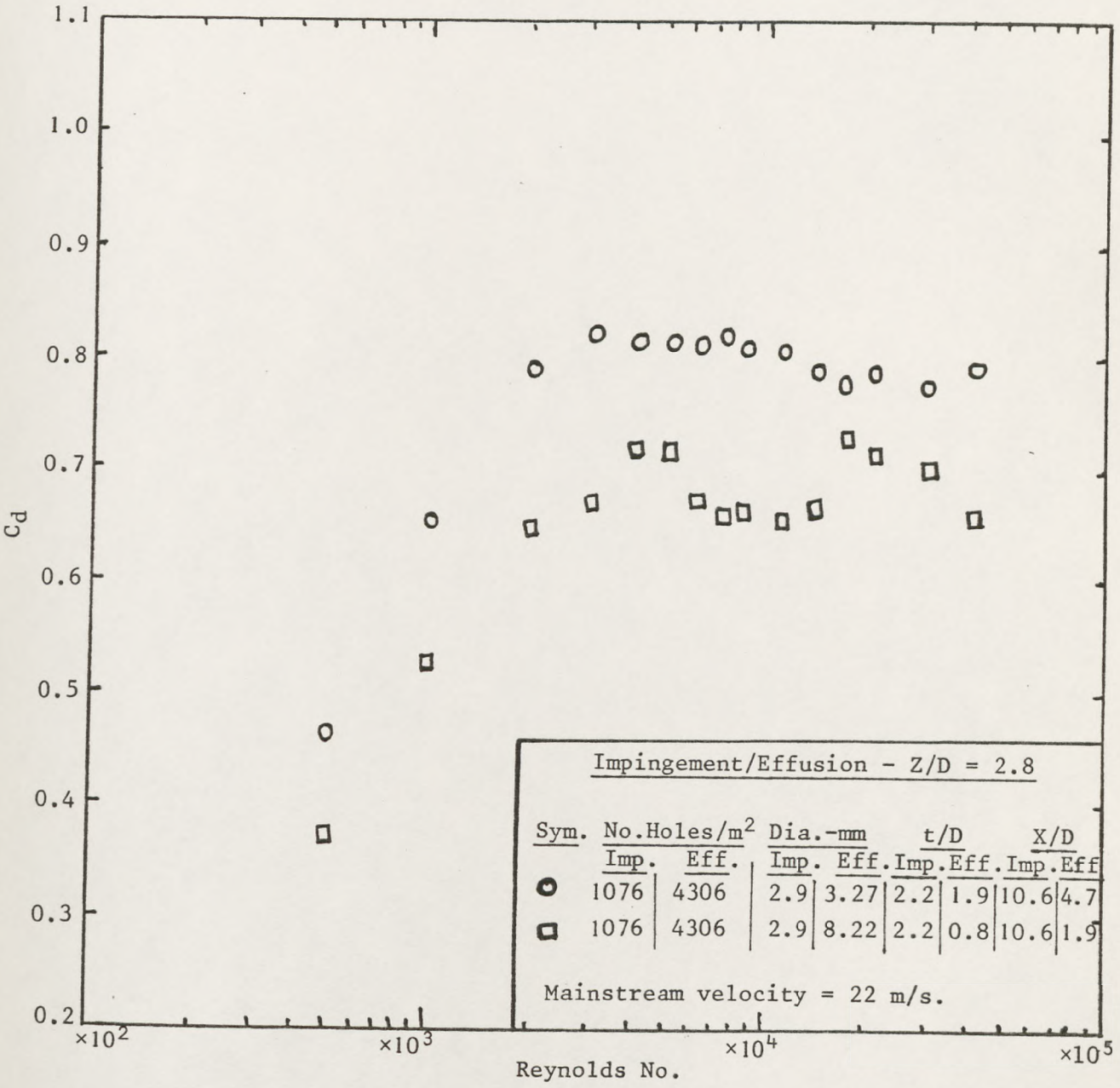

Fig. 3.43: Effect of effusion holes diameter on impingement holes C_d

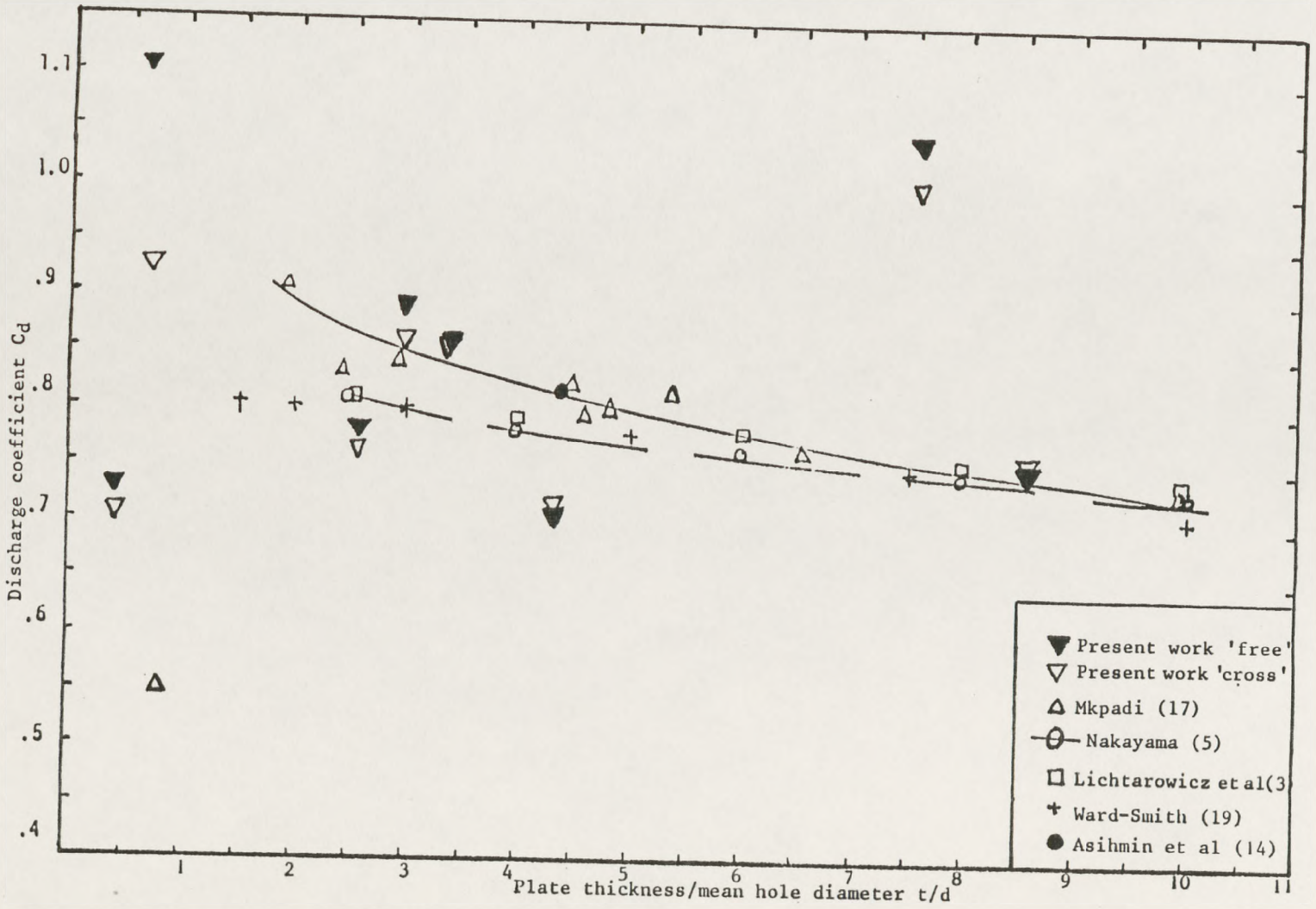

Fig. 3.44: Influence of plate thickness on discharge coefficient

3.7 APPENDIX

UNIVERSITY OF LEEDS
DEPARTMENT OF FUEL AND ENERGY
GAS TURBINE COMBUSTOR WALL COOLING PROGRAMME

EFFUSION PLATE DISCHARGE COEFFICIENT TEST(Free_Discharge)

NO. OF PLT. HOLES:400.0 HOLES MEAN DIAMETER:0.7469510mm
HOLE PITCH: 7.619998mm PLATE ()P/P: 3.0000% PLATE THN.: 6.350mm
HOLES LAYOUT FORMAT: in-line PLATE-MATERIAL: nimonic-75
PLATE THICK. TO DIA. RATIO-t/d: 8.501 HOLE PITCH TO DIA. RATIO-x/d:10.201
ATMOS. PRESS.: 766.25mmHg at TEMP.: 17.0C EXP. DATE:19/ 1/83 Drill

F=ROTA. INDICATED VOLUME FLOWRATE; C=ACTUAL COOLANT MASS FLOW.;
G=COOLANT MASS FLOW RATE PER WALL AREA-Kg/(s m*2); REYS. NO.=REYNOLDS NUMBER
CDr=RAW DISCHARGE COEFF.; CDc=DISCHARGE COEFF.(COMPRESSIBILITY EFFECT CORRECTED);
TC=ROTA. COOLANT TEMP; TC1=PLENUM CHAMBER COOLANT TEMP.; TP=PLATE TEMP.
VEL=COOLANT HOLE VELOCITY; MACH NUMBER OF HOLE COOLANT

F-l/min	C-Kg/s	G	REYS. NO.	CDr	CDc
1400.0	0.04879	2.10055	0.12E+05	0.61026	0.73899
1200.0	0.03693	1.59001	0.88E+04	0.68166	0.76844
1000.0	0.02714	1.16838	0.64E+04	0.70069	0.75420
800.0	0.01946	0.83765	0.46E+04	0.71900	0.74883
700.0	0.01632	0.70251	0.39E+04	0.72697	0.74848
600.0	0.01355	0.58323	0.32E+04	0.72583	0.74107
500.0	0.01095	0.47139	0.26E+04	0.72550	0.73567
400.0	0.00855	0.36818	0.20E+04	0.72376	0.73008
350.0	0.00742	0.31960	0.18E+04	0.67665	0.68176
300.0	0.00631	0.27167	0.15E+04	0.66050	0.66430
250.0	0.00522	0.22462	0.12E+04	0.63415	0.63687
200.0	0.00414	0.17841	0.98E+03	0.60774	0.60954
150.0	0.00309	0.13303	0.73E+03	0.57952	0.58058
100.0	0.00206	0.08860	0.49E+03	0.51970	0.52022
50.0	0.00102	0.04412	0.24E+03	0.41957	0.41973

TC-K	TC1-K	TP-K	VEL-m/s	MACH NO.	TOTAL PRESS. LOSS
289.3	286.0	285.4	146.61	0.43E+00	5.028
289.3	287.8	286.2	131.81	0.39E+00	4.228
289.5	287.8	286.9	107.39	0.32E+00	4.055
289.6	287.7	287.3	82.56	0.24E+00	3.902
289.7	287.7	287.5	70.91	0.21E+00	3.838
289.7	287.6	287.6	59.88	0.18E+00	3.847
289.5	287.6	287.7	49.07	0.14E+00	3.850
289.5	287.6	287.7	38.74	0.11E+00	3.864
288.9	287.6	287.8	33.71	0.99E-01	4.276
289.1	287.6	287.8	28.75	0.85E-01	4.438
289.0	287.6	287.9	23.84	0.70E-01	4.730
289.0	287.6	287.9	18.99	0.56E-01	5.061
288.9	287.7	288.0	14.20	0.42E-01	5.466
288.8	287.8	288.1	9.47	0.28E-01	6.554
288.6	287.8	288.2	4.72	0.14E-01	9.521

EFFECTIVE MEANS OF CD: CORRECTED-(CDc)
STANDARD: DEVIATION-(SD), ERROR-(SE), & RELATIVE ERROR-(RE) IN EFFECTIVE MEAN CDc

	CDc
EFF.MEAN	0.75261
St.Dev	0.01064
St.Error	0.00532
Re.Error	0.01414

Table 3.6A: Sample of a 'free-discharge' computer result output of a single effusion wall (17222 m^{-2} holes)

UNIVERSITY OF LEEDS
DEPARTMENT OF FUEL AND ENERGY
GAS TURBINE COMBUSTOR WALL COOLING PROGRAMME

EFFUSION PLATE DISCHARGE COEFFICIENT TEST(Cross_Flow_Discharge)

NO. OF PLT. HOLES:400.0 HOLES MEAN DIAMETER:0.7469510mm
HOLE PITCH: 7.619998mm PLATE ()P/P: 3.0000% PLATE THN.: 6.350mm
HOLES LAYOUT FORMAT: in-line PLATE-MATERIAL: nimonic-75
PLATE THICK. TO DIA. RATIO-t/d: 8.501 HOLE PITCH TO DIA. RATIO-x/d:10.201
ATMOS. PRESS.: 769.30mmHg at TEMP.: 17.0C EXP. DATE:19/ 1/83 Drill

F=ROTA. INDICATED VOLUME FLOWRATE; C=ACTUAL COOLANT MASS FLOW.;
G=COOLANT MASS FLOW RATE PER WALL AREA-Kg/(s m**2); REYS. NO.=REYNOLDS NUMBER
CDr=RAW DISCHARGE COEFF.; CDc=DISCHARGE COEFF.(COMPRESSIBILITY EFFECT CORRECTED);
TC=ROTA. COOLANT TEMP; TC1=PLENUM CHAMBER COOLANT TEMP.; TP=PLATE TEMP.
VEL=COOLANT HOLE VELOCITY; MACH NUMBER OF HOLE COOLANT
VELr & RNr =RATIOS OF VELOCITY & REYNOLD NO. REPECTIVELY

F-l/min	C-Kg/s	G	REYS. NO.	CDr	CDc
1400.0	0.04869	2.09649	0.12E+05	0.61817	0.74564
1200.0	0.03658	1.57485	0.87E+04	0.68198	0.76704
1000.0	0.02722	1.17192	0.65E+04	0.70284	0.75611
800.0	0.01952	0.84042	0.46E+04	0.72863	0.75810
700.0	0.01640	0.70600	0.39E+04	0.72222	0.74386
600.0	0.01359	0.58529	0.32E+04	0.72835	0.74351
500.0	0.01096	0.47202	0.26E+04	0.72609	0.73619
400.0	0.00859	0.37003	0.20E+04	0.67853	0.68526
350.0	0.00746	0.32117	0.18E+04	0.67847	0.68358
300.0	0.00634	0.27299	0.15E+04	0.65678	0.66061
250.0	0.00525	0.22584	0.12E+04	0.62939	0.63214
200.0	0.00417	0.17958	0.99E+03	0.58735	0.58922
150.0	0.00311	0.13402	0.74E+03	0.53531	0.53646
100.0	0.00207	0.08909	0.49E+03	0.44379	0.44440
50.0	0.00103	0.04447	0.24E+03	0.30860	0.30882

TC-K	TC1-K	TP-K	VEL-M/S	MACH NO.	TOTAL PRESS. LOSS	VELr	RNr
289.6	288.0	290.3	147.13	0.43E+00	4.925	9.998	0.125
289.7	287.9	291.6	130.71	0.38E+00	4.225	8.870	0.094
289.6	287.8	292.3	107.35	0.32E+00	4.037	7.275	0.070
289.5	287.7	293.2	82.64	0.24E+00	3.825	5.597	0.050
288.8	287.5	293.7	70.84	0.21E+00	3.876	4.797	0.042
288.6	287.5	294.2	59.82	0.18E+00	3.828	4.048	0.035
288.5	287.5	294.9	48.92	0.14E+00	3.845	3.311	0.028
288.3	287.5	295.6	38.66	0.11E+00	4.258	2.615	0.022
288.1	287.6	296.1	33.72	0.99E-01	4.259	2.284	0.019
287.8	287.6	296.6	28.76	0.85E-01	4.477	1.947	0.016
287.6	287.7	296.9	23.88	0.70E-01	4.787	1.617	0.013
287.4	287.9	297.3	19.05	0.56E-01	5.348	1.289	0.011
287.3	287.8	298.1	14.24	0.42E-01	6.234	0.964	0.008
287.0	288.0	299.2	9.49	0.28E-01	8.616	0.643	0.005
286.5	288.8	300.2	4.75	0.14E-01	16.750	0.322	0.003

EFFECTIVE MEANS OF CD: CORRECTED-(CDc)
STANDARD: DEVIATION-(SD), ERROR-(SE), & RELATIVE ERROR-(RE) IN EFFECTIVE MEAN CDc

	CDc
EFF.MEAN	0.75672
St.Dev	0.00761
St.Error	0.00380
Re.Error	0.01005

Fig. 3.6B: Sample of 'cross-flow discharge' computer result output of a single effusion wall (17222 m^{-2} holes)

UNIVERSITY OF LEEDS
DEPARTMENT OF FUEL AND ENERGY
Gas Turbine Combustor Wall Cooling Programme

30- 1 IMPINGEMENT PLATE DISCHARGE COEFFICIENT TEST-(Free_Discharge)

PLATE COMBINATION:-IMP.:NO. HOLES:225.0 HOLES M.DIA.:0.9860330mm PITCH:10.159997mm
()P/P: 3.0000% THICK.: 3.321MM FORMAT: in-line MAT.:nimonic-75
EFFUSION:NO. HOLES:225.0 HOLES M.DIA.:2.1952219mm H. PITCH:10.159997mm
()P/P: 0.1000% THICK.: 6.507mm FORMAT: offset MAT.: nimonic-75
SEP.GAP(Z): 4.49mm Z/D: 4.56 X/D:10.304 IMP. PLATE THICK. TO DIA. RATIO-t/d: 3.37
ATMOS. PRESS.: 755.15mmHg AT TEMPERATURE: 19.5 Deg.C EXP. DATE:16/ 3/83 Laser

F=ROTA. INDICATED VOLUME FLOWRATE; C=ACTUAL COOLANT MASS FLOW.;
G=COOLANT MASS FLOW RATE PER WALL AREA-Kg/(s m*2); REYS. NO.=REYNOLDS NUMBER
CDr=RAW DISCHARGE COEFF.; CDc=DISCHARGE COEFF.(COMPRESSIBILITY EFFECT CORRECTED);
TC=ROTA. COOLANT TEMP; TC1=PLENUM CHAMBER COOLANT TEMP.; TP=PLATE TEMP.
VEL=COOLANT HOLE VELOCITY; MACH NUMBER OF HOLE COOLANT

F-l/min	C-Kg/s	G	REYS. NO.	CDr	CDc
1400.0	0.04802	2.06755	0.15E+05	0.76465	0.90712
1200.0	0.03607	1.55317	0.11E+05	0.81818	0.90996
1000.0	0.02664	1.14699	0.84E+04	0.84691	0.90169
800.0	0.01922	0.82746	0.61E+04	0.86274	0.89299
700.0	0.01614	0.69481	0.51E+04	0.85822	0.88021
600.0	0.01331	0.57307	0.42E+04	0.85777	0.87305
500.0	0.01088	0.46845	0.34E+04	0.82842	0.83912
400.0	0.00848	0.36514	0.27E+04	0.82102	0.82766
350.0	0.00735	0.31643	0.23E+04	0.81297	0.81803
300.0	0.00624	0.26865	0.20E+04	0.81251	0.81613
250.0	0.00516	0.22227	0.16E+04	0.79645	0.79902
200.0	0.00410	0.17671	0.13E+04	0.78627	0.78793
150.0	0.00307	0.13199	0.97E+03	0.78270	0.78363
100.0	0.00204	0.08765	0.64E+03	0.73551	0.73595
50.0	0.00102	0.04373	0.32E+03	0.70315	0.70326

TC-K	TC1-K	TP-K	VEL-m/s	MACH NO.	TOTAL PRESS. LOSS
292.1	292.0	291.7	166.70	0.49E+00	3.565
292.1	291.9	291.8	142.91	0.42E+00	3.241
292.1	291.5	291.7	114.74	0.34E+00	3.091
292.2	291.5	291.7	87.29	0.26E+00	3.015
292.3	291.6	291.9	74.57	0.22E+00	3.037
292.3	291.7	292.0	62.39	0.18E+00	3.039
291.3	291.5	292.2	51.42	0.15E+00	3.186
291.0	291.5	292.1	40.43	0.12E+00	3.225
290.7	291.4	292.0	35.14	0.10E+00	3.270
290.7	291.5	292.0	29.94	0.87E-01	3.272
290.7	291.6	292.1	24.84	0.73E-01	3.365
290.5	291.7	292.1	19.79	0.58E-01	3.426
290.4	291.8	292.2	14.81	0.43E-01	3.448
290.3	291.8	292.2	9.85	0.29E-01	3.773
290.0	291.9	292.3	4.92	0.14E-01	4.034

EFFECTIVE MEANS OF CD: CORRECTED-(CDc)
STANDARD: DEVIATION-(SD), ERROR-(SE), & RELATIVE ERROR-(RE) IN EFFECTIVE MEAN CDc

	CDc
EFF.MEAN	0.89417
St.Dev	0.01364
St.Error	0.00557
Re.Error	0.01245

Table 3.6C: Sample of 'free-discharge' computer result output for impingement/effusion combined system (9688/9688 m^{-2} holes)

UNIVERSITY OF LEEDS
DEPARTMENT OF FUEL AND ENERGY
Gas Turbine Combustor Wall Cooling Programme

30- 1 IMPINGEMENT PLATE DISCHARGE COEFFICIENT TEST-(Cross_Flow_Discharge)

PLATE COMBINATION:-IMP.:NO. HOLES:225.0 HOLES M.DIA.:0.9860330mm PITCH:10.159997mm
()P/P: 3.0000% THICK.: 3.321MM FORMAT: in-line MAT.:nimonic-75
EFFUSION:NO. HOLES:225.0 HOLES M.DIA.:2.1952219mm H. PITCH:10.159997mm
()P/P: 0.1000% THICK.: 6.507mm FORMAT: offset MAT.: nimonic-75
SEP.GAP(Z): 4.49mm Z/D: 4.56 X/D:10.304 IMP. PLATE THICK. TO DIA. RATIO-t/d: 3.37
ATMOS. PRESS.: 756.15mmHg AT TEMPERATURE: 21.0 Deg.C EXP. DATE:17/ 3/83 Laser

F=ROTA. INDICATED VOLUME FLOWRATE; C=ACTUAL COOLANT MASS FLOW.;
G=COOLANT MASS FLOW RATE PER WALL AREA-Kg/(s m*2); REYS. NO.=REYNOLDS NUMBER
CDr=RAW DISCHARGE COEFF.; CDc=DISCHARGE COEFF.(COMPRESSIBILITY EFFECT CORRECTED);
TC=ROTA. COOLANT TEMP; TC1=PLENUM CHAMBER COOLANT TEMP.; TP=PLATE TEMP.
VEL=COOLANT HOLE VELOCITY; MACH NUMBER OF HOLE COOLANT
VELr & RNr =RATIOS OF VELOCITY & REYNOLD NO. REPECTIVELY

F-l/min	C-Kg/s	G	REYS. NO.	CDr	CDc
1400.0	0.04782	2.05911	0.15E+05	0.74186	0.88523
1200.0	0.03599	1.54966	0.11E+05	0.79618	0.88934
1000.0	0.02657	1.14379	0.83E+04	0.81959	0.87572
800.0	0.01917	0.82531	0.60E+04	0.85180	0.88242
700.0	0.01608	0.69231	0.50E+04	0.85431	0.87636
600.0	0.01335	0.57494	0.42E+04	0.84862	0.86423
500.0	0.01082	0.46586	0.34E+04	0.82064	0.83139
400.0	0.00847	0.36452	0.27E+04	0.81005	0.81680
350.0	0.00733	0.31559	0.23E+04	0.79451	0.79970
300.0	0.00623	0.26813	0.20E+04	0.78303	0.78685
250.0	0.00515	0.22177	0.16E+04	0.76156	0.76426
200.0	0.00409	0.17628	0.13E+04	0.77879	0.78046
150.0	0.00306	0.13170	0.96E+03	0.69617	0.69722
100.0	0.00203	0.08746	0.64E+03	0.59386	0.59441
50.0	0.00101	0.04362	0.32E+03	0.43213	0.43232

TC-K	TC1-K	TP-K	VEL-M/S	MACH NO.	TOTAL PRESS. LOSS	VELr	RNr
295.9	294.4	295.8	164.92	0.48E+00	3.726	7.398	0.111
295.9	294.9	296.6	142.46	0.41E+00	3.366	6.370	0.083
294.8	295.1	297.3	114.74	0.33E+00	3.233	5.116	0.061
294.0	295.0	297.7	87.73	0.25E+00	3.067	3.923	0.045
293.6	294.9	297.9	74.93	0.22E+00	3.055	3.351	0.037
293.1	294.8	298.1	63.04	0.18E+00	3.083	2.828	0.031
293.0	294.8	298.4	51.58	0.15E+00	3.227	2.315	0.025
293.0	295.0	298.9	40.73	0.12E+00	3.286	1.824	0.020
293.0	295.1	299.3	35.40	0.10E+00	3.376	1.588	0.017
292.9	295.3	299.7	30.18	0.88E-01	3.446	1.354	0.015
292.8	295.5	300.2	25.04	0.73E-01	3.586	1.124	0.012
292.8	295.6	300.7	19.96	0.58E-01	3.473	0.894	0.010
292.6	295.9	301.8	14.95	0.43E-01	4.095	0.670	0.007
292.6	296.1	302.9	9.94	0.29E-01	5.253	0.445	0.005
292.6	296.4	304.6	4.97	0.14E-01	9.033	0.224	0.002

EFFECTIVE MEANS OF CD: CORRECTED-(CDc)
STANDARD: DEVIATION-(SD), ERROR-(SE), & RELATIVE ERROR-(RE) IN EFFECTIVE MEAN CDc

	CDc
EFF.MEAN	0.87888
St.Dev	0.00809
St.Error	0.00330
Re.Error	0.00752

**********&&&&&&&&&&&&&&**********%%%%%%%%%%%%%%%%

Table 3.6D: Sample of 'cross-flow discharge' computer result output of impingement/effusion combined system (9688/9688 m^{-2} holes)

CHAPTER 4

Nomenclature

Nu	=	Nusselt number
Re	=	Reynolds number
Pr	=	Prandtl number
H,h	=	Heat transfer coefficient of convection - W/m^2K
D	=	Total maximum diameter of Rigid mesh pore - m
K	=	Thermal conductivity of coolant - W/mK
Q,q	=	Heat transfer rate - W
A,Z	=	Rigidmesh material area, or surface area - m^2
T_p,t	=	Rigidmesh material temperature - K
T,t	=	Coolant temperature - K
E	=	Emissivity
V	=	Volume of material - m^2
G,$\dot{M}$	=	Coolant flow rate per unit surface area - kg/sm^2
μ	=	Dynamic viscosity - Ns/m^2 or Pas or kg/ms
S	=	Total cross-section area available for flow - m^2
X or x	=	Axial distance downstream of wall leading edge - m
p	=	Porosity
n	=	Distance
B	=	Defined in equation 4.17B
e	=	Exponential
C_p	=	Specific heat capacity - J/kgK
R	=	Definition of equation 4.29
ρ	=	Density
U	=	Velocity
σ	=	Stefan-Boltzmann constant (56.7×10^{-9} W/m^2K^4)
W	=	Radiosity
P	=	Pressure

C,n = Constant in equations 4.38 and 4.39

η = Cooling effectiveness

Subscripts:

b,rb,o = back of wall

f,c = coolant or fluid

p = Rigid Mesh material

i,h = inside of wall

w = wall

g,RF = mainstream

n = exchange or constant

e = in log

ov = overall

ad = adiabatic

tb = thermal boundary layer

1 = upstream

2 = surface of wall or downstream

3 = plenum wall

CHAPTER 4

TRANSPIRATION SYSTEM

4.1 INTRODUCTION

The concept of transpiration cooling is an old one but its application had been delayed for reasons outlined in section 1.6.6. Transpiration cooling occurs when the surface to be cooled is uniformly porous. When liquid is employed as coolant, the system is sometimes referred to as sweat cooling. Sweat cooling was first proposed by H. Oberth in 1929 and the first experiment was carried out by Goddard in 1930. Moore and Grootenhuis (1) first suggested the application of sweat cooling in gas turbines. Liquids as opposed to air have many thermodynamic advantages and a water-cooled turbine was built in Germany during the war (2). However the formidable problems posed in designing a reliable liquid-circulating system for high speed turbine rotors and other mechanical problems associated with the application of liquid as coolant showed in the early days that liquid cooling raises more problems than it overcomes. These shortcomings until recently had left dormant the use of liquid as a coolant. Jacob and Fieldhouse (3) carried out investigation on sweat cooling forcing water through a porous metal disc and found that the convective heat transfer to the wall from the mainstream was reduced by 79%. More recently El-Masri (4) has presented what he called two-phase partially-flooded and completely-flooded modes for sweat cooling in gas turbine blades.

The requirement for energy saving, simplicity, light weight and low cost in turbines, most especially in aero-engines, makes the use of compressor delivery air, as the turbine hot section

coolant, a very attractive one. The application of air, forced through a porous material, as coolant in a gas turbine engine was appreciated and first assessed by Duwez and Wheeler (4). By forcing a small amount of air through a porous bronze cylinder exposed to high temperature combustion gas, Duwez and Wheeler showed the high cooling potential offered by transpiration system. Wheeler and Duwez (5) showed that the heat transfer coefficients to the surface of a porous wall, using hydrogen and nitrogen, are approximately the same. Bland (6) discussed the mathematical theory of the flow of a gas in a porous solid using data of Ref. 19.

Apart from the works of Bayley et al (7), Nealy and Reider (8) and Wassell and Bhangu (9), most works done on transpiration cooling system were focused on turbine nozzle guide vanes and blades application (10-15). Nealy and Reider used complex, diffusion-bonded sheet structures called Lamilloy while Wassell and Bhangu used sophisticated, brazed laminates called Transply in their investigation. Both Lamilloy and Transply are not available commercially and data from the work carried out on them are very hard to come by. Essman et al (16) investigated the durability of Lamilloy combustors using an Allison TF41 turbofan engine. Their investigation showed that thermal stress cracking in the air hole inserts, along with erosion at the material cross-over tube attachments, developed in the combustor after a period of tests, equivalent to 1000 hours of field service. Such durability tests on Transply have not been reported in the literature.

Bayley et al (7) used commercially available material called Rigidmesh to investigate the cooling performance of transpiration system applied to a Rolls Royce 'Dart' combustor. Smith et al (17)

used different grades of Rigidmesh and a grade of Rigimesh sintered material, as a porous plate, to investigate the heat transfer to a transpiration cooled turbine combustor. Goldstein et al (18) used sintered stainless steel porous material as an injection slot to study film cooling effectiveness on a blank plate downstream of the injection.

Transpiration cooling system is the most promising system for optimum wall cooling. Despite this, data on the cooling effectiveness performance of transpiration cooled systems under realistic conditions are limited, particularly for combustion chamber applications (20). It is against this background and the need to compare the performance of both effusion (single) wall and impingement-effusion combined wall cooling with the transpiration cooling system that the present work was carried out. The experimental apparatus has been described in Chapter 2. Three grades of commercially available Porosint RigidMesh were used in the investigation. These grades were RM50A, RM50B and RM10A and their pictures taken under microscope are shown in plates 4.1 to 4.3 respectively.

4.1.1 Production, Characteristics and Instrumentation of the Transpiration Wall

The material used in this investigation is a porous sintered stainless steel, commercially produced by Sheepbridge Sintered Products Ltd. The trade name of the porous wall is Porosint Rigid Mesh and comes in grades which are a measure of its pore size. It consists essentially of rigidising woven mesh, produced by sintering together stainless steel wires. Sintering improves the strength and ensures that the uniformity of the weave is

maintained. The sheets produced by sintering are then rolled to modify the shape of the apertures in the original weave (38). This rolling process improves the rigidity and strength of the material by welding together many layers of wire mesh. Rigid Mesh is suitable for working at room temperature up to 773 K. It is made from stainless steel type AISI 316.

The pictures of the three grades of Rigid Mesh, taken under a microscope with a magnification of × 80 (plates 4.1 to 4.3) reveal that the surfaces were very rough and that the characteristics of each plate are quite different. The materials exhibit characteristics which show that the compressed wire mesh construction is similar to an array of very many small holes of random directional outlet angles. Other characteristics of the Rigid Mesh, as specified by the manufacturer (39), are tabulated in table 4.1.

TABLE 4.1

Rigid Mesh Grade	Pore Size (μm)	Thickness (mm)	UTS Pa	Permeability P (kg.m.s)
RM 50A	50	1.09	232	14.4
RM 50B	50	0.92	77	550.0
RM 10A	10	0.95	185	14.1

Table 4.1: Characteristics of three grades of Rigid Mesh

The permeability, P, is defined as

$$P = \frac{\dot{v}t\mu}{A_e \Delta P} = \frac{Gt\mu}{\varepsilon\rho \Delta P} \qquad \ldots (1A)$$

where $\dot{v}$ = Volumetric flow rate - m^3/s

t = Porous wall thickness - m

ΔP = Pressure loss - Pa

μ = Fluid viscosity - kg/ms

A_e = Effective area - m^2

A = Porous wall area - m^2

G = Coolant flow per unit surface area - kg/sm^2

ρ = Coolant density - kg/m^3

Thickness measurements of the three walls show that the manufacturer's quoted thicknesses were only nominal and the true measured mean values are:

a) RM 50A = 1.304 mm

b) RM 50B = 0.897 mm

c) RM 10A = 0.905 mm.

The test wall was a square section of 152.4 mm by 152.4 mm welded to stainless steel flanges, 25.4 mm wide at all its four edges. The flanges carry perforated holes which allow 2BA screws to pass through, and enable the Rigid Mesh test section to be bolted to the outlet of the plenum as described in Chapter 2 for perforated plates. The test wall was instrumented with five Type K mineral insulated grounded junction thermocouples attached with a welded strap to the rear of the test plate to give good thermal contact. They could not be brazed or welded to the Rigid Mesh at the thermocouple tip due to the problem of locally blocking the porous surface. The thermocouples were in a line 25.4 mm apart on the duct centre line. The coolant boundary layer temperature profiles were measured by traversing three 1.6 mm diameter mineral insulated grounded junction type K thermocouples normal to the test surface as described

in Chapter 2 for perforated plates. The tests were carried out at a gas temperature of 750 K with the coolant at room temperature giving a coolant to hot gas density ratio of approximately 2.5.

4.2 HEAT TRANSFER CONSIDERATIONS IN TRANSPIRATION COOLED SYSTEMS

Transpiration cooling achieves its high cooling effectiveness through three major heat transfer processes. These are:

(1) Radiative heat transfer to the plenum chamber at the back-side,

(2) Interstitial heat transfer, and

(3) Film heat transfer.

4.2.1 Radiative Heat Transfer at the Back-side of the Test Wall

There is radiative heat at the back of the test wall. This radiation at the condition of testing is small and was computed using the Gray and Muller (22) radiosity method, detailed in Chapter 5. The radiative heat, Q_{rb}, at the back of the wall is

$$Q_{rb} = f(A,E,R_1,W,\rho)$$

Analysis results in

$$Q_{rb} = \frac{AE}{1-E}\left[\frac{(0.952 - 0.953\,E)\,T_p^4 - (0.952 - 0.952\,E)\,T_3^4}{(0.952 + 0.047\,E)}\right] \quad \ldots (4.5)$$

The Rigid Mesh material is of stainless steel type AISI 316. In the absence of any data on Porosint emissivity, the correlation produced in Chapter 5 for stainless steel had been made use of, and reproduced here as

$$E = 0.6179 + 2.40933 \times 10^{-4}\, T_p \quad \ldots (4.6)$$

where E = Emissivity of stainless steel

T_p = Test wall temperature

4.2.2 Interstitial Heat Transfer

In cooling processes where the coolant is made to flow through the wall before being ejected at the gas side, heat is transferred by convection between the wall and the coolant. The internal heat removed in this way by the coolant, in transpiration cooling, represents a significant proportion of the high cooling performance displayed by this system. This significant heat transfer process has led to the development of complex materials such as Lamilloy (8,29,30) and Transply (9). Both Lamilloy and Transply have many internal coolant passages to enhance the internal heat removed by the coolant to the neglect of back-side heat transfer to the coolant at its approach to the holes. Internal heat transfer, a specific feature of transpiration cooling, has been investigated by many workers. Bayley and Turner (23) determined the internal heat transfer coefficient of porous wall - Rigimesh and Rigidmesh - by applying currents of up to 2000 amps to the wall and blowing air through a tunnel. The coefficient of heat transfer, h_i, obtained was defined as

$$h_i = \frac{q}{\Delta T V}$$

where q = rate of heat transfer

ΔT = mean temperature difference between coolant and material

V = volume of material

Bayley et al (7) presented a correlation for the internal Nusselt number as:

$$Nu_i = 0.35\, Re_i \qquad \ldots (4.7)$$

From fig. 4.19 of (7), both internal Nusselt and Reynolds numbers were correlated as

$$Nu_i = \frac{h_i (V/S)^2}{k_f} \qquad \ldots (4.8)$$

$$Re_i = \frac{G(V/S)}{\mu_f} \qquad \ldots (4.9)$$

Combining equations 4.8 and 4.9 with 4.7, the internal heat transfer coefficient may be shown as in equation 4.10.

$$h_i = 0.35 \frac{G.K_f}{\mu_f (V/S)} \qquad \ldots (4.10)$$

The major problem with the above equation is in the determination of (V/S). One approach to its determination is the weighing method employed in the determination of the surface area of coal pores (41). The mass (m_1) of the material is first determined. The material is soaked in a fluid of suitable viscosity - water - and the new mass (m_2) of the material is again determined.

From m_1, the volume, V, of the solid material is determined as

$$V = \frac{m_1}{\rho} \qquad \ldots (4.10A)$$

where ρ = density of the material = 8238 kg/m^3 for AISI 316 (42).

From m_2, the total volume (V_p) of the pores may be determined as

$$m_2 - m_1 = \delta_m \qquad \ldots (4.10B)$$

$$\therefore \quad V_p = \frac{\delta_m}{\rho_w} \qquad \ldots (4.10C)$$

where δ_m = mass of fluid - kg

ρ_w = density of fluid; water was employed and this is at 20 °C, 998 kg/m^3.

Table 4.2 shows the results obtained for (V/S) in the present work.

TABLE 4.2

	RM50A	RM50B	RM10A
Mass of material - kg	0.1789	0.0972	0.1307
Volume, V, of material - m^3	2.1716×10^{-5}	1.1799×10^{-5}	1.5866×10^{-5}
δ_m - kg	0.0024	0.0051	0.0011
Total volume, V_p, of pores - m^3	2.4048×10^{-6}	5.1102×10^{-6}	1.1022×10^{-6}
Pore size, r, - m	50×10^{-6}	50×10^{-6}	10×10^{-6}
Volume (V_e) of a pore (assumed spherical) - m^3	6.545×10^{-14}	6.545×10^{-14}	5.236×10^{-16}
Number of pores $n = (\frac{V_p}{V_e})$	3.674×10^{7}	7.8078×10^{7}	2.105×10^{9}
Total surface area (S) of pore = $4n\pi r^2$ - m^2	0.2886	0.6132	0.6613
(V/S)	7.5246×10^{-5}	1.9241×10^{-5}	2.399×10^{-5}

Table 4.2: The determination of (V/S)

The error in weighing was ± 0.01%. The value of (V/S) above is less than that of Bayley et al (7). For a RM40A and RM30B, Bayley et al used the value of (V/S) of 1.27×10^{-4} and 1.78×10^{-4} respectively, without stating how the values were arrived at. The present value of (V/S) is about a factor of 7 less than that of Bayley.

Smith and Watts (17) assuming constant physical properties of coolant and solid as well as constant heat flux from wall to the coolant, correlate internal heat transfer coefficient for Rigidmesh and Rigimesh, for practical design purposes, as

$$h_i = 2.2045 \times 10^6 \, G^{0.9} \qquad \ldots (4.11)$$

where h_i = Internal heat transfer coefficient per unit volume

G = Coolant mass flow rate per unit surface area

Epifanov and Leontjev (24) using porous turbine blade and employing the Runge-Kutta method, numerically determined the heat transfer inside the porous wall. The heat transfer inside a porous wall has been considered by Holman (25), Colladay and Stepka (26) and Curry (27) as being purely conductive. Rigorously, the heat transfer in a porous wall may be derived by assuming conduction processes.

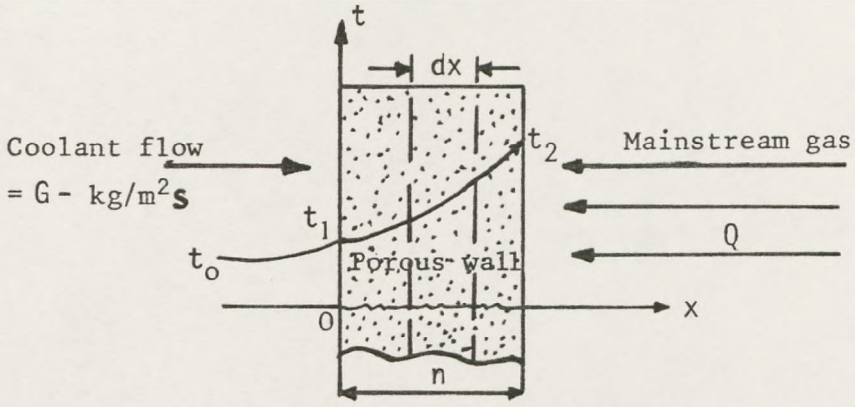

Fig. 4.1: Transpiration cooling of a plane porous plate

Considering fig 4.1, it is assumed that the temperature field inside the porous wall is one-dimensional. Assuming the physical properties of the coolant to be constant, it is necessary to find the temperature distribution in the porous wall.

Take a small element dx, the heat transfer in the plate between point x and x + dx, from Fourier's law, is

$$q_x = -KA\frac{dt}{dx} \qquad \ldots (4.12)$$

and $$q_{x+dx} = -KA\frac{d}{dx}\left(t + \frac{dt}{dx}dx\right) \quad \ldots (4.13)$$

Now the porosity, p, of the above wall is defined as

$$p = \frac{\text{Volume of the pores}}{\text{Total volume of wall material}} \equiv \frac{\text{Effective area}}{\text{Total area of wall}}$$

Take the solid area for heat conduction as Z. It follows that

$$Z = 1 - p \quad \ldots (4.14)$$

But Z = A in equation 4.13, therefore

$$Z = A = 1 - p \quad \ldots (4.15)$$

Substituting for A, from equation 4.15, equations 4.12 and 4.13 may be rewritten as

$$q_x = -K(1 - p)\frac{dt}{dx} \quad \ldots (4.12B)$$

and $$q_{x+dx} = -K(1 - p)\frac{d}{dx}\left(t + \frac{dt}{dx}dx\right) \quad \ldots (4.13B)$$

The heat extracted by the fluid to cool the element dx is

$$dq = q_x - q_{x+dx} = \dot{M} C_p dt \quad \ldots (4.16)$$

or, substituting and differentiating, we have

$$-K(1 - p)\frac{dt}{dx} + K(1 - p)\frac{dt}{dx} + K(1 - p)\frac{d^2t}{dx^2}dx = \dot{M} C_p dt \quad \ldots (4.16B)$$

where K = Thermal conductivity of the wall material

$\dot{M}$ = Coolant mass flow rate

C_p = Specific heat capacity of the fluid

At $0 \leq x \leq n$, equation 4.16B gives

$$\frac{d^2t}{dx^2} - \frac{\dot{M}C_p}{K(1-p)} \frac{dt}{dx} = 0 \qquad \ldots (4.17)$$

Now let

$$B = \frac{\dot{M}C_p}{K(1-p)} \qquad \ldots (4.17B)$$

The general solution of equation 4.17 is

$$t = C_1 e^{Bx} + C_2 \qquad \ldots (4.18)$$

Boundary condition for the above equation is

$$\text{at } x = 0, \quad t = t_1; \quad x = n, \quad t = t_2 \qquad \ldots (4.19)$$

For the above conditions, the values of the constants, C_1 and C_2, are

$$C_1 = \frac{t_2 - t_1}{e^{Bn} - 1} e^{Bx}; \quad C_2 = t_1 - \frac{t_2 - t_1}{e^{Bn} - 1}$$

Equation 4.18, on substituting for C_1 and C_2, yields for the origin,

$$t = t_1 + \frac{t_2 - t_1}{e^{Bn} - 1} (e^{Bx} - 1) \qquad \ldots (4.20)$$

For the case of $-\infty \leq x \leq 0$, equation 4.16B gives

$$\frac{d^2t}{dx^2} - B_f \frac{dt}{dx} = 0 \qquad \ldots (4.21)$$

where $B_f = \frac{\dot{M}C_p}{K_f}$ (for this case, $p = 0$)

K_f = Thermal conductivity of the coolant

The general solution for equation 4.21 is

$$t_f = C_3 e^{B_f x} + C_4 \qquad \ldots (4.22)$$

Boundary condition for the above equation is

$$\left.\begin{aligned} &\text{at } x = -\infty, \quad t_f = t_o \\ &\text{at } x = 0, \quad K_f \frac{dt_f}{dx} = K(1 - p)\frac{dt}{dx} \end{aligned}\right\} \qquad \ldots (4.23)$$

For the above condition, the constants of equation 4.22 are

$$C_3 = \frac{t_2 - t_1}{e^{Bn} - 1} \quad \text{and} \quad C_4 = t_o$$

Substituting, equation 4.22 gives

$$t_f = t_o + \frac{t_2 - t_1}{e^{Bn} - 1} e^{B_f x} \qquad \ldots (4.24)$$

Based on equation 4.24, the temperature t_1 in equation 4.20 may be eliminated. At $x = 0$,

$$t_f = t_1 = t_o + (t_{w2} - t_o)e^{-Bn} \qquad \ldots (4.25)$$

By substituting for t_1 in equation 4.20, the temperature distribution in the porous wall is

$$\frac{t - t_o}{t_2 - t_o} = e^{-Bn(1-x/n)} \qquad \ldots (4.26)$$

Knowing t_1 from equation 4.25 and the temperature at the surface of the wall, t_2, the heat transfer in the porous wall may be expressed as

$$Q_1 = \dot{M} C_p (t_2 - t_o) \qquad \ldots (4.27A)$$

From Newton's law of cooling, Q_1 may be represented as

$$Q_1 = h_i A(t - t_o) \qquad \ldots (4.27B)$$

Combining equations 4.27A and 4.27B, the heat transfer coefficient in the wall can be shown to be

$$h_i = \frac{\dot{M}C_p}{A}\left(\frac{t_2 - t_o}{t - t_o}\right) \qquad \ldots (4.28)$$

For improved computation of h_i, the mean temperature inside the wall should be preferred. Representing the dimensionless temperature in equation 4.26 by R, the mean temperature in the wall for a given value of Bn is

$$\overline{R} = \frac{1}{n}\int_o^n R\,dx$$

$$\overline{R} = \frac{\overline{t} - t_o}{t_2 - t_1} = \frac{1}{Bn}(1 - e^{-Bn}) \qquad \ldots (4.29)$$

From equation 4.29, the heat transfer coefficient in the wall is

$$\overline{h_i} = \frac{\dot{M}C_p}{A}\left(\frac{t_2 - t_o}{\overline{t} - t_o}\right) = GC_p\left(\frac{t_2 - t_o}{\overline{t} - t_o}\right) \qquad \ldots (4.30)$$

$$\simeq \text{const. } G \text{ (for a constant operating temp.)}$$

where A = Effective area for fluid flow.

The above derivation is liable to error because of the assumptions made. But the correlation of Smith et al is of the same format as in equation 4.30. The correlation, equation 4.11, was said to have an error of ± 20%.

In the analysis of the work reported here, the correlations of Bayley et al and Smith et al have been adopted.

4.2.3 Film Heat Transfer

The coolant after removing heat in the interstitial of the porous wall ejects into the mainstream in the form of micro-diameter jets at variable pore outlet angles. The coolant jets are quickly deflected, coalesce and remain attached to the wall's surface as a protective cool film.

In the case of attached film, the convection to the wall from the mainstream may be very small and at a high coolant flow rate the convection may be reduced to zero. At a zero convection to the wall, the temperature of the entire wall is the same as that of the coolant at inlet. When this stage is reached, the ideal cooling mechanism of transpiration system is said to have been achieved (1).

In determining the convective heat transfer to the surface of the porous wall from the mainstream, Grootenhuis employed the Naiver-Stokes equation and the energy balance equation, while Torii et al (28) used the heat balance approach. Bayley et al (7) compute convective heat to the porous surface by assuming fully developed turbulent fluid flow in a pipe with no influence of the transpiration film on the heat transfer coefficient. They solved the forced convection equation 4.31,

$$Nu = 0.023\, Re^{0.8}\, Pr^{0.4} \qquad \ldots (4.31)$$

where both Reynolds number, Re, and Prandtl number, Pr, are based on the physical properties of the mainstream. Torii et al (28) and, more recently, Guo-Rui (40) have shown that equation 4.31 under-predicts the film heat transfer coefficient to the transpiration wall surface by up to 50%. The correlation used by Torii et al may be represented as in equation 4.32,

$$h = \rho_w C_p U_w \left(\frac{T_w - T_c}{T_g - T_w}\right) \quad \ldots (4.32)$$

where h = Local heat transfer coefficient

ρ_w = Fluid density based on wall surface temperature

C_p = Specific heat capacity of fluid

U_w = Velocity of fluid perpendicular to the surface of the wall

T_w = Wall surface temperature

T_c = Coolant temperature upstream of test wall

T_g = Mainstream temperature

Both Torii et al and Grootenuis, in the application of their correlation to the computation of heat transfer to the wall surface from the mainstream, have assumed that the coolant temperature at outlet from the wall attains the wall's surface temperature. This assumption has been made by all workers of transpiration cooling. It is part of the purpose of the work reported here to confirm whether or not this assumption is justified.

To compute the heat transfer to the surface in the work reported here, a heat balance on the porous wall has been carried out and from this the convection to the surface was computed. The process of heat balance analysis applied to the transpiration wall is fully detailed in Chapter 5 with the convection in the holes replaced by the correlation of Smith et al. Few investigations of transpiration cooling have been carried out at the high gas temperature of the present work. Under the present conditions, radiative heat loss to the duct wall and radiative heat gain from the combustion product gases have to be taken into account. The procedure used is fully described in Chapter 5. For the radiative

heat transfer, Q_{RF}, the correlation employed in Chapter 5 for effusion cooling and restated in equation 4.33 has been made use of.

$$Q_{RF} = A\sigma \frac{(1 + E)}{2} E_f T_g^{1\cdot5} [T_g^{2\cdot5} - T_p^{2\cdot5}] \quad \ldots (4.33)$$

where E = Emissivity of test wall, equation 4.6

E_f = Flame/hot gas emissivity

The emissivity of the hot gas is as in equation 5.35 of Chapter 5. If the test wall is cooler or hotter than the duct walls in which the test has been conducted, radiative heat is exchanged between the test wall and the duct. The net effect of this is radiative cooling and a higher cooling performance by the test wall than will generally be the case. To eliminate the radiative cooling effect, the radiative exchange between the test wall and its surrounding walls was computed. This correlation is as analysed in Chapter 5 and restated in equation 4.34,

$$Q_n = \frac{AE}{(1 - E)} (\sigma T_p - W_1) \quad \ldots (4.34)$$

where W_1 = Radiosity leaving the duct walls and analysed in Chapter 5.

By computing all the heat transfer in the cooling system, the convection, Q_f, to the wall surface was deduced as in equation 4.35,

$$Q_f = Q_{rb} + Q_i + Q_n - Q_{RF} \quad \ldots (4.35)$$

From equation 4.35, the local heat transfer coefficient is represented as

$$H_f = \frac{Q_f}{A(T_g - T_p)} \quad \ldots (4.36)$$

4.3 PRESSURE DROP AND COOLANT MASS FLOW IN POROUS WALL

Successful application of transpiration cooling requires not only a heat transfer analysis of the system but also a knowledge of the pressure drop across the porous wall and the fluid flow characteristics. The flow through the porous wall, such as employed in the present work, is complicated by the fact that the method of manufacture of the wall is such that the pores are not necessarily continuous through the wall.

Some of the pores terminate midway through the wall (32) and the higher the permeability of the wall the greater the proportion of continuous pores. Because of the non-continuity of some of the pores, the flow may change from laminar to turbulent. If the flow through the wall is laminar, the pressure drop across the wall will be proportional to the coolant flow rate as shown in equation 4.37A,

$$\dot{M} \alpha (P_1 - P_2) \qquad \ldots (4.37A)$$

Investigators of transpiration cooling system (7,31,32) have shown, however, that the pressure drop across the porous wall may be correlated as in equation 4.37B,

$$\dot{M} = f(P_1, P_2, T, n) \qquad \ldots (4.37B)$$

$$\dot{M} = C\left(\frac{P_m dP}{T^m}\right)^n \qquad \ldots (4.38)$$

where $\dot{M} = G$ = Coolant mass flow rate per unit surface area

C = Constant

P_m = Mean pressure

dP = Pressure loss $(P_1 - P_2)$

P_1 = Upstream pressure of test wall

P_2 = Downstream pressure of test wall

Now the mass flow rate of the coolant may be correlated as in equation 4.38B,

$$G = C_D A(2\rho\, dP)^n \qquad \ldots (4.38B)$$

where C_D = Discharge coefficient

A = Total test area

The density, ρ, is

$$\rho = \frac{P_1}{RT} \qquad \ldots (4.38C)$$

Equation 4.38B is the equation for correlating fluid flow in the effusion wall where the exponent n takes the value of 0.5.

Combining equation 4.38C with equation 4.38B at constant temperature, T, of coolant, equation 4.38D is obtained.

$$G = C(P_1\, dP)^n \qquad \ldots (4.38D)$$

where C is a constant.

Equation 4.38D is similar to equation 4.38. The present work was done at constant coolant temperature, T, and equation 4.38D may be expressed as

$$\log G = \log C + n \log (P_1\, dP) \qquad \ldots (4.39)$$

The constant C is the parameter which indicates the permeability of the test wall while the index n in equation 4.38D is largely to do with the viscosity effect of the fluid as it flows through the wall. The values of C and n will be determined under cross-flow condition in this work.

4.4 OVERALL AND ADIABATIC COOLING EFFECTIVENESS

To quantify the performance of the transpiration system, previous workers have normally expressed their result in a dimensionless temperature form as in equation 4.40,

$$\eta_{ov} = \frac{T_g - T_w}{T_g - T_c} \qquad \ldots (4.40)$$

where η_{ov} = Overall cooling effectiveness

T_g = Mainstream gas temperature

T_w = Temperature of the porous wall

T_c = Coolant temperature upstream of wall

In conventional cooling systems using slot injection, it is usual to express the cooling effectiveness in terms of an adiabatic wall temperature. The adiabatic wall temperature is the temperature, T_{ad}, of the fluid at the proximity of the wall. Adiabatic cooling effectiveness is defined as

$$\eta_{ad} = \frac{T_g - T_{ad}}{T_g - T_c} \qquad \ldots (4.41)$$

The adiabatic temperature which is regarded as the wall temperature with no heat within the wall is measured by traversing the boundary layer measuring thermocouples until they touch the wall. This is confirmed by physically moving the thermocouples to touch the wall's surface. The temperatures indicated at different coolant flow rates were then recorded. The temperatures of the wall were taken as those indicated by the five thermocouples attached to the rear of the test wall.

Both the adiabatic and overall cooling effectiveness of the transpiration system are presented in the result.

4.5 ANALYSIS OF DATA

A computer program has been developed to analyse the data obtained in this work. The format of the computer program is similar to that developed for perforated plates and is shown in Chapter 5.

4.6 EXPERIMENTAL RESULTS AND DISCUSSION

4.6.1 Boundary Layer Temperature Profiles

The boundary layer temperature profiles for the three Rigidmesh grades for a range of coolant injections per unit surface area, G, are shown in figs. 4.1-9 for three axial positions, downstream of the leading edge, of 25.4, 76.2 and 127 mm respectively.

The temperature profiles have been expressed in a non-dimensional form, T_{tb}, to give thermal boundary layer profile, as in equation 4.42.

$$T_{tb} = \frac{T - T_w}{T_g - T_w} \qquad \ldots (4.42)$$

where T = Local gas temperature in the boundary layer

T_w = Measured wall temperature at the axial location of the traverse (see Chapter 2)

T_g = Gas temperature upstream of test section

The graphs for the thermal boundary layer at the leading edge for the three Rigidmesh grades show a thin boundary layer at this location, with RM50A and RM10A giving similar profiles, slightly different from that of RM50B. Thereafter the temperature profiles at locations 76.2 and 127 mm demonstrate a rapid thickening of the thermal boundary layer with high coolant flow rate (G) giving the

thickest. To show the influence of coolant flow rate, axial distance and characteristics of transpiration material on thermal boundary layer thickness, the distance at which T_{tb} equals 0.9 has been determined. This distance for each coolant injection is presented in table 4.3.

TABLE 4.3

Rigidmesh	Axial Distance - mm	G - kg/sm^2 → 0.13	0.27	0.6	1.6
		Distance in mm at which T_{tb} = 0.9			
RM50A	25.4	2	4	6	10
	76.2	5	10	15	23
	127.0	7	15	22	33
RM10A	25.4	1.5	1.5	3	6
	76.2	2	5	9	15
	127.0	5	9	15	25
RM50B	25.4	2	2	5	11
	76.2	5	7	17	27
	127.0	8	13	26	39

Table 4.3: Thermal boundary layer thickness

Table 4.3 shows the similarity in boundary layer thickness with axial distance. It also demonstrates increased thickness with increasing axial distance for the three grades of rigidmesh. In all respects the profiles for RM50A and RM50B are generally similar. This may be due to the fact that both have the same pore sizes of

50 micron, while that of RM10A is only 10 micron. The similarity between RM10A and RM50A at the leading edge may be put down to the fact that both have nearly the same permeability while that of RM50B is about a factor of 43 greater. Because of the large permeability of RM50B, one would expect the profiles of this wall to be different from the rest but this was not the case. The reason for this may be found in the manufacture of the wall materials. The pictures of the surface of the wall materials taken under magnified microscope (see transpiration plate - 1,2,3 in appendix) reveal numerous micro-pores with differing opening angles. The pictures also show significant surface roughness. The opening on RM50B is much larger than the rest and this will lead to a reduction in jet stirring of the boundary layer in comparison with RM50A and RM10A. This characteristic will give RM50B improved film protection of the surface and hence good cooling effectiveness. As the pore size of RM10A is smaller than the rest, the jets leaving the surface of this wall will easily be deflected and coalesce and will not give as much boundary layer stirring. This may explain why the boundary layer for this particular wall is thin. One would expect a better film protection from this wall than will be the case for RM50A. Figure 4.10 shows the comparison of the thermal boundary layer profile for the three walls at two coolant injection rates, 1.6 and 0.27 kg/m^2, and at axial distance of 127 mm. At a distance of less than 5 mm from the wall, the profiles converge to nearly the same point for all the plates at a lower coolant injection rate of 0.27 kg/sm^2 while at a high coolant injection rate the local temperature at the surface of RM50A is much higher than the rest. This is an indication of hot gas entrainment to the surface of RM50A and hence poor film protection.

Figure 4.11 shows the profile of film temperature with coolant injection for the three walls. Almost all previous workers on the transpiration system take the coolant outlet temperature as being equal to the wall temperature in the computation of convective heat transfer to this surface (1,28). However the results of figure 4.11 show that this is a wrong assumption and hence predictions based on this assumption will also be wrong. This figure also confirms the improved film protection of RM50B and worst protection for RM50A.

4.6.2 Cooling Effectiveness

Figures 4.12-14 show the overall and adiabatic cooling effectiveness for RM50A, RM10A and RM50B respectively at three axial locations with coolant injection. For RM50A, fig. 4.12, the overall cooling effectiveness for the three axial locations can be represented by a single curve. This is an indication of the uniformity of coolant heat removal in the wall. The adiabatic cooling effectiveness does increase with distance but this does not result in a corresponding influence on the overall cooling effectiveness. For walls RM10A and RM50B, figs. 4.13 and 4.14, the overall cooling effectiveness shows some influence of axial distance for the various coolant flow rates examined. The adiabatic cooling effectiveness, η_a, for the three locations is also represented on these graphs and for the three Rigid Mesh types there is a significant improvement in η_a with axial distance.

The comparison between overall and adiabatic cooling effectiveness indicates the proportion of the effectiveness that is due to interstitial heat removal by the coolant. The heat removal from the wall is shown to be significant at a low coolant flow rate of below 0.8 kg/sm^2 while the cooling effectiveness is predominantly

due to good film protection at flow rates greater than 0.8 kg/sm^2. Figs. 4.15, 4.16 and 4.17 give the dimensionless axial development of overall and adiabatic cooling effectiveness at two coolant injection rates of 0.583 and 0.27 kg/sm^2. The overall cooling effectiveness displays an approximately flat profile except for coolant at 0.27 kg/sm^2. This flat profile is not repeated in the adiabatic cooling effectiveness; instead there is an improvement with axial distance due to the growth in the boundary layer thickness.

Figure 4.18 compares the three Rigid Mesh types for the overall and adiabatic cooling effectiveness, while fig. 4.19 gives this comparison as the axial profile at two coolant injections of G = 0.583 and 0.269 kg/sm^2 respectively. Figure 4.18 shows that at lower coolant injection rates of below 0.8 kg/m^{2}s, the overall cooling effectiveness of transpiration wall RM50B is the best of the three walls, while that of RM50A is the worst. This result is not totally confirmed by the adiabatic profiles, however, but it still shows that for RM50A the adiabatic effectiveness is still the worst. The result here is a reflection of the film protection shown in the thermal boundary layer profiles of figures 4.1-14. The result shown in fig. 4.19 for the cooling effectiveness as a function of axial distance confirms the near flat profile of axial overall cooling effectiveness while that of the adiabatic improves with axial distance. The difference between η for 0.583 kg/sm^2 and 0.269 kg/sm^2 is only about 10%, while that for the adiabatic effectiveness is up to 40%.

The main feature of figs. 4.18 and 4.19 is that film cooling is the dominant process of transpiration cooling at G values greater than or equal to 0.269 kg/sm^2 at thermal locations of 127 mm and

this is confirmed by the closeness of cooling points at this location in fig.4.19.

Figure 4.20 compares the present work overall cooling effectiveness results at thermal location 127 mm for various coolant injections G - kg/sm^2 with those of other workers. The present results for both RM50B and RM10A are superior to those of the rest. It is only the upper limit data of the Lamilloy (8) wall and the result of Jakob (3), in which nitrogen was used as coolant, that match the present results of RM50A at high coolant injection rate.

For the same coolant injection below 0.8 kg/sm^2, the worst results of the present investigation are superior to those of Lamilloy (8), Transply (9) and Bayley et al (7). The data of Transply are for five different designs and although all fall below the present results, they do indicate that a high cooling effectiveness can be achieved at low G values. The same is true for Lamilloy for which the maximum and minimum cooling effectiveness for a range of designs was represented.

4.6.3 Heat Transfer Processes

The heat transfer within the transpiration wall has been shown to be of importance in the good cooling performance of this cooling technique. The results of the heat removed in the porous walls are presented in figs. 4.21-23. Generally the figures indicate that with a decrease in coolant injection there is an increase in the heat removed in the wall. This is the process that compensated for the deterioration in the heat sink provided by the surface coolant film at low G. The profiles of this heat transfer in RM50A and RM10A do not show the sort of continuous curve evident at coolant injection rates greater than 0.4 kg/sm^2. For RM50A there was an initial

increase up to a point, then a fall-off with increase in coolant injection. That of RM10A is a sharp fall-off then an increase and a continuous trend of decreases with increase in coolant injection rate. RM50B shows, in fig.4.23, a continuous trend of heat removal fall-off with coolant injection increases. The reason for the rise and fall, at low coolant injection rates below 0.4 kg/sm^2, of heat removal in RM50A and R10A may be found in the fluid flow aerodynamics. The early region indicates a laminar fluid flow followed by a transition region and the continuous sections of the graph are regions of turbulent flow.

Figure 4.24 shows the results of the heat transfer coefficients in the wall according to correlations of Smith and Watts (17) and Bayley et al (7). For the three walls, for the range of G values examined, the heat transfer coefficient, according to the correlation of (17), may be represented by a single line, while each transpiration wall gives a different heat transfer coefficient with Bayley's correlation. Generally, the coefficient increases with increases in coolant injection rates. To resolve the problem of heat transfer coefficient posed by these two correlations, a separate investigation, where the coefficient is measured directly for the range of coolant injections examined here, has been arranged for the future in the ongoing research in this field.

The results of film heat transfer coefficient for the three walls are presented in fig.4.25 as a function of G at thermal location 127 mm. The figure indicates a higher heat transfer to the surface of RM50A from the mainstream than the other two walls. For RM50B, the result shows a more uniform trend of heat transfer to the wall than the other walls, with a sharp increase at G less than 0.4 kg/sm^2.

The profile of RM10A is similar to that of RM50A, with both showing a rise at G greater than 0.2 kg/sm^2, followed by a continuous fall at coolant injection rates above 0.3 kg/sm^2. This trend of RM10A and RM50A indicates a change in the film gas flow aerodynamics, that is from laminar to transition then to turbulence in the vicinity of the wall. In summary, fig. 4.25 indicates that the coolant film protection at high coolant injection rate is very effective to the extent that the convective heat transfer to the wall from the mainstream is reduced to a mere trickle. For the three walls, at low coolant injection rates, there is a high heat transfer to the wall's surface. It can be concluded that at high coolant flow rates film protection of the wall is the dominant factor responsible for the wall cooling performance while at low coolant injection, heat removal from the wall is responsible for the transpiration wall cooling performance.

Figure 4.26 shows the axial profiles of the film heat transfer coefficient for the three walls at $0.566 \leqslant G - kg/sm^2 \leqslant 0.61$ and $0.265 \leqslant G - kg/sm^2 \leqslant 0.273$. The results for RM50B at both G values and RM10A at G = 0.6 kg/sm^2 show a continuous improvement of the film protection downstream of the leading edge. This results from the development of the film cooling boundary layer. For RM50A at both G values and RM10A at G = 0.27, the film heat transfer coefficient first decreases then increases with axial distance. These effects can be found back to very small differences in the axial variation in the overall cooling effectiveness in figs. 4.15-17 and could be due to temperature measurement errors.

Figure 4.27 shows the comparison between the film heat transfer obtained using the heat balance process discussed in sections 4.2.1 to 4.2.3, with the correlation of Torii et al (28). The difference

between the present results and those obtained using Torii's correlation is about a factor of 4. The reason for this may be that Torii et al's work was carried out at a low temperature of 50 °C and adequate attention to changes at high temperature in fluid transport properties was not given. The viscosity and thermal conductivity of gases at temperatures greater than 50 °C increase to about 0.8 power (35) of the absolute temperature while the density varies inversely with the first power of the temperature.

Finally, the irregularities in the profiles of heat transfer for both RM50A and RM10A may be due to their low permeability. In 'sintered wire', as is the case in this investigation, the lower the permeability the less are the chances of pores' continuity from one side of the 'sheet' to the other, that is, some of the pores are dead ends (32) which enhances the three flow regimes of laminar, transition and turbulence. The larger the permeability, the greater the chances of all the pores being continuous from one side to the other, which enhances a single flow pattern through the wall. RM50B has large permeability and hence a different behaviour from RM50A which has the same pore size but a permeability much less than that of RM50B.

4.6.4 Pressure Loss and Coolant Correlation

Figure 4.28 shows the profiles of the pressure loss as the coolant flows through the wall in accordance with equation 4.37A. The figure indicates that, except at low coolant injection regimes, the profiles for the three walls are mostly straight lines. The change of gradient at low coolant injection rates may be attributed to the effect of cross-flow. The results also show that RM10A is a high pressure loss wall while RM50B is of very low pressure loss.

The results of equation 4.38D are presented in fig.4.29. Apart from RM50B, the plot is fairly linear. The best straight lines through the data have been drawn using the least square fit method. There is a small scatter of the data, which is most pronounced in RM50B. The reason for the scatter in RM50B may partly be associated with small particle blockage in localised areas and also the effect of cross-flow. The coolant air was filtered before reaching the test wall but this may not get rid of micro-particles.

The constant C and exponent n of equation 4.38D were determined using least square (43), and their values are presented in table 4.4.

TABLE 4.4

	RM50A	RM10A	RM50B
C	1.65×10^{-7}	1.52×10^{-7}	1.36×10^{-11}
n	0.761 ± 0.01	0.706 ± 0.02	1.47 ± 0.1
C (at G > 0.5 kg/sm^2)			1.78×10^{-6}
n (at G > 0.5 kg/sm^2)			0.766 ± 0.03

Table 4.4: Values of constant C and exponent n in equation 4.38D

The values of C and n for RM50A and RM10A are of the same magnitude with an error of ± 0.01 and ± 0.02 respectively for n, while values for RM50B are completely different. The reason for this may be due in part to RM50B's very low pressure loss characteristics coupled with high permeability. For RM50B there is a discontinuity in the data in fig.4.28 between G = 0.4 and 0.5 kg/sm^2 and this gives the high value for n in fig.4.29. The reason for the discontinuity

is not known. The values of C and n for $G > 0.5$ kg/sm^2 are also shown in table 4.4 when the values of C and n are in close agreement with the other Rigid Mesh design. It may be concluded that in the coolant flow pressure loss relationship, the value of n in Rigid Mesh is higher than its value of 0.5 in the effusion wall, but lower than the value of unity for laminar flow.

4.7 CONCLUSIONS

(1) Transpiration cooling results in a thermal boundary layer whose thickness increases with axial distance and no steady state thickness was found within the present 127 mm measurement limit.

(2) The cooling effectiveness of the transpiration wall is a function of the wall's permeability; the higher this parameter, the better the wall's cooling effectiveness.

(3) Film cooling is a major proportion of the overall cooling effectiveness at all coolant injection rates and is the dominant process at $G > 0.8$ kg/sm^2.

(4) Transpiration wall cooling cuts the cooling air requirement for effective wall protection compared with conventional methods by a factor of 4.

(5) Heat removal in transpiration walls is an important contributor to high overall cooling effectiveness at low G values.

(6) The flow aerodynamics in the wall as well as in the film boundary layer are a function of the characteristics of the sintered porous walls.

(7) Empirical correlation relating coolant injection flow rate to wall pressure loss in Rigid Mesh in the presence of cross-flow has been proposed.

4.8 REFERENCES

1. Grootenhuis, P., 'The mechanism and application of effusion cooling', J. Roy. Aero. Soc., Vol. 63, pp. 73-89, Feb. 1959.

2. Bayley, F.J., and Turner, A.B., 'The heat transfer performance of porous gas turbine blades', J. Roy. Aero. Soc., Vol. 72, pp. 1087-1094, Dec. 1968.

3. Jacob, M., and Fieldhouse, I.B., 'Cooling by forcing a fluid through a porous plate in contact with a hot gas stream', Proc. 2nd Symp. on Heat Trans. and Fluid Mech., ASME, pp. 191-200, 1949.

4. Duwez, P., and Wheeler, H.L., 'Experimental study of cooling by injection of a fluid through a porous material', J. Aero. Sciences, Vol. 15, No. 9, pp. 509-521, Sept. 1948.

5. Wheeler, H.L., and Duwez, P., 'Heat transfer through sweat cooled porous tubes', Jet Propulsion, pp. 519-524, Oct. 1955.

6. Bland, D.R., 'Mathematical theory of the flow of a gas in a porous solid and of the associated temperature distributions', Proc. of Royal Soc., Vol. 221 A, pp. 1-28, 1954.

7. Bayley, F.J., Cornforth, J.W., and Turner, A.B., 'Experiments on a transpiration cooled combustion chamber', Proc. Instn. Mech. Engrs., 1973.

8. Nealy, D.A., and Reider, S.B., 'Evaluation of laminated porous wall materials for combustor liner cooling', Trans. ASME - J. Eng. Power, Vol. 102, pp. 268-276, April 1980.

9. Wassell, A.B., and Bhangu, J.K., 'The development and application of improved combustor wall cooling techniques', ASME Paper 80-GT-66.

10. Wolf, J., and Moskowitz, S., 'Development of the transpiration air-cooled turbine for high-temperature dirty gas streams', ASME - J. Eng. Power, Vol. 105, pp. 821-825, Oct. 1983.

11. Bayley, F.J., 'Performance and design of transpiration-cooled turbine blading', AGARD CP No. 229, High Temp. Problems in Gas Turbine Engines, Feb. 1978.

12. Morris, A.W.H., Bullard, J.B., and Wigg, L.D., 'Experimental evaluation of a transpiration cooled nozzle guide vane', AGARD CP No. 229, High Temp. Problems in Gas Turbine Engines, Feb. 1978.

13. Andrews, S.J., Ogden, H., and Marshall, J., 'Some experiments on an effusion cooled turbine nozzle blade', NGTE CP No. 267, Note No. NT132, May 1954.

14. Bartoo, E.R., Schafer, Jr., L.J., and Richards, H.T., 'Experimental investigation of coolant-flow characteristics of a sintered porous turbine blade', NACA RM E51K02, 6 Feb., 1952.

15. Koh, J.C.Y., and Stevens, R.L., 'Enhancement of cooling effectiveness by porous materials in coolant passage', ASME - J. Heat Transfer, pp. 309-311, May 1975.

16. Essman, D.J., Vogel, R.E., Tomlinson, J.G., and Novick, A.S., 'TF41/Lamilloy accelerated mission test', AIAA-81-1349, AIAA/SAE/ASME 17th Joint Prop. Conf., 27-29 July, 1981.

17. Smith, I.E., and Watts, M.J., 'Radiation heat transfer to a porous surface cooled by a transpiring flow', Combustion and Heat Transfer in Gas Turbine Systems, edited by E. R. Nonter, Perg. Press, pp. 207-228, 1971.

18. Goldstein, R.J., Shavit, G., and Chen, T.S., 'Film-cooling effectiveness with injection through a porous section', Trans. ASME - J. Heat Transfer, pp. 353-361, Aug. 1965.

19. Grootenhuis, P., Mackworth, R.C.A., and Saunders, D.A., 'Heat transfer to air passing through heated porous metals', Instn. Mech. Engrs., Proc. Gen. Discussion on Heat Transfer, pp. 363-366, March 1951.

20. Andrews, G.E., and Asere, A.A., 'Transpiration cooling of gas turbine combustion chamber walls', First UK National Heat Transfer Conference, Leeds, I. Chem. E. Symposium Series No. 86, pp. 1047-1056, 1984.

21. Sparrow, E.M., and Ortiz, M.C., 'Heat transfer coefficients for the upstream face of a perforated plate positioned normal to an oncoming flow', Int. J. Heat Mass Transfer, Vol. 25, No. 1, pp. 127-135, 1982.

22. Gray, W.A., and Muller, R., 'Engineering Calculations in Radiative Heat Transfer', Pergamon Press, Oxford, 1974.

23. Bayley, F.J., and Turner, A.B., 'Transpiration-cooled turbines', AGARD CP173-71, High Temp. Turbines Conf., 1970.

24. Epifanov, V.M., and Leontjev, A.I., 'Heat and mass transfer in transpiration cooled turbine blade', Proc. 7th Int. Heat Transf. Conf., Vol. 6, pp. 61-65, 1982.

25. Holman, J.P., 'Heat Transfer', 5th Edition, McGraw Hill International Book Company, 1981.

26. Colladay, R.S., and Stepka, F.S., 'Examination of boundary conditions for heat transfer through a porous wall', NASA TN D-6405, 1971.

27. Curry, D.M., 'Two-dimensional analysis of heat and mass transfer in porous media using the strongly implicit procedure', NASA TN D-7608, 1974.

28. Torii, K., Nishiwaki, N., and Hirata, M., 'Heat transfer and skin friction in turbulent boundary layer with mass injection', Proc. 3rd Int. Heat Transfer Conference, pp. 34-48, 1966.

29. Nealy, D.A., 'Combustor cooling - Old problems and new approaches', A Project Squid Workshop, Gas Turbine Combustor Design Problems, Ed. by A.H. Lefebvre, Hemisphere Publishing Corp., 1980.

30. Nealy, D.A., Reider, S.B., and Mongia, H.C., 'Alternate cooling configuration for gas turbine combustion system', AGARD CPP-390, Heat Transfer and Cooling in Gas Turbines, Paper 25, 1985.

31. Anderson, R.D., and Nealy, D.A., 'Final Report - Task I and II, Evaluation of laminated porous material for high temperature air-cooled turbine blades', NASA CR-72281, Jan. 1967.

32. Green, Jr., L., and Duwez, P., 'Fluid flow through porous metals', ASME - J. Applied Mech., Vol. 18, pp. 39-45, March 1951.

33. Bayley, F.J., and Cornforth, J.W., 'Design and performance of transpiration-cooled combustion systems', Proc. Instn. Mech. Engrs., Vol. 191, 1977.

34. Andrews, G.E., Asere, A.A., and Mkpadi, M.C., 'Transpiration and full coverage discrete hole film cooling', I. Chem. E., 11th Annual Research Meeting Proceedings, pp. 92-96, 1984.

35. Kays, W.M., 'Convective Heat and Mass Transfer', McGraw-Hill Book Company, New York, London, 1966.

36. Librizzi, J., and Cresci, R.J., 'Transpiration cooling of a turbulent boundary layer in an axisymmetric nozzle', AIAA Journal, Vol. 2, No. 4, April 1964.

37. Manning, G.B., Moskowitz, S., and Cole, R., 'Performance comparison between transpiration air cooled turbine 3000 ^{o}F (1649 ^{o}C) stator vanes and solid uncooled vanes', ASME Paper No. 84-GT-121.

38. Bates, R., 'Manufacture, properties and applications of sintered metal filters', Filtration, Uplands Press Ltd., Purley, Surrey, March/April 1964.

39. Andrews, G.E., Asere, A.A., and Mkpadi, M.C., 'Transpiration cooling: Contribution of film cooling to the overall cooling'. To be presented at ASME - International Gas Turbine Conference Dussendolf, 1986.

40. Guo-Rui, H., 'A theoretical analysis and experimental study of flow and heat transfer in a transpiration cooled passage', ASME Paper 85-IGT-137. Presented at the Int. Gas Turbine Symposium and Exposition, in Beijing, China, 1-7 Sept., 1985.

41. Asere, A.A., 'The breakage of coal during combustion in a fluidised bed', B.Sc. Dissertation, Dept. of Fuel and Energy, Leeds University, June 1981.

42. Incropera, F.P., and Dewitt, D.P., 'Fundamentals of Heat Transfer', John Wiley & Sons, New York, 1981.

43. Taylor, J.R., 'An Introduction to Error Analysis in the Study of Uncertainties in Physical Measurements', University Science Books, USA, 1982.

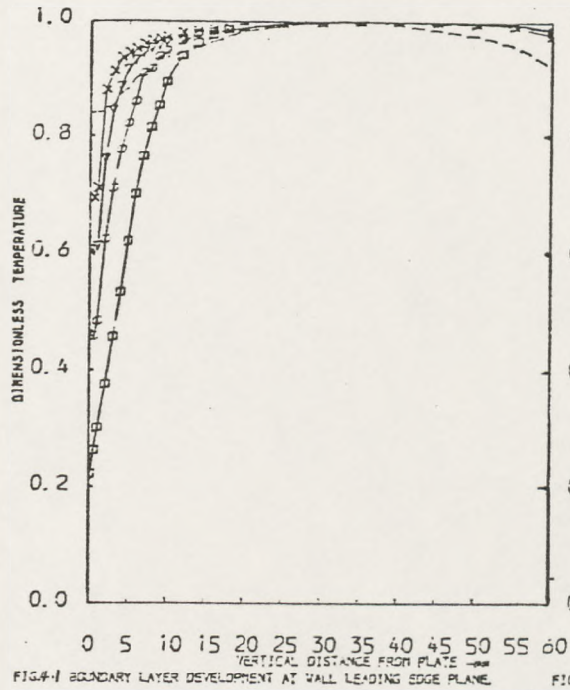

FIG.4.1 BOUNDARY LAYER DEVELOPMENT AT WALL LEADING EDGE PLANE

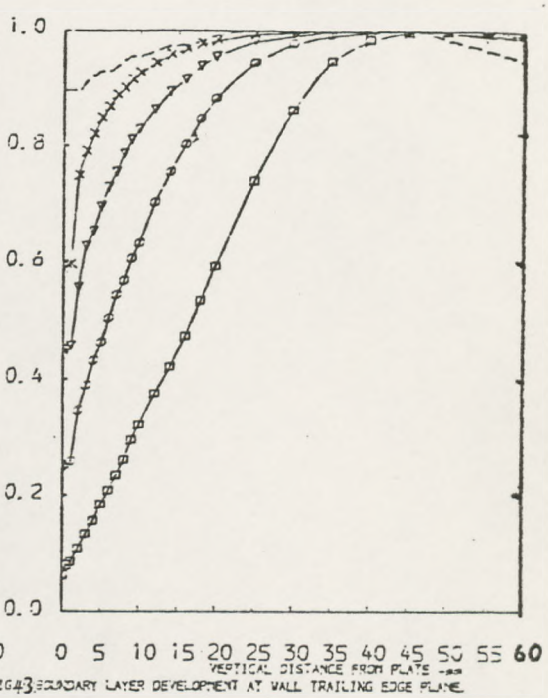

FIG.4.3 BOUNDARY LAYER DEVELOPMENT AT WALL TRAILING EDGE PLANE

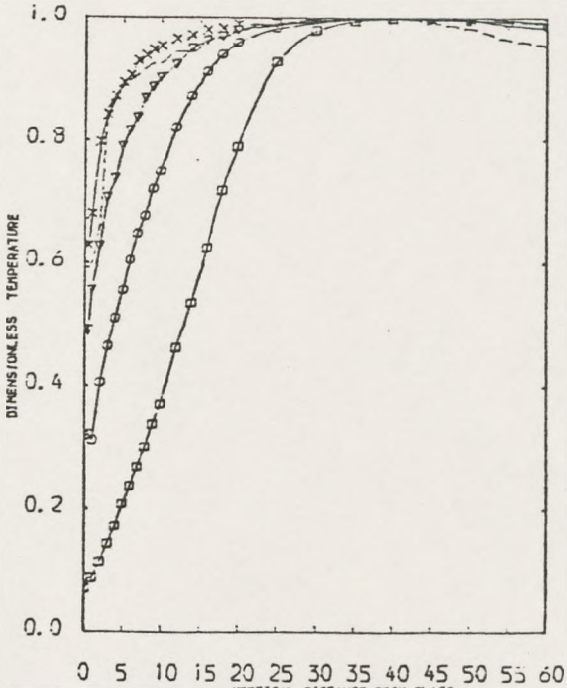

FIG.4.2. BOUNDARY LAYER DEVELOPMENT AT WALL CENTRE PLANE

TRANSPIRATION PLATE HISTORY

PERMEABILITY COEFFICIENT-$X10^{-10}m^2$ - 1.45

PORE SIZE-(micron) - 50

PLATE THICKNESS-(mm) 1.3045

WALL MATERIAL-(s. steel) RMSOA

COMBUSTOR MAINSTREAM TEMPERATURE-763k

COOLANT TEMPERATURE-292k

COOLANT FLOW RATE-$Kg/s.m^2$

p - 1.552

o - 0.574

▼ - 0.268

x - 0.131

- - 0.0

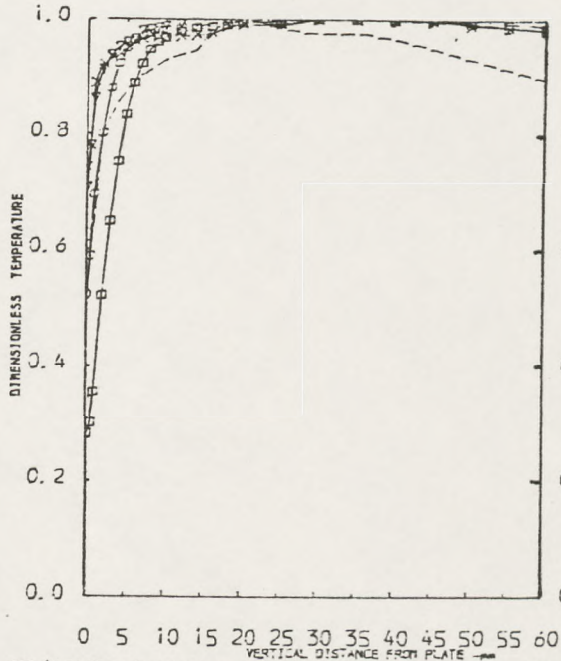

FIG.44 BOUNDARY LAYER DEVELOPMENT AT WALL LEADING EDGE PLANE.

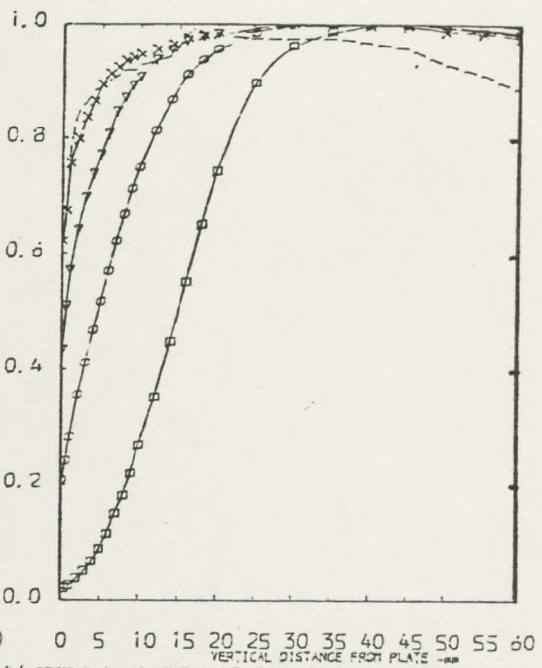

FIG.46. BOUNDARY LAYER DEVELOPMENT AT WALL TRAILING EDGE PLANE.

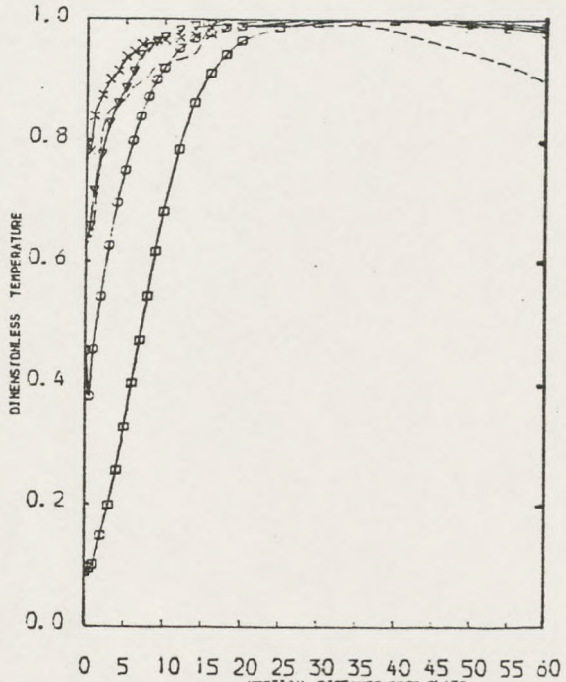

FIG45. BOUNDARY LAYER DEVELOPMENT AT WALL CENTRE PLANE.

TRANSPIRATION PLATE HISTORY

PERMEABILITY COEFFICIENT-$x10^{-10}$ m^2- 1.14

PORE SIZE-(micron) - 10

PLATE THICKNESS-(mm) 0.9051

WALL MATERIAL-(s. steel) RM10A

COMBUSTOR MAINSTREAM TEMPERATURE-765K

COOLANT TEMPERATURE-292.9K

COOLANT FLOW RATE-$Kg/s.m^2$

□ - 1.690

○ - 0.610

▽ - 0.273

× - 0.133

- - 0.0

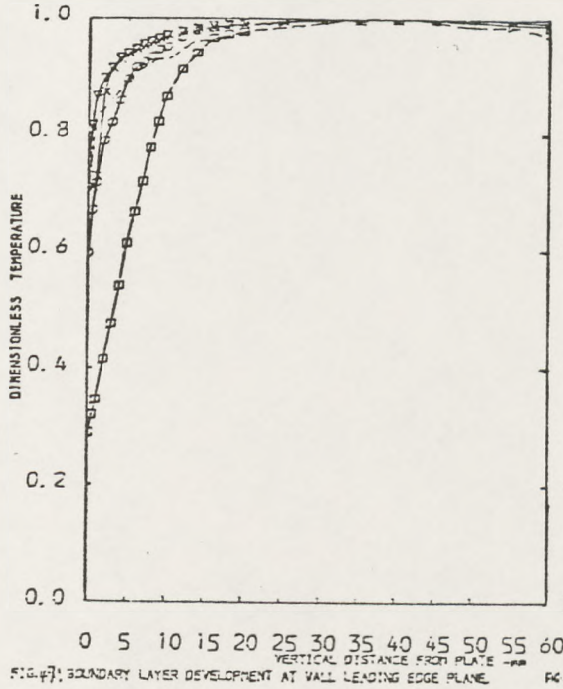

FIG 4.7 BOUNDARY LAYER DEVELOPMENT AT WALL LEADING EDGE PLANE

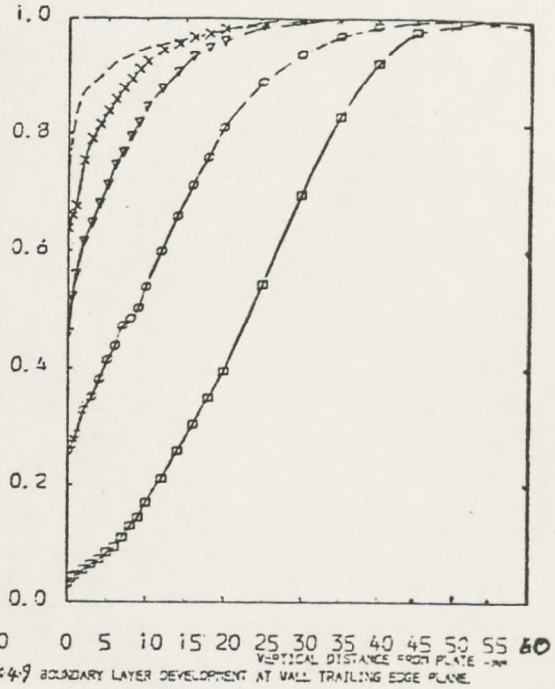

FIG 4.9 BOUNDARY LAYER DEVELOPMENT AT WALL TRAILING EDGE PLANE

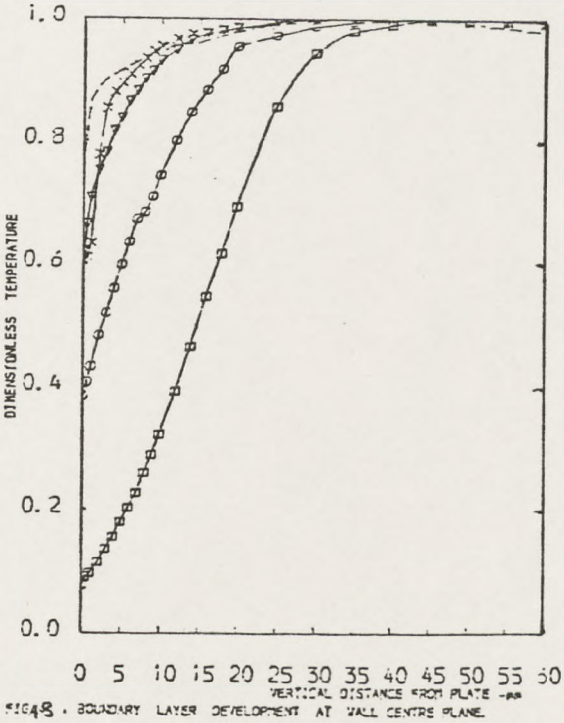

FIG 4.8 BOUNDARY LAYER DEVELOPMENT AT WALL CENTRE PLANE

TRANSPIRATION PLATE HISTORY

PERMEABILITY COEFFICIENT-$X10^{-10}$ m^2 - 55.0

PORE SIZE-(micron) - 50

PLATE THICKNESS-(mm) 0.8974

WALL MATERIAL-(s. steel) RMSOB

COMBUSTOR MAINSTREAM TEMPERATURE-769K

COOLANT TEMPERATURE-295k

COOLANT FLOW RATE-Kg/s.m^2

□ - 1.528

○ - 0.566

▼ - 0.265

x - 0.130

- - 0.0

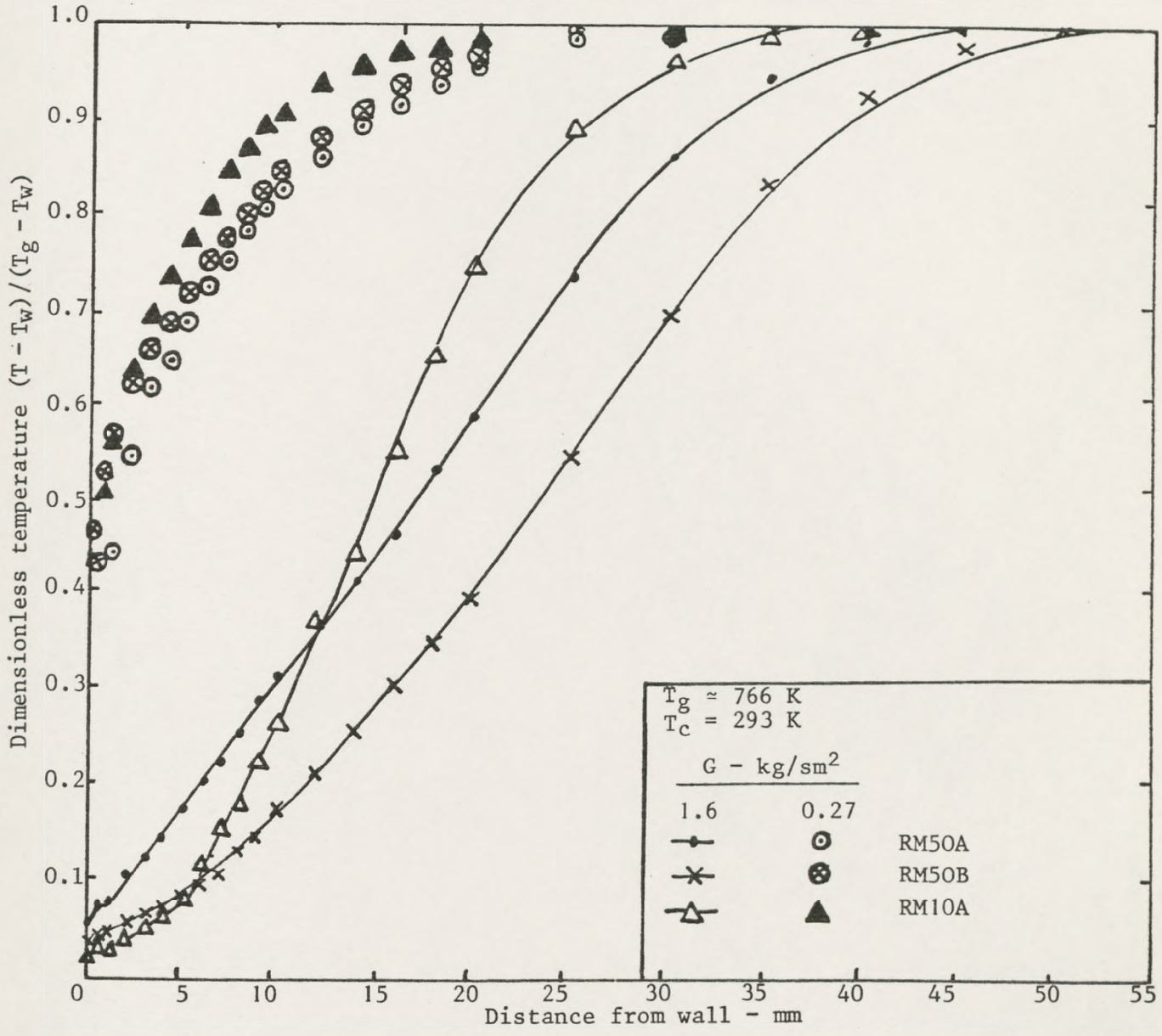

Fig. 4.10: Comparison of temperature profiles for two coolant injection rates at X = 127 mm.

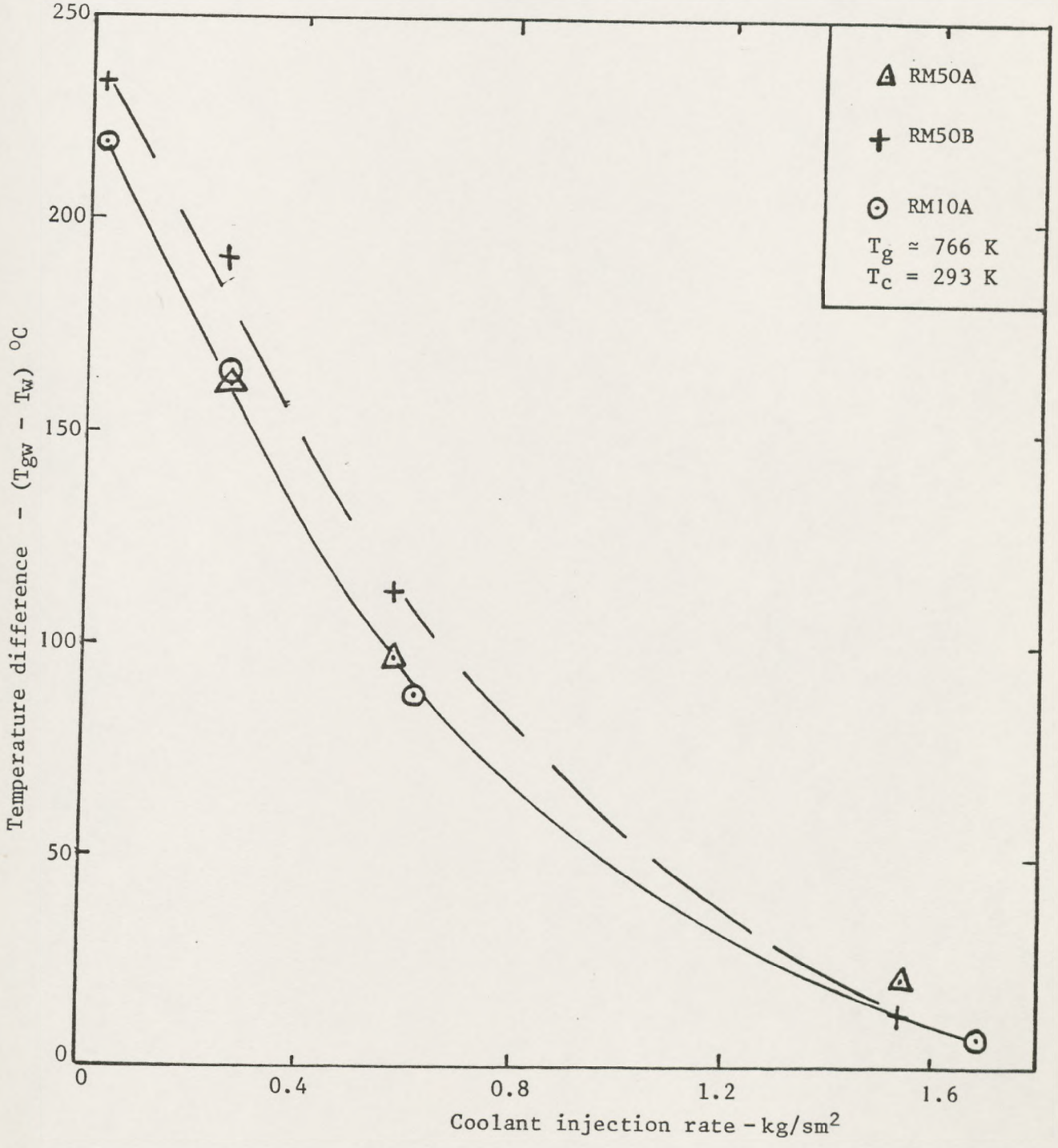

Fig. 4.11: Film temperature profile

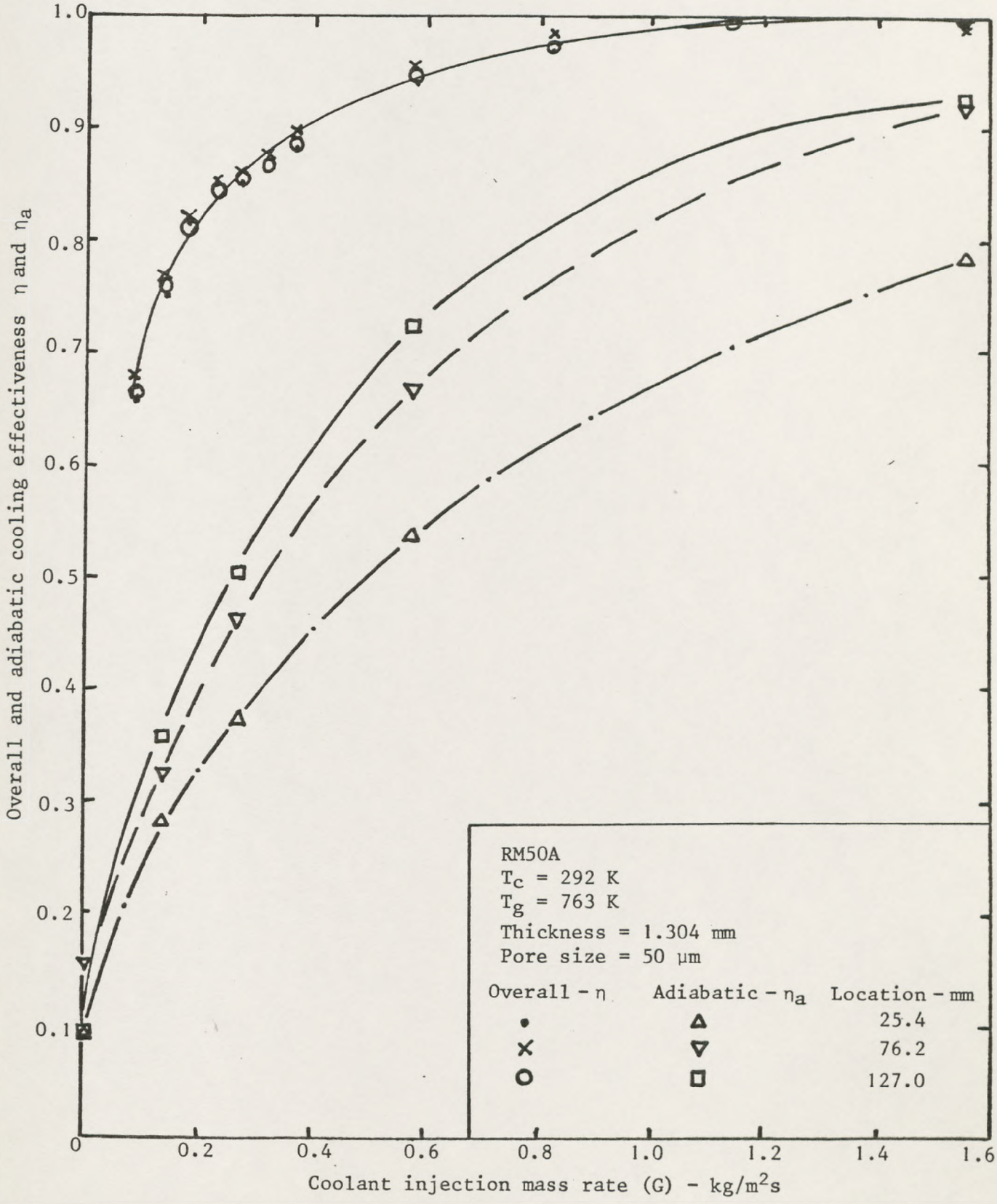

Fig. 4.12: Development of overall and adiabatic cooling effectiveness of RM50A at three thermal stations from leading edge.

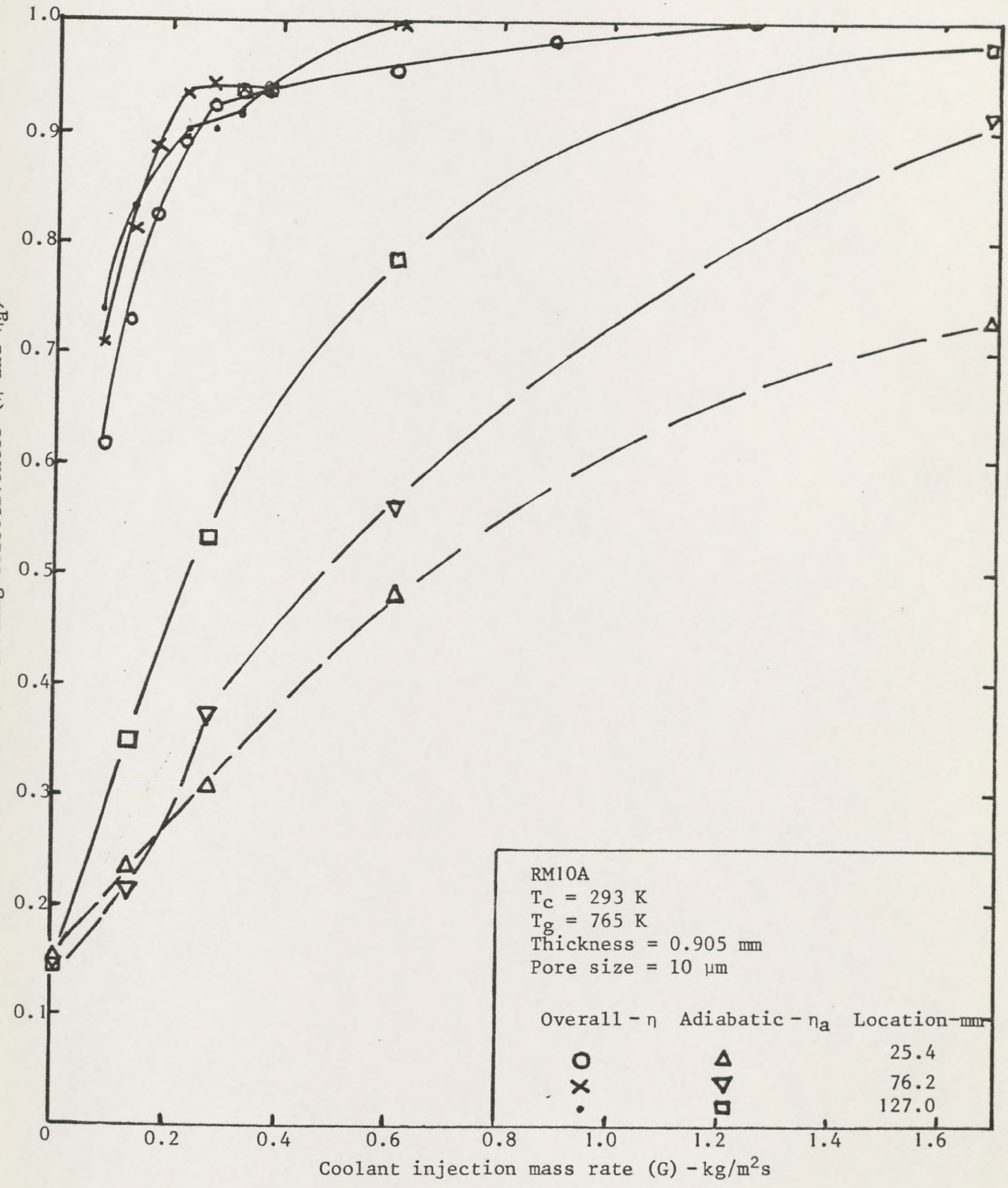

Fig. 4.13: Development of overall and adiabatic cooling effectiveness of RM10A at three thermal stations from leading edge.

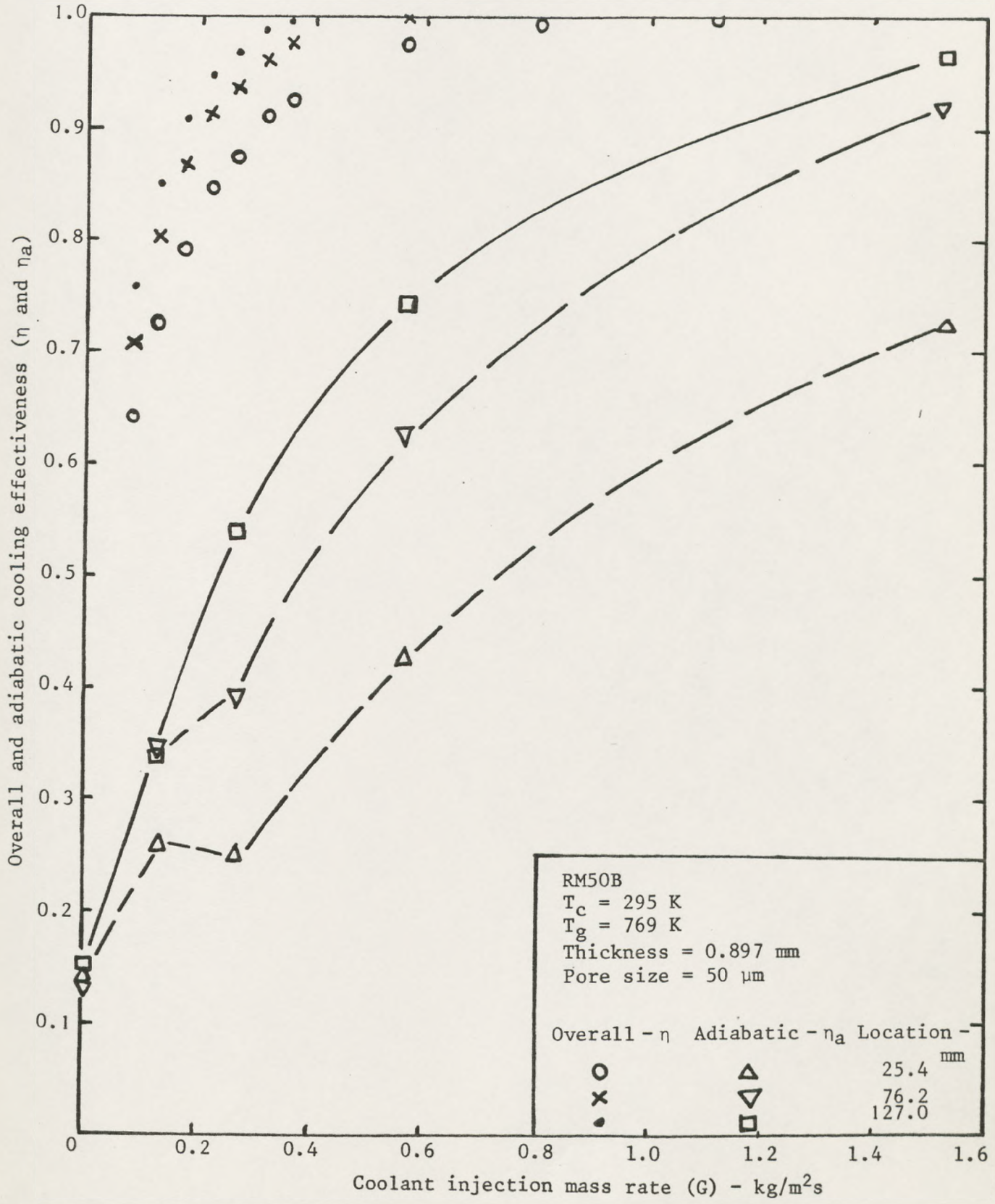

Fig. 4.14: Development of overall and adiabatic cooling effectiveness of RM50B at three thermal stations from leading edge.

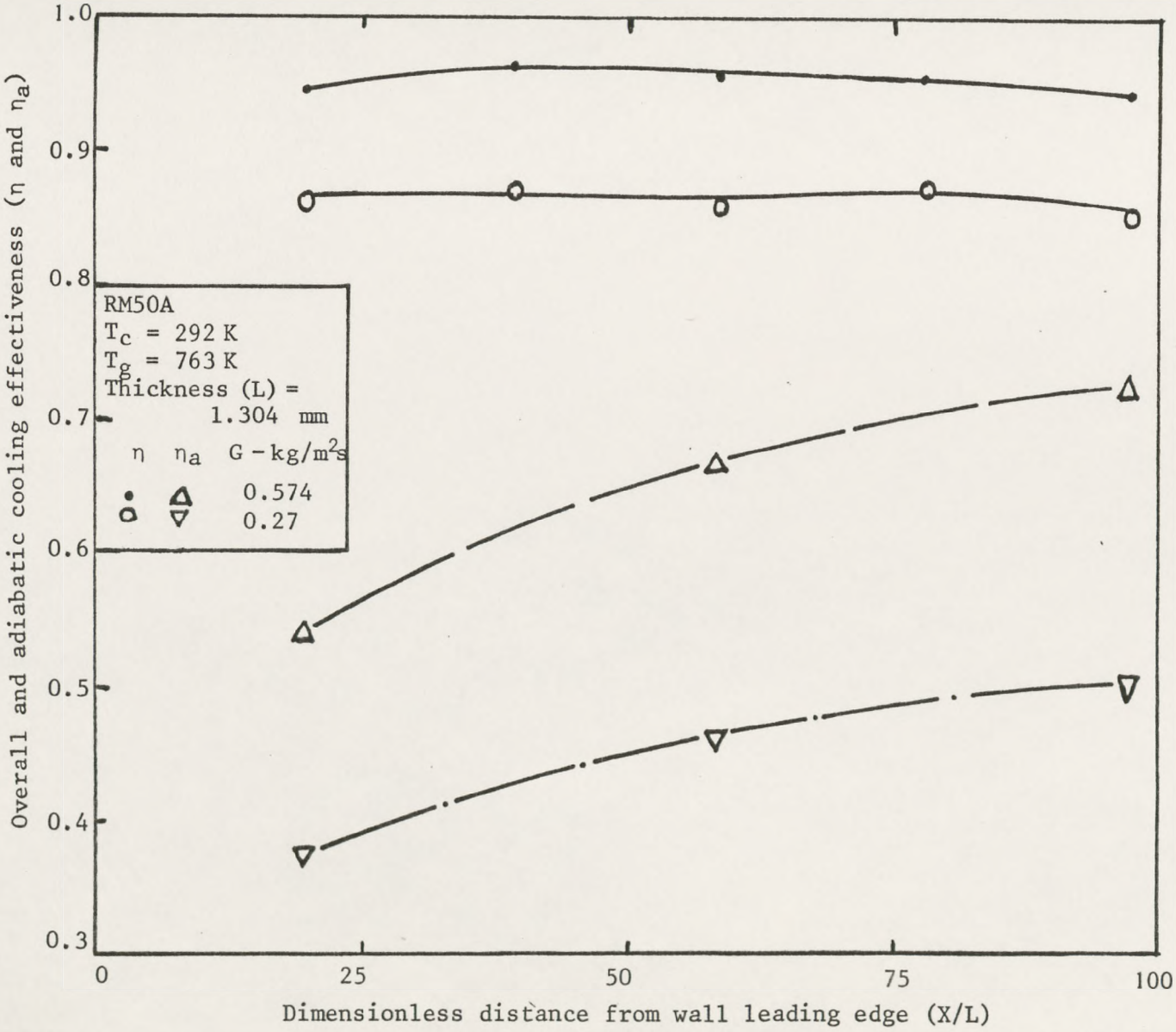

Fig. 4.15: Axial development of overall and adiabatic cooling effectiveness for two coolant injection rates (G).

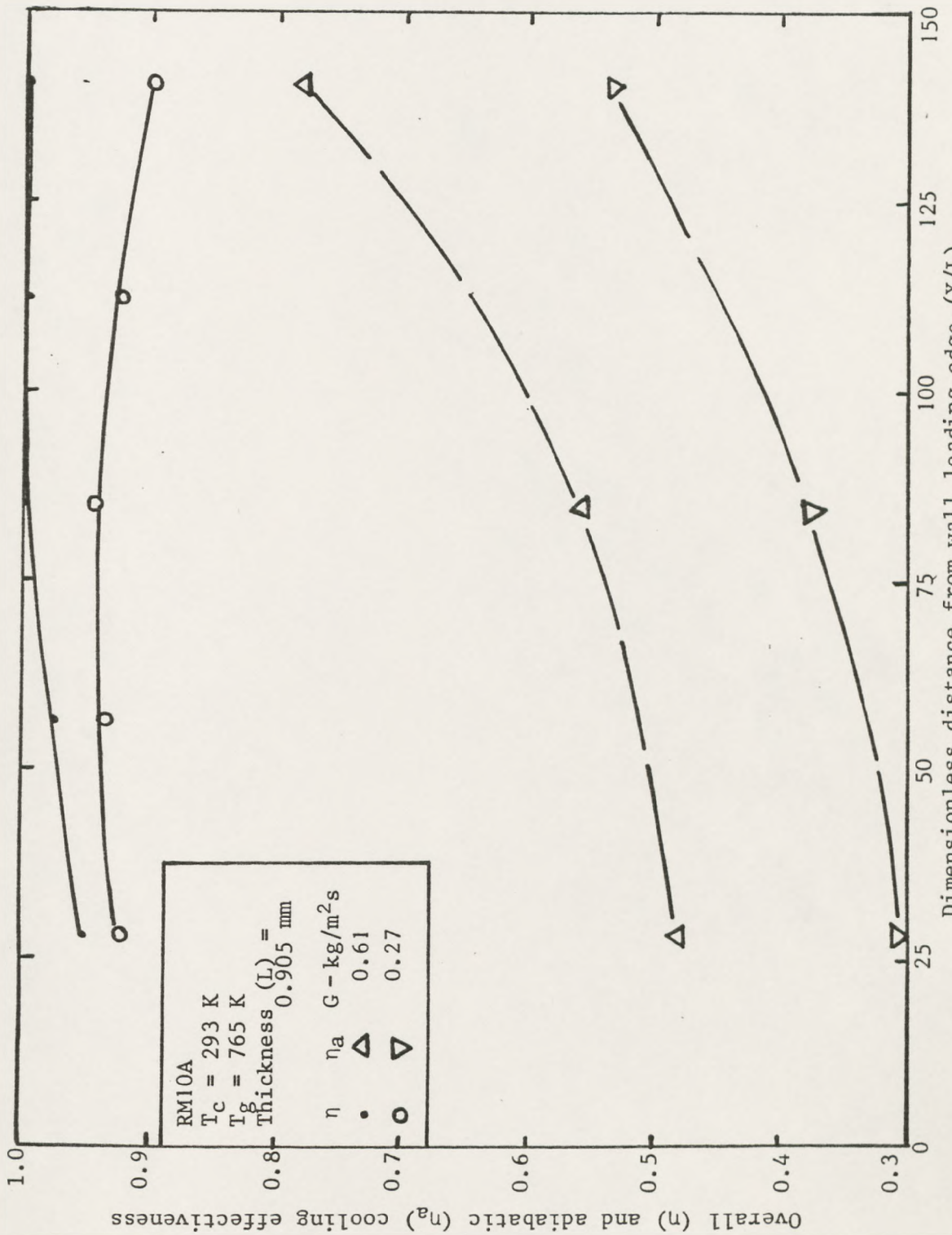

Fig. 4.16: Axial development of overall and adiabatic cooling effectiveness for two coolant injection rates (G)

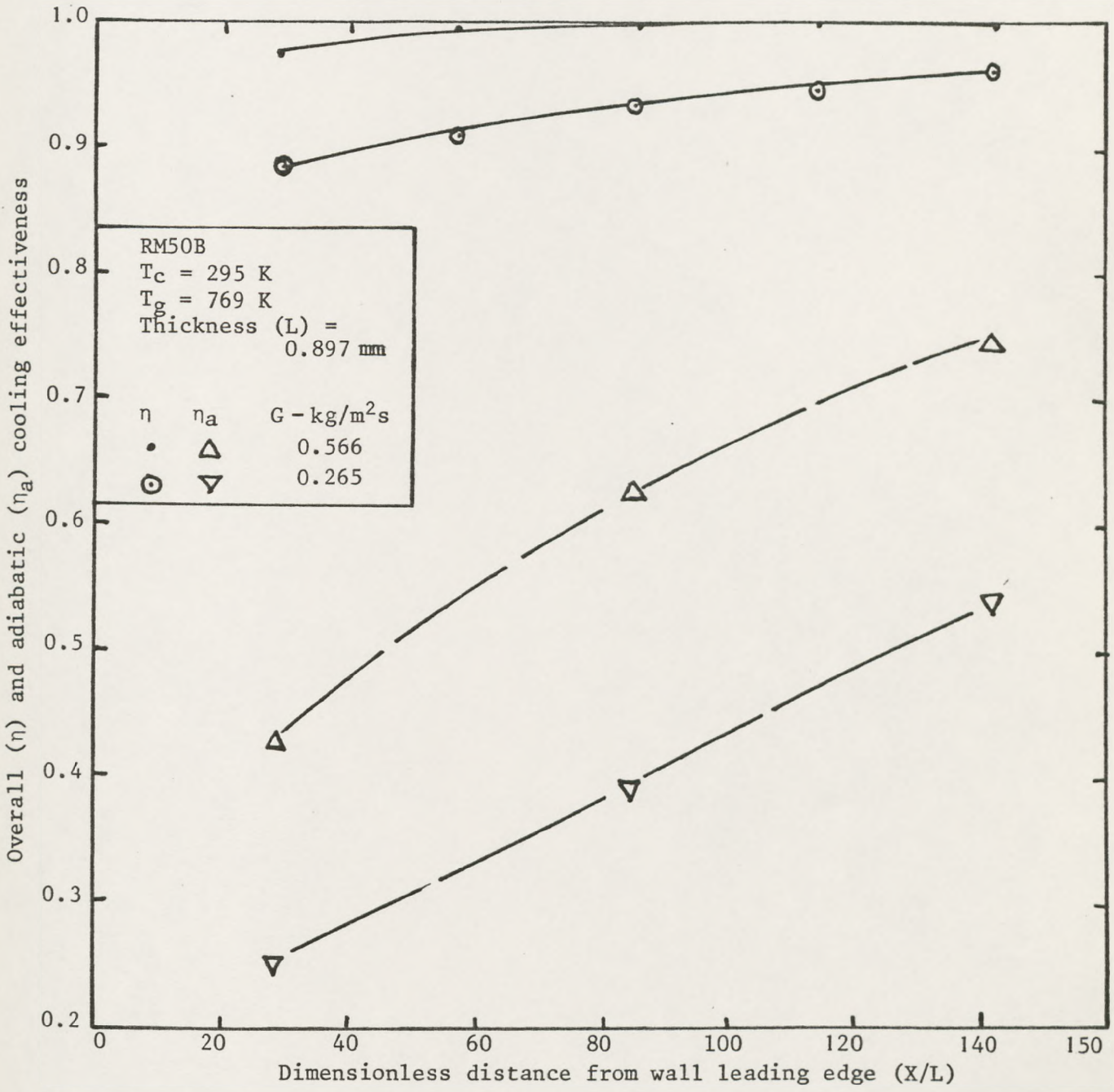

Fig. 4.17: Axial development of overall and adiabatic cooling effectiveness for two coolant injection rates (G).

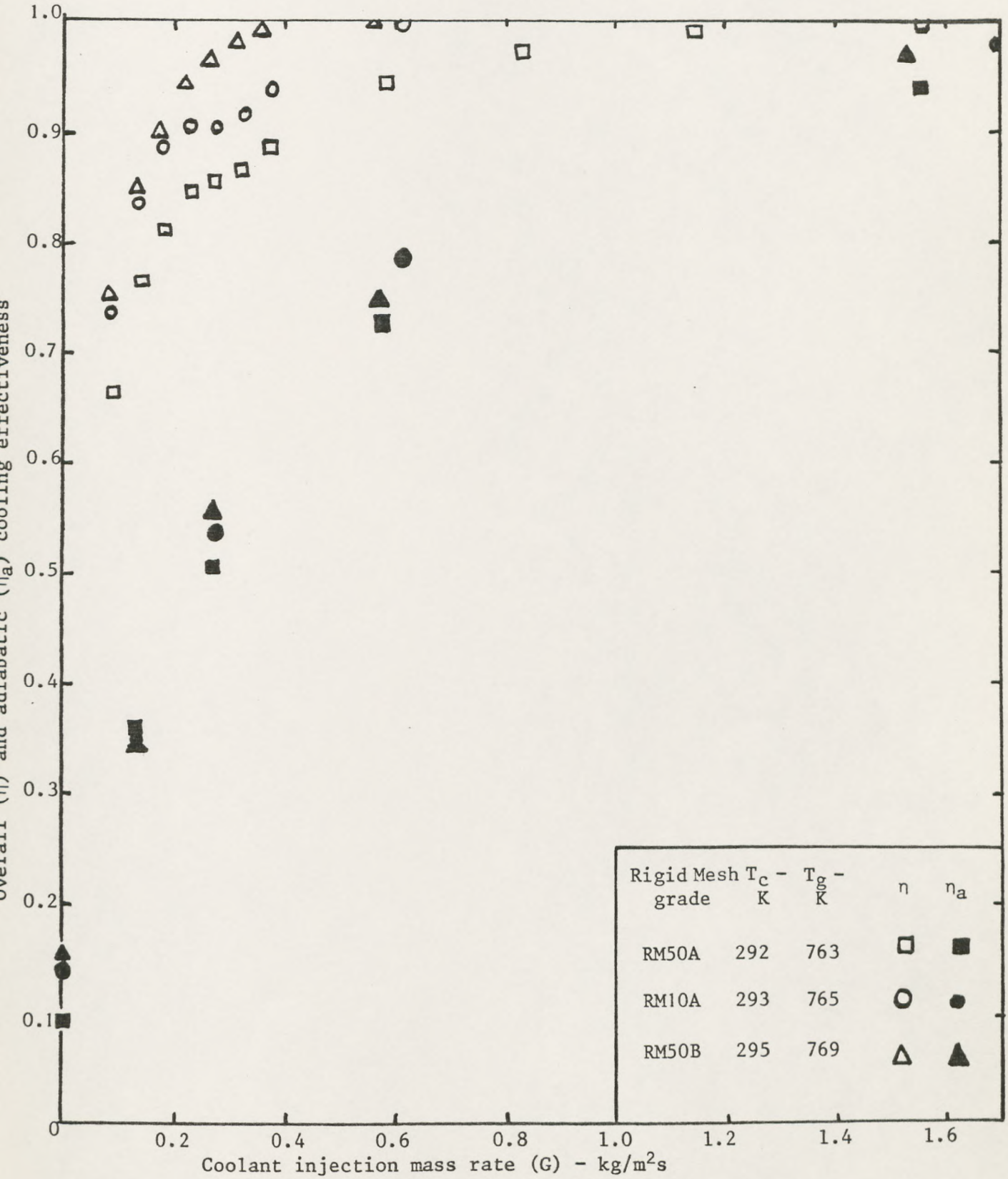

Fig. 4.18: Comparison of cooling effectiveness of three grades of Rigid Mesh at thermal station 5 (X = 127 mm).

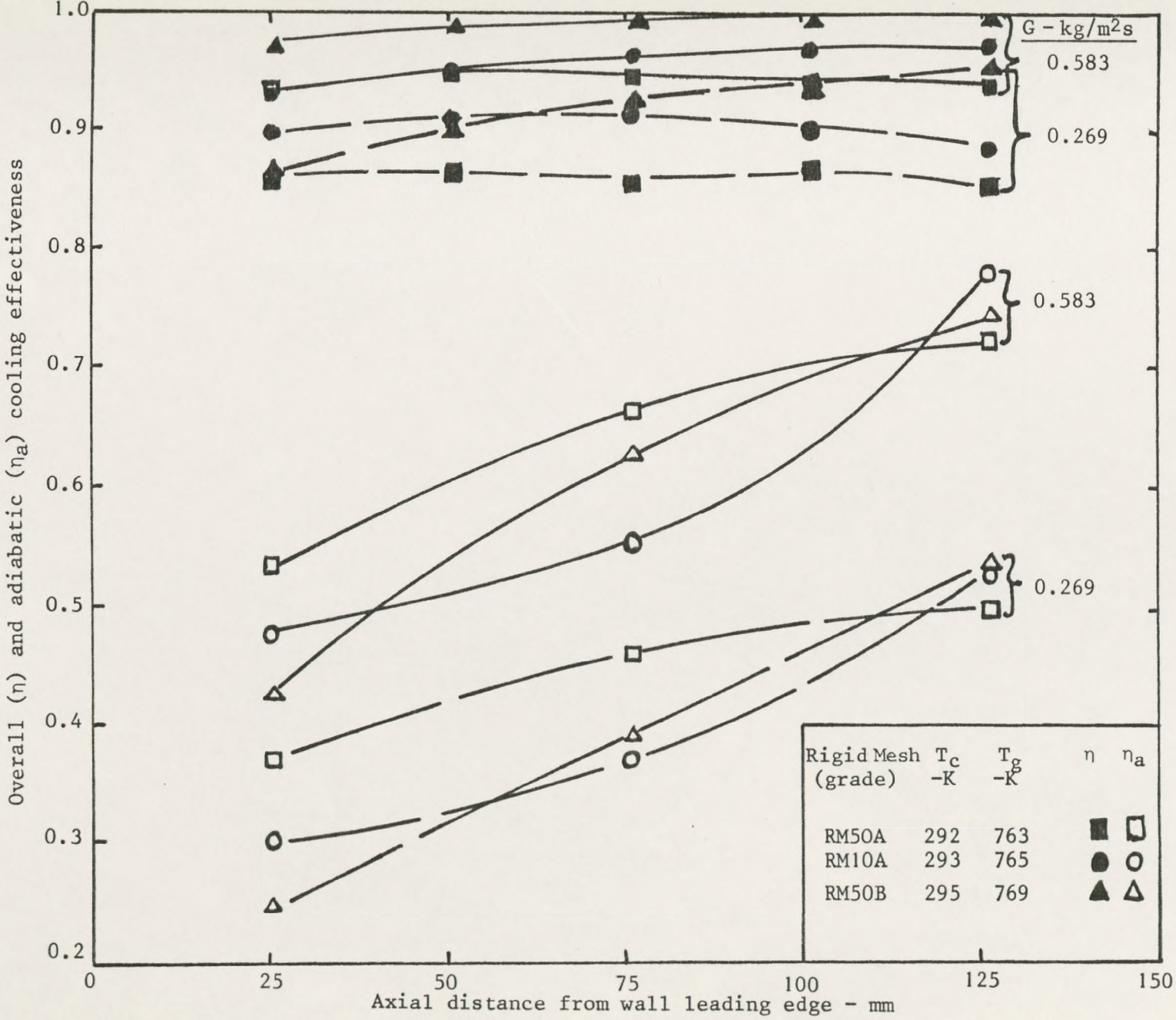

Fig. 4.19: Comparison of axial profile of cooling effectiveness of 3 Rigid Mesh grades at two coolant injections (G).

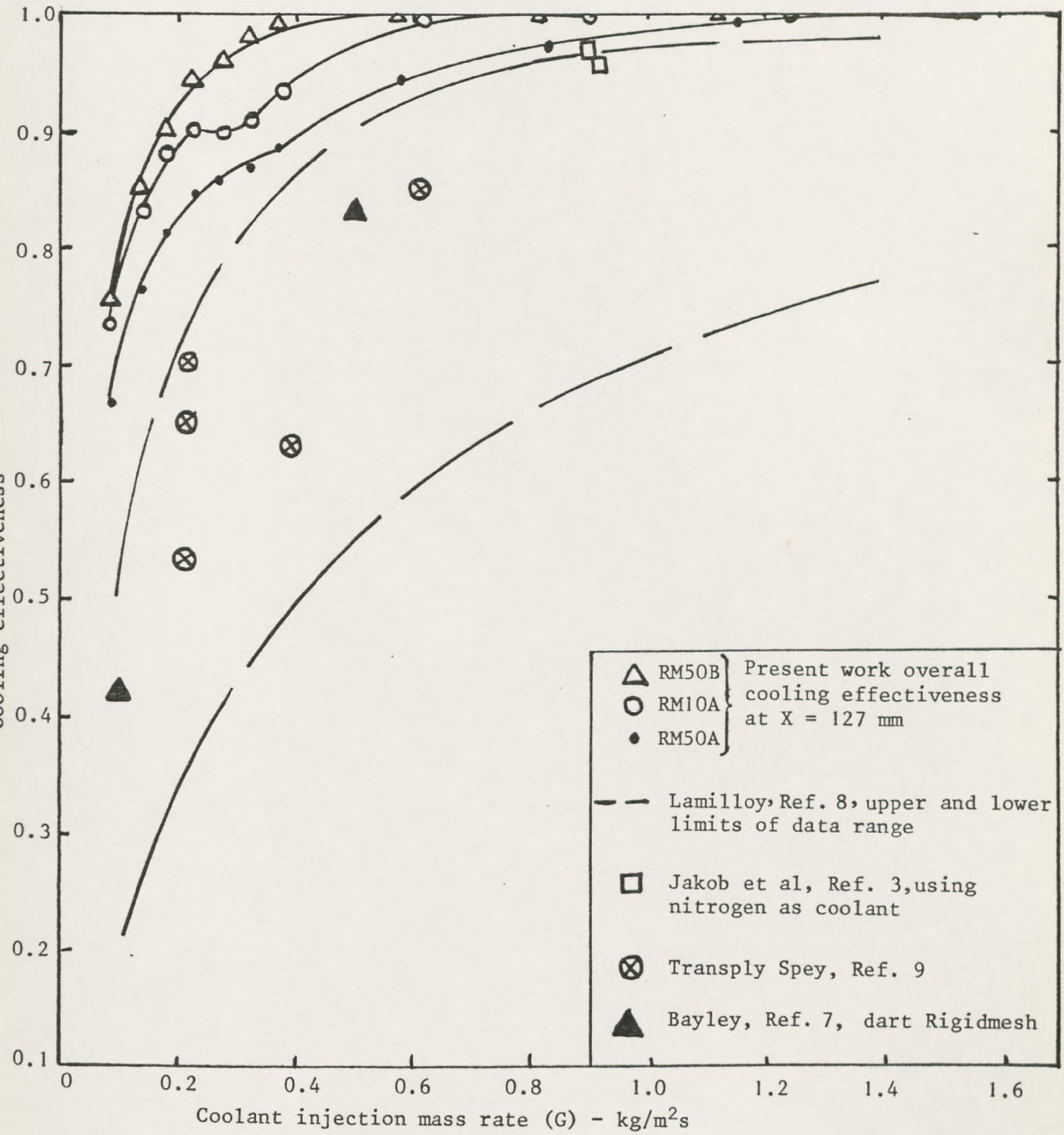

Fig. 4.20: Cooling effectiveness as a function of coolant injection

Fig. 4.21: Interstitial convective heat transfer with coolant injection.

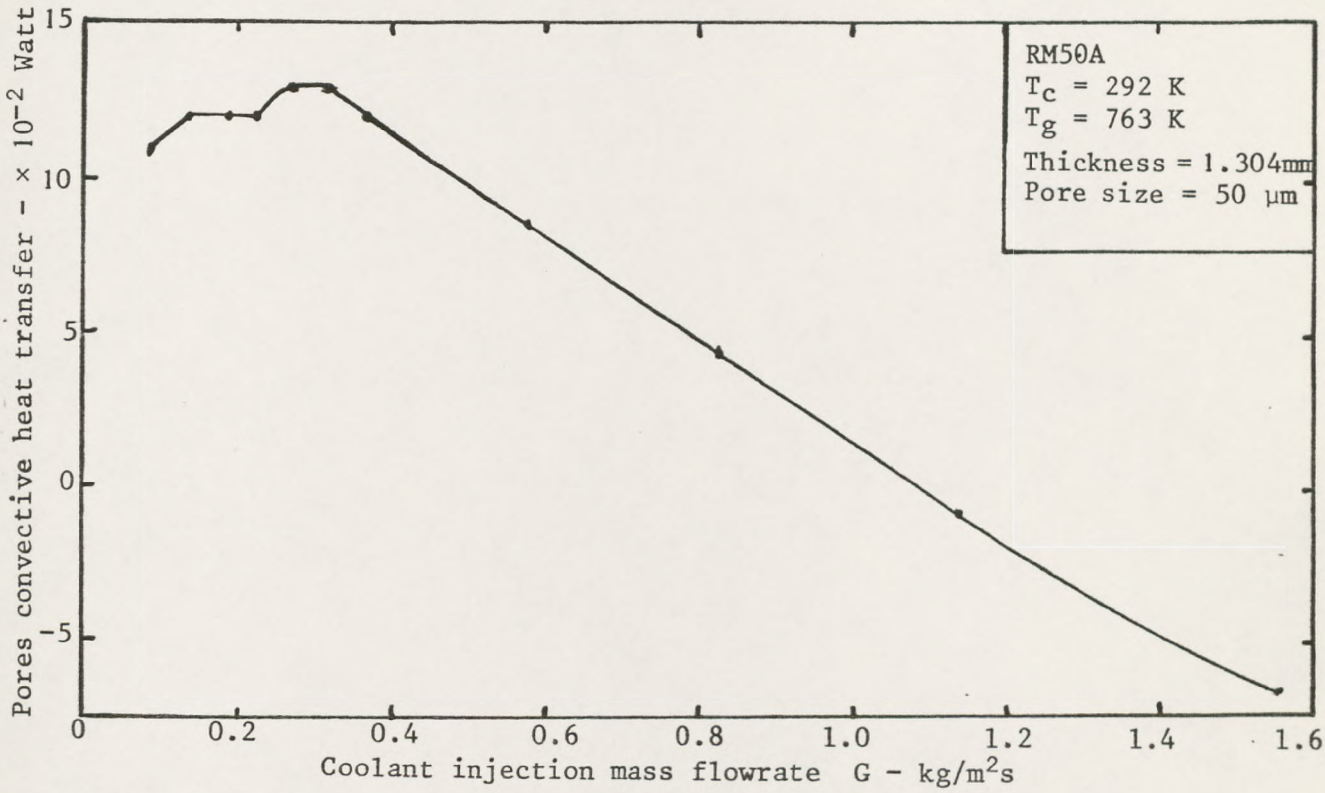

Fig. 4.22: Interstitial convective heat transfer with coolant injection.

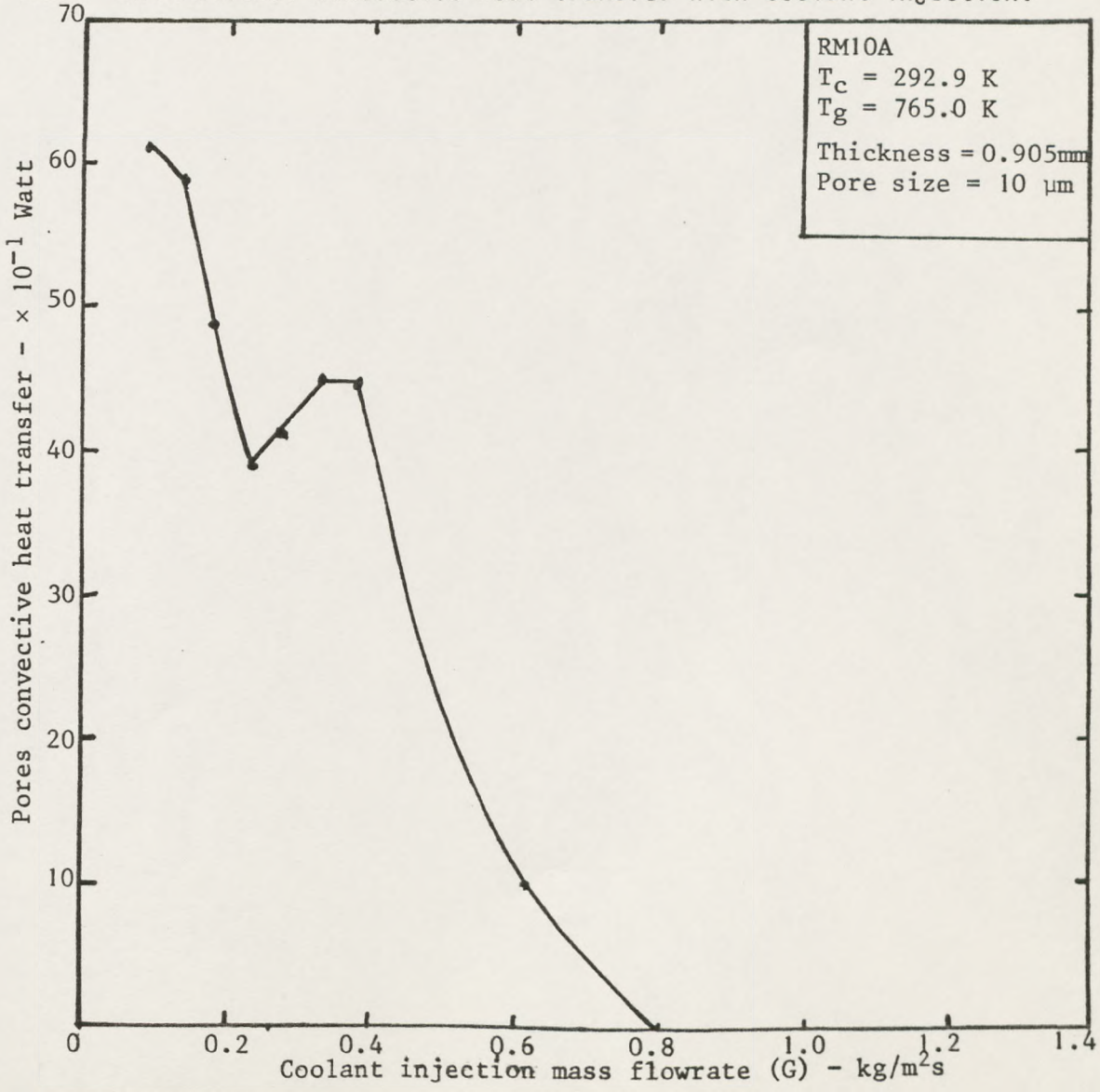

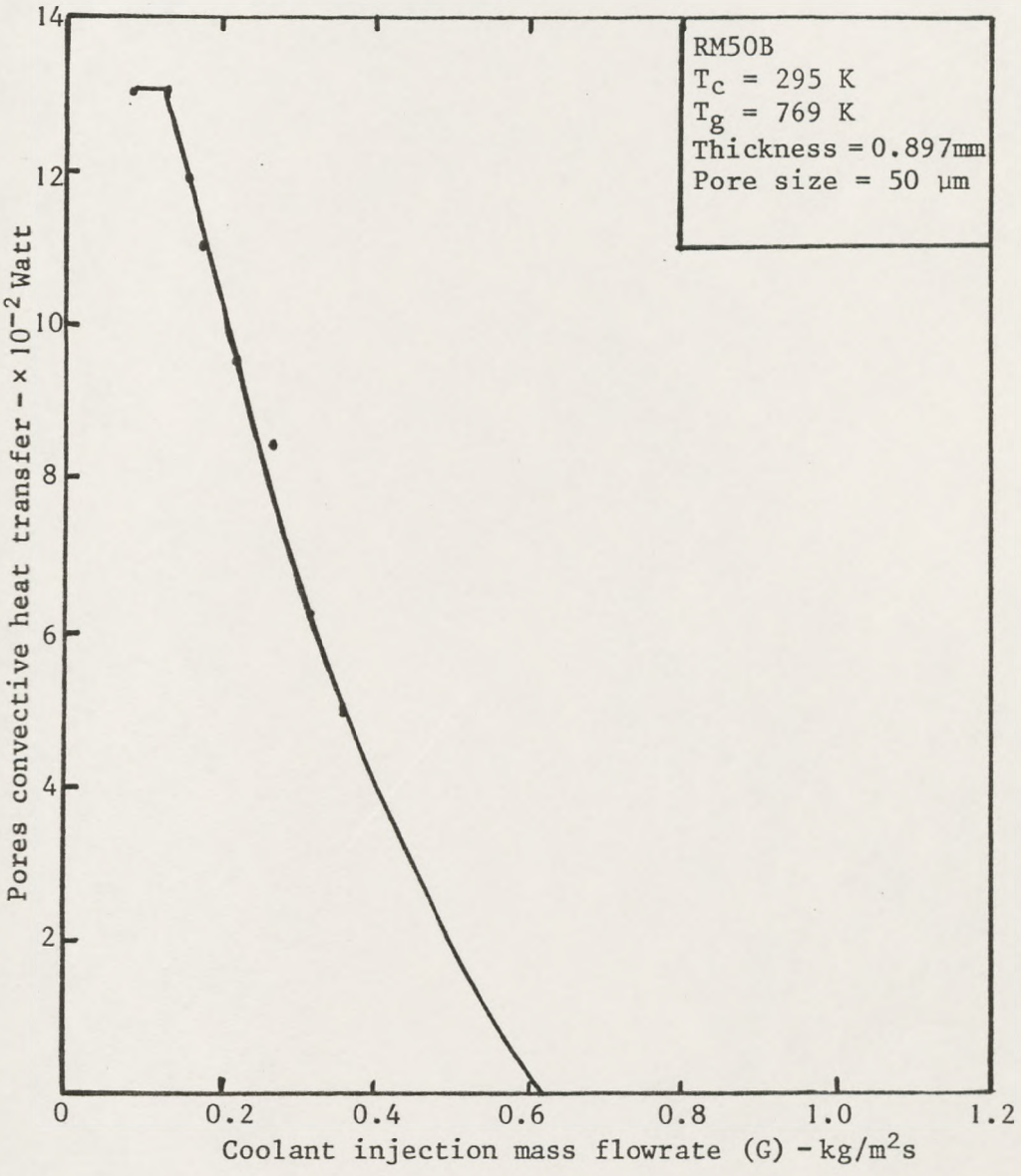

Fig. 4.23: Interstitial convective heat transfer with coolant injection

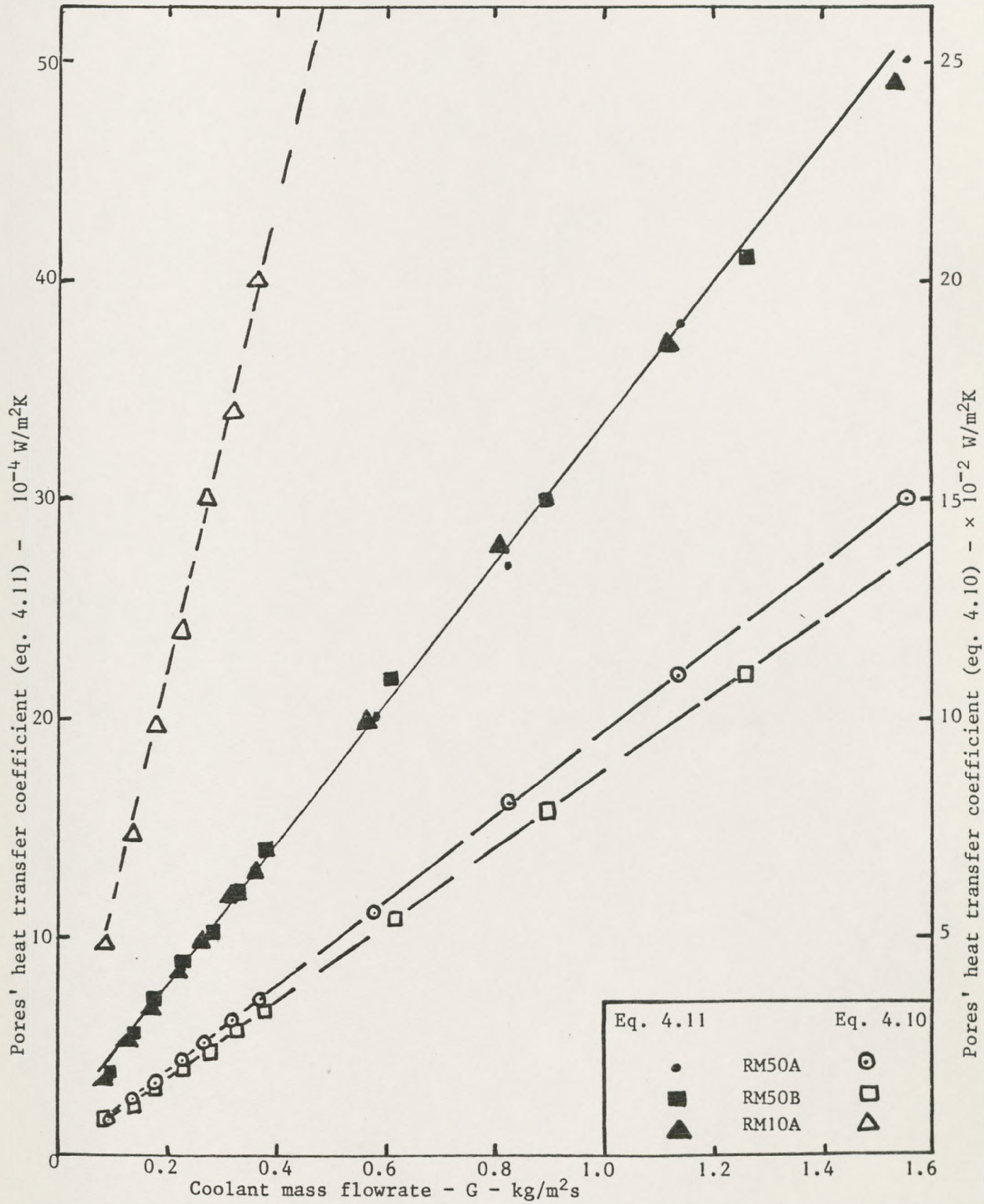

Fig. 4.24: Development of heat transfer coefficient with coolant injection using two correlating equations

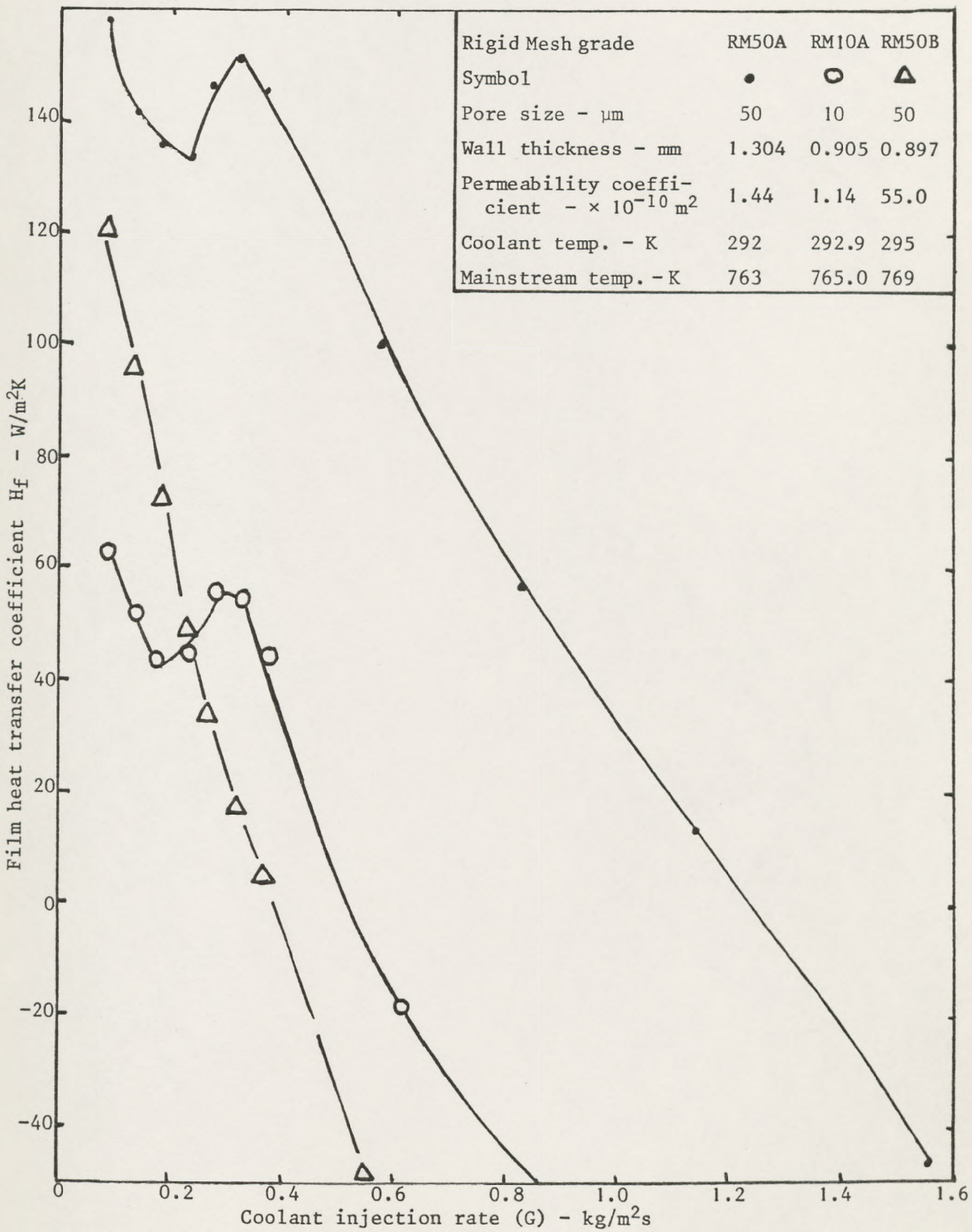

Fig. 4.25: Comparison of film heat transfer coefficient dependency on coolant injection for the three grades of Rigid Mesh at X = 127 mm.

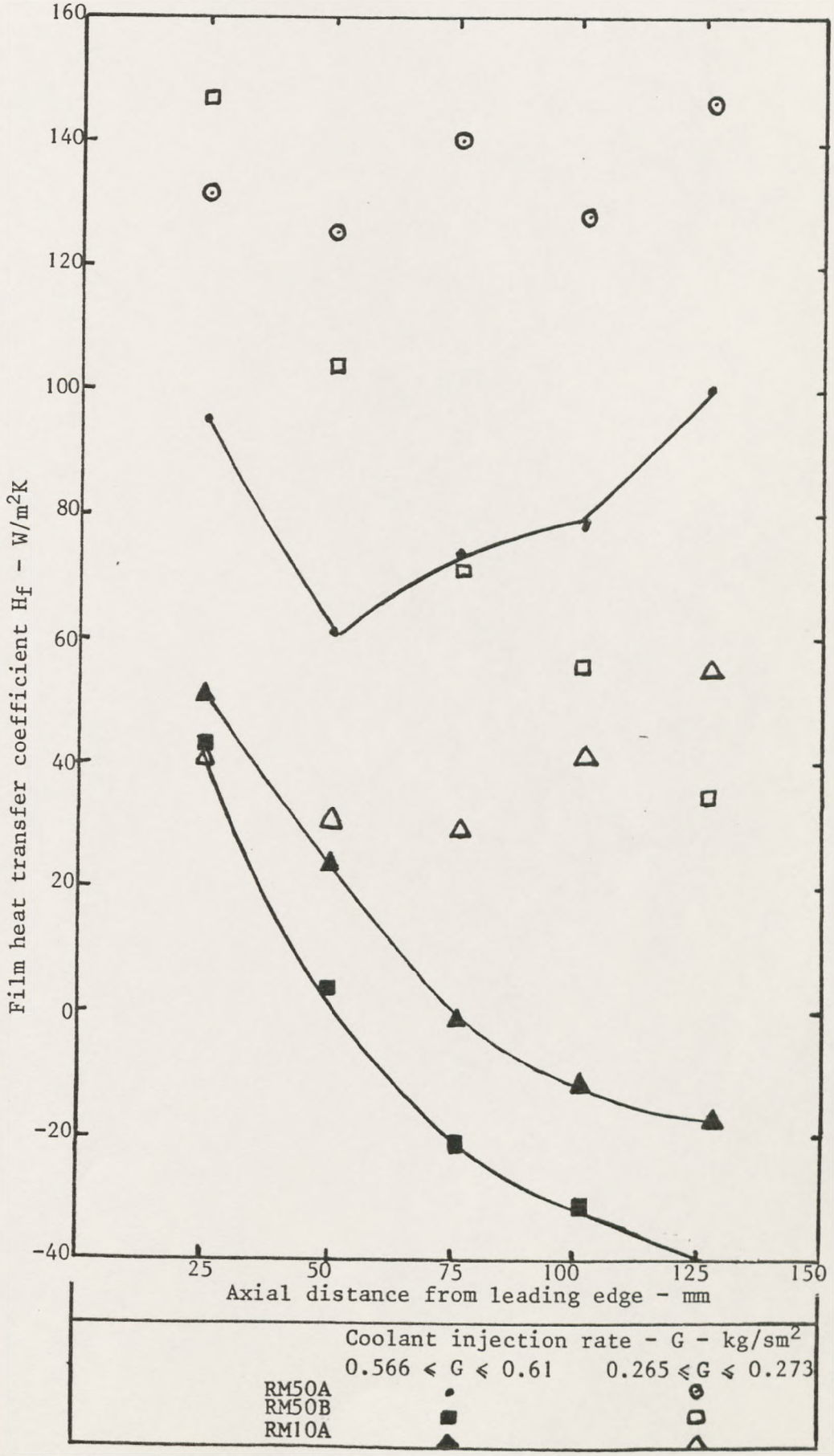

Fig. 4.26: Axial profile of film heat transfer coefficient at two G values

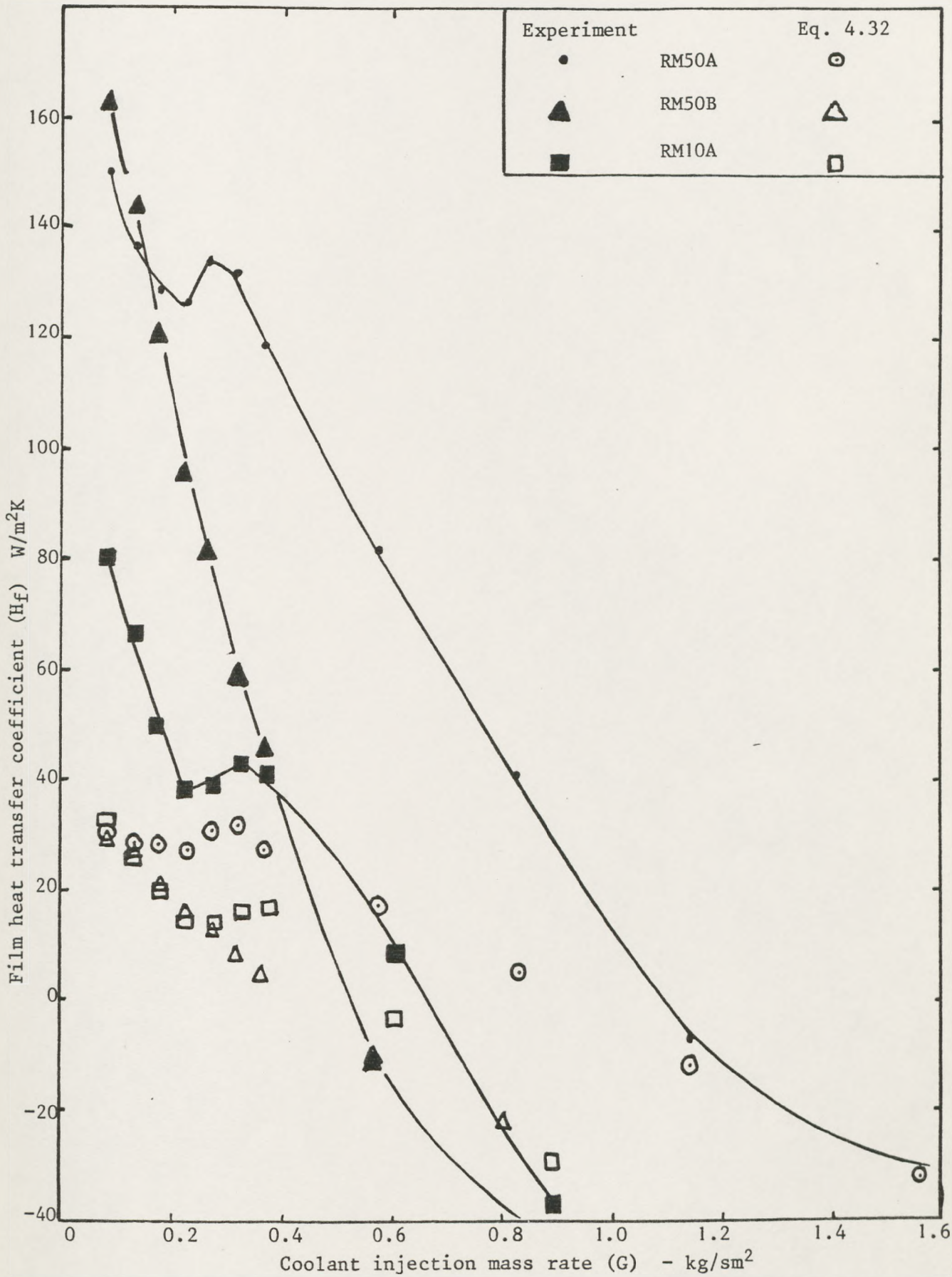

Fig. 4.27: Comparison of average film heat transfer coefficient with the correlation of Ref. 28.

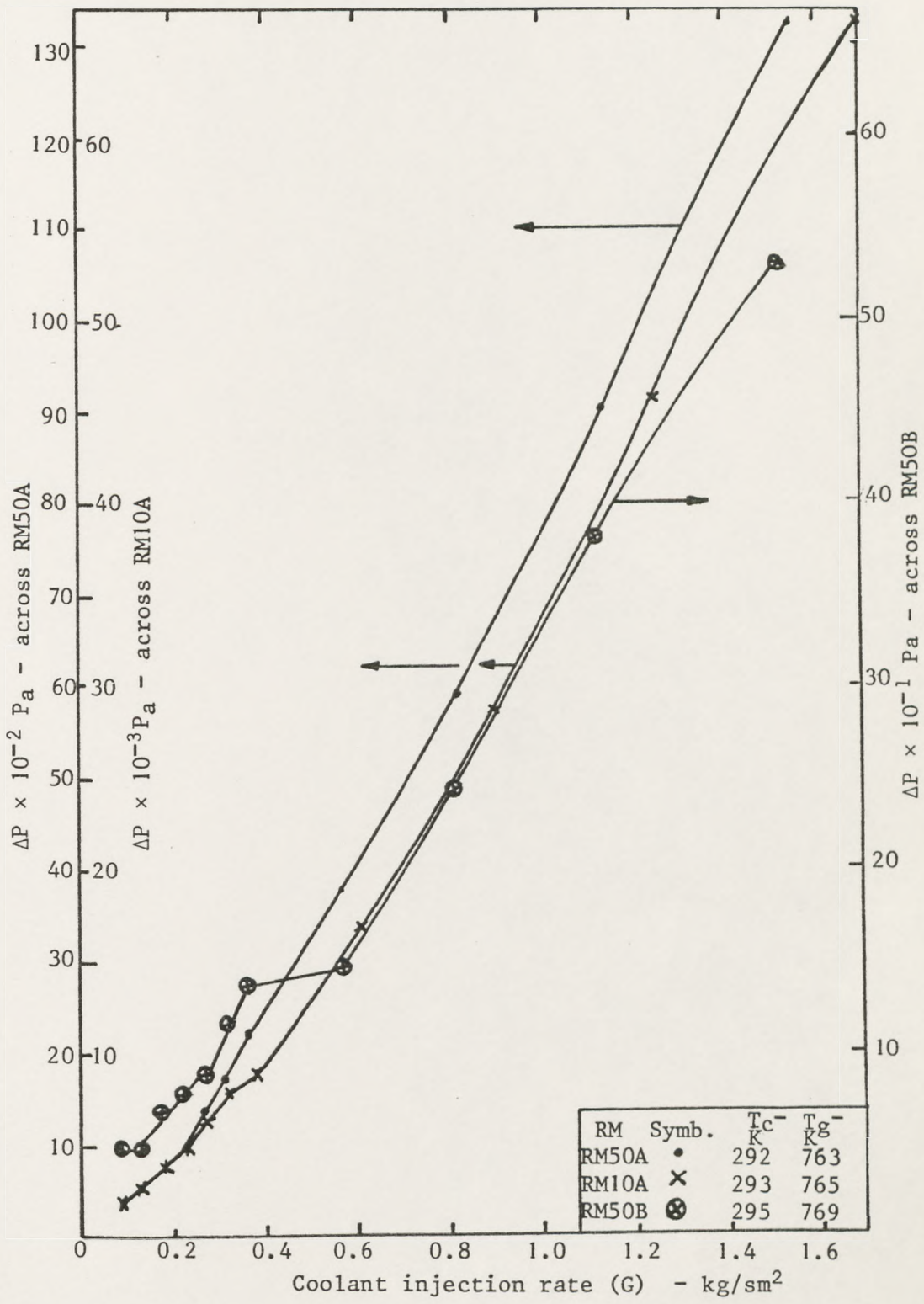

Fig. 4.28: Profile of pressure loss across transpiration wall.

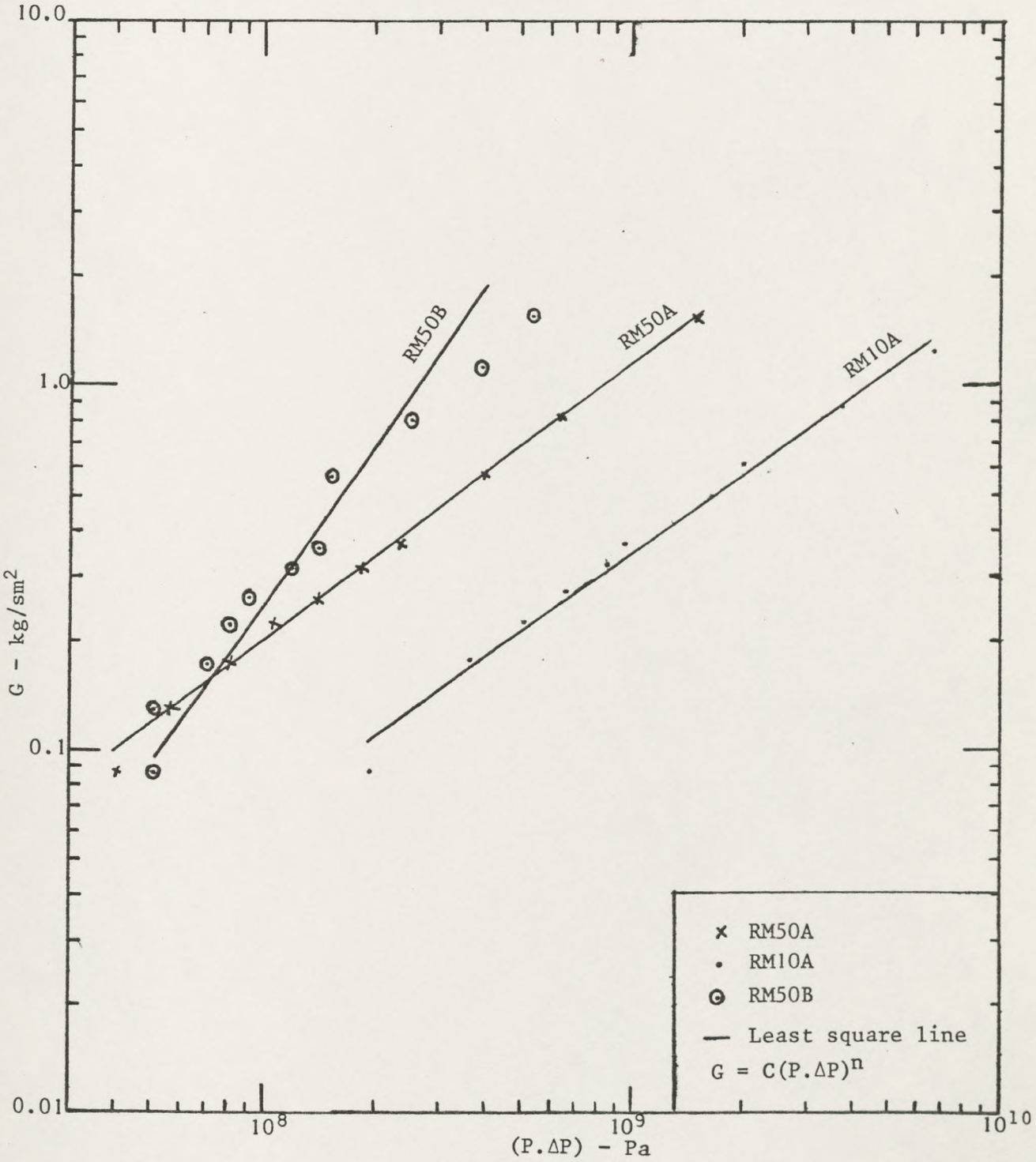

Fig. 4.29: Dependency of coolant injection rate on pressure loss across Rigid Mesh.

4.10 APPENDIX

Plate (4.1): The Rigid Mesh RM50A; 1.3039 mm thick

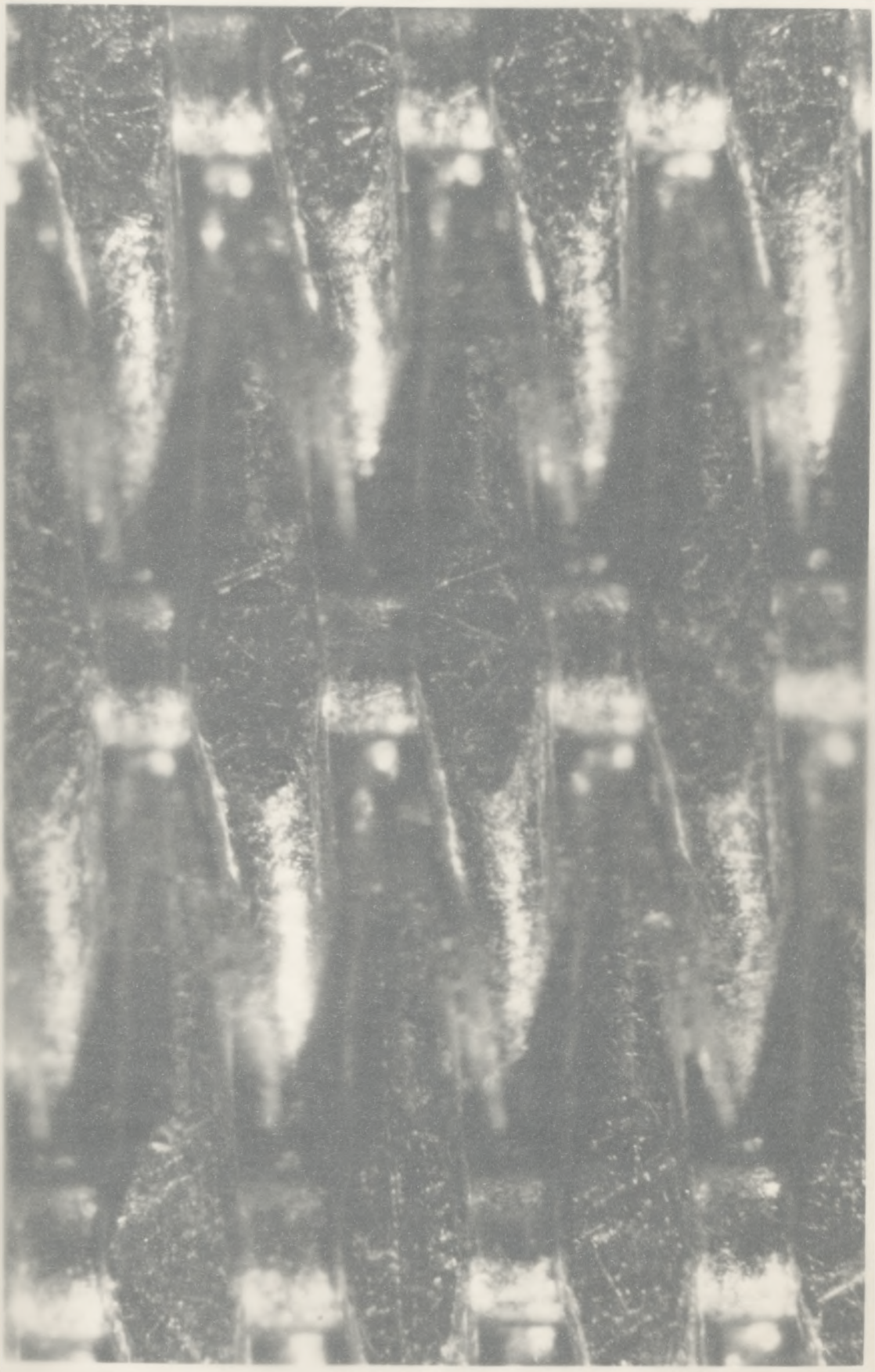

Plate (4.1): The Rigid Mesh RM50A; 1.3039 mm thick

Plate (4.2): The Rigid Mesh RM10A; 0.9051 mm thick

Plate (4.2): The Rigid Mesh RM10A; 0.9051 mm thick

Plate (4.3): The Rigid Mesh RM50B; 0.8974 mm thick

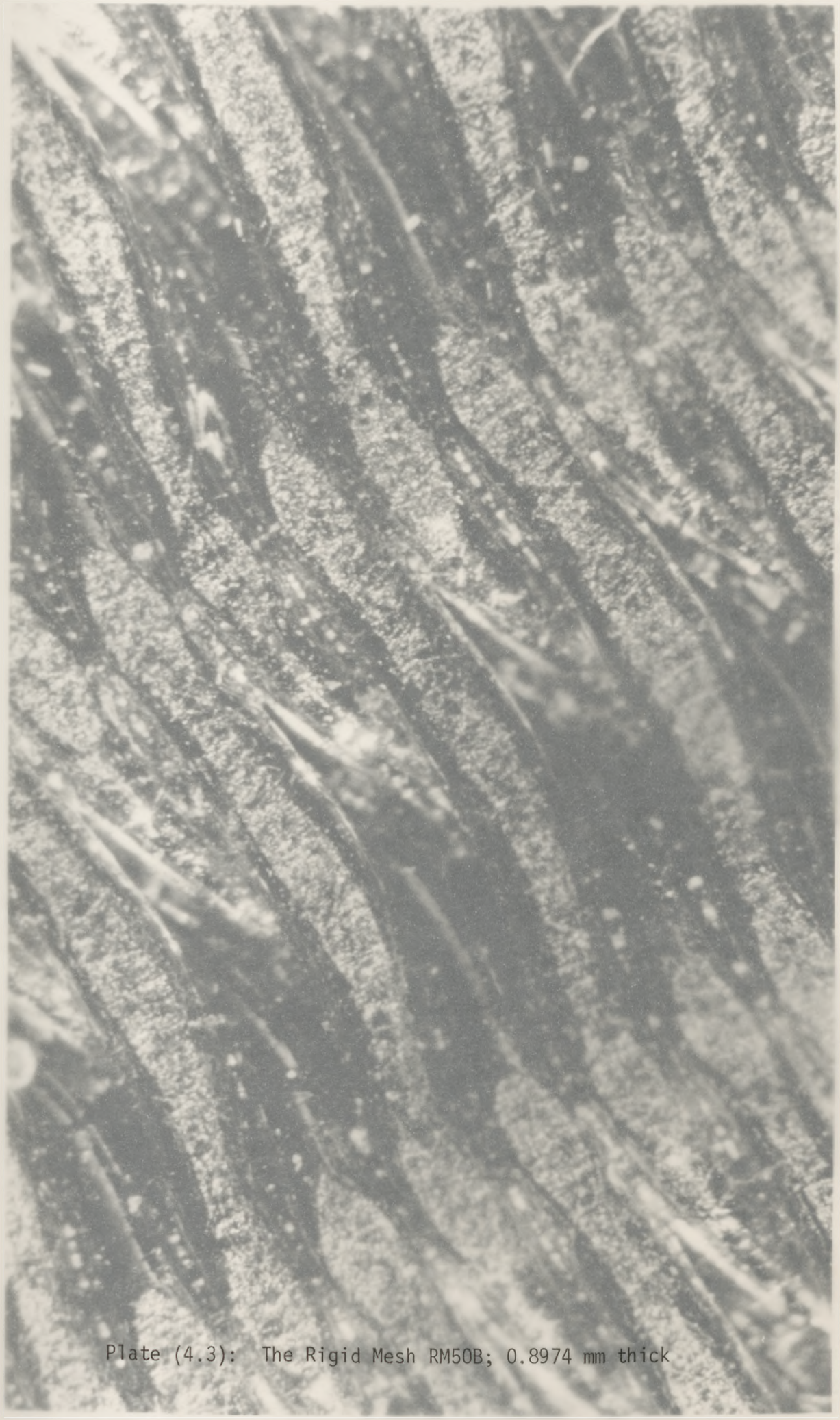

Plate (4.3): The Rigid Mesh RM50B; 0.8974 mm thick

CHAPTER 5

Nomenclature

Nu	=	Nusselt number
Re	=	Reynolds number
Pr	=	Prandtl number
H	=	Convective heat transfer coefficient - W/m^2K
A	=	Area - m^2
P	=	Pressure - Pa
K_p	=	Thermal conductivity - W/mK
p	=	Hole's pitch - m
T	=	Temperature - K
Q	=	Convective heat transfer - W
u	=	Velocity - m/s
ρ	=	Density - kg/m^2
D	=	Hole's mean diameter - m
μ	=	Dynamic viscosity - Ns/m^2
N	=	Total number of holes
$\dot{M}, \dot{m}$	=	Mass flow rate - kg/s
π	=	3.1415927
C_p	=	Specific heat capacity - J/kgK
E	=	Emissivity
W	=	Radiosity
σ	=	Stefan-Boltzmann constant
F	=	View factor
α	=	Radius ratio
ϕ	=	Parameter in equation 5.22 = $0.0065\ Re_1^{-\frac{1}{6}}$
r	=	Radius of tube - m - effective fuel/air ratio
L	=	Axial distance/mean beam length - m
R_{NU}	=	Ratio of average Nusselt to fully developed Nusselt numbers

t = Plate thickness - m

l_m = Luminosity factor

Mc = Mach number

γ = Ratio of specific heats

Z = Distance in the direction of cross-stream or hole pitch

M = Blowing rate

V = Mean velocity of jet

Δt = Temperature error

Subscripts:

cb = back-side of effusion wall

pl = test plate

c = coolant, for temperatures

1 = test wall

2,d,w = duct wall

3,ple = plenum

rb = back-side

s = evaluated at the wall

ch = in the holes

in = inlet to the holes

f = mainstream/flame

rf = hot gas stream

p = with emissivity designates test wall

g = mainstream

e2 = stainless steel

22 = duct wall to duct wall

12 = test wall to duct wall

21 = duct wall to test wall

g2 = gas stream to duct walls

n	=	exchange between test wall and duct walls
c	=	mainstream or film for heat
o,t,out	=	outlet or exit
j	=	jet
h	=	hole
fl	=	fluxmeter
wh	=	Whitaker
ccb	=	Chilton and Colburn

CHAPTER 5

HEAT TRANSFER IN FULL COVERAGE DISCRETE HOLE FILM COOLING: A THEORETICAL CONSIDERATION

5.1 INTRODUCTION

To design a long service-life cooling system for a gas turbine combustor, it is essential to know both the flame tube metal temperature and cooling effectiveness at the condition for which the combustor is to be used. In order to obtain these parameters, the heat transfer coefficient at the flame side of the cooled flame-tube for a given coolant flow rate at a given performance level is required. Using the average convective heat transfer coefficient for Full Coverage Discrete Hole Film Cooling System (DHFC), at the condition of use, the metal temperature and cooling effectiveness can be predicted with accuracy.

Conventional procedures (1,2) for treating turbulent flow convective heat transfer in a pipe are inadequate when applied to a DHFC cylindrical combustor. This inadequacy arises because the boundary layer on the film cooled flame-side of the combustor is strongly disturbed by the coolant injection. This disturbance results in a convective heat transfer coefficient considerably different from that which would be obtained if a conventional approach were employed. Also the influence of hole size combined with mainstream fluid velocity may act to decrease the turbulence at the surface of the DHFC combustor, creating laminarization which will lead to a different convective heat transfer coefficient from that of the conventional approach.

To account accurately for the convective heat transfer to a DHFC combustor flame-side from the hot gas stream, full account

must be made of the heat transfer to the cooling air from the moment it makes contact with the perforated wall on the back-side, to the time it leaves as jets on the flame-side of the wall. If the heat transfer processes are clarified and a heat balance is carried out on the wall, accurate convective heat transfer coefficients at the surface of the DHFC can easily be found. With this coefficient, both metal temperature and cooling effectiveness of the DHFC combustor may be predicted with confidence. It is the objective of this chapter to accomplish this task.

The investigation reported here made use of a flat plate. The test area of the plate was 152.4 by 152.4 mm, simulating a portion of a large gas turbine combustor wall.

To describe the theory of heat transfer process, the sequence of individual coolant processes must be identified.

5.2 COOLANT PROCESSES

As the coolant flows from the back of the flame-tube to the flame surface of the wall, four major operations are carried out by the coolant.

(a) Removal of heat from the coolant side or back-side of the full coverage discrete hole film cooling combustor wall.

(b) Removal of heat from the wall by convection as the coolant passes through the DHFC-wall holes en route to the flame surface.

(c) The protective film cooling action of the coolant on the flame-side from the mainstream hot flame gases.

(d) The absorption of the radiative fluxes from the high temperature flame gases.

The above coolant processes have been divided into three major areas with the heat transfer processes in each area identified. The heat transfer processes as well as the areas where the processes take place are the subject of the sections below.

5.3 ANALYSIS OF THE HEAT TRANSFER PROCESSES

The heat transfer processes are as shown in fig. 5.4. These are considered in respect of the part of the wall where they occur.

5.3.1 Back-side of the Full Coverage Discrete Hole Film Cooling Wall

The coolant at the back wall is subjected to two main heat transfer processes. These are:

5.3.1A Convective heat transfer, and

5.3.1B Radiative heat transfer.

5.3.1A.1 Convective heat transfer (Q_{cb}) at the back-side

Heat is transferred by convection to the coolant as it makes contact with the wall and flows towards the holes, fig. 5.1. Many investigators of full coverage discrete hole film cooling in gas turbines have only considered the film cooling part of the process and not given consideration to convective heat transfer to coolant approaching a bank of holes or within the holes. Choe et al (3) worked on heat transfer in full coverage film cooled surface, obtaining Stanton values using superposition method. Kasagi et al (4) used liquid crystal to determine the film cooled wall temperature. Other works such as that of Mayle et al (5) and Furuhama et al (6) also concentrated entirely on the film cooling process.

Work on heat transfer by convection to the fluid approaching

an array of holes is very scanty in the literature and the only work done which is relevant to the work presented here was that of Sparrow et al(7,84). Sparrow et al did work on fluid en route to perforated holes on a circular disc using mass analogy to obtain a general correlation for the convective heat transfer coefficient. However it is the work of reference 7 that is of relevance to the present work. The correlation of (7) is presented here as:

$$Nu = 0.881\ Re^{0.476}\ Pr^{\frac{1}{3}} \qquad \ldots (5.1)$$

The Nusselt number is based on the ratio of unperforated total area (A) to the total pitch (p) of the holes and the above equation may therefore be expressed as

$$Nu = \frac{H_{cb}\ A}{p\ K_p} \qquad \ldots (5.2)$$

Substituting equation (2) into equation (1) and rearranging, we have

$$H_{cb} = 0.881\ Re^{0.476}\ Pr^{\frac{1}{3}}\ p.K_p/A \qquad \ldots (5.3)$$

From the above equations the convective heat removed by the coolant from the back of the effusion test wall, figs. 5.1 and 5.2, is presented here as

$$Q_{cb} = H_{cb}\ A(T_{p1} - T_c) \qquad \ldots (5.4)$$

The Reynolds number of the fluid as in equation 5.1 is based on the mean holes diameter (D) and is related to the total number of perforations as

$$Re = \frac{\rho u D}{\mu} \cdot N \qquad \ldots (5.5)$$

The velocity, u, of the fluid flow is related to the total coolant mass flow rate, $\dot{m}$, as

$$u = \frac{4\dot{m}}{\rho\pi D^2} \qquad \ldots (5.6)$$

Combining equations 5.5 and 5.6, the Reynolds number can be shown to be

$$Re = \frac{4\dot{m}}{\pi\mu D} \cdot N \qquad \ldots (5.7)$$

The coolant Prandtl number (Pr) is given as

$$Pr = \frac{C_p\mu}{K_p} \qquad \ldots (5.8)$$

Using equations 5.1, 5.3, 5.4, 5.7 and 5.8, the convective heat transfer, Q_{cb}, by the coolant by scrubbing the effusion wall-back on its approach to the holes can be shown to be related to the coolant mass flowrate, plate holes' size and concentration as

$$Q_{cb} = 0.988\,\dot{m}^{0.476}\left(\frac{N}{D}\right)^{0.476} C_p{}^{0.333} K_p{}^{0.667} \mu^{-0.143} P.(T_{p1} - T_c) \qquad \ldots (5.9)$$

T_{p1} = Effusion plate temperature in Kelvin.

T_c = HERE PLENUM TEMP.

5.3.1A.2 Specific heat capacity - C_p

Since the specific heat capacity, C_p, of the coolant air depends on the temperature of the air, a correlation in which the temperature plays a role is necessary for an accurate heat transfer correlation. Also as the temperature of the coolant varies from room temperature to as high as 1000 K, data for this temperature range are required. Using US National Bureau of Standards' (8) data for air, at temperatures from 273 K to 2000 K, a curve-fitted polynomial equation was derived.

This correlating equation for the specific heat capacity, C_p, employed in equations 5.1, 5.3, 5.4, 5.8 and 5.9 is

$$C_p = 1063.3 - 5.7194 \times 10^{-14} T_c^5 + 4.2538 \times 10^{-10} T_c^4 - 1.1417 \times 10^{-6} T_c^3 + 1.3637 \times 10^{-3} T_c^2 - 0.5117 T_c \quad (J/kgK) \qquad \ldots (5.10)$$

5.3.1A.3 Viscosity - μ

The viscosity (μ) of the coolant air used is also temperature dependent and an appropriate correlation involving temperature for viscosity is required. The correlation for viscosity of air according to Sunderland's formula (9) and employed by Mkpadi (10) is

$$\mu = \frac{150 \times 10^{-8} \times T_c^{1.5}}{(T_c + 124)} \quad (Ns/m^2) \qquad \ldots (5.11)$$

where T_c = the coolant temperature in K.

However the above correlation has been superseded by the work of Watson (11) and his analytical correlation for the viscosity of air. Equation 5.11 may have uncertainties of up to 8% at temperatures above 300 K. Watson's correlation for the viscosity of air is applicable from 270-2200 K with uncertainties of: 0.25% from 270-600 K, 1.0% from 610-1600 K and 2.0% from 1610-2200 K. Coolant air is employed in this work at temperatures of about 288 up to 773 K. Employing Watson's correlation will therefore result in uncertainty of 1.0% compared with 8.0% if equation 5.11 is employed. Watson's correlating formula for the viscosity of air (μ) is presented here as

$$\mu = 10^{-6} T_c^{-0.5} R^{-1} \quad (Ns/m^2) \qquad \ldots (5.12)$$

where $R = A_1 + A_2 S + A_3 S^2 + A_4 S^3 + A_5 S^4$

$S = 100 T_c^{-1}$

A_{1-5} are constants, with

A_1 = 0.55279544

A_2 = 2.8108916

A_3 = -13.50834

A_4 = 39.353086

A_5 = -41.419387

T_c = Fluid temperature in Kelvin.

5.3.1A.4 Thermal conductivity - K_p

The coolant air thermal conductivity, K_p, depends on the temperature of the air and a correlation that is representative of the coolant temperature must be found. To satisfy this need, the data of US National Bureau of Standards (8) for air, at temperatures 273 to 2000 K, have been curve fitted using the NAGFE (12) package. The empirical equation produced was found to be accurate to within ± 1.0%. The correlating polynomial is presented here as

$$K_p = -0.7231 \times 10^{-14} T_c^4 + 0.3126 \times 10^{-10} T_c^3 - 0.6331 \times 10^{-7} T_c^2 + 0.1081 \times 10^{-3} T_c - 0.1265 \times 10^{-2} \quad \text{- W/(mK)} \quad \ldots (5.13)$$

where T_c = Coolant temperature in Kelvin.

5.3.1B Radiative heat transfer, Q_{rb}, at DHFC back-side

The test surface in this work, a flat plate, is of Nimonic-75. As stated in Chapter 2, the plate-effusion wall is bolted to the end part of the plenum to leave a 152.4 × 152.4 mm test section. During testing, radiative heat is lost from the back of the test section to the surfaces of the plenum wall, the incoming coolant and the plenum grid plate. Applying radiative heat transfer in an enclosure, fig. 5.3, and using the radiosity method as detailed by Gray et al (13), the view factors were determined (14,15). The

plenum walls, figure 5.3 (2,3), were treated as one surface. Vermaculate was used as insulator with the outer surface of it covered smoothly with auto-stick cement. The mean emissivity, E_3, of this cement was determined to be 0.74 (10).

The radiative heat loss at the back of the test plate, Q_{rb}, using Gray et al, is

$$Q_{rb} = f(A, E_1, R_1, W_1, \rho) \qquad \ldots (5.14)$$

From the characteristics of opaque materials and Kirchoff's Law, it can be shown that

$$\rho = 1 - E_1 \qquad \ldots (5.14B)$$

From 5.14 then,

$$R_1 = \sigma T_{p1}^4 \qquad \ldots (5.15)$$

W_1 = net radiative flux or radiosity leaving the test plate surface

Considering that the other surface, radiating back to the test wall is only the plenum walls, fig. 5.3(3),

$$W_1 = E_1 R_1 + F_{13}(1 - E_1) W_3 \qquad \ldots (5.16)$$

$$W_3 = E_3 R_3 + F_{31}(1 - E_3) W_1 + F_{33}(1 - E_3) W_3 \qquad \ldots (5.17)$$

where $R_3 = \sigma T_3^4$ $\qquad \ldots (5.18)$

W_3 = Radiosity from the plenum wall

F_{13}, F_{31} and F_{33} are view factors whose values have been determined as 1.0, 0.143 and 0.851 respectively.

Combining equations 5.14, 5.15, 5.16, 5.17 and 5.18 and substituting for E_3 and the view factors, gives

$$Q_{rb} = \frac{A E_1 \sigma}{(1 - E_1)} \left[\frac{(0.952 - 0.953 E_1) T_{p1}^4 - (0.952 - 0.952 E_1) T_3^4}{(0.952 + 0.047 E_1)} \right] \qquad \ldots (5.19)$$

where A = Test plate area - m^2

σ = Stefan-Boltzmann constant = 56.7×10^{-9} - $W/(m^2K^4)$

E_1 = Nimonic-75's emissivity

T_{pl} = Test plate temperature - K

T_3 = Measured plenum wall temperature - K.

The emissivity of Nimonic-75, E_1, is a function of temperature:

$$E_1 = f(T_{pl}) \qquad \ldots (5.20)$$

To derive a correlating equation for the emissivity, E_1, which is a function of temperature, the data of emissivity for Nimonic-75, oxidised at a temperature greater than 800 K (16), have been computer curve fitted. A five degree polynomial empirical equation, with uncertainty of less than $\pm$ 0.1% on the tabulated data at metal temperature up to 2000 K, has been derived as in equation 5.21:

$$E_1 = 2.6227 \times 10^{-15} T_{pl}^5 - 1.2267 \times 10^{-11} T_{pl}^4 + 2.2842 \times 10^{-8} T_{pl}^3 - 2.087 \times 10^{-5} T_{pl}^2 + 9.3087 \times 10^{-3} T_{pl} - 0.9386 \qquad \ldots (5.21)$$

Substituting equation 5.21 into equation 5.19, the radiative heat transfer at the back of the DHFC plate is evaluated. The calculation shows that this radiative heat loss is small relative to other components.

5.3.2 The Effusion Plate Holes

The internal hole heat transfer is the only wall heat transfer mode that has normally been considered. The hole length to diameter ratios are relatively small and hence entry effects are of importance.

5.3.2A.1 Convective heat transfer, Q_{ch}, inside the holes

The problem involved in computing convective heat transfer inside the holes is the thermal entry effect which renders orthodox equations for fully developed flow heat transfer in pipes inapplicable.

Thermal entry effect results when a fluid flowing adiabatically in a conduit enters a region where the temperature is different from that of the fluid. The cross-section at this point is termed the entrance. In theory the temperature gradient in the fluid is infinite. The resulting local heat transfer coefficient and the Nusselt number are likewise infinite and decrease rapidly in the direction of the fluid flow. The thermal entry effect also has a marked dependence on Prandtl number of the fluid and generally increases as the Prandtl number decreases (17,18).

In the present application of heat transfer in short holes there is not only a thermal entry effect but also an aerodynamic entry effect. The present geometry involves sharp edged hole entry which will generate flow separation. In the length of holes being considered, fully developed turbulent or laminar flow will not be achieved. It is considered that it is the aerodynamic entry effects which dominate the short hole heat transfer.

Heat transfer in the entrance regions of pipes has been the subject of considerable research. Deissler (19) studied the effects of turbulent heat transfer at the entrance of smooth pipes using fluid of variable properties. He used the integral equation to solve for the heat transfer. Roberts et al (20) investigated heat transfer to air at the entrance of a heated annulus. They suggested that the heat transfer may be correlated as:

$$Nu = \left\{ \frac{Re\, Pr^{\frac{1}{3}} (1 + 0.01X)\phi}{1 - \left[\frac{4\phi(1 + 0.01X)X}{Pr^{\frac{2}{3}}(1 + \alpha)} \right]} \right\} \quad \ldots (5.22)$$

where $\phi = 0.0065\, Re_1^{-\frac{1}{6}}$

$X = L/D$

α = Radius ratio

Re = Duct flow Reynolds number

Re_1 = Momentum thickness Reynolds number

L = Axial distance

D = Diameter of annulus

Pr = Prandtl number

Sellars et al (21) investigated heat transfer to laminar fluid flow at the entrance of a round tube with constant heat flux and proposed that the heat transfer should be correlated as

LAMINAR

$$Nu = 1.6393\, X^{-\frac{1}{3}} \quad \ldots (5.23)$$

where $X = (L/r)(Re\, Pr)^{-1}$

L = Axial distance along the tube

r = Radius of the tube

Re = Reynolds number of fluid

Pr = Prandtl number

Sieder and Tate (22) working with liquids proposed, for the thermal entry effect, an equation of the form

LAMINAR

$$Nu = 1.86\left(\frac{Re\, Pr}{L/D}\right)^{\frac{1}{3}} \left(\frac{\mu}{\mu_s}\right)^{0.14} \quad \text{for} \quad \begin{array}{l} 0.48 < Pr < 16{,}700 \\ 0.0044 < (\mu/\mu_s) < 9.75 \\ L/D \geq 60 \end{array} \quad \ldots (5.24)$$

where Re = Reynolds number of fluid based on pipe diameter

Pr = Prandtl number

L = Length of pipe

D = Pipe diameter

μ = Dynamic viscosity of fluid at bulk temperature

μ_s = Dynamic viscosity of fluid evaluated at wall temperature

Kobata et al (33) used a 2-D straight channel to investigate turbulent flows in the entrance region of a pipe. Khalil (23), Lin et al (24) and Jicha et al (25) employed numerical methods in computing heat transfer in their work on thermal entry effect for a fluid flowing in a tube. Al-Arabi (26) investigating thermal entry effect for turbulent flows of liquid and air at pipe entries, suggested that the available data for the heat transfer coefficient (H) may be correlated by equation 5.25, which was stated to be applicable for $Re > 7000$ and $(X/D) > 3$.

$$H = \frac{h_L}{h_\infty} = 1 + 1.683\left(\frac{D}{X}\right)^{0.577} \qquad \ldots (5.25)$$

where h_L = Average heat transfer coefficient for pipe length L

h_∞ = Asymptotic heat transfer coefficient

X/D = Ratio of axial distance to pipe diameter

Lloyd et al (27) working on heat transfer in a short tube, applied equation 5.25 to correlate their heat transfer data. From their experimental result, it has been estimated that equation 5.25 only fits the data at $X \geq 1.7$ m and below this value the equation over-predicts the results. Heat transfer in small holes applicable in turbine blades cooling systems has been investigated by Trushin (28). Using copper plates with 400 perforated holes for each, thicknesses from 1-4 mm and holes' diameters ranging from 0.6 to 1.4 mm, he obtained a heat transfer equation as:

$$Nu = 1.1\ Re^{0.5} \qquad \text{... (5.26)}$$

$$Re \leq 10^4$$

and

$$Nu = 0.0023\ Re^{1.17} \qquad \text{... (5.27)}$$

$$Re > 10^4$$

where Nu = Nusselt number based on thickness of plate

Re = Reynolds number based on plate thickness

Mills (29) investigated local heat transfer characteristics for turbulent air flow at the entrance of circular pipes of length to diameter ratio ranging from 0.25 to 320 and having variable entrance format. In all, twelve series of the entrance format were investigated. The relevant heat transfer correlation for the present sharp edged entry is given by equation 5.28,

$$Nu = 0.023\ Re^{0.8}\ Pr^{0.333}\ R_{NU} \qquad \text{... (5.28)}$$

where

$$R_{NU} = \frac{\text{Nusselt number (average - } Nu_{AV})}{\text{Nusselt number (fully developed flow - } Nu_f)} \qquad \text{... (5.29)}$$

The correlation for Mills' fourth series has been chosen because the work reported here has holes all of sharp-edge entrance and in computing the heat transfer in the holes this correlation was employed. Another reason why the correlation was chosen is that Mills' work was done on pipes of length (L) to diameter (D) ratio (L/D) of 0.25 to 320, which are the ranges used in the work presented here, whereas most of the others are only applicable for $L/D \geq 60$. The parameter R_{NU} of equation 5.29 is a function of (L/D)

$$R_{NU} = f\left(\frac{L}{D}\right) \qquad \text{... (5.30)}$$

The data of Mills for series 4 have been curve-fitted to derive correlating equations for R_{NU} as:

for $(L/D) \leq 2.0$,

$$R_{NU} = 0.13197(\frac{L}{D})^3 - 0.7544(\frac{L}{D})^2 + 1.03993(\frac{L}{D}) + 2.2378 \quad \ldots (5.31)$$

for $(L/D) > 2.0$,

$$R_{NU} = 1 - 49.281(\frac{D}{L})^4 + 58.6032(\frac{D}{L})^3 - 26.476(\frac{D}{L})^2 + 7.48122(\frac{D}{L}) \quad \ldots (5.32)$$

$L \equiv t$ - thickness of test plate in this work.

It can be shown from equation 5.28 that the average convective heat transfer coefficient (H_{ch}) in the holes is

$$H_{ch} = 0.023\, Re^{0.8}\, Pr^{0.333}\, R_{NU}\, K_p/D \quad \ldots (5.33)$$

Knowing the temperature of the coolant fluid at the holes' inlet and that of the wall, the convective heat transfer, Q_{ch}, to the coolant can be computed. In the work presented here, the coolant temperature at the holes' inlet is unknown. The temperature (T_{in}) may however be predicted using either equation 5.4 or 5.9. Having obtained T_{in}, the convective heat transfer is given as

$$Q_{ch} = H_{ch}\, A_{ch}\, (T_{pl} - T_{in}) \quad \ldots (5.34)$$

where A_{ch} = Total area

$= N\pi Dt$

N = Total number of holes

T_{in} = Coolant holes' inlet temperature - K

t = hole length $\equiv$ plate thickness

The prediction of T_{in} is discussed in section 5.5.

5.3.2A.2 Comparison of surveyed holes' heat transfer correlations

The correlation proposed by Sieder and Tate, Sellar et al, Trushin and Mills (employed in this work) for thermal entry effect are compared in table 5.1. In addition, the empirical correlation of Le Grieves et al (74) shown below has been added. Le Grieves et al worked with short holes effusion cooling system and suggested the heat transfer in the holes be correlated in terms of Stanton number. This has been expressed as a Nusselt number, equation 5.34B, for the 17,222 m^{-2} holes effusion plate (L/D = 8.314) on which the theoretical computations of tables 1 and 2 are based.

$$Nu = 0.263\ Re^{0.6} \qquad \ldots (5.34B)$$

for Pr = 0.7
L/D = 8.314

The results of the theoretical computation are shown graphically in figs. 5.5 and 5.6 as Nusselt number as a function of coolant flowrate and Reynolds number. For all the correlations it is seen that the heat extracted increases with coolant flowrate as well as increase in Reynolds number. This trend is of course expected. Apart from Trushin's correlation, the theoretical predictions tend to converge at low coolant flowrate and as the flow approaches laminar state. At high coolant flow, the differences in the correlation are most evident with a huge jump for Trushin's correlation.

The Al-Arabi (26) correlation, which Lloyd et al (27) made use of, has been theoretically compared with the correlation employed in this work, in table 5.2 with Le Grieves et al, Trushin and McAdam's correlations. It is possible to normalize other

correlations to conform with the dimensionless heat transfer coefficient of Al-Arabi, by dividing the Nusselt numbers of other correlations by standard developed pipe-flow correlation (76,77), given by equation 5.B1.

$$Nu_\infty = 0.023\ Re^{0.8}\ Pr^{0.4} \qquad \ldots (5.B1)$$

or, for Pr = 0.7, we have

$$Nu_\infty = 0.019942\ Re^{0.8} \qquad \ldots (5.B2)$$

Table 5.2 shows that the value of h/h_∞ according to Al-Arabi as well as the correlation employed in the work reported here are constant for both coolant flowrates and Reynolds numbers.

The correlation employed for this work is only a factor of 1.1 greater than Al Arabi's but a factor of 1.8 and 3.5 less for Le Grieves et al and Trushin respectively. The present correlation of Mills' data, as shown by table 5.2, is almost mid-way in the range of all the other three correlations.

It will be shown in the next section that it is likely that the correlations of Le Grieves et al (74) and Trushin (28) apply to the overall heat transfer in a perforated plate. This means that they include the back-side approach flow heat transfer. However, neither of these two references give any significant details of the measurement techniques. For the other data, it is clear from the description of the measurement technique that only the internal tube heat transfer was considered and the back-side was insulated. This is generally the situation for all the short hole or tube entry length heat transfer investigations. The data of Mills are considered to be the best for the present purpose as his hole sizes are closer

TABLE 5.1

Coolant Flow Rate - kg/m^2s	Reynolds Number	Nusselt Number				
		Le Grieves et al	Sieder & Tate	Seller et al	Trushin	Present Work (Mills)
0.842	4.4×10^3	40.36	13.36	9.34	72.97	26.7
0.583	3.1×10^3	32.72	11.89	8.32	61.25	20.4
0.365	1.9×10^3	24.39	10.097	7.06	47.95	13.79
0.27	1.4×10^3	20.31	9.12	6.38	41.16	10.8
0.178	0.092×10^3	15.78	7.93	5.55	33.37	7.72

Table 5.1: Theoretical comparison of thermal entry effect for various literature correlations with that employed in the current work. (L/D = 8.314, Pr = 0.7)

TABLE 5.2

Coolant Flow Rate kg/m^2s	Reynolds Number	Le Grieves et al (74) h/h_∞	Al-Arabi (26) & Lloyd (27) h/h_∞	Trushin (28) h/h_∞	McAdams (72) h/h_∞	Present Work (Mills) h/h_∞
0.842	4.4×10^3	2.46	1.50	4.45	1.23	1.63
0.583	3.1×10^3	2.64	1.50	4.95	1.23	1.65
0.365	1.9×10^3	2.91	1.50	5.73	1.23	1.65
0.270	1.4×10^3	3.10	1.50	6.28	1.23	1.65
0.178	0.9×10^3	3.37	1.50	7.12	1.23	1.65

Table 5.2: Theoretical comparison of dimensionless heat transfer coefficient in 17,222 m^{-2} holes plate for various survey correlations. (L/D = 8.314; Pr = 0.7)

to those of interest in film cooling than for many investigators who used quite long diameter pipes.

The correlation of Al-Arabi was based on a review of several workers' work, including Sieder and Tate and Sellar et al. Table 5.2 reveals that the correlation employed for heat transfer in holes in the work reported here is higher than this correlation but applies to smaller holes. The slight difference between the two coefficients may be due to the fact that the universal correlation of Al-Arabi is only efficient for conditions of Re > 7000 and L/D > 3. That of Mills covers all the conditions operative in the present work and hence the justification for employing the correlation.

The most widely used correlation for thermal entry effect and heat transfer in tubes in the industry is the correlation given by McAdams (72). McAdams recommended that for a sharp-edged entry, such as is the case in the present work, the heat transfer in the tube should be correlated as in equation 5.B3.

$$\frac{h}{h_\infty} = 1 + \left(\frac{L}{D}\right)^{-0.7} \qquad \ldots (5.B3)$$

The theoretical results of equation 5.B3, shown in table 5.2, indicate that this correlation will under-predict the present work by 25% and that of Al-Arabi by 18%. It may be concluded in the light of present correlations that industrial estimations of heat transfer in tubes, as applicable in the present work, using McAdams' correlation have been under-estimated by up to 21.5%.

5.3.2A.3 Bulk holes' heat transfer correlation

None of the investigators of drilled hole cooling systems has given more than a token reference to heat transfer at the back-side

of the unit considered. However some workers have presented a single correlation to typify heat transfer at both the back-side and the holes of the cooling system. The only work of significance in this area for 90^{o} holes is that of Le Grieves et al and Trushin.

The heat transfer at the back of the effusion wall was recognized and given attention by Andrews et al (14,75). The trend of that investigation led to the separate presentation and analysis of what actually happens prior to the holes. To justify the claim that a bulk correlation for both the back and holes of the cooling wall were presented by other workers, a bulk correlation for the present work is here developed by combining the correlation of Sparrow et al with that of Mills.

From equation 5.1, we have for the back-side:

$$Nu_s = 0.881\ Re^{0.476}\ Pr^{\frac{1}{3}} \qquad \ldots (5.1S)$$

(The above Nusselt number by Sparrow was based on the ratio of unperforated total area to the total pitch of the holes.)

From equation 5.28 for the holes we have:

$$Nu_M = 0.023\ Re^{0.8}\ Pr^{\frac{1}{3}}\ R_{NU} \qquad \ldots (5.28)$$

For the 17,222 m^{-2} holes plate of L/D = 8.314, $R_{Nu} = 1.60847$

$$\therefore \quad Nu_M = 0.037\ Re^{0.8}\ Pr^{\frac{1}{3}} \qquad \ldots (5.28B)$$

Defining bulk heat transfer at the holes as Nusselt number, Nu_B, we have:

$$Nu_B = Nu_s + Nu_M \qquad \ldots (5.C1)$$

Substituting from equations 5.1S and 5.28B, we have:

$$Nu_B = (0.881\ Re^{0.476} + 0.037\ Re^{0.8})Pr^{\frac{1}{3}} \qquad \ldots (5.C2)$$

For a Prandtl number of 0.7, we have:

$$Nu_B = (0.782243 + 0.03285\ Re^{0.324})Re^{0.476} \quad \ldots (5.C3)$$

The theoretical computation of equation 5.C3 is presented in table 5.3 as a comparison with the correlations of Le Grieves et al and Trushin. Correlation of equation 5.C3 compares very well with that of Trushin but only marginally with that of Le Grieves, as the deviation from Trushin's correlation is only around 11% while for Le Grieves et al it is around 42%. Equation 5.C3 agrees within 5% with Trushin's at turbulent flow region while the deviation widens as the coolant flow tends towards laminarization. The wide difference between equation 5.C3 and that of Le Grieves may be because much attention has not been given to convective heat transfer by coolant scrubbing of the back-wall as it approaches the holes.

TABLE 5.3

Coolant Flow Rate - kg/m^2s	Reynolds Number	Nusselt Number		
		Le Grieves et al	Trushin	Present Work (Eq. 5.C3)
0.842	4.4×10^3	40.36	72.97	69.42
0.582	3.1×10^3	32.72	61.25	56.31
0.365	1.9×10^3	24.39	47.95	42.24
0.270	1.4×10^3	20.31	41.16	35.40
0.178	0.9×10^3	15.78	33.37	27.86

Table 5.3: Comparison of proposed bulk short holes heat transfer correlation with those available in the literature. ($17{,}222\ m^{-2}$ holes effusion plate; L/D = 8.314, Pr = 0.7)

Since the derivation of equation 5.C2 takes into account detailed back-side heat transfer and thermal entry effects in short tubes, as well as the fluid Prandtl number, which may vary with temperature increases, it is suggested that this equation may be used in cases where detailed back-side heat transfer analysis is not undertaken.

5.3.3 Flame-side of the Full Coverage Discrete Hole Film Cooling System

The coolant air leaves the plate's holes in the form of jets penetrating into the mainstream. The magnitude of the degree of penetration is a function of the coolant to mainstream density ratio, velocity ratio, holes' size and the plate holes' pitch. As the jets penetrate into the mainstream, the cross-flow upstream is retarded with a build-up of pressure at this end. This leads to the deflection of the jets back towards the wall. The jets interact and coalesce (30) forming a blanket of cool layer of gas over the surface of the test wall. The effectiveness of the wall's protection is a function of the cooling potential left in the coolant after reaching the flame side. Jets that penetrate deeper into the mainstream before being deflected will entrain the hot gas, allowing the mainstream to flow between the penetrating jets and create regimes of detachment at the surface of the wall. The problems of penetration, entrainment and detachment with reattachment are functions of coolant mass flowrate and lead to high heat transfer coefficient (31,32) at the surface of the wall. At high coolant flowrate, the coolant will penetrate deeper into the mainstream before being deflected. However, because of the high cooling

potential left in the coolant, the effect of entrainment of the hot stream will not significantly affect the cooling protection offered to the wall. At low flowrate, the coolant cooling potential will be significantly reduced due to heat transfer from the back-side and holes of the plate. At the flame-side, the jets exhausted will easily be deflected and remain attached to the wall's surface but the protection offered in this case is impaired.

On this side of the test wall, as shown in fig. 5.4, three major heat transfer processes exist. These are:

5.3.3A Radiative heat transfer from the hot gas stream;

5.3.3B Radiative heat exchange between the test wall and the duct walls; and

5.3.3C Convective heat transfer from the hot gas stream to the wall.

To fully account for the heat transfer processes above, the temperature (T_g) of the mainstream must be accurately known. This temperature, in the consideration of the heat processes below, is a subject of special consideration later in this chapter but is used before then as a fully accurate stream temperature.

5.3.3A Radiative heat transfer, Q_f, from the hot gas stream

Knowing the mainstream gas temperature, T_g, and the emissivity of the test section, the radiation from the stream incident on the plate can be computed with accuracy, but only if the emissivity of the mainstream is known. A mean emissivity, E_f, of the stream can be determined to a high degree of accuracy using the approach of Reeves (35), Herbert (36), Lefebvre et al (37,38), Kretchmer et al (39) and Odgers (40). The emissivity has been correlated as:

$$E_f = 1 - \exp[-0.2864\ l_m P(rL)^{0.5} T_g^{-1.5}] \quad \ldots (5.35)$$

where l_m = Luminosity factor of flame

Using data of Kretchmer et al (39) and Odgers (40), an equation for flame luminosity factor has been deduced as

$$l_m = 0.0691(0.01\rho - 3.48)^{2.71} \quad \ldots (5.36)$$

where ρ = Density of fuel burnt - kg/m^3

P = Combustor total pressure - Pa

r = Effective fuel/air (37) ratio by mass

L = Mean beam length - m

The mean beam length has been taken as the combustor diameter by Lefebvre et al (37). In the work reported here, the beam length for the combustor used has been determined as 0.0446 m (10).

Herbert, in his evaluation of radiative heat transfer from gas turbine combustor mainstream, stated that radiation be correlated as:

$$Q_{rf} = \sigma\left(\frac{1 + E_p}{2}\right)(E_f T_g^4 - T_{pl}^4) \quad \ldots (5.37)$$

Lefebvre et al have correlated the radiation as in equation 5.38. This correlation is now widely used and is presented here as:

$$Q_{rf} = A\sigma\left(\frac{1 + E_p}{2}\right)E_f T_g^{1.5}[T_g^{2.5} - T_{pl}^{2.5}] \quad \ldots (5.38)$$

The above equation is employed in the work presented here.

5.3.3B Radiative heat, Q_n, exchange between the test wall and the duct walls

The duct walls are cooled, separately, by air and, since the test wall is mounted as a part of these walls - fig. 5.3, there is

a temperature difference between the two components. The effect of the wall temperature difference in this work is very significant when the application of the results to a practical cylindrical combustor is considered. The duct exchanges radiative heat with the test wall as a result of the difference in temperature. In determining the net radiation by the test plate to the duct, the radiosity method of Gray et al (13) has been employed. The net radiation, Q_n, is given as

$$Q_n = \frac{AE_p}{(1 - E_p)} (\sigma T_{p1}^4 - W_1) \qquad \ldots (5.39)$$

$$W_1 = E_p \sigma T_{p1}^4 + (1 - E_p) W_2 F_{12} (1 - E_{12}) + (1 - E_p) E_{g1} \sigma T_g^4 \qquad \ldots (5.40)$$

$$W_2 = E_{e2} \sigma T_d^4 + (1 - E_{e2}) W_d F_{21} (1 - E_{21}) + (1 - E_{e2}) W_2 F_{22} (1 - E_{22}) + (1 - E_{e2}) E_{g2} \sigma T_g^4 \qquad \ldots (5.41)$$

where $W_2 = W_d$ = radiosity leaving the duct walls.

Substituting equation 5.41 into equation 5.40, it can be shown that

$$W_1 = \frac{Z_3 + Z_4}{Z_5} \qquad \ldots (5.42)$$

and

$$Q_n = \frac{AE_p(\sigma T_{p1}^4 Z_5 - Z_3 - Z_4)}{Z_5(1 - E_p)} \qquad \ldots (5.43)$$

where $Z_5 = 1 - F_{22}(1 - E_{e2})(1 - E_{22}) - F_{21}(1 - E_p)(1 - E_{e2})(1 - E_{12})(1 - E_{21})$ ... (5.43A)

$$Z_4 = [\sigma E_{e2} T_d^4 + \sigma E_{g2} T_g^4 (1 - E_{e2})] (1 - E_p)(1 - E_{12}) \qquad \ldots (5.43B)$$

$$Z_3 = [\sigma E_p T_{p1}^4 + \sigma E_{g1} T_g^4 (1 - E_p)][1 - F_{22}(1 - E_p)(1 - E_{22})] \qquad \ldots (5.43C)$$

Parameters F_{12}, F_{21} and F_{22} are view factors of the test wall and the duct walls. Taking the duct walls as a single surface, according to (31),

$$AF_{12} = A_d F_{21} \quad \ldots (5.44)$$

where A = Area of the test wall

A_d = Area of the duct walls

F_{12} = View factor of test wall

F_{21} = View factor of duct wall

Since the test wall is a flat plate and connot see itself, $F_{12} = 1$. However the duct wall can see itself and hence the component F_{22}. The value of F_{21} has been determined (14,15) as 0.106. For the duct wall the sum of F_{21} and F_{22} must be unity (13) and so $F_{22} = 0.894$.

Parameters $(1 - E_{e2})$ and $(1 - E_p)$ are the duct and test walls' absorptivities. $(1 - E_{12})$, $(1 - E_{21})$ and $(1 - E_{22})$ are the hot gas transmissivities. The duct walls' material is stainless steel and its emissivity, E_{e2}, has been correlated by curve fitting the data of ref. (16) for 18/8 (304) stainless steel as rolled and oxidized at 873 K. The emissivity which was linear with temperature, with uncertainty of less than $\pm 0.5\%$, is given as

$$E_{e2} = 0.6179 + 2.40933 \times 10^{-4} T_d \quad \ldots (5.45)$$

where T_d = the duct wall mean temperature - K.

To find the flame emissivities, E_{12}, E_{21}, E_{22} and E_{g2}, equation 5.35 is employed as

$$E_{g2} = E_f \quad \ldots (5.35b)$$

$$E_{12} = 1 - \exp[-0.2864\, l_m\, P(rl_{12})^{0.5}\, T_g^{-1.5}] \quad \ldots (5.46)$$

$$E_{21} = 1 - \exp[-0.2864\, l_m\, P(rl_{21})^{0.5}\, T_g^{-1.5}] \quad \ldots (5.47)$$

$$E_{22} = 1 - \exp[-0.2864\, l_m\, P(rl_{22})^{0.5}\, T_g^{-1.5}] \quad \ldots (5.48)$$

Equations 5.46 to 5.48 are easily computed if the unknowns, l_{12}, l_{21} and l_{22}, which are beam lengths relative to the test and duct walls surface, are determined. The values of these beam lengths have been calculated (14,16) as $l_{12} = 0.04214$, $l_{21} = 0.04214$ and $l_{22} = 0.0745$. Substituting these values into the above equations, the required emissivities are easily obtained. Finally, substituting back into equation 5.43, the net radiation from the test wall to the duct walls is obtained. Having determined the radiative exchange the convective heat at the surface of the wall must be determined. It is this heat transfer process to which the next section addresses itself.

5.3.3C Convective heat transfer, Q_c, from the hot gas stream to the wall

Convective heat transfer by the mainstream to film cooled surface has been investigated extensively (41-51). Most of these investigations are for turbine blade application and nearly all of the work done so far has been done at conditions of very low temperature far removed from practical turbine engine conditions.

Two approaches of computing heat transfer coefficient at the film cooled wall surface are currently in use. These correlations are

(a) heat transfer coefficient computed from the knowledge of the adiabatic wall temperature (41,42,49), and

(b) heat transfer coefficient computed using the principle of superposition (44-47).

In the quest for better representative correlation for this local heat transfer, other researchers have applied direct measurement techniques such as liquid crystal (4), mass transfer analogy

using naphthalene (49) and swollen polymer measurement (50,51) to determine the surface heat transfer coefficient.

The above methods, even though they are widely applied, have defects when employed in real situations, and in the case of a combustor wall cooling with heat transfer within the wall. The methods may be used if a procedure is available to reliably predict the hole outlet temperature; such a procedure has been presented in the present work. The new method of heat transfer measurement using swollen polymer has the drawback of not being suitable in situations of changing fluid physical properties (52) or density ratio effect as is the case with combustor coolant. At the present time no single correlation has been found that offers a very high degree of reliability, especially for the full coverage discrete hole film cooling combustor. All of the work applies to one or two rows of holes.

In the present work, the heat transfer by convection from the hot stream to the film cooled surface is computed by employing the heat balance on the test wall. The determination of the heat transfer coefficient of convection is the focus of the next section.

5.3.3C.1 Heat balance and flame side convective heat transfer coefficient, H_c

The heat balance on the film cooled wall takes into account all the heat transfer processes on the test wall, fig. 5.4. At steady state, the heat balance on the wall is

$$Q_{cb} + Q_{rb} + Q_{ch} + Q_n = Q_c + Q_{rf} \qquad \ldots (5.49)$$

The unknown parameter in equation 5.49 is Q_c. Rearranging,

$$Q_c = Q_{cb} + Q_{rb} + Q_{ch} + Q_n - Q_{rf} \qquad \ldots (5.50)$$

Substituting values for the heat transfer processes on the right-hand side of equation 5.50, the convective heat transfer to the test wall surface from the hot gas stream and flame is determined. With Q_c known, the mean coefficient of convection, H_c, is easily predicted as in equation 5.51.

$$H = \frac{Q_c}{A(T_g - T_{pl})} \qquad \ldots (5.51)$$

where H_c = mean coefficient of convection - W/m^2K

A = test surface area - m^2

T_g = corrected mainstream temperature - K (as discussed in section 5.4)

The above predicted values of mean heat transfer coefficient of convection, based on thermal stations on the test wall, serve as a basis for modelling the test wall results to a condition equivalent to a cylindrical combustor.

The main gas stream temperature, T_g, is a very important parameter in the accurate computation of the heat transfer processes on the flame side of the film cooled wall. Its determination is the subject of the next section.

5.3.3C.2 Error in Q_c and H_c

The accuracy of Q_c depends largely on the accuracy of the correlations applied to the computation of heat transfer Q_{cb} at the back of the plate and in the holes Q_{ch} as shown by equation 5.50. The correlation of Sparrow et al used in computing Q_{cb} has an overall uncertainty of less than ± 5% and that of Mills, employed in the computation of Q_{ch}, has an overall maximum uncertainty of less than ± 3%. The uncertainty in Q_{rf} is ± 2%. Since Q_{rb} and

Q_n of equation 5.50 are ignored during modelling, section 5.7, the global error in Q_c is ± 10%. However the relative error between two plates of different geometries is much less than the above magnitude for Q_c.

The error in the film heat transfer coefficient depends on the accuracy of Q_c and the mainstream temperature, T_g. The error involved in the measurement of T_g is negligible at low temperature work of 700-900 K but it is significant at high temperature work of 1400-2000 K. The error, as detailed in the next section, is up to ± 3% at high temperature. Taking T_g's uncertainty into account, the error involved in H_c is ± 7%. This is an error in the absolute magnitude of H_c and the uncertainty in the relative effect of the hole diameter will bring the uncertainty in H_c down to about ± 3%.

5.4 MAIN GAS STREAM TEMPERATURE, T_g, MEASUREMENT AND CORRECTION

In the measurement of the main gas stream temperature in this work, thermocouples were employed. Two main types of thermocouple which were used are:

(a) the type K, Chrome-Alumel, grounded junction mineral insulated 1.6 mm diameter thermocouple, and

(b) Pt/Pt 13% Rh thermocouple, mineral insulated.

The type K thermocouple was used for low temperature work, that is mainstream temperature range of 600 to 800 K, while the Pt/Pt 13% Rh thermocouple was employed at high temperature work of 810 to 2000 K mainstream temperature. The advantages in using a thermocouple to determine the mainstream temperature are simplicity, rapidity of read-out and lower cost. Against this background is the error associated with thermocouple temperature measurement of

flowing gas stream. This error is a function of the convection, radiation, conduction, velocity and surface reaction effects. This error source has been investigated extensively (53-58) and is considered briefly below.

(i) Convection error. The convection error is associated with the flow velocity over the thermocouple. The convective heat transfer to the thermocouple from the hot stream varies approximately as a square root of the mass flow rate of the fluid. The correlating equation for this error for a wire normal to the flow has been given by Williamson et al (58) as

$$Nu = 0.477\left(\frac{\dot{M}D}{\mu}\right)^{0.5} Pr^{0.3} \qquad (5.52)$$

where Nu = Nusselt number

$\dot{M}$ = Mass flow rate of gas

D = Diameter of thermocouple wire

μ = Viscosity of gas

Pr = Prandtl number based on fluid

The above error may be reduced by increasing the gas flow rate over the thermocouple junction and reducing the thermocouple diameter. Neither of these techniques was possible in the present work.

(ii) Radiation error. As the thermocouple gets hotter than the fluid container, it loses heat by radiation to the surrounding surfaces which it sees. This error is correlated by Stottmann (55) as

$$\Delta t = CE(T_g^4 - T_w^4) \qquad \ldots (5.53)$$

where Δt = Temperature departure

C = Constant

E = Emissivity of the thermocouple junction

T_g = Fluid temperature

T_w = Container wall temperature

The fourth power effect of the temperature on radiation loss as well as the thermocouple emissivity are the paramount parameters in the estimation of this error. The error may be reduced by reducing the emissivity of the junction, by applying resistance heating and by increasing the wall temperature, T_w, in equation 5.53.

(iii) Conduction error. This occurs if the heat transfer from the junction to the support is significant. By maintaining the thermocouple support at nearly the same temperature as the junction, keeping the wire thermal conductivity low and keeping the cross-sectional area of the wire small, the above error may be eliminated. In the present work, the thermocouple's body was immersed in the hot gas and conduction errors were small.

(iv) Surface catalysis. Surface reaction occurs on Pt/Rh thermocouples in hot gases containing unburnt fuel and oxygen. This leads to higher temperatures being indicated by the thermocouple than what the true temperature of the gas is. This error mainly occurs on bare wire and may be eliminated by either coating the wire with aluminium oxide or sheeting it. In the present work, a mineral insulated Pt/Rh thermocouple was used and the junction was not exposed to the hot gas.

(v) Gas Radiation Error. This error is insignificant at low pressures up to atmospheric but prominent at high pressures.

Aware of these errors, a means of correcting the indicated thermocouple temperature in the work reported here was developed.

At Rolls Royce a correlation has been developed by Foxcroft (59) for the same purpose in their turbine combustor. This correlation, which we modified to take account of emissivities of the two types of thermocouples mentioned above, has been employed in this work. To use the modified equation to correct for the mainstream temperature, the Mach number, Mc, of the mainstream was computed with a guessed mainstream temperature near that indicated. The value of this Mc was then used to upgrade the gas stream indicated temperature. A new Mc was then calculated using the upgraded temperature. This new Mc value was then used to compute the temperature error (difference between actual and indicated temperature). Using the result obtained, a corrected value of mainstream temperature was computed. The modified correlation is given as

$$\Delta t = \frac{3.369 \times 10^{-8} E_m T_{g_n}^{-0.18} (T_{g_n}^4 - T_w^4)}{(M_c P)^{0.5}} \qquad \ldots (5.54)$$

where Δt = the temperature error - K

E_m = Emissivity of thermocouple junction (type K = 0.8 to 0.95 Pt/Pt 13% Rh = 0.25-0.3 intensive use in rough atmosphere = 0.5)

T_{g_n} = Mainstream indicated temperature - K

T_w = Mean wall temperature - K

P = Combustor total pressure at plane of test - Pa

$$Mc = \frac{(R T_{g_n}/\gamma)^{0.5} \dot{M}}{P A_c} \qquad \ldots (5.55)$$

where Mc = Mach number

A_c = Combustor cross-sectional area = $\pi D_c^2/4$

D_c = Combustor hydraulic diameter - m

R = Gas constant

γ = Ratio of specific heats, taken as 1.4

$\dot{M}$ = Mainstream mass flow rate

Actual mainstream temperature is given as:

$$T_g = T_{gn} + \Delta t \qquad \ldots (5.56)$$

The value of the mainstream temperature, T_g, given in equation 5.56 was employed in the computation of heat transfer processes at the film cooled wall flame side. A computer program was used to carry out the mainstream temperature. At low temperature work, equation 5.54 has an uncertainty of ± 1.0% while at high temperature the uncertainty is as high as ± 3.0%. These errors take into account the ± 0.1% manufacturers' thermocouple error which, when amplified for digital output, results in ± 0.4% uncertainty.

5.5 EFFUSION HOLES' COOLANT INLET AND OUTLET TEMPERATURES

In the computation of convective heat transfer in the holes the coolant temperature T_{in} at inlet is unknown. However this temperature may be predicted by equating heat transfer to the fluid as it approaches the holes to the correlating equation 5.9 derived from (7). The heat transfer to the fluid is

$$Q_{co} = \dot{M}C_p(T_{in} - T_c) \qquad \ldots (5.57)$$

Now

$$Q_{co} = Q_{cb}$$

$$T_{in} = Q_{cb}(\dot{M}C_p)^{-1} + T_c \qquad \ldots (5.58)$$

where $\dot{M}$ = Coolant mass flow rate - kg/s

C_p = Coolant specific heat capacity as in equation 5.10

T_c = Coolant temperature measured in the plenum - K

T_{in} = Predicted coolant holes inlet temperature

The coolant outlet jet temperature, T_t, is not monitored but its knowledge is significant in understanding the aerodynamics of the coolant fluid at the flame side of the test wall. Such knowledge as the inlet to outlet coolant density ratio, jet velocity, blowing rate and jet penetration into the cross-stream will be lost if information on T_t is not available. To deduce T_t the heat transfer to the coolant in a pipe flow, Q_p, is equated to the correlation deduced from Mills (29), equation 5.34.

$$Q_p = \dot{M}C_p(T_t - T_{in}) \qquad \ldots (5.59)$$

(Heat transfer to fluid in the holes)

$$Q_p = Q_{ch} = \dot{M}C_p(T_t - T_{in})$$

Rearranging, T_t is predicted as

$$T_t = Q_{ch}(\dot{M}C_p)^{-1} + T_{in} \qquad \ldots (5.60)$$

where C_p = Coolant specific heat capacity as in equation 5.10 but based on temperature T_{in}

With the prediction of the above temperatures is associated the complex mechanism of coolant jet penetration and mixing processes. Penetration of cross-stream by coolant jets is the focus of the next section.

5.6 JETS' PENETRATION INTO AND DEFLECTION BY MAINSTREAM WITH OUTLET DENSITY AND VELOCITY PREDICTIONS

5.6.1 Jets' Penetration and Deflection by Mainstream

Because of the convenience of small temperature differences, the majority of film cooled experiments reported to date in the literature have been performed with low density ratios of approximately

unity. Those that were performed at high density ratio use alternative coolant gases (e.g. freon) to simulate density variation but it has been found that density variation of this sort has implications for hole size and coolant pressure loss (60). The reason for this is that in essence the technique allows the velocity and the density of the coolant to be varied independently but density variation in a practical turbine is brought about by temperature increases. The effect of temperature increase on coolant is a reduction in its density and an increase in its velocity. Hence both density and velocity are linked. This effect of density variation leads to penetration of coolant jets into the cross-stream in practical situations, much of the same sort as in the work reported here. The penetration, deflection and attachment of the jets to the test wall surface is of significance in the performance of a full coverage discrete hole cooling design. The knowledge of coolant penetrating distance also helps in the understanding of the flow aerodynamics at the test wall. Jiji et al (61), Kennedy et al (62), Shaw et al (63), Button (64,65), Andreopoulos (66), Keffer et al and Keffer (67,68) have all investigated the effect of jet penetration into a cross-stream. For a simple round free jet discharging into a stagnant fluid, the extent of jet penetration is given (69) as

$$Y = 6.3\left(\frac{\rho_c}{\rho_g}\right)^{0.5} \frac{u_g}{u_o} D \qquad \ldots (5.61)$$

where Y = Jet trajectory from the hole exit

ρ_c = Coolant jet density

ρ_g = Stagnant fluid density

u_g = Jet exit velocity

u_o = Jet velocity on the axis

D = Jet diameter at exit $\equiv$ hole's diameter

Equation 5.61 shows that the jet length, Y, from hole exit is a function of the coolant density as well as the hole size, D. If D is small, equation 5.61 implies less penetration, assuming all other conditions are constant.

In this work, the jets are discharging into a flowing cross-stream and equation 5.61 cannot adequately account for the true value of Y. Button (64,65) investigated a jet of air in a cross-flow using cotton threads, and showed that the jet was deflected by the cross-stream and that there was an area of recirculation downstream of the jet inlet. The implication of recirculation will lead to the development of a hot spot on the combustor surface. Gregoric et al (70) used salt water to investigate the discharge of multiple jets in a cross-flow. They reported the development of vortexes by the jets and also noted reduction in the level of entrainment compared with a single jet. Gregoric et al correlated their data with equation 5.62:

$$Y = 0.78\, R^{-0.98} N^{0.17} X^{0.52} D_o^{0.48} \qquad \ldots (5.62)$$

where Y = Jets' length from exit

$R = \dfrac{\text{Mainstream velocity}}{\text{Jet velocity}}$

N = Number of jets

X = Horizontal co-ordinate

D_o = Jet diameter at exit

Shaw et al (63) investigated the effect of pressure ratio on the penetration of an under-expanded sonic jet in a cross-stream, and showed that there was a negative pressure downstream of the deflected jet which resulted in recirculation and entrainment. They propose an analytic correlation as:

$$Y = 0.755\left(\frac{P_j}{P_s}\right)^{0.5} D \qquad \ldots (5.63)$$

Equation 5.63 can, of course, be shown to be

$$Y = 0.755\left(\frac{\rho_j T_j}{\rho_s T_s}\right)^{0.5} D \qquad \ldots (5.64)$$

where Y = Jet length from exit

P_j = Total pressure of jet

P_s = Cross-stream static pressure

D = Jet diameter

Isaac et al (71) showed, from their work on multiple jets, that the rear jet trajectory is significantly modified by the presence of the front jet while Andreopoulos (66) concluded that the vortex formed by the deflected jet has a stabilizing effect on fluid turbulence.

At the present time there is no one correlation that adequately or reliably accounts for multiple jets, such as encountered in this work, trajectory into a turbulent cross-stream. To account for the cross-stream effect on jet trajectory, the work of Keffer and Baines (67) has been found to be more relevant, though with a drawback. Keffer and Baines (67) determined the trajectory and diffusion characteristics of a single jet for outlet jet velocity to mainstream velocity ratios of 2, 4, 6, 8 and 10.

The plot of Keffer et al's work, with slight modification, gives

$$\frac{Z}{DR} = 5.5\left(\frac{Y}{DR}\right)^{2.175} \qquad \ldots (5.65A)$$

Rearranging, $Y = 0.45665\, Z^{0.4598}\, (DR)^{0.5402}$

$$R = \frac{\rho_o u_o^2}{\rho_g u_g^2} \qquad \ldots (5.65B)$$

Substituting,

$$Y = 0.457\, Z^{0.46} \left(\frac{D\rho_o}{\rho_g}\right)^{0.54} \left(\frac{u_o}{u_g}\right)^{1.08} \quad \ldots (5.66)$$

where Y = Jet trajectory - mm

Z = Distance to the direction of the cross-stream

D = Jet diameter at hole's exit - mm

ρ_o = Coolant jet density at outlet - kg/m^3

ρ_g = Mainstream density at plane of test

u_o = Jet velocity at outlet - m/sec

u_g = Mainstream velocity - m/sec

Equation 5.66 was used in obtaining the penetration depth of coolant jets into the mainstream before deflection in the work reported here. The distance, Z, for the purpose of this work has been replaced by a hole pitch, while the jet diameter was assumed to be equal to the hole diameter at exit. Both the jets' density and velocity at outlet were predicted.

5.6.2 Jets' Outlet Density and Velocity Prediction

The blowing rate, which is the ratio of coolant to mainstream mass velocities, is an important parameter in the estimation of the performance of any cooling system. In this work, both the density and velocity of the coolant at outlet are not directly measured but are predicted from heat balance developed above. The density of the jets at outlet is predicted by equation 5.67.

$$\rho_o = \frac{P}{R\,T_t} \quad \ldots (5.67)$$

where ρ_o = Predicted coolant jets outlet density - kg/m^3

P = Upstream total pressure - Pa

R = Gas constant

T_t = Coolant jets' outlet temperature from section 5.5

The velocity of the coolant is predicted from the continuity equation as

$$V_o = \frac{\dot{M}}{\rho_o A_h} \qquad \ldots (5.68)$$

where V_o = Mean velocity of jets at outlet - m/s

$\dot{M}$ = Coolant mass flowrate - kg/s

A_h = Total cross-sectional area of holes - m^2

Using the above parameters, the blowing rate of the coolant is correlated as

$$M = \frac{\rho_o V_o}{\rho_g V_g} \qquad \ldots (5.69)$$

where M = Dimensionless blowing rate

$\rho_o V_o$ = Mass velocity of coolant

$\rho_g V_g$ = Mass velocity of mainstream

The predictions above were made in order of the thermal stations on the test wall.

The application of test results to cylindrical combustors needs some modelling and this requirement is dealt with below.

5.7 MODELLING OF FLAT PLATE RESULT FOR CYLINDRICAL COMBUSTOR

The work reported here made use of a flat test plate which simulates a small part of an annular gas turbine combustor. To enhance the reliability of the application of the results obtained to a cylindrical combustor employed in both industrial and aero-engines, correction is made in the heat transfer processes. The aim of this modelling was to eliminate the duct heat transfer which does not occur in a cylindrical combustor. The focal points

of the modelling of the results are:

(a) In a full cylindrical combustor using an effusion cooling system, the radial temperature of the wall at a given location will be fairly similar. Since the material for construction is the same, the emissivity and the absorptivity of the wall at this location will also be the same.

(b) In accordance with statement (a), the wall will only be receiving radiation from the hot gas stream.

(c) The radiation at the back of the cylindrical combustor will be entirely to the coolant if there is any. For this work the radiation is small and is neglected.

Having the above main points in mind, the modelling of the results for a cylindrical combustor starts by setting to zero the radiative exchange in the heat balance, equation 5.50. The value of radiative heat at the back of the effusion wall was also set to zero. From the resulting convective heat transfer from the hostile hot stream to the test wall, Q_c, a corrected value of wall temperature and hence cooling effectiveness for a cylindrical combustor was obtained. From the corrected temperature, a new value of convective heat transfer coefficient, H_c, was computed. The final heat balance equation is given as:

$$Q_c = Q_{cb} + Q_{ch} - Q_{rf} \qquad \ldots (5.70)$$

5.8 COMPUTER PROGRAM

To handle the large amount of data collected and to process it for the cooling effectiveness of the effusion wall, the heat transfer in the system and the modelling of the results, a computer

program was written. The program incorporates all the heat transfer processes detailed in the previous sections. It operates by reading the data, processes the data for a flat plate, and predicts the plenum temperature from the radiative heat loss from the back-side as

$$\dot{M}C_p(T_{ple} - T_c) = Q_{rb} \quad \ldots (5.71)$$

$$T_{ple} = Q_{rb}(\dot{M}C_p)^{-1} + T_c \quad \ldots (5.72)$$

where T_{ple} = Plenum temperature - K

The program then commenced modelling by setting the radiative heat transfer processes as stated above to zero and reprocessed the results, using the predicted temperature of the coolant for a cylindrical combustor. The detailed results for both flat plate and cylindrical combustor are then output. The computer program layout is as shown in the flowchart in section 5.10.

5.9 FLAT NON-PERFORATED SURFACE HEAT TRANSFER

The heat transfer measurement of a flat non-perforated surface was carried out at the same time as the injection through the perforated surface. This was done using the flux meter as dimensioned and depicted in Chapter 2. Coolant air at a constant flowrate is made to pass through the flux meter, which sits next to the test plate at one end and exhaust to the surrounding at the other end. Applying Newton's law of cooling (72,73), the heat transfer to the flux meter wall by the hot combustion gases is, for wall heating,

$$Q_{f1} = H_{f1} A_{f1} (T_g - T_{f1}) \quad \ldots (5.73)$$

where Q_{fl} = Convective heat transfer to the wall - W

H_{fl} = Convective heat transfer coefficient - W/m^2K

A_{fl} = Surface area of the flux meter in contact with mainstream - m^2

T_g = Mainstream temperature - K

T_{fl} = Flux meter measured surface wall temperature - K

The heat transfer coefficient is the unknown parameter of the right-hand part of equation 5.73. The heat transfer to the flux meter is equal to the heat removed by the flowing air. This heat to the air is given as:

$$Q_{fl} = \dot{M}_{fl} C_p (T_{out} - T_{in}) \qquad \ldots (5.74)$$

where $\dot{M}_{fl}$ = Flux meter corrected air mass flow rate - kg/s

C_p = Specific heat capacity of air computed as in equation 5.10 but based on mean temperature of the air $(T_{out} + T_{in})/2$

T_{out} = Flux meter air outlet temperature (monitored) - K

T_{in} = Flux meter air inlet temperature (monitored) - K

Combining equations 5.73 and 5.74, it can be shown that

$$H_{fl} = \dot{M}_{fl}(T_{out} - T_{in})[A_{fl}(T_g - T_{fl})]^{-1} \qquad \ldots (5.75)$$

5.9.1 Comparison of Measured Flat Plate Heat Transfer with Surveyed Correlations

Heat transfer to a flat plate has been widely investigated (2,79,80). For turbulent flow over a flat plate, Chilton and Colburn (80) suggested that the heat transfer be correlated as in equation 5.76:

$$Nu_{cb} = 0.0296\ Re^{0.8}\ Pr^{0.333} \qquad \ldots (5.76)$$

On the basis of the experimental work of Zhukauskas and Ambrazyavichyus (79), Whitaker (2) has recently proposed that for turbulent boundary layer the local Nusselt number on a flat plate be correlated as:

$$Nu_{wh} = 0.029\ Re^{0.8}\ Pr^{0.43} \qquad \ldots (5.77)$$

For air, Pr = 0.72. These two equations have constants of 0.0265 and 0.0252 respectively and thus equation 5.76 is over 5% greater than equation 5.77.

In the present work, high turbulence is generated using three inline Jet Mix (81) flame stabilisers. The above correlations' application is problematic in the method of choosing the characteristic dimension for the Nusselt and Reynolds number. The major problem is the point at which the starting point for fully developed flow is defined and hence determining the characteristic dimension on which both the Nusselt and Reynolds numbers are based. However no matter what length is chosen, the coefficient of heat transfer on the flat plate is, as is shown later, not strongly dependent on this dimension due to the power exponent of 0.2 for this dimension.

The length, L, of the flux meter used is 0.0762 m. Using this length, the heat transfer coefficients according to Chilton and Colburn (80), and Whitaker (2) may be shown respectively as in equations 5.76B and 5.77B.

$$H_{ccb} = 0.0296\ Re^{0.8}\ Pr^{0.333}\ \frac{K}{L} \qquad \ldots (5.76B)$$

$$H_{wh} = 0.029\ Re^{0.8}\ Pr^{0.43}\ \frac{K}{L} \qquad \ldots (5.77B)$$

where H_{ccb} = Flat plate heat transfer coefficient based on Chilton and Colburn's correlation - W/m^2K

H_{wh} = Flat plate heat transfer coefficient based on Whitaker's correlation - W/m^2K

K = Thermal conductivity of fluid - W/mK

L = 0.0762 m - flux meter length

Tables 5.4 and 5.5 show the results of heat transfer coefficient, H_{fl}, obtained in the present work, at low and high temperature work respectively, according to equation 5.75. Tables 5.6 and 5.7 compare these results with correlations available in the literature. At low temperature work, table 5.6 shows that H_{ccb} over-predicts experimentally obtained convective coefficient (H_{fl}) by 9% while H_{wh} over-predicts it by ± 3.3%. At high temperature work, H_{ccb} over-predicts H_{fl} by 44.3% while H_{wh} over-predicts it by 38.8%. It is well-known that correlations from literature cannot be expected to predict results, at this sort of temperature, to better than 30% accuracy (73).

Because of the disagreement that exists in determining the characteristic dimension, L, (79) one might choose the hydraulic diameter, D, which in the present work is greater than L by 25%. The value of D is 0.1016 m and may be substituted for L in equation 5.76B and 5.77B to give

$$H_{ccb_1} = 0.0296\ Re^{0.8}\ Pr^{0.333}\ \frac{K}{D} \qquad \ldots (5.76C)$$

$$H_{wh_1} = 0.029\ Re^{0.8}\ Pr^{0.43}\ \frac{K}{D} \qquad \ldots (5.77C)$$

Table 5.8 shows the results of equations 5.76C and 5.77C compared with equations 5.76B and 5.77B. The results indicate a difference of approximately 5% between using L and D. This difference is small and it may be concluded that the characteristic dimension chosen for a turbulent heat transfer to a flat plate is not of major

TABLE 5.4

$\dot{M}_{fl}$ - kg/s	C_p - J/kgK	T_{out} - K	T_{in} - K	A_{fl} - m^2	T_g - K	T_{fl} - K	H_{fl} - W/m^2K
0.00288	1.01×10^3	395.5	304.0	0.009677	768.6	431.2	81.4
0.00239	1.01×10^3	409.8	307.6	0.009677	765.1	444.2	79.3
0.00221	1.01×10^3	414.7	309.0	0.009677	765.0	450.2	77.4
0.00208	1.01×10^3	420.3	310.3	0.009677	766.2	454.6	76.7
0.00205	1.01×10^3	420.3	311.4	0.009677	766.2	451.9	74.3

Table 5.4: Flat plate experimental heat transfer coefficient

TABLE 5.5

$\dot{M}_{fl}$ - kg/s	C_p - J/kgK	T_{out} - K	T_{in} - K	A_{fl} - m^2	T_g - K	T_{fl} - K	H_{fl} - W/m^2K
0.00424	1.02×10^3	569.2	319.2	0.009677	1821.2	673.2	97.4
0.00425	1.02×10^3	573.2	320.5	0.009677	1821.3	694.2	100.5
0.00425	1.03×10^3	699.2	346.9	0.009677	1837.3	818.2	157.0

Table 5.5: Flat plate experimental heat transfer coefficient

TABLE 5.6

Re	Pr	K - W/mK	Heat Transfer Coefficient W/m^2K		
			H_{ccb}	H_{wh}	Experimental - H_{fl}
4.7×10^4	0.7047	0.0561	84.2	79.8	81.4
4.7×10^4	0.7045	0.0559	83.9	79.4	79.3
4.8×10^4	0.7045	0.0559	85.4	80.8	77.4
4.8×10^4	0.7041	0.0560	85.5	80.9	76.7
4.8×10^4	0.7041	0.0560	85.5	80.9	74.3

Table 5.6: Comparison of experimental heat transfer coefficient to a flat plate with survey literature correlations at low temperature work

TABLE 5.7

Re	Pr	K - W/mK	Heat Transfer Coefficient W/m^2K		
			H_{ccb}	H_{wh}	Experimental - H_{fl}
5.2×10^4	0.8636	0.0949	165.2	159.6	97.4
5.1×10^4	0.8721	0.0940	161.7	156.3	100.5
5.0×10^4	0.8692	0.0951	160.9	155.5	157.0

Table 5.7: Comparison of experimental heat transfer coefficient to a flat plate with survey literature correlations at high temperature work

significance as long as it is within the length of the surface of the plate under investigation.

5.9.2 Comparison of Flat Plate Heat Transfer with Fully Developed Turbulent Pipe Flow Correlations

For turbulent fully developed flow, McAdams (72) suggested the heat transfer to the wall be correlated as

$$Nu = 0.023\ Re^{0.8}\ Pr^{0.4} \qquad \ldots (5.78)$$

Dittus and Boelter (82), working with turbulent liquid flow in tubes, suggested that, for heat transfer from the fluid to the wall, the heat flow may be correlated as in equation 5.79.

$$Nu_d = 0.0265\ Re_d^{0.8}\ Pr^{0.3} \qquad \ldots (5.79)$$

Working with air flow in a tube, Mills (29) correlated his data using least square method and proposed that convective heat transfer to the wall, for a fully developed turbulent flow, be correlated as

$$Nu = 0.0397\ Re^{0.73}\ Pr^{0.33} \qquad \ldots (5.80)$$

Using the hydraulic diameter, D (= 0.1016 m), of the combustor employed in the present work, the predictions of the above correlations as well as those of Chilton and Colburn, and Whitaker are compared in table 5.9 with experimental results for low temperature work. The Reynolds number, Prandtl number and the thermal conductivity of the fluid are as in table 5.6.

Table 5.9 shows that Chilton and Colburn's correlation is within ± 3% of the result of the present work. The correlation of Dittus and Boelter under-predicts the experimental result by 7% while correlations of McAdams and Mills under-predict it by more than 20%. Whitaker's correlation using the hydraulic diameter is

TABLE 5.8

Correlation of Chilton and Colburn		Correlation of Whitaker	
H_{ccb} - W/m^{2}K	H_{ccbl} - W/m^{2}K	H_{wh} - W/m^{2}K	H_{whl} - W/m^{2}K
84.2	79.5	79.8	75.3
83.9	79.2	79.4	75.0
85.4	80.6	80.8	76.3
85.5	80.7	80.9	76.4
85.5	80.7	80.9	76.4

Table 5.8: Comparison of heat transfer coefficient on a flat plate using both heat transfer surface length, L, and hydraulic diameter, D.

TABLE 5.9

Convective Heat Transfer Coefficient - W/m^{2}K					
Chilton & Colburn[1]	McAdams[2]	Dittus & Boelter[3]	Whitaker[4]	Mills[5]	Experimental
79.5	60.4	72.0	75.3	50.3	81.4
79.2	60.1	71.8	75.0	50.1	79.3
80.6	61.1	73.0	76.3	50.9	77.4
80.7	61.2	73.1	76.4	51.0	76.7
80.7	61.2	73.1	76.4	51.0	74.3

1 $Nu = 0.0296\ Re^{0.8}\ Pr^{0.33}$ 2 $Nu = 0.023\ Re^{0.8}\ Pr^{0.4}$

3 $Nu = 0.0265\ Re^{0.8}\ Pr^{0.3}$ 4 $Nu = 0.029\ Re^{0.8}\ Pr^{0.43}$

5 $Nu = 0.0397\ Re^{0.73}\ Pr^{0.33}$

Table 5.9: Comparison of flat plate heat transfer coefficient with fully developed turbulent flow correlations of other workers

within ± 2% of this result. It can be concluded, therefore, that the correlation of Whitaker (2) is closest to the present measured result and may be employed in situations where the temperature cannot be measured directly.

The mean value of H_{f1} has been compared with experimental values of film heat transfer coefficient, H_c, at the surface of the effusion wall of varying geometries for very low coolant injection or no blowing condition. H_{f1} was found to be higher than these values of H_c. This difference arose because of two major reasons:

(a) a high degree of surface roughness and hence high skin friction on the surface of the perforated wall, and

(b) high natural convection taking place on the other side of the perforated wall at no injection state.

Condition (a) will typify the nature of boundary layer development (83) on the perforated surface without coolant injection. The skin friction and boundary layer on the perforated wall are parameters which quantify the heat transfer coefficient to the wall's surface. Condition (b) will in the same manner affect H_c at no injection state. It can be concluded that, at no injection state, the heat transfer coefficient on a perforated plate will not be the same as that for a non-perforated flat plate.

The results of the heat transfer processes as analysed in this chapter for the effusion cooling system are detailed in Chapter 6.

5.10 COMPUTER PROGRAM FLOW SHEET

A detailed computer program and samples of two operating temperature results are shown in the appendix.

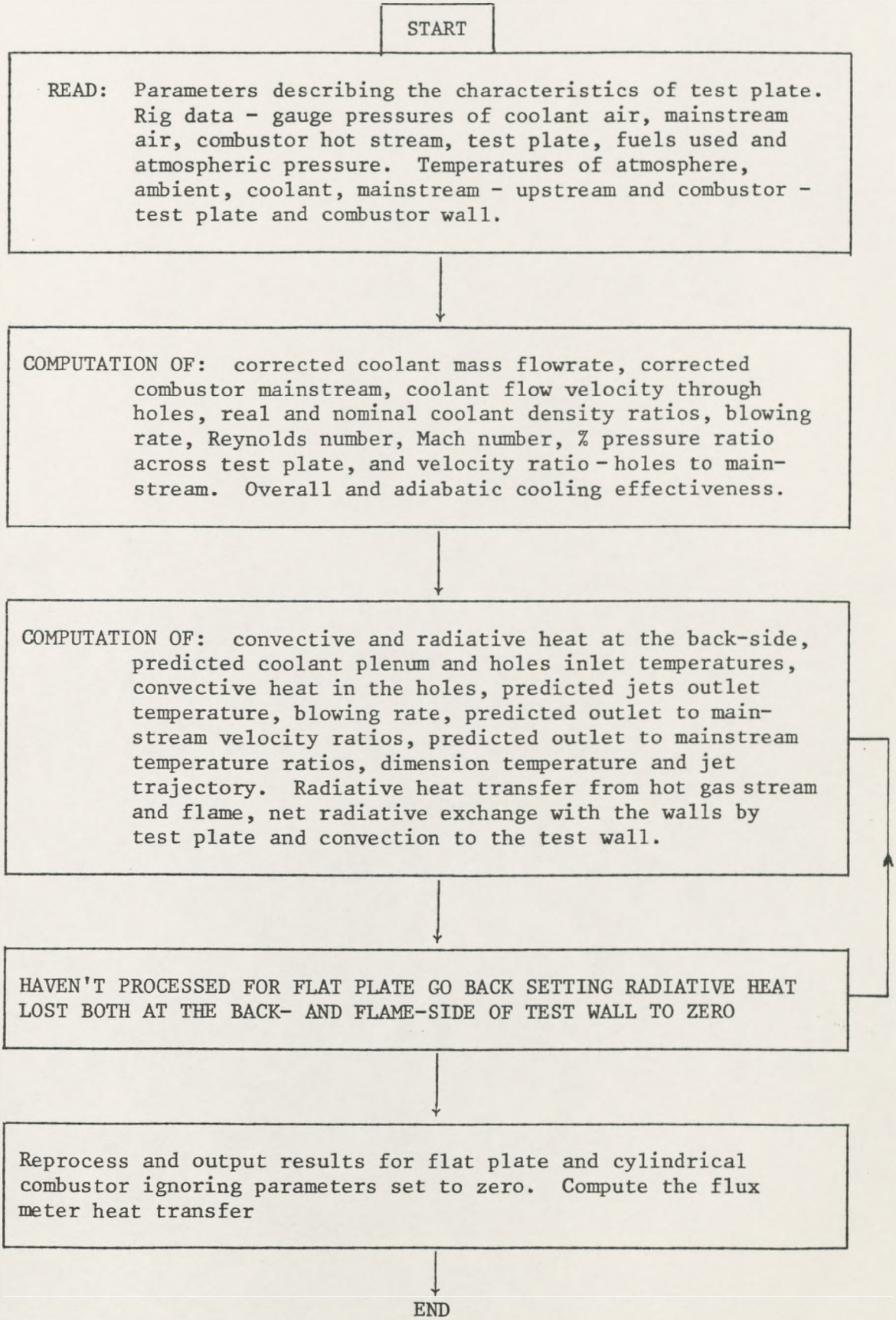

5.11 REFERENCES

1. Colburn, A.P., 'A method of correlating forced convection heat transfer data and a comparison with fluid friction', Transactions of the American Inst. Chem. Eng., Vol. XXIX, pp. 174-210, 1933.

2. Whitaker, S., 'Forced convection heat transfer correlations for flow in pipes, past flat plates, single cylinders, single spheres, and for flow in packed beds and tube bundles', AIChE Journal, Vol. 18, No. 2, pp. 361-371, March 1972.

3. Choe, H., Kays, W.M., and Moffat, R.J., 'Turbulent boundary layer on a full-coverage film-cooled surface - an experimental heat transfer study with normal injection', NASA CR-2642, 1976.

4. Kasagi, N., Hirata, M., and Kumada, M., 'Studies of full-coverage film cooling, Part 1: Cooling effectiveness of thermally conductive wall', ASME paper 81-GT-37, 1981.

5. Mayle, R.E., and Camarata, F.J., 'Multihole cooling film effectiveness and heat transfer', ASME J. Heat Transfer, pp. 534-538, 1975.

6. Furuhama, K., Moffat, R.J., and Frota, M.N., 'Heat transfer and turbulence measurements of a film-cooled flow over a convexly curved surface', 83-Tokyo-IGTC-16.

7. Sparrow, E.M., and Ortiz, M.C., 'Heat transfer coefficients for the upstream face of a perforated plate positioned normal to an oncoming flow', Int. J. Heat Mass Transfer, Vol. 25, No. 1, pp. 127-135, 1982.

8. US National Bureau of Standards Circ. 564, 1955.

9. Reid, C.R., and Sherwood, T.K., 'The properties of gases and liquids: their estimation and correlation', McGraw-Hill Book Company Inc., 1958.

10. Mkpadi, M.C., 'Full coverage effusion cooling of gas turbine combustion chamber', Ph.D. thesis, Dept. of Fuel and Energy, University of Leeds, Leeds, 1982.

11. Watson, J.T.R., 'Thermal conductivity of gases in metric units', Department of Trade and Industry, National Engineering Laboratory, 1973.

12. E02AFH - Chebyshev - Series - NAG Fortran Library Routine Document, NAGF LIB: 1790/0: MK8, IBM, 28 Jan., 1981.

13. Gray, W.A., and Muller, R., 'Engineering Calculations in Radiative Heat Transfer', Pergamon Press, Oxford, 1974.

14. Andrews, G.E., Gupta, M.L., and Mkpadi, M.C., 'Combustor wall temperature predictions for blank, perforated and combined impingement and effusion plate systems', Rept. No. GEA/HT/6, Dept. of Fuel and Energy, University of Leeds, 1981.

15. Andrews, G.E., Gupta, M.L., and Mkpadi, M.C., 'Combined radiative and convective heat transfer in an enclosure', First UK National Heat Transfer Conference, I.Chem.E. Symposium Series No. 86, pp. 979-988, 1984.

16. Sulley, A.H., Bander, E.A., and Waterhouse, R.B., 'Some measurements of the total emissivity of metal and pure refractory oxides and the variation of emissivity with temperature', Brit. J. Appl. Phys. Vol. 3, pp. 99-101, 1952.

17. Sparrow, E., Hallman, T., and Siegel, R., 'Turbulent heat transfer in the thermal entrance region of a pipe with uniform heat flux', Appl. Scientific Research, Sect. A, Vol. 7, No. 1, 1957.

18. Martin, B.W., and Fargie, D., 'Effect of temperature-dependent viscosity on laminar forced convection in the entrance region of a circular pipe', Proc. Instn. Mech. Engrs., Vol. 186 24/72, 1972.

19. Deissler, R.G., 'Analysis of turbulent heat transfer and flow in the entrance regions of smooth passages', NACA Tech. Note 3016, 1953.

20. Roberts, A., and Barrow, H., 'Turbulent heat transfer to air in the vicinity of the entry of an internally heated annulus', Proc. Instn. Mech. Engrs., Vol. 182, Pt. 3H, 1967-68.

21. Sellars, J.R., Tribus, M., and Klein, J.S., 'Heat transfer to laminar flow in a round tube or flat conduit - The Graetz problem extended', Trans. ASME, pp. 441-448,Feb. 1956.

22. Sieder, E., and Tate, G., 'Heat transfer and pressure drop of liquids in tubes', Ind. Eng. Chem.,Vol. 28, pp. 1429-1435, Dec. 1936.

23. Khalil, E.E., 'Heat transfer to turbulent pipe flows with swirl and following a sudden enlargement', Proc. 7th Int. Heat Transfer Conf., Vol. 3, 1982.

24. Lin, T., and Shah, V.L., 'Numerical solution of heat transfer to yield Power Law fluids flowing in the entrance region', Proc. 6th Int. Heat Transfer Conf., Vol. 5, 1978.

25. Jicha, M., and Ramik, Z., 'Turbulent boundary layer heat transfer in the entrance region of a pipe', Proc. 7th Int. Heat Transfer Conf., Vol. 3, 1982.

26. Al-Arabi, M., 'Turbulent heat transfer in the entrance region of a tube', Heat Transfer Engineering, Vol. 3, pp. 76-83, 1982.

27. Lloyd, S., and Brown, A., 'Fluid flow and heat transfer characteristics in the entrance regions of circular pipes', ASME - Paper 85-GT-121, 1985.

28. Trushin, V.A., 'Results of analysis of experimental data from study of heat transfer in holes typical for turbine blade perforations by the local similarity method', Izvestiya VUZ, Aviatsionnaya Tekhnika, Vol. 23, No. 3, pp. 120-122, 1980.

29. Mills, A.F., 'Experimental investigation of turbulent heat transfer in the entrance region of a circular conduit', J. Mech. Eng. Science, Vol. 4, No. 1, pp. 63-77, 1962.

30. Afejuku, W.O., Hay, N., and Lampard, D., 'Measured coolant distributions downstream of single and double rows of film cooling holes', ASME - J. Eng. Power, Vol. 105, pp. 172-177, 1983.

31. Baughn, J.W., Hoffman, M.A., Takahashi, R.K., and Launder, B.E., 'Local heat transfer downstream of an abrupt expansion in a circular channel with constant wall heat flux', Trans. ASME - J. Heat Transfer, Vol. 106, pp. 789-796, 1984.

32. Clifford, R.J., Jones, T.V., and Dunne, S.T., 'Techniques for obtaining detailed heat transfer coefficient measurements within gas turbine blade and vane cooling passages', ASME - Paper 83-GT-58, 1983.

33. Kobata, T., Yoshino, Y., Masuda, S., and Ariga, I., 'Turbulent flows in entrance region of two-dimensional straight channel with inlet disturbance', Bulletin of the JSME, Vol. 26, No. 220, pp. 1711-1718, 1983.

34. Hengyue, W., Shaoyan, G., Dengyun, L., and Yaxian, Y., 'Method of calculation and calculated curves of film-cooled wall temperature', Eng. Thermophysics in China, Vol. 1, pp. 95-110, 1980.

35. Reeves, D., 'Flame radiation in industrial gas turbine combustion chamber', NGTE: M.285, Oct. 1956.

36. Herbert, M.V., 'Some notes on heat transfer in combustion chambers', NGTE, Note No. NT 196, 1955.

37. Lefebvre, A.H., and Herbert, M.V., 'Heat transfer processes in gas turbine combustion chambers', Proc. Inst. Mech. Eng., Vol. 174, No. 12, pp. 463-478, 1960.

38. Lefebvre, A.H., 'Radiation from flames in gas turbines and rocket engines', 12th Symposium (Int.) on Combustion, pp. 1247-1253, 1968.

39. Kretschmer, D., and Odgers, J., 'A simple method for the prediction of wall temperatures in gas turbines', ASME - Paper 78-GT-90, 1978.

40. Odgers, J., 'Problems due to multifuel operation of gas turbine combustors'. A Project Squid Workshop - Gas Turbine Combustor Design Problems. Ed. A.H. Lefebvre, Hemisphere Pub. Corp., London, 1980.

41. Goldstein, R.J., 'Film cooling', Advances in Heat Transfer, Vol. 7, Academic Press, New York and London, pp. 321-379, 1971.

42. Goldstein, R.J., and Chen, H.P., 'Film cooling on a gas turbine blade near the end wall', ASME - Paper 84-GT-42, 1984.

43. Goldstein, R.J., and Yoshida, T., 'The influence of a laminar boundary layer and laminar injection on film cooling performances', Trans. ASME - J. Heat Transfer, Vol. 104, pp. 355-362, 1982.

44. Crawford, M.E., Choe, H., Kays, W.M., and Moffat, R.J., 'Full-coverage film cooling heat transfer study - Summary of data for normal-hole injection and 30° slant-hole injection', NASA CR-2648, 1976.

45. Metzger, D.E., Carper, H.J., and Swank, L.R., 'Heat transfer with film cooling near non-tangential injection slots', J. Eng. Power, Vol. 90, 1968.

46. Metzger, D.E., Takeuchi, D.I., and Kuenstler, P.A., 'Effectiveness and heat transfer with full-coverage film cooling', ASME - J. Eng. Power, pp. 180-184, 1973.

47. Eckert, E.R.G., 'Analysis of film cooling and full-coverage film cooling of gas turbine blades', 83-Tokyo-IGTC-15, 1983.

48. Dunn, M.G., 'Turbine heat flux measurements: Influence of slot injection on vane trailing edge heat transfer and influence of rotor on vane heat transfer', ASME - Paper 84-GT-175, 1984.

49. Kumada, M., Hirata, M., and Kasagi, 'Studies of full-coverage film cooling. Part 2: Measurement of local heat transfer coefficient', ASME - Paper 81-GT-38, 1981.

50. Hay, N., Lampard, D., and Saluja, C.L., 'Application of the swollen polymer technique to the study of heat transfer on film cooled surfaces', Proc. 7th Int. Heat Transfer Conf., Vol. 4, pp. 503-508, 1982.

51. Saluja, C.L., Lampard, D., Hay, N., and Burns, I., 'The determination of heat transfer coefficients on film cooled flat surfaces using the swollen polymer technique', First UK National Conf. Heat Transf., I. Chem. E. Symp. Series, Vol. 2, No. 86, pp. 893-906, 1984.

52. MacLeod, N., Discussion on paper, 'The use of electronic speckle-pattern interferometry for convective mass-transfer measurement: Studies of transfer to a turbulent air jet impinging on a plane surface', presented at the 11th Annual Research Meeting of I. Chem. E., Bath, 1984.

53. Moffat, R.J., 'Gas temperature measurement', Temperature, Its Measurement and Control in Science and Industry, Rheinhold, New York, pp. 553-571, 1962.

54. Glawe, G.E., Johnson, R.C., and Krause, L.N., 'Intercomparison of several pyrometers in a high-temperature gas stream', Temperature, Its Measurement and Control in Science and Industry, Vol. 3, Pt. 2, Reinhold, New York, pp. 601-605, 1962.

55. Stottmann, P., 'Temperature measurements with thermocouples including errors caused by catalytic effects', AGARD-CP-73-71, Proc. No. 73, 1971.

56. Green, S.J., and Hunt, T.W., 'Accuracy and response of thermocouples for surface and fluid temperature measurements', Temperature, Its Measurement and Control in Science and Industry, Vol. 3, Pt. 2, Reinhold, New York, pp. 695-722, 1962.

57. Holderness, F.H., Tilston, J.R., and MacFarlane, J.J., 'Electrical compensation for radiation loss in thermocouples', NGTE, Note No. NT 758, 1969.

58. Williamson, R.C., and Stanforth, C.M., 'Measurement of jet engine combustion temperature by the use of thermocouples and gas analysis', SAE, 1969.

59. Foxcroft, J.S., 'The measurement of combustion chamber exit temperature', Rolls Royce Ltd., 1971.

60. Andrews, G.E., Discussion on paper - 'Measured coolant distributions downstream of single and double rows of film cooling holes', ASME - J. Eng. Power, Vol. 105, p. 177, 1983.

61. Jiji, L.M., and Moghadam, S.M., 'Theoretical and experimental investigation of 3-D buoyant turbulent jets', Proc. 7th Int. Heat Transfer Conf., Vol. 2, pp. 425-430, 1982.

62. Kennedy, L.A., and Chang, R.H., 'Measurements of velocity and temperature profiles of a heated surface jet discharging into a cross flow', Proc. 7th Int. Heat Transf. Conf., Vol. 6, pp. 111-115, 1982.

63. Shaw, C.S., and Margason, R.J., 'An experimental investigation of a highly underexpanded sonic jet ejecting from a flat plate into a subsonic crossflow', NASA TN D-7314, 1973.

64. Button, B.L., 'Effectiveness measurements for a cooling film disrupted by a single jet', ASME - Paper 83-GT-250, 1983.

65. Button, B.L., 'Effectiveness measurements for a cooling film disrupted by a single jet with wall plunging', AGARD - CPP - 390, 1985.

66. Andreopoulos, J., 'Measurements in a jet-pipe flow issuing perpendicularly into a cross stream', ASME - J. Fluids Engineering, Vol. 104, pp. 493-499, 1982.

67. Keffer, J.F., and Baines, W.D., 'A round turbulent jet in a cross-wind', J. Fluid Mech., Vol. 15, pt. 4, pp. 481-497, 1963.

68. Keffer, J.F., 'The physical nature of the subsonic jet in a cross-stream', NASA SP-128, 1969.

69. Andrews, G.E., Asere, A., and Mkpadi, M.C., 'Transpiration and full coverage discrete hole film cooling', I. Chem. E., 11th Annual Research Meeting, pp. 92-96, 1984.

70. Gregoric, M., Davis, L.R., and Bushnell, D.J., 'An experimental investigation of merging buoyant jets in a crossflow', ASME - J. Heat Transfer, Vol. 104, pp. 236-240, May 1982.

71. Isaac, K.M., and Schetz, J.A., 'Analysis of multiple jets in a cross-flow', ASME - J. Fluids Eng., Vol. 104, pp. 489-492, 1982.

72. McAdams, W.H., 'Heat Transmission', 3rd Ed., McGraw-Hill Kogakusha Ltd., London, 1954.

73. Incropera, F.P., and Dewitt, D.P., 'Fundamentals of Heat Transfer', John Wiley & Sons, New York, 1981.

74. Le Grieves, E., Nicolas, J.J., and Genot, J., 'Internat aero-dynamics and heat transfer problems associated to film cooling of gas turbines', ASME Paper No. 79-GT-57.

75. Andrews, G.E., Gupta, M.L., and Mkpadi, M.C., 'Full coverage discrete hole wall cooling: Cooling effectiveness', ASME Paper No. 84-GT-212, 1984.

76. Bayley, F.J., Cornforth, J.W., and Turner, A.B., 'Experiments on a transpiration cooled combustion chamber', Proc. Instn. Mech. Engrs., Vol. 187, 1973.

77. Holman, J.P., 'Heat Transfer', 5th Ed., McGraw Hill Inter. Book Company, 1981.

78. Topping, J., 'Errors of Observation and Their Treatment', 3rd Ed., Chapman and Hall Limited, London, 1969.

79. Zhukauskas, A.A., and Ambrazyavichyus, A.B., 'Heat transfer of a plate in a liquid flow', Int. J. Heat Mass Transfer, Vol. 3, pp. 305-309, 1961.

80. Chilton, T.H., and Colburn, A.P., 'Mass transfer (absorption) coefficients, prediction from data on heat transfer and fluid friction', Ind. Eng. Chem., Vol. 26, No. 11, pp. 1183-1187, Nov. 1934.

81. Andrews, G.E., Abdul-Aziz, M.M., and Al-Dabbagh, N.A., 'Mixing and fuel atomisation effects on premixed combustion performance', ASME Paper 83-GT-55, 1983.

82. Dittus, F.W., and Boelter, L.M.K., Univ. Calif. Publs. Eng., 2:443, 1930.

83. Schlichting, H., 'Boundary Layer Theory'. Translated by J. Kestin, 7th Ed., McGraw Hill Book Company, 1979.

84. Sparrow, E.M., and Gurdal, U., 'Heat transfer at an upstream-facing surface washed by fluid en route to an aperture in the surface', Int. J. Heat and Mass Transfer, Vol. 24, No. 5, pp. 851-857, 1981.

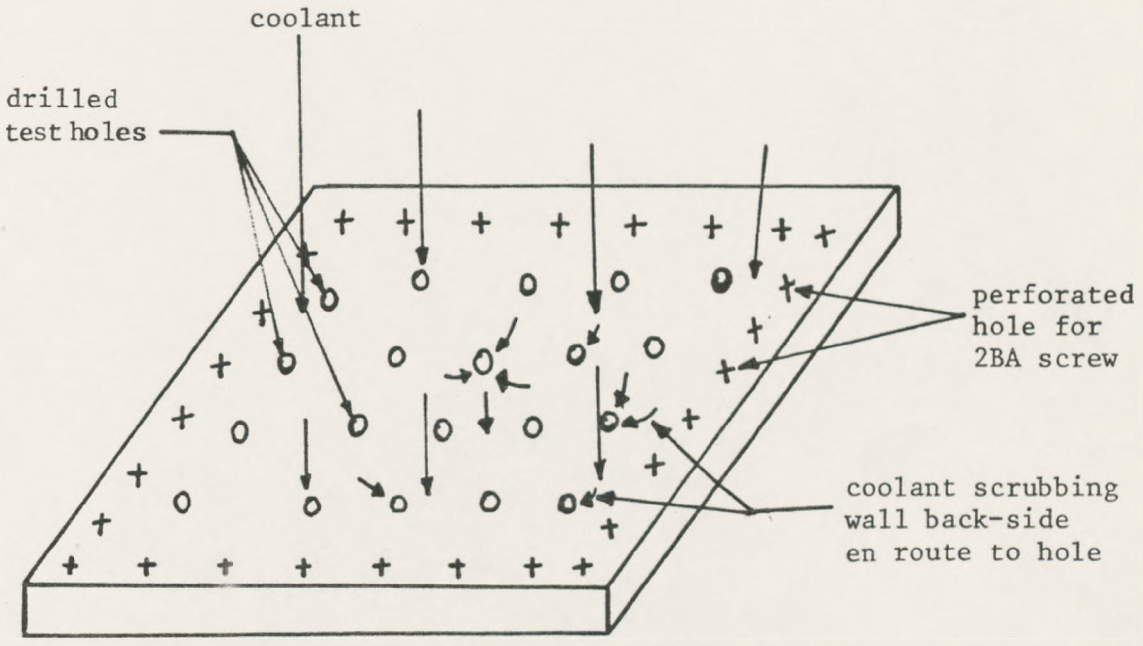

Fig. 5.1: Effusion plate

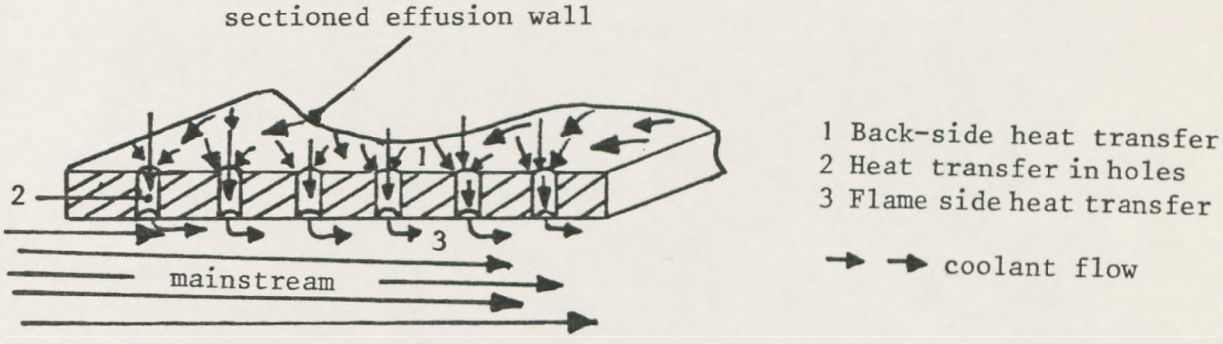

Fig. 5.2: Heat transfer processes in full coverage discrete hole film cooling system

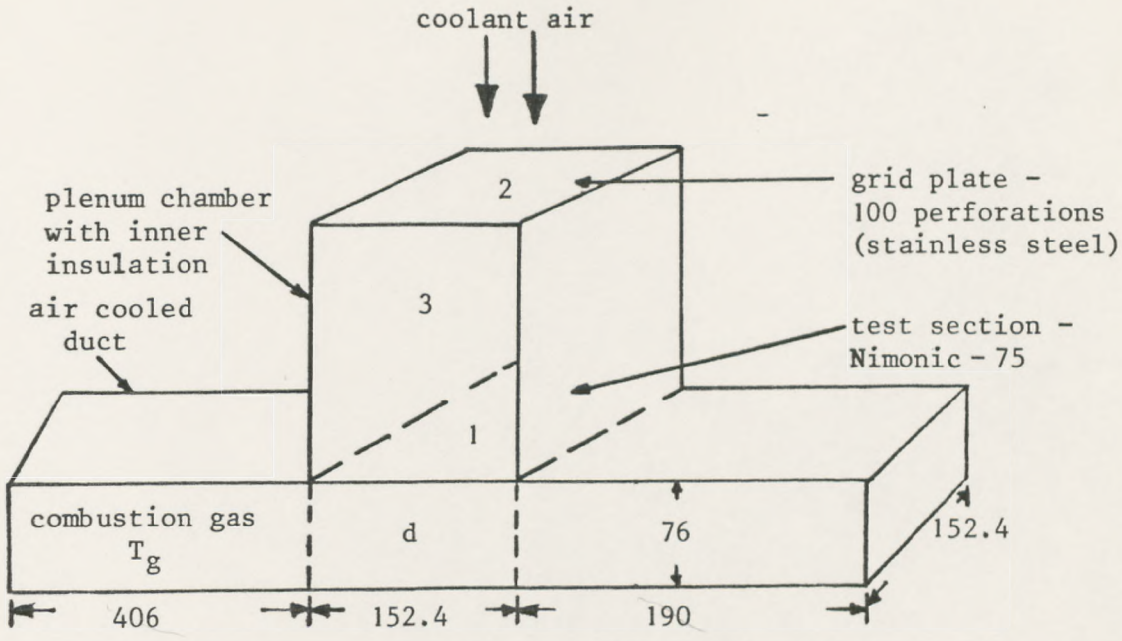

Fig. 5.3: Radiative volume

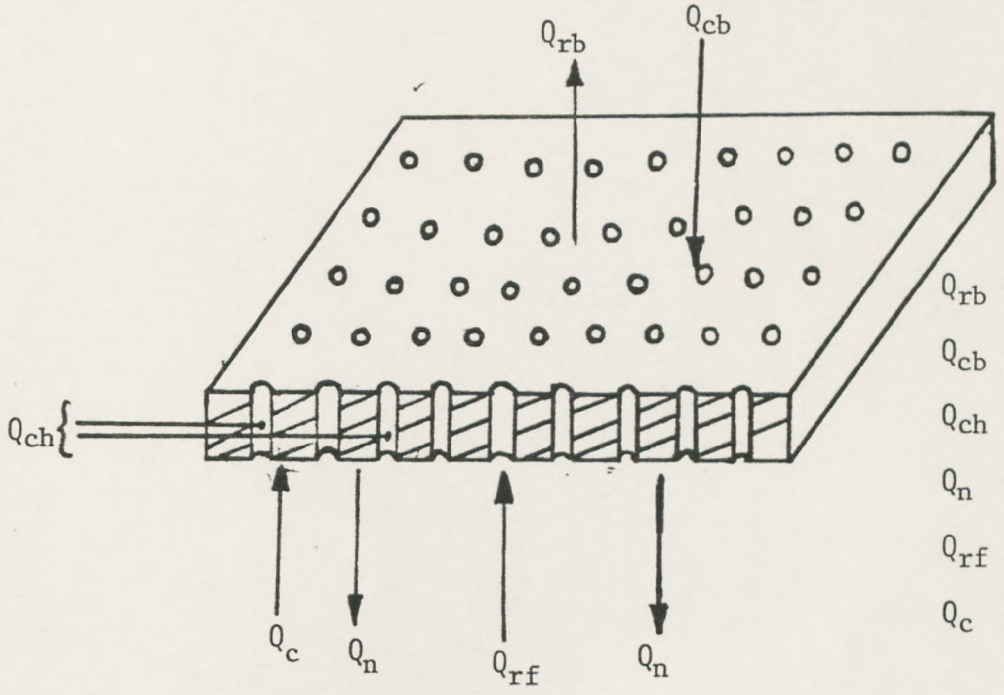

Fig. 5.4: Heat balance on effusion wall

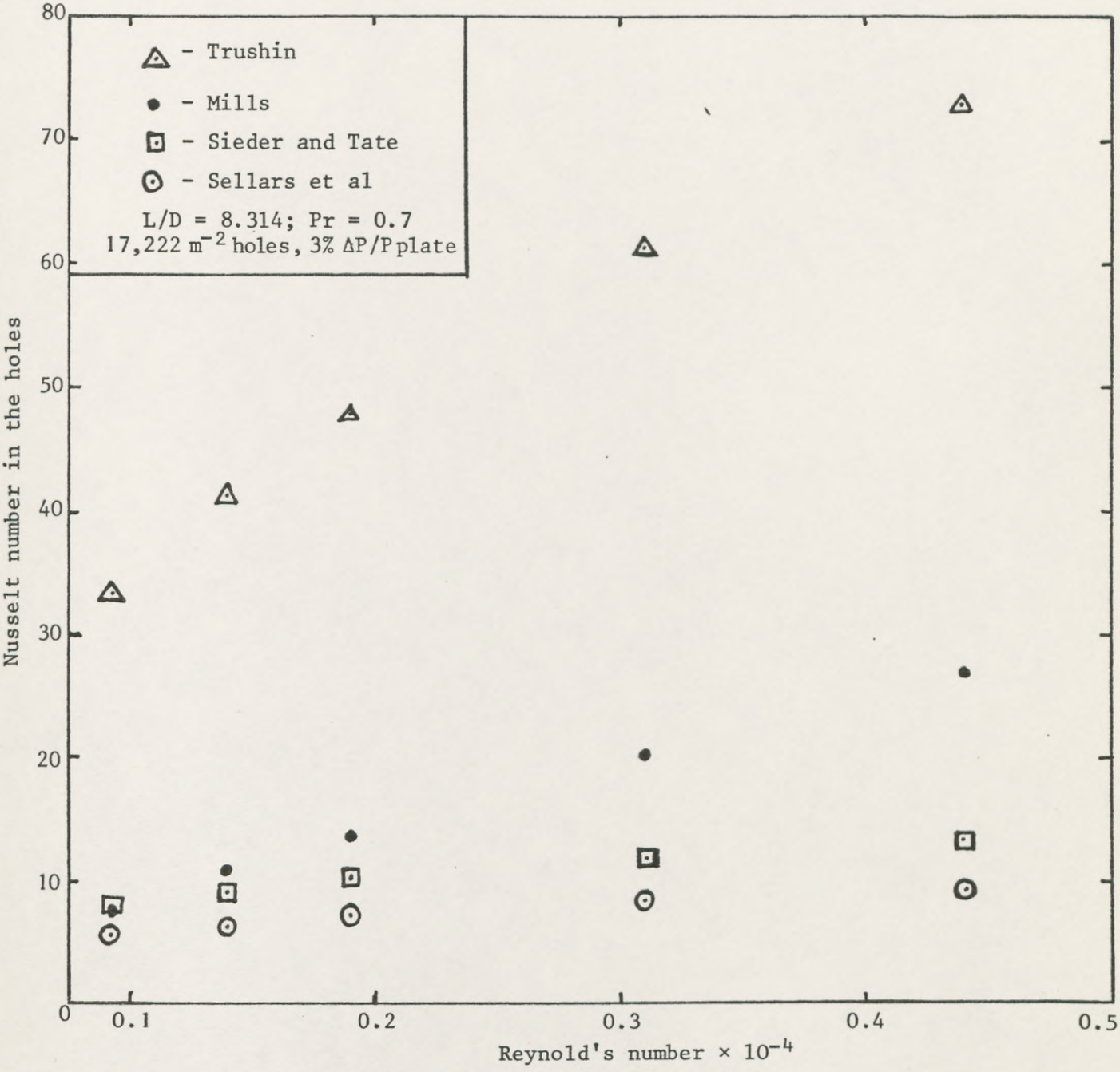

Fig. 5.5: Comparison of heat transfer correlation employed for computing holes with those used by other workers from literature.

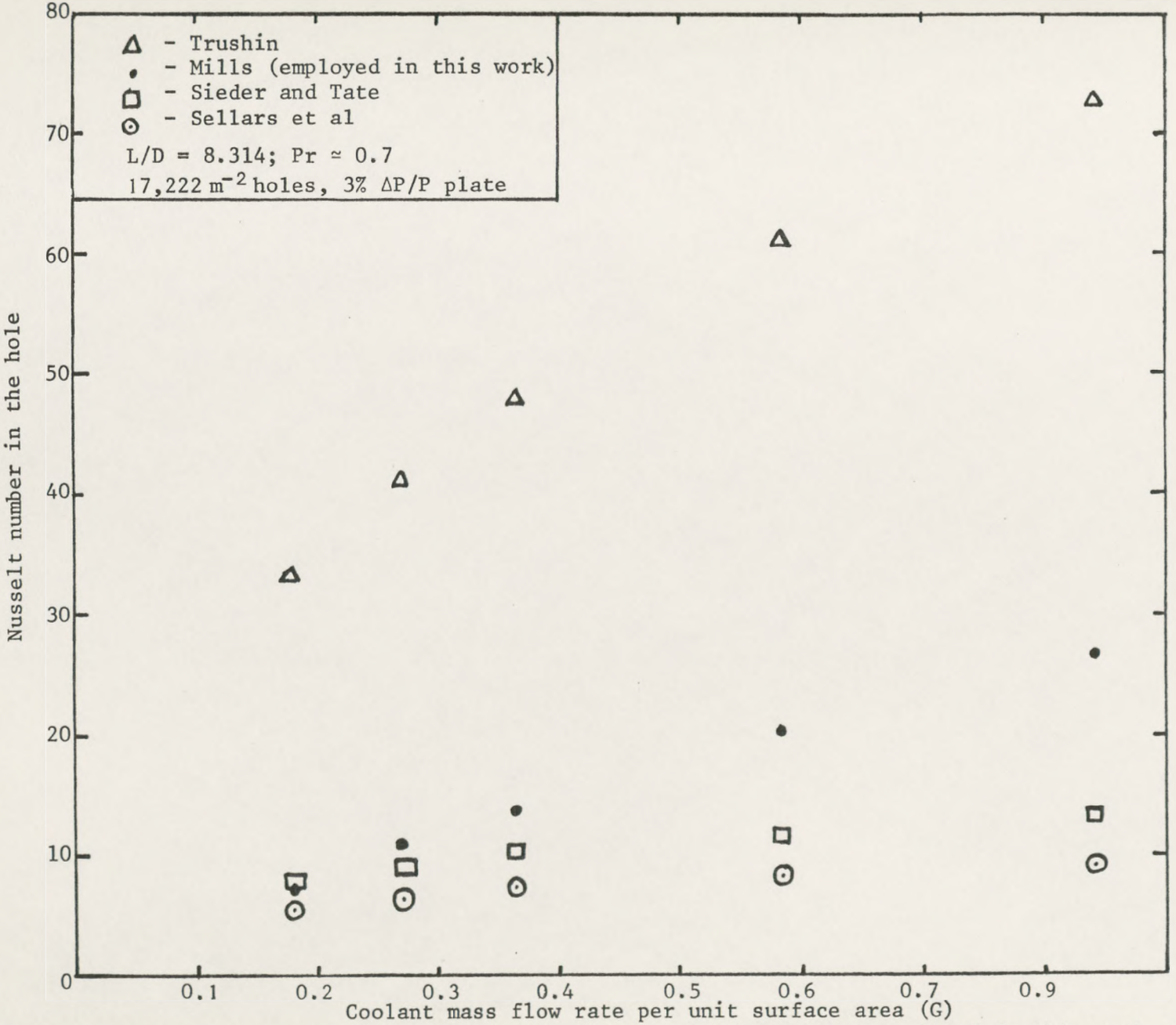

Fig. 5.6: Comparison of various holes heat transfer correlations with that employed in this work, for varying coolant injection rates.

5.13 A P P E N D I X

```
C THE NAME OF THIS PROGRAM IS "AB-83 FORTRAN",FOR PROCESSING IT USES,
C TWO DATA FILES . IT IS EXECUTED THROUGH EXEC "MARS'
C  OR "AAA EXEC", or 'a5' exec
C PROGRAM FOR COMPLETE ANALYSIS OF COOLING EFFECTIVENESS IN TURBINE
C COMBUSTOR
      DIMENSION UR(20),D2(20),C(20),G(20),D3(20),DPT(20),PR(20),VI(20),
     *P2(20),P7(20),AP3(20),P4(20),PP(20),P6(20),TC(20),TPC(20),TIC(20),
     *TC1(20),TV(20),P3(20),TG(20),TPH1(20),TPH2(20),TPH3(20),TPH4(20),
     *TPH5(20),T9(20),VM(20),V1(20),FC(20),F1(20),AD1(20),AT(20),BL(20),
     *S(20),S1(20),U(20),U1(20),Y(20),Y1(20),RE(20),RF1(20),H(20),G1(20)
     *,H1(20),T10(20),BLMT(20),BLR(20),AD2(20),PRA(20),AVT(20),TH1(20),
     *TH2(20),TH3(20),TH4(20),TH5(20),E1(20),E2(20),E3(20),E4(20),
     *E5(20),AM(20),FP(20),FK(20),TOP(20),OP(20),DUP(20),T11(20),DR3(20)
     *,SFR(20),PP2(20),AVTH(20),P8(20),FMF(20),P5(20),SQT(20),TIL(20),
     *TW1(20),TW2(20),TW3(20),TWM(20),T5(20),T6(20),UB1(20),TPG(20),
     *DF(20),FMM(20),TMV(20),QFM(20),CPF(20),HAV(20),RETMP(20),HIMP(20),
     *PRT(20),PRT1(20),PRT2(20),PLS(20),VMS(20),VRT(20),DR2(20),VM2(20)
      DIMENSION THCL(20),CAP(20),PRAT(20),WHCR(20),Q1B(20),Q2B(20),
     *W3B(20),W4B(20),W5B(20),W9(20),B1N(20),B2N(20),B3N(20),B4N(20),
     *B5N(20),BN(20),E1P(20),E2P(20),E3P(20),E4P(20),E5P(20),R1B(20),
     *R2B(20),R3B(20),R4B(20),R5B(20),RMB(20),T1N(20),T2N(20),T3N(20),
     *T4N(20),T5N(20),TN(20),F1D(20),F2D(20),F3D(20),F4D(20),F5D(20),
     *FLD(20),HTH(20),W1H(20),W2H(20),W3H(20),W4H(20),W5H(20),WH(20),
     *HN1(20),HN2(20),HN3(20),HN4(20),HN5(20),HN(20),F1AR(20),F2AR(20),
     *F3AR(20),TUE(20),EE2(20),EG1(20),EG2(20),E12(20),E21(20),E22(20),
     *Z31(20),Z32(20),Z33(20),Z34(20),Z35(20),Z41(20),Z42(20),Z43(20),
     *Z44(20),Z45(20),Z51(20),Z52(20),Z53(20),Z54(20),Z55(20),Q1F(20),
     *W2F(20),W3F(20),W4F(20),W5F(20),WMF(20),W1CT(20),W2CT(20),W3CT(20)
     *,W4CT(20),W5CT(20),WCT(20),H1F(20),H2F(20),H3F(20),H4F(20),H5F(20)
     *,HMF(20),C1P(20),C2P(20),C3P(20),C4P(20),C5P(20),TU1(20),TU2(20),
     *TU3(20),TU4(20),TU5(20),TU(20),S1C(20),Y1C(20),U1C(20),REC(20),
     *TCL(20),PRCT(20),CPC(20),CNU(20),HC0(20),C10(20),C20(20),C30(20),
     *C4W(20),C5W(20),CVW(20),HNL(20),CD(20),CPR(20),CCR(20),CD1(20)
      DIMENSION T1F(20),T2F(20),T3F(20),T4F(20),T5F(20),TRLE(20),CEP(20)
     *,R1F(20),R2F(20),R3F(20),R4F(20),R5F(20),RF(20),T1P(20),T2P(20),
     *T3P(20),T4P(20),T5P(20),TPP(20),E1R(20),E2R(20),E3R(20),E4R(20),
     *E5R(20),E1E(20),E2E(20),E3E(20),E4E(20),E5E(20),T1A(20),TW4(20)
      DIMENSION VV01(20),VV02(20),VV03(20),VV04(20),VV05(20),DD01(20),
     *DD02(20),DD03(20),DD04(20),DD05(20),Y1Z(20),Y2Z(20),Y3Z(20),
     *YYP1(20),YYP2(20),YYP3(20),YYP4(20),Y4Z(20),Y5Z(20),VVV(20),
     *YYP5(20),VV11(20),VV12(20),VV13(20),VV14(20),H8(20),TG8(20),
     *VV15(20),DD11(20),DD12(20),DD13(20),DD14(20),DD15(20),VR3(20),
     *TT1R(20),TT2R(20),TT3R(20),TT4R(20),TT5R(20),AMR(20),PRQ(20),
     -T1R(20),T2R(20),T3R(20),T4R(20),T5R(20),IP(20),TDZ(20),TOP2(20),
     *WBRH(20),TKTP(20),H1V(20),H2V(20),H3V(20),H4V(20),H5V(20),DDM(20),
     *VOM(20),HVM(20),BMO(20),TG2(20),TG3(20),T2A(20),T3A(20),TG1(20),
     -E8(20),E9(20),T8P(20),T9P(20),E5X(20),BB7(20),H7(20),TG7(20),
     *T7P(20),E7(20)
      CHARACTER * 70,AB,AR,AH,AMA,AS,ASE,SDR
1000  READ(1,*,END=7777)N
      ABR1=0.0
      ISET=0
      READ(1,575)ASE
575   FORMAT(A70)
C  ATMOS. PRESSURE-PL(AS OBT. FROM T.L) IN MMHG ,ATMOS. TEMP.-TL-CENT;
C  MEAN PLATE HOLE DIA.-D- IN MM; TOTAL NUMBER OF HOLES-THN-; PLATE
C  THICKNESS-TKN-IN MM; PLATE HOLE PITCH-PTH-IN MM; DESIGNED PLATE PRE-
C  SSURE DROP-IPD-; J,KRM ARE DATE NUMBERS ; FLUX-METER HEAT TRANSF.
C  SURFACE AREA-IN SW. METER.
      READ(1,*)IP,NP,AB,THNI,DI,PTH1,TPD1,TKNI,AR,AH,THN,D,PTH,TPD,TKN,
     *AMA,AS,GZ,J,K,M,PL,TL,AF,SDR
      WRITE(7,3)AB,THN,D,SDR,PTH,TPD,TKN,AMA,AS,J,K,M,PL,TL
      WRITE(7,4)
      D=D*1E-03
      PTH=PTH*1E-03
      TKN=TKN*1E-03
      PL=PL*0.0136
      READ(1,*)L
      DO 21,I=1,L
      IF(AB.EQ.'(High_Temp._Work)') GOTO 7114
      READ(1,*)AT(I),TV(I),TOP(I),TC(I),TPG(I),T5(I),T6(I),TPH1(I),
     *TPH2(I),TPH3(I),TPH4(I),TPH5(I),TIC(I),T9(I),T10(I),T11(I),TW1(I),
     *TW2(I),TW3(I),TW4(I),TG1(I),TG2(I),TG3(I),T1A(I),T2A(I),T3A(I),
     *PR(I),OP(I),P3(I),P4(I),P5(I),P6(I),P7(I),P8(I),FC(I),FK(I),FP(I),
     *FMF(I),PP(I),TPC(I)
      GOTO 7115
7114  READ(1,*)AT(I),TV(I),TOP(I),TOP2(I),TC(I),TPG(I),T5(I),T6(I),
     *TPH1(I),TPH2(I),TPH3(I),TPH4(I),TPH5(I),TIC(I),T9(I),T10(I),T11(I)
     *,TW1(I),TW2(I),TW3(I),TW4(I),TG2(I),T2A(I),PR(I),OP(I),P3(I),
     *P4(I),P5(I),P6(I),P7(I),P8(I),FC(I),FK(I),FP(I),FMF(I),PP(I),
     *TPC(I)
C    T(1-3)A    ADIABATIC WALL TEMP.'THIS IS THE FILM TEMPERATURE SEEN
C BY THE TEST WALL',--AT THE CENTRAL PLANE OF THE TEST WALL
C MOLECULAR WEIGHT-(B)-OF AIR DEFINED,TOP2=Kerosine Temp.
7115  TG(I)=TG2(I)
9680  B=28.96
C PRESSURE AT ROTAMETER(PR) AS WELL AS ALL OTHER PRESSURES ARE GAUGE
C PRESSURES HENCE FOR ABSOLUTE PRESSURE ADD ATMOS. PRESSURE(AP3)- AND
C SINCE MEASUREMENTS ARE IN MM2O CONVERT TO PASCALS BY MULT. BY 9803.92
C PLATE PRESSURE DROP DURING CO TEST(PP) AND HOT RUN (P6) CONVERTED
C ALL TEMPERATURES ARE IN CENT. ADD 273.16 TO GIVE KELVIN-K
      TIL(I)=TL(I)
      P=9803.92
      PLS(I)=P*(P6(I)-P7(I))
      AP3(I)=PL
      T=273.16
      TIC(I)=TIC(I)+T
      PP(I)=PP(I)*P
      P5(I)=P*(P5(I)+AP3(I))
      PR(I)=PR(I)*25.4E-03
      PR(I)=P*(PR(I)+AP3(I))
C COOLANT AIR TEMPERATURE AT ROTAMETER IS TC
      TC(I)=TC(I)+T
C GAS CONSTANT R AND DENSITY D2 BOTH OF COOLANT AIR AT ROTAMETER
      R=8314.0/B
      D2(I)=PR(I)/(TC(I)*R)
C COOLANT MEASURED FLOWRATE,FC, AT ROTAMETER IS CONVERTED FROM LITERS
C PER MIN. TO M2/S
      FC(I)=FC(I)*1E-03/60.0
C MANUFACTURED CONDITION OF ROTAMETER IS 15 C ,1ATMOSPHERE(CP) HENCE
```

```
FILE: AB        FORTRAN  A   LEEDS UNIVERSITY VM/SP RELEASE 3

C ACTUAL COOLANT FLOW RATE AT ROTAMETER IS F1                                   AB 01110
      CT=15.0+T                                                                 AB 01120
      CP=101.325E03                                                             AB 01130
      F1(I)=FC(I)*SQRT((CP*TC(I))/(CT*PR(I)))                                   AB 01140
C DIMENSIONS OF TEST PLATE AND HENCE AREA(ARE)- MUST BE COMPUTED                AB 01150
C C=COOLANT MASS FLOWRATE-KG/S; G=COOLANT MASS FLOWRATE PER UNIT PLATE          AB 01160
C AREA; G1= G  PER BAR -- COMBUSTOR STATIC PRESSURE IN BAR(P7) IS USED          AB 01170
C NOTE THAT P7 IS RECONVERTED TO PASCALS                                        AB 01180
      ARE=(0.1524)**2                                                           AB 01190
      C(I)=D2(I)*F1(I)                                                          AB 01200
      P7(I)=P*(P7(I)+AP3(I))/1.0E05                                             AB 01210
      G(I)=C(I)/ARE                                                             AB 01220
      G1(I)=G(I)/P7(I)                                                          AB 01230
      P7(I)=P7(I)*1.0E05                                                        AB 01240
C PLENUM CHAMBER FLUID DENSITY(D3),static absolute PRESSURE(P2), AND            AB 01250
C TEMPERATURE(TC1)                                                              AB 01260
C COMPUTED;T5 & T6-PLENUM CHAMBER TEMPS. AT 235MM & 55MM TO PLATE FACE          AB 01270
      T5(I)=T5(I)+T                                                             AB 01280
      T6(I)=T6(I)+T                                                             AB 01290
      TC1(I)=(T5(I)+T6(I))/2.0                                                  AB 01300
      P2(I)=P*(P6(I)+AP3(I))                                                    AB 01310
      D3(I)=P2(I)/(TC1(I)*R)                                                    AB 01320
C FROM MEAN PLATE HOLE DIAMETER D, AND TOTAL NUMBERS OF HOLES  THN, THE         AB 01330
C TOTAL CROSS SECTIONAL AREA OF HOLES IS COMPUTED                               AB 01340
      TW1(I)=TW1(I)+T                                                           AB 01350
      TW2(I)=TW2(I)+T                                                           AB 01360
      TW3(I)=TW3(I)+T                                                           AB 01370
      PI=3.14159                                                                AB 01380
      Z=PI*D**2*THN/4.0                                                         AB 01390
      TW4(I)=TW4(I)+T                                                           AB 01400
      TWM(I)=(TW1(I)+TW2(I)+TW3(I)+TW4(I))/4.0                                  AB 01410
C CD=RAW PLATE DISCHARGE COEFFICIENT,CCR=COMPRESIBILITY CD CORRECTION           AB 01420
C FACTOR AFTER Y.NAKAYAMA; CD1=CORRECTED DISCHARGE COEFFICIENT                  AB 01430
C VELOCITY-V1, MASS VELOCITY-VM, REYNOLDS NUMBER-RE, MACH NUMBER-H,             AB 01440
C SPECIFIC HEAT RATIO-W, ALL OF COOLANT THROUGH TEST PLATE HOLES ARE            AB 01450
C COMPUTED. THE VISCOSITY-U, OF THE COOLANT IS COMPUTED USING WATSON            AB 01460
C METHOD                                                                        AB 01470
997   V1(I)=C(I)/(D3(I)*Z)                                                      AB 01480
      VM(I)=C(I)/Z                                                              AB 01490
      ARA=Z/ARE                                                                 AB 01500
      A1=0.55279544                                                             AB 01510
      A2=2.8108916                                                              AB 01520
      A3=-13.50834                                                              AB 01530
      A4=39.353086                                                              AB 01540
      A5=-41.419387                                                             AB 01550
      S(I)=100.0/TC1(I)                                                         AB 01560
      Y(I)=A1+A2*S(I)+A3*S(I)**2+A4*S(I)**3+A5*S(I)**4                          AB 01570
      U(I)=1E-06*SQRT(TC1(I))/Y(I)                                              AB 01580
      RE(I)=4.0*C(I)/(PI*D*U(I)*THN)                                            AB 01590
      W=1.4                                                                     AB 01600
      H(I)=SQRT(R*TC1(I)/Q)*C(I)/(P2(I)*Z)                                      AB 01610
      P6(I)=P*P6(I)                                                             AB 01620
      TG(I)=TG(I)+T                                                             AB 01630
      TP6(I)=TPG(I)+T                                                           AB 01640
      TPH1(I)=TPH1(I)+T                                                         AB 01650
      TPH2(I)=TPH2(I)+T                                                         AB 01660
      TPH3(I)=TPH3(I)+T                                                         AB 01670
      TPH4(I)=TPH4(I)+T                                                         AB 01680
      TPH5(I)=TPH5(I)+T                                                         AB 01690
      FC(I)=FC(I)*60.0/(1E-03)                                                  AB 01700
C ************************************************************************    AB 01710
C *        MAINSTREAM              FLOW                    SEGMENT           *AB 01720
C ************************************************************************    AB 01730
C DENSITY OF AIR AT BOTH ATMOS.(AD1) AND AT VENTURI UPSTREAM(AD2),COMPUTA       AB 01740
C ATMOS. TEMPERATURE-AT-,AIR DENSITY AT 273.16K,& 760MMHG=10.34MH2O IS          AB 01750
C 1.293-KG/M3                                                                   AB 01760
      SD=1.293                                                                  AB 01770
      STP=10.34                                                                 AB 01780
      TV(I)=TV(I)+T                                                             AB 01790
      AT(I)=AT(I)+T                                                             AB 01800
      AD1(I)=SD*AP3(I)*T/(AT(I)*STP)                                            AB 01810
C DENSITY, USING STATIC PRESSURE(P4), TEMPERATURE(TV) OF AIR AT VENTURI         AB 01820
C UPSTREAM PIPE COMPUTED                                                        AB 01830
      P4(I)=P4(I)+AP3(I)                                                        AB 01840
      AD2(I)=AD1(I)*P4(I)*AT(I)/(TV(I)*AP3(I))                                  AB 01850
C USING CD=0.92839, ZR=0.9911, EX=0.994725, THROAT DIA.=63.76667MM,             AB 01860
C THROAT CROSS-SECT. AREA=0.003194M2, UPSTREAM PIPE DIA.=150.54912MM,           AB 01870
C E=1.0165; MULT. CONST. FOR AIR MASS FLOWRATE(AM) THRO' VENT.=0.0042:          AB 01880
C PRESSURE DROP AT THROAT IS-P3                                                 AB 01890
      P3(I)=P*P3(I)                                                             AB 01900
      AM(I)=0.0042*SQRT(AD2(I)*P3(I))                                           AB 01910
C                 ++++++++++++++++++++++++++++++++++                            AB 01920
C                 +                                +                            AB 01930
C                 : COMBUSTOR  FLOWRATE EVALUATION :                            AB 01940
C                 +                                +                            AB 01950
C                 ++++++++++++++++++++++++++++++++++                            AB 01960
C USING PROPANE M-FLOWRATE(FP), KEROSINE FLOWRATE(FK), & AIR FLOW THRO.         AB 01970
C VENTURI(AM),THE COMBUSTOR MAINSTREAM FLOW(SFK) IS COMPUTED. DENSITIES         AB 01980
C OF PROPANE(DOP),USING PROPANE INLET TEMP.(TOP)& PRESSURE(OP), AND             AB 01990
C KEROSINE(DOK), ARE FIRST COMPUTED. ROP=PROPANE GAS CONSTANT(R).               AB 02000
      TOP(I)=TOP(I)+T                                                           AB 02010
      ROP=188.0                                                                 AB 02020
      OP(I)=P*(OP(I)*25.4E-03+AP3(I))                                           AB 02030
      DOP(I)=OP(I)/(ROP*TOP(I))                                                 AB 02040
      DOK=820.1                                                                 AB 02050
      FP(I)=FP(I)*DOP(I)*1E-03/60.0                                             AB 02060
      FK(I)=FK(I)*DOK*1E-03/60.0                                                AB 02070
      SFK(I)=AM(I)+FP(I)+FK(I)                                                  AB 02080
C DENSITY OF MAINSTREAM(DPT) AT PLANE OF TEST USING COMB. STATIC PRESS.         AB 02090
C (P7) AND MAINSTREAM TEMP.(TG) IS COMPUTED                                     AB 02100
      DPT(I)=P7(I)/(R*TG(I))                                                    AB 02110
C DENSITY RATIO (DR) COMPUTED.                                                  AB 02120
      DR(I)=D2(I)/DPT(I)                                                        AB 02130
C USING COMBUST.CROSS SECTIONAL AREA(CCA), MAINSTREAM BLOWING RATE(BLMT)AR      AB 02140
C &BLOW. RATIO(BLR) ARE COMPUTED. BOTH REYNOLD(RE1) AND MACH(H1) NUMBERSAR      AB 02150
C COMPUTED ;NOTE FOR CCA HYDRAULIC DIA. ACCORDING TO PERRY HAD BEEN USEDAR      AB 02160
      CCA=0.0081073                                                             AB 02170
      S1(I)=100.0/TIC(I)                                                        AB 02180
      Y1(I)=A1+A2*S1(I)+A3*S1(I)**2+A4*S1(I)**3+A5*S1(I)**4                     AB 02190
      U1(I)=1E-06*SQRT(TIC(I))/Y1(I)                                            AB 02200
```

FILE: AB FORTRAN A LEEDS UNIVERSITY VM/SP RELEASE 3

```
C   COMBUSTOR HYDRAULIC DIAMETER = 0.1016                                   AB 02210
      ME1(I)=4*SFR(I)/(PI*0.1016*U1(I))                                     AB 02220
      H1(I)=SQRT(R*TIC(I)/G)*SFR(I)/(P5(I)*CCA)                             AB 02230
C     ================================================================    AB 02240
C     +  TEMPERATURE          CORRECTION              ZONE              +   AB 02250
C     ================================================================    AB 02260
C  BELOW TO CONVERT P7 TO ATMOSPHERE DIVIDE BY 101325---reconvert to ABLAB 02270
C  -am Velocity AND VRT=Velocity Ratio                                      AB 02280
C % RATIO OF gauge press. in the plenum to ATMOSPHERIC PRESS.=(PRT)         AB 02290
C % RATIO OF PRESS. LOSS ACROSS PLATE TO upstream static absolute press AB 02300
C of plenum-PRT1- and combustor -PRT2-                                      AB 02310
      EM=0.875                                                              AB 02320
      IF(TG(I).GT.1200.0) EM=0.30                                           AR 02330
      IF(TG(I).GT.1200.0) GOTO 2007                                         AB 02340
C////////////////////////////////////                                       AB 02350
      H8(I)=SQRT(R*(TG(I)+20.0)/G)*SFR(I)/(P7(I)*CCA)                       AR 02360
      BB1(I)=3.369E-08*EM*TG(I)**(-0.18)*(TG(I)**4-TWM(I)**4)/(SQRT(H8(IAB 02370
     *)*P7(I)))                                                             AB 02380
      TG8(I)=BB1(I)+TG(I)                                                   AB 02390
      H8(I)=SQRT(R*TG8(I)/G)*SFR(I)/(P7(I)*CCA)                             AB 02400
      BB1(I)=3.369E-08*EM*TG(I)**(-0.18)*(TG(I)**4-TWM(I)**4)/(SQRT(H8(IAB 02410
     *)*P7(I)))                                                             AB 02420
      BB7(I)=BB1(I)                                                         AB 02430
      GOTO 2001                                                             AB 02440
C//////////////////////////                                                 AB 02450
2007  H7(I)=SQRT(R*(TG(I)+200.0)/G)*SFR(I)/(P7(I)*CCA)                      AB 02460
      BB7(I)=3.369E-08*EM*TG(I)**(-0.18)*(TG(I)**4-TWM(I)**4)/(SQRT(H7(IAB 02470
     *)*P7(I)))                                                             AB 02480
      TG7(I)=BB7(I)+TG(I)                                                   AB 02490
      H7(I)=SQRT(R*TG7(I)/G)*SFR(I)/(P7(I)*CCA)                             AB 02500
      BB7(I)=3.369E-08*EM*TG(I)**(-0.18)*(TG(I)**4-TWM(I)**4)/(SQRT(H7(IAB 02510
     *)*P7(I)))                                                             AB 02520
C//////////////////////////                                                 AB 02530
2001  TG(I)=TG(I)+BB7(I)                                                    AB 02540
C nominal blowing rate ratio-BLR1- ,mass velocity of plenum coolant-VM2-AB 02550
C calculated                                                                AB 02560
      BLMT(I)=SFR(I)/CCA                                                    AB 02570
      BLR(I)=VM(I)/BLMT(I)                                                  AB 02580
      VMS(I)=SFR(I)/(DPT(I)*CCA)                                            AB 02590
      VRT(I)=V1(I)/VMS(I)                                                   AB 02600
      PRT1(I)=100.0*PLS(I)/P2(I)                                            AB 02610
      WRITE(7,5)FC(I),P6(I),TC(I),TG(I),C(I),G(I),G1(I),V1(I),VMS(I)        AB 02620
21    CONTINUE                                                              AB 02630
      WRITE(7,6)                                                            AB 02640
      DO 31,I=1,L                                                           AB 02650
      IF(TC(I).LT.303.0.AND.TPG(I).GT.350.0) GOTO 7017                      AB 02660
      DR2(I)=P7(I)/(DPT(I)*R*TC(I))                                         AB 02670
      GOTO 7007                                                             AB 02680
7017  DR(I)=PR(I)/(DPT(I)*R*TPG(I))                                         AB 02690
      DR2(I)=P7(I)/(DPT(I)*R*TPG(I))                                        AB 02700
C//////////////////////////////                                             AB 02710
7007  AMR(I)=100.0*C(I)/(SFR(I)+C(I))                                       AB 02720
C//////////////////////////////                                             AB 02730
      WRITE(7,7)DR(I),DR2(I),BLR(I),RE(I),H(I),RE1(I),H1(I),PRT1(I),        AB 02740
     *VRT(I)                                                                AB 02750
7     FORMAT(1H ,3(2X,F5.2),4(2X,E8.2),2(2X,F7.4))                          AB 02760
31    CONTINUE                                                              AB 02770
3     FORMAT(1H1,16X,'UNIVERSITY OF LEEDS'/,13X,'DEPARTMENT OF FUEL AND AB 02780
     *ENERGY'/,8X,'Gas Turbine Combustor Wall Cooling Programme'/1H0,7X,AB 02790
     *'EFFUSION   PLATE    TEST -',A30                                      AB 02800
     */,1X,'-------------------------------------------------------------AB 02810
     *-------------------------'                                           AB 02820
     */,2X,'NO. OF PLT. HOLES:',F5.1,3X,'HOLES MEAN DIAMETER:',F9.7,'mm'AB 02830
     *,2X,A20                                                             AB 02840
     */,2X,'HOLE PITCH:',F11.7,'mm',3X,'PLATE ()P/P:',F7.4,'%',2X,'PLATEAB 02850
     * THN.:',F6.3,'mm'                                                   AB 02860
     */,2X,'HOLES LAYOUT FORMAT: ',A30,4X,'PLATE-MATERIAL: ',A10         AB 02870
     */,2X,'EXP. DATE:',I2,'/',I2,'/',I2,3X,'ATMOS. PRESS.:',F7.2,'mmHg'AB 02880
     *,2X,'AT TEMP.:',F5.1,1X, 'Deg. C'                                  AB 02890
     */,1X,'-------------------------------------------------------------AB 02900
     *---------------------------')                                       AB 02910
4     FORMAT(1H ,1X,'FC-COOLANT FLOWRATE AS MEASURED AT ROTAMETER-l/min'AB 02920
     *       /,2X,'TC-K=COOLANT TEMP. AT ROTAMETER, TG-K=MAINSTREAM FLOWAB 02930
     * TEMP. AT TEST PLANE'/,2X,'CM-Kg/s=COOLANT MASS FLOWRATE, G-Kg/(s=AB 02940
     *2)=C. MASS FLOW/TEST PLATE AREA'                                    AB 02950
     */,2X,'G!-Kg/(m2sBar)=COOLANT MASS FLOW. /Meter Sq./Sec./Bar'        AB 02960
     */,2X,'V & Vm=m/s=VEL. COOL. & MAINST.THRU. HOLES & COMBUSTOR;BLR=BAR 02970
     *LOWING RATE RATIO'                          /,2X,'DR=DENSITY RATIO(DAR 02980
     *1/D2); PPD-Pa=PLENUM STATIC GAUGE PRESSURE'                         AB 02990
     */,2X,'nDr=NOMINAL DENSITY RATIO:'                                  AB 03000
     */,2X,'RE-1&2=REYNOLDS NUMBER FOR COOLANT THRU. PLATE & MAINSTREAM AB 03010
     *AT TEST PLANE'/,2X,'H 1&2=MACH NUMBERS OF BOTH COOLANT & MAINSTREAAB 03020
     *M AS FOR RE ABOVE'/,2X,'%Pr & Vrt =(%Press Loss Across Plate/UpstrAB 03030
     *eam (plenum) Absolute Press.)* & V/Vm'                              AB 03040
     * /,1X,'-------------------------------------------------------------AB 03050
     *---------------------------      ' /1H ,3X,'FC-l/min.',3X,'PPD-Pa',4AB 03060
     *X,'TC-K',4X,'TG-K',3X,'CM-Kg/s',6X,'G',7X,'G1',6X,'V-m/s',2X,'Vm-mAR 03070
     */s')                                                                AB 03080
5     FORMAT(1H ,2X,F7.1,6X,F7.1,2(1X,F7.1),2X,F7.5,2(3X,F6.3),3X,F6.2,2AB 03090
     *X,F5.2)                                                             AB 03100
6     FORMAT(1H0,4X,'DR',5X,'nDr',3X,'BLR',7X,'RE',8X,'H',7X,             AB 03110
     *'RE1',8X,'H1',7X,'%Pr',6X,'Vrt')                                    AB 03120
55    WRITE(7,12)                                                          AB 03130
C +----------+--------------------+--------------------+-------------+AB 03140
C +       COOLING             EFFECTIVENESS              SEGMENT      +AB 03150
C +----------+--------------------+--------------------+-------------+AB 03160
C   TPH-(1 TO 5) ARE TEST PLATE TEMPERATURE AT INCREASING DISTANCE FROM AB 03170
C  LEADING EDGE,AND E-(1 TO 5) ARE COOLING EFFECTIVENESS                    AB 03180
      DO 30,I=1,L                                                          AB 03190
      IF(TC(I).LT.303.0.AND.TPG(I).GT.350.0) TC(I)=TPG(I)                  AR 03200
      E1(I)=(TG(I)-TPH1(I))/(TG(I)-TC(I))                                  AR 03210
      E2(I)=(TG(I)-TPH2(I))/(TG(I)-TC(I))                                  AB 03220
      E3(I)=(TG(I)-TPH3(I))/(TG(I)-TC(I))                                  AR 03230
      E4(I)=(TG(I)-TPH4(I))/(TG(I)-TC(I))                                  AB 03240
      E5(I)=(TG(I)-TPH5(I))/(TG(I)-TC(I))                                  AB 03250
      WRITE(7,14)TC(I),TPH1(I),E1(I),TPH2(I),E2(I),TPH3(I),E3(I),TPH4(I)AB 03260
     *,E4(I),TPH5(I),E5(I)                                                AB 03270
14    FORMAT(1H ,1X,F5.1,4X,F7.1,2X,F5.3,4(2X,F7.1,2X,F5.3))               AB 03280
30    CONTINUE                                                             AR 03290
      WRITE(7,42)                                                          AB 03300
```

```
FILE: AB        FORTRAN  A   LEEDS UNIVERSITY VM/SP RELEASE 3

   42    FORMAT(1H ,2X,'-------------------------------------------------------AB 03310
        *----------------------------'                                          AB 03320
        */1H0,18X,'ADIABATIC COOLING EFFECTIVENESS.'                           AB 03330
        */,19X,'-------------------------------'                               AB 03340
        */,2X,'TGc=COMBUSTOR MAINSTREAM TEMP.;G!=G/(PRESSURE)-Kg/(m2sec.barAB 03350
        *);Tal(,c,t)=ADIABATIC'                                                AB 03360
        */,2X,'WALL TEMP. AT LEADING EDGE, CENTRAL, & TRAILING EDGE ;Ea=ADIAB 03370
        *ABATIC COOLING EFFECTIVENESS'                                         AB 03380
        */,2X,'For High Temp. Work Tac=central thermocouple- Only Feature' AB 03390
        *-------------------------------------------------------------------AB 03400
        *----------------------------')                                       AB 03410
         IF(AB.EQ.'(High_Temp._Work)') GOTO 990                                AB 03420
         WRITE(7,7447)                                                         AB 03430
 7447    FORMAT(1H ,4X,'TGc-K',5X,'G!',12X,'Tal-K',6X,'E',11X,'Tac-K',7X,'EAB 03440
        -',11X,'Tat-K',7X,'E')                                                 AB 03450
         GOTO 991                                                              AB 03460
  990    WRITE(7,7457)                                                         AB 03470
 7457    FORMAT(1H ,10X,'TGC-K',11X,'G!',11X,'Tac-K',10X,'E')                  AB 03480
  991    DO 9443,I=1,L                                                         AB 03490
         IF(AB.EQ.'(High_Temp._Work)'.AND.C(I).EQ.0.0) GOTO 9443               AB 03500
         IF(TG(I).GT.1200.0) GOTO 993                                          AB 03510
         T1A(I)=T1A(I)+T                                                       AB 03520
         E7(I)=(TG(I)-T1A(I))/(TG(I)-TC(I))                                    AB 03530
         T3A(I)=T3A(I)+T                                                       AB 03540
         E9(I)=(TG(I)-T3A(I))/(TG(I)-TC(I))                                    AB 03550
  993    T2A(I)=T2A(I)+T                                                       AB 03560
         E8(I)=(TG(I)-T2A(I))/(TG(I)-TC(I))                                    AB 03570
         IF(AB.EQ.'(High_Temp._Work)') GOTO 994                                AB 03580
         WRITE(7,9444)TG(I),G1(I),T1A(I),E7(I),T2A(I),E8(I),T3A(I),E9(I)       AB 03590
 9444    FORMAT(1H ,1X,F7.1,2X,F6.3,3(8X,F7.1,4X,F5.3))                        AB 03600
         GOTO 9443                                                             AB 03610
  994    WRITE(7,995)TG(I),G1(I),T2A(I),E8(I)                                  AB 03620
  995    FORMAT(1H ,8X,F7.1,8X,F6.3,8X,F7.1,7X,F5.3)                           AB 03630
 9443    CONTINUE                                                              AB 03640
 9687    WRITE(7,17)                                                           AB 03650
   17    FORMAT(1H ,2X,'-------------------------------------------------------AB 03660
        *----------------------------'                                          AB 03670
        */1H0,8X,'CONVECTIVE HEAT TRANSFER AT THE BACK OF TEST WALL'           AB 03680
        */,12X,'-------------------------------------'                         AB 03690
        */,2X,'W(1-5)B-WATT =CONVECTIVE HEAT TRANSFER - BASED ON WALL THERMAB 03700
        *OCOUPLE STATIONS,'                                                    AB 03710
        */,2X,'WHILE WB IS THE MEAN AT THE BACK OF TEST WALL; QHCB-W/M*2.K AB 03720
        * = CONVECTIVE HEAT'                                                   AB 03730
        */,2X,'TRANSFER COEFFICIENT; BN=NUSSELT NUMBER'                        AB 03740
        */,2X,'-------------------------------------------------------------AB 03750
        *---------------------'                                                AB 03760
        */,6X,'W1B',6X,'Q2B',6X,'W3B',6X,'Q4B',6X,'Q5B',6X,'QHCB',7X,'QB',8AB 03770
        *X,'BN')                                                               AB 03780
         GOTO 301                                                              AB 03790
  582    WRITE(7,600)                                                          AB 03800
  600    FORMAT(1H0,2X,'CONVECTIVE HEAT TRANSFER AT THE BACK OF TEST WALL-BAB 03810
        *ased On Predicted Wall Temp.'                                         AB 03820
        */,2X,'-------------------------------------------------------------- AB 03830
        *-----------'                                                          AB 03840
        */,2X,'W(1-5)B-WATT =CONVECTIVE HEAT TRANSFER - BASED ON WALL THERMAB 03850
        *OCOUPLE STATIONS,'                                                    AB 03860
        */,2X,'WHILE WB IS THE MEAN AT THE BACK OF TEST WALL; QHCB-W/M*2.K AB 03870
        * = CONVECTIVE HEAT'                                                   AB 03880
        */,2X,'TRANSFER COEFFICIENT; BN=NUSSELT NUMBER'                        AB 03890
        */,2X,'-------------------------------------------------------------AB 03900
        *---------------------'                                                AB 03910
        */,6X,'W1B',6X,'Q2B',6X,'W3B',6X,'Q4B',6X,'Q5B',6X,'QHCB',7X,'QB',8AB 03920
        *X,'BN')                                                               AB 03930
C              !++++++++++-----------+++++++++++++++++++++++++!                AB 03940
C              +                                               +                AB 03950
C              !  HEAT              TRANSFER          SEGMENT  !                AB 03960
C              +                                               +                AB 03970
C              !-----------++++++++++++++++++++++++++++++++++++!                AB 03980
C    AHA=TEST PLATE AREA - TOTAL HOLES CROSS-SECTIONAL AREA                    AB 03990
C -------------------------------------------------------------------------AB 04000
C !  CONVECTIVE HEAT TRANSFER AT BLACK OF TEST PLATE-----CASE-1A              !AB 04010
C -------------------------------------------------------------------------AB 04020
C THCL & CAP ARE THERMAL CONDUCTIVITY & SPECIFIC HEAT CAPACITY OF FLUID AB 04030
C RESPECTIVELY; PRAT=PRANDTL NO.;POH=AREA/(TOTAL PITCH);                       AB 04040
C  USING SPARROW ET AL-INT. J. H&M TRF.,VOL.25,PP127-35,1982. CONVECTIVEAB 04050
C  HEAT TRANSFER COEFFICIENT FOR PLATE BACK SIDE WAS COMPUTED.                 AB 04060
  301    DO 75,I=1,L                                                           AB 04070
         IF(ABR1.EQ.1.0.AND.C(I).EQ.0.0) GOTO 302                              AB 04080
         IF(C(I).EQ.0.0) GOTO 511                                              AB 04090
         AHA=ARE-Z                                                             AB 04100
         POH=AHA/(PTH*THN)                                                     AB 04110
         THCL(I)=-0.7231E-14*TC1(I)**4+0.3126E-10*TC1(I)**3-0.6331E-07*TC1(AB 04120
        *I)**2+0.1081E-03*TC1(I)-0.1265E-02                                    AB 04130
         CAP(I)=1063.3-5.7194E-14*TC1(I)**5+4.2538E-10*TC1(I)**4-1.1417E-06AB 04140
        **TC1(I)**3+1.3637E-03*TC1(I)**2-0.5117*TC1(I)                         AB 04150
         PRAT(I)=CAP(I)*U(I)/THCL(I)                                           AB 04160
C        CASE-1==QB & CONFECTIVE HEAT TRANSFER COEFFICIENT-QHCB CALCULATION AB 04170
         QHCB(I)=0.881*RE(I)**0.476*PRAT(I)**0.333*THCL(I)/POH                 AB 04180
         W1B(I)=QHCB(I)*AHA*(TPH1(I)-TC1(I))                                   AB 04190
         Q2B(I)=QHCB(I)*AHA*(TPH2(I)-TC1(I))                                   AB 04200
         W3B(I)=QHCB(I)*AHA*(TPH3(I)-TC1(I))                                   AB 04210
         W4B(I)=QHCB(I)*AHA*(TPH4(I)-TC1(I))                                   AB 04220
         Q5B(I)=QHCB(I)*AHA*(TPH5(I)-TC1(I))                                   AB 04230
         QB(I)=(Q1B(I)+W2B(I)+Q3B(I)+W4B(I)+Q5B(I))/5.0                        AB 04240
         IF(ABR1.EQ.1.0) GOTO 1307                                             AB 04250
         T7P(I)=TPH1(I)                                                        AB 04260
         T8P(I)=TPH3(I)                                                        AB 04270
         T9P(I)=TPH5(I)                                                        AB 04280
C NUSSELT NUMBER-(D-N) BASED ON HOLE MEAN DIAMETER & WALL THERMAL              AB 04290
C STATIONSCOMPUTED                                                             AB 04300
 1307    B1N(I)=Q1B(I)*D/(AHA*THCL(I)*(TPH1(I)-TC1(I)))                        AB 04310
         B2N(I)=W2B(I)*D/(AHA*THCL(I)*(TPH2(I)-TC1(I)))                        AB 04320
         B3N(I)=Q3B(I)*D/(AHA*THCL(I)*(TPH3(I)-TC1(I)))                        AB 04330
         B4N(I)=W4B(I)*D/(AHA*THCL(I)*(TPH4(I)-TC1(I)))                        AB 04340
         B5N(I)=Q5B(I)*D/(AHA*THCL(I)*(TPH5(I)-TC1(I)))                        AB 04350
         BN(I)=(B1N(I)+B2N(I)+B3N(I)+B4N(I)+B5N(I))/5.0                        AB 04360
         WRITE(7,71)Q1B(I),W2B(I),Q3B(I),W4B(I),Q5B(I),WHCB(I),WB(I),BN(I)     AB 04370
   71    FORMAT(1H ,5(2X,F7.1),2(2X,F8.1),2X,F8.2)                             AB 04380
   75    CONTINUE                                                              AB 04390
  511    WRITE(7,19)                                                           AB 04400
```

```
   19    FORMAT(1H ,2X,'-------------------------------------------------------------AB 04410
        *-------------------------'                                                   AB 04420
        */1HO,8X,'TEST WALL BACK RADIATIVE HEAT TRANSFER TO COOLANT'                  AB 04430
        */,15X,'---------------------------------------'                             AB 04440
        */,2X,'R(1-5)B-WATT =RADIATIVE HEAT TRANSFER TO COOLANT-BASED ON THAB 04450
        *ERMOCOUPLE STATIONS'                                                         AB 04460
        */,2X,'UN TEST WALL; RMB-WATT=MEAN OF THE RADIATION TO COOLANT'               AB 04470
        */,2X,'-------------------------------------------------------------AB 04480
        *-------------------'                                                         AB 04490
        */8X,'R1B',8X,'R2B',8X,'R3B',8X,'R4B',8X,'R5B',8X,'RMB')                      AB 04500
         GOTO 80                                                                      AB 04510
  302    WRITE(7,601)                                                                 AB 04520
  601    FORMAT(1H ,2X,'-------------------------------------------------------------AB 04530
        *-------------------------'                                                   AB 04540
        */1HO,2X,'TEST WALL BACK RADIATIVE HEAT TRANSFER TO COOLANT-Based OAB 04550
        *n Predicted Wall Temp.'                                                      AB 04560
        */,2X,'-------------------------------------------------------------AB 04570
        *-------------------'                                                         AB 04580
        */,2X,'R(1-5)B-WATT =RADIATIVE HEAT TRANSFER TO COOLANT-BASED ON THAB 04590
        *ERMOCOUPLE STATIONS'                                                         AB 04600
        */,2X,'UN TEST WALL; RMB-WATT=MEAN OF THE RADIATION TO COOLANT'               AB 04610
        */,2X,'-------------------------------------------------------------AB 04620
        *-------------------'                                                         AB 04630
        */8X,'R1B',8X,'R2B',8X,'R3B',8X,'R4B',8X,'R5B',8X,'RMB')                      AB 04640
C ---------------------------------------------------------------------AB 04650
C : COMPUTATION OF RADIATIVE HEAT TRANSFER AT THE BACK OF PLATE-CASE-1b:AB 04660
C ---------------------------------------------------------------------AB 04670
C E1-5P=NIMONIC-75 CURVE FITTED EMISSIVITY EQUATION; RMB=MEAN RADIATIVE AB 04680
C HEAT TRANSFER                                                                       AB 04690
   80    DO 85,I=1,L                                                                  AB 04700
        IF(ABR1.EQ.1.0.AND.C(I).EQ.0.0) GOTO 513                                     AB 04710
        IF(C(I).EQ.0.0) GOTO 85                                                      AB 04720
C  NEW EMISSIVITY EQUATION BASED ON TEMPERATURE IN KELVIN                            AB 04730
        E1P(I)=2.6227E-15*TPH1(I)**5-1.2267E-11*TPH1(I)**4+2.2842E-08*TPH1AB 04740
       *(I)**3-2.0874E-05*TPH1(I)**2+9.3087E-03*TPH1(I)-0.9386                       AB 04750
        E2P(I)=2.6227E-15*TPH2(I)**5-1.2267E-11*TPH2(I)**4+2.2842E-08*TPH2AB 04760
       *(I)**3-2.0874E-05*TPH2(I)**2+9.3087E-03*TPH2(I)-0.9386                       AB 04770
        E3P(I)=2.6227E-15*TPH3(I)**5-1.2267E-11*TPH3(I)**4+2.2842E-08*TPH3AB 04780
       *(I)**3-2.0874E-05*TPH3(I)**2+9.3087E-03*TPH3(I)-0.9386                       AB 04790
        E4P(I)=2.6227E-15*TPH4(I)**5-1.2267E-11*TPH4(I)**4+2.2842E-08*TPH4AB 04800
       *(I)**3-2.0874E-05*TPH4(I)**2+9.3087E-03*TPH4(I)-0.9386                       AB 04810
        E5P(I)=2.6227E-15*TPH5(I)**5-1.2267E-11*TPH5(I)**4+2.2842E-08*TPH5AB 04820
       *(I)**3-2.0874E-05*TPH5(I)**2+9.3087E-03*TPH5(I)-0.9386                       AB 04830
C  STEFAN-BOLTZMANN CONSTANT HERE IS DEFINED AS--0.                                  AB 04840
        U=56.7E-09                                                                   AB 04850
        IF(ABR1.EQ.0) GOTO 6666                                                      AB 04860
        R1B(I)=(AHA*E1P(I)/(1.0-E1P(I)))*(U*((0.952-0.953*E1P(I))*TPH1(I)*AB 04870
       **4-(0.952-0.953*E1P(I))*TPH1(I)**4)/(0.952+0.047*E1P(I)))                    AB 04880
        R2B(I)=(AHA*E2P(I)/(1.0-E2P(I)))*(U*((0.952-0.953*E2P(I))*TPH2(I)*AB 04890
       **4-(0.952-0.953*E2P(I))*TPH2(I)**4)/(0.952+0.047*E2P(I)))                    AB 04900
        R3B(I)=(AHA*E3P(I)/(1.0-E3P(I)))*(U*((0.952-0.953*E3P(I))*TPH3(I)*AB 04910
       **4-(0.952-0.953*E3P(I))*TPH3(I)**4)/(0.952+0.047*E3P(I)))                    AB 04920
        R4B(I)=(AHA*E4P(I)/(1.0-E4P(I)))*(U*((0.952-0.953*E4P(I))*TPH4(I)*AB 04930
       **4-(0.952-0.953*E4P(I))*TPH4(I)**4)/(0.952+0.047*E4P(I)))                    AB 04940
        R5B(I)=(AHA*E5P(I)/(1.0-E5P(I)))*(U*((0.952-0.953*E5P(I))*TPH5(I)*AB 04950
       **4-(0.952-0.953*E5P(I))*TPH5(I)**4)/(0.952+0.047*E5P(I)))                    AB 04960
        GOTO 5555                                                                    AB 04970
 6666   R1B(I)=(AHA*E1P(I)/(1.0-E1P(I)))*(U*((0.952-0.953*E1P(I))*TPH1(I)*AB 04980
       **4-(0.952-0.953*E1P(I))*TC1(I)**4)/(0.952+0.047*E1P(I)))                     AB 04990
        R2B(I)=(AHA*E2P(I)/(1.0-E2P(I)))*(U*((0.952-0.953*E2P(I))*TPH2(I)*AB 05000
       **4-(0.952-0.953*E2P(I))*TC1(I)**4)/(0.952+0.047*E2P(I)))                     AB 05010
        R3B(I)=(AHA*E3P(I)/(1.0-E3P(I)))*(U*((0.952-0.953*E3P(I))*TPH3(I)*AB 05020
       **4-(0.952-0.953*E3P(I))*TC1(I)**4)/(0.952+0.047*E3P(I)))                     AB 05030
        R4B(I)=(AHA*E4P(I)/(1.0-E4P(I)))*(U*((0.952-0.953*E4P(I))*TPH4(I)*AB 05040
       **4-(0.952-0.953*E4P(I))*TC1(I)**4)/(0.952+0.047*E4P(I)))                     AB 05050
        R5B(I)=(AHA*E5P(I)/(1.0-E5P(I)))*(U*((0.952-0.953*E5P(I))*TPH5(I)*AB 05060
       **4-(0.952-0.953*E5P(I))*TC1(I)**4)/(0.952+0.047*E5P(I)))                     AB 05070
 5555   RMB(I)=(R1B(I)+R2B(I)+R3B(I)+R4B(I)+R5B(I))/5.0                              AB 05080
        WRITE(7,74)R1B(I),R2B(I),R3B(I),R4B(I),R5B(I),RMB(I)                         AB 05090
   74   FORMAT(1H ,6(4X,F7.1))                                                       AB 05100
   85   CONTINUE                                                                     AB 05110
        WRITE(7,37)                                                                  AB 05120
   37   FORMAT(1H ,2X,'-------------------------------------------------------------AB 05130
        *-------------------------'                                                   AB 05140
        */1H1,14X,'PREDICTED COOLANT"S HOLES INLET & PLENUM TEMPERATURES'            AB 05150
        */,15X,'-------------------------------------------------'                   AB 05160
        */,2X,'T(1-5)n-K =COOLANT"S HOLES INLET TEMPERATURE -- BASED ON WALAB 05170
        *L"S THERMAL STATIONS'                                                       AB 05180
        */,2X,'mTin-K = MEAN INLET COOLANT"S TEMPERATURE.; pTp-K = PREDICTEAB 05190
        *D PLENUM TEMPERATURE'                                                       AB 05200
        */,15X,'mTp-k = MEASURED PLENUM TEMPERATURE'                                 AB 05210
        */,2X,'-------------------------------------------------------------AB 05220
        *-------------------'                                                        AB 05230
        */,5X,'T1n-K',4X,'T2n-K',4X,'T3n-K',4X,'T4n-K',4X,'T5n-K',4X,'mTin-AB 05240
        *k',3X,'plp-K',4X,'mTp-K')                                                   AB 05250
         GOTO 117                                                                    AB 05260
  513   WRITE(7,311)                                                                 AB 05270
  311   FORMAT(1H ,2X,'-------------------------------------------------------------AB 05280
        *-------------------------'                                                   AB 05290
        */1H1,2X,'PREDICTED COOLANT"S HOLES INLET TEMPERATURE -Based On PreAB 05300
        *dicted Wall Temp.'                                                          AB 05310
        */,2X,'-------------------------------------------------------------AB 05320
        *-------------------'                                                        AB 05330
        */,2X,'T(1-5)n-K =COOLANT"S HOLES INLET TEMPERATURE -- BASED ON WALAB 05340
        *L"S THERMAL STATIONS'                                                       AB 05350
        */,2X,'mTin-K = MEAN INLET COOLANT"S TEMPERATURE and pTp-K = PLENUMAB 05360
        * TEMPERATURE'                                                              AB 05370
        */,2X,'-------------------------------------------------------------AB 05380
        *-------------------'                                                        AB 05390
        */,7X,'T1n-K',6X,'T2n-K',6X,'T3n-K',6X,'T4n-K',6X,'T5n-K',6X,'mTin-AB 05400
        *K',5X,'plp-K')                                                              AB 05410
C ********************************************************************** AB 05420
C + PREDICTION OF FLUID DISTRIBUTION & HOLES INLET TEMPERATURE-CASE-1 + AB 05430
C ********************************************************************** AB 05440
C  IN THIS PROCESS COMBINED CONVECTIVE(USING SPARROW ET AL) & RADIATIVE AB 05450
C  HEAT TRANSFER TO THE FLUID ARE USED. TIN=INLET TEMPERATURE BASED ON  AB 05460
C  THERMOCOUPLE LOCATIONS ON THE PLATE                                               AB 05470
  117   DO 95,I=1,L                                                                  AB 05480
        IF(ABR1.EQ.1.0.AND.C(I).EQ.0.0) GOTO 305                                     AB 05490
        IF(C(I).EQ.0.0) GOTO 401                                                     AB 05500
```

FILE: AB FORTRAN A LEEDS UNIVERSITY VM/SP RELEASE 3

```
      T1N(I)=Q1B(I)/(C(I)*CAP(I))+TC1(I)                                    AB 05510
      T2N(I)=Q2B(I)/(C(I)*CAP(I))+TC1(I)                                    AB 05520
      T3N(I)=Q3B(I)/(C(I)*CAP(I))+TC1(I)                                    AB 05530
      T4N(I)=Q4B(I)/(C(I)*CAP(I))+TC1(I)                                    AB 05540
      T5N(I)=Q5B(I)/(C(I)*CAP(I))+TC1(I)                                    AB 05550
      TN(I)=(T1N(I)+T2N(I)+T3N(I)+T4N(I)+T5N(I))/5.0                        AB 05560
      IF(ABR1.EQ.1.0) GOTO 519                                              AB 05570
C  PREDICTION OF PLENUM AIR TEMPERATURE USING CONVECTIVE HEAT TRANSFER      AB 05580
C  VALUE                                                                    AB 05590
      CEP(I)=1063.3-5.7194E-14*TC(I)**5+4.253RE-10*TC(I)**4-1.1417E-06*TAB 05600
     *C(I)**3+1.3637E-03*TC(I)**2-0.5117*TC(I)                              AB 05610
      TPLE(I)=RMB(I)/(C(I)*CEP(I))+TC1(I)                                   AB 05620
      IF(TPLE(I).GT.TN(I)) TPLE(I)=TN(I)                                    AB 05630
      WRITE(7,171)T1N(I),T2N(I),T3N(I),T4N(I),T5N(I),TN(I),TPLE(I),TC1(IAB 05640
     *)                                                                     AB 05650
  171 FORMAT(1H ,8(2X,F7.1))                                                AB 05660
      GOTO 95                                                               AB 05670
  519 WRITE(7,512)T1N(I),T2N(I),T3N(I),T4N(I),T5N(I),TN(I),TC1(I)           AB 05680
  512 FORMAT(1H ,7(4X,F7.1))                                                AB 05690
   95 CONTINUE                                                              AB 05700
  401 WRITE(7,49)                                                           AB 05710
   49 FORMAT(1H ,2X,'-------------------------------------------------------AB 05720
     *----------------------------'                                         AB 05730
     */1H0,16X,'HOLES CONVECTIVE HEAT TRANSFER TO COOLANT'                  AB 05740
     */,17X,'-----------------------------------------'                     AB 05750
     */,2X,'Hhc-W/M**2.K = CONVECTIVE HEAT TRANSFER COEFFICIENT; Q(1-5)H-AB 05760
     *WATT = CONVECTION IN THE'                                             AB 05770
     */,2X,'HOLES BASED ON WALL THERMOCOUPLE STATIONS ON WALL"S THERMOCOAB 05780
     *UPLE STATIONS;'                                                       AB 05790
     */,2X,'WH-W =MEAN HOLE CONVECTION;  NUS.#= HOLE"S NUSSELT NO. BASEDAB 05800
     * ON WALL"S THICKNESS,'                                                AB 05810
     -/,12X,'QB/WH=BACK TO HOLE CONV. COEFF.'                               AB 05820
     */,2X,'-------------------------------------------------------------AB 05830
     *----------------------------'                                         AB 05840
     */,7X,'Hhc',6X,'Q1h',7X,'Q2h',8X,'Q3h',7X,'Q4h',7X,'Q5h',7X,'Qh',7XAB 05850
     *,'NUS.#',4X,'QB/QH')                                                  AB 05860
      GOTO 82                                                               AB 05870
  305 WRITE(7,605)                                                          AB 05880
  605 FORMAT(1H ,2X,'-------------------------------------------------------AB 05890
     *----------------------------'                                         AB 05900
     */1H0,4X,'HOLES CONVECTIVE HEAT TRANSFER TO COOLANT-Based On PrediAB 05910
     *cted Wall Temp.'                                                      AB 05920
     */,5X,'-----------------------------------------------------------AB 05930
     *----------'                                                          AB 05940
     */,2X,'Hhc-W/M**2.K = CONVECTIVE HEAT TRANSFER COEFFICIENT; Q(1-5)H-AB 05950
     *WATT = CONVECTION IN THE'                                             AB 05960
     */,2X,'HOLES BASED ON WALL THERMOCOUPLE STATIONS ON WALL"S THERMOCOAB 05970
     *UPLE STATIONS;'                                                       AB 05980
     */,2X,'WH-W =MEAN HOLE CONVECTION;  NUS.#= HOLE"S NUSSELT NO. BASEDAB 05990
     * ON WALL"S THICKNESS,'                                                AB 06000
     -/,12X,'QB/WH=BACK TO HOLE CONV. COEFF.'                               AB 06010
     */,2X,'-------------------------------------------------------------AB 06020
     *----------------------------'                                         AB 06030
     */,7X,'Hhc',6X,'Q1h',7X,'Q2h',8X,'Q3h',7X,'Q4h',7X,'Q5h',7X,'Qh',7XAB 06040
     *,'NUS.#',4X,'QB/QH')                                                  AB 06050
C                                                                           AB 06060
C -----------------------------------------------------------------------AB 06070
C : COMPUTATION OF CONVECTIVE HEAT PICKED UP IN PLATE HOLES--CASE-2     :AB 06080
C -----------------------------------------------------------------------AB 06090
C   RTD=RATIO OF THICKNESS OF PLATE TO HOLES MEAN DIAMETER; RNU=NUSSELT AB 06100
C  AVG./NUSSELT FULL---MILLS DATA FOR SHARP 90 DEG. EDGE SERIES HAS BEENAB 06110
C  CURVE FITIED; HTH=CONVECTIVE HEAT TRANSFER COEFFICIENT;QTH=AVG CONVECAB 06120
C CTION TRANSFER;                                                           AB 06130
C USING MILLS DATA--CURVE FITTED EQUATION--FOR SHARP 90-DEG. EDGE SERIESAB 06140
C 4 -NUSSELT.AVG./NUSSELT.FULLY-DEV.=RNU;HTH=CONVECTIVE COEFFICIENT;QTH AB 06150
C                                                                           AB 06160
   82 RTD=TKN/D                                                             AB 06170
      RDT=1.0/RTD                                                           AB 06180
      DO 96,I=1,L                                                           AB 06190
      IF(ABR1.EQ.1.0.AND.C(I).EQ.0.0) GOTO 307                              AB 06200
      IF(C(I).EQ.0.0) GOTO 60                                               AB 06210
      IF(RTD.GE.2.001) GOTO 747                                             AB 06220
      RNU=0.131971*RTD**3-0.75444*RTD**2+1.03993*RTD+2.2378                 AB 06230
      GO TO 757                                                             AB 06240
  747 RNU=1.0-49.2818*RDT**4+58.6032*RDT**3-26.476*RDT**2+7.48122*RDT       AB 06250
      IF(RNU.EQ.0.0) GOTO 444                                               AB 06260
  757 HTH(I)=0.023*RE(I)**0.8*PRAT(I)**0.333*RNU*THCL(I)/D                  AB 06270
      TAH=PI*D*TKN*THN                                                      AB 06280
      W1H(I)=HTH(I)*TAH*(TPH1(I)-T1N(I))                                    AB 06290
      W2H(I)=HTH(I)*TAH*(TPH2(I)-T2N(I))                                    AB 06300
      W3H(I)=HTH(I)*TAH*(TPH3(I)-T3N(I))                                    AB 06310
      W4H(I)=HTH(I)*TAH*(TPH4(I)-T4N(I))                                    AB 06320
      W5H(I)=HTH(I)*TAH*(TPH5(I)-T5N(I))                                    AB 06330
      WH(I)=(W1H(I)+W2H(I)+W3H(I)+W4H(I)+W5H(I))/5.0                        AB 06340
      WBRH(I)=WB(I)/WH(I)                                                   AB 06350
C NUSSELT NUMBER(HN)- BASED ON WALL THICKNESS AND ABOVE HEAT COMPUTATIONAB 06360
      THCL(I)=-0.7231E-14*TN(I)**4+0.3126E-10*TN(I)**3-0.6331E-07*TN(I)*AB 06370
     **2+0.1081E-03*TN(I)-0.1265E-02                                        AB 06380
      HN1(I)=W1H(I)*TKN/(TAH*THCL(I)*(TPH1(I)-T1N(I)))                      AB 06390
      HN2(I)=W2H(I)*TKN/(TAH*THCL(I)*(TPH2(I)-T2N(I)))                      AB 06400
      HN3(I)=W3H(I)*TKN/(TAH*THCL(I)*(TPH3(I)-T3N(I)))                      AB 06410
      HN4(I)=W4H(I)*TKN/(TAH*THCL(I)*(TPH4(I)-T4N(I)))                      AB 06420
      HN5(I)=W5H(I)*TKN/(TAH*THCL(I)*(TPH5(I)-T5N(I)))                      AB 06430
      HN(I)=(HN1(I)+HN2(I)+HN3(I)+HN4(I)+HN5(I))/5.0                        AB 06440
      WRITE(7,121)HTH(I),W1H(I),W2H(I),W3H(I),W4H(I),W5H(I),WH(I),HN(I),AB 06450
     *WBRH(I)                                                               AB 06460
  121 FORMAT(1H ,8(2X,F8.2),2X,F7.3)                                        AB 06470
   96 CONTINUE                                                              AB 06480
   60 WRITE(7,57)                                                           AB 06490
   57 FORMAT(1H ,2X,'-------------------------------------------------------AB 06500
     *----------------------------'                                         AB 06510
     */,1H0,2X,'RADIATIVE HEAT LOST FROM TEST WALL FLAME SURFACE TO OTHEAB 06520
     *R COMBUSTOR SURFACES.'                                                AB 06530
     */,3X,'-----------------------------------------------------------AB 06540
     *----------'                                                          AB 06550
     */,2X,'W(1-5)H-WATT =RADIATIVE LOSS-BASED ON WALL"S THERMOCOUPLE STAB 06560
     *ATIONS, WMH-WATT=MEAN RADIATION'                                      AB 06570
     */,12X,'F/AR = FUEL/AIR RATIO'                                         AB 06580
     */,2X,'-------------------------------------------------------------AB 06590
     *----------------------------'                                         AB 06600
```

```
     */,9X,'W1F',8X,'Q2F',8X,'W3F',8X,'Q4F',8X,'W5F',8X,'QMF',8X,'F/AR')AB 06610
      GOTO 84                                                          AR 06620
307   WRITE(7,607)                                                     AR 06630
607   FORMAT(1H ,2X,'-------------------------------------------------AB 06640
     *----------------'                                                AB 06650
     */,1HO,2X,'RADIATIVE HEAT EXCHANGE BY TEST WALL FLAME SURFACE WITH AB 06660
     *OTHER COMBUSTOR SURFACES.'                                       AB 06670
     */,10X,'-Based On Predicted Wall Temperature.'                    AB 06680
     */,3X,'-------------------------------------------------------AB 06690
     *----------------'                                               AB 06700
     */,2X,'G(1-5)F-WATT =RADIATIVE LOSS-BASED ON WALL"S THERMOCOUPLE STAB 06710
     *ATIONS, WMF-WATT=MEAN RADIATION'                                 AB 06720
     */,12X,'F/AR = FUEL/AIR RATIO'                                   AB 06730
     */,2X,'-------------------------------------------------------AB 06740
     *----------------'                                               AB 06750
     */,9X,'W1F',8X,'Q2F',8X,'Q3F',8X,'Q4F',8X,'W5F',8X,'QMF',8X,'F/AR')AB 06760
C                                                                     AB 06770
C ---------------------------------------------------------------------AB 06780
C ! RADIATIVE HEAT LOST AT PLATE FLAME FACE-!Q1-5F!-QMF-! CASE-C     !  AB 06790
C ---------------------------------------------------------------------AB 06800
C  F1-3AR=FUEL/AIR RATIO,1-FOR PROPANE ONLY,2-FOR KEROSINE;3-FOR EFFECTIAB 06810
C VE FUEL/AIR RATIO; ULM=FLAME LUMINOSITY EQUATION USING ODGERS ET AL; AB 06820
C COMBUSTION EFFICIENCE IS TAKING AS 85%-FOR FUEL/AIR RATIO-;EE2=STAINL.AB 06830
C E-G1,G2,12,21,& 22,ARE FLAME AND EXCHANGE EMISSIVITIES;MEAN BEAM LENGHAB 06850
C T USED ARE THOSE CALCULATED USING GRAY ET AL METHOD & ARE :LG1=0.0446,AR 06860
C LG2=0.0667, L12=0.04214, L21=0.04214 AND L22=0.0745;EMISSIVITY EWN. ISAB 06870
C BASED ON REVES,LEFEBVRE ET AL , KRITCHER ET AL & ODGERS.           AR 06880
84    FLG1=0.0446                                                     AR 06890
      FLG2=0.0667                                                     AR 06900
      FL12=0.04214                                                    AR 06910
      FL21=0.04214                                                    AR 06920
      FL22=0.0745                                                     AR 06930
      IF(ISET.EQ.1)GOTO 332                                           AR 06940
      DO 98,I=1,L                                                     AB 06950
      IF(ABR1.EQ.1.0.AND.C(I).EQ.0.0) GOTO 308                        AB 06960
      IF(C(I).EQ.0.0) GOTO 98                                         AB 06970
      TGE(I)=TG(I)**(-1.5)                                            AB 06980
      F1AR(I)=FP(I)/AM(I)                                             AB 06990
      F2AR(I)=FK(I)/(AM(I)+FP(I))                                     AB 07000
      F3AR(I)=F1AR(I)+0.85*F2AR(I)                                    AB 07010
      IF(FK(I).EW.0.0) F3AR(I)=F1AR(I)                                AB 07020
      ULM=0.0691*(0.01*DOK-3.48)**2.71                                AB 07030
      IF(FK(I).EW.0.0) ULM=1.0                                        AB 07040
      ULM=1.0                                                         AB 07050
      EE2(I)=0.6179+2.40933E-04*TWM(I)                                AB 07060
      EG1(I)=1.0-EXP(-0.2864*ULM*P7(I)*(F3AR(I)*FLG1)**0.5*TGE(I))    AB 07070
      EG2(I)=1.0-EXP(-0.2864*ULM*P7(I)*(F3AR(I)*FLG2)**0.5*TGE(I))    AB 07080
      E12(I)=1.0-EXP(-0.2864*ULM*P7(I)*(F3AR(I)*FL12)**0.5*TGE(I))    AB 07090
      E21(I)=1.0-EXP(-0.2864*ULM*P7(I)*(F3AR(I)*FL21)**0.5*TGE(I))    AB 07100
      E22(I)=1.0-EXP(-0.2864*ULM*P7(I)*(F3AR(I)*FL22)**0.5*TGE(I))    AB 07110
C                                                                     AB 07120
C      ++++++++++++++++++++++++++++++++++++++++++++++++++++++++++++++ AB 07130
C      +     FOR VALUES OF Z3-,Z4-,Z5-, COMPUTATION COMMENCE      +   AB 07140
C      ++++++++++++++++++++++++++++++++++++++++++++++++++++++++++++++ AB 07150
C   NOTE THE ABOVE PARAMETERS ARE FOR COMPUTING RADIATIVE HEAT LOSS   AB 07160
C                                                                     AB 07170
      Z31(I)=(E1P(I)*0*TPH1(I)**4+(1.0-E1P(I))*EG1(I)*0*TG(I)**4)*(1.0-0AB 07180
     *.894*(1.0-E1P(I))*(1.0-F22(I)))                                 AB 07190
      Z32(I)=(E2P(I)*0*TPH2(I)**4+(1.0-E2P(I))*EG1(I)*0*TG(I)**4)*(1.0-0AB 07200
     *.894*(1.0-E2P(I))*(1.0-E22(I)))                                 AB 07210
      Z33(I)=(E3P(I)*0*TPH3(I)**4+(1.0-E3P(I))*EG1(I)*0*TG(I)**4)*(1.0-0AB 07220
     *.894*(1.0-E3P(I))*(1.0-E22(I)))                                 AB 07230
      Z34(I)=(E4P(I)*0*TPH4(I)**4+(1.0-E4P(I))*EG1(I)*0*TG(I)**4)*(1.0-0AB 07240
     *.894*(1.0-E4P(I))*(1.0-E22(I)))                                 AB 07250
      Z35(I)=(E5P(I)*0*TPH5(I)**4+(1.0-E5P(I))*EG1(I)*0*TG(I)**4)*(1.0-0AB 07260
     *.894*(1.0-E5P(I))*(1.0-E22(I)))                                 AB 07270
      Z41(I)=(EE2(I)*0*TWM(I)**4+(1.0-EE2(I))*EG2(I)*0*TG(I)**4)*(1.0-E1AB 07280
     *P(I))*(1.0-E12(I))                                              AB 07290
      Z42(I)=(EE2(I)*0*TWM(I)**4+(1.0-EE2(I))*EG2(I)*0*TG(I)**4)*(1.0-E2AB 07300
     *P(I))*(1.0-E12(I))                                              AB 07310
      Z43(I)=(EE2(I)*0*TWM(I)**4+(1.0-EE2(I))*EG2(I)*0*TG(I)**4)*(1.0-E3AB 07320
     *P(I))*(1.0-E12(I))                                              AB 07330
      Z44(I)=(EE2(I)*0*TWM(I)**4+(1.0-EE2(I))*EG2(I)*0*TG(I)**4)*(1.0-E4AB 07340
     *P(I))*(1.0-E12(I))                                              AB 07350
      Z45(I)=(EE2(I)*0*TWM(I)**4+(1.0-EE2(I))*EG2(I)*0*TG(I)**4)*(1.0-E5AB 07360
     *P(I))*(1.0-E12(I))                                              AB 07370
      Z51(I)=1.0-0.894*(1.0-EE2(I))*(1.0-E22(I))-0.106*(1.0-E1P(I))*(1.0AB 07380
     *-EE2(I))*(1.0-E12(I))*(1.0-E21(I))                              AB 07390
      Z52(I)=1.0-0.894*(1.0-EE2(I))*(1.0-E22(I))-0.106*(1.0-E2P(I))*(1.0AB 07400
     *-EE2(I))*(1.0-E12(I))*(1.0-E21(I))                              AB 07410
      Z53(I)=1.0-0.894*(1.0-EE2(I))*(1.0-E22(I))-0.106*(1.0-E3P(I))*(1.0AB 07420
     *-EE2(I))*(1.0-E12(I))*(1.0-E21(I))                              AB 07430
      Z54(I)=1.0-0.894*(1.0-EE2(I))*(1.0-E22(I))-0.106*(1.0-E4P(I))*(1.0AB 07440
     *-EE2(I))*(1.0-E12(I))*(1.0-E21(I))                              AB 07450
      Z55(I)=1.0-0.894*(1.0-EE2(I))*(1.0-E22(I))-0.106*(1.0-E5P(I))*(1.0AB 07460
     *-EE2(I))*(1.0-E12(I))*(1.0-E21(I))                              AB 07470
      AP=ARE                                                          AB 07480
C                                                                     AB 07490
      Q1F(I)=AP*E1P(I)*(0*TPH1(I)**4*Z51(I)-Z31(I)-Z41(I))/(Z51(I)*(1.0-AB 07500
     *E1P(I)))                                                        AB 07510
      Q2F(I)=AP*E2P(I)*(0*TPH2(I)**4*Z52(I)-Z32(I)-Z42(I))/(Z52(I)*(1.0-AB 07520
     *E2P(I)))                                                        AB 07530
      Q3F(I)=AP*E3P(I)*(0*TPH3(I)**4*Z53(I)-Z33(I)-Z43(I))/(Z53(I)*(1.0-AB 07540
     *E3P(I)))                                                        AB 07550
      Q4F(I)=AP*E4P(I)*(0*TPH4(I)**4*Z54(I)-Z34(I)-Z44(I))/(Z54(I)*(1.0-AB 07560
     *E4P(I)))                                                        AB 07570
      Q5F(I)=AP*E5P(I)*(0*TPH5(I)**4*Z55(I)-Z35(I)-Z45(I))/(Z55(I)*(1.0-AB 07580
     *E5P(I)))                                                        AB 07590
      QMF(I)=(Q1F(I)+Q2F(I)+Q3F(I)+Q4F(I)+Q5F(I))/5.0                 AB 07600
      WRITE(7,174)Q1F(I),Q2F(I),Q3F(I),Q4F(I),Q5F(I),QMF(I),F3AR(I)   AB 07610
174   FORMAT(1H ,6(4X,F7.1),4X,F8.4)                                  AB 07620
98    CONTINUE                                                        AB 07630
      IF(ABR1.EQ.0.0) GOTO 335                                        AB 07640
C      ++++++++++++++++++++++++++++++++++++++++++++++++++++++++++++++ AB 07650
C      +     NEW VALUES OF Z3-,Z4-,Z5-, COMPUTATION COMMENCE      +   AB 07660
C      ++++++++++++++++++++++++++++++++++++++++++++++++++++++++++++++ AB 07670
C   NOTE THE ABOVE PARAMETERS ARE FOR COMPUTING RADIATIVE HEAT LOSS   AB 07680
332   DO 330,I=1,L                                                    AB 07690
      IF(C(I).EQ.0.0) GOTO 337                                        AB 07700
```

FILE: AB FORTRAN A LEEDS UNIVERSITY VM/SP RELEASE 3

```
      Z31(I)=(E1P(I)*0*TPH1(I)**4+(1.0-E1P(I))*EG1(I)*0*TG(I)**4)*(1.0-0AB 07710
     *.894*(1.0-E1P(I))*(1.0-E22(I)))                                    AB 07720
      Z32(I)=(E2P(I)*0*TPH2(I)**4+(1.0-E2P(I))*EG1(I)*0*TG(I)**4)*(1.0-0AB 07730
     *.894*(1.0-E2P(I))*(1.0-E22(I)))                                    AB 07740
      Z33(I)=(E3P(I)*0*TPH3(I)**4+(1.0-E3P(I))*EG1(I)*0*TG(I)**4)*(1.0-0AB 07750
     *.894*(1.0-E3P(I))*(1.0-E22(I)))                                    AB 07760
      Z34(I)=(E4P(I)*0*TPH4(I)**4+(1.0-E4P(I))*EG1(I)*0*TG(I)**4)*(1.0-0AB 07770
     *.894*(1.0-E4P(I))*(1.0-E22(I)))                                    AB 07780
      Z35(I)=(E5P(I)*0*TPH5(I)**4+(1.0-E5P(I))*EG1(I)*0*TG(I)**4)*(1.0-0AB 07790
     *.894*(1.0-E5P(I))*(1.0-E22(I)))                                    AB 07800
      E1E(I)=0.6179+2.40933E-04*TPH1(I)                                  AB 07810
      E2E(I)=0.6179+2.40933E-04*TPH2(I)                                  AB 07820
      E3E(I)=0.6179+2.40933E-04*TPH3(I)                                  AB 07830
      E4E(I)=0.6179+2.40933E-04*TPH4(I)                                  AB 07840
      E5E(I)=0.6179+2.40933E-04*TPH5(I)                                  AB 07850
      Z41(I)=(E1E(I)*0*TPH1(I)**4+(1.0-E1E(I))*EG2(I)*0*TG(I)**4)*(1.0-EAB 07860
     *1P(I))*(1.0-E12(I))                                                AB 07870
      Z42(I)=(E2E(I)*0*TPH2(I)**4+(1.0-E2E(I))*EG2(I)*0*TG(I)**4)*(1.0-EAB 07880
     *2P(I))*(1.0-E12(I))                                                AB 07890
      Z43(I)=(E3E(I)*0*TPH3(I)**4+(1.0-E3E(I))*EG2(I)*0*TG(I)**4)*(1.0-EAB 07900
     *3P(I))*(1.0-E12(I))                                                AB 07910
      Z44(I)=(E4E(I)*0*TPH4(I)**4+(1.0-E4E(I))*EG2(I)*0*TG(I)**4)*(1.0-EAB 07920
     *4P(I))*(1.0-E12(I))                                                AB 07930
      Z45(I)=(E5E(I)*0*TPH5(I)**4+(1.0-E5E(I))*EG2(I)*0*TG(I)**4)*(1.0-EAB 07940
     *5P(I))*(1.0-E12(I))                                                AB 07950
      Z51(I)=1.0-0.894*(1.0-E1E(I))*(1.0-E22(I))-0.106*(1.0-E1P(I))*(1.0AB 07960
     *-E1E(I))*(1.0-E12(I))*(1.0-E21(I))                                 AB 07970
      Z52(I)=1.0-0.894*(1.0-E2E(I))*(1.0-E22(I))-0.106*(1.0-E2P(I))*(1.0AB 07980
     *-E2E(I))*(1.0-E12(I))*(1.0-E21(I))                                 AB 07990
      Z53(I)=1.0-0.894*(1.0-E3E(I))*(1.0-E22(I))-0.106*(1.0-E3P(I))*(1.0AB 08000
     *-E3E(I))*(1.0-E12(I))*(1.0-E21(I))                                 AB 08010
      Z54(I)=1.0-0.894*(1.0-E4E(I))*(1.0-E22(I))-0.106*(1.0-E4P(I))*(1.0AB 08020
     *-E4E(I))*(1.0-E12(I))*(1.0-E21(I))                                 AB 08030
      Z55(I)=1.0-0.894*(1.0-E5E(I))*(1.0-E22(I))-0.106*(1.0-E5P(I))*(1.0AB 08040
     *-E5E(I))*(1.0-E12(I))*(1.0-E21(I))                                 AB 08050
      AP=ARE                                                             AB 08060
      Q1F(I)=0.0                                                         AB 08070
      Q2F(I)=0.0                                                         AB 08080
      Q3F(I)=0.0                                                         AB 08090
      Q4F(I)=0.0                                                         AB 08100
      Q5F(I)=0.0                                                         AB 08110
      QMF(I)=0.0                                                         AB 08120
330   CONTINUE                                                           AB 08130
337   IF(ISET.EQ.1.AND.ABR1.EQ.0.0) GOTO 333                             AB 08140
      DO 338,I=1,L                                                       AB 08150
      IF(C(I).EQ.0.0) GOTO 308                                           AB 08160
      WRITE(7,331)Q1F(I),Q2F(I),Q3F(I),Q4F(I),Q5F(I),QMF(I),F3AR(I)      AB 08170
331   FORMAT(1H ,6(4X,F7.1),4X,F8.4)                                     AB 08180
338   CONTINUE                                                           AB 08190
335   WRITE(7,58)                                                        AB 08200
58    FORMAT(1H ,2X,'-----------------------------------------------------AB 08210
     *----------------------------------------')                         AB 08220
     */1H1,20X,'CONVECTIVE HEAT TRANSFER FROM COMBUSTION GAS TO TEST WALAB 08230
     *L'/,21X,'-----------------------------------------------------------AB 08240
     *'/,2X,'Q(1-5)ct & Qct-WATT=CONVECTION FROM GAS STREAM TO TEST WALLAB 08250
     * --BASED ON WALL THERMOCOUPLE STATIONS - Qct IS MEAN;'              AB 08260
     */,2X,'H(1-5)g & HMg-W/M*2.K =ARE BOTH CONVECTIVE HEAT TRANSFER CUEAB 08270
     *FFICIENT -BASED ON WALL THERMOCOUPLES- & HMg IS MEAN.'             AB 08280
     */,2X,'Nu.l=NUSSELT NO. BASED ON TEST WALL LENGTH'                 AB 08290
     */,2X,'-----------------------------------------------------------AB 08300
     *----------------------------------'                               AB 08310
     */,6X,'H1g',5X,'Q1ct',6X,'H2g',5X,'Q2ct',5X,'H3g',5X,'Q3ct',6X,'H4gAB 08320
     *',6X,'Q4ct',6X,'H5g',5X,'Q5ct',5X,'HMg',6X,'Qct',5X,'Nu.l')        AB 08330
      GOTO 80                                                            AB 08340
308   WRITE(7,608)                                                       AB 08350
608   FORMAT(1H ,2X,'-----------------------------------------------------AB 08360
     *----------------------------------'                               AB 08370
     */1H1,5X,'CONVECTIVE HEAT TRANSFER FROM COMBUSTION GAS TO TEST WALLAB 08380
     * -Based On Predicted Wall Temperature.'                            AB 08390
     */,6X,'-----------------------------------------------------------AB 08400
     *----------------------------------'                               AB 08410
     * /,2X,'Q(1-5)ct & Qct-WATT=CONVECTION FROM GAS STREAM TO TEST WALLAB 08420
     * --BASED ON WALL THERMOCOUPLE STATIONS - Qct IS MEAN;'              AB 08430
     */,2X,'H(1-5)g & HMg-W/M*2.K =ARE BOTH CONVECTIVE HEAT TRANSFER CUEAB 08440
     *FFICIENT -BASED ON WALL THERMOCOUPLES- & HMg IS MEAN.'             AB 08450
     */,2X,'Nu.l=NUSSELT NO. BASED ON TEST WALL LENGTH'                 AB 08460
     */,2X,'-----------------------------------------------------------AB 08470
     *----------------------------------'                               AB 08480
     */,6X,'H1g',5X,'Q1ct',6X,'H2g',5X,'Q2ct',5X,'H3g',5X,'Q3ct',6X,'H4gAB 08490
     *',6X,'Q4ct',6X,'H5g',5X,'Q5ct',5X,'HMg',6X,'Qct',5X,'Nu.l')        AB 08500
C                                                                        AB 08510
C &&&&&&&&&&&&&&&&&&&&&&&&&&&&&&&&&&&&&&&&&&&&&&&&&&&&&&&&&&&&&&&&&&&&&AB 08520
C &  CONVECTIVE HEAT TRANSFER FROM HOT COMBUSTOR MAINSTREAM TO TEST   & AB 08530
C &                    WALL-:QCT:----------CASE-C1                    & AB 08540
C &&&&&&&&&&&&&&&&&&&&&&&&&&&&&&&&&&&&&&&&&&&&&&&&&&&&&&&&&&&&&&&&&&&&&AB 08550
C   H1-5F,HMF : ARE CONVECTIVE HEAT TRANSFER COFFFICIENT--WALL THERMOCOUAB 08560
C   -PLE STATIONS & MEAN; TCL=THERMAL CONDUTIVITY BASED ON INLET TEMP.  AB 08570
C   HNL=NUSSELT #-BASED ON TEST WALL LENGHT; ELT=TEST WALL LENGHT IN M .AB 08580
86    ELT=0.1524                                                         AB 08590
      DO 101,I=1,L                                                       AB 08600
      IF(ABR1.EQ.1.0.AND.Q1H(I).EQ.0.0) GOTO 309                         AB 08610
      IF(Q1H(I).EQ.0.0) GOTO 222                                         AB 08620
      TCL(I)=-0.7231E-14*TN(I)**4+0.3126E-10*TN(I)**3-0.6331E-07*TN(I)**AB 08630
     *2+0.1081E-03*TN(I)-0.1265E-02                                      AB 08640
      R1F(I)=AP*0*(1.0+E1P(I))*EG1(I)*TG(I)**1.5*(TG(I)**2.5-TPH1(I)**2.AB 08650
     *5)/2.0                                                             AB 08660
      R2F(I)=AP*0*(1.0+E2P(I))*EG1(I)*TG(I)**1.5*(TG(I)**2.5-TPH2(I)**2.AB 08670
     *5)/2.0                                                             AB 08680
      R3F(I)=AP*0*(1.0+E3P(I))*EG1(I)*TG(I)**1.5*(TG(I)**2.5-TPH3(I)**2.AB 08690
     *5)/2.0                                                             AB 08700
      R4F(I)=AP*0*(1.0+E4P(I))*EG1(I)*TG(I)**1.5*(TG(I)**2.5-TPH4(I)**2.AB 08710
     *5)/2.0                                                             AB 08720
      R5F(I)=AP*0*(1.0+E5P(I))*EG1(I)*TG(I)**1.5*(TG(I)**2.5-TPH5(I)**2.AB 08730
     *5)/2.0                                                             AB 08740
      RF(I)=(R1F(I)+R2F(I)+R3F(I)+R4F(I)+R5F(I))/5.0                     AB 08750
      IF(C(I).EQ.0.0) GOTO 484                                           AB 08760
      Q1CT(I)=W1B(I)+R1B(I)+W1H(I)+Q1F(I)-R1F(I)                         AB 08770
      Q2CT(I)=W2B(I)+R2B(I)+W2H(I)+Q2F(I)-R2F(I)                         AB 08780
      Q3CT(I)=W3B(I)+R3B(I)+W3H(I)+Q3F(I)-R3F(I)                         AB 08790
      Q4CT(I)=W4B(I)+R4B(I)+W4H(I)+Q4F(I)-R4F(I)                         AB 08800
```

```
FILE: AB        FORTRAN  A   LEEDS UNIVERSITY VM/SP RELEASE 3

      W5CT(I)=W5B(I)+R5B(I)+W5M(I)+W5F(I)-R5F(I)                          AB 08810
      WCT(I)=(W1CT(I)+W2CT(I)+W3CT(I)+W4CT(I)+W5CT(I))/5.0               AB 08820
      H1F(I)=Q1CT(I)/(AP*(TG(I)-TPH1(I)))                                AB 08830
      H2F(I)=Q2CT(I)/(AP*(TG(I)-TPH2(I)))                                AB 08840
      H3F(I)=Q3CT(I)/(AP*(TG(I)-TPH3(I)))                                AB 08850
      H4F(I)=Q4CT(I)/(AP*(TG(I)-TPH4(I)))                                AB 08860
      H5F(I)=Q5CT(I)/(AP*(TG(I)-TPH5(I)))                                AB 08870
      HMF(I)=(H1F(I)+H2F(I)+H3F(I)+H4F(I)+H5F(I))/5.0                    AB 08880
      HNL(I)=HMF(I)*ELT/TCL(I)                                           AB 08890
      WRITE(7,176)H1F(I),Q1CT(I),H2F(I),W2CT(I),H3F(I),Q3CT(I),H4F(I),   AB 08900
     *W4CT(I),H5F(I),Q5CT(I),HMF(I),WCT(I),HNL(I)                        AB 08910
  176 FORMAT(1H ,13(2X,F7.1))                                            AB 08920
  101 CONTINUE                                                           AB 08930
  222 WRITE(7,59)                                                        AB 08940
   59 FORMAT(1H ,2X,'-------------------------------------------------AB 08950
     *----------------------------------------------------------------' AB 08960
     */1H0,12X,'PREDICTED COOLANT"S HOLES OUTLET TEMPERATURE AND FLOW DIAB 08970
     *STRIBUTION'                                                        AB 08980
     */,13X,'-------------------------------------------------AB 08990
     *-------'                                                           AB 09000
     */,2X,'T-(1 TO 5)o=OUTLET TEMPERATURE BASED ON HEAT TRANSFER FROM TAB 09010
     *HERMAL LOCATIONS 1 TO 5 OF TEST WALL,'                             AB 09020
     */,2X,'mTo = MEAN OUTLET TEMPERATURE; T(1 to 5)r = OUTLET TO PLENUMAB 09030
     *COOLANT TEMP. RATIO & Trm IS THE MEAN'                             AB 09040
     -/,5X,'To/Tp = Ratio Of Outlet To Plenum Temperature'              AB 09050
     */,2X,'-------------------------------------------------AB 09060
     *----------------------------------------------------'              AB 09070
     */,4X,'T1o-K',3X,'T2o-K',3X,'T3o-K',3X,'T4o-K',3X,'T5o-K',3X,'mTo-KAB 09080
     *',5X,'T1r',6X,'T2r',6X,'T3r',6X,'T4r',6X,'T5r',5X,'Trm',6X,'To/Tp'AB 09090
     -)                                                                 AB 09100
      GOTO 64                                                           AB 09110
  309 WRITE(7,609)                                                      AB 09120
  609 FORMAT(1H ,2X,'-------------------------------------------------AB 09130
     *----------------------------------------------------------------' AB 09140
     */1H0,2X,'PREDICTED COOLANT"S HOLES OUTLET TEMPERATURE AND FLOW DISAB 09150
     *TRIBUTION-Based On Predicted Wall Temp.'                           AB 09160
     */,3X,'-------------------------------------------------AB 09170
     *-------------------------------------'                            AB 09180
     */,2X,'T-(1 TO 5)o=OUTLET TEMPERATURE BASED ON HEAT TRANSFER FROM TAB 09190
     *HERMAL LOCATIONS 1 TO 5 OF TEST WALL,'                             AB 09200
     */,2X,'mTo = MEAN OUTLET TEMPERATURE; T(1 to 5)r = OUTLET TO PLENUMAB 09210
     *COOLANT TEMP. RATIO & Trm IS THE MEAN'                             AB 09220
     -/,5X,'To/Tp = Ratio Of Outlet To Plenum Temperature'              AB 09230
     */,2X,'-------------------------------------------------AB 09240
     *----------------------------------------------------'              AB 09250
     */,4X,'T1o-K',3X,'T2o-K',3X,'T3o-K',3X,'T4o-K',3X,'T5o-K',3X,'mTo-KAB 09260
     *',5X,'T1r',6X,'T2r',6X,'T3r',6X,'T4r',6X,'T5r',5X,'Trm',6X,'To/Tp'AB 09270
     *)                                                                 AB 09280
C  ##################################################################### AB 09290
C  #      PREDICTION OF COOLANT OUTLET TEMPERATURE---CASE Cb           # AB 09300
C  ##################################################################### AB 09310
C  THE PREDICTION BELOW IS BASED ON CONVECTIVE HEAT COMPUTATION USING    AB 09320
C  MILL'S THERMAL ENTRY MODEL; THE TEMPERATURE-TO1-, IS BASED ON WALL    AB 09330
C  THERMAL STATIONS                                                      AB 09340
C5555555555555555555555555555555555555555555555555555555555555555555 AB 09350
   64 DO 102,I=1,L                                                      AB 09360
      IF(ABR1.EQ.1.0.AND.C(I).EQ.0.0) GOTO 314                          AB 09370
      IF(C(I).EQ.0.0) GOTO 404                                          AB 09380
      C1P(I)=1063.3-5.7194E-14*T1N(I)**5+4.2538F-10*T1N(I)**4-1.1417E-06AB 09390
     **T1N(I)**3+1.3637E-03*T1N(I)**2-0.5117*T1N(I)                     AB 09400
      C2P(I)=1063.3-5.7194E-14*T2N(I)**5+4.2538F-10*T2N(I)**4-1.1417E-06AB 09410
     **T2N(I)**3+1.3637E-03*T2N(I)**2-0.5117*T2N(I)                     AB 09420
      C3P(I)=1063.3-5.7194E-14*T3N(I)**5+4.2538E-10*T3N(I)**4-1.1417E-06AB 09430
     **T3N(I)**3+1.3637E-03*T3N(I)**2-0.5117*T3N(I)                     AB 09440
      C4P(I)=1063.3-5.7194E-14*T4N(I)**5+4.2538E-10*T4N(I)**4-1.1417E-06AB 09450
     **T4N(I)**3+1.3637E-03*T4N(I)**2-0.5117*T4N(I)                     AB 09460
      C5P(I)=1063.3-5.7194L-14*T5N(I)**5+4.2538F-10*T5N(I)**4-1.1417E-06AB 09470
     **T5N(I)**3+1.3637E-03*T5N(I)**2-0.5117*T5N(I)                     AB 09480
      IF(ABR1.EQ.1.0) GOTO 9001                                         AB 09490
      TDZ(I)=TC1(I)                                                     AB 09500
C-------------------------------------------------------------------AB 09510
 9001 TO1(I)=(W1H(I)/(C(I)*C1P(I)))+T1N(I)                              AB 09520
      TO2(I)=(W2H(I)/(C(I)*C2P(I)))+T2N(I)                              AB 09530
      TO3(I)=(W3H(I)/(C(I)*C3P(I)))+T3N(I)                              AB 09540
      TO4(I)=(W4H(I)/(C(I)*C4P(I)))+T4N(I)                              AB 09550
      TO5(I)=(W5H(I)/(C(I)*C5P(I)))+T5N(I)                              AB 09560
      TO(I)=(TO1(I)+TO2(I)+TO3(I)+TO4(I)+TO5(I))/5.0                    AB 09570
      TRTP(I)=TO(I)/TPLF(I)                                             AB 09580
C##################################################################AB 09590
C  T(1-5)R& IR ARE COOLANT TEMPERATURE PROFILE FROM PLENUM TO HOLES OUT-AB 09600
C  LET, NORMINAL PLENUM TEMPERATURE TC1 HAS BEEN USED FOR COMPUTATION.   AB 09610
C  ----------------------------------------------------------------AB 09620
      IF(ABR1.EQ.1.0) GOTO 9002                                         AB 09630
      T1R(I)=(TPH1(I)-TO1(I))/(TPH1(I)-TC1(I))                          AB 09640
      T2R(I)=(TPH2(I)-TO2(I))/(TPH2(I)-TC1(I))                          AB 09650
      T3R(I)=(TPH3(I)-TO3(I))/(TPH3(I)-TC1(I))                          AB 09660
      T4R(I)=(TPH4(I)-TO4(I))/(TPH4(I)-TC1(I))                          AB 09670
      T5R(I)=(TPH5(I)-TO5(I))/(TPH5(I)-TC1(I))                          AB 09680
      GOTO 9004                                                         AB 09690
 9002 T1R(I)=(TPH1(I)-TO1(I))/(TPH1(I)-TDZ(I))                          AB 09700
      T2R(I)=(TPH2(I)-TO2(I))/(TPH2(I)-TDZ(I))                          AB 09710
      T3R(I)=(TPH3(I)-TO3(I))/(TPH3(I)-TDZ(I))                          AB 09720
      T4R(I)=(TPH4(I)-TO4(I))/(TPH4(I)-TDZ(I))                          AB 09730
      T5R(I)=(TPH5(I)-TO5(I))/(TPH5(I)-TDZ(I))                          AB 09740
 9004 TR(I)=(T1R(I)+T2R(I)+T3R(I)+T4R(I)+T5R(I))/5.0                    AB 09750
C   ################################################################## AB 09760
C ----------------------------------------------------------------AB 09770
C  COOLANT MASS DISTRIBUTION BASED ON PREDICTED INLET & OUTLET TEMP.   AR 09780
C ----------------------------------------------------------------AB 09790
      T1F(I)=(TO1(I)+T1N(I))/2.0                                        AB 09800
      CAP(I)=1063.3-5.7194E-14*T1F(I)**5+4.2538E-10*T1F(I)**4-1.1417E-06AR 09810
     **T1F(I)**3+1.3637E-03*T1F(I)**2-0.5117*T1F(I)                     AR 09820
      F1D(I)=Q1H(I)/(CAP(I)*ARE*(TO1(I)-T1N(I)))                        AR 09830
      T2F(I)=(TO2(I)+T2N(I))/2.0                                        AR 09840
      CAP(I)=1063.3-5.7194E-14*T2F(I)**5+4.2538F-10*T2F(I)**4-1.1417E-06AB 09850
     **T2F(I)**3+1.3637E-03*T2F(I)**2-0.5117*T2F(I)                     AR 09860
      F2D(I)=Q2H(I)/(CAP(I)*ARE*(TO2(I)-T2N(I)))                        AB 09870
      T3F(I)=(TO3(I)+T3N(I))/2.0                                        AR 09880
      CAP(I)=1063.3-5.7194E-14*T3F(I)**5+4.2538F-10*T3F(I)**4-1.1417E-06AR 09890
     **T3F(I)**3+1.3637E-03*T3F(I)**2-0.5117*T3F(I)                     AB 09900
```

```
FILE: AB       FORTRAN  A   LEEDS UNIVERSITY VM/SP RELEASE 3

      F3D(I)=Q3M(I)/(CAP(I)*ARE*(TO3(I)-T3N(I)))                        AB 09910
      T4F(I)=(TO4(I)+T4N(I))/2.0                                        AB 09920
      CAP(I)=1063.3-5.7194E-14*T4F(I)**5+4.2538E-10*T4F(I)**4-1.1417E-06AB 09930
     **T4F(I)**3+1.3637E-03*T4F(I)**2-0.5117*T4F(I)                     AB 09940
      F4D(I)=Q4M(I)/(CAP(I)*ARE*(TO4(I)-T4N(I)))                        AB 09950
      T5F(I)=(TO5(I)+T5N(I))/2.0                                        AB 09960
      CAP(I)=1063.3-5.7194E-14*T5F(I)**5+4.2538E-10*T5F(I)**4-1.1417E-06AB 09970
     **T5F(I)**3+1.3637E-03*T5F(I)**2-0.5117*T5F(I)                     AB 09980
      F5D(I)=Q5M(I)/(CAP(I)*ARE*(TO5(I)-T5N(I)))                        AB 09990
      WRITE(7,97)TO1(I),TO2(I),TO3(I),TO4(I),TO5(I),TO(I),T1R(I),T2R(I),AB 10000
     *T3K(I),T4R(I),T5R(I),TR(I),TRTP(I)                                AB 10010
 97   FORMAT(1H ,6(1X,F7.1),7(2X,F7.3))                                 AB 10020
 102  CONTINUE                                                          AB 10030
 404  WRITE(7,61)                                                       AB 10040
 61   FORMAT(1H ,2X,'-------------------------------------------------AB 10050
     *-------------------'                                              AB 10060
     */,1H0,4X,'CONVECTIVE HEAT--2 TRANSFER TO TEST WALL FROM COMBUSTOR AB 10070
     *MAINSTREAM'                                                       AB 10080
     */,5X,'-------------------------------------------------------AB 10090
     *------'                                                          AB 10100
     */,2X,'THE CONVECTIVE HEAT HERE IS BASE ON MILL"S LONG CALMING SECTAB 10110
     *ION SERIES EWUATION'                                             AB 10120
     */,2X,'NUM=NUSSELT NUMBER; CHo-W/(M*2.K)=CONVECTIVE HEAT TRANSFER CAB 10130
     *UEFFICIENT; W-(1 TO 5)M-WATTS'                                   AB 10140
     */,2X,'=CONVECTIVE HEAT TRANSFER AS PER TEST WALL THERMAL STATIONS AB 10150
     *1 TO 5; WM=MEAN CONVECTIVE HEAT.'                                AB 10160
     */,2X,'-------------------------------------------------------AB 10170
     *-----------------------------------'                            AB 10180
     */,6X,'NUM.',7X,'CHo',6X,'Q1M',7X,'Q2M',7X,'Q3M',7X,'Q4M',6X,'Q5M',AB 10190
     *8X,'WM')                                                         AB 10200
      GOTO 68                                                          AB 10210
 314  WRITE(7,619)                                                     AB 10220
 619  FORMAT(1H ,2X,'-------------------------------------------------AB 10230
     *-------------------'                                              AB 10240
     */,1H0,4X,'CONVECTIVE HEAT--2 TRANSFER TO TEST WALL FROM COMBUSTOR AB 10250
     *MAINSTREAM'                                                      AB 10260
     */,5X,'-------------------------------------------------------AB 10270
     *------'                                                          AB 10280
     */,2X,'THE CONVECTIVE HEAT HERE IS BASE ON MILL"S LONG CALMING SECTAB 10290
     *ION SERIES EWUATION'                                             AB 10300
     */,2X,'NUM=NUSSELT NUMBER; CHo-W/(M*2.K)=CONVECTIVE HEAT TRANSFER CAB 10310
     *UEFFICIENT; W-(1 TO 5)M-WATTS'                                   AB 10320
     */,2X,'=CONVECTIVE HEAT TRANSFER AS PER TEST WALL THERMAL STATIONS AB 10330
     *1 TO 5; WM=MEAN CONVECTIVE HEAT.'                                AB 10340
     */,2X,'-------------------------------------------------------AB 10350
     *-----------------------------------'                            AB 10360
     */,6X,'NUM.',7X,'CHo',6X,'Q1M',7X,'Q2M',7X,'Q3M',7X,'W4M',6X,'Q5M',AB 10370
     *8X,'WM')                                                         AB 10380
C MMMMMMMMMMMMMMMMMMMMMMMMMMMMMMMMMMMMMMMMMMMMMMMMMMMMMMMMMMMMMMMMMMAB 10390
C +   CONVECTIVE HEAT TRANSFER TO TEST WALL FROM COMB. MAINSTREAM    +  AB 10400
C MMMMMMMMMMMMMMMMMMMMMMMMMMMMMMMMMMMMMMMMMMMMMMMMMMMMMMMMMMMMMMMMMMAB 10410
C THE CONVECTIVE HEAT COMPUTED BELOW IS BASED ON MILL'S LONG CALMING    AB 10420
C SECTION SERIES;CNU=NUSSELT NO.,REC=REYNOLDS NO.,PRCT=PRANDTL NO.,    AB 10430
C HCO=CONVECTION COEFFICIENT,C1-5W & CVW =CONVECTION TRANSFER          AB 10440
C   COMBUSTOR HYDRAULIC DIAMETER = 0.1016;                             AB 10450
C YT=VALUE OF NUSSELT NO. RATIO FROM MILL'S DATA FOR THE COMBUSTOR     AB 10460
 68   CCA=0.0081073                                                    AB 10470
      YT=1.57                                                          AB 10480
      DEM=0.1016                                                       AB 10490
      DO 103,I=1,L                                                     AB 10500
      IF(C(I).EQ.0.0) GOTO 103                                         AB 10510
      S1C(I)=100.0/TG(I)                                               AB 10520
      Y1C(I)=A1+A2*S1C(I)+A3*S1C(I)**2+A4*S1C(I)**3+A5*S1C(I)**4       AB 10530
      U1C(I)=1E-06*SQRT(TG(I))/Y1C(I)                                  AB 10540
      TCL(I)=-0.7231E-14*TG(I)**4+0.3126E-10*TG(I)**3-0.6331E-07*TG(I)**AB 10550
     *2+0.1081E-03*TG(I)-0.1265E-02                                    AB 10560
      REC(I)=4*SFR(I)/(PI*0.1016*U1C(I))                               AB 10570
      CPC(I)=1063.3-5.7194E-14*TG(I)**5+4.253RE-10*TG(I)**4-1.1417E-06*TAB 10580
     *G(I)**3+1.3637E-03*TG(I)**2-0.5117*TG(I)                         AB 10590
      PRCT(I)=CPC(I)*U1C(I)/TCL(I)                                     AB 10600
      CNU(I)=0.023*REC(I)**0.8*PRCT(I)**0.333*YT                       AB 10610
      HCO(I)=CNU(I)*TCL(I)/DEM                                         AB 10620
      C1W(I)=PI*DEM*ELT*HCO(I)*(TG(I)-TPH1(I))                         AB 10630
      C2W(I)=PI*DEM*ELT*HCO(I)*(TG(I)-TPH2(I))                         AB 10640
      C3W(I)=PI*DEM*ELT*HCO(I)*(TG(I)-TPH3(I))                         AB 10650
      C4Q(I)=PI*DEM*ELT*HCO(I)*(TG(I)-TPH4(I))                         AB 10660
      C5W(I)=PI*DEM*ELT*HCO(I)*(TG(I)-TPH5(I))                         AB 10670
      CVW(I)=(C1W(I)+C2Q(I)+C3W(I)+C4Q(I)+C5W(I))/5.0                  AB 10680
      WRITE(7,99)CNU(I),HCO(I),C1Q(I),C2W(I),C3Q(I),C4Q(I),C5Q(I),CVQ(I)AB 10690
 99   FORMAT(1H ,8(3X,F7.1))                                           AB 10700
 103  CONTINUE                                                         AB 10710
      IF(ABR1.EQ.1.0) GOTO 315                                         AB 10720
      WRITE(7,271)                                                     AB 10730
 271  FORMAT(1H ,2X,'-------------------------------------------------AB 10740
     *----------'                                                      AR 10750
     */1H1,16X,'RADIATIVE HEAT TRANSFER FROM FLAME'                    AR 10760
     */,17X,'-----------------------------------'                     AR 10770
     */,2X,'R(1 TO 5)F-WATTS = RADIATIVE HEAT TRANSFER FROM FLAME TO WALAR 10780
     *L-BASED ON WALL'                                                 AB 10790
     */,2X,'THERMAL STATIONS ; Rmf-WATT = MEAN FLAME RADIATION'        AR 10800
     */,2X,'Ep & Eg = EMISSIVITIES OF TEST WALL AND THE FLAME RESPECTIVEAB 10810
     *LY'                                                              AB 10820
     */,2X,'-------------------------------------------------------AR 10830
     *------------------------'                                        AR 10840
     */,9X,'R1F',7X,'R2F',9X,'R3F',7X,'R4F',8X,'R5F',8X,'Rmf',6X,'Ep',  AR 10850
     *7X,'Eg',6X,'%Rf/Wc')                                            AB 10860
      GOTO 91                                                          AR 10870
 315  WRITE(7,617)                                                     AR 10880
 617  FORMAT(1H ,2X,'-------------------------------------------------AB 10890
     *----------'                                                      AB 10900
     */1H1,2X,'RADIATIVE HEAT TRANSFER FROM FLAME -Based On Predicted WaAR 10910
     *ll Temperature'                                                  AR 10920
     */,3X,'-------------------------------------------------------AB 10930
     *------------------'                                             AB 10940
     */,2X,'R(1 TO 5)F-WATTS = RADIATIVE HEAT TRANSFER FROM FLAME TO WALAB 10950
     *L-BASED ON WALL'                                                 AB 10960
     */,2X,'THERMAL STATIONS ; Rmf-WATT = MEAN FLAME RADIATION'        AB 10970
     */,2X,'-------------------------------------------------------AB 10980
     *------------------'                                             AB 10990
     */,9X,'R1F',7X,'R2F',9X,'R3F',7X,'R4F',8X,'R5F',8X,'Rmf',7X,'%Rf/WcAB 11000
```

FILE: AB FORTRAN A LEEDS UNIVERSITY VM/SP RELEASE 3

```
     *')                                                                    AB 11010
C :::::::::::::::::::::::::::::::::::::::::::::::::::::::::::::::::::::::: AB 11020
C :    COMPUTATION OF RADIATIVE HEAT TRANSFER FROM MAINSTREAM          :   AB 11030
C :::::::::::::::::::::::::::::::::::::::::::::::::::::::::::::::::::::::: AB 11040
C R(1-5)F=W = FLAME RADIATION TO PLATE                                      AB 11050
91    DO 272,I=1,L                                                          AB 11060
      IF(ABR1.EQ.1.0.AND.C(I).EQ.0.0) GOTO 128                              AB 11070
      IF(C(I).EQ.0.0) GOTO 272                                              AB 11080
      IF(ABR1.EQ.1.0) GOTO 2271                                             AB 11090
      PRW(I)=100.0*RF(I)/QCT(I)                                             AB 11100
      WRITE(7,270)R1F(I),R2F(I),R3F(I),R4F(I),R5F(I),RF(I),E1P(I),EG1(I)AB 11110
     -,PRQ(I)                                                               AB 11120
270   FORMAT(1H ,6(4X,F7.2),2(2X,F7.4),2X,F7.2)                             AB 11130
      GOTO 272                                                              AB 11140
2271  WRITE(7,2270)R1F(I),R2F(I),R3F(I),R4F(I),R5F(I),RF(I),PRW(I)          AB 11150
2270  FORMAT(1H ,7(4X,F7.2))                                                AB 11160
272   CONTINUE                                                              AB 11170
      ISET=1                                                                AB 11180
      IF(ABR1.EQ.1.0) GOTO 333                                              AB 11190
      GOTO 332                                                              AB 11200
C   ------------------------------------------------------------            AB 11210
C   :           PREDICTION OF TEST WALL TEMPERATURE            :            AB 11220
C   ------------------------------------------------------------            AB 11230
333   DO 274,I=1,L                                                          AB 11240
      IF(C(I).EQ.0.0) GOTO 274                                              AB 11250
      W1CT(I)=W1B(I)+R1B(I)+W1H(I)+Q1F(I)-R1F(I)                            AB 11260
      W2CT(I)=W2B(I)+R2B(I)+W2H(I)+Q2F(I)-R2F(I)                            AB 11270
      W3CT(I)=W3B(I)+R3B(I)+W3H(I)+Q3F(I)-R3F(I)                            AB 11280
      W4CT(I)=W4B(I)+R4B(I)+W4H(I)+Q4F(I)-R4F(I)                            AB 11290
      W5CT(I)=W5B(I)+R5B(I)+W5H(I)+Q5F(I)-R5F(I)                            AB 11300
      T1P(I)=TG(I)-(W1CT(I)/(H1F(I)*AP))                                    AB 11310
      T2P(I)=TG(I)-(W2CT(I)/(H2F(I)*AP))                                    AB 11320
      T3P(I)=TG(I)-(W3CT(I)/(H3F(I)*AP))                                    AB 11330
      T4P(I)=TG(I)-(W4CT(I)/(H4F(I)*AP))                                    AB 11340
      T5P(I)=TG(I)-(W5CT(I)/(H5F(I)*AP))                                    AB 11350
      TPM(I)=(T1P(I)+T2P(I)+T3P(I)+T4P(I)+T5P(I))/5.0                       AB 11360
      E1(I)=(TG(I)-T1P(I))/(TG(I)-TC(I))                                    AB 11370
      E2(I)=(TG(I)-T2P(I))/(TG(I)-TC(I))                                    AB 11380
      E3(I)=(TG(I)-T3P(I))/(TG(I)-TC(I))                                    AB 11390
      E4(I)=(TG(I)-T4P(I))/(TG(I)-TC(I))                                    AB 11400
      E5(I)=(TG(I)-T5P(I))/(TG(I)-TC(I))                                    AB 11410
      IF(AB.EQ.'(High_Temp._Work)') GOTO 274                                AB 11420
      T1A(I)=(T1P(I)-TC(I))*((T1A(I)-TC(I))/(T7P(I)-TC(I)))+TC(I)           AB 11430
      T3A(I)=(T5P(I)-TC(I))*((T3A(I)-TC(I))/(T9P(I)-TC(I)))+TC(I)           AB 11440
      E7(I)=(TG(I)-T1A(I))/(TG(I)-TC(I))                                    AB 11450
      E9(I)=(TG(I)-T3A(I))/(TG(I)-TC(I))                                    AB 11460
      T2A(I)=(T3P(I)-TC(I))*((T2A(I)-TC(I))/(T8P(I)-TC(I)))+TC(I)           AB 11470
      E8(I)=(TG(I)-T2A(I))/(TG(I)-TC(I))                                    AB 11480
274   CONTINUE                                                              AB 11490
C                                                                           AB 11500
C     ++++++++++++++++++++++++++++++++++++++++++++++++++++++++++++++++++++AB 11510
C     +       COMPUTATION OF JET VELOCITY & VELOCITY RATIOS              +AB 11520
C     ++++++++++++++++++++++++++++++++++++++++++++++++++++++++++++++++++++AB 11530
C                                                                           AB 11540
484   WRITE(7,140)                                                          AB 11550
140   FORMAT(1H ,2X,'-------------------------------------------------------AB 11560
     *-------------------------'                                            AB 11570
     */1H1,9X,'COOLANT JET OUTLET VELOCITY AND JET VELOCITY TO MAINSTREAAB 11580
     *M VELOCITY RATIOS'                                                    AB 11590
     */,10X,'-----------------------------------------------------------AR 11600
     *---------------'                                                      AB 11610
     */,8X,'V0(1 TO 5)-M/S = COOLANT JET OUTLET VELOCITY-BASED ON WALL TAB 11620
     *HERMAL STATIONS'                                                      AB 11630
     */,8X,'V(1 TO 5)R = COOLANT JET OUTLET VELOCITY TO MAINSTREAM VELOCAB 11640
     *ITY RATIOS'                                                           AB 11650
     */,23X,'Vrt = VELOCITY RATIO AS ABOVE'                                AB 11660
     */,2X,'-------------------------------------------------------------AR 11670
     *-------------------------------'                                      AB 11680
     */,5X,'V01',5X,'V1R',5X,'V02',5X,'V2R',5X,'V03',5X,'V3R',5X,'V04',5AB 11690
     *X,'V4R',5X,'V05',5X,'V5R',6X,'Vrt')                                   AB 11700
      GOTO 127                                                              AB 11710
128   WRITE(7,129)                                                          AB 11720
129   FORMAT(1H ,2X,'-------------------------------------------------------AB 11730
     *-------------------------'                                            AB 11740
     */1H0,9X,'COOLANT JET OUTLET VELOCITY AND JET VELOCITY TO MAINSTREAAB 11750
     *M VELOCITY RATIOS'                                                    AB 11760
     */,10X,'-----------------------------------------------------------AB 11770
     *---------------'                                                      AB 11780
     */,21X,'-Based On Wall temperature Prediction'                         AB 11790
     */,22X,'-----------------------------------'                          AB 11800
     */,8X,'V0(1 TO 5)-M/S = COOLANT JET OUTLET VELOCITY-BASED ON WALL TAB 11810
     *HERMAL STATIONS'                                                      AB 11820
     */,8X,'V(1 TO 5)R = COOLANT JET OUTLET VELOCITY TO MAINSTREAM VELOCAB 11830
     *ITY RATIOS'                                                           AB 11840
     */,23X,'Vrt = VELOCITY RATIO AS ABOVE'                                AB 11850
     */,2X,'-------------------------------------------------------------AB 11860
     *-------------------------------'                                      AR 11870
     */,5X,'V01',5X,'V1R',5X,'V02',5X,'V2R',5X,'V03',5X,'V3R',5X,'V04',5AB 11880
     *X,'V4R',5X,'V05',5X,'V5R',6X,'Vrt')                                   AB 11890
127   DO 45,I=1,L                                                           AB 11900
      IF(ABR1.EQ.1.0.AND.C(I).EQ.0.0) GOTO 123                              AR 11910
      IF(C(I).EQ.0.0) GOTO 196                                              AR 11920
      DD01(I)=P2(I)/(T01(I)*R)                                              AB 11930
      DD02(I)=P2(I)/(T02(I)*R)                                              AB 11940
      DD03(I)=P2(I)/(T03(I)*R)                                              AB 11950
      DD04(I)=P2(I)/(T04(I)*R)                                              AR 11960
      DD05(I)=P2(I)/(T05(I)*R)                                              AR 11970
      DOM(I)=(DD01(I)+DD02(I)+DD03(I)+DD04(I)+DD05(I))/5.0                  AB 11980
      DD11(I)=DD01(I)/DPT(I)                                                AR 11990
      DD12(I)=DD02(I)/DPT(I)                                                AB 12000
      DD13(I)=DD03(I)/DPT(I)                                                AB 12010
      DD14(I)=DD04(I)/DPT(I)                                                AB 12020
      DD15(I)=DD05(I)/DPT(I)                                                AR 12030
      VV01(I)=C(I)/(DD01(I)*Z)                                              AR 12040
      VV02(I)=C(I)/(DD02(I)*Z)                                              AB 12050
      VV03(I)=C(I)/(DD03(I)*Z)                                              AR 12060
      VV04(I)=C(I)/(DD04(I)*Z)                                              AR 12070
      VV05(I)=C(I)/(DD05(I)*Z)                                              AB 12080
      VOM(I)=(VV01(I)+VV02(I)+VV03(I)+VV04(I)+VV05(I))/5.0                  AB 12090
      BMO(I)=VOM(I)*DOM(I)/BLMT(I)                                          AB 12100
```

```
FILE: AB       FORTRAN  A   LEEDS UNIVERSITY VM/SP RELEASE 3

      D3(I)=P2(I)/(T(1(I)*R)                                                    AB 12110
      V1(I)=C(I)/(D3(I)*Z)                                                      AB 12120
      VRT(I)=V1(I)/VMS(I)                                                       AB 12130
      VV11(I)=VVU1(I)/VMS(I)                                                    AB 12140
      VV12(I)=VVU2(I)/VMS(I)                                                    AB 12150
      VV13(I)=VVU3(I)/VMS(I)                                                    AB 12160
      VV14(I)=VVU4(I)/VMS(I)                                                    AB 12170
      VV15(I)=VVU5(I)/VMS(I)                                                    AB 12180
      YYP1(I)=6.3*D*(VVO1(I)/VMS(I))*SQRT(TG(I)/TO1(I))*1000.0                  AB 12190
      YYP2(I)=6.3*D*(VVO2(I)/VMS(I))*SQRT(TG(I)/TO2(I))*1000.0                  AB 12200
      YYP4(I)=6.3*D*(VVO4(I)/VMS(I))*SQRT(TG(I)/TO4(I))*1000.0                  AB 12210
      YYP5(I)=6.3*D*(VVO5(I)/VMS(I))*SQRT(TG(I)/TO5(I))*1000.0                  AB 12220
      A1AZ=25.4E-3                                                              AB 12230
      A2AZ=50.8E-3                                                              AB 12240
      A3AZ=76.2E-3                                                              AB 12250
      A4AZ=101.6E-3                                                             AB 12260
      A5AZ=127E-3                                                               AB 12270
      Y1Z(I)=456.65*PTH**(0.4598)*(D*DD11(I))**(0.5402)*VV11(I)*W1.0804 AB 12280
      Y2Z(I)=456.65*PTH**(0.4598)*(D*DD12(I))**(0.5402)*VV12(I)**1.0804 AB 12290
      Y3Z(I)=456.65*PTH**(0.4598)*(D*DD13(I))**(0.5402)*VV13(I)**1.0804 AB 12300
      Y4Z(I)=456.65*PTH**(0.4598)*(D*DD14(I))**(0.5402)*VV14(I)**1.0804 AB 12310
      Y5Z(I)=456.65*PTH**(0.4598)*(D*DD15(I))**(0.5402)*VV15(I)**1.0804 AB 12320
      IF(TPG(I).LT.350.0) GOTO 5757                                             AB 12330
      DR2(I)=D3(I)/DPT(I)                                                       AB 12340
5757  YYP3(I)=456.65*PTH**(0.4598)*(D*DR2(I))**(0.5402)*VV13(I)**1.0804 AB 12350
      WRITE(7,141)VVO1(I),VV11(I),VVO2(I),VV12(I),VVO3(I),VV13(I),              AB 12360
     *VVO4(I),VV14(I),VVO5(I),VV15(I),VRT(I)                                    AB 12370
141   FORMAT(1H ,5(2X,F6.2,2X,F6.3),3X,F6.2)                                    AB 12380
45    CONTINUE                                                                  AB 12390
196    WRITE(7,142)                                                             AB 12400
142   FORMAT(1H ,2X,'-------------------------------------------------------AB 12410
     *-----------------------------------'                                      AB 12420
     */1H0,14X,'JET OUTLET DENSITY TO FLAME DENSITY RATIOS'                     AB 12430
     */,15X,'-----------------------------------------'                        AB 12440
     */,2X,'D1OF(1 TO 5) = RATIOS OF OUTLET COOLANT JET DESITY TO THAT OAR 12450
     *F MAINSTREAM-BASED'                                                       AR 12460
     */,8X,'ON WALL THERMAL STATIONS ;nDr = NORMINAL DENSITY RATIO, BLo=AB 12470
     *OUTLET BLOWING RATE'                                                      AB 12480
     */,2X,'-------------------------------------------------------------AR 12490
     *--------------------'                                                     AB 12500
     */,7X,'D1of',6X,'D2of',6X,'D3of',6X,'D4of',6X,'D5of',6X,'nDr',5X,  AR 12510
     *'BLo')                                                                    AB 12520
      GOTO 125                                                                  AB 12530
123   WRITE(7,124)                                                              AB 12540
124   FORMAT(1H ,2X,'-------------------------------------------------------AR 12550
     *-----------------------------------'                                      AB 12560
     */1H0,4X,'JET OUTLET DENSITY TO FLAME DENSITY RATIOS-Based On Wall AB 12570
     *Temp. Prediction'                                                         AB 12580
     */,3X,'-------------------------------------------------------------AR 12590
     *--------------------'                                                     AB 12600
     */,2X,'D1OF(1 TO 5) = RATIOS OF OUTLET COOLANT JET DESITY TO THAT OAR 12610
     *F MAINSTREAM-BASED'                                                       AB 12620
     */,6X,'ON WALL THERMAL STATIONS ;nDr = NORMINAL DENSITY RATIO,BLo= AB 12630
     *OUTLET BLOWING RATE'                                                      AB 12640
     */,2X,'-------------------------------------------------------------AB 12650
      *--------------------'                                                    AB 12660
      */,7X,'D1of',6X,'D2of',6X,'D3of',6X,'D4of',6X,'D5of',6X,'nDr',5X,  AB 12670
      *'BLo')                                                                   AB 12680
C                                                                               AB 12690
C  ::::::::::::::::::::::::::::::::::::::::::::::::::::::::::::::::::::::: AB 12700
C  :     JET  DENSITY RATIO BLOCK BASED ON JET OUTLET TEMPERATURE     : AB 12710
C  ::::::::::::::::::::::::::::::::::::::::::::::::::::::::::::::::::::::: AB 12720
C                                                                               AB 12730
125   DO 44,I=1,L                                                               AB 12740
      IF(ABR1.LG.1.0.AND.C(I).EQ.0.0) GOTO 120                                  AB 12750
      IF(C(I).EQ.0.0) GOTO 159                                                  AB 12760
      WRITE(7,48)DD11(I),DD12(I),DD13(I),DD14(I),DD15(I),DR2(I),BMO(I)  AB 12770
48    FORMAT(1H ,6(5X,F5.2),3X,F6.3)                                            AB 12780
44    CONTINUE                                                                  AB 12790
159   WRITE(7,53)                                                               AB 12800
53    FORMAT(1H ,2X,'-------------------------------------------------------AR 12810
     *--------------------------'                                               AB 12820
     */1H0,6X,'COOLANT JETS OUTLET TO MAINSTREAM TEMPERATURE RATIOS AND AB 12830
     *JET PENETRATIONS'                                                         AR 12840
     */,7X,'-------------------------------------------------------------AB 12850
     *-------------'                                                           AB 12860
     */,2X,'T(1 TO 5)R = COOLANT JET OUTLET TO MAINSTREAM TEMPERATURE RAAR 12870
     *TIOS;'                                                                    AB 12880
     */,2X,'Y(1 TO 5)P = MAINSTREAM PENETRATION BY JET-mm;-BASED ON WALLAR 12890
     * THERMAL STATIONS'                                                        AB 12900
     -/,20X,'nYp=Nominal Jet Penetration-mm'                                    AB 12910
     */,2X,'-------------------------------------------------------------AB 12920
     *-----------------'                                                        AB 12930
     */,4X,'T1r',6X,'Y1p',4X,'T2r',5X,'Y2p',4X,'T3r',5X,'Y3p',4X,'T4r',5AR 12940
     *X,'Y4p',4X,'T5r',5X,'Y5p',3X,'nYp')                                       AR 12950
      GOTO 122                                                                  AR 12960
120    WRITE(7,126)                                                           AB 12970
126   FORMAT(1H ,2X,'-------------------------------------------------------AB 12980
     *--------------------------'                                               AB 12990
     */1H1,6X,'COOLANT JETS OUTLET TO MAINSTREAM TEMPERATURE RATIOS AND AB 13000
     *JET PENETRATIONS'                                                         AB 13010
     */,7X,'-------------------------------------------------------------AB 13020
     *-------------'                                                           AB 13030
     */,20X,'-Based On Wall Temperature Prediction'                             AB 13040
     */,21X,'-----------------------------------'                               AB 13050
     */,2X,'T(1 TO 5)R = COOLANT JET OUTLET TO MAINSTREAM TEMPERATURE RAAR 13060
     *TIOS;'                                                                    AB 13070
     */,2X,'Y(1 TO 5)P = MAINSTREAM PENETRATION BY JET-mm;-BASED ON WALLAR 13080
     * THERMAL STATIONS'                                                        AB 13090
     -/,20X,'nYp=Norminal Jet Penetration-mm'                                   AB 13100
     */,2X,'-------------------------------------------------------------AB 13110
     *-----------------'                                                        AB 13120
     */,4X,'T1r',6X,'Y1p',4X,'T2r',5X,'Y2p',4X,'T3r',5X,'Y3p',4X,'T4r',5AB 13130
     *X,'Y4p',4X,'T5r',5X,'Y5p',3X,'nYp')                                       AB 13140
C                                                                               AB 13150
C  ********************************************************************** AB 13160
C  *  JET OUTLET TO MAINSTREAM TEMPERATURE RATIOS & JET PENETRATION   * AB 13170
C  ********************************************************************** AB 13180
C                                                                               AB 13190
122   DO 155,I=1,L                                                              AB 13200
```

```
      IF(ABR1.EQ.1.0.AND.C(I).EQ.0.0) GOTO 414                          AB 13710
      IF(C(I).EQ.0.0) GOTO 56                                           AB 13720
      TT1R(I)=T01(I)/TG(I)                                              AB 13730
      TT2R(I)=T02(I)/TG(I)                                              AB 13740
      TT3R(I)=T03(I)/TG(I)                                              AB 13750
      TT4R(I)=T04(I)/TG(I)                                              AB 13760
      TT5R(I)=T05(I)/TG(I)                                              AB 13770
      WRITE(7,54)TT1R(I),Y1Z(I),TT2R(I),Y2Z(I),T13R(I),Y3Z(I),TT4R(I),  AB 13780
     *Y4Z(I),TT5R(I),Y5Z(I),YYP3(I)                                     AB 13790
   54 FORMAT(1H ,5(3X,F5.3,2X,F5.1),2X,F5.1)                            AB 13800
  155 CONTINUE                                                          AB 13810
   56 WRITE(7,279)                                                      AB 13820
  279 FORMAT(1H ,2X,'-------------------------------------------------------AB 13830
     *-------------------------'                                        AB 13840
     */1H1,5X,'PREDICTED TEMPERATURE AND COOLING EFFECTIVENESS FOR CYLINAB 13850
     -DRICAL COMBUSTOR'                                                 AB 13860
     */,6X,'-------------------------------------------------------------AB 13870
     -------------'                                                     AB 13880
     */,2X,'T(1 TO 5)p-K = PREDICTED TEST WALL TEMPERATURE -BASED ON WALAB 13890
     *L THERMAL STATIONS.'                                              AB 13900
     */,2X,'E = CORRESPONDING WALL COOLING EFFECTIVENESS; G!=COOLANT MASAB 13910
     *S FLOW(Kg/(s.m2.bar))'                                            AB 13920
     */,2X,'-------------------------------------------------------------AB 13930
     *-------------------------------------------'                      AB 13940
     *                    /,16X,'25.4mm',9X,'50.8mm',11X,'76.2mm',9X, '101.AB 13950
     *6mm',10X,'127mm'/,4X,'G!',7X,'T1p-K',4X,'E',6X,'T2p-K',4X,'E',6X, AB 13960
     *'T3p-K',5X,'E',5X,'T4p-K',5X,'E',5X,'T5p-K',4X,'E')               AB 13970
      DO 2222,I=1,L                                                     AB 13980
      IF(C(I).EQ.0.0) GOTO 2222                                         AB 13990
      WRITE(7,275)G1(I),T1P(I),E1(I),T2P(I),E2(I),T3P(I),E3(I),T4P(I),  AB 14000
     *E4(I),T5P(I),E5(I)                                                AB 14010
  275 FORMAT(1H ,1X,F6.3,3X,F7.1,2X,F5.3,4(2X,F7.1,2X,F5.3))            AB 14020
 2222 CONTINUE                                                          AB 14030
 C/////////////////                                                     AB 14040
      IF(Ab.EQ.'(High_Temp._Work)') GOTO 9689                           AB 14050
      WRITE(7,7742)                                                     AB 14060
 7742 FORMAT(1H ,2X,'-------------------------------------------------------AB 14070
     *-------------------------'                                        AB 14080
     */1H0,12X,'CYLINDRICAL COMBUSTOR ADIABATIC COOLING EFFECTIVENESS.' AB 14090
     */,13X,'-------------------------------------------------------'   AB 14100
     */,2X,'TGc=COMBUSTOR MAINSTREAM TEMP.;G!=G/(PRESSURE) kg/(m2sec.barAB 14110
     *);Ta(l,c,t)=ADIABATIC'                                            AB 14120
     */,2X,'WALL TEMP. AT LEADING EDGE, CENTRAL, & TRAILING EDGE ; E=ADIAB 14130
     *ABATIC COOLING EFFECTIVENESS'                                     AB 14140
     */,1X,'-------------------------------------------------------------AB 14150
     *-------------------------------')                                 AB 14160
      WRITE(7,900)                                                      AB 14170
  900 FORMAT(1H ,4X,'TGc-K',5X,'G!',11X,'Tal-K',6X,'E',11X,'Tac-K',7X,'EAR 14180
     -',11X,'Tat-K',7X,'E')                                             AB 14190
  901 DO 9446,I=1,L                                                     AB 14200
      IF(C(I).EQ.0.0) GOTO 9446                                         AB 14210
      WRITE(7,9447)TG(I),G1(I),T1A(I),E7(I),T2A(I),E8(I),T3A(I),E9(I)   AB 14220
 9447 FORMAT(1H ,1X,F7.1,2X,F6.3,3(8X,F7.1,4X,F5.3))                    AB 14230
 9446 CONTINUE                                                          AB 14240
 9689 WRITE(7,23)                                                       AB 14250
   23 FORMAT(1H ,2X,'-------------------------------------------------------AB 14260
     *-------------------------'                                        AB 14270
      IF(ABR1.EQ.1.0) GOTO 414                                          AB 14280
      ABR1=1.0                                                          AB 14290
      DO 525,I=1,L                                                      AB 14300
      TC1(I)=TPLE(I)                                                    AB 14310
      TPH1(I)=T1P(I)                                                    AB 14320
      TPH2(I)=T2P(I)                                                    AB 14330
      TPH3(I)=T3P(I)                                                    AB 14340
      TPH4(I)=T4P(I)                                                    AB 14350
      TPH5(I)=T5P(I)                                                    AB 14360
  525 CONTINUE                                                          AB 14370
      GO TO 582                                                         AB 14380
  414 WRITE(7,32)                                                       AB 14390
   32 FORMAT(1H ,2X,'-------------------------------------------------------AB 14400
     *-------------------------'                                        AB 14410
     */1H0,19X,'FLUX-METER HEAT TRANSFER'/,20X,'----------------------'AB 14420
     *'                    /,2X,'Tg=COMBUSTOR GAS TEMP.;T-(in,ot,pl)=COOLANAB 14430
     *T INLET,OUTLET &PLATE TEMP.'/,2X,'Cpf=SP. HEAT CAPACITY(J/KgK); FMAB 14440
     *M=COOL. MASS FLOWRATE(Kg/sec.)'/,2X,'Hav=AVERAGE CONV. HEAT TRANSFAB 14450
     *ER COEFF.(W/m2K); Q=HEAT TRANSFER-(W)'/,2X,'---------------------AB 14460
     *-------------------------------------------------'/,5X,'Tg-K',3X,'TiAB 14470
C                                                                       AB 14480
C                :-+-+-+-+-+-+-+-+-+-+-+-+-+-+-+-+-+-+-+-+-+-+-+-:     AB 14490
C                 :  FLUX-METER     HEAT        TRANSFER    :          AB 14500
C                  :                SEGMENT                 :          AB 14510
C                   :-+-+-+-+-+-+-+-+-+-+-+-+-+-+-+-+-+-+-+-+-+-+-+-:  AB 14520
C   FLUX-METER COOLANT VOLUME FLOWRATE-FMF-LT/MIN (CON. TO M2/SEC. IN   AB 14530
C   PROG. BODY); COOLANT DENSITY-DF-; FLUX-METER COOL. MASS FLOWRATE-    AB 14540
C  -FMM-; 1-(9,10,11)-ARE TEMPS. FLUX-METER COOL. INLET,OUTLET & PLATE; AB 14550
C   FILM TEMP. FOR EVALUATING COOLANT SP.HEAT-(CPF)- IS-TMV-;FLUX-METER AB 14560
C   PLATE FACE AREA-AF-;FLUX-METER HEAT TRANSFER/M2 & AVRAGE CONVECTIVE AB 14570
C   HEAT TRANSFER COEFFICIENT ARE -QFM- & -HAV-                         AB 14580
      TC(I)=T1L(I)                                                      AB 14590
      DO 70,I=1,L                                                       AB 14600
      IF(C(I).EQ.0.0) GOTO 70                                           AB 14610
      P8(I)=P*(P8(I)+AP3(I))                                            AB 14620
      FMF(I)=FNF(I)*1E-03*SQRT((CP*TC(I))/(C1*P8(I)))/60.0              AB 14630
      DF(I)=P8(I)/(TC(I)*R)                                             AB 14640
      FMM(I)=DF(I)*FMF(I)                                               AB 14650
      T9(I)=T9(I)+T                                                     AB 14660
      T10(I)=T10(I)+T                                                   AB 14670
      T11(I)=T11(I)+T                                                   AB 14680
      TMV(I)=(T9(I)+T10(I))/2.0                                         AB 14690
      CPF(I)=1063.3-5.7194E-14*TMV(I)**5+4.2538E-10*TMV(I)**4-1.1417E-06AB 14700
     **TMV(I)**3+1.3637E-03*TMV(I)**2-0.5117*TMV(I)                     AB 14710
      QFM(I)=FMM(I)*CPF(I)*(T10(I)-T9(I))                               AB 14720
      HAV(I)=QFM(I)/(AF*(TG(I)-T11(I)))                                 AB 14730
      H1V(I)=H1F(I)/HAV(I)                                              AB 14740
      H2V(I)=H2F(I)/HAV(I)                                              AB 14750
      H3V(I)=H3F(I)/HAV(I)                                              AB 14760
      H4V(I)=H4F(I)/HAV(I)                                              AB 14770
      H5V(I)=H5F(I)/HAV(I)                                              AB 14780
      HVM(I)=HMF(I)/HAV(I)                                              AB 14790
      WRITE(7,24)TG(I),T9(I),T10(I),T11(I),CPF(I),FMM(I),HAV(I),QFM(I)  AB 14800
   24 FORMAT(1H ,4(2X,F6.1),2X,E9.3,2X,E9.3,2X,F6.1,2X,F7.2)            AB 14810
   70 CONTINUE                                                          AB 14820
      WRITE(7,25)                                                       AB 14830
      ABR1=0.0                                                          AB 14840
      GO TO 1000                                                        AB 14850
  444 PRINT *,'THE VALUE OF RNU IS 0.0 .HENCE PROGRAM IS TERMINATING, BYAB 14860
     *E, BYE'                                                           AB 14870
 7777 STOP                                                              AB 14880
   12 FORMAT(1H ,1X,'-------------------------------------------------------AB 14890
     *-------------------------'                                        AB 14900
     *                  /1H ,2X,'TPH(1 to 5)-K=TEST PLATE FLAMESIDE TEMPAB 14910
     *. AT INCREASING DISTANCE FROM LEAD.'     /,2X,'EDGE, E=COOLING EFFAB 14920
     *ECTIVENESS AT INCREASING DIST. FROM PLATE LEADING EDGE'           AB 14930
     */,1X,'-------------------------------------------------------------AB 14940
     *-------------------------'                                        AB 14950
     *                    /,16X,'25.4mm',9X,'50.8mm',11X,'76.2mm',9X, '101.AB 14960
     *6mm',10X,'127mm'/,2X,'TC-K',8X,   'TPH1',4X,'E',6X,'TPH2',4X,'E',7AB 14970
     *X,'TPH3',4X,'E',7X,'TPH4',4X,'E',7X,'TPH5',4X,'E')                AB 14980
   25 FORMAT(1H ,'$$$$$$$$$$$$$$$$$$$$$$$$$$$$$$$$$$$$$$$$$$$$$$$$$$$$AB 14990
     **********')                                                       AB 15000
      END                                                               AB 15010
                                                                        AB 15020
```

UNIVERSITY OF LEEDS
DEPARTMENT OF FUEL AND ENERGY
Gas Turbine Combustor Wall Cooling Programme

TABLE 5.A1

EFFUSION PLATE TEST -(Low_Temp._Work)

NO. OF PLT. HOLES:225.0 HOLES MEAN DIAMETER:0.9996065mm DCM=1
HOLE PITCH: 10.1592770mm PLATE (P/D: 5.00005 PLATE THK.: 3.321mm
HOLES LAYOUT FORMAT: in-line PLATE-MATERIAL: Nimonic-75
EXP. DATE:28/ 2/85 ATMOS. PRESS.: 762.70mmHg AT TEMP.: 19.5 Deg. C

FC=COOLANT FLOWRATE AS MEASURED AT ROTAMETER-l/min
TC-r=COOLANT TEMP. AT ROTAMETER, TG-K=MAINSTREAM FLOW TEMP. AT TEST PLANE
CH-Kg/s=COOLANT MASS FLOWRATE, G-Kg/(sm2)=G. MASS FLOW/TEST PLATE AREA
G!-Kg/(m2sBar)=COOLANT MASS FLOW. /Meter Sq./Sec./Bar
V & Vm-m/s=VEL. COOL. & MAINST.THRO. HOLES & COMBUSTOR;BLR=BLOWING RATE RATIO
DR=DENSITY RATIO(D1/D2); PPD-Pa=PLENUM STATIC GAUGE PRESSURE
nDr=NOMINAL DENSITY RATIO;
RE-1&2=REYNOLDS NUMBER FOR COOLANT THRO. PLATE & MAINSTREAM AT TEST PLANE
H 1&2=MACH NUMBERS OF BOTH COOLANT & MAINSTREAM AS FOR RE ABOVE
SPr & Vrt =(SPress Loss Across Plate/Upstream (plenum) Absolute Press.) & V/Vm

FC-l/min.	PPD-Pa	TC-r	TG-K	CH-Kg/s	G	G!	V-m/s	Vm-m/s
7 .0	6225.5	292.9	1003.9	0.01643	0.707	0.695	73.92	37.34
409.0	1951.0	294.2	1003.0	0.00950	0.366	0.360	40.73	37.21
300.0	1156.9	294.0	998.8	0.00624	0.269	0.264	30.48	37.07
200.0	588.2	293.6	999.7	0.00411	0.177	0.174	20.53	37.12
100.0	264.7	293.6	999.3	0.00204	0.088	0.086	11.24	37.10
0.0	1.0	293.4	998.9	0.00000	0.000	0.000	0.00	37.10

DR	nDr	BLR	RE	H	RE1	H1	SPr	Vrt
4.27	3.19	6.57	0.501E+04	0.21E+00	0.34E+05	0.61E-01	5.7592	1.9795
3.50	3.18	3.41	0.261E+04	0.12E+00	0.34E+05	0.61E-01	1.8724	1.0948
3.35	3.17	2.51	0.191E+04	0.87E-01	0.34E+05	0.61E-01	1.1150	0.8221
3.27	3.17	1.65	0.128E+04	0.59E-01	0.34E+05	0.61E-01	0.5654	0.5530
3.21	3.17	0.92	0.561E+03	0.30E-01	0.34E+05	0.61E-01	0.2479	0.3030
3.19	3.18	0.00	0.00E+00	0.00E+00	0.34E+05	0.61E-01	0.0000	0.0000

TPH(1 to 5)-K=TEST PLATE FLAMESIDE TEMP. AT INCREASING DISTANCE FROM LEAD.
EDGE, E=COOLING EFFECTIVENESS AT INCREASING DIST. FROM PLATE LEADING EDGE

	25.4mm		50.8mm		76.2mm		101.6mm		127mm	
TC-K	TPH1	E	TPH2	E	TPH3	E	TPH4	E	TPH5	E
292.9	591.2	0.589	592.2	0.579	576.2	0.602	556.2	0.630	545.2	0.645
294.2	621.2	0.539	619.2	0.542	608.2	0.557	592.2	0.580	589.2	0.584
294.0	634.2	0.517	630.2	0.523	619.2	0.539	605.2	0.558	603.2	0.561
293.6	652.2	0.492	644.2	0.501	638.2	0.512	626.2	0.529	624.2	0.532
293.6	689.2	0.440	684.2	0.447	677.2	0.457	666.2	0.472	665.2	0.474
293.4	740.2	0.367	745.2	0.360	745.2	0.360	734.2	0.372	735.2	0.374

ADIABATIC COOLING EFFECTIVENESS.

TGc=COMBUSTOR MAINSTREAM TEMP.;G!=G/(PRESSURE)-Kg/(m2sec.bar);Ta(l,c,t)=ADIABATIC WALL TEMP. AT LEADING EDGE, CENTRAL, & TRAILING EDGE ;Ea=ADIABATIC COOLING EFFECTIVENESS For High Temp. Work Tac-central thermocounle- Only Feature

Tgc-K	G!	Tal-K	E	Tac-K	E	Tat-K	E
1003.9	0.695	824.2	0.253	757.2	0.347	721.2	0.398
1003.0	0.360	764.2	0.337	773.2	0.324	695.2	0.434
998.8	0.264	761.2	0.337	783.2	0.306	733.2	0.377
999.7	0.174	853.2	0.236	819.2	0.256	796.2	0.288
999.3	0.086	847.2	0.216	844.2	0.220	841.2	0.224
998.9	0.000	833.2	0.164	866.2	0.188	869.2	0.184

PREDICTED TEMPERATURE AND COOLING EFFECTIVENESS FOR CYLINDRICAL COMBUSTOR

T(1 TO 5)p-K = PREDICTED TEST WALL TEMPERATURE -BASED ON WALL THERMAL STATIONS.
E = CORRESPONDING WALL COOLING EFFECTIVENESS; G!=COOLANT MASS FLOW(Kg/(s.m2.bar))

	25.4mm		50.8mm		76.2mm		101.6mm		127mm	
G!	T1p-K	E	T2p-K	E	T3p-K	E	T4p-K	E	T5p-K	E
0.695	591.8	0.589	593.0	0.578	573.0	0.604	547.1	0.642	532.5	0.663
0.360	629.3	0.527	626.7	0.531	612.3	0.551	590.6	0.582	586.4	0.588
0.264	647.4	0.499	642.1	0.506	627.5	0.527	608.1	0.554	605.3	0.558
0.174	673.8	0.462	665.9	0.473	655.1	0.488	638.3	0.512	635.4	0.516
0.066	731.5	0.380	725.2	0.388	716.2	0.401	701.6	0.422	700.3	0.424

CYLINDRICAL COMBUSTOR ADIABATIC COOLING EFFECTIVENESS.

TGc=COMBUSTOR MAINSTREAM TEMP.;G!=G/(PRESSURE)-Kg/(m2sec.bar);Ta(l,c,t)=ADIABATIC WALL TEMP. AT LEADING EDGE, CENTRAL, & TRAILING EDGE ; E=ADIABATIC COOLING EFFECTIVENESS

Tgc-K	G!	Tal-K	E	Tac-K	E	Tat-K	E
1003.9	0.695	825.2	0.251	751.9	0.354	699.6	0.428
1003.0	0.360	775.8	0.321	779.4	0.315	691.4	0.440
998.8	0.264	779.3	0.311	795.6	0.288	736.2	0.373
999.7	0.174	865.3	0.190	844.9	0.219	813.3	0.264
999.3	0.086	906.4	0.132	900.3	0.140	892.9	0.151

CONVECTIVE HEAT TRANSFER AT THE BACK OF TEST WALL-Based On Predicted Wall Temp.

W(1-5)B-WATT =CONVECTIVE HEAT TRANSFER - BASED ON WALL THERMOCOUPLE STATIONS, WHILE QB IS THE MEAN AT THE BACK OF TEST WALL; QHCR-W/M*2.K = CONVECTIVE HEAT TRANSFER COEFFICIENT; BN=NUSSELT NUMBER

W1B	W2B	W3B	W4B	W5B	QHCB	QB	BN
790.2	793.6	738.6	647.7	627.4	119.1	723.5	4.48
637.6	634.3	604.6	560.1	551.5	89.2	598.0	3.22
577.0	567.5	541.1	506.2	501.1	78.3	538.4	2.76
499.5	487.3	470.8	445.2	440.9	66.2	468.7	2.22
379.7	363.0	352.1	334.3	332.6	53.0	350.5	1.49

PREDICTED COOLANT'S HOLES INLET TEMPERATURE -Based On Predicted Wall Temp.

T(1-5)n-K =COOLANT'S HOLES INLET TEMPERATURE -- BASED ON WALL'S THERMAL STATIONS =Tin-K = MEAN INLET COOLANT'S TEMPERATURE and pTp-K = PLENUM TEMPERATURE

T1n-K	T2n-K	T3n-K	T4n-K	T5n-K	=Tin-K	pTp-K
351.8	352.0	343.7	344.4	341.9	347.8	303.9
393.1	392.5	389.0	383.8	382.8	383.3	318.3
419.5	416.0	413.8	408.2	407.4	413.4	327.7
467.0	464.1	460.1	453.9	452.9	459.6	346.5
606.6	602.7	597.7	589.1	588.3	596.9	427.9

HOLES CONVECTIVE HEAT TRANSFER TO COOLANT-Based On Predicted Wall Temp.

Hhc-W/M*2.K = CONVECTIVE HEAT TRANSFER COEFFICIENT; W(1-5)H-WATT = CONVECTION IN THE HOLES BASED ON WALL THERMOCOUPLE STATIONS ON WALL'S THERMOCOUPLE STATIONS; WH-W =MEAN HOLE CONVECTION; HNUS.#= HOLE'S NUSSELT NO. BASED ON WALL'S THICKNESS, QB/WH=BACK TO HOLE CONV. COEFF.

Hhc	W1h	W2h	W3h	W4h	W5h	Wh	HNUS.#	QB/WH
1016.30	572.25	574.71	534.87	483.49	454.37	523.94	112.96	1.381
611.51	338.85	336.03	320.30	296.69	292.15	316.80	61.86	1.848
484.21	258.95	254.71	242.82	227.17	224.88	241.70	46.48	2.223
355.96	172.78	163.58	162.87	154.02	152.51	162.15	31.31	2.891
221.41	64.86	63.53	61.61	58.49	58.20	61.34	15.84	5.715

TABLE 5.A2

```
CONVECTIVE HEAT TRANSFER FROM COMBUSTION GAS TO TEST WALL -Based On Predicted Wall Temperature.
-----------------------------------------------------------------------------------------------
.5)ct & Qct-WATT=CONVECTION FROM GAS STREAM TO TEST WALL --BASED ON WALL THERMOCOUPLE STATIONS - Uct IS MEAN:
.5)g & HMg-W/M*2.K =ARE BOTH CONVECTIVE HEAT TRANSFER COEFFICIENT -BASED ON WALL THERMOCOUPLES- & HMg IS MEAN.
.=NUSSELT NO. BASED ON TEST WALL LENGTH
--------------------------------------------------------------------------------------------------------------------
H1g     Q1ct     H2g     Q2ct     H3g     Q3ct     H4g     Q4ct     H5g     Q5ct     HMg     Uct     Nu.l
140.1   1341.3   141.2   1347.2   125.1   1251.7   106.4   1128.6   96.7    1058.9   121.9   1275.5  621.7
110.5   958.9    108.8   950.7    99.7    994.8    87.3    835.9    85.0    822.7    98.2    894.6   456.1
100.1   817.4    97.0    803.5    88.6    764.6    78.6    713.4    77.2    705.9    88.3    760.9   389.0
86.5    654.0    82.3    638.0    76.9    615.3    69.1    580.3    67.9    574.3    76.5    612.5   308.9
67.6    420.3    64.6    411.1    60.5    397.8    54.4    376.3    53.9    374.3    60.2    396.0   197.6
--------------------------------------------------------------------------------------------------------------------

EDICTED COOLANT"S HOLES OUTLET TEMPERATURE AND FLOW DISTRIBUTION-Based On Predicted Wall Temp.
---------------------------------------------------------------------------------------------
1 TO 5)o=OUTLET TEMPERATURE BASED ON HEAT TRANSFER FROM THERMAL LOCATIONS 1 TO 5 OF TEST WALL,
 = MEAN OUTLET TEMPERATURE: T(1 to 5)r = OUTLET TO PLENUMCOOLANT TEMP. RATIO & Trm IS THE MEAN
To/Tp = Ratio Of Outlet To Plenum Temperature
------------------------------------------------------------------------------------------------------------------
1o-K    T2o-K   T3o-K   T4o-K   T5o-K   mTo-K   T1r     T2r     T3r     T4r     T5r     Trm     To/Tp
86.3    386.7   381.0   373.6   367.4   379.4   0.701   0.701   0.700   0.699   0.698   0.700   1.248
32.5    431.5   426.3   418.3   416.8   425.1   0.608   0.608   0.607   0.604   0.604   0.606   1.335
60.3    458.1   452.0   444.0   442.9   451.5   0.553   0.552   0.551   0.548   0.548   0.550   1.378
508.0   504.1   498.8   490.6   489.2   498.1   0.461   0.460   0.458   0.456   0.455   0.458   1.438
530.9   632.6   626.4   616.4   615.5   625.6   0.245   0.244   0.243   0.240   0.239   0.242   1.462
------------------------------------------------------------------------- ----------------------------------------

DIATIVE HEAT TRANSFER FROM FLAME -Based On Predicted Wall Temperature
---------------------------------------------------------------------
1 TO 5)F-WATTS = RADIATIVE HEAT TRANSFER FROM FLAME TO WALL-BASED ON WALL
ERMAL STATIONS ; Rmf-WATT = MEAN FLAME RADIATION
----------------------------------------------------------------------------
   R1F      R2F      R3F      R4F      R5F      Rmf      %Rf/Qc
  21.19    21.15    21.77    22.51    22.90    21.91     1.63
  19.56    19.65    20.14    20.85    20.98    20.24     1.99
  18.59    18.78    19.31    19.96    20.06    19.34     2.17
  17.64    17.95    18.36    13.97    19.08    18.40     2.43
  15.20    15.43    15.86    16.48    16.54    15.91     2.66
----------------------------------------------------------------------------

     COOLANT JET OUTLET VELOCITY AND JET VELOCITY TO MAINSTREAM VELOCITY RATIOS
     --------------------------------------------------------------------------
                  -Based On Wall temperature Prediction
                  -------------------------------------
    VO(1 TO 5)-M/S = COOLANT JET OUTLET VELOCITY-BASED ON WALL THERMAL STATIONS
    V(1 TO 5)R = COOLANT JET OUTLET VELOCITY TO MAINSTREAM VELOCITY RATIOS
                 Vrt = VELOCITY RATIO AS ABOVE
----------------------------------------------------------------------------------------
VO1     V1R     VO2     V2R     VO3     V3R     VO4     V4R     VO5     V5R     Vrt
95.59   2.560   95.67   2.562   94.76   2.524   92.43   2.475   91.39   2.447   2.01
57.64   1.549   57.52   1.546   56.81   1.527   55.76   1.499   55.55   1.493   1.14
45.42   1.225   45.70   1.219   44.61   1.203   43.82   1.182   43.70   1.179   0.87
33.19   0.894   32.94   0.887   32.59   0.878   32.05   0.864   31.96   0.861   0.61
20.68   0.558   20.55   0.554   20.35   0.548   20.02   0.540   19.99   0.539   0.37
----------------------------------------------------------------------------------------
          COOLANT JETS OUTLET TO MAINSTREAM TEMPERATURE RATIOS AND JET PENETRATIONS
          -------------------------------------------------------------------------
                       -Based On Wall Temperature Prediction
                       -------------------------------------
    T(1 TO 5)R = COOLANT JET OUTLET TO MAINSTREAM TEMPERATURE RATIOS:
    Y(1 TO 5)P = MAINSTREAM PENETRATION BY JET-mm;-BASED ON WALL THERMAL STATIONS
                      nYp=Norminal Jet Penetration-mm
    ------------------------------------------------------------------------------
     T1r     Y1p    T2r     Y2p    T3r     Y3p    T4r     Y4p    T5r     Y5p   nYp
     0.385   6.1    0.385   6.1    0.379   6.0    0.372   6.0    0.368   5.9   6.7
     0.431   3.3    0.430   3.3    0.425   3.2    0.417   3.2    0.416   3.2   3.9
     0.461   2.4    0.459   2.4    0.453   2.4    0.445   2.4    0.443   2.4   3.0
     0.508   1.6    0.504   1.6    0.499   1.6    0.491   1.6    0.489   1.6   2.1
     0.637   0.9    0.633   0.9    0.627   0.9    0.617   0.9    0.616   0.9   1.3
    ------------------------------------------------------------------------------

                   FLUX-METER HEAT TRANSFER
                   ------------------------
    Tg=COMBUSTOR GAS TEMP.;T-(in,ot,pl)=COOLANT INLET,OUTLET &PLATE TEMP.
    Cpf=SP. HEAT CAPACITY(J/KgK); FMM=COOL. MASS FLOWRATE(Kg/sec.)
    Hav=AVERAGE CONV. HEAT TRANSFER COEFF.(W/m2K); Q=HEAT TRANSFER-(W)
    ------------------------------------------------------------------
      Tg-K    Tin-K   Tot-K   Tpl-K   Cpf         FMM          Hav     Q
     1003.9   310.7   455.7   482.2   0.101E+04   0.235E-02    68.3    344.64
     1003.0   312.8   461.9   491.2   0.101E+04   0.213E-02    64.9    321.26
      998.8   313.8   465.3   495.2   0.101E+04   0.208E-02    65.5    319.32
      999.7   313.7   466.5   496.2   0.101E+04   0.206E-02    65.3    318.07
      999.3   315.9   474.2   504.2   0.101E+04   0.204E-02    68.2    326.78
$$$$$$$$$$$$$$$$*****************************@@@@@@@@@@@@@@&&&**********************
```

UNIVERSITY OF LEEDS
DEPARTMENT OF FUEL AND ENERGY
Gas Turbine Combustor Wall Cooling Programme

TABLE 5.B1

EFFUSION PLATE TEST -(High_Temp._Work)

NO. OF PLT. HOLES:225.0 HOLES MEAN DIAMETER:0.9996065mm LASER
HOLE PITCH: 10.1599970mm PLATE ()P/P: 3.0000% PLATE THK.: 3.321mm
HOLES LAYOUT FORMAT: in-line PLATE-MATERIAL: Nimonic-75
EXP. DATE: 7/ 3/85 ATMOS. PRESS.: 740.50mmHg AT TEMP.: 17.5 Deg. C

FC-COOLANT FLOWRATE AS MEASURED AT ROTAMETER-l/min
TC-K=COOLANT TEMP. AT ROTAMETER, TG-K=MAINSTREAM FLOW TEMP. AT TEST PLANE
CM-Kg/s=COOLANT MASS FLOWRATE, G-Kg/(sm2)=C. MASS FLOW/TEST PLATE AREA
G!-Kg/(m2sBar)=COOLANT MASS FLOW. /Meter Sq./Sec./Bar
V & Vm-m/s=VEL. COOL. & MAINST.THRO. HOLES & COMBUSTOR;BLR=BLOWING RATE RATIO
DR=DENSITY RATIO(D1/D2); PPD-Pa=PLENUM STATIC GAUGE PRESSURE
nDr=NOMINAL DENSITY RATIO;
RE-1&2=REYNOLDS NUMBER FOR COOLANT THRO. PLATE & MAINSTREAM AT TEST PLANE
H 1&2=MACH NUMBERS OF BOTH COOLANT & MAINSTREAM AS FOR RE ABOVE
%Pr & Vrt =(%Press Loss Across Plate/Upstream (plenum) Absolute Press.) & V/Vm

FC-l/min.	PPD-Pa	TC-K	TG-K	CM-Kg/s	G	G!	V-m/s	Vm-m/s
400.0	4862.7	294.4	1821.2	0.00888	0.382	0.387	94.01	79.65
300.0	3607.8	294.4	1821.3	0.00642	0.276	0.280	70.83	79.48
200.0	2352.9	294.6	1837.3	0.00411	0.177	0.179	46.78	78.66
0.0	2352.9	294.6	1837.3	0.00000	0.000	0.000	0.00	78.66

DR	nDr	BLR	RE	H	RE1	H1	%Pr	Vrt
3.04	2.46	3.04	0.15E+04	0.18E+00	0.52E+05	0.59E-01	4.5993	1.1804
2.83	2.46	2.20	0.11E+04	0.13E+00	0.51E+05	0.60E-01	3.4295	0.8911
2.63	2.48	1.43	0.68E+03	0.88E-01	0.50E+05	0.59E-01	2.2307	0.5947
2.48	2.48	0.00	0.00E+00	0.00E+00	0.50E+05	0.59E-01	2.2307	0.0000

TPH(1 to 5)-K=TEST PLATE FLAMESIDE TEMP. AT INCREASING DISTANCE FROM LEAD. EDGE, E=COOLING EFFECTIVENESS AT INCREASING DIST. FROM PLATE LEADING EDGE

	25.4mm		50.8mm		76.2mm		101.6mm		127mm	
TC-K	TPH1	E	TPH2	E	TPH3	E	TPH4	E	TPH5	E
674.2	1135.2	0.598	1149.2	0.586	1149.2	0.586	1120.2	0.611	1116.2	0.615
672.2	1151.2	0.583	1157.2	0.578	1155.2	0.580	1129.2	0.602	1134.2	0.598
672.2	1193.2	0.553	1195.2	0.551	1193.2	0.553	1171.2	0.572	1174.2	0.569
672.2	1193.2	0.553	1195.2	0.551	1193.2	0.553	1171.2	0.572	1174.2	0.569

ADIABATIC COOLING EFFECTIVENESS.

TGc=COMBUSTOR MAINSTREAM TEMP.;G!=G/(PRESSURE)-Kg/(m2sec.bar);Ta(l,c,t)=ADIABATIC WALL TEMP. AT LEADING EDGE, CENTRAL, & TRAILING EDGE ;Ea=ADIABATIC COOLING EFFECTIVENESS
For High Temp. Work Tac-central thermocouple- Only Feature

TGC-K	G!	Tac-K	E
1821.2	0.387	1523.2	0.260
1821.3	0.280	1530.2	0.253
1837.3	0.179	1610.2	0.195

PREDICTED TEMPERATURE AND COOLING EFFECTIVENESS FOR CYLINDRICAL COMBUSTOR

T(1 TO 5)p-K = PREDICTED TEST WALL TEMPERATURE -BASED ON WALL THERMAL STATIONS.
E = CORRESPONDING WALL COOLING EFFECTIVENESS; G!=COOLANT MASS FLOW(Kg/(s.m2.bar))

	25.4mm		50.8mm		76.2mm		101.6mm		127mm	
G!	T1p-K	E	T2p-K	E	T3p-K	E	T4p-K	E	T5p-K	E
0.387	1284.3	0.468	1304.0	0.451	1304.0	0.451	1262.0	0.488	1255.8	0.493
0.280	1324.4	0.432	1332.5	0.425	1329.8	0.428	1293.2	0.460	1300.6	0.453
0.179	1395.2	0.379	1397.6	0.377	1395.2	0.379	1367.5	0.403	1371.4	0.400

CONVECTIVE HEAT TRANSFER AT THE BACK OF TEST WALL-Based On Predicted Wall Temp.

Q(1-5)B-WATT =CONVECTIVE HEAT TRANSFER - BASED ON WAL_ THERMOCOUPLE STATIONS, WHILE QB IS THE MEAN AT THE BACK OF TEST WALL; QHCB-W/M*2.K = CONVECTIVE HEAT TRANSFER COEFFICIENT; BN=NUSSELT NUMBER

Q1B	Q2B	Q3B	Q4B	Q5B	QHCB	QB	BN
1548.7	1613.3	1613.3	1475.5	1455.2	142.4	1541.2	2.44
1335.9	1359.2	1351.5	1245.5	1266.8	125.7	1311.8	2.06
1123.4	1129.2	1123.4	1055.8	1065.4	105.8	1099.4	1.64

PREDICTED COOLANT"S HOLES INLET TEMPERATURE -Based On Predicted Wall Temp.

T(1-5)n-K =COOLANT"S HOLES INLET TEMPERATURE -- BASED ON WALL"S THERMAL STATIONS
mTin-K = MEAN INLET COOLANT"S TEMPERATURE and pTp-K = PLENUM TEMPERATURE

T1n-K	T2n-K	T3n-K	T4n-K	T5n-K	mTin-K	pTp-K
970.9	977.6	977.6	963.4	961.4	970.2	812.5
1050.5	1053.7	1052.6	1037.8	1040.8	1047.1	863.3
1177.0	1178.3	1177.0	1162.4	1164.5	1171.8	934.7

TABLE 5.B2

```
         HOLES CONVECTIVE HEAT TRANSFER TO COOLANT-Based On Predicted Wall Temp.
         -----------------------------------------------------------------------
        Hhc-W/M*2.K = CONVECTIVE HEAT TRANSFER COEFFICIENT: Q(1-5)H-WATT = CONVICTION IN THE
        HOLES BASED ON WALL THERMOCOUPLE STATIONS ON WALL"S THERMOCOUPLE STATIONS:
        QH-W =MEAN HOLE CONVECTION:  NUS.#= HOLE"S NUSSELT NO. BASED ON WALL"S THICKNESS,
                    QB/QH=BACK TO HOLE CONV. COEFF.
        ----------------------------------------------------------------------------------
           Hhc      Q1h       Q2h       Q3h       Q4h       Q5h       Qh       NUS.#    QB/QH
          822.59   604.80    630.05    630.05    576.21    568.29    601.88    41.29    2.561
          649.44   417.51    424.79    422.38    389.26    395.71    409.97    30.94    3.200
          471.43   241.39    242.65    241.39    226.86    228.92    236.24    20.84    4.654
         ---------------------------------------------------------------------------------

   CONVECTIVE HEAT TRANSFER FROM COMBUSTION GAS TO TEST WALL -Based On Predicted Wall Temperature.
   ----------------------------------------------------------------------------------------------
Q(1-5)ct & Qct-WATT=CONVECTION FROM GAS STREAM TO TEST WALL --BASED ON WALL THERMOCOUPLE STATIONS - Qct IS MEAN;
H(1-5)m $ HMg-W/M*2.K =ARE BOTH CONVECTIVE HEAT TRANSFER COEFFICIENT -BASED ON WALL THERMOCOUPLES- $ HMg IS MEAN.
Nu.l=NUSSELT NO. BASED ON TEST WALL LENGTH
-------------------------------------------------------------------------------------------------------------------
   H1g     Q1ct     H2g    Q2ct     H3g    Q3ct     H4g    Q4ct     H5g    Q5ct    HMg     Qct      Nu.
  162.9   2031.1   176.8  2123.8   176.8  2123.8   148.3  1926.3   144.5  1897.2   161.8  2020.4    37
  141.8   1636.6   147.0  1668.3   145.2  1657.8   123.4  1513.5   127.6  1542.5   137.0  1603.8    27
  121.9   1252.2   123.3  1259.6   121.9  1252.2   106.8  1165.9   108.9  1178.2   116.6  1221.6    2
-------------------------------------------------------------------------------------------------------------------

 PREDICTED COOLANT"S HOLES OUTLET TEMPERATURE AND FLOW DISTRIBUTION-Based On Predicted Wall Temp.
 ------------------------------------------------------------------------------------------------
T-(1 TO 5)o=OUTLET TEMPERATURE BASED ON HEAT TRANSFER FROM THERMAL LOCATIONS 1 TO 5 OF TEST WALL,
mTo = MEAN OUTLET TEMPERATURE; T(1 to 5)r = OUTLET TO PLENUMCOOLANT TEMP. RATIO & Trm IS THE MEAN
   To/Tp = Ratio Of Outlet To Plenum Temperature
-----------------------------------------------------------------------------------------------------------------
 T1o-K   T2o-K   T3o-K   T4o-K   T5o-K   mTo-K     T1r      T2r      T3r      T4r      T5r      Trm      To/Tp
1030.9  1040.0  1040.0  1020.7  1017.8  1029.9    0.416    0.420    0.420    0.411    0.409    0.415    1.268
1106.9  1111.1  1109.7  1090.6  1094.4  1102.6    0.345    0.347    0.346    0.339    0.340    0.344    1.277
1227.0  1228.5  1227.0  1209.5  1211.9  1220.8    0.245    0.245    0.245    0.239    0.240    0.243    1.306
-----------------------------------------------------------------------------------------------------------------

 RADIATIVE HEAT TRANSFER FROM FLAME -Based On Predicted Wall Temperature
 ---------------------------------------------------------------------------
R(1 TO 5)F-WATTS = RADIATIVE HEAT TRANSFER FROM FLAME TO WALL-BASED ON WALL
THERMAL STATIONS ; Rmf-WATT = MEAN FLAME RADIATION
---------------------------------------------------------------------------
    R1F        R2F        R3F        R4F        R5F        Rmf       %Rf/Qc
  122.33     119.57     119.57     125.41     126.25     122.63      3.61
  116.79     115.63     116.01     121.22     120.18     117.97      3.82
  112.59     112.23     112.59     116.71     116.12     114.05      3.66
-----------------------------------------------------------------------------

       COOLANT JET OUTLET VELOCITY AND JET VELOCITY TO MAINSTREAM VELOCITY RATIOS
       --------------------------------------------------------------------------
                   -Based On Wall temperature Prediction
                    -----------------------------------
      VO(1 TO 5)-M/S = COOLANT JET OUTLET VELOCITY-BASED ON WALL THERMAL STATIONS
      V(1 TO 5)R = COOLANT JET OUTLET VELOCITY TO MAINSTREAM VELOCITY RATIOS
                       Vrt = VELOCITY RATIO AS ABOVE
------------------------------------------------------------------------------------
  VO1     V1R     VO2     V2R     VO3     V3R     VO4     V4R     VO5     V5R     Vrt
143.66   1.804  144.92   1.820  144.92   1.820  142.23   1.786  141.84   1.781    1.42
112.86   1.420  113.29   1.425  113.15   1.424  111.19   1.399  111.59   1.404    1.11
 81.11   1.031   81.21   1.032   81.11   1.031   79.95   1.016   80.11   1.018    0.79
----------------------------------------------------------------------------------

          JET OUTLET DENSITY TO FLAME DENSITY RATIOS-Based On Wall Temp. Prediction
          -------------------------------------------------------------------------
        D1OF(1 TO 5) = RATIOS OF OUTLET COOLANT JET DESITY TO THAT OF MAINSTREAM-BASED
            ON WALL THERMAL STATIONS ;nDr = NORMINAL DENSITY RATIO,BLo= OUTLET BLOWING RATE
        ------------------------------------------------------------------------
              D1of       D2of       D3of       D4of       D5of       nDr      BLo
              1.68       1.67       1.67       1.70       1.70       2.14     3.036
              1.55       1.54       1.54       1.57       1.57       1.99     2.199
              1.39       1.39       1.39       1.41       1.41       1.82     1.433
        ------------------------------------------------------------------------
            COOLANT JETS OUTLET TO MAINSTREAM TEMPERATURE RATIOS AND JET PENETRATIONS
            -------------------------------------------------------------------------
                          -Based On Wall Temperature Prediction
                           ------------------------------------
       T(1 TO 5)R = COOLANT JET OUTLET TO MAINSTREAM TEMPERATURE RATIOS;
       Y(1 TO 5)P = MAINSTREAM PENETRATION BY JET-mm;-BASED ON WALL THERMAL STATIONS
                            nYp=Norminal Jet Penetration-mm
       ----------------------------------------------------------------------------
         T1r      Y1p    T2r      Y2p    T3r      Y3p    T4r      Y4p    T5r      Y5p   nYp
         0.566    3.3    0.571    3.3    0.571    3.3    0.560    3.3    0.559    3.3    3.8
         0.608    2.5    0.610    2.5    0.609    2.5    0.599    2.4    0.601    2.4    2.8
         0.668    1.6    0.669    1.6    0.668    1.6    0.658    1.6    0.660    1.6    1.9
        ---------------------------------------------------------------------------

                          FLUX-METER HEAT TRANSFER
                          ------------------------
       Tg=COMBUSTOR GAS TEMP.;T-(in,ot,pl)=COOLANT INLET,OUTLET &PLATE TEMP.
       Cpf=SP. HEAT CAPACITY(J/KgK); FMM=COOL. MASS FLOWRATE(Kg/sec.)
       Hav=AVERAGE CONV. HEAT TRANSFER COEFF.(W/m2K); Q=HEAT TRANSFER-(W)
       ----------------------------------------------------------------------
         Tg-K    Tin-K    Tot-K    Tpl-K     Cpf        FMM          Hav      Q
        1821.2   319.2    569.2    673.2  0.102E+04  0.424E-02      97.4  1082.02
        1821.3   320.5    573.2    694.2  0.102E+04  0.425E-02     100.5  1095.80
        1837.3   346.9    699.2    818.2  0.103E+04  0.425E-02     157.0  1548.56
      $$$$$$$$$$$$$$$$$$************************@@@@@@@@@@@@@@&&********************
```

CHAPTER 6

Nomenclature

DHFC	=	Full coverage discrete holes film cooling
T_{BL}	=	Thermal boundary layer dimensionless temperature
T	=	Local gas temperature in the boundary layer - K
T_w	=	Measured wall temperature - K
T_g	=	Mainstream gas temperature - K
G	=	Coolant air mass flow rate - kg/sm^2
T_c	=	Coolant air temperature - K
η	=	Overall cooling effectiveness
η_{ad}	=	Adiabatic cooling effectiveness
T_{gw}	=	Adiabatic wall temperature - K
Q_{cb}	=	Back-side wall convective heat transfer - W
Q_{ch}	=	Holes' convective heat transfer - W
Q_{RA}	=	(Q_{cb}/Q_{ch})
T_{out} or T_{cout}	=	Coolant jets' outlet temperature - K
T_{ple}	=	Coolant plenum temperature - K
T_{RAT}	=	(T_{out}/T_{ple})
H_{CF}	=	Film heat transfer coefficient
M	=	Blowing rate - ratio of coolant mass velocity to mainstream mass velocity
H_D	=	Dimensionless temperature eq. 6.6.
Y	=	Jet penetration distance - mm
t	=	Walls' thickness - mm
D	=	Holes' mean diameter - mm
n	=	Number of holes
$\Delta P/P$	=	Design pressure loss
X	=	Axial distance along test wall from the leading edge - mm or Holes' pitch
α	=	Angle of inclination of hole

CHAPTER 6

FULL COVERAGE DISCRETE HOLE FILM COOLING SYSTEM - EXPERIMENTAL INVESTIGATION RESULTS

6.1 INTRODUCTION

A range of full coverage discrete hole film cooling (effusion cooling) geometries has been investigated. These were a continuation of the series investigated by Mkpadi (7). All the experimental results of Mkpadi have been reprocessed using the new heat balance computer program discussed in Chapter 5 and compared with the present results at the end of this chapter. The effusion cooling geometries had the following aims:

(a) To extend the range of hole sizes investigated by Mkpadi (7) for a fixed number of holes in a uniform square array. The 4306 m^{-2}, 0.0027% design pressure loss wall was used for this work. Mkpadi's results showed that as the hole size was increased, the cooling effectiveness increased due to improvement in the film cooling. The present work used a much larger hole size than those of Mkpadi to investigate the ultimate performance that could be achieved by maximising the film cooling performance. It was designed to achieve a similar jet penetration and hence film cooling performance as the 21960 m^{-2}, 0.1% wall which had the best film performance of the designs tested by Mkpadi.

(b) Most of the work of Mkpadi was carried out with a constant wall thickness of 6.35 mm. It was a major objective of the present work to determine the importance of the wall thickness in the overall cooling performance. As discussed in Chapter 5, the convective cooling

of the hole approach flow is very significant in the wall cooling, and this is independent of the thickness. The influence of wall thickness was investigated at a 3% design pressure loss for the 9688 m^{-2} and 17,222 m^{-2} holes configuration and at 0.1% design pressure loss for the 26,910 m^{-2} holes configuration. In the present work, the information on the walls of 3.2 mm and 0.7 mm thickness is presented and compared, towards the end of the chapter, with the previous work of Mkpadi for the 6.35 mm thickness.

(c) The influence of the number of holes was investigated by Mkpadi mainly at a 3% design pressure loss and only two hole numbers were investigated at a 0.1% design pressure loss. It was considered likely that the optimum number of holes could be different at 0.1% pressure loss, due to the greater importance of the film cooling. This information was important in relation to the optimum configuration for impingement/effusion cooling, where the effusion wall would have a low pressure loss. Consequently 9688 and 17,222 m^{-2} designs at 0.1% design pressure loss were tested and compared with the 4306 and 26,910 m^{-2} data of Mkpadi. These tests were all at 6.35 mm wall thickness.

(d) All the previous work of Mkpadi and most of the present work was carried out on square arrays of 90° holes. Improvement in film cooling occurs if inclined holes are used. To determine the magnitude of this improvement, a 30° inclined hole staggered arrays 9688 m^{-2} system was tested at a 3% design pressure loss. The objective of this work was to investigate the maximum effusion cooling performance that could be achieved for a 3% design pressure loss. The 9688 m^{-2} design was shown by Ref. 7 to have the optimum cooling performance at 3% design pressure loss, 6.35 mm thick wall

and 90° hole.

One of the techniques used to investigate the film cooling performance by Ref. 7 was to determine the temperature profile in the coolant boundary layer. It was shown in this work and Ref. 11 that for systems with a high wall pressure loss or high effusion hole velocity, the jets 'stirred' the boundary layer and entrained hot gases into the wall region, a process shown in fig. 6.1. This was detected in the boundary layer temperature profile by a higher temperature adjacent to the wall than further away, followed by a temperature rise to the mainstream temperature. This appeared as a 'trough' in the temperature profile and the presence of this was a simple method for detecting the presence of excessive 'jet stirring' leading to poor film cooling. This type of thermal boundary layer for a 4306 m^{-2}, 3% pressure loss wall is shown in fig. 6.2. In the present work the absence of such a trough in a thermal boundary layer profile will be taken as an indication of good boundary layer film cooling aerodynamics.

In the present work it has been realised that the temperature of the gas adjacent to the wall could be used as a quantitative measure of the local cooling effectiveness in the absence of any wall heat transfer. This will be referred to as a 'pseudo' adiabatic cooling effectiveness using the temperature adjacent to the wall, T_{gw}, as an equivalent adiabatic wall temperature. Most investigators of film cooling have used adiabatic test configurations of either the mass transfer or very low temperature difference types. The problem with the present technique was that a single point gas temperature adjacent to the wall was used, whereas adiabatic film cooling effectiveness is known to be highly variable with axial and

spanwise directions. In the present work the traverse positions were aligned on the centre of the square hole arrays and hence measured the minimum adiabatic cooling effectiveness. Comparison of these would give a more quantitative indication of the film cooling performance than the simple absence or presence of a trough and the magnitude of the trough in the thermal boundary layer profile. However, problems of aligning the thermocouple traverses with the hole array make comparisons between different geometries difficult.

The procedure for testing the designed effusion walls has been discussed in Chapter 2. The first rig, on which some of the works reported here were carried out, has no facility for controlling the air flow to the duct wall to match the test wall temperature with that of the duct due to thermal distortion problems at high temperature. The new rig - Mk IV - has this facility, a process that helps in attaining more realistic cooling effectiveness (Chapter 2) by reducing the wall to duct wall radiative interchange.

A temperature bias of the mainstream to one side of the combustor at high temperature > 1000 K was sometimes encountered in the old rig - Mk III - due to fuel distribution problems in the jet mix flame stabilizers. A counter-rotating three swirler stabilizer was sometimes used on the combustor which was less prone to fuel maldistribution. For this combustor the temperature traverse across the mainstream at high temperature was measured. Figure 6.3 shows the two temperature traverse profiles carried out to ascertain a uniform temperature distribution in Mk IV at high mainstream temperature.

Two traverses between the combustor walls, in steps of 5 mm, were carried out and the results presented graphically in fig. 6.3

are mean values of the data collected. The results show that uniformity of temperature distribution in the mainstream was attained within 5 mm of the air cooled duct, either side of the mainstream. The effusion cooling results presented here were carried out in two temperature regimes. Mainstream temperatures from $500\ K \leqslant T_g \leqslant 1000\ K$ are classified as 'low temperature work', while mainstream temperatures of $T_g \geqslant 1005\ K$ are classified as 'high temperature work'.

Discrete hole full coverage film cooling (DHFC) or effusion cooling were investigated for different holes' densities, thicknesses, layout formats and design pressure loss ($\Delta P/P\%$). The test geometries will be referred to by their design pressure loss at a 700 K and $G = 0.4\ kg/sm^2$ design condition. Thus a 3% design pressure loss wall will be referred to as a 3% wall. Also the number of each plate's holes has been expressed in terms of the number per unit area, n. A 100 holes plate on a test area of 152.4 by 152.4 mm thus has an n of 4,306 holes per m^2. Subsequent sections of this chapter present the experimental results for n of 4,306, 9,688, 17,222 and 26,910 m^{-2} holes. The centre line thermocouple locations on the effusion walls at 25 mm intervals are referred to as thermal stations, e.g. the first wall (leading edge) thermocouple becomes thermal station one, 25 mm downstream of the leading edge.

6.2 THERMAL BOUNDARY LAYER PROFILES

The thermal boundary layer profiles on the test wall were determined by measuring the temperatures in the boundary layer at the plane of the test wall using the thermocouple traverse arrangement described in Chapter 2. In the early part of the work reported here,

one single thermocouple was used, located at the centre of the test wall. Later work used three thermocouples as discussed in Chapter 2. The thermocouples were located on the centre-line of the test wall at 25 mm (leading edge region), 76 mm (centre region) and 127 mm (trailing edge region) from the wall leading edge. The thermal boundary layer (4) temperature profile was expressed in a dimensionless form according to equation 6.1.

$$T_{BL} = \frac{T - T_w}{T_g - T_w} \qquad \ldots (6.1)$$

where T_{BL} = Thermal boundary layer dimensionless temperature

T = Local gas temperature in the boundary layer

T_w = Measured wall temperature at the axial location of traverse

T_g = Gas temperature downstream of the test wall

6.2.1 4306 m^{-2}, 0.0027% Design Pressure Loss, DHFC Wall

Figure 6.4 shows the results of the 4306 m^{-2} effusion holes wall. The development of the boundary layer at all coolant flow rates was very rapid. The thickening of the boundary layer at a high coolant flow rate of 1.56 kg/sm^2 resulted in a thickness of greater than 38 mm. At lower coolant flow rates, the boundary layer thickness was around 22 mm. There was no sign of any trough in the temperature profile and hence no entrainment of hot mainstream gas into the proximity of the test wall. This indicates that as the jets were deflected they coalesced and remained attached to the wall throughout the ranges of coolant flow rates investigated. It may be expected from these results that the cooling performance of the wall will be good due to a good film cooling. This will be assessed further in sections 6.3 and 6.5.

6.2.2 9688 m^{-2} Holes DHFC Wall

6.2.2.1 Wall thickness

Figures 6.5 and 6.6 show the results of the thermal boundary layer growth on 3%, 9688 m^{-2} holes effusion wall with wall thicknesses of 6.35 mm and 3.32 mm respectively. The results are for the central region traverse position.

Figure 6.5 shows that at high coolant flow rate (G), greater than 0.8 kg/sm^2, there is a trough in the profile indicating the presence of three-dimensional jet stirring of the boundary layer. In contrast with fig. 6.5, fig. 6.6 displays no trough in the boundary layer profiles for all the G values investigated. In spite of this apparently better film for the thinner wall, the boundary profile shows higher temperature in the wall region in fig. 6.6 than in fig. 6.5 and this is reflected in the lower adiabatic cooling effectiveness discussed later (fig. 6.30) for the thinner wall. However there is no reason why the wall thickness should have any major influence on the film cooling, except for any density ratio changes due to the lower wall heat transfer. This is confirmed by the computed film heat transfer coefficient, especially at low G, as discussed later (fig. 6.53). It is considered that the reason for the apparent difference in the thermal boundary layer is probably the difficulty of ensuring that the traverses are in the same position relative to the holes.

6.2.2.2 Density ratio

Mkpadi (7) showed that for a 3% design pressure loss the 9688 m^{-2} design was the optimum for a high cooling effectiveness and a low manufacturing cost. Although combined impingement/effusion systems are required for the highest cooling effectiveness in the

main flame tube, this type of double wall system is not considered suitable for the transition duct cooling. Consequently, a single wall design is required which must have the full combustor flame tube pressure loss across it of 3%. Also the 3.2 mm thick wall was more suitable for the more complex geometry of an industrial gas turbine transitional duct. Consequently, this design was chosen for tests over a wider range of test conditions.

The effect of different operating temperatures will produce different coolant to mainstream density ratios. The 3.32 mm thick wall was tested at various gas to coolant temperatures (T_g/T_c) ratios. The thermal boundary layer profiles at different temperature ratios are presented in figs. 6.7 to 6.17. In this part of the work, three traversing thermocouples were employed and the results are presented according to the plane of location of the traverse. Figures 6.7 to 6.9 of temperature ratios 1.95, 3.4 and 2.64 respectively, at the leading edge of the wall, show a significant trough in the profiles at G values greater than 0.3 kg/sm^2. This suggests entrainment of and recirculation with the hot gas stream by the coolant jets. This is most acute at mainstream temperatures greater than 600 K.

Figures 6.10 to 6.14 present the results at the wall centre-line of boundary layer profiles for T_g/T_c of 1.95, 2.64, 2.43 and 2.71 with coolant temperature ranging from 293 K to 673 K while mainstream hot gas temperature ranges from 572 K to 1827 K. Figures 6.10 to 6.12 bear the same similarity to those profiles at the leading edge of the test wall but with a thicker overall boundary layer due to the accumulation of coolant. However at very high coolant and mainstream temperatures, figs. 6.13 and 6.14, the profiles are significantly different from the lower mainstream temperature. The evidence of three-dimensional jet stirring has disappeared and

the overall boundary layer was much thinner. The increase in mainstream temperature was achieved at constant mass flow, so that when the kerosine burners were used, T_g increased with an associated increase in the mainstream hot gas velocity, V_g, but the blowing rate remained constant. It would appear that blowing rate is not a good parameter to characterise the film performance; the velocity ratio or dynamic head ratio is probably to be preferred.

The figures for mainstream temperatures of less than 1010 K, irrespective of coolant temperatures, of interest compare well with results of figure 6.5 for the thick plate and support the conclusion that the traverse in fig. 6.6 was at a different relative position to the effusion holes.

Only one thermocouple was employed for traversing at temperatures greater than 1010 K, and this was at the centre. Figures 6.15 to 6.17 show the results of the boundary layer profiles at the trailing end of the test wall. The results show a trough in the profile at high G values as for the other locations. Depending on the magnitude of heat picked up by the coolant at the back and inside the wall, these conditions of test may not yield high cooling performance.

6.2.2.3 0.1% design pressure loss

Figure 6.18 shows the thermal boundary layer profiles as a function of centre-line vertical distance from the test wall, for a 9688 m^{-2} holes, 0.1% design pressure loss and 6.5 mm thick effusion wall. Comparison with fig. 6.5 for the equivalent 3% pressure loss wall results shows a much reduced jet stirring at high G value and low temperature adjacent to the wall at high G. This better film cooling performance should lead to a higher cooling performance when

compared with the 3%, 6.35 mm thick, 9688 m^{-2} holes wall.

6.2.3 17,222 m^{-2} Holes, 3% Design Pressure Loss DHFC Wall

This work investigates the effects of two wall thicknesses, 6.35 and 3.29 mm, on the thermal boundary layer growth on the wall when tested at the same operating condition. Figures 6.19 and 6.20 show the wall centre-line thermal boundary layer profiles. These profiles display hot stream entrainment characteristics by showing troughs at all values of G greater than 0.18 kg/sm^2 with the magnitude of the trough increasing with G. The apparently worse results for the thinner wall, in terms of a deeper trough, were probably due to differences in traverse location. Comparison with the equivalent 9688 m^{-2} geometry in fig. 6.5 show that the temperatures are lower in the wall region indicating that the larger number of holes has improved the film protection for both wall thicknesses.

6.2.4 26,910 m^{-2} Holes, 0.1% Design Pressure Loss DHFC Wall

Two wall thicknesses, in addition to that studied by Mkpadi (7), were investigated in this category of holes' density of DHFC wall. The thicknesses were 3.37 mm and 0.69 mm compared with 6.35 mm of Ref. 7. The thermal boundary layer results are shown in figs. 6.21 to 6.26. Three traversing thermocouples were employed and the locations investigated were leading edge region, 25 mm from the leading edge of a test wall, the central region, 76 mm from the leading edge of the test wall, and the trailing edge region, 127 mm from the leading edge of the test wall.

The results show a rapid thickening of the boundary layer from the leading edge to 76 mm axial distance downstream. Beyond this

location there is deceleration in the thickening of the boundary layer. Generally the boundary layers are thin with the thickness varying between 17 mm to 35 mm for the profiles to reach a value of $T_{BL} = 0.99$. In all respects, the profiles for the two walls' thicknesses are similar with little indication of stirring of the boundary layer. The profiles are also similar to those of transpiration walls, discussed in Chapter 4, and it is possible that the film cooling performance of these walls may well be as good. Comparison with figs. 6.21 and 6.22 shows a considerably thinner boundary layer, illustrating the strong influence of the lower design pressure loss on the film thickness and the much lower temperature adjacent to the wall. Comparison of fig. 6.23 with fig. 6.4 shows that the 4306 m^{-2}, large hole design has a similar boundary layer, although not quite as good as the 26,910 m^{-2} in fig. 6.23.

6.3 OVERALL AND ADIABATIC COOLING EFFECTIVENESS

The overall cooling effectiveness was measured using the five centre-line thermocouples on the effusion wall. These thermocouples were flush with the flame side of the test plates and then vacuum welded. This mode of installing the thermocouples minimised the errors that may result (1) in temperature measurements in solid metals. The only significant error source is that specified by the thermocouple manufacturers and the amplification of its measurement through digital read-out as discussed in Chapter 5. The error involved was found to be less than ± 0.4%. The thermocouples were mounted on the centre of the square hole arrays and hence measured the maximum temperature, if there was any temperature gradient. The overall cooling effectiveness is defined as:

$$\eta = \frac{T_g - T_w}{T_g - T_c} \qquad \ldots (6.2)$$

where η = Overall cooling effectiveness

T_g = Mainstream gas temperature

T_w = Test wall temperature

T_c = Coolant gas temperature

The error of the gas stream temperature, T_g, in equation 6.1 has been discussed in Chapter 5 and the final error of η is small (3) and mainly associated with the uncertainties correction procedures discussed in Chapter 5, which are highest for the high temperature tests.

There is a difference between the temperature of the test wall and the gas in the immediate proximity of the wall. At high coolant mass injection rate, G, this difference (ΔT), for high cooling performance wall designs, is expected to be small and high at low G values. Figure 6.27 shows the results of ΔT for all the walls investigated at the standard low temperature condition T_g = 750 K and T_c = 290 K. As expected, the temperature of the film in the proximity of the wall for low G values was high due to the thin boundary layer and hence rapid mixing between the coolant air and the hot mainstream for all the walls. At high G values the film temperature is relatively low for most of the wall except the 9688 m^{-2} holes 3% walls which show an increase in ΔT with G, due to enhanced jet stirring. This agrees with the thermal boundary layer profile and the conclusion there that a poor cooling performance is anticipated. The 26,910 hole walls have a low film temperature at high G values which again confirms the thermal boundary layer conclusion that a high cooling performance for this density holes'

wall is expected. For good boundary layer film cooling, ΔT decreases as G is increased, indicating that the film remains attached to the wall with little jet stirring.

The gas temperature adjacent to the wall, T_{gw}, is similar to the wall temperature in studies of adiabatic wall film cooling (2). The procedure for the measurement of the temperature adjacent to the wall, T_{gw}, was the same as discussed for the transpiration system, Chapter 4. Using this temperature, the adiabatic cooling effectiveness was defined as in equation 6.3.

$$\eta_{ad} = \frac{T_g - T_{gw}}{T_g - T_c} \qquad \ldots (6.3)$$

where η_{ad} = Adiabatic effectiveness

T_{gw} = Temperature of the gas in the immediate proximity of the test wall

The error in η_{ad} is directly related to the error in T_{gw}, as the other temperature errors are relatively small. As has already been discussed, the main problem in the determination of T_{gw} is that it will vary between the holes and it is difficult for the boundary layer traverse to be located at the same position relative to the holes for each traverse.

6.3.1 η and η_{ad} - 4306 m^{-2} Holes, 0.0027% Design Pressure Loss Full Coverage Discrete Hole Film Cooling (DHFC) Wall

The 0.0027% plate overall cooling effectiveness as a function of coolant mass injection rate, G - kg/sm^2, at thermal station 5, is presented in fig. 6.26. The results indicate a rapid growth of the cooling effectiveness with coolant injection and at G values greater than 1.0 kg/sm^2, the wall behaves as an ideal transpiration system. The axial development of the overall cooling effectiveness

at two values of G is shown in fig. 6.29. The results indicate a strong axial development of effectiveness downstream of the test wall leading edge, with no sign of an equilibrium cooling effectiveness independent of axial distance. This good cooling performance confirms the conclusion for the thermal boundary layer result.

The adiabatic effectiveness measurement was made at only one location. This was at the centre-line of the test wall. Figure 6.28 shows the results of the adiabatic effectiveness as a function of coolant injection rate. For all values of G, the results showed a continuous increase and at no point was an equilibrium state reached. The results when compared with the overall effectiveness were lower. This was due to the film temperature at the wall shown in fig. 6.27. The continuous increase in the adiabatic effectiveness with G lends support to the conclusion that there was very little interaction and mixing between the coolant jets and the mainstream. From these results it may be concluded that the coolant jets after deflection by the mainstream coalesce and remain attached to the test wall surface. Comparison of fig. 6.28 with similar results for the transpiration wall in Chapter 4 shows that this discrete hole system has similar characteristics.

6.3.2A η and η_{ad} - 9688 m^{-2} holes DHFC wall

The results of the overall cooling effectiveness for three plates, two of which are of the same design pressure loss of 3% but different thickness (t) (6.35 mm and 3.32 mm) and the other of 0.1% design pressure loss, are presented in fig. 6.30. Considering the walls of the same design pressure loss, the results showed that the effectiveness, η, of the thick wall (t/D = 6.78) was superior to that of the thin wall (t/D = 3.32), increasing from 5% at a low G

value of 0.4 kg/sm^2 to 13% at G values greater than 1.0 kg/sm^2.

The low pressure loss wall (0.1% design pressure loss) had an effectiveness much superior to either of the 3% walls. Its superiority, at low G values of less than 0.2 kg/sm^2, was 15% compared with the 3%, 6.35 mm thick wall and 19% compared with the 3%, 3.32 mm thick wall, at the same G value. The values of η were not as high as for the very large hole 4306 m^{-2} system and hence the cooling performance was inferior in spite of the larger number of holes.

Also on fig. 6.30 are the adiabatic cooling effectiveness, η_{ad}, of these three walls at the wall centre-line. The magnitude of the difference between η and η_{ad} is a rough measure of the degree of heat transfer at the back and within the walls by the coolant. For the 3% walls the profiles of the adiabatic effectiveness are similar to those of η. However the difference in η_{ad} between the two designs, apparently due to wall thickness, is more likely to be associated with differences in the traverse positions relative to the holes, as discussed in relation to the boundary layer traverses. The 0.1% results show much higher values of η_{ad} at high G than for the 3% walls and this is the main reason for the much higher overall cooling effectiveness at high G. At low G values (< 0.2), all three designs exhibit a similar low η_{ad} and hence the overall η must be dominated by internal wall cooling in this region.

Figure 6.31 shows the axial development of the overall cooling effectiveness at a G value of 0.2 kg/sm^2. The 0.1% wall results maintain its superior cooling performance over the others at all axial positions. A stronger axial dependence of η from the leading edge downstream of the test wall was displayed by the 0.1%, 6.35 mm wall due mainly to the strong axial gradient of the film cooling, η_{ad}.

Figure 6.32 shows results, at the fifth thermal station, of the cooling effectiveness for three mainstream and coolant operating temperatures. The work was carried out using the 3%, 3.32 mm thick wall. High G values, for the mainstream temperature of 1827 K, were not investigated due to an unacceptable level of combustion generated noise. The results at low temperature of 772 K were superior to the others. The high temperature results with radiation from the hot gases set at zero do not account for the differences between η at high and low temperatures.

For conditions at 1634 K, and at low G value, the no-radiative effect effectiveness was almost the same as η at 772 K condition but with only a small reduction in the magnitude of the difference at high G values. This analysis shows that radiation from the flame is a significant factor that will lower the cooling effectiveness at high combustion temperature.

Figure 6.33 shows the results of both low and high temperature work at thermal station 2. Here the results of the 1634 K test condition were superior to those of low temperature work at G values below 0.35 kg/sm^2. At higher G values, however, the 772 K test conditions were superior to the rest. The effectiveness at 1827 K test condition was significantly lower than the rest though there is a tendency of improvement with higher G. Figures 6.34 and 6.35 show the axial development of the cooling effectiveness at the three test conditions, for two G values. The high temperature results have a lower axial dependence of cooling effectiveness than the 772 K results. This may indicate a reduced axial development of the boundary layer thickness. The much thinner boundary layers have already been referred to and these may be responsible for the

reduced overall cooling effectiveness.

6.3.2B Density ratio effect on cooling effectiveness

The 3.32 mm thick wall was investigated for density ratio effect on cooling effectiveness by varying the coolant air temperature. Previous workers have investigated the density ratio effect using gases of different thermodynamic properties from the mainstream, a process that will alter other design characteristics (6). Figure 6.36 shows the density ratio results of overall cooling effectiveness as a function of G at thermal station 5. The results show that the cooling effectiveness of density ratio 2.64 and 3.40 were superior to the rest above G value of 0.18 kg/sm^2. The influence of the density ratio is complex and fig. 6.37 shows that there is no simple relationship between density ratio and cooling effectiveness. Figure 6.36 shows that at T_g = 1000 K, the two density ratios, with different T_c, gave very similar η. However, for a constant T_c of 293 K, the three values of T_g show different η but no consistent trend. The two higher temperature results have lower effectiveness than for the lower value of T_g. Two factors influence this: hole Reynolds number (Re), and the high velocity cross flow. The high coolant temperature reduces the Re at a fixed G due to the increase in viscosity. This will reduce the internal wall heat transfer which is a function of Re. The mainstream velocity is increased in direct proportion to the temperature change due to the kerosine combustion as the mass flow is set by the stabilizer, 0.047 approach Mach number. This does not change $\rho_g u_g$ and hence the blowing rate and the low cooling effectiveness at high temperature indicates that blowing rate is not a good correlating parameter and a velocity ratio or dynamic head ratio may be preferable. The

difference in the thermal boundary layer thickness has already been noted.

6.3.3 η and η_{ad} - 17,222 m^{-2} Holes, 3% Design Pressure Loss DHFC Wall

This full coverage discrete hole film cooling wall geometry was investigated for thicknesses of 6.35 mm and 3.32 mm. The holes were in a square array and at 90°. Both designs were investigated only at low temperature. This work was undertaken as part of a series of walls of different thickness to establish whether the optimum number of holes was influenced by thickness.

Figure 6.38 shows the results of the overall and adiabatic cooling effectiveness as a function of coolant air mass flow at thermal station 5. The overall cooling effectiveness of the thicker wall was superior to that of the thin wall at all G values investigated. However, the difference was not as great as for the same change in wall thickness for the 9688 m^{-2} design as shown in fig. 6.30. The adiabatic effectiveness of the thinner wall was unexpectedly higher than that of the thick wall at all values of G above 0.3 kg/sm^2, with a low value between $0.12 \leqslant G \leqslant 0.3$. This performance may be traced back to figs. 6.19 and 6.20 where it was shown that the boundary layers were significantly different, indicating that the traverse location relative to the jet was different and hence the temperature adjacent to the wall was at a different location.

Figure 6.39 shows the overall cooling effectiveness as a function of axial distance from wall leading edge. The thick wall performs better than the thin wall but at a distance of 100 mm from the leading edge both effectivenesses had reached their equilibrium value. Comparison with fig. 6.31 for the 9688 m^{-2} system shows that an equilibrium value was not reached within the 127 mm test

length. This phenomenon may be controlled by the number of upstream holes. The equilibrium point in fig. 6.39 is two-thirds of the test section, which corresponds to approximately 14 upstream holes in the direction of the cross-flow. In fig. 6.31, the hole array is 15 × 15 and hence at thermal station 5 there are only 13 upstream holes. This conclusion is only applicable to the 3% pressure loss designs and may be different as the pressure loss is reduced.

6.3.4 η and η_{ad} - 26,910 m^{-2} Holes, 0.1% Design Pressure Loss DHFC Wall

In this low pressure loss design two thicknesses were investigated, 3.37 mm and 0.69 mm. Figure 6.40 shows the results of the overall and adiabatic cooling effectiveness for both walls as a function of coolant mass injection, G, at thermal station 5. The results for the two walls are very close both for overall and adiabatic effectiveness, with the thicker wall being slightly better at G values less than 0.4 kg/sm^2, while it is the thinner wall at G greater than 0.45 kg/sm^2. Generally, the results confirm the conclusion in previous sections that they behave in a similar way to a transpiration wall, as the adiabatic results tend towards the overall results at high G. This indicates that the change in heat transfer due to the reduction in wall thickness has a small influence as the overall heat transfer is dominated by the high film cooling effectiveness.

Figure 6.41 shows the axial profiles of the overall and adiabatic cooling effectiveness at two G values of 0.177 kg/sm^2 and 0.363 kg/sm^2. At G value of 0.177 kg/sm^2, the thicker wall overall cooling effectiveness was superior to that of the thinner wall. This is also the case for the adiabatic effectiveness except at distance

127 mm. At G value of 0.363 kg/sm^2, there was little difference between the two walls' overall cooling effectiveness while the adiabatic effectiveness of the thicker wall was superior up to a distance of 119 mm from the wall leading edge. It may be concluded that for this geometry wall thickness it is not an important feature of the overall cooling effectiveness and hence can be shown purely on mechanical requirement.

6.4 HEAT TRANSFER AT THE BACK AND INSIDE THE WALL FOR FULL COVERAGE DISCRETE HOLE FILM COOLING WALL

The results of the heat transfer at the back-side and inside the holes of the DHFC wall have been expressed as a ratio (Q_{RA}) of the former to the latter (Q_{cb}/Q_{ch}). The ratio of the plenum coolant temperature to that of the outlet jets on the hot gas face of the wall is also a measure of the magnitude of the heat transferred to the coolant in its journey to this side of the wall. This outlet temperature of the coolant jets at the wall gas side was predicted not measured and the method of prediction was detailed in Chapter 5. The temperature ratio was defined as in equation 6.4, and its magnitude is a reflection of the combined heat transfer due to Q_{cb} and Q_{ch}.

$$T_{RAT} = \frac{T_{out}}{T_{ple}} \qquad \ldots (6.4)$$

where T_{RAT} = Coolant jet outlet to plenum temperature ratio

T_{out} = Coolant outlet temperature

T_{ple} = Coolant plenum temperature

6.4.1 Q_{RA} and T_{RAT} - 4306 Holes, 0.0027% Design Pressure Loss DHFC Wall

Figure 6.42 shows the results of the dimensionless heat transfer at the back-side and inside of the 4306 m^{-2} DHFC wall as a function of coolant mass injection rate - G kg/sm^2. The results indicate that the heat transfer at the back-side is very significant at all coolant injection rates less than G value of 1.0. The heat transfer in the holes, however, is dominant at values of G greater than 1.0.

Figure 6.43 shows the results of the temperature rise of the coolant as it passes through the wall from the plenum. The results indicate a larger increase in coolant temperature at low G values. However, the magnitude of the temperature change was small, especially at high G. This confirms the low wall heat transfer due to the high film cooling effectiveness discussed previously. It may be concluded that at high coolant injection, film protection of the wall is predominant while heat removal from the wall at low G values is as significant as film protection.

6.4.2 Q_{RA} and T_{RAT} - 9688 m^{-2} Holes, DHFC Wall

Figure 6.44 shows the results of heat transfer from the back-side and in the holes of 9688 wall geometry as a function of coolant mass injection rate G for three plates, two of the same design pressure loss of 3% but different thickness - 6.35 mm and 3.32 mm, and the other of 0.1% design pressure loss. The figure indicates that at all G values the heat transfer at the back-side of the 3%, 3.32 mm wall is higher than that in the holes, while back-side heat transfer is only superior to that in the hole at G value less than 0.4 kg/sm^2 for both the 3%, 6.35 mm thick and 0.1%, 6.5 mm thick walls.

Figure 6.45 shows the results of T_{RAT} for the three walls as a function of coolant injection. The results indicate a nearly equal magnitude of temperature rise for the two walls of the same geometry but different thicknesses. The situation is slightly different for the 0.1% wall as the results indicate that temperature rise in the wall is only significant at G value less than 0.5 kg/sm^2. This is an indication that at high coolant injection the film protection is effective.

The increase in Q_{cb}/Q_{ch} in fig. 6.44 with decrease in wall thickness for the same hole size or design pressure loss is due to the decrease in Q_{ch} with Q_{cb} remaining the same for both wall thicknesses. However for the same hole t/d of approximately 3, the 0.1% design pressure loss wall shows much lower values of Q_{cb}/Q_{ch} than for the 3% design but similar value for the same thickness (t). This indicates that for the same total hole length an increase in hole diameter reduces Q_{cb} and Q_{ch} in similar proportion and hence the ratio remains constant. The temperature ratios in fig. 6.45 show that the reduced wall thickness for the 3% pressure loss creates only a small loss in the total heat transfer which explains the relatively small influence of the wall thickness on the overall cooling effectiveness in fig. 6.30. For the lower pressure loss wall, fig. 6.45 shows much lower total heat transfer due to the lower Reynolds number (Re), but significantly higher than for the very low pressure loss 4306 m^{-2} design in fig. 6.43.

For the density ratio investigation carried out on the wall with 3.32 mm thickness, the Q_{cb}/Q_{ch} results are presented in fig. 6.46. The results show that at all coolant injection rates the back-side heat transfer was superior to the holes' heat transfer. The results

show that Q_{cb}/Q_{ch} is only influenced if the coolant temperature changes due to the different Re dependence of Q_{cb} and Q_{ch}. At a fixed G the results show that Q_{cb}/Q_{ch} increases as T_c increases. For a constant T_c, Q_{cb}/Q_{ch} is not influenced by the density ratio, as expected, as this should only influence the film heat transfer.

6.4.3 Q_{RA} and T_{RAT} - 17,222 m^{-2} Holes, 3% Design Pressure Loss DHFC Wall

The results of heat transfer at the back-side and inside the 17,222 holes geometry for two thicknesses is presented in fig. 6.47. The results show that heat picked up by the coolant at the back-side of the thin wall is a greater proportion of the heat transfer than is the case for the thick wall. In the thick wall, the heat transfer in the holes is more significant. For both walls, back-side heat transfer is very significant at G values below 0.3 kg/sm^2.

Figure 6.48 shows the profiles of T_{RAT} as a function of coolant injection rate. The results indicate that the temperature rise of the coolant within the thin wall is less than for the thick wall but the difference is small considering the hole length has been halved. These results help to explain why the overall effectiveness of the thick wall was slightly better than that of the thick wall in fig. 6.38.

6.4.4 Q_{RA} and T_{RAT} - 26,910 m^{-2} Holes, 0.1% Design Pressure Loss DHFC Wall

Figure 6.49 shows the profiles of Q_{cb}/Q_{ch} for two wall thicknesses for this low pressure design geometry. The results show that the back-side heat transfer in the thin wall is the predominant process in the overall heat transfer. For the thicker wall, heat removed within the wall is higher than the back-side heat transfer

at G values greater than 1.1 kg/sm^2.

Figure 6.50 shows T_{RAT} as a function of coolant injection, G. For the thin wall, the temperature rise of the coolant is less than is the case for the thick wall. However, as in fig. 6.48, the difference is not large even though the thin wall here, 0.7 mm, has almost negligible internal hole heat transfer and the temperature rise is almost entirely due to Q_{cb}. This explains the small influence of wall thickness on the overall cooling effectiveness in fig. 6.40.

6.5 FILM HEAT TRANSFER COEFFICIENT (H_{CF})

The determination of the convective heat transfer from the hot gas stream and the film heat transfer coefficient have been discussed and analysed in Chapter 5. The results for the film heat transfer coefficient for all the full coverage discrete hole film cooling (DHFC) walls investigated in the present work are presented in this section.

6.5.1 H_{CF} - 4306 m^{-2} Holes, 0.0027% Design Pressure Loss DHFC Wall

The results of the film heat transfer coefficient on this geometry are shown in fig. 6.51 as a function of coolant mass injection rate G. The results indicate a decreasing H_{CF} with increasing coolant injection. This dependence of H_{CF} on G is a characteristic of transpiration cooling as discussed in Chapter 4. These results confirm the transpiration behaviour, discussed in previous sections on this geometry. The negative results at high G are due to inaccuracies in heat balance when the heat removed in the wall is very low so that H_{CF} is low and the heat gained by convection from the wall is high.

Figure 6.52 shows the axial profiles of the film heat transfer coefficient at two G values. The results indicate that the convective heat transfer to the wall at the leading edge is high and decreases axially downstream of the wall. The steep gradient of the decrease implies the increasing improvement of the coolant film downstream of the leading edge of the test wall.

6.5.2A H_{CF} - 9688 m^{-2} holes, DHFC wall

The results of the film heat transfer coefficient for three walls, two of 3% design pressure loss geometry and the other of 0.1% design pressure loss geometry, are shown in figure 6.53 as a function of coolant injection G at thermal station 5. The result of a flat plate heat transfer coefficient as discussed in Chapter 5 is also presented as a straight broken line. The results show that the film heat transfer coefficient of the 3% wall geometry was not strongly influenced by the wall thickness at low G, as discussed previously for the thermal boundary layer profiles. The low pressure loss wall has a very low film heat transfer coefficient due to the superior thermal boundary layer characteristics. Consequently the increase in the overall cooling effectiveness for this design compared with the 3%, in fig. 6.30, was due to the superior film cooling.

The results of the axial profiles of the film heat transfer coefficient at coolant injection of 0.2 kg/sm^2 are shown in fig. 6.54. The profiles show a decreasing axial convective heat transfer to the wall as the thermal boundary layer grows more effective.

6.5.2B Density ratio effect on film convective heat transfer coefficient

As discussed in section 6.3.2B, fig. 6.55 shows the results of the film heat transfer coefficient at different norminal density

ratios as a function of coolant mass injection G. The results indicate an influence of density ratio on H_{CF} but there was no consistent trend. The results indicate that when the coolant temperature was constant, varying T_g did not influence H_{CF}. However at T_g = 1000 K, the two coolant temperatures give different H_{CF}. Further work is required to account for the density ratio influence.

Figure 6.56 shows the axial profiles of the film heat transfer coefficient for $0.36 \leqslant G \leqslant 0.383$ for all the density ratios investigated. H_{CF} was generally lower the greater the magnitude of the density ratio within the operating temperature regimes of less than 1010 K.

6.5.3 H_{CF} - 17,222 m^{-2} Holes, 3% Design Pressure Loss DHFC Wall

The results of H_{CF} for the two walls investigated are shown in fig. 6.57 as a function of G at thermal station 5. Presented with these results are the results of flat blank plate represented by a straight broken line. The influence of wall thickness is only small on H_{CF}, as expected. The values are lower than for the 9688 m^{-2} design in fig. 6.53, demonstrating the improved film cooling due to the greater number of holes. The near constant value of H_{CF} at high G indicates that the thermal boundary layer is not being 'stirred' as G increases.

Figure 6.58 shows the results of the axial profiles of the two walls' H_{CF} at G value of 0.2 kg/sm^2. The results show a high convective heat transfer at the leading edge due to intense mixing but this high value of H_{CF} decreases downstream until 100 mm away from the leading edge. Beyond 100 mm a near constant H_{CF} was found, indicating that the thermal boundary layer was fully developed.

6.5.4 H_{CF} - 26,910 m^{-2} Holes, 0.1% Design Pressure Loss DHFC Wall

The results of the work done on two wall thicknesses are presented in fig. 6.59 as a function of G at thermal station 5 and in fig. 6.60 as axial profiles at two G values of 0.177 and 0.363 kg/sm^2 respectively. Figure 6.60 shows that for both walls H_{CF} results are lower than that for flat plate convective heat transfer coefficient of 78 W/m^2K. After an initial increase of H_{CF} for the thicker wall, both walls' H_{CF} decreases with increasing G, indicating that a transpiration type of film cooling had been achieved. The lower results for the thinner wall may not be valid and may only reflect problems with the wall heat transfer correlations for these geometries.

The axial results show that for the two G values considered, the thermal boundary layer only reaches an equilibrium situation with no change in H_{CF} with axial distance at approximately the 125 mm position.

6.6 EFFECT OF BLOWING RATE ON COOLING EFFECTIVENESS AND FILM HEAT TRANSFER COEFFICIENT

The blowing rate, M, has been used by many investigators for the correlation of film cooling performance. M has been defined in Chapter 5 (see equation 5.72). The cooling effectiveness and film heat transfer coefficient results as a function of M, for all the DHFC walls investigated, are discussed in this section.

6.6.1 M - 4306 m^{-2} Holes, 0.0027% Design Pressure Loss Wall

The results of the dependency of cooling effectiveness and film heat transfer coefficient on M are shown in figs. 6.61 and 6.62.

The large hole size and low design pressure loss result in very low blowing rates, which is the main reason for the very good film cooling characteristics and hence low value of H_{CF}.

6.6.2 M - 9688 m^{-2} Holes DHFC Wall

Figures 6.63 and 6.64 show the results of film heat transfer coefficient and cooling effectiveness dependency on M for two 3% walls and one 0.1% wall. These show that for the 3% design pressure loss, the values of M are very high whereas for the 0.1% design pressure loss they are much lower for the same range of G. However, although the film heat transfer coefficient is low for the 3% pressure loss walls, the values are not as low as for the 0.1% design at the same M. This blowing rate does not correlate the film or 'adiabatic' film effectiveness data and fig. 6.64 shows it is even worse at correlating the overall film cooling effectiveness data.

Figures 6.65 and 6.66 show the results for the 3%, 3.32 mm wall at different density ratios. The cooling effectiveness results at thermal station 5 are shown in fig. 6.65. This shows no real improvement in the data correlation compared with fig. 6.36. The results of the H_{CF} are presented in fig. 6.66 and for this too, no real improvement over fig. 6.55 is visible. Consequently, it may be concluded that blowing rate is a poor correlating parameter for the influence of hole size and density ratio.

6.6.3 M - 17,222 m^{-2} Holes, 3% Design Pressure Loss Wall

The results for the two walls investigated in this geometry both for the H_{CF} and cooling effectiveness are presented in figs. 6.67 and 6.68. Wall thickness does not influence the blowing rate,

but the results do show again that for a 3% design pressure loss, low H_{CF} are only obtained at low M.

6.6.4 M - 26,910 m^{-2} Holes, 0.1% Design Pressure Loss Wall

Figure 6.69 shows the results of the cooling effectiveness dependency on M. This shows that for the same M the thinner wall has the higher cooling effectiveness, which is the reverse of the situation when comparison was made at the same G as in fig. 6.40. The reason is the use of the computed hole outlet M and the higher wall heat transfer, fig. 6.70, with the thicker wall producing a higher M. This again shows that M is not a good correlating parameter.

6.7 DIMENSIONLESS TEMPERATURE (H_D) AND JET PENETRATION DEPTH (Y)

The dimensionless temperature for different coolant systems is another method of assessing the cooling performance of the system in comparison with the transpiration cooling wall. The nearer the dimensionless temperature is to zero, for a particular geometry, the nearer its performance compares with transpiration cooling. This dimensionless temperature is defined as

$$H_D = \frac{T_w - T_{cout}}{T_w - T_{ple}} \qquad \ldots (6.6)$$

where H_D = Dimensionless temperature

T_w = Measured wall temperature

T_{cout} = Predicted coolant jets' outlet temperature (see Chapter 5)

T_{ple} = Plenum chamber coolant temperature

For a transpiration wall it is generally assumed that T_{cout} is equal to T_w and hence H_D should be zero.

The jets' penetration depth (Y) into the mainstream has been analysed and defined in Chapter 5, equation 5.69. In that equation, Y is for one hole pitch.

6.7.1 H_D and Y - 4306 m^{-2} Holes, 0.0027% DHFC Wall

The results of H_D at station 5 as a function of G are shown in fig. 6.71. For this design the results show that H_D tends to a low value at low G, but it is a long way from zero. Thus the contribution of internal wall cooling to the high cooling effectiveness is not as great as for a transpiration system, even though the overall cooling effectiveness is high. Figure 6.72 shows the jet penetration to be very small at all G and this is the reason for the good film cooling performance which does approximate to that of a transpiration system and, as already discussed, is the main contributor to the high overall cooling effectiveness.

6.7.2 H_D and Y - 9688 m^{-2} Holes, DHFC Wall

Figure 6.73 shows the results of the three walls investigated. Two of these walls were of a 3% design pressure loss and the other of a 0.1% wall. Figure 6.73 shows that H_D is lower for the 3% pressure loss walls than the 0.1% pressure loss, demonstrating the higher internal wall cooling due to the higher Reynolds number. Figure 6.73 also shows that the thicker 3% wall has a lower H_D than the thinner, demonstrating that wall thickness does have a significant influence on the internal wall heat transfer which accounts for the significant difference in the overall cooling effectiveness.

Figure 6.74 shows the results of Y with G. The results show a high penetration for the 3% wall but low Y for the 0.1% wall. The difference between no wall heating, norminal Y, and actual Y

illustrates the relatively small influence of internal wall heat transfer in reducing the jet penetration and improving film effectiveness. The much lower Y values for 0.1% are a reflection of its good film cooling characteristics, which are responsible for the high wall cooling effectiveness.

6.7.3 H_D and Y - 17,222 m^{-2} Holes, 3% Design Pressure Loss, DHFC Wall

Figure 6.75 shows the results of H_D for the two walls investigated, as a function of G. The results show that the thicker wall of the two has its value of H_D closer to zero than that of the thin wall. This again shows that wall thickness has a measurable influence on the internal wall cooling, however the influence is not large as has already been discussed.

The jet penetration, fig. 6.76, Y, is quite large, again indicating the relatively poor film aerodynamics of the 3% design pressure loss options.

6.7.4 H_D and Y - 26,910 m^{-2} Holes, 0.1% Design Pressure Loss, DHFC Wall

Figure 6.77 shows the results of H_D for the two walls investigated as a function of G at the fifth thermal station. The results indicate that both walls have a relatively poor internal heat transfer as has been found for the 0.1% design pressure loss systems. Wall thickness difference, which is very large in this case, shows a very significant deterioration in the internal wall cooling, with much lower H_D for the thicker wall.

The jet penetration, fig. 6.78, was very small for both thicknesses, again indicating good film aerodynamics and hence low H_{CF}

and high adiabatic cooling effectiveness, as has already been discussed. The good film cooling compensates for the low internal wall cooling to give a high overall cooling effectiveness.

6.8 COMPARISON AND GRAPHICAL DESIGN CORRELATIONS

The main objective of this section is to compare the present work with that of other people and to present empirical graphical correlations for design purposes. The main comparison will be with the work of Mkpadi (7), using the same test facility as the present work.

6.8.1 Comparison of the 0.0027% Wall With Other Works in the Literature

The cooling performance of the 4306 m^{-2} holes, 0.0027% design pressure loss wall is compared in fig. 6.79 with other works, as well as with the results of RM50A Rigid Mesh investigated in the present work, and reported in Chapter 4. Figure 6.79 shows that the present results compare well with those of the RM50A at G values greater than 0.8 kg/sm^2. This shows that this design approximates to a transpiration situation at high G. At low G values the present results are below those of RM50A.

Mkpadi (7) studied two main holes' density of DHFC wall, 4306 m^{-2} and 26,910 m^{-2}. Mkpadi's data for both plates' geometry for 0.1% design pressure loss have been reprocessed using the computer program developed for the present work. The results of Mkpadi's work at the same operating conditions as the present are shown in fig. 6.79. The results of his 0.1% design pressure loss 4306 m^{-2} holes wall are well below the results of the 0.0027% wall but the 0.1% pressure loss 26,910 m^{-2} wall performs better than the present

wall at G values less than 0.3 kg/sm^2. This indicates that it is not just the design pressure loss that is important but also the number of holes or hole diameter and jet penetration is one method of including hole size and jet velocity in any correlation. At G > 0.3 kg/sm^2, the present work is much superior to the 0.1% 26910 m^{-2}.

Lamilloy has been reported in Chapter 5 to be a complex transpiration wall developed by Detroit Diesel Allison (8) of the USA. The upper and lower limits of the cooling effectiveness of Lamilloy are presented in fig. 6.79. The present results compare well with the upper limit. At all values of G below 0.84 kg/sm^2, Lamilloy upper limit is superior to 0.0027% wall while at G > 0.84 kg/sm^2, the 0.0027% wall performs better than the upper limit of the Lamilloy.

Transply (10) has also been discussed in Chapter 5 as another complex porous wall developed by Rolls-Royce for the Spey engine. The results of five different designs of the Transply are shown in fig. 6.79. Except for one type of the designs, the present results are much better than those of the Transply.

Bayley et al (9), using Rigidmesh for the Rolls-Royce 'Dart' engine combustor, investigated the cooling performance of a transpiration system. Their results are shown in fig. 6.79. The present results compare very well with these results.

It may be concluded that if a low pressure loss can be tolerated for a single wall combustor, the present design should be preferred over existing transpiration designs for its freedom from manufacturing complexity and blockages.

6.8.2 Comparison of the Performance of the 3% Design Pressure Loss DHFC Wall with Other Cooling Works

The present work's results on 3% design pressure loss walls of two types of holes' concentration and thicknesses are compared with results of various cooling design systems in fig. 6.80. Mkpadi's (7) data for DHFC 3% design pressure loss, after reprocessing, are compared in fig. 6.80 with the present work. The results of the 6.35 mm thick 17,222 m^{-2} wall of the present work compare very well with Mkpadi's work on the 26,910 m^{-2} holes wall of the same thickness, with only 4% improvement at high G values over the present work. The results of the 9688 m^{-2}, 6.35 mm thick wall show it does not perform as well as the above walls but at low G values the difference is less than 3%, for both high density holes' walls, rising to 10% at high G values. Both 17,222 m^{-2} and 9688 m^{-2}, 6.35 mm thick walls of the present work perform better than the 4306 m^{-2} holes wall (t = 6.35 and 3.2 mm) results. Rigid Mesh RM50A, upper limit of Lamilloy's results, and three designs of the Transply results are more superior to the results of the present work, but the 17,222 m^{-2} wall was superior to two designs of Transply and lower limits of Lamilloy at all G values. The 6.35 mm thick 9688 m^{-2} holes wall was only superior to one design of the Transply and to the lower limit of the Lamilloy at all G values less than 0.91 kg/sm^2.

In the 3.2 mm thickness range, the present work for the 17,222 m^{-2} holes wall was superior to the lower limit of Lamilloy at all G values, to all results of Mkpadi for a 4306 m^{-2} wall (both thicknesses) and to the 9688 m^{-2} of the present work. The 9688 m^{-2} holes (3.2 mm thick) was superior in performance to the results of Mkpadi for the 3.2 mm thick, 4306 m^{-2} holes wall at all G values,

to the 6.35 mm thickness at all G values below 1.2 kg/sm^2 and to the lower limit of the Lamilloy at all G values below 0.5 kg/sm^2. It may be concluded that for a 3% design pressure loss single wall combustor, the influence of the number of holes is most significant at high G and the optimum number will be discussed in the next section. Also fig. 6.80 shows that the influence of wall thickness was significant for the 3% design pressure loss option.

6.8.3 Empirical Graphic Correlation of the Influence of Holes' Density per Square Metre on the Wall Cooling Performance

The results of the cooling performance of the present investigation on walls of 6.35 mm thickness and 3% design pressure loss are presented in fig. 6.81 as a function of wall holes' density. Again the reprocessed results of Mkpadi (7) have been included for completeness. The results show that at G of up to a value of 0.3 kg/sm^2, there is no advantage in using higher density of holes than 9688 m^{-2} and hence this value of n is possibly the optimum density of holes at low G values. At higher G values, the density of holes becomes more important. However, the 3% walls were designed for low G values and their performance at high G was not important.

The results of the 3% design pressure loss, 3.3 mm thick wall cooling performance are presented in fig. 6.82. Mkpadi's reprocessed data for 4306 m^{-2} are also included. The results show that n = 9688 m^{-2} remains the optimum number at G values up to 0.2, but at higher G, n was more important than in fig. 6.81.

Figure 6.83 presents results of the wall cooling performance of 6.35 mm thickness and 0.1% design pressure loss. Mkpadi's reprocessed results are also included. The results show that at

all values of G, holes' density is important, although results at 17,222 m^{-2} are required to establish whether the optimum number lies in the present range of n.

The reasons for the influence of n on the overall cooling effectiveness are mainly two - internal and film cooling. Firstly, the internal hole surface area, A_s, for a fixed total hole area per unit surface area, A, is increased according to equation 6.7

$$A_s = (4\pi nA)^{0.5}\, t \qquad \ldots (6.7)$$

where n = holes' density

t = wall thickness.

Hence, the heat transfer will be increased in proportion to this area. This is offset somewhat by the lower hole Reynolds number (Re) and hence the holes' convective heat transfer coefficient for the same G. The back-side heat transfer also increases with n; again this is offset by lower Re. Thus the influence of n on the overall internal wall heat transfer is complex but may be summarized by comparing the temperature rise ratio as in fig. 6.84 or the non-dimensional temperature, H_D, as in fig. 6.85.

The influence of n on internal cooling is relatively small, but there was a much larger influence on the film cooling as shown by comparison of the H_{CF} value for the 3% design in fig. 6.86 and the 0.1% design in fig. 6.87. This was mainly due to the much reduced jet penetration, fig. 6.88, as n was increased. This was due to the strong influence of n, through the reduced hole diameter, D, on Y as shown by equation 5.66 in Chapter 5. A second factor influencing the improved film aerodynamics was the greater number of upstream holes at any fixed axial position as n was increased. This helped the axial film cooling to develop quickly.

The heat removed from the wall may be shown by the bulk heat transfer correlation deduced in Chapter 5, equation 5.C2.

$$N_u = \left[0.881\ Re^{0.476}\ \frac{X}{t} + 0.023\ Re^{0.8}\ R_{Nu}\right] Pr^{\frac{1}{3}} \quad \ldots (5.C2)$$

The holes' Re is given as (Chapter 3):

$$Re = \left(\frac{4}{\pi An}\right)^{0.5} \frac{G}{\mu} \quad \ldots (6.8A)$$

Combining equations 5.C2 and 6.8A gives

$$N_u = \left[0.881\left(\frac{4}{\pi An}\right)^{0.238}\left(\frac{G}{\mu}\right)^{0.476}\ \frac{X}{t} + 0.023\left(\frac{4}{\pi An}\right)^{0.4}\ \left(\frac{G}{\mu}\right)^{0.8}\ R_{Nu}\right] Pr^{\frac{1}{3}}$$

$$= \left[K_b\left(\frac{1}{An}\right)^{0.238}\left(\frac{X}{t}\right) + K_h\left(\frac{1}{An}\right)^{0.4}\right] Pr^{\frac{1}{3}} \quad \ldots (6.8B)$$

$$N_u = \frac{hD}{K} \quad \ldots (6.8C)$$

The rate of heat removed, Q, from the wall is given as

$$Q = \frac{K\,N_u}{D} \cdot A\,\Delta T \quad \ldots (6.8D)$$

where $A = n\pi tD$ = Total area of holes

K = Coolant thermal conductivity

ΔT = Temperature difference of coolant between inlet and outlet

t = Wall thickness

n = Total number of holes

h = Bulk convective heat transfer coefficient

Substituting into Q gives

$$Q = n\pi t\,K\,\Delta T\,N_u$$

$$= n\,K_c\,\Delta T\left[K_b\,X\left(\frac{1}{An}\right)^{0.238} + t\,K_h\left(\frac{1}{An}\right)^{0.4}\right] \quad \ldots (6.9)$$

where K_c, K_b and K_h are constants.

The holes' pitch is given, from Chapter 3, as

$$X = \frac{1}{n^{0.5}} \qquad \ldots (6.10)$$

The ratio of heat transfer from the back-side to that of the holes (Q_{cb}/Q_{ch}) can be correlated using equations 6.9 and 6.10 as

$$\frac{Q_{cb}}{Q_{ch}} = n K_c \Delta T \left[\frac{K_b}{t K_h} \cdot \frac{A^{0.162}}{n^{0.388}} + 1\right] \qquad \ldots (6.11)$$

Equation 6.11 shows that increasing the number of holes increases the heat removed from the wall. Figures 6.84 and 6.85 show that this is the case. Figure 6.85 shows that even though the wall temperature is low, the heat removed from the wall, with increasing n, is high and amounts to approximately 45% at low G for the 26,910 m^{-2} holes in comparison with the 4306 m^{-2} holes. This phenomenon indicates that as the holes' number is increased, the wall will approach a transpiration system.

6.8.4 Comparison of the Cooling Performance of the 0.1% Design Pressure Loss DHFC Wall with Other Cooling Works

Figure 6.89 shows the comparison between various holes density DHFC wall investigated in the present work with the work of Mkpadi (7), Lamilloy, Transply and Rigid Mesh RM50A (Chapter 4). The only works that were better than those of the present 26,910 m^{-2} holes geometry are the works on RM50A (Chapter 4), the upper limit of Lamilloy and two designs of Transply. The 9688 holes wall of the present work was superior in its cooling performance to the work of Mkpadi on the 0.1%, 4306 m^{-2} holes wall, as previously discussed.

6.8.5 Empirical Correlation of Cooling Effectiveness with Dimensionless Wall Thickness

Figure 6.90 shows the correlation of cooling effectiveness with dimensionless thickness for 9688 m^{-2} holes walls investigated in the present work. The correlation shows that walls smaller in thickness than the present 6.35 mm but thicker than the 3.32 mm wall, for the 3% design pressure loss, can be designed with considerable ease with nearly as high cooling effectiveness as that of the 6.35 mm wall.

Figure 6.91 shows the cooling effectiveness of 17,222 m^{-2} inline holes, 3% design pressure loss wall, as a function of t/D. The correlation shows the influence of t/D was relatively small.

The graphical correlation of 26,910 m^{-2} holes, 0.1% design pressure loss wall cooling performance with dimensionless thickness is presented in fig. 6.92. Data for the thickest wall (6.35 mm) of Mkpadi (7) has been reprocessed and included in the results for completeness. The graph shows that there is no significant influence of wall thickness, indicating a very low contribution of internal short hole cooling for low pressure loss walls.

6.8.6 Comparison and Pressure Effect on Cooling Effectiveness of 3% and 0.1% Design Pressure Loss Walls

Figure 6.93 shows the results of all DHFC walls investigated, at two thicknesses and 3% design pressure loss, in comparison with the work of Mkpadi, as a function of the actual measured hot pressure loss. Figure 6.93 clearly shows that all the test walls were designed for 3% $\Delta P/P$ at low G. Their performance at high G is not of practical relevance as $\Delta P/P$ is too high. At all pressure losses ($\Delta P/P\%$) greater than 3%, results show the 26,910 m^{-2} holes

wall performs better than the present work, but has a poor performance in comparison with both the 17,222 m^{-2} and 9688 m^{-2} walls at all $\Delta P/P\%$ values less than 3. Except for $\Delta P/P\%$ greater than 8 and G values greater than 0.85 kg/sm^2 for the 6.35 mm thick, 4306 m^{-2} wall of Ref. 7, the 3.3 mm thick, 9688 m^{-2} wall of the present work is superior to the 4306 m^{-2} wall of Ref. 7.

Figure 6.94 shows the wall performance results of 0.1% design pressure loss as a function of $\Delta P/P\%$ and G values. The 26,910 m^{-2}, 6.35 mm thick wall of Ref. 7 performs better at all $\Delta P/P\%$ values except for the present work on 26,910 m^{-2}, 0.69 mm thick wall. The results of Ref. 7 for 4306 m^{-2} holes, 6.35 mm thick wall performance are poor when compared with the present results at all values of $\Delta P/P\%$ greater than 0.1 and G values greater than 0.32 kg/sm^2. Figure 6.94 shows that at high G values these low design pressure loss walls have a practical low pressure loss. Hence, it would be feasible to use these designs, still with an impingement wall, at G values near unity, which is the level relevant to current coolant usage. Thus at conventional coolant flow rate, fig. 6.94 shows that cooling effectiveness in the 0.8-0.9 region would easily be achieved. These figures are extremely difficult to match with the best of current film cooling techniques.

6.9 THE 9688 m^{-2} INCLINED STAGGERED HOLES, 3% DESIGN PRESSURE LOSS, DHFC WALL

This wall geometry has its holes inclined to the direction of mainstream flow at 30° but could be turned round such that the holes' inclination to the direction of mainstream flow is 150°. Both the above positions were investigated. Inclined holes have

dominated the literature on film cooling due to their extensive use in turbine blade cooling, where 30° is a typical angle of inclination. Very little previous work has been published for large arrays of inclined holes, as most of the work has been for single or double rows of inclined holes for turbine blade applications. It was the intention in the present work to investigate a full coverage inclined hole design for the same hole configuration as the 90° hole direction used in the rest of the present work. For a 3% design pressure loss wall, it has been shown that an n of 9688 m^{-2} was the optimum number of holes. This value of n was therefore chosen to investigate the improvement in cooling effectiveness that could be achieved by using 30° inclined holes. The test wall was manufactured by laser drilling, a technique that makes the use of full coverage inclined holes feasible at a reasonable cost. The thickness was 3.34 mm, but this gave a hole length of 6.69 mm due to the 30° inclination.

6.9.1 Thermal Boundary Layer Profile

For the wall positioned at 30° holes inclination to the direction of mainstream flow, figures 6.95, 6.96 and 6.97 show the thermal boundary layer profiles at locations 25 mm, 76 mm and 127 mm from the wall's leading edge over a range of coolant mass flow rates G. The boundary layer is quite thin and shows an increasing axial thickness downstream of the wall's leading edge. At the wall region the existence of a flat profile for all the three traverse locations is an indication of film attachment to the wall and points to an initial good adiabatic cooling effectiveness. The results on fig. 6.95 indicate that there is entrainment and recirculation of hot gas in the wall region at high G values and

this can only mean poor cooling effectiveness and high convective heat transfer at the leading edge region. However, further downstream these disappear, indicating a good final adiabatic film cooling effectiveness. The boundary layer thickness is comparable with the low pressure loss designs discussed earlier.

For the wall positioned at 150° to the mainstream flow direction, figs. 6.98 to 6.100 show the results of the thermal boundary layer at the three traverse locations, as in the previous case. At low G values the profiles of the boundary layer are similar to those of the 30° case, but at high G values the boundary layer thickness is quite large and much greater. In the wall region, at low G values, the temperature of the gas is low while at the same region for the 30° position the gas temperature is higher. At G values above 0.58, the gas temperature adjacent to the wall increases indicating a change in the aerodynamics, also reflected in the increased thickness. Low gas temperature at the wall was found at the leading edge region, for high G values, while at the trailing edge this temperature was high. Compared with the 30° position at high G values, the temperature of the gas at the wall was the reverse of the 150° one. This means that at low G values the adiabatic cooling effectiveness values for the 150° position will be higher than those of the 30°, while at high G values the adiabatic effectiveness will have an axial dependence which are of opposite trends for the two angles.

The prominent jet stirring entrainment characteristics displayed at the leading edge of the 30° position do not occur in the 150° position but show up at the trailing edge. It is considered that the improved film aerodynamics at the leading edge

and at low G values were due to the impingement action of the oncoming mainstream flow which forced the cooling jet to spread sidewards and thus to form a more uniform cooling layer between the jets. At high G values the jets separate and are reversed backward rather than spread sidewards, thus giving a deterioration in film performance. The deterioration of the film aerodynamics with axial distance for the 150° injection was considered to be due to the reduction of the approach flow in the wall region spreading the jets sidewards.

6.9.2 η and η_{ad} - 9688 m^{-2} Inclined Staggered Holes, 3% Design Pressure Loss DHFC Wall

The overall and adiabatic cooling effectiveness at two thermal stations are shown in fig. 6.101 as a function of G and in fig. 6.102 at three G values as a function of axial distance from the wall leading edge, for both 30° and 150° positions. In fig. 6.101, the results show that the cooling effectiveness of the 150° position at thermal station one is superior to that of the 30° but the 30° position shows a dominant superiority at high G values as expected from the boundary layer results.

The axial development of cooling effectiveness of the 150° injection in fig. 6.102 was superior to that of the 30° for all the three G values up to 75 mm and throughout the axial length of the wall at G values of 0.36 kg/sm^2. The 30° position however performs better at beyond 88 mm at a G value of 0.875 kg/sm^2. It is in this G region that the boundary layer profile showed the 150° jets had separated from the wall.

Figure 6.101 shows the overall and adiabatic cooling effectiveness of the 30° and 150° positions at both leading and

trailing edge regions of the wall as a function of G. The adiabatic effectiveness at the trailing edge for 30° injection was superior to that of the 150° position. At the leading edge it was the 150° position adiabatic effectiveness that was superior to that of the 30° and at high G values performs better than the 30° trailing edge one, as well as being very close to its own overall cooling effectiveness. In the low G values region, the adiabatic effectiveness of the 30° at the trailing edge is better than that of 150° but at the leading edge it is the opposite.

Figure 6.102 also compares the axial adiabatic effectiveness of the two positions as well as with their overall cooling effectiveness. The results of the adiabatic effectiveness for both positions show that for the two G values of 0.17 and 0.36 kg/sm^2, the 150° position performs better. At high G values the 30° injection adiabatic effectiveness is, in the initial region, much worse than for 150° but at the trailing edge is much higher. This change was also reflected in the boundary layer traverse.

6.9.3 Heat Transfer at the Back and Inside the Wall of the 9688 m^{-2} Inclined Staggered Holes, 3% Design Pressure Loss DHFC Wall

It will be assumed in this section that the internal wall heat transfer was unaffected by the hole angle, i.e. it behaved as a 90° hole of the same length. This is unlikely to be a valid assumption, but reliable overall internal wall heat transfer data are not available. The only investigation for internal wall cooling is the data of Kumada et al (11), who provided a correlation for the back-side heat transfer for 30° inclined holes. This may be shown to be a factor of four lower than the correlation of Sparrow for 90° holes, used in the present work. The reason for the reduced heat

transfer may be associated with a change in the hole entry aerodynamics with inclined holes. These are more likely to have a biased entry profile, with most of the flow entering from the leading edge hole lip so that only part of the hole circumference is exposed to high velocity coolant flow. Changes in the hole entry aerodynamics are also likely to influence the internal wall cooling. It is recommended that future work should investigate this heat transfer geometry so that the current heat balance model can be improved.

Figure 6.103 shows the results of the heat transfer at the back-side and inside the holes at 30° and 150° positions as a function of G. Hole direction should have no influence as there is no way of introducing this into the heat balance. The results indicate that at low G values the back heat transfer is significant while at high G values the holes' heat transfer comes into prominence. It may be concluded that the heat removed from the wall is not a contributing factor to the difference in cooling effectiveness displayed by the wall in the two positions investigated.

As discussed in section 6.4, the result of T_{RAT} is shown in fig. 6.104 as a function of G. The results show that the T_{RAT} for both walls' positions is the same at low G values and in general very similar.

6.9.4 Film Heat Transfer Coefficient H_{CF} of 9688 m^{-2} Inclined Staggered Holes, 3% Design Pressure Loss DHFC Wall

The results of the film heat transfer coefficient for the two positions are shown in fig. 6.105 for two thermal stations as

a function of G. The results show that for the 150° position, the film heat transfer at thermal station one, for low values of G up to 0.35 kg/sm^2, rises, but beyond this value of G there is a decrease in the value of H_{CF} up to a G value of 1.0 kg/sm^2 when it starts to rise again. However, in the case of the 30° position, at thermal station one, the results show that H_{CF} increases for all values of G. These agree with the cooling effectiveness at this thermal station, fig. 6.101, where the 150°'s effectiveness case is better than those of the 30° position. At thermal station five, the results show a slow development of H_{CF} for both positions up to G value of 0.4 kg/sm^2, but at all values of G greater than 0.4, there is a very steep rise in H_{CF} for position 150° while in the case of 30° position, a gradual rise in H_{CF} is shown. These indicate that the film at this station will be poor due to coolant jet separation as previously discussed and hence the poor effectiveness at high G values for position 150° but better for position 30°. This is confirmed to be the case in figures 6.101 and 6.102.

Figure 6.106 shows the axial profiles of H_{CF} for the two wall positions at three G values. At a high G value of 0.84 kg/sm^2, the results show a sharp axial increase for the 150° injection, whereas H_{CF} drops with axial distance for wall position 30°. At a G value of 0.36 kg/sm^2, the results indicate higher H_{CF} with axial distance for wall position 30° than for 150°, while for G equals 0.17, the results alternate. This indicates a high axial cooling effectiveness where H_{CF} is low and poor effectiveness where H_{CF} is high. This is shown to be the case if figs. 6.101 and 6.102.

6.9.5 Blowing Rate, M, Effect on Cooling Effectiveness and Film Heat Transfer Coefficient

For the two wall positions the results of H_{CF} and η with η_{ad} are shown in figures 6.107 and 6.108 respectively. The results are similar to those of fig. 6.105. At a blowing rate of just over 3.0, these results show that for 150° injection, a sharp change in the boundary layer aerodynamics occurs, which has already been discussed.

6.9.6 Dimensionless Temperature, H_D, and Jets' Penetration, Y

The results of H_D for the two wall positions are shown in fig. 6.109 as a function of G. It indicates that for both positions the approach to a transpiration state is the same, slightly better than for 9688 m^{-2}, 90° holes, 3% pressure loss but better when compared with 0.1% pressure loss, fig. 6.73.

The results of Y are shown in fig. 6.110 assuming that the jet velocity is the component of the hole velocity normal to the hole angle and not the jet outlet velocity. The low penetration at low G is the reason for the good film performance here.

6.9.7 Comparison of 9688 m^{-2} Inclined Staggered Holes, 3.343 mm Thick, 3% Design Pressure Loss Wall with Walls of the Same Holes' Density

The length of the holes of the inclined staggered holes geometry is 6.69 mm and those geometries with nearly the same holes' length in this design family are the 6.4 mm and 6.5 mm thick walls of 3% and 0.1% respectively. These walls have been chosen because with the same holes' length, the internal wall heat transfer to coolant will be similar and the differences in cooling effectiveness

will be mainly due to film cooling boundary layer aerodynamic effects.

6.9.7A Comparison of η and η_a of three walls

The results of the overall cooling effectiveness for the three walls are compared in fig. 6.111. This shows that the inclined hole results are superior to the equivalent 3% pressure loss design with 90° holes at all G values below 0.7 kg/sm^2. However, the low 0.1% pressure loss design matches the performance of the inclined wall at low G values but it performs better at high values of G.

Figure 6.112 shows the comparison of the walls' adiabatic effectiveness for various values of G. Again at low G values the inclined wall performs better than both 90° holes walls and remains superior to the performance of the 3%, 90° holes wall at all values of G. The η_{ad} for the 0.1% wall is the best of all the designs at high G.

It may be concluded that at low G values the present 3% design pressure loss inclined hole results give acceptable cooling effectiveness results and could provide a viable gas turbine transitional duct design for a 3% design pressure loss requirement. The 0.1% pressure loss 90° system matches the performance of the inclined system for much lower manufacturing cost.

6.9.7B Comparison of H_{CF} of three walls

The results of the film heat transfer coefficient, H_{CF}, for the three walls are presented in fig. 6.113. The figure shows that the 90° holes, 3% pressure loss wall H_{CF} is highest of the three walls, followed by the two inclined wall positions, while

the 0.1% design has least value for H_{CF}, for all values of G indicating it has the best film aerodynamics.

Since the results of the inclined holes wall at the two positions of investigation show superiority in cooling effectiveness to that of the 90°, 3% design pressure loss, 6.35 mm thick wall, and the latter's performance has been shown to be better than those of the 3.32 mm thick wall, figs. 6.30 and 6.31, it may be concluded that the inclined staggered holes, 3% design pressure loss, 3.3 mm thick wall, has cooling performance far superior to that of the 90° holes, 3% design pressure loss, 3.3 mm thick wall. If a 3% design pressure single wall is required, and a combined impingement/effusion system is not practical, then it is clear that inclined hole systems are preferable. However, the present finding that upstream injection is superior to downstream at low G is new and has not been realised by any other investigators.

6.10 REFERENCES

1. Moffat, R.J., 'Temperature measurement in solids', ISA Paper, 68-514, 1968.

2. Andrews, G.E., Asere, A.A., and Mkpadi, M.C., 'Transpiration cooling: Contribution of film cooling to the overall cooling effectiveness'. To be presented at the International Gas Turbine Conference, Dusseldorf, ASME, 1986.

3. Taylor, J.R., 'An Introduction to Error Analysis - The Study of Uncertainties in Physical Measurements', University Science Books, 1982.

4. Incropera, F.P., and Dewitt, D.P., 'Fundamentals of Heat Transfer', John Wiley & Sons, New York, 1981.

5. Hennecke, D.K., 'Heat transfer problems in aero-engines', Heat and Mass Transfer in Rotating Machinery, Edited by D.E. Metzger and N.H. Afgan, Hemisphere Pub. Corp., pp. 353-379, 1984.

6. Andrews, G.E., 'Discussion on "Double rows of film cooling holes"', J. Eng. Power, Vol. 105, p. 177, 1983.

7. Mkpadi, M.C., 'Full coverage effusion cooling of gas turbine combustion chamber', Ph.D. thesis, Dept. of Fuel and Energy, University of Leeds, 1982.

8. Nealy, D.A., and Reider, S.B., 'Evaluation of laminated porous wall materials for combustor liner cooling', ASME - Paper No. 79-GT-100.

9. Bayley, F.J., Cornforth, J.W., and Turner, A.B., 'Experiments on a transpiration cooled combustion chamber', Proc.I.Mech., Vol. 187, pp. 158-169, 1973.

10. Wassell, A.B., and Bhangu, J.K., 'The development and application of improved combustor wall cooling techniques', ASME - Paper No. 80-GT-66.

11. Kumada, M., Hirata, M., and Kasagi, N., 'Studies of full-coverage film cooling. Part 2: Measurement of local heat transfer coefficient', ASME - Paper No. 81-GT-38.

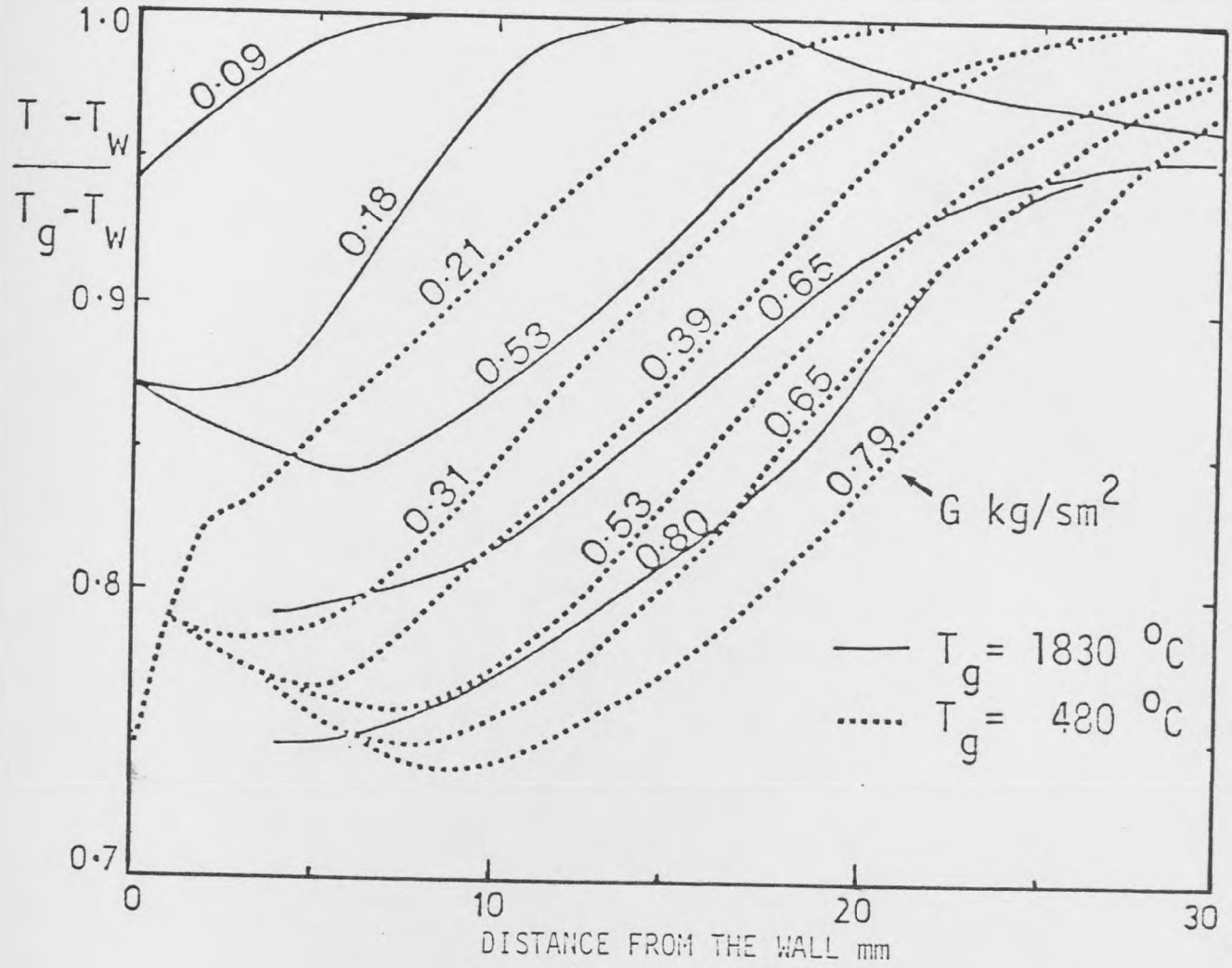

FIG.(6.1): NON DIMENSIONAL TEMPERATURE PROFILES AT TWO GAS TEMPERATURES.

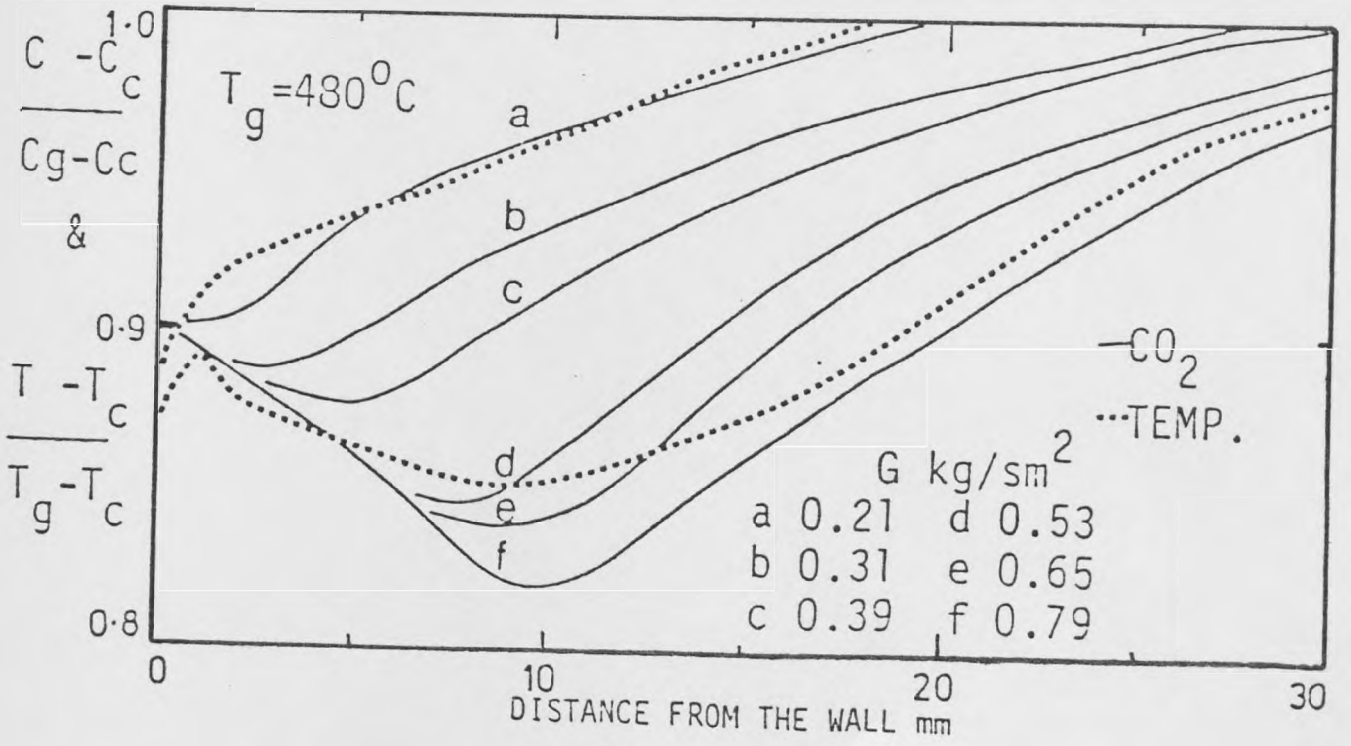

FIG.(6.2): NON DIMENSIONAL CO_2 AND TEMPERATURE PROFILES.

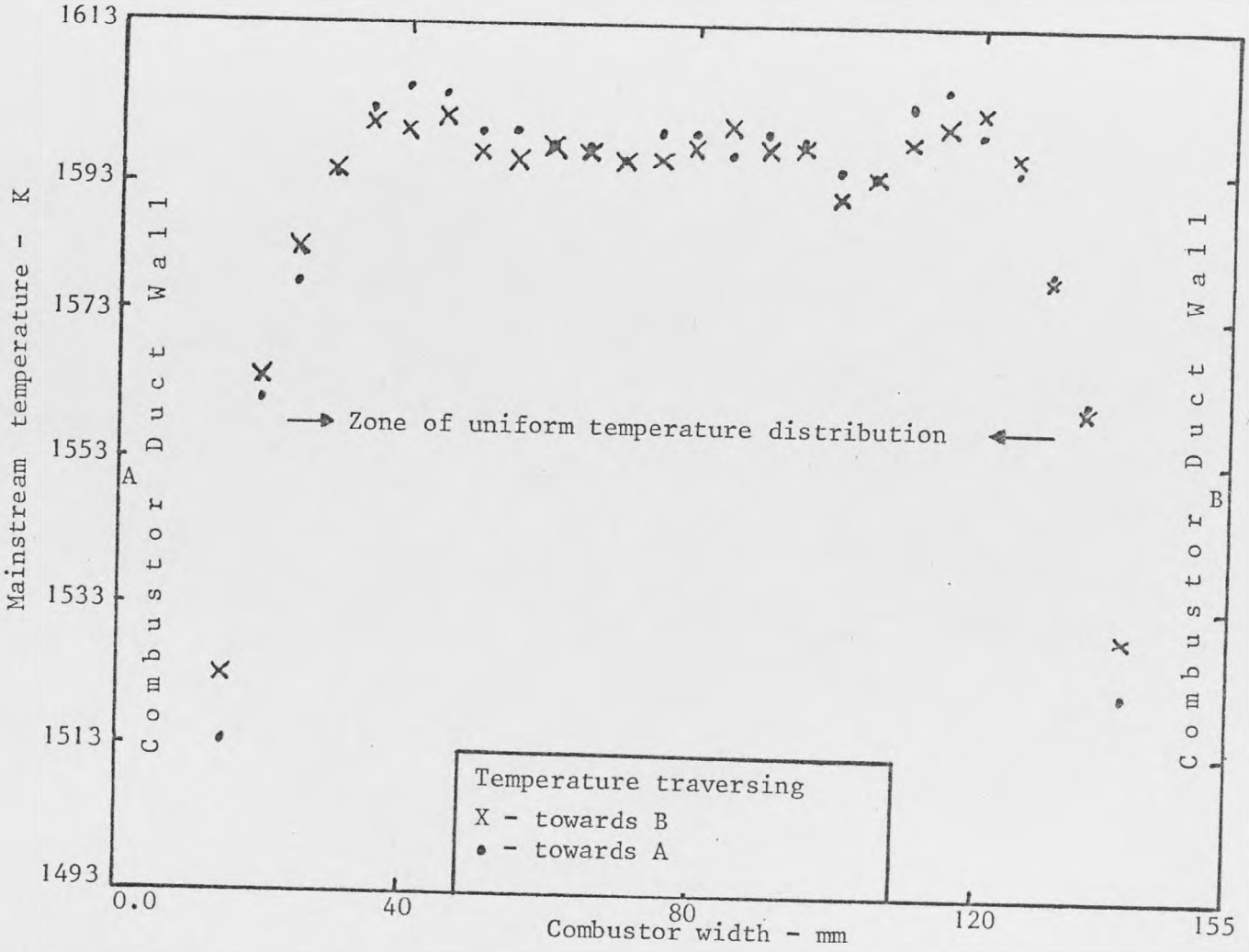

Fig. 6.3: Combustor mainstream temperature distribution profile

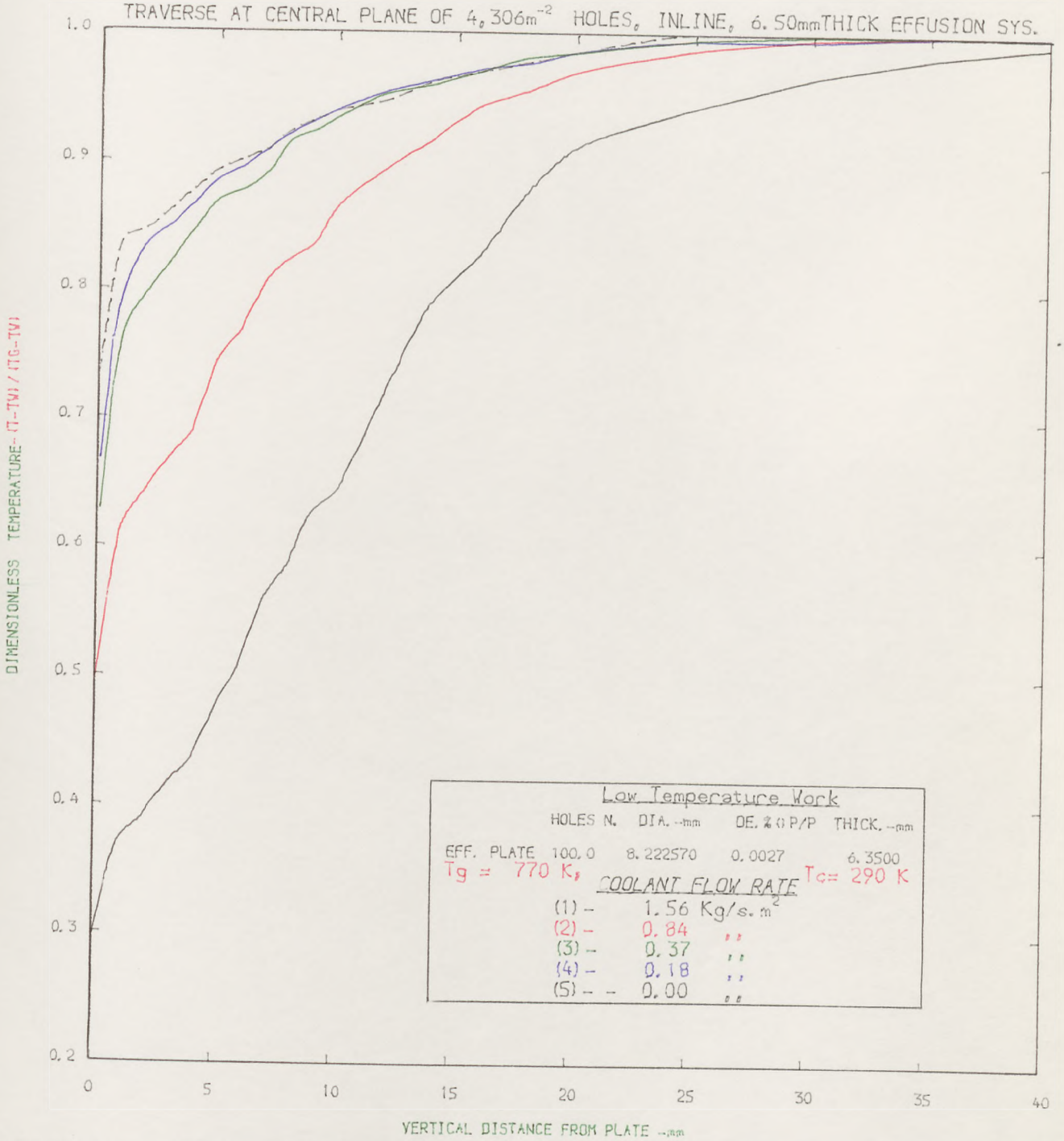

FIG. (6.4) : THERMAL BOUNDARY LAYER DEVELOPMENT AT CENTRAL PLANE OF WALL.

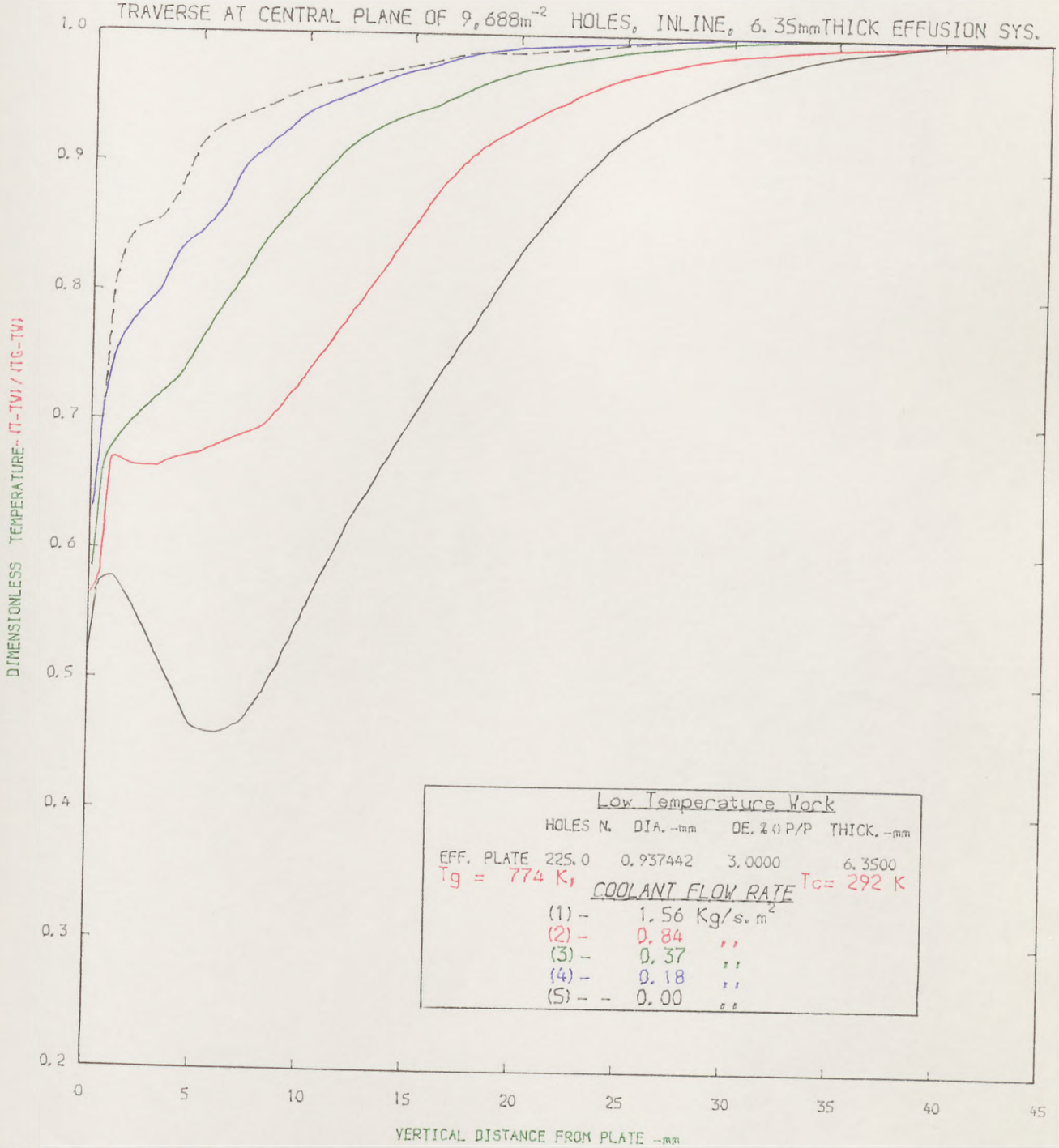

FIG. (6.5) : THERMAL BOUNDARY LAYER DEVELOPMENT AT CENTRAL PLANE OF WALL.

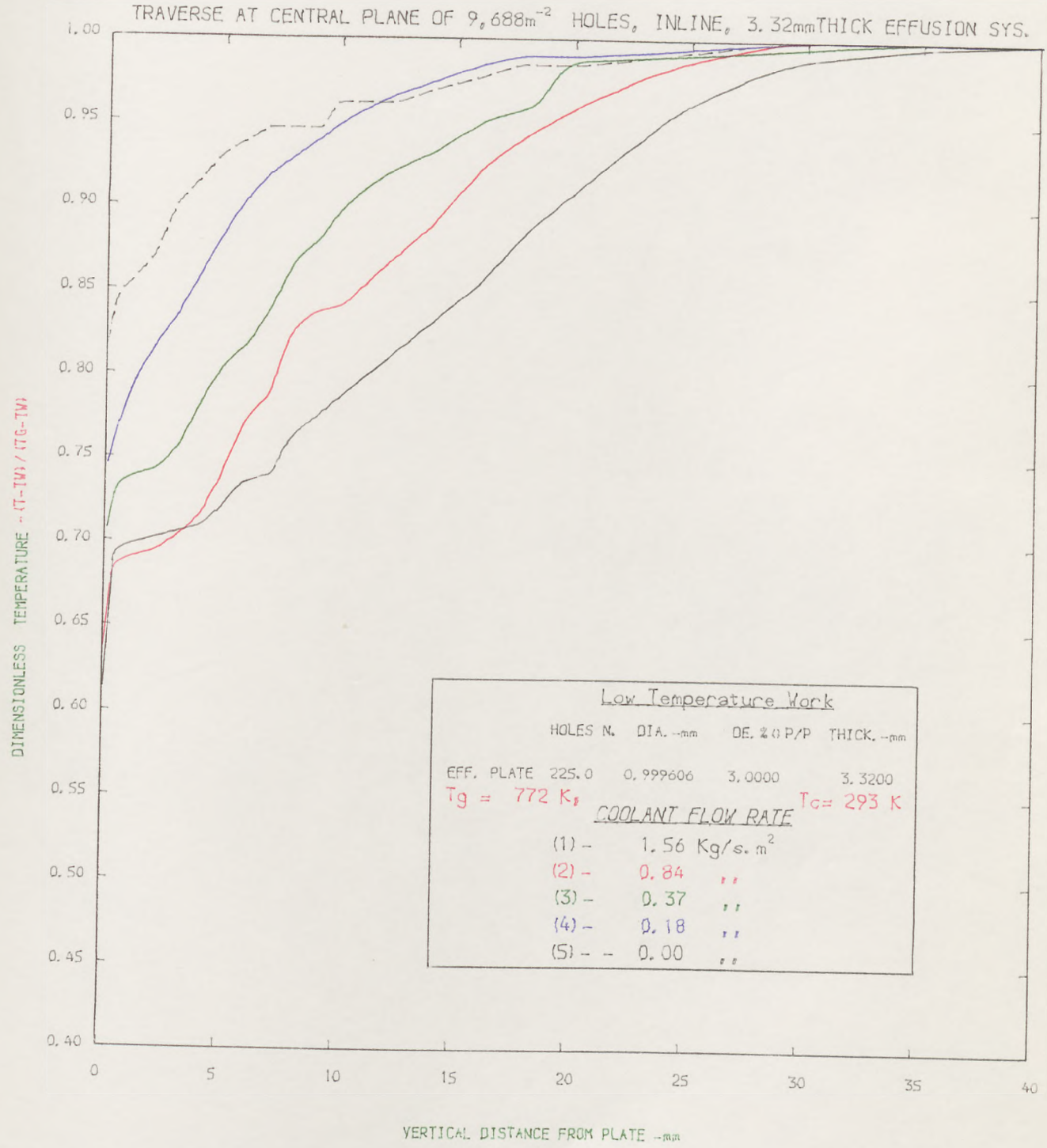

FIG. (6.6) : THERMAL BOUNDARY LAYER DEVELOPMENT AT CENTRAL PLANE OF WALL.

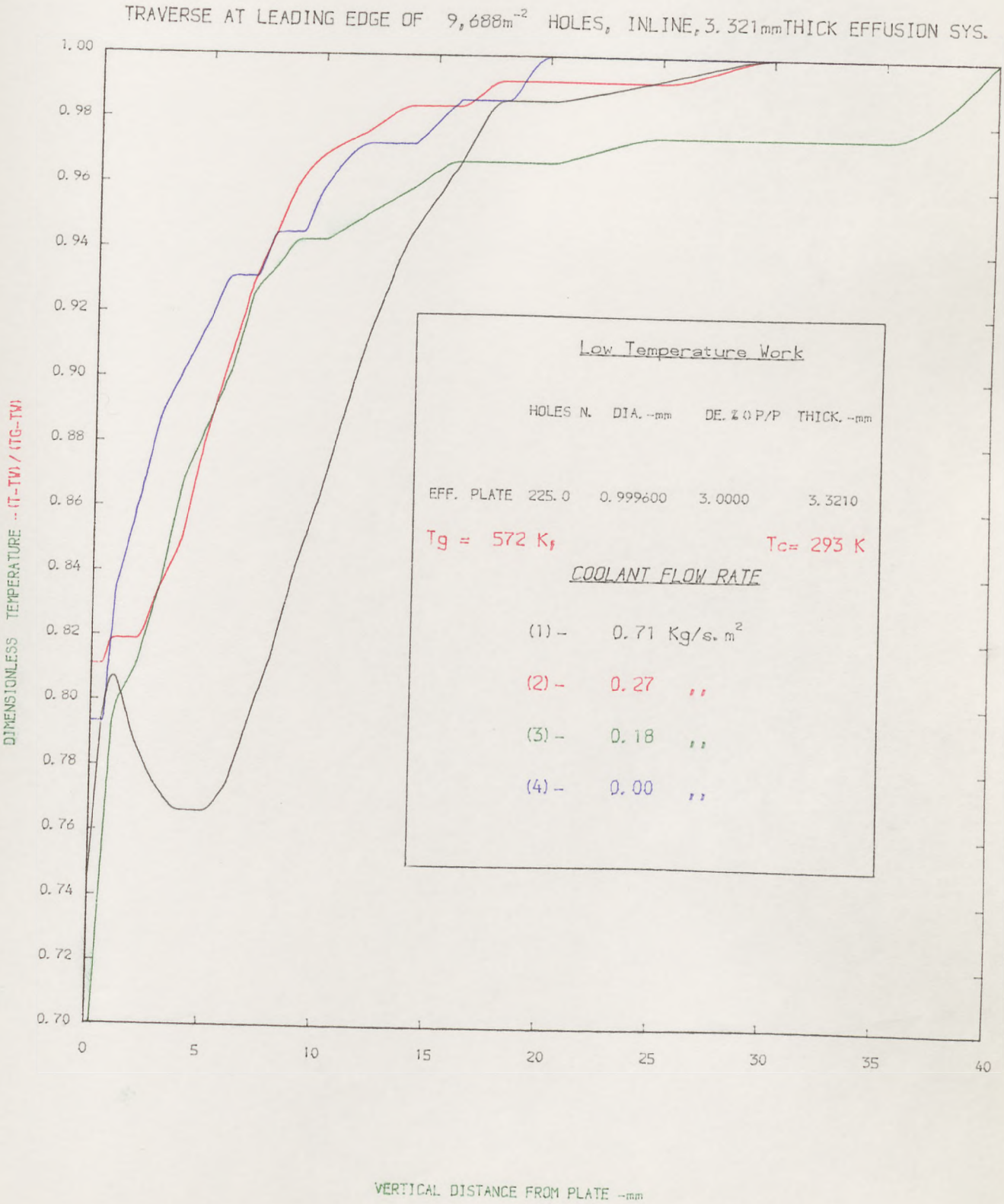

FIG. (6.7). THERMAL BOUNDARY LAYER DEVELOPMENT NEAR LEADING EDGE OF WALL.

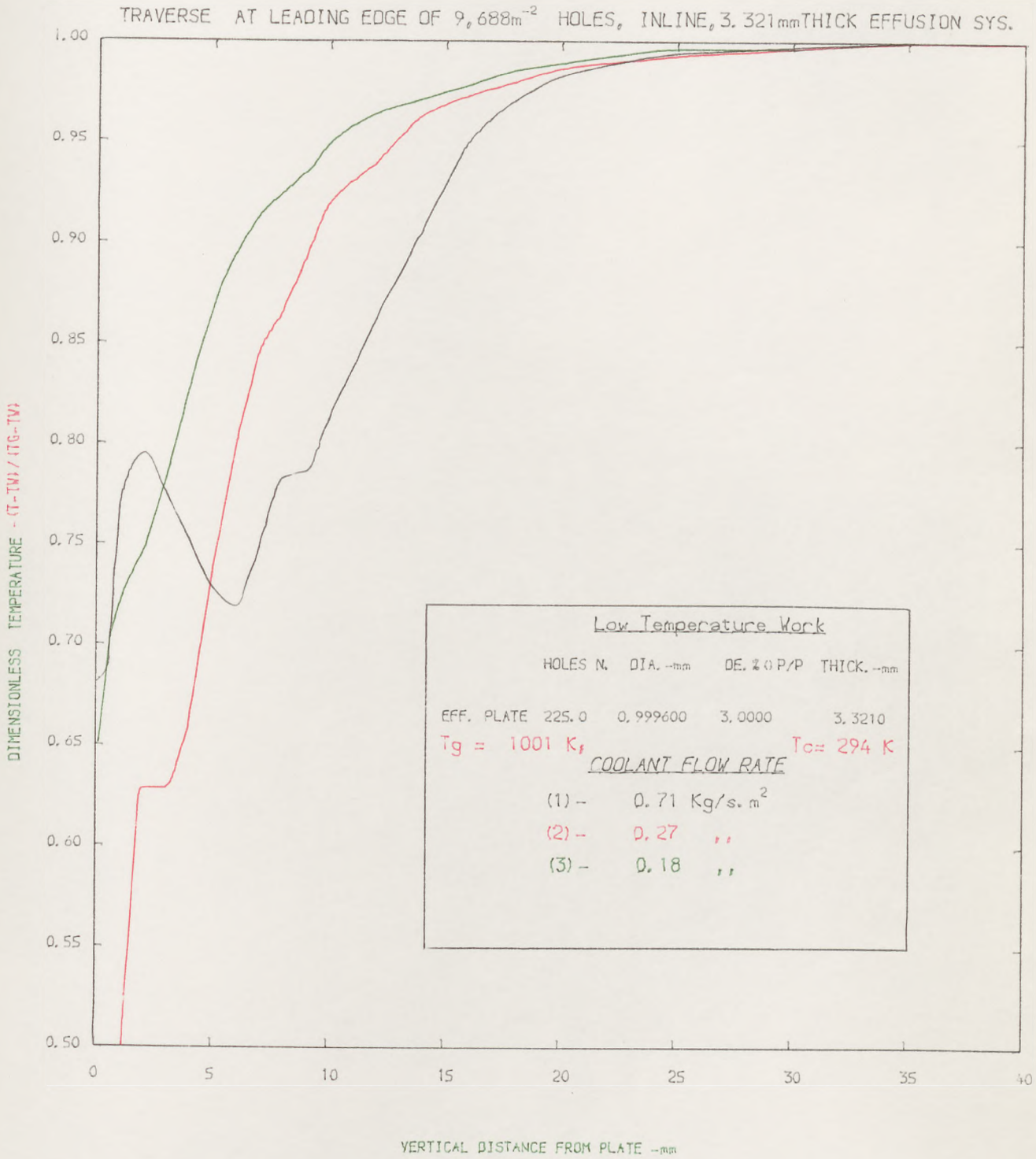

FIG. (6.8) : THERMAL BOUNDARY LAYER DEVELOPMENT NEAR LEADING EDGE OF WALL.

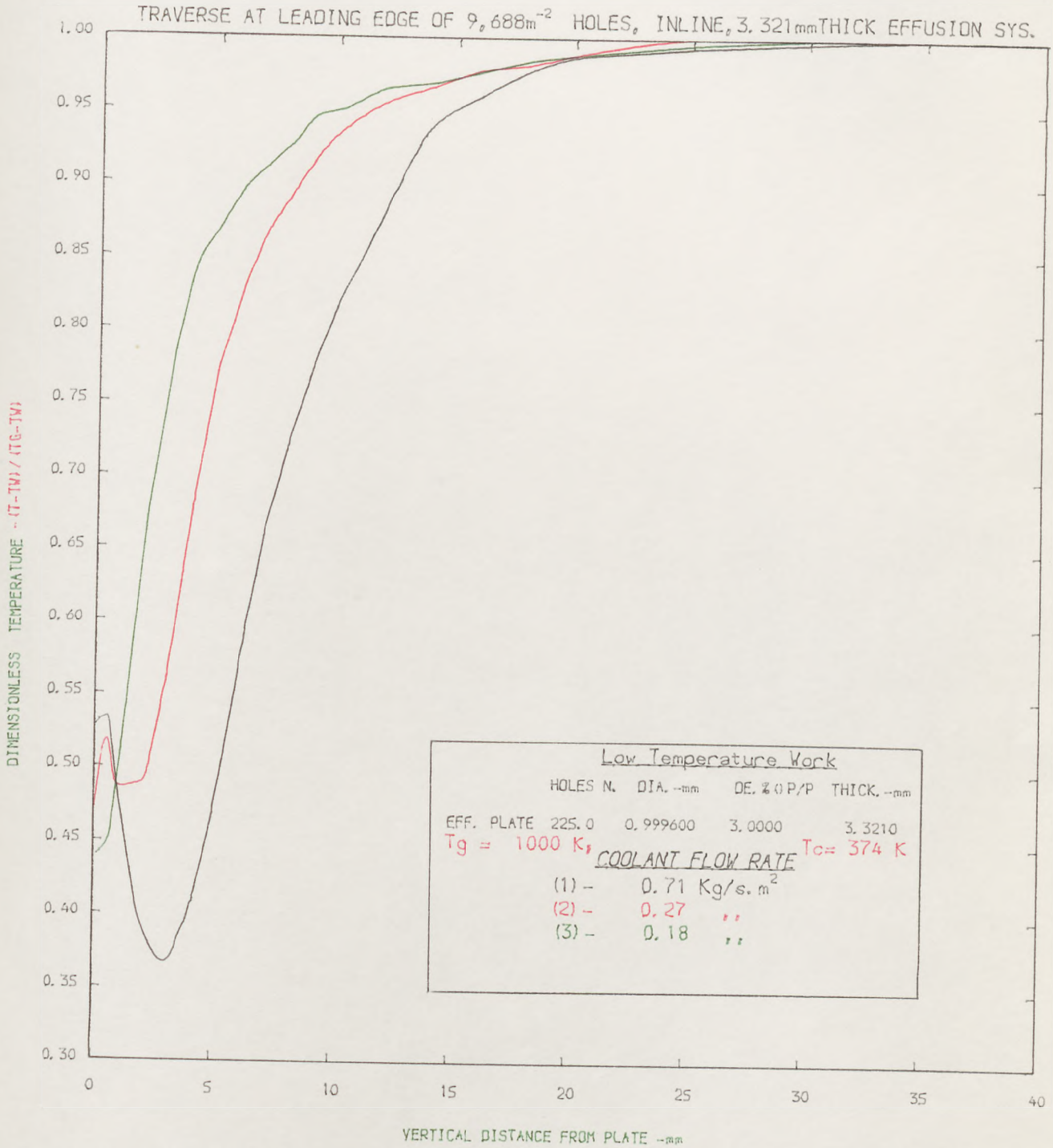

FIG. (6.9) : THERMAL BOUNDARY LAYER DEVELOPMENT NEAR LEADING EDGE OF WALL.

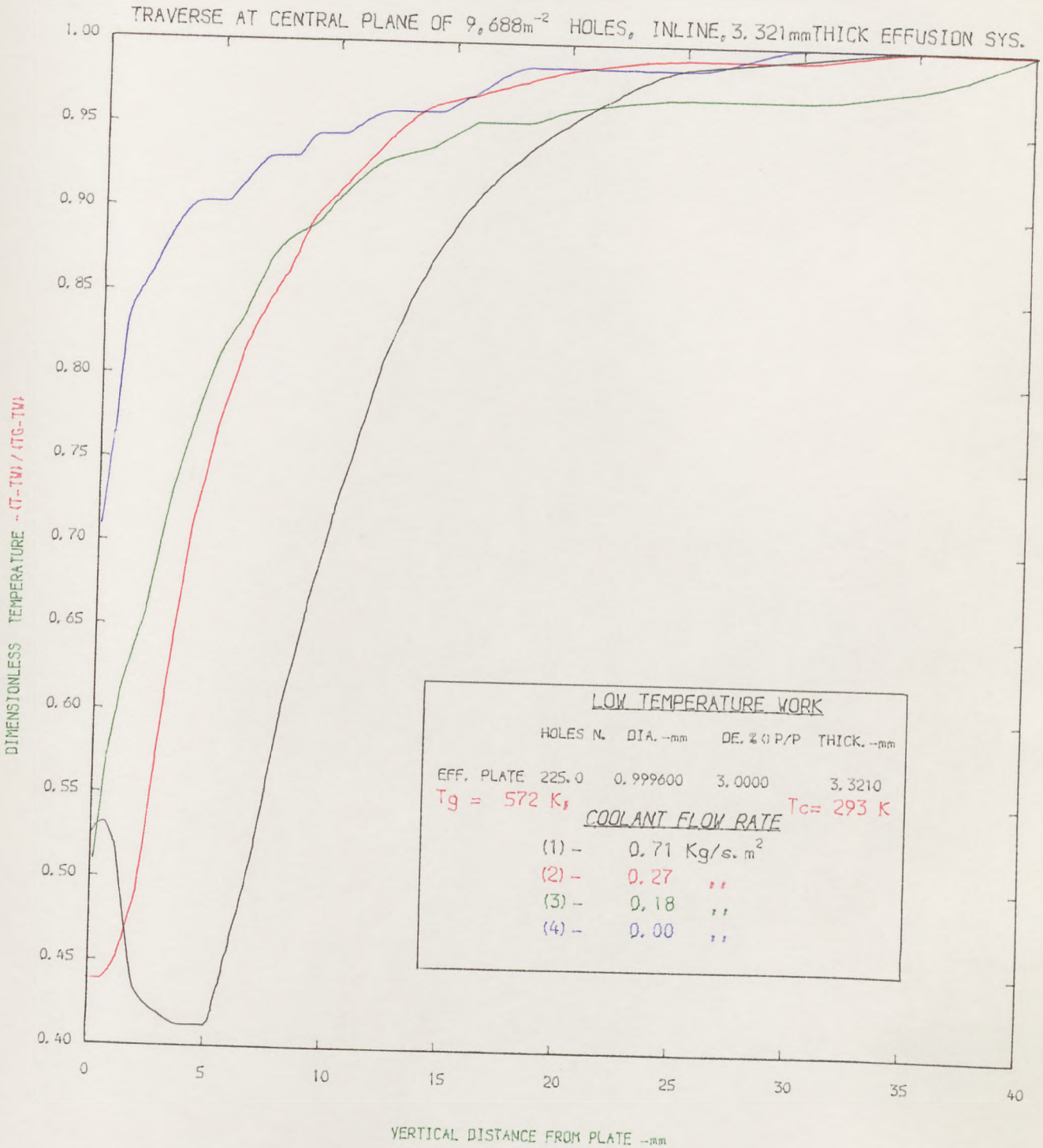

FIG. (6.10) : THERMAL BOUNDARY LAYER DEVELOPMENT AT CENTRAL PLANE OF WALL.

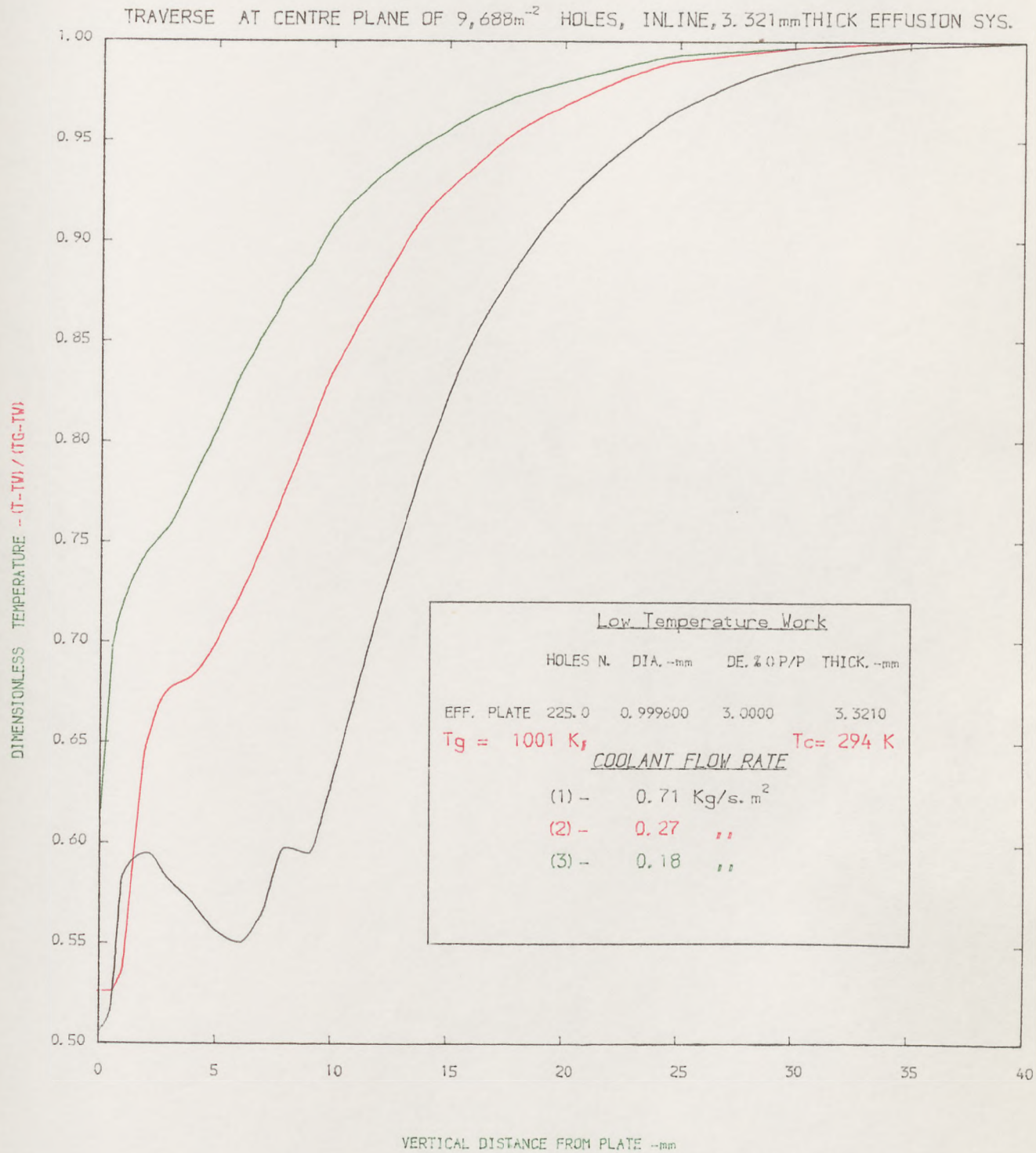

FIG. (6.11). THERMAL BOUNDARY LAYER DEVELOPMENT AT CENTRAL PLANE OF WALL.

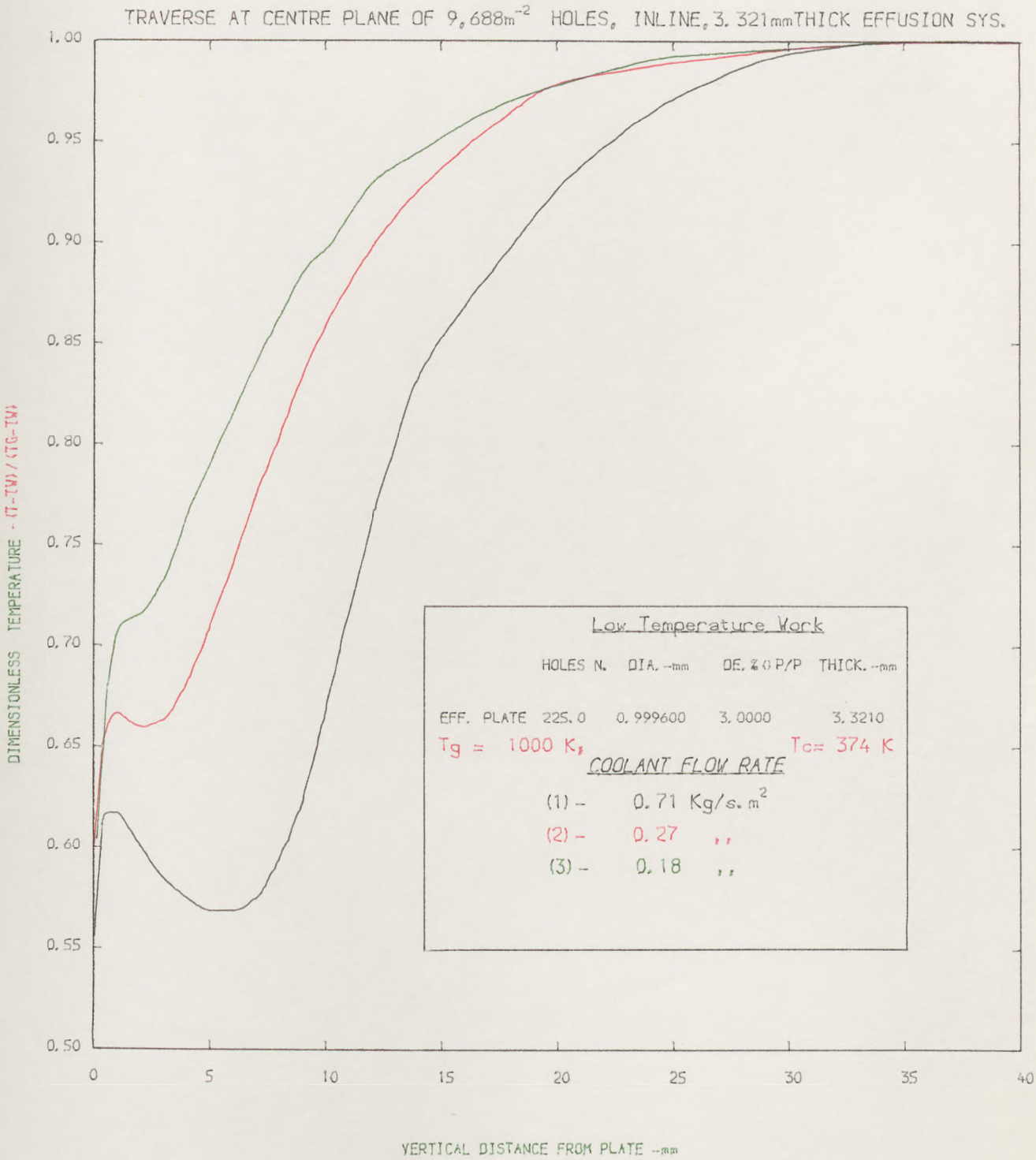

FIG. (6.12) : THERMAL BOUNDARY LAYER DEVELOPMENT AT CENTRAL PLANE OF WALL.

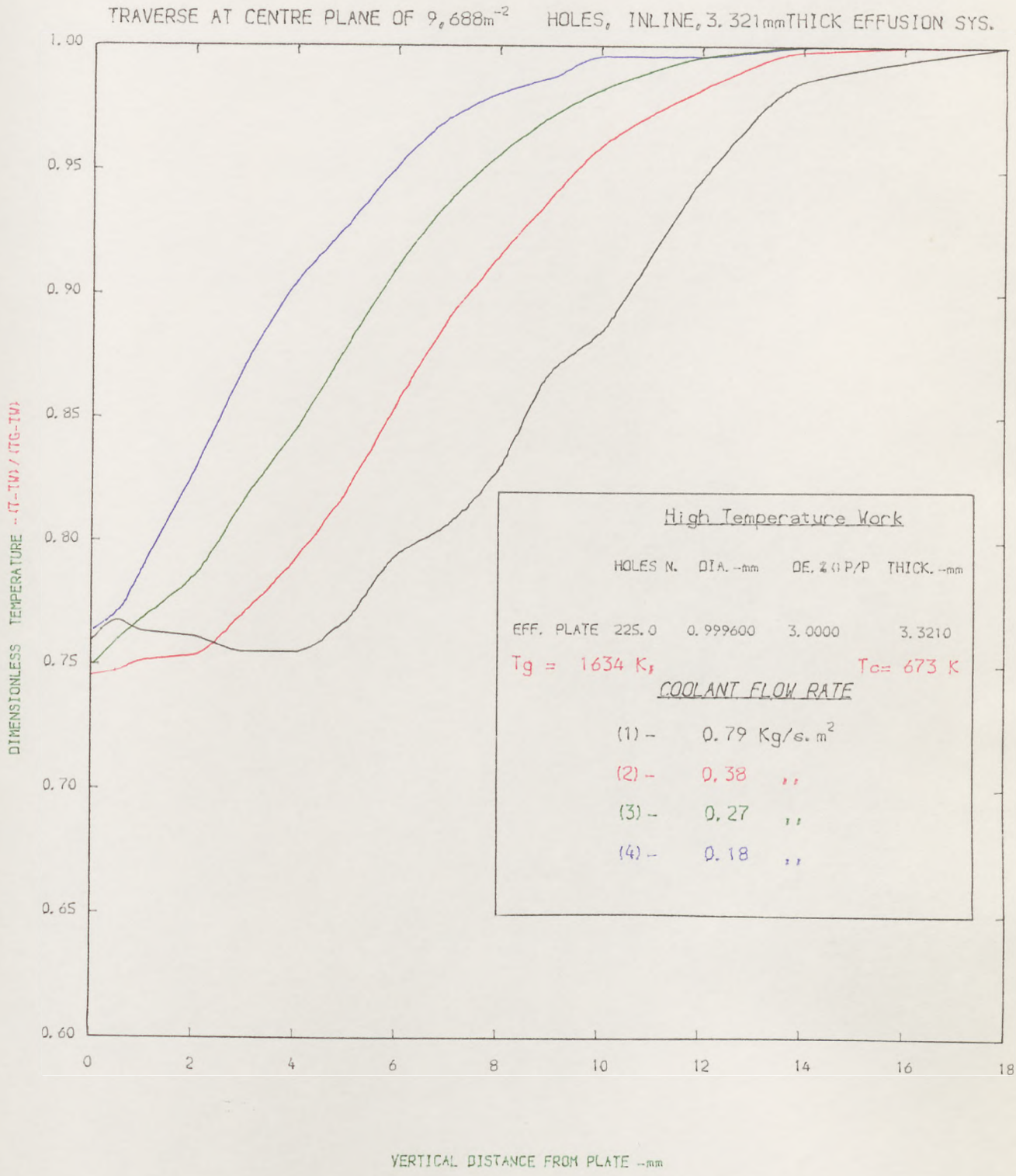

FIG. (6.13). THERMAL BOUNDARY LAYER DEVELOPMENT AT CENTRAL PLANE OF WALL.

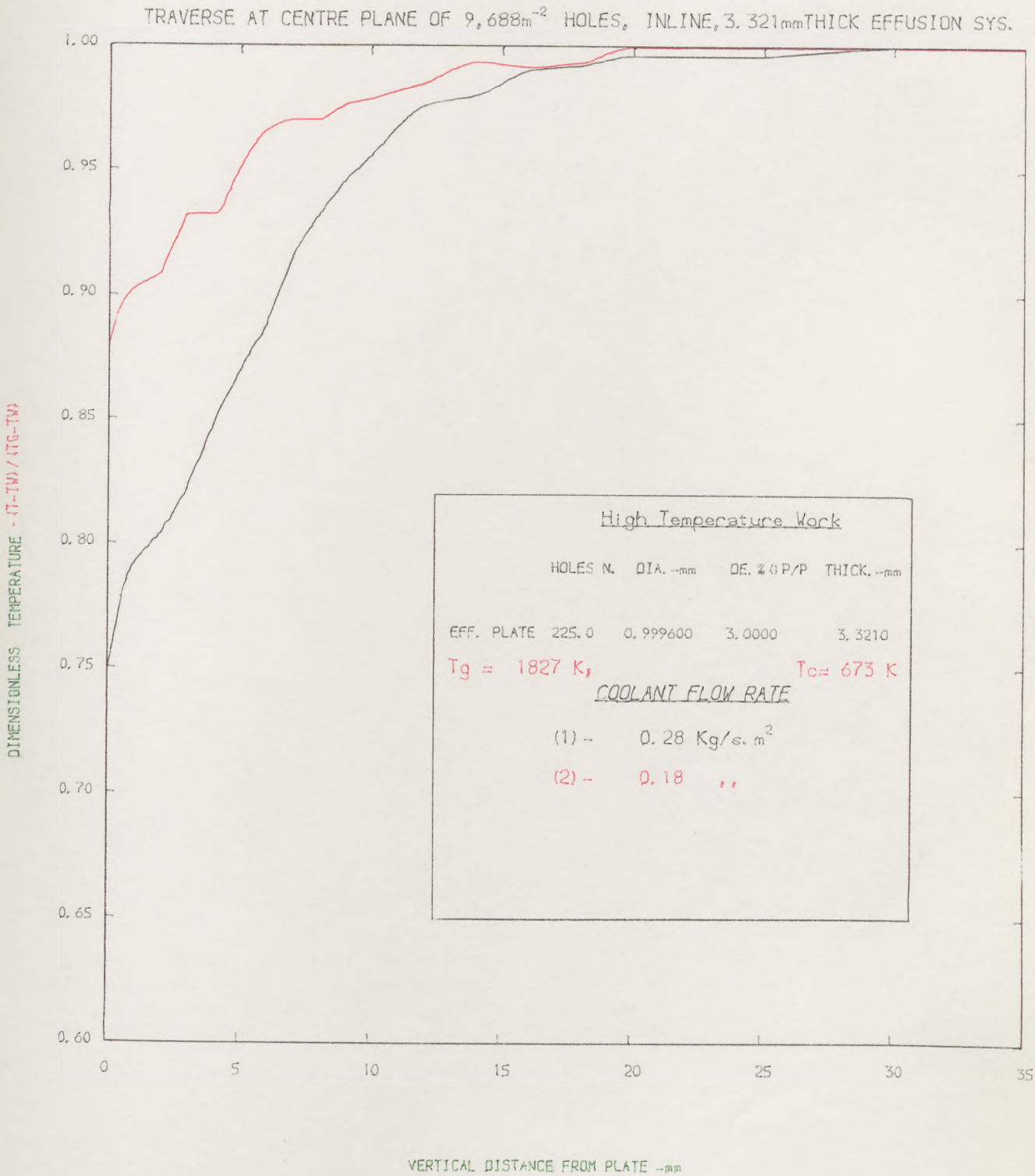

FIG. (6.14) : THERMAL BOUNDARY LAYER DEVELOPMENT AT CENTRAL PLANE OF WALL.

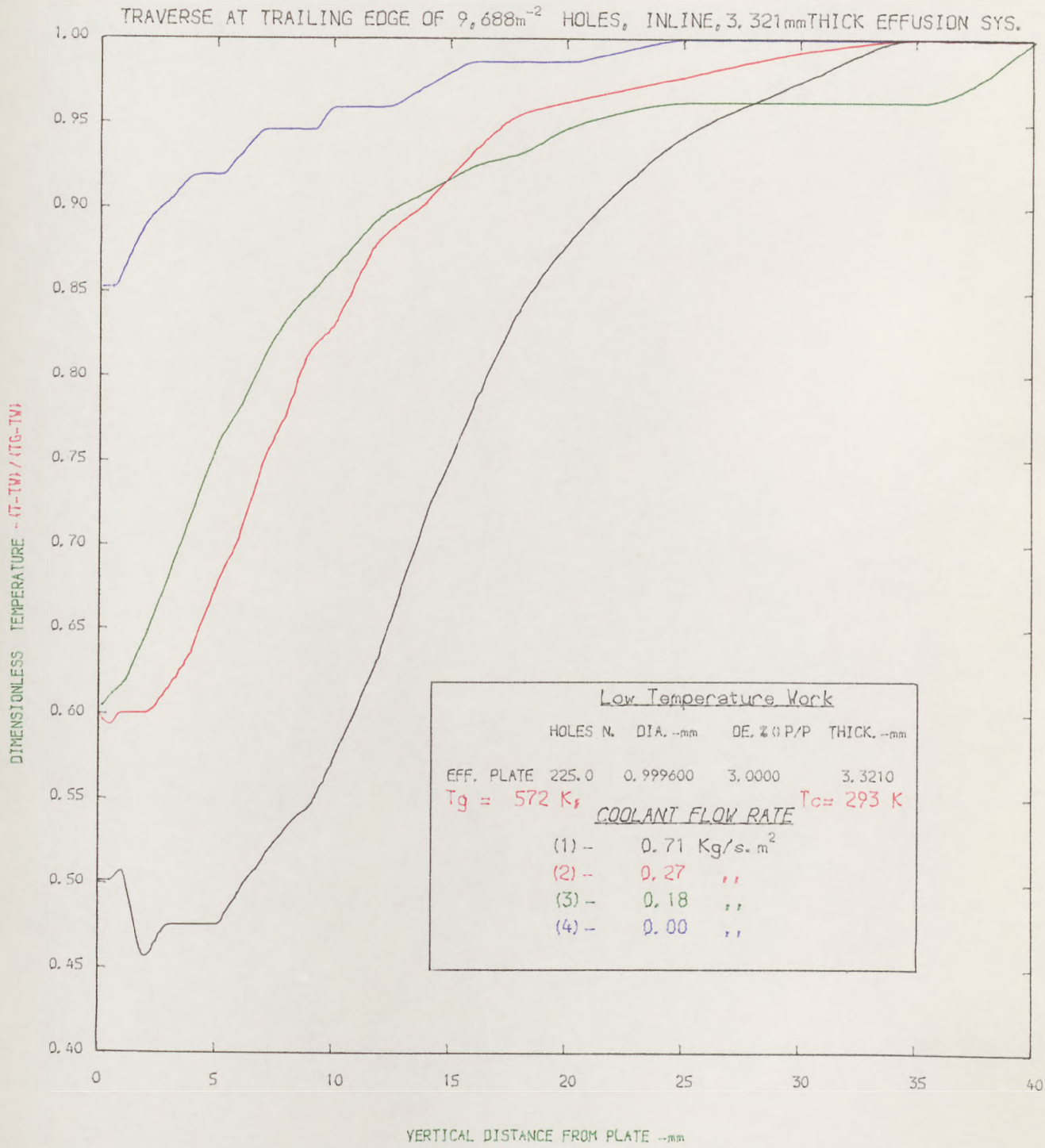

FIG. (6.15). THERMAL BOUNDARY LAYER DEVELOPMENT NEAR TRAILING EDGE OF WALL

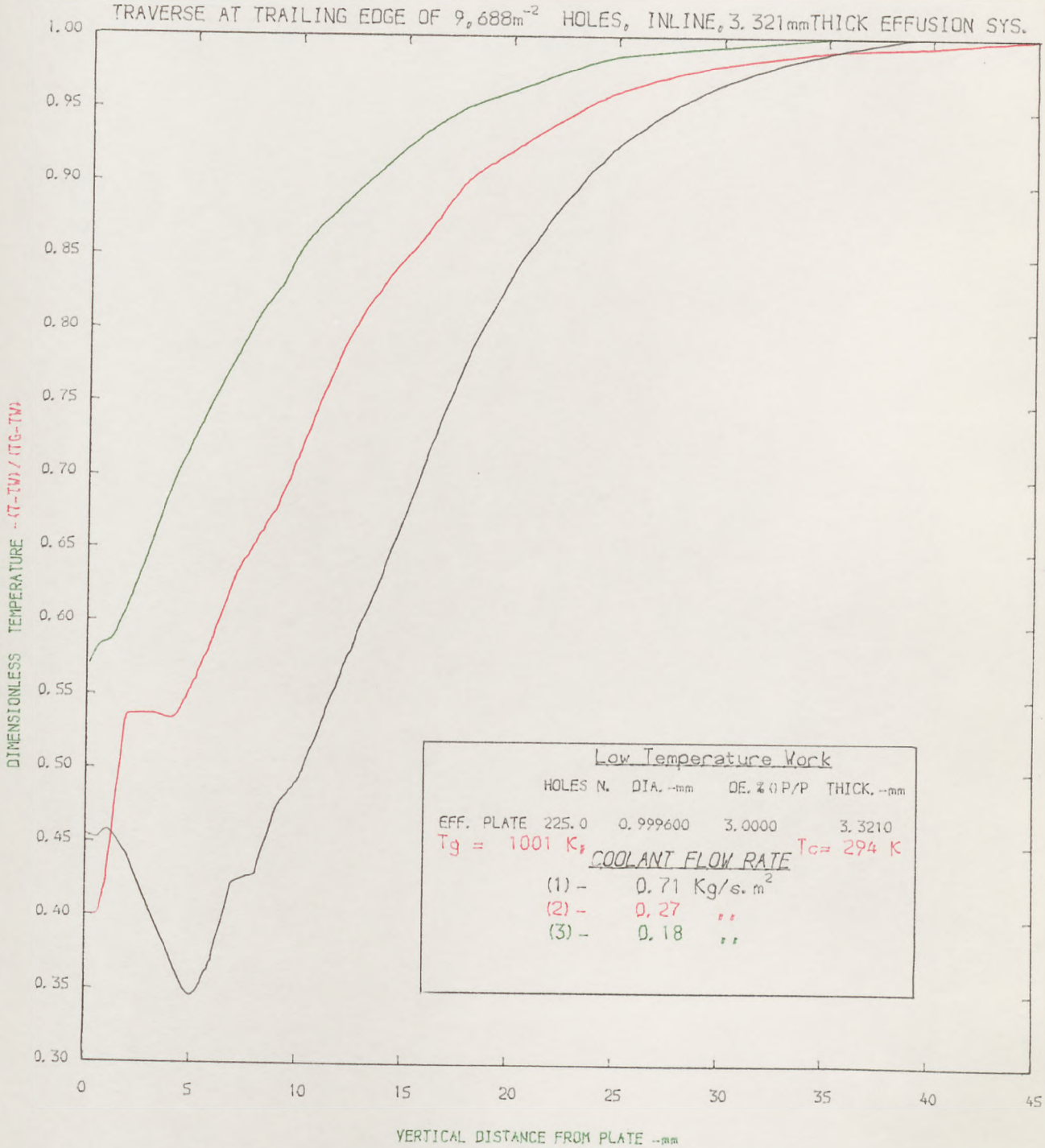

FIG. (6.16) : THERMAL BOUNDARY LAYER DEVELOPMENT AT TRAILING EDGE OF WALL.

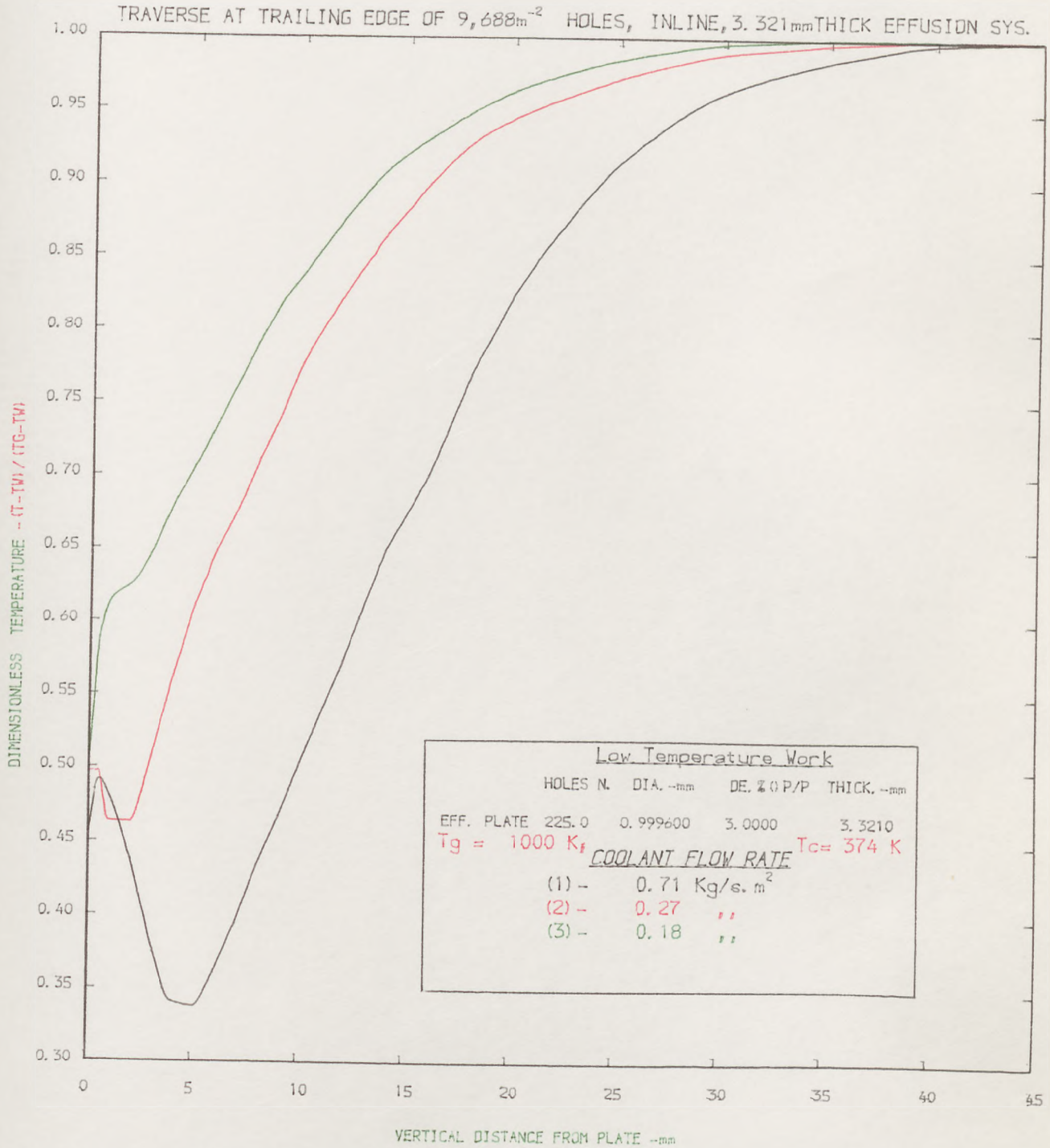

FIG. (6.17) : THERMAL BOUNDARY LAYER DEVELOPMENT AT TRAILING EDGE OF WALL.

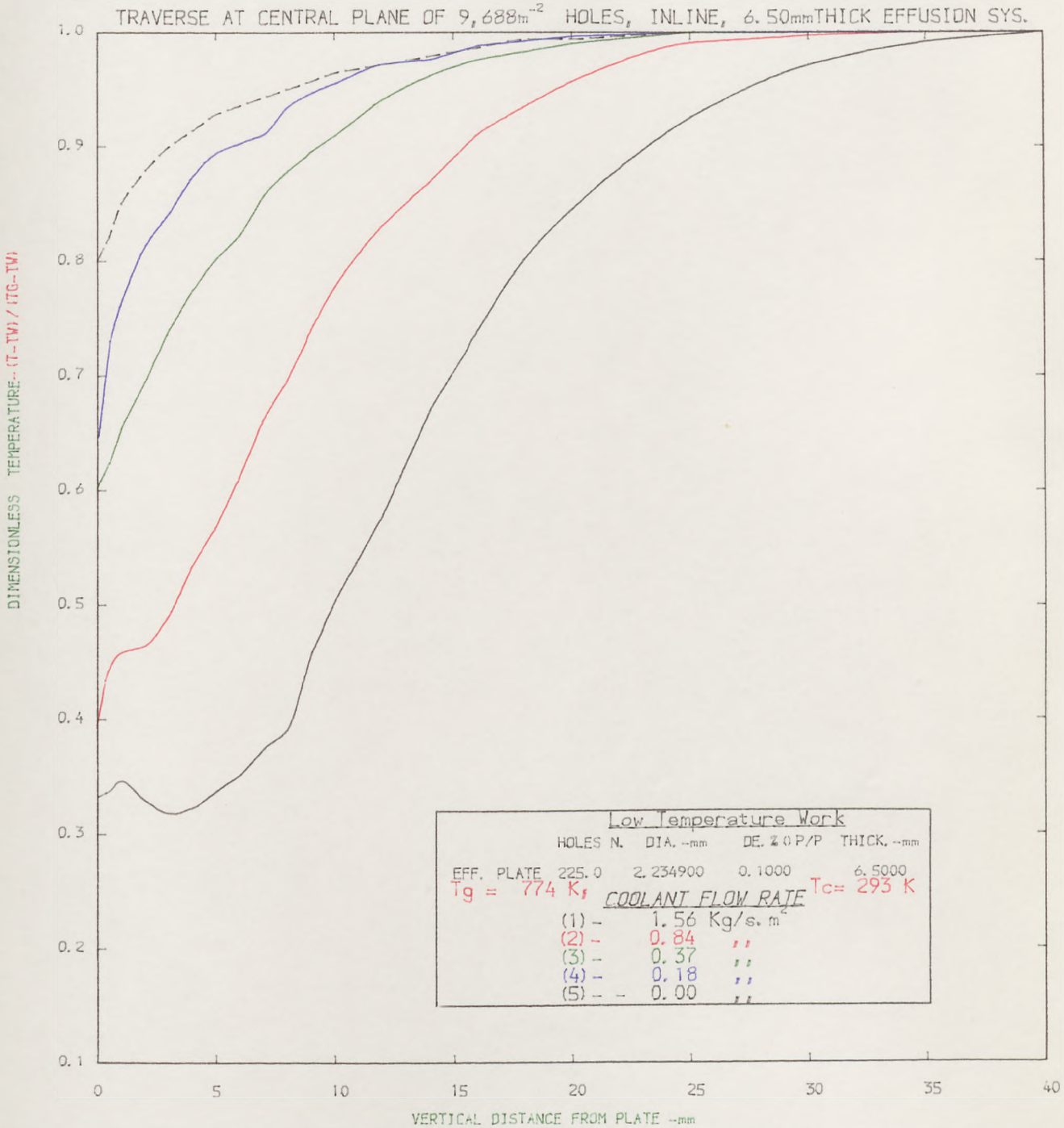

FIG. (6.18) : THERMAL BOUNDARY LAYER DEVELOPMENT AT CENTRAL PLANE OF WALL.

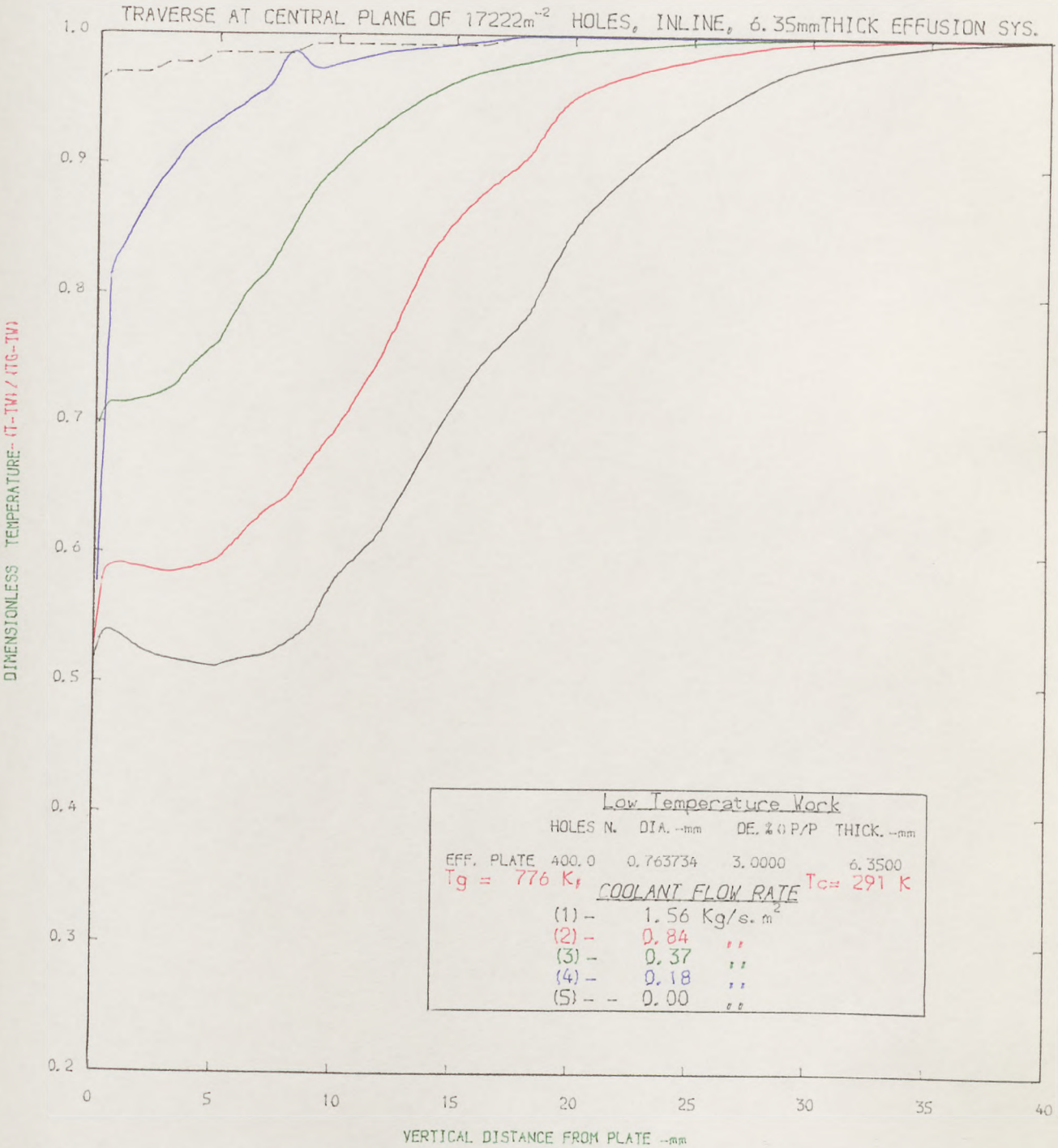

FIG. (6.19) : THERMAL BOUNDARY LAYER DEVELOPMENT AT CENTRAL PLANE OF WALL.

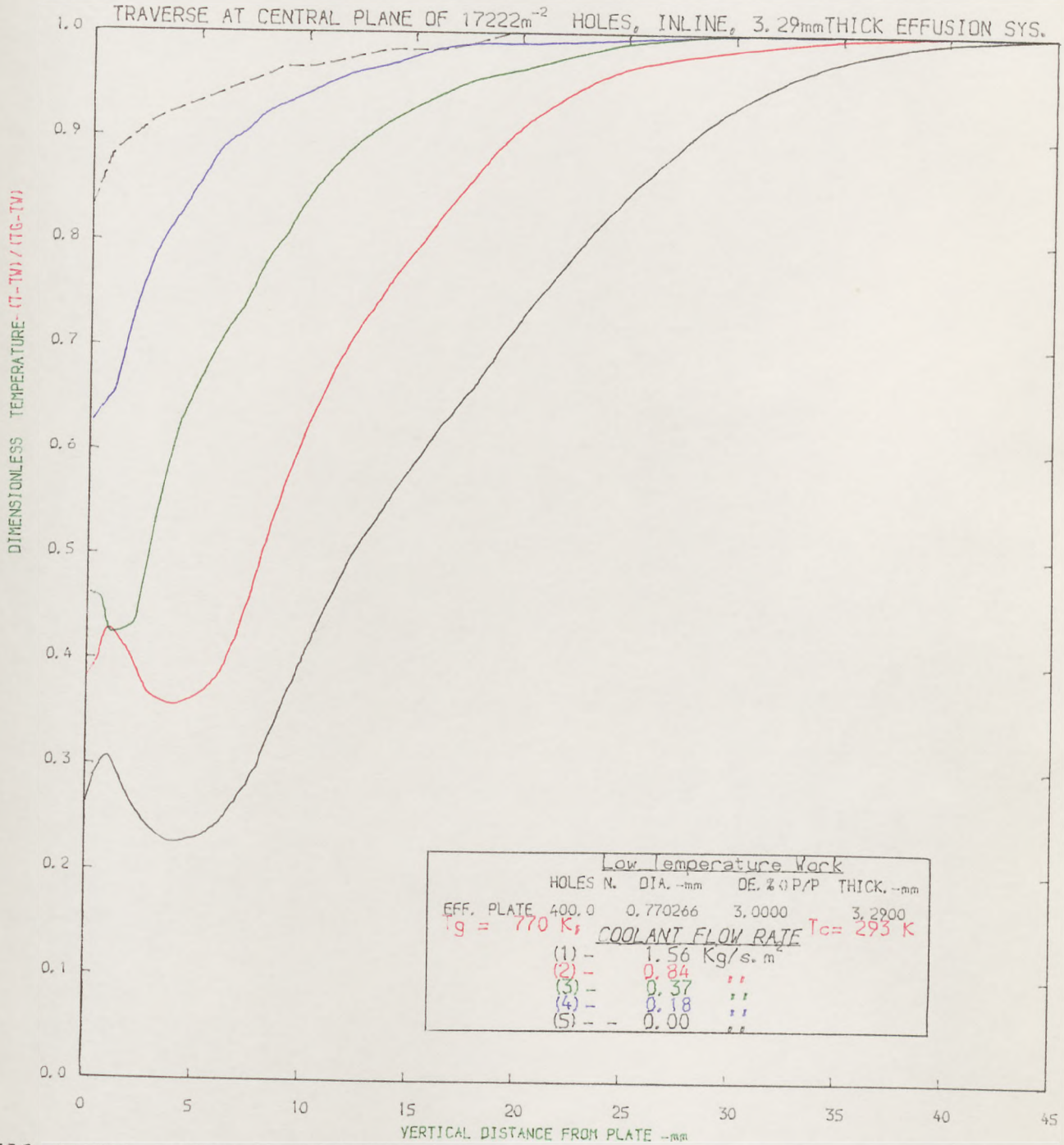

FIG. (6.20). THERMAL BOUNDARY LAYER DEVELOPMENT AT CENTRAL PLANE OF WALL.

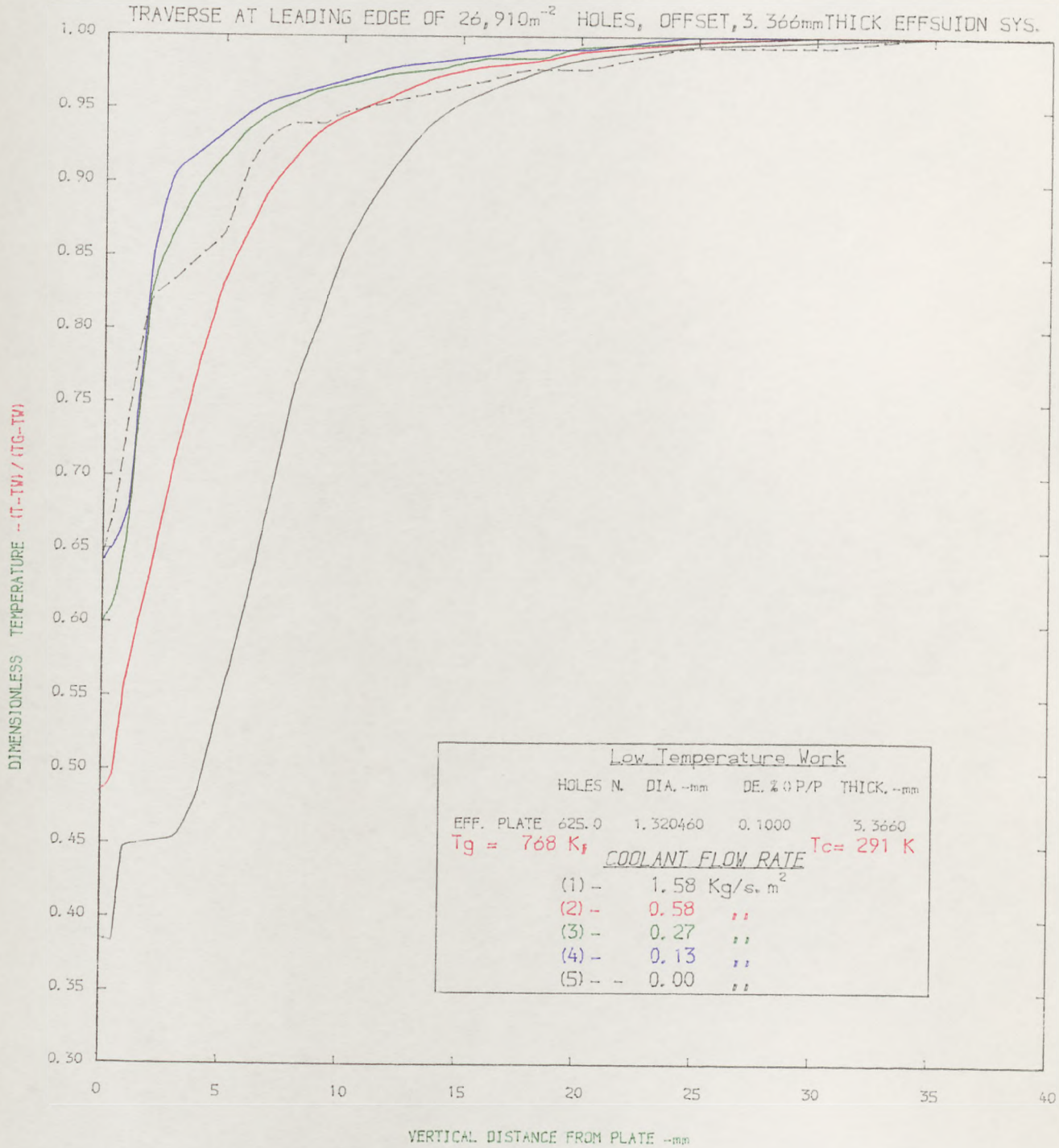

FIG. (6.21) : THERMAL BOUNDARY LAYER DEVELOPMENT NEAR LEADING EDGE OF WALL.

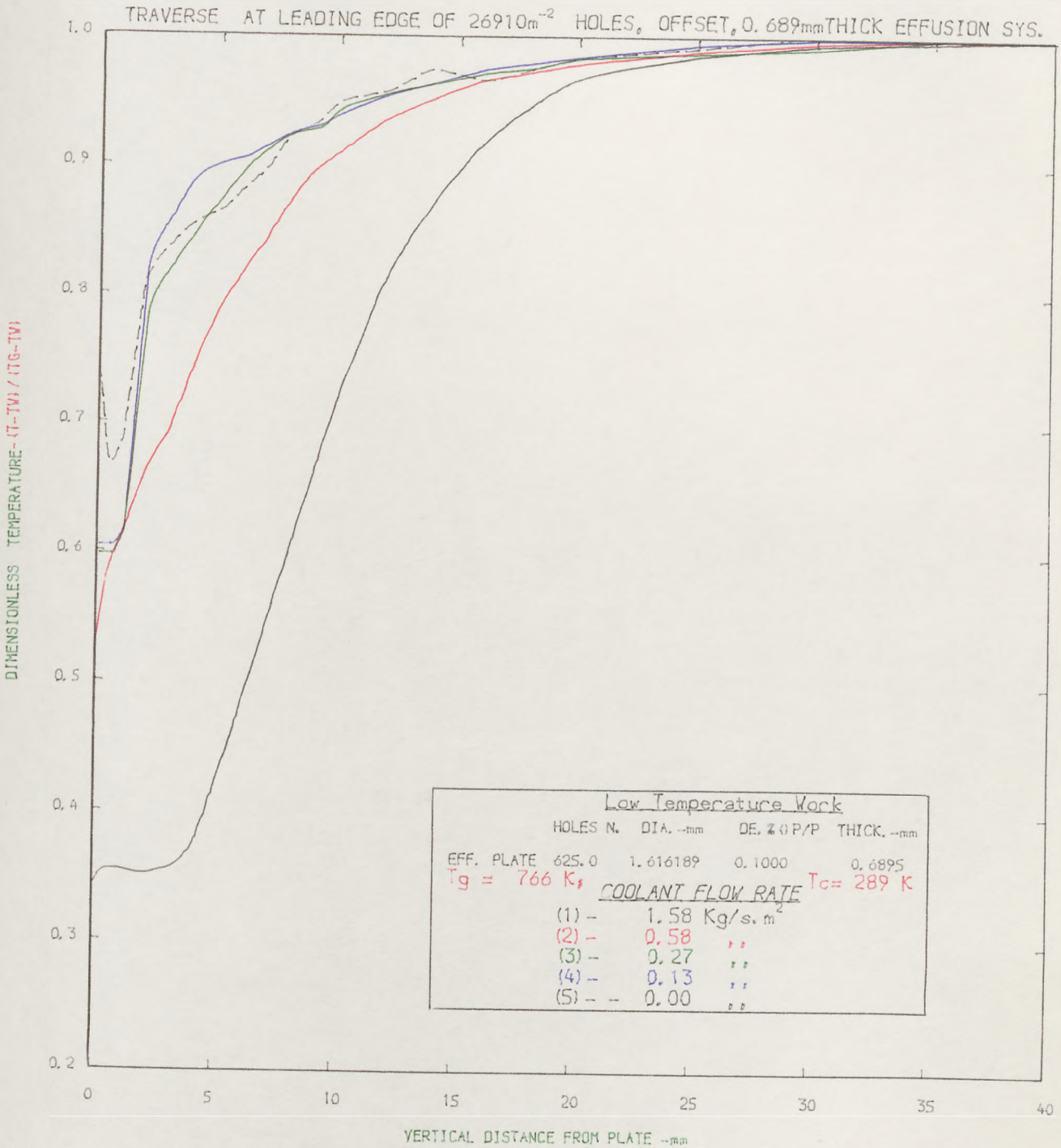

FIG. (6.22) : THERMAL BOUNDARY LAYER DEVELOPMENT NEAR LEADING EDGE OF WALL.

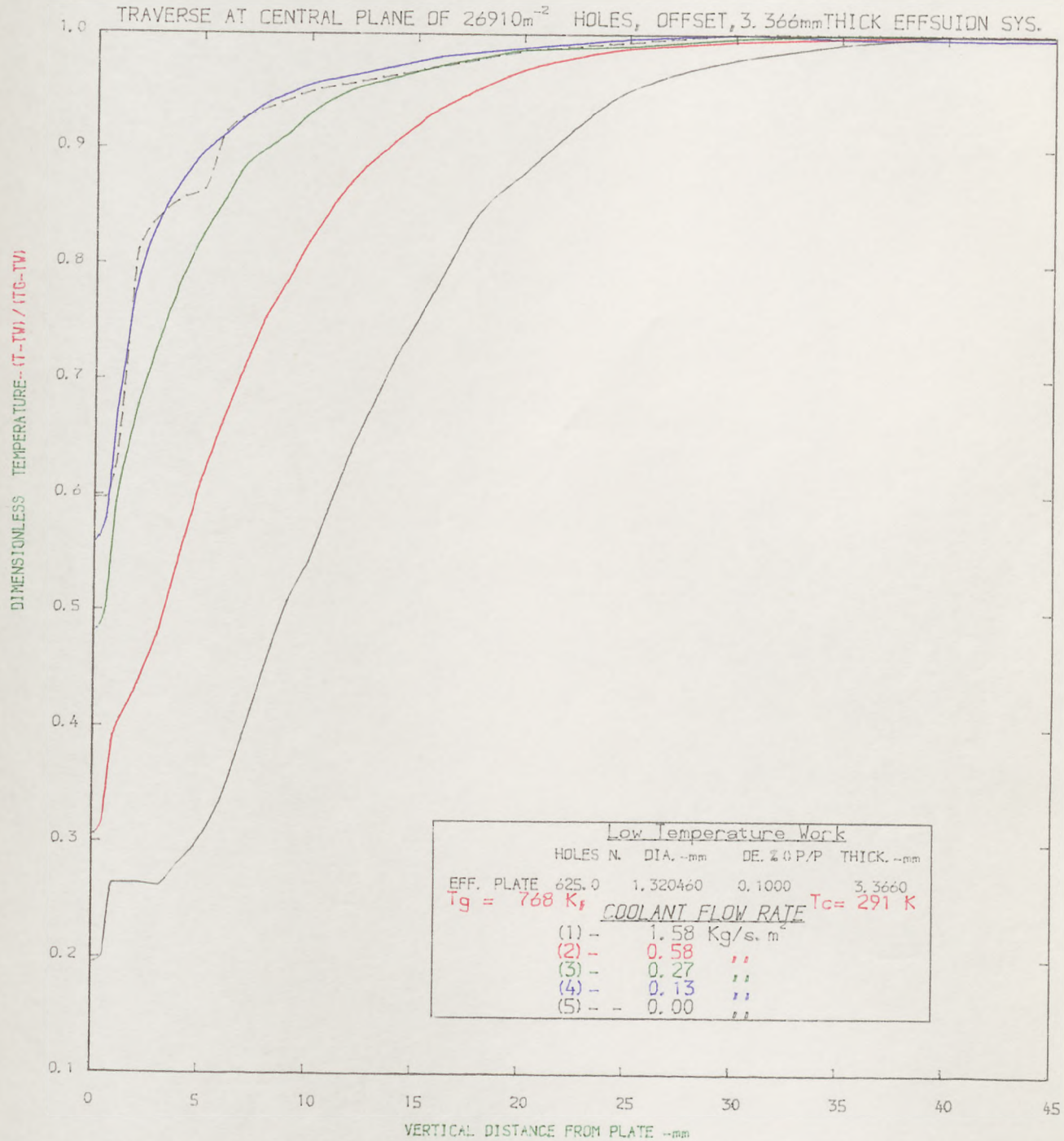

FIG. (6.23) : THERMAL BOUNDARY LAYER DEVELOPMENT AT CENTRAL OF WALL.

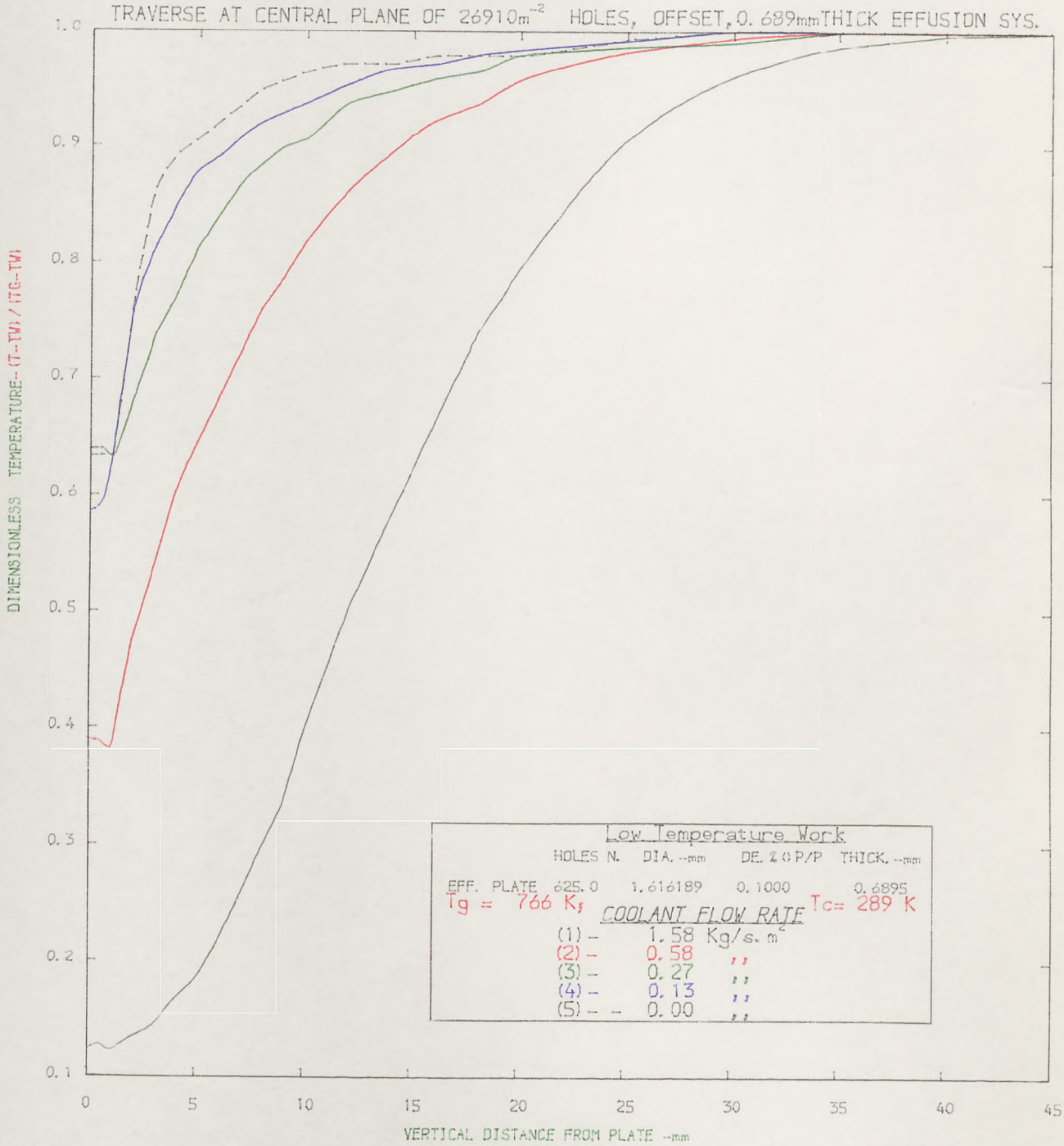

FIG. (6.24) : THERMAL BOUNDARY LAYER DEVELOPMENT AT CENTRAL OF WALL.

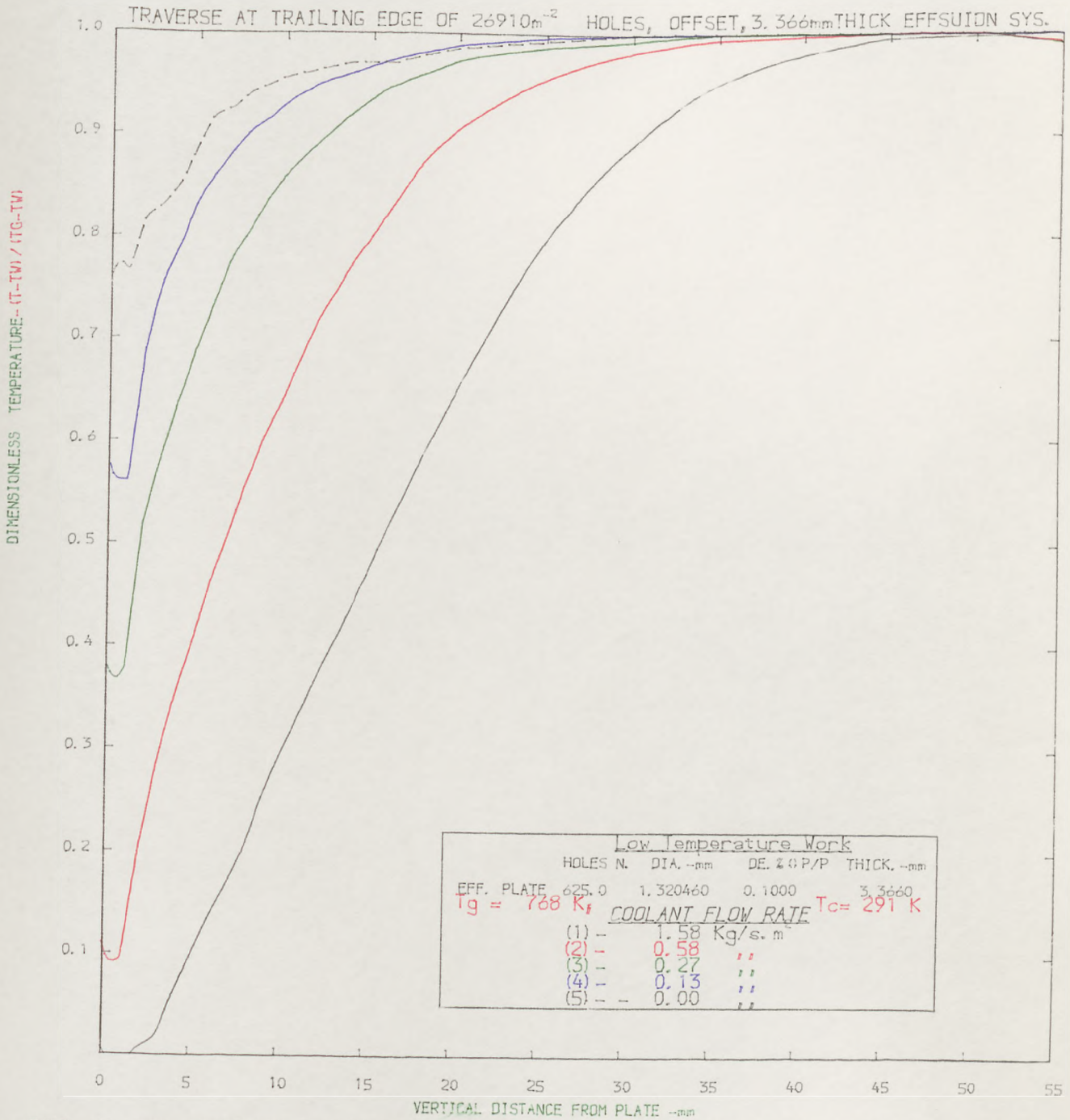

FIG. (6.25) : THERMAL BOUNDARY LAYER DEVELOPMENT NEAR TRAILING EDGE OF WALL

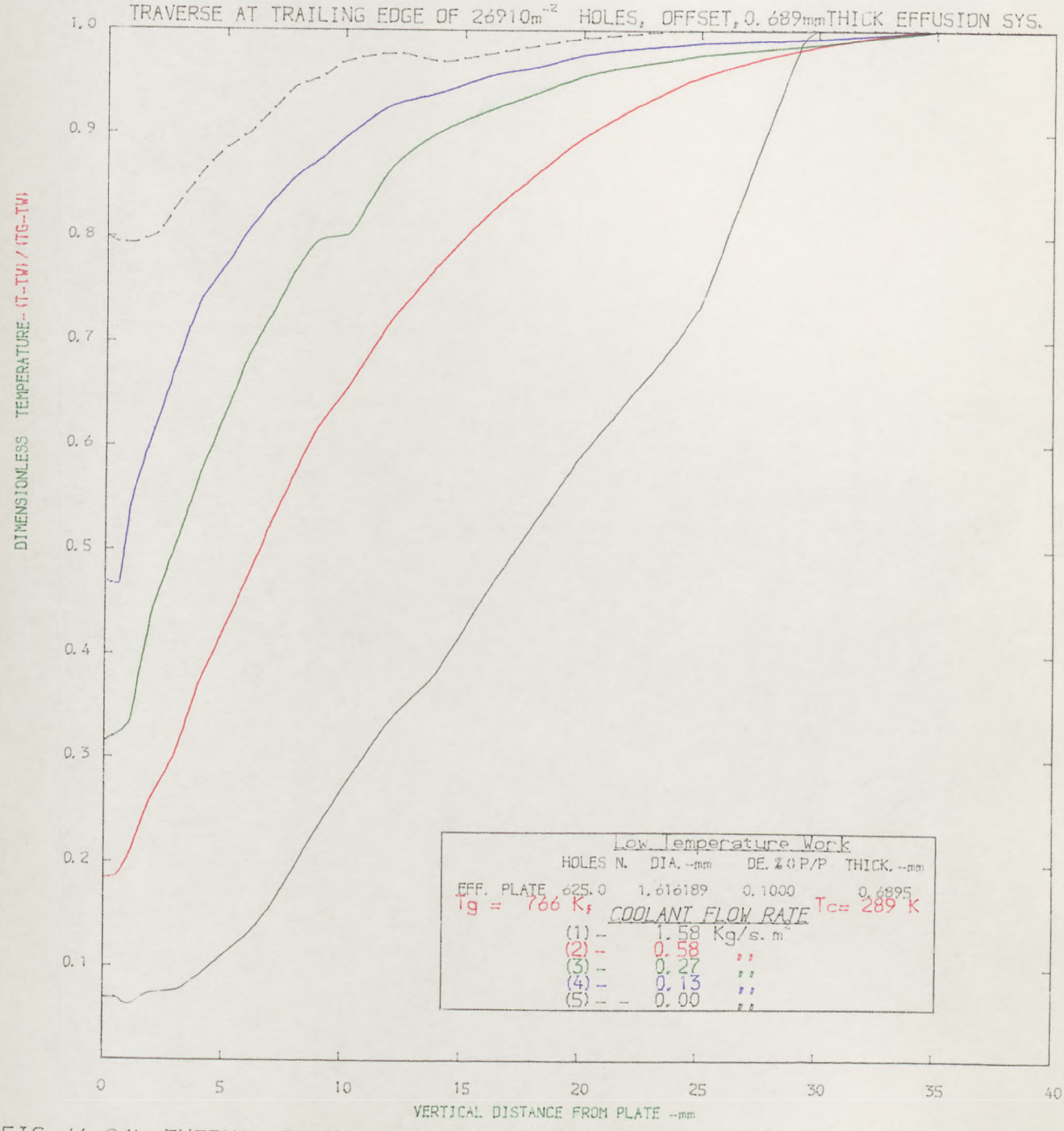

FIG. (6.26) : THERMAL BOUNDARY LAYER DEVELOPMENT NEAR TRAILING EDGE OF WALL

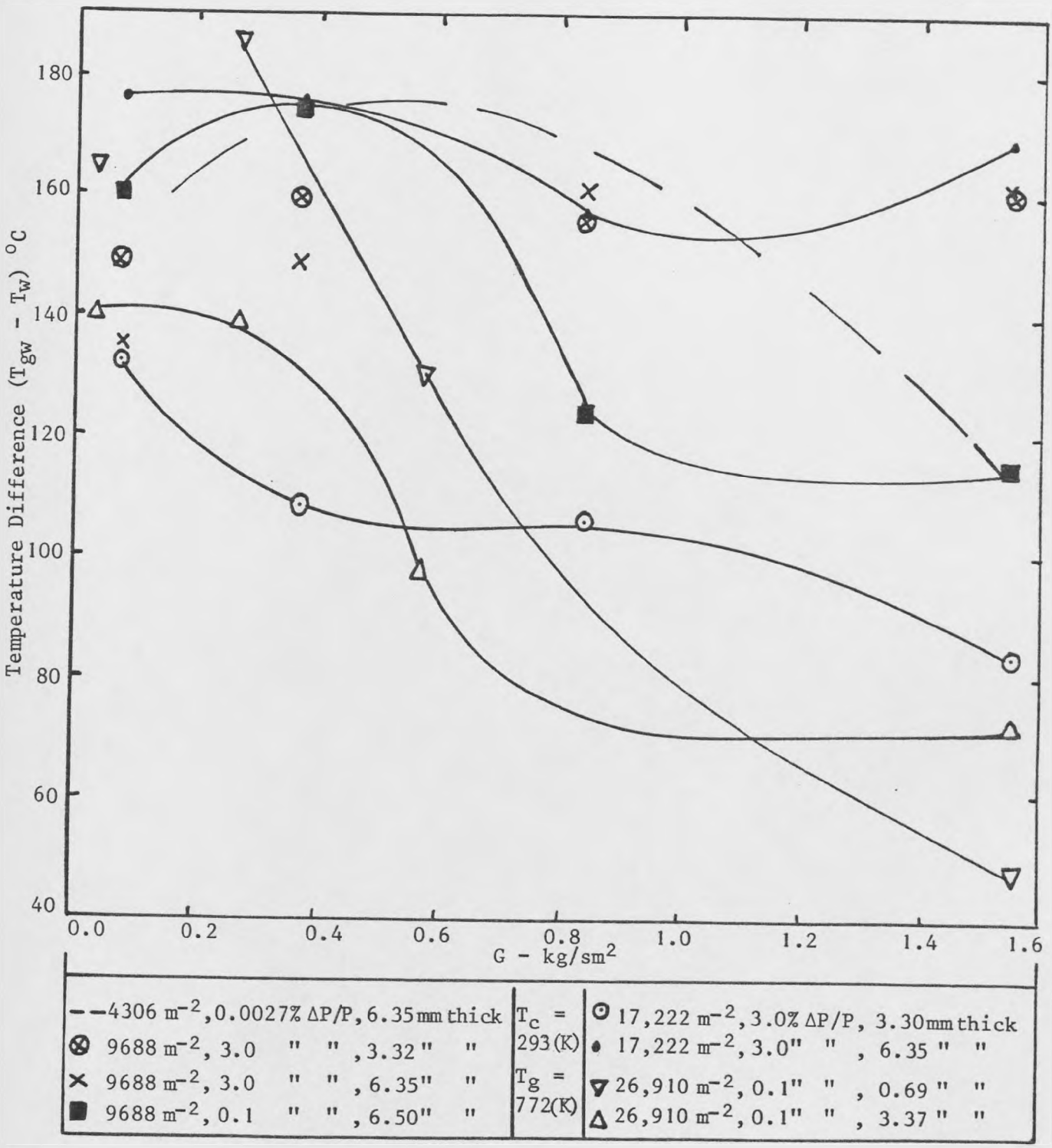

Fig. 6.27: Film temperature profile

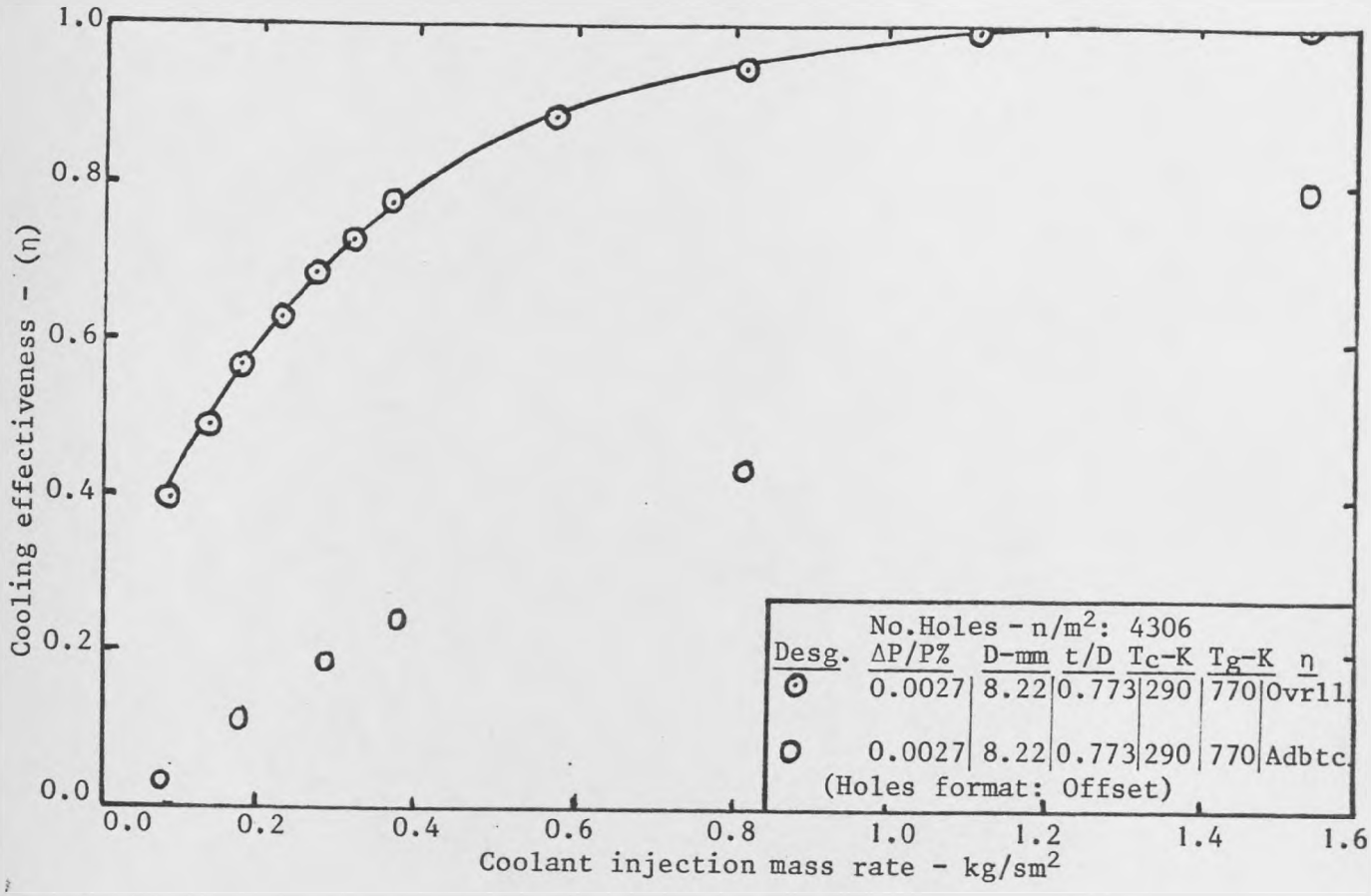

Fig. 6.28: Dependency of overall and adiabatic effectiveness on coolant injection at station 5

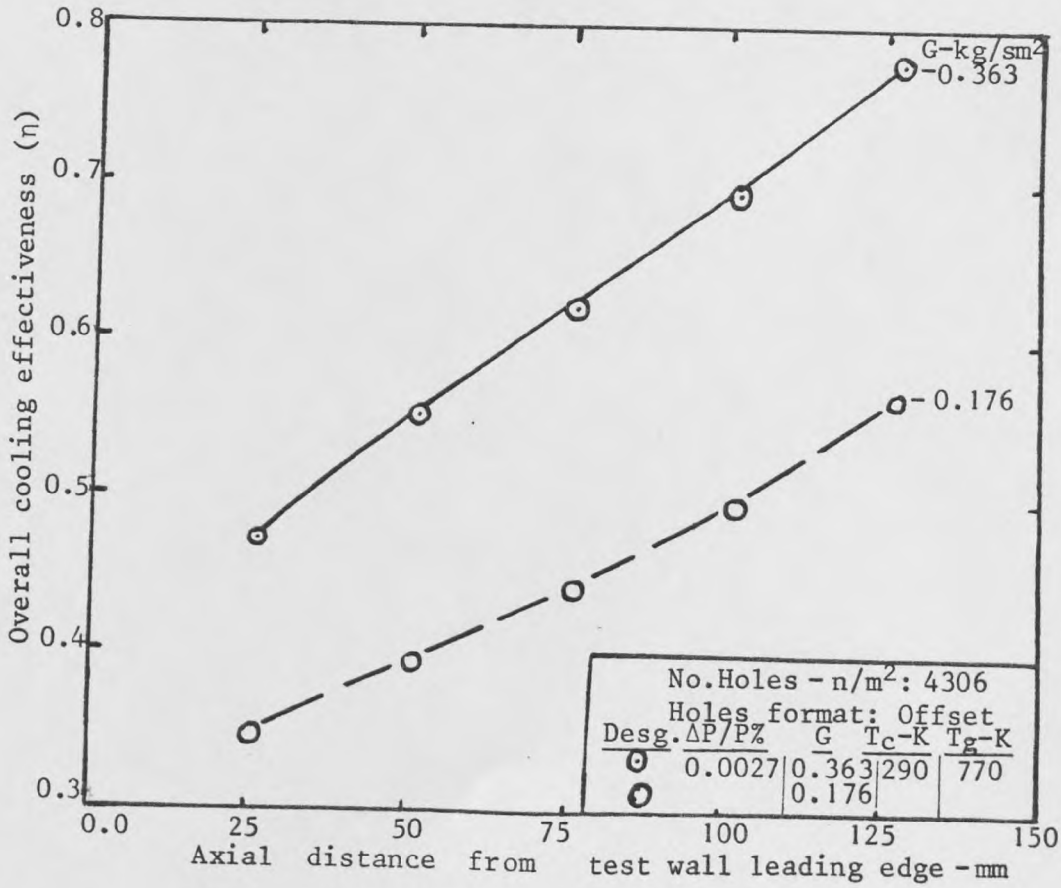

Fig. 6.29: Axial profile of overall cooling effectiveness at two coolant injection rates

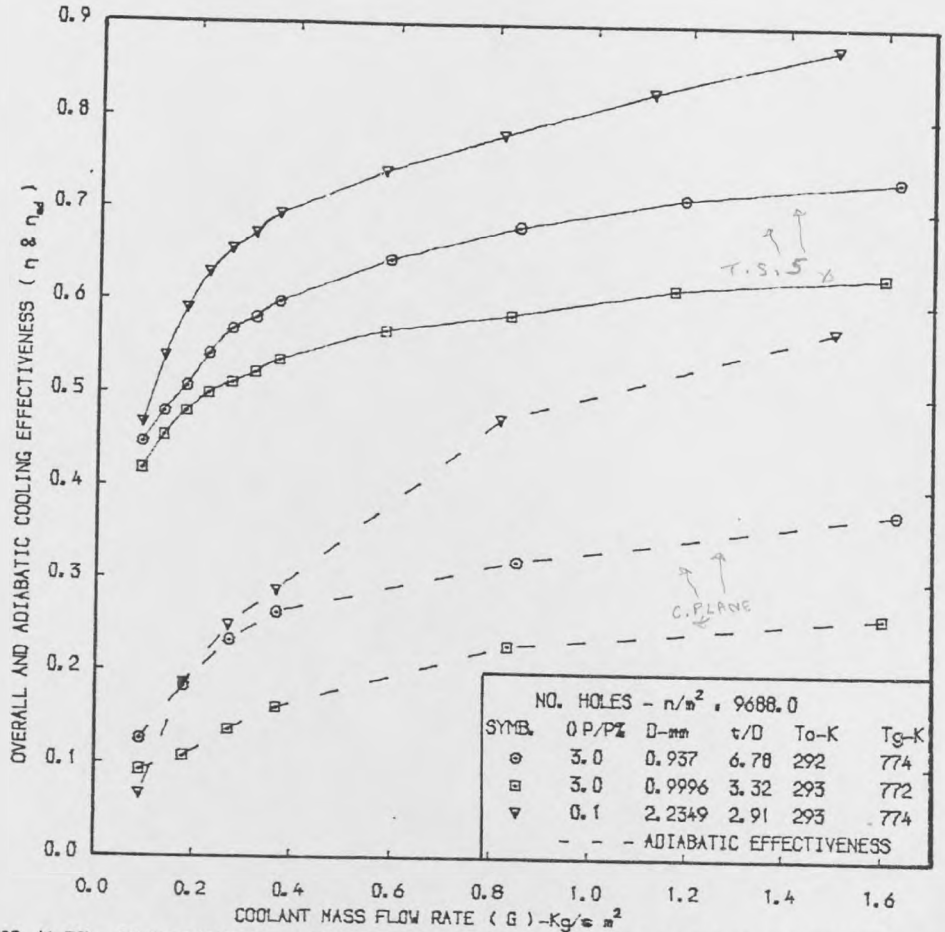

FIG. (6.30) : DEVELOPMENT OF COOLING EFFECTIVENESS WITH COOLANT INJECTION AT STATION 5

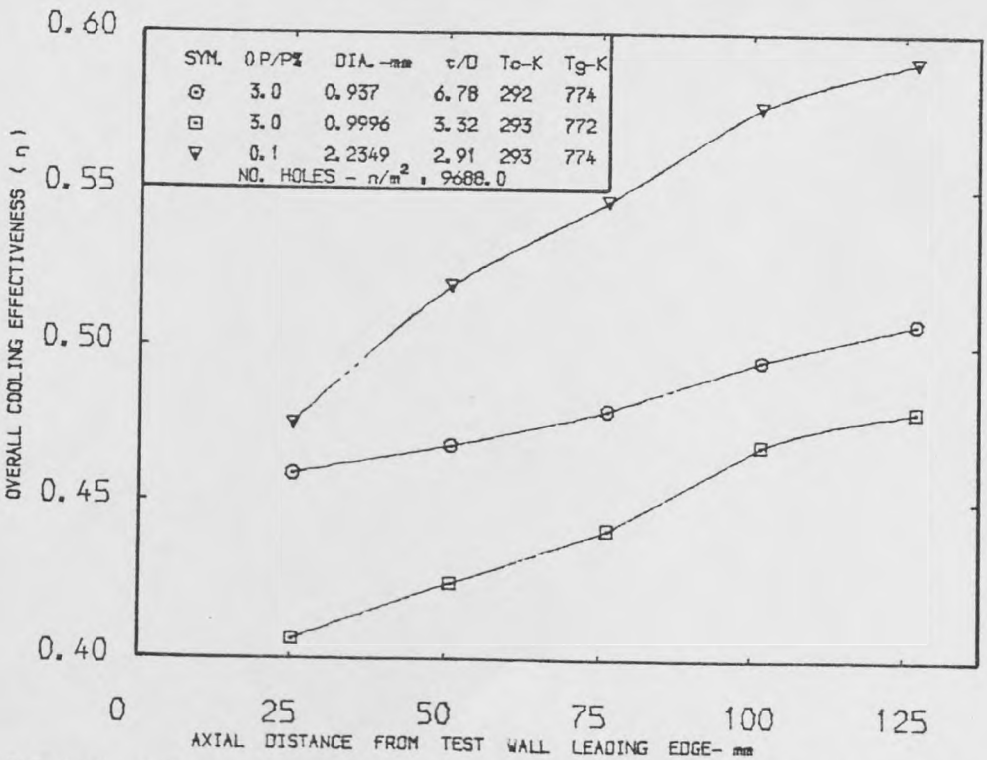

FIG. (6.31) : AXIAL DEVELOPMENT OF OVERALL COOLING EFFECTIVENESS AT COOLANT INJECTION RATE G = 0.2 Kg/s m²

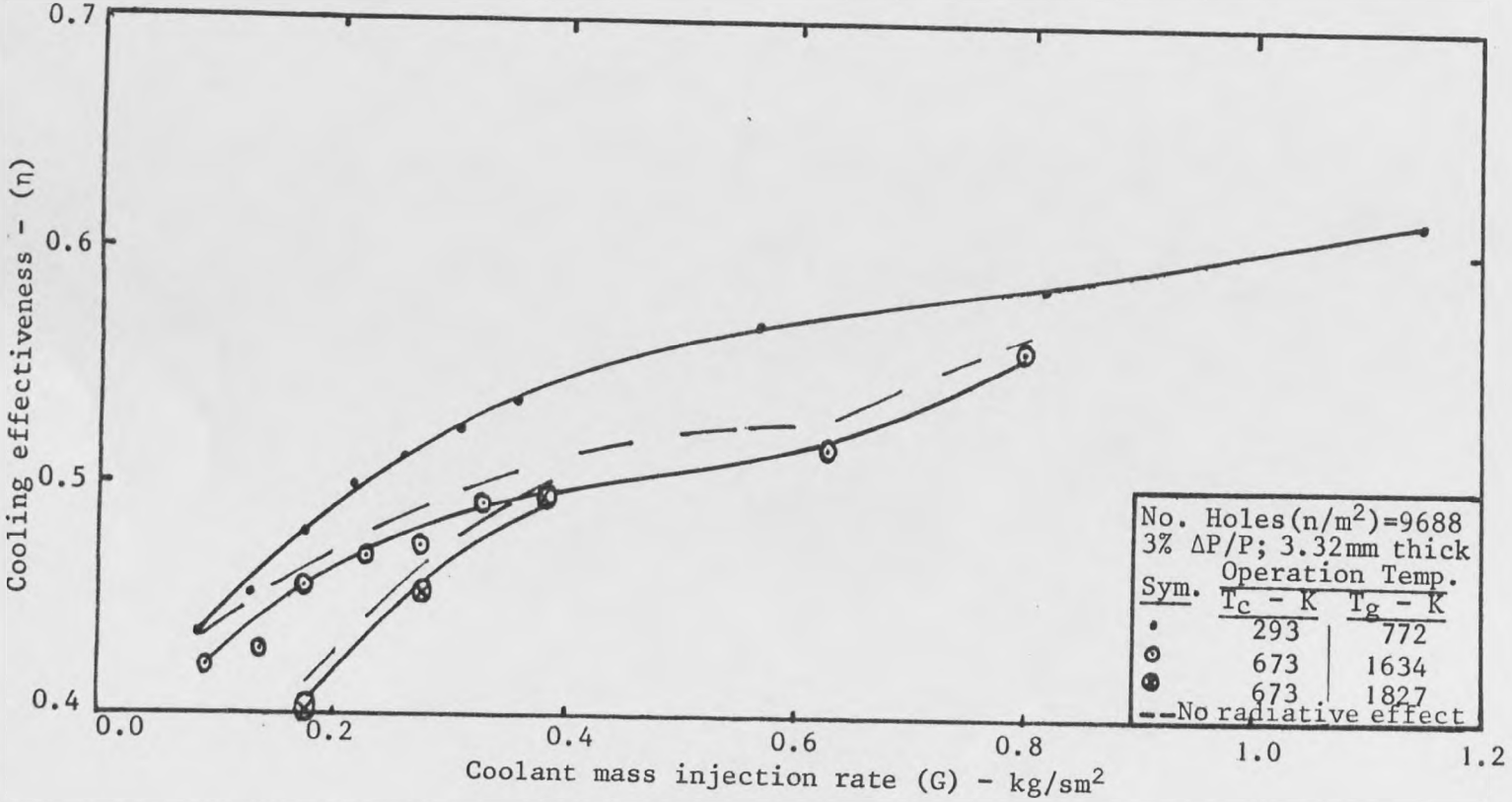

Fig. 6.32: Variation of cooling effectiveness with coolant injection at three operating temperatures at thermal station 5

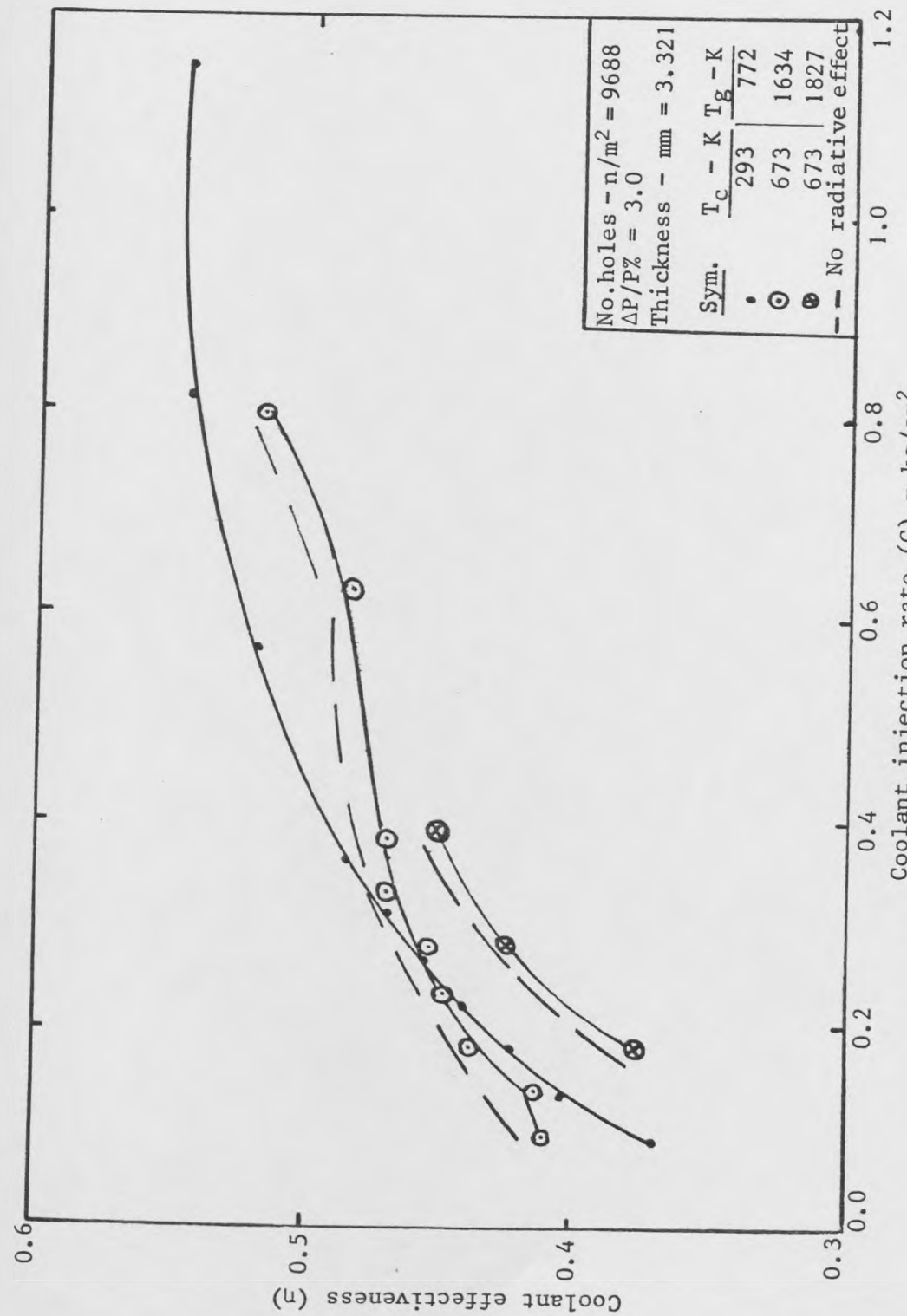

Fig. 6.33: Variation of cooling effectiveness with coolant injection at various operating temperatures at the second thermal station

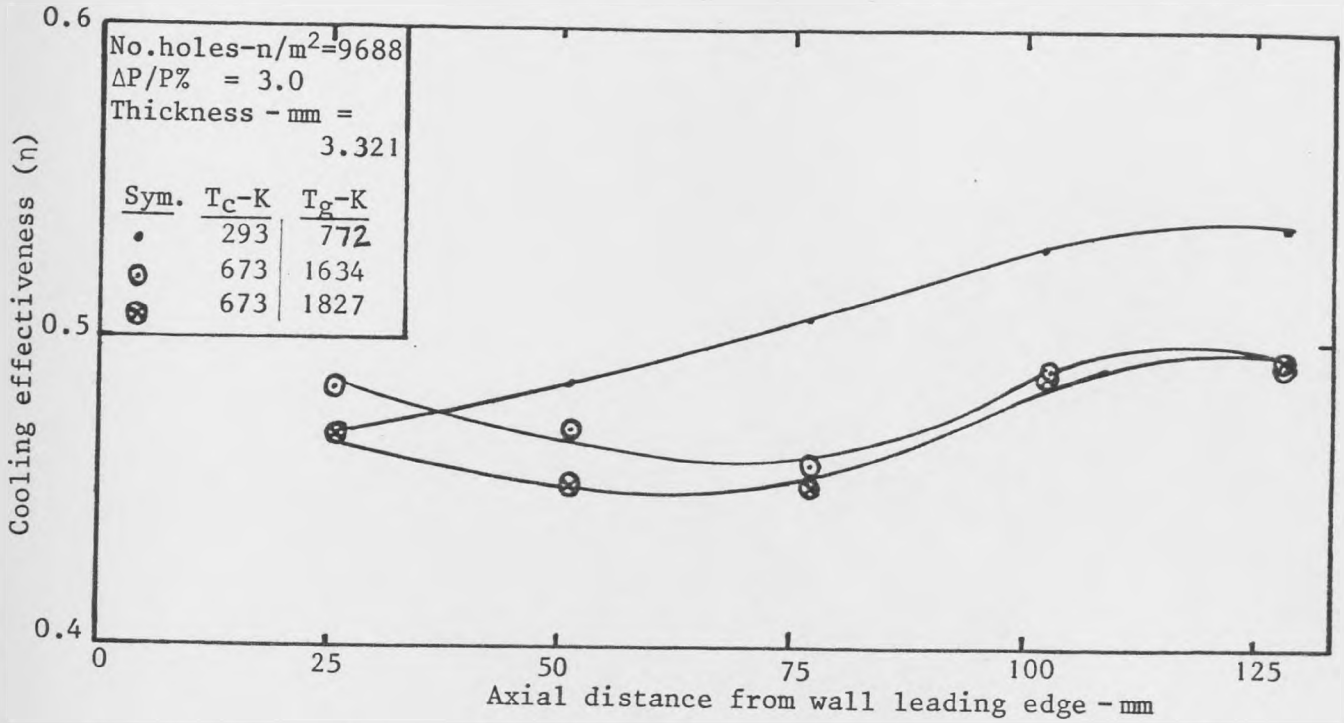

Fig. 6.34: Axial overall cooling effectivness for cylindrical combustor at coolant injection rate of $0.36 \leqslant G \leqslant 0.387$

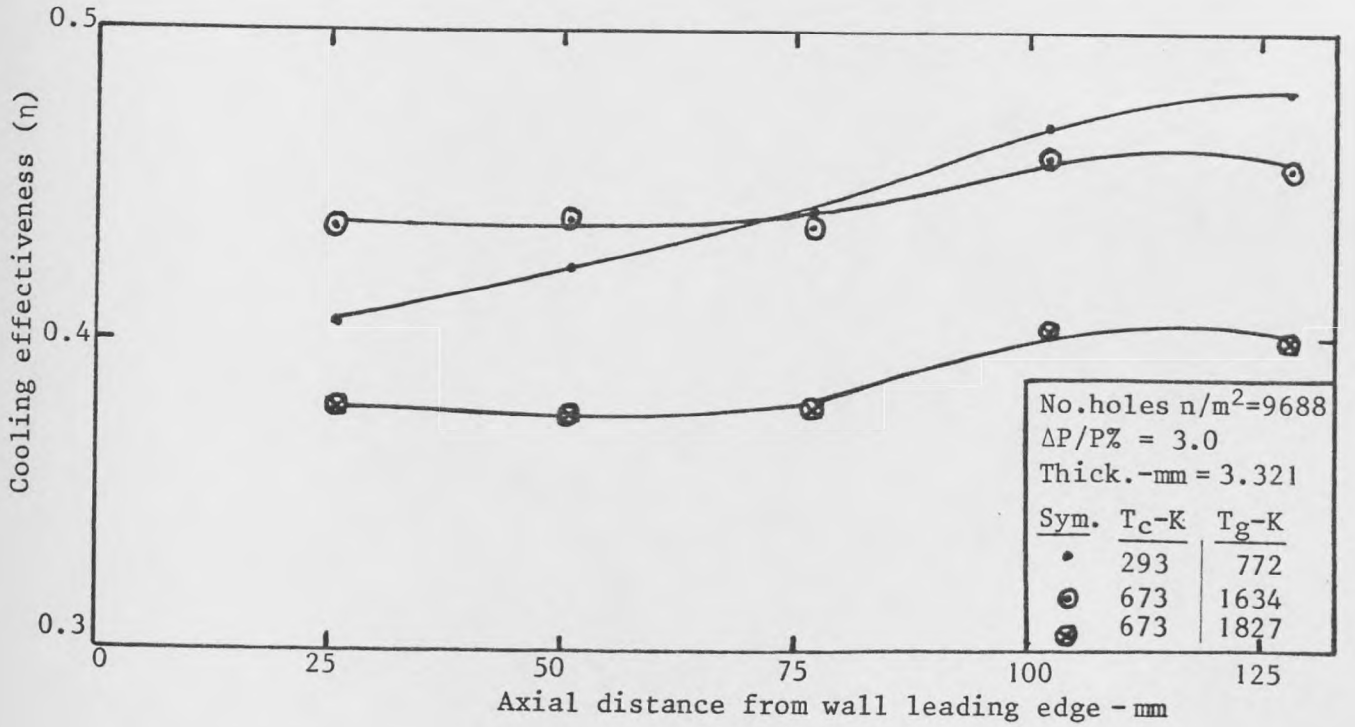

Fig. 6.35: Axial overall cooling effectiveness for cylindrical combustor at coolant injection rate of $0.174 \leqslant G \leqslant 0.179$

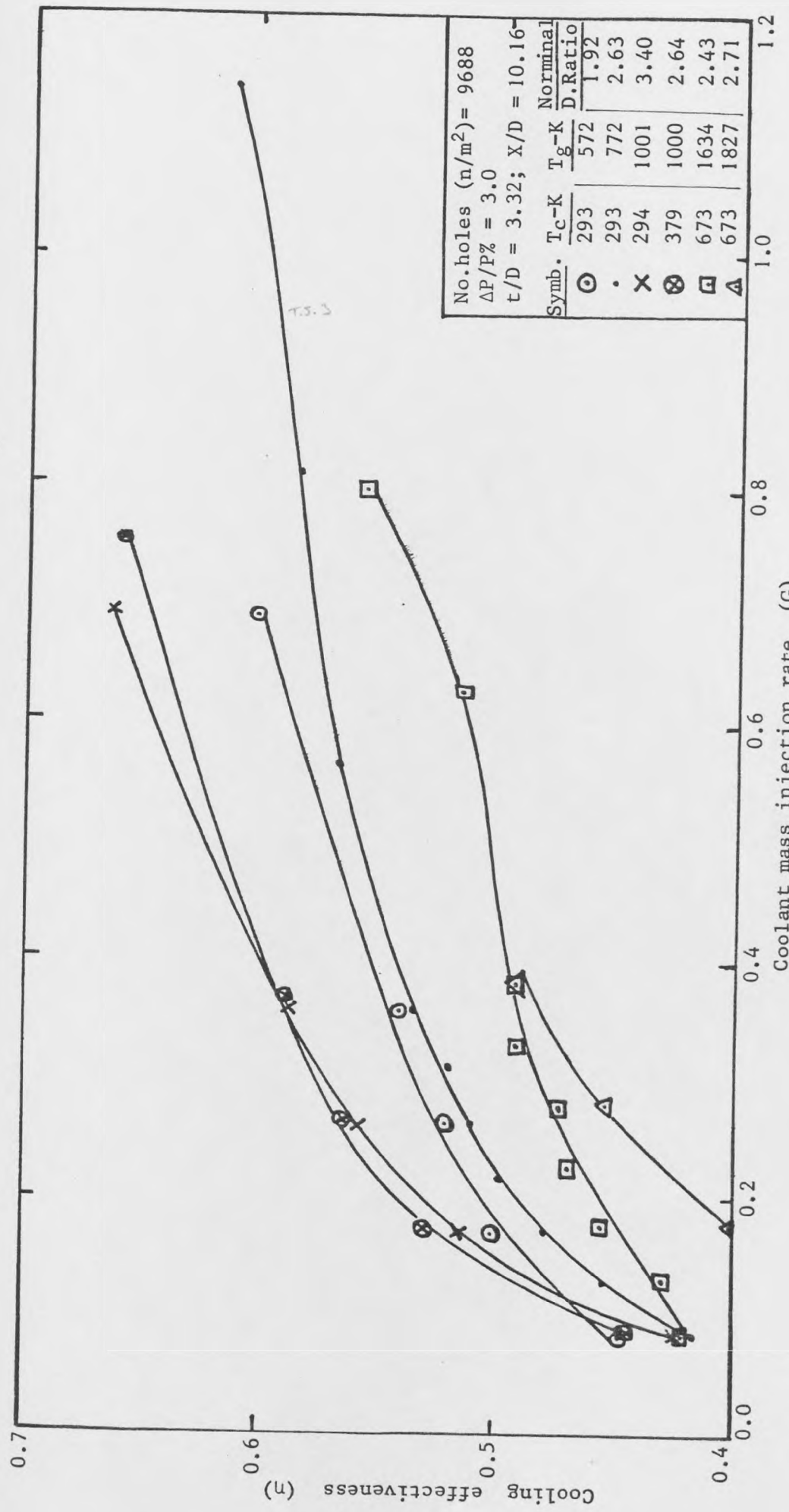

Fig. 6.36: Cooling effectiveness profiles at different norminal density ratios at thermal station 5

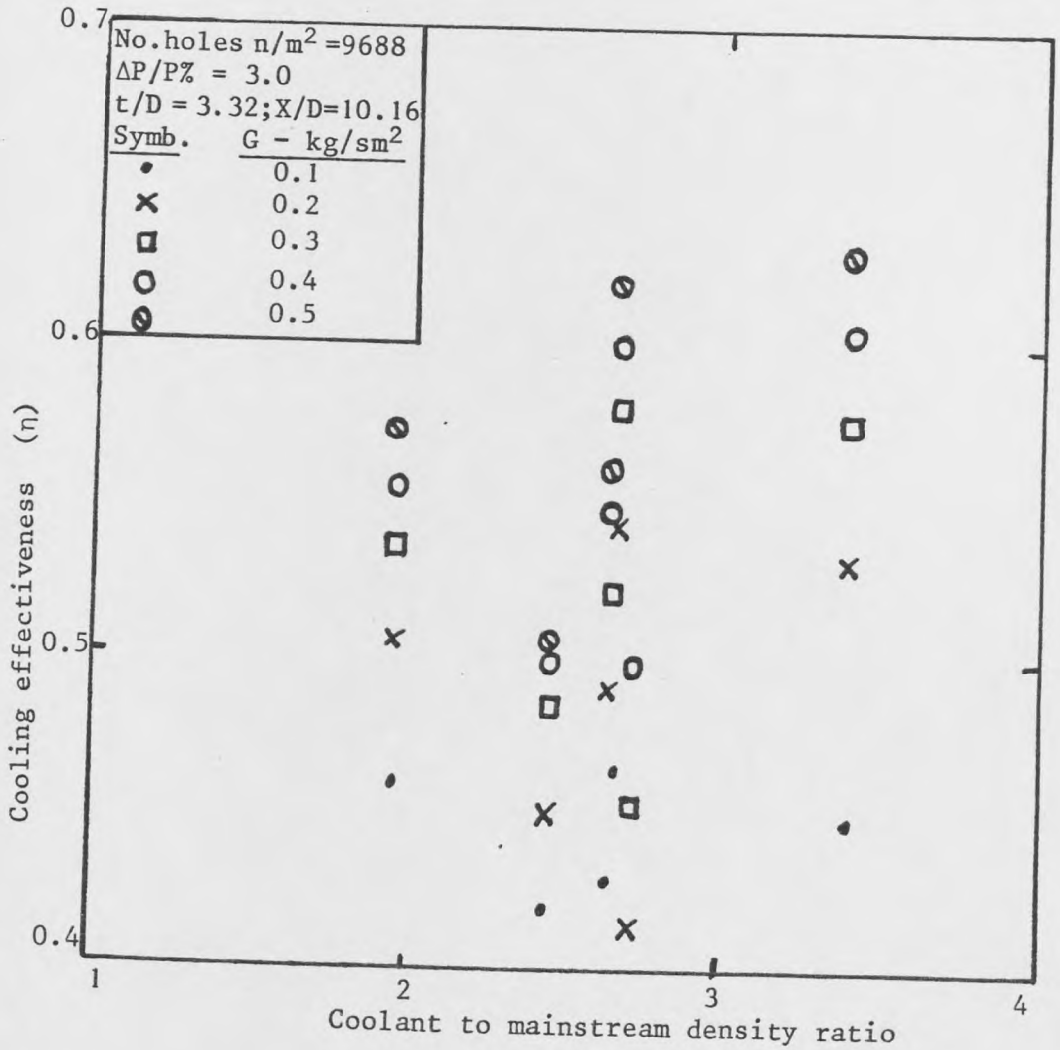

Fig. 6.37: Density ratio effect on cooling effectiveness for a 9688/m² holes cylindrical type effusion system at various coolant injection rates

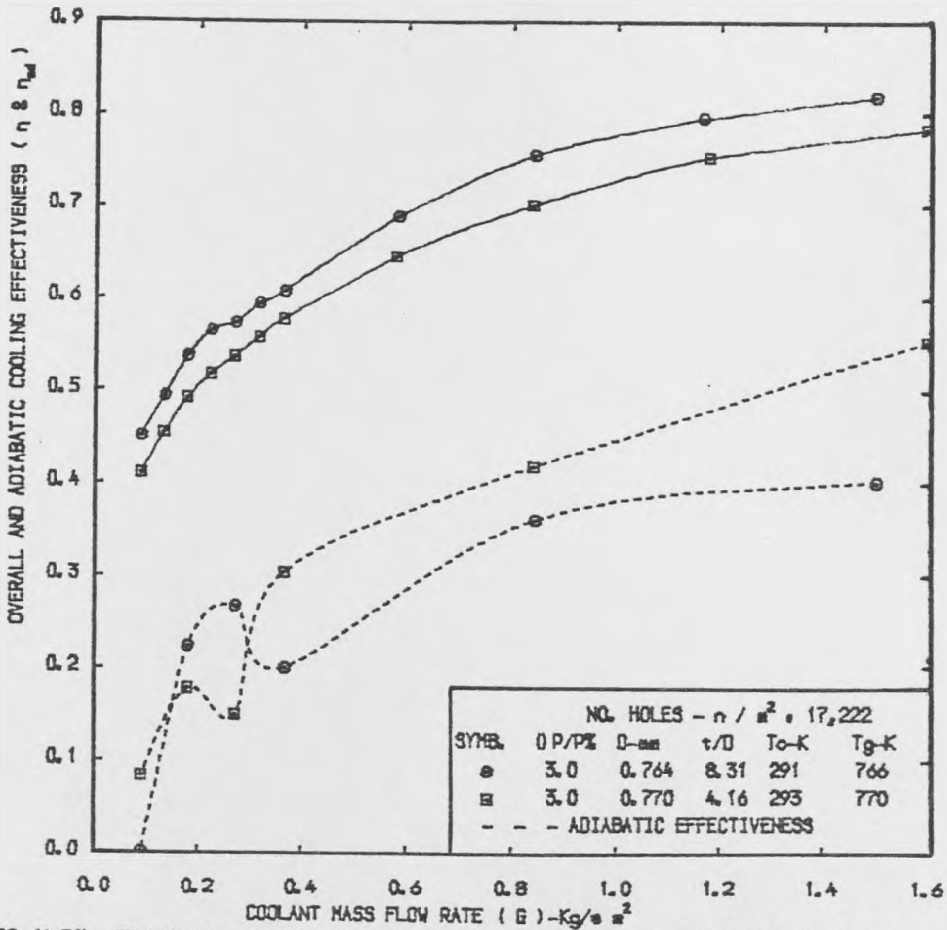

FIG. (6.38) : DEVELOPMENT OF COOLING EFFECTIVENESS WITH COOLANT INJECTION AT STATION 5

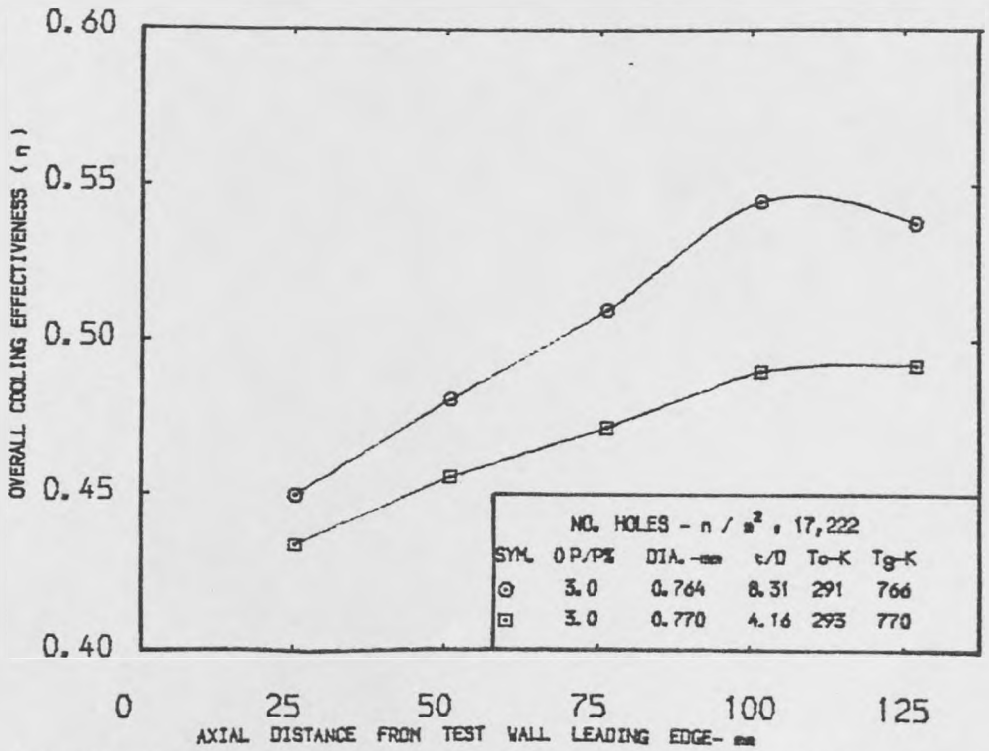

FIG. (6.39) : AXIAL DEVELOPMENT OF OVERALL COOLING EFFECTIVENESS AT COOLANT INJECTION RATE G = 0.2 Kg/s m²

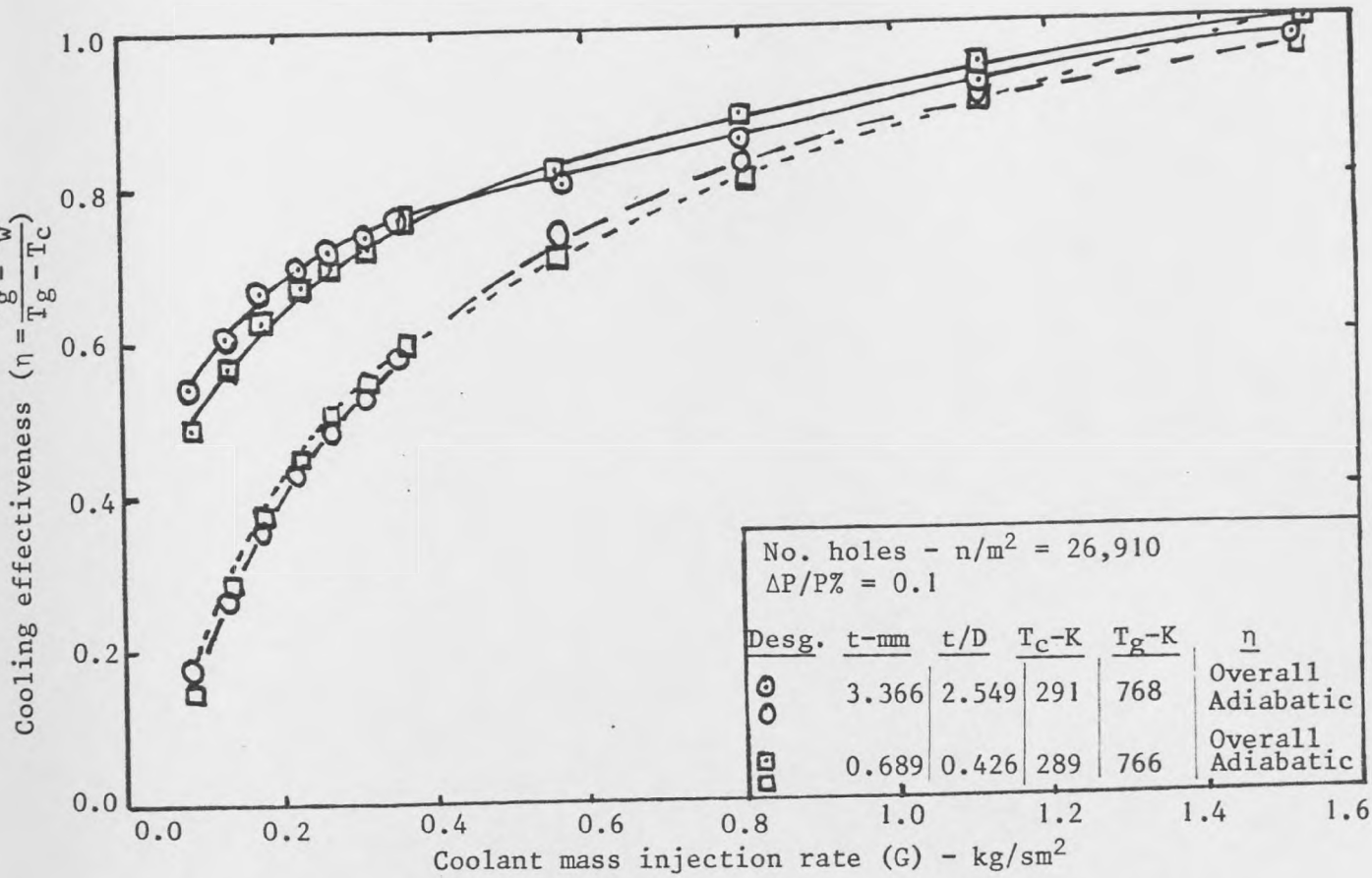

Fig. 6.40: Dependency of overall and adiabatic cooling effectivenesses on coolant injection at station 5

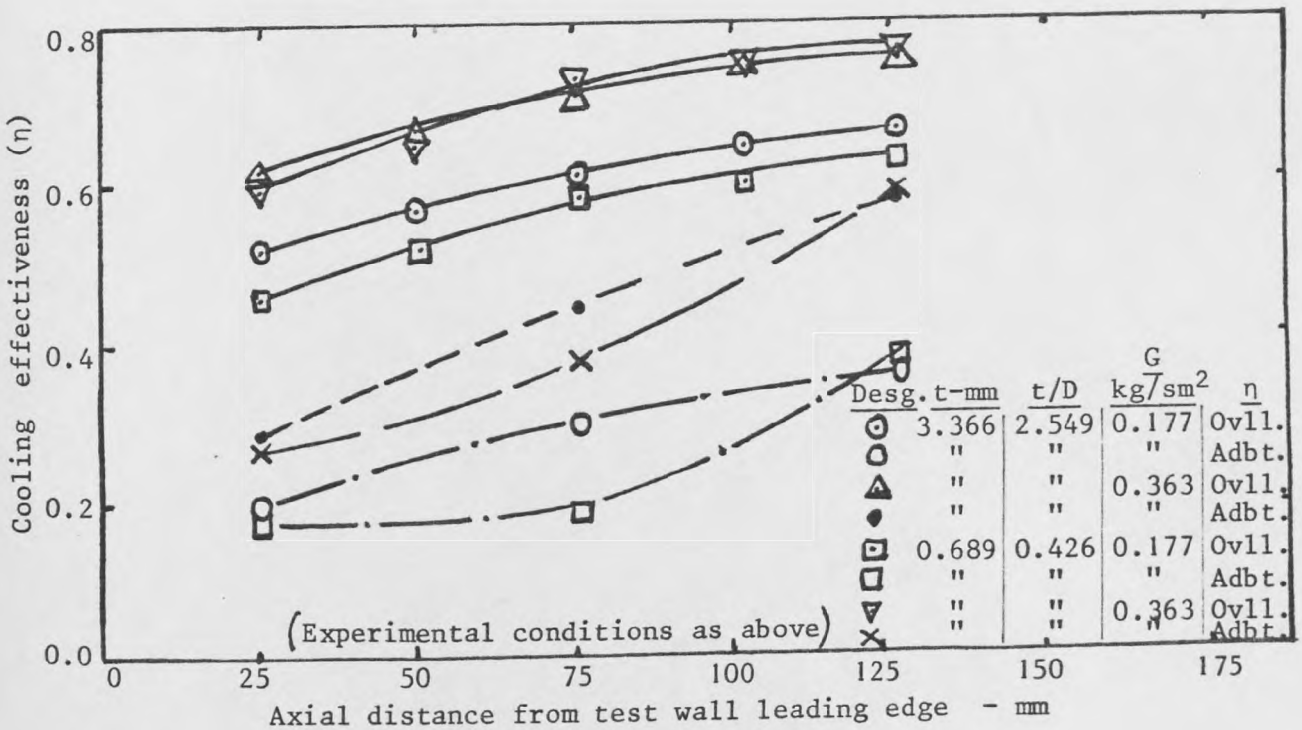

Fig. 6.41: Axial profile of cooling effectiveness (η) at two injection rates (G)

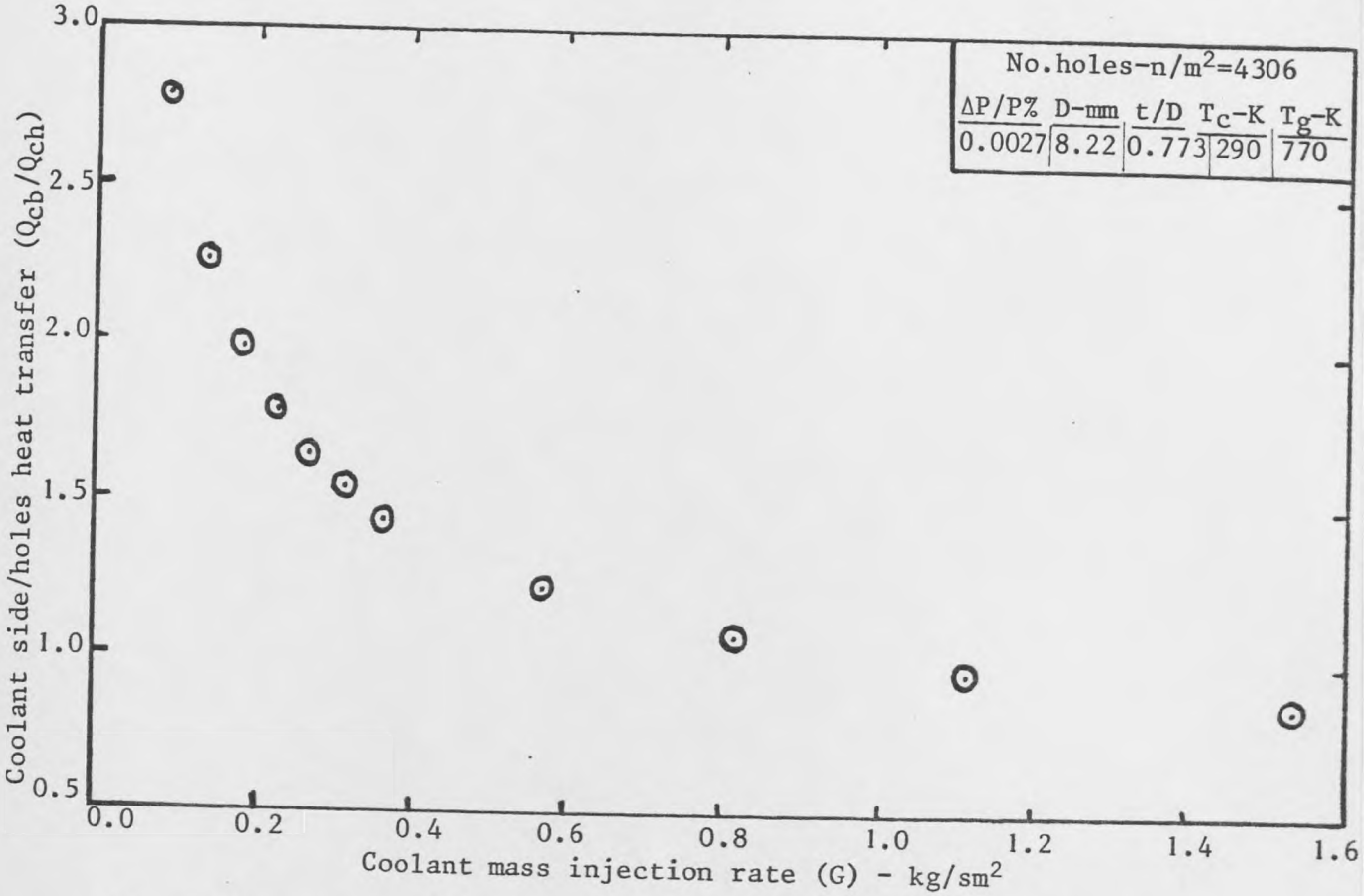

Fig. 6.42: The profile of pre-flame side heat transfer with coolant injection

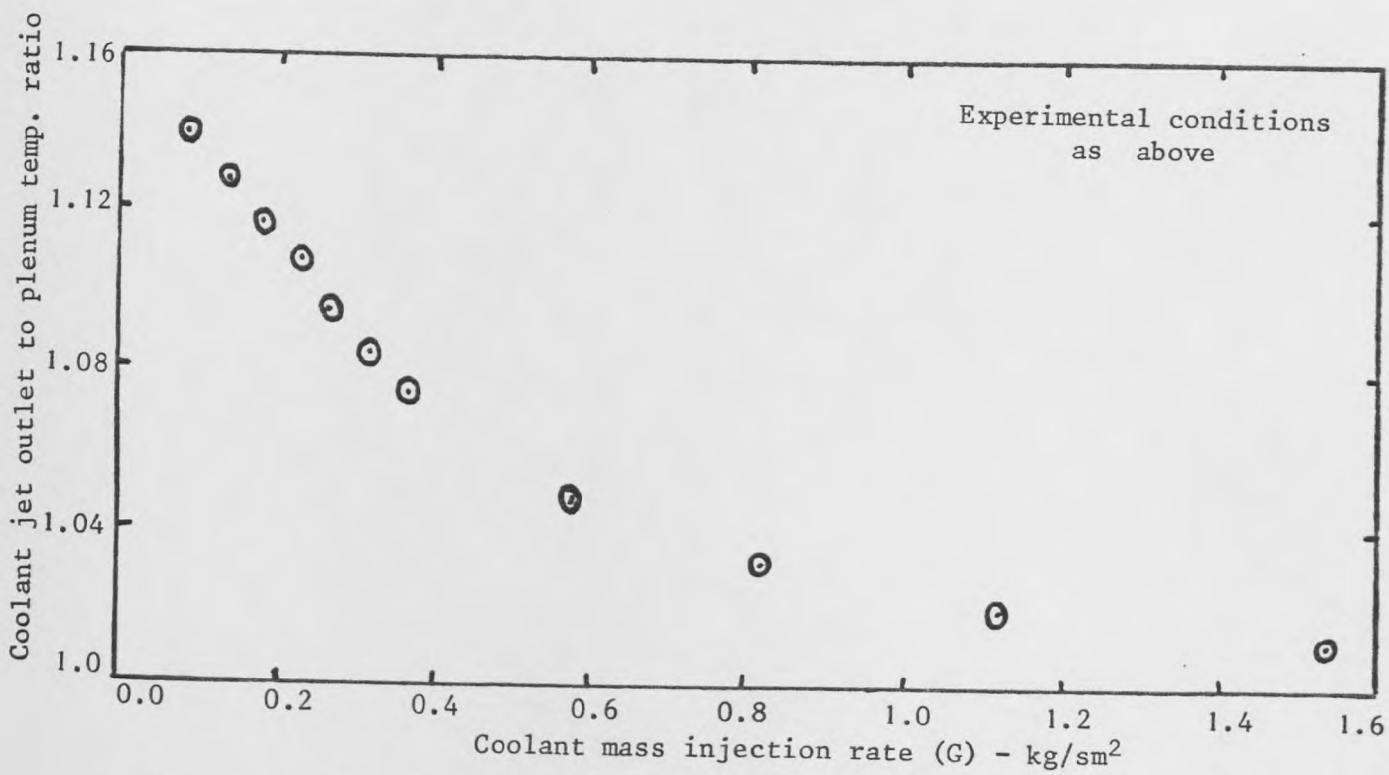

Fig. 6.43: The temperature history of plenum chamber coolant en route to test wall flame-side

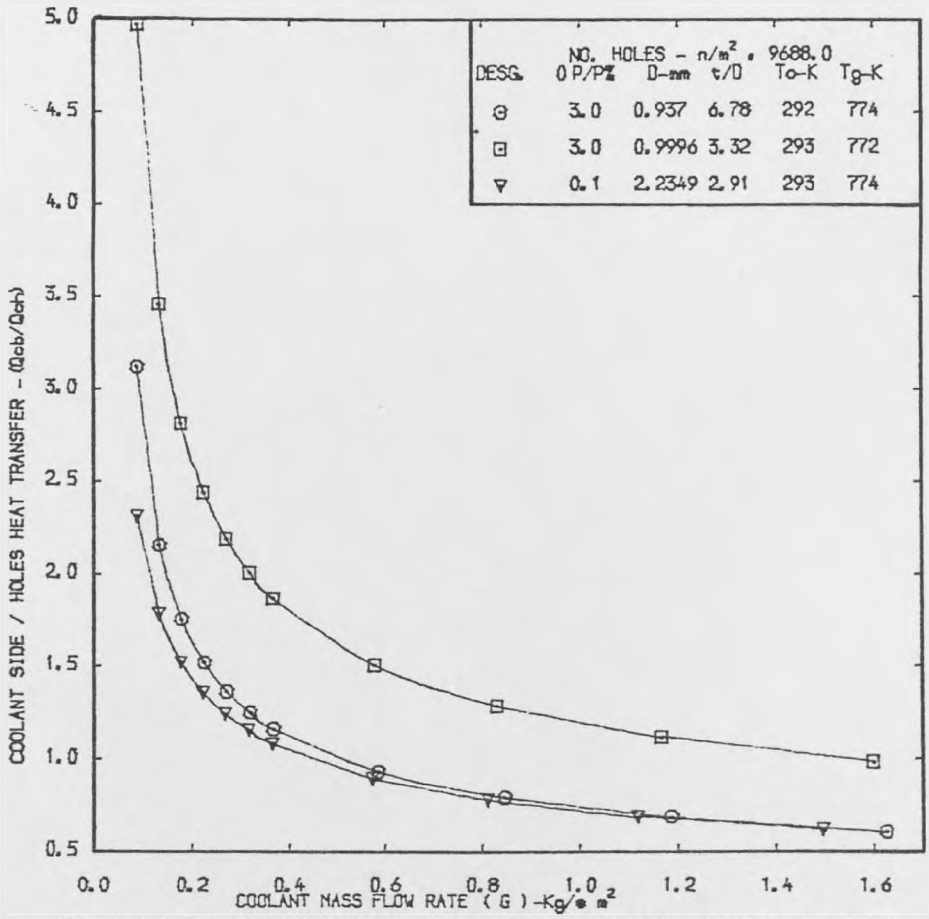

FIG. (6.44) : THE PROFILE OF PRE-FLAME SIDE HEAT TRANSFER WITH COOLANT INJECTION

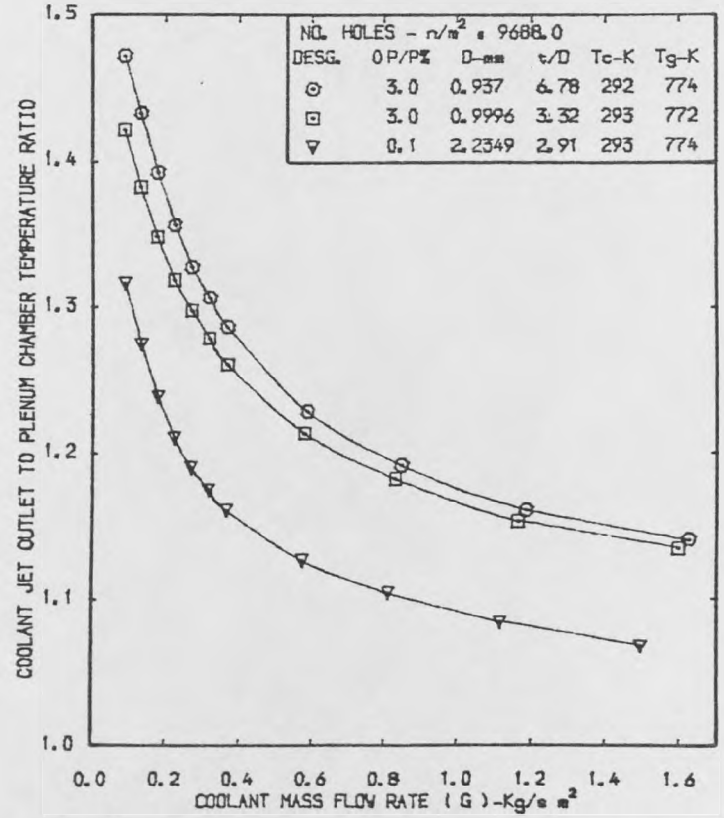

FIG. (6.45) : THE TEMPERATURE HISTORY OF PLENUM CHAMBER COOLANT ENROUTE TO TEST WALL FLAME-SIDE

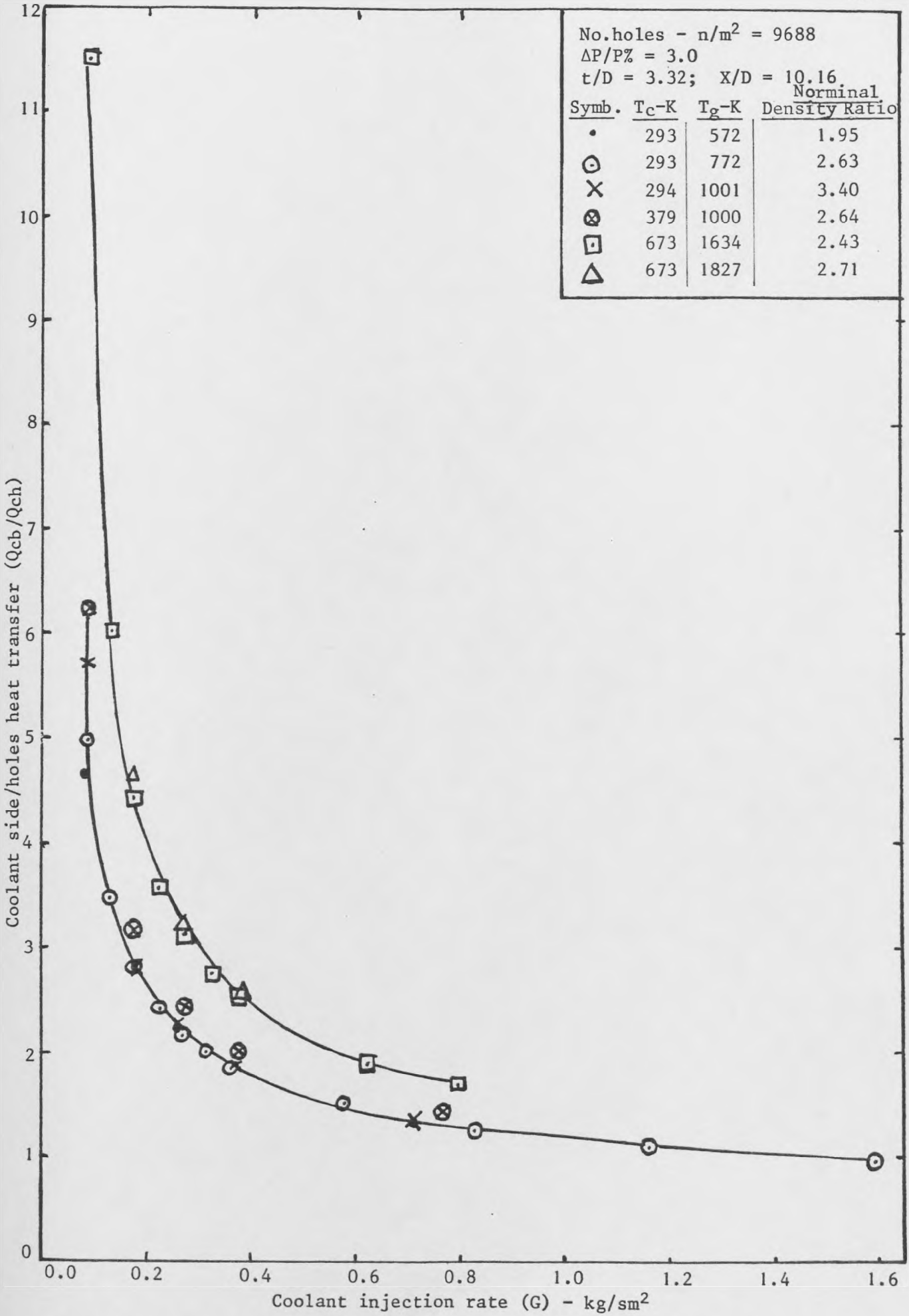

Fig. 6.46: Comparison of back and holes heat transfer of 9688 holes effusion wall at various coolant and cross-stream temperatures

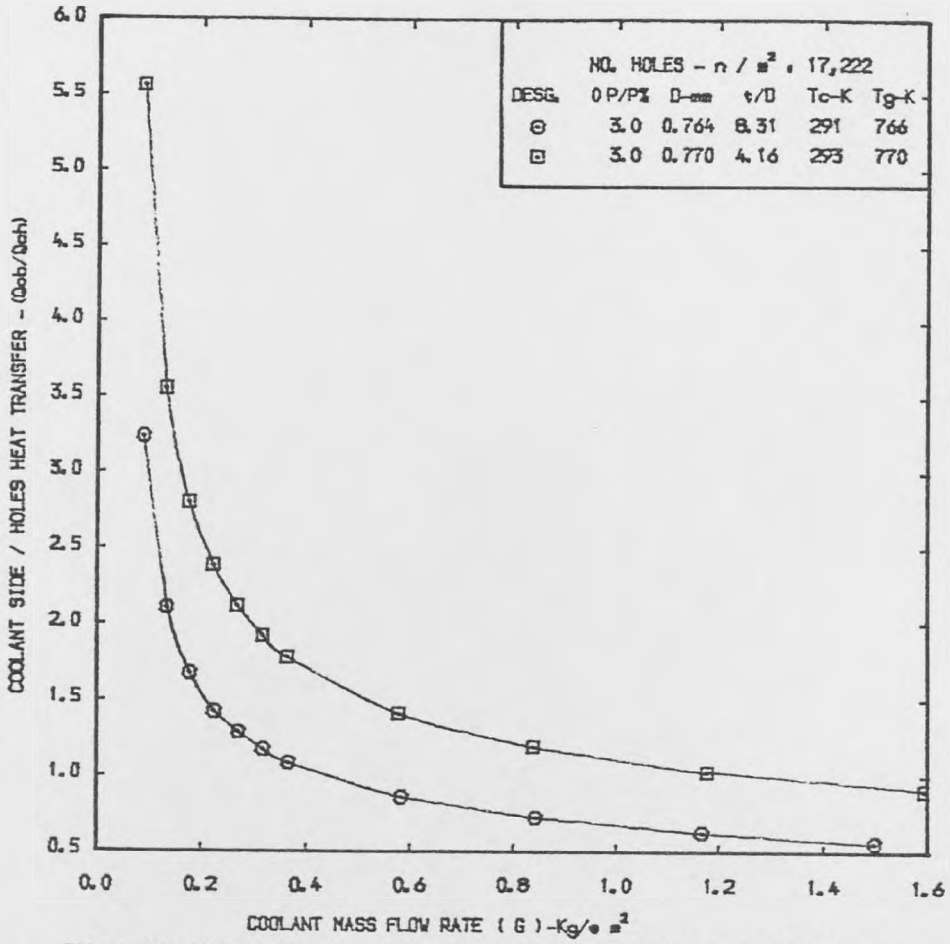

FIG. (6.47) : THE PROFILE OF PRE-FLAME SIDE HEAT TRANSFER WITH COOLANT INJECTION

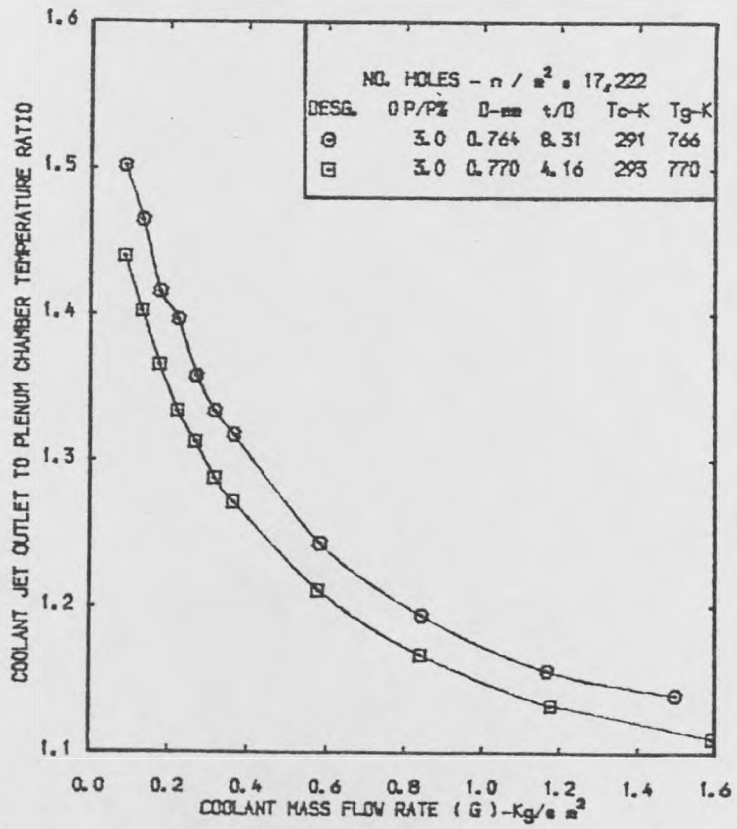

FIG. (6.48) : THE TEMPERATURE HISTORY OF PLENUM CHAMBER COOLANT ENROUTE TO TEST WALL FLAME-SIDE

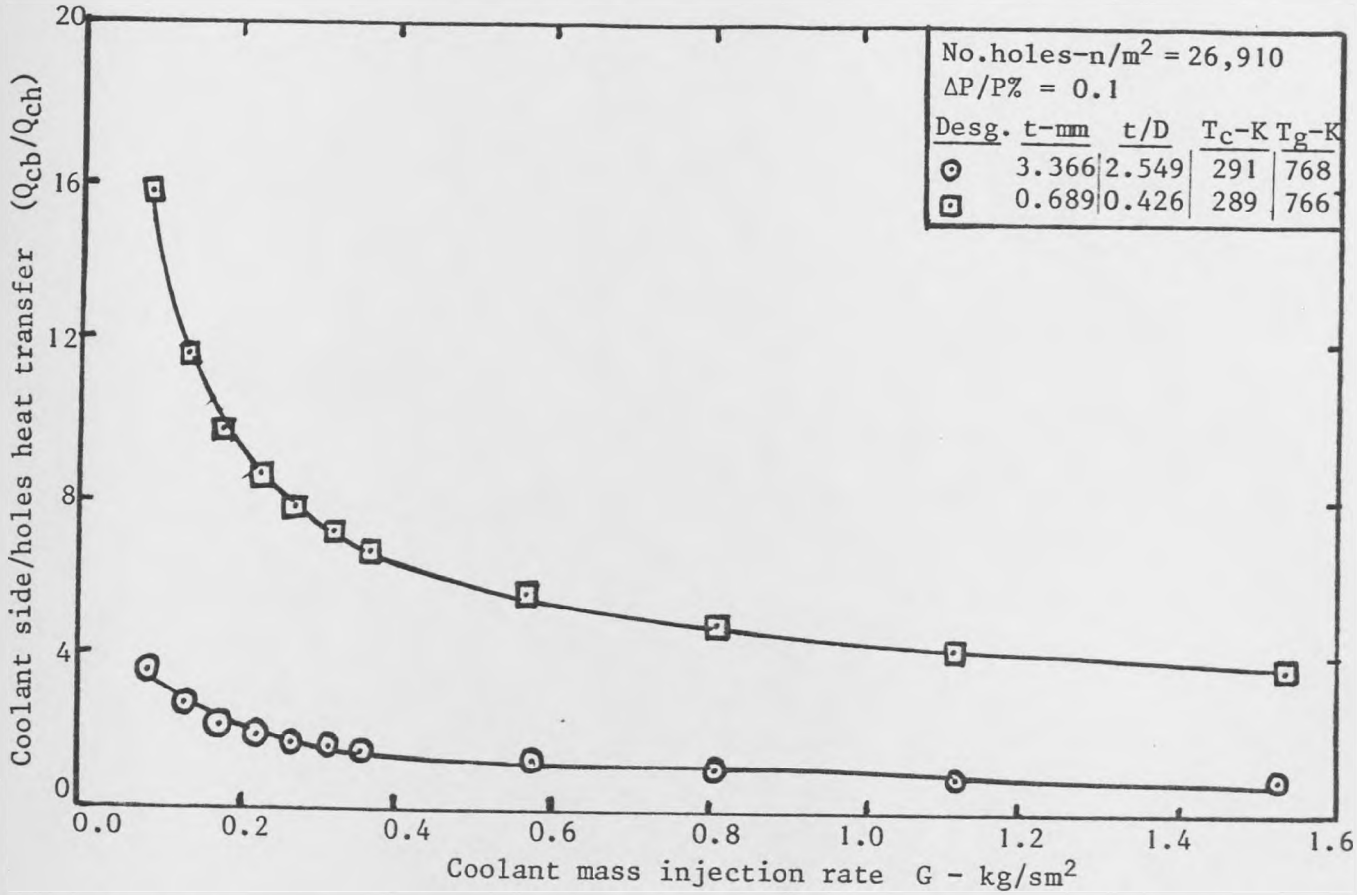

Fig. 6.49: The profile of pre-flame side heat transfer with coolant injection

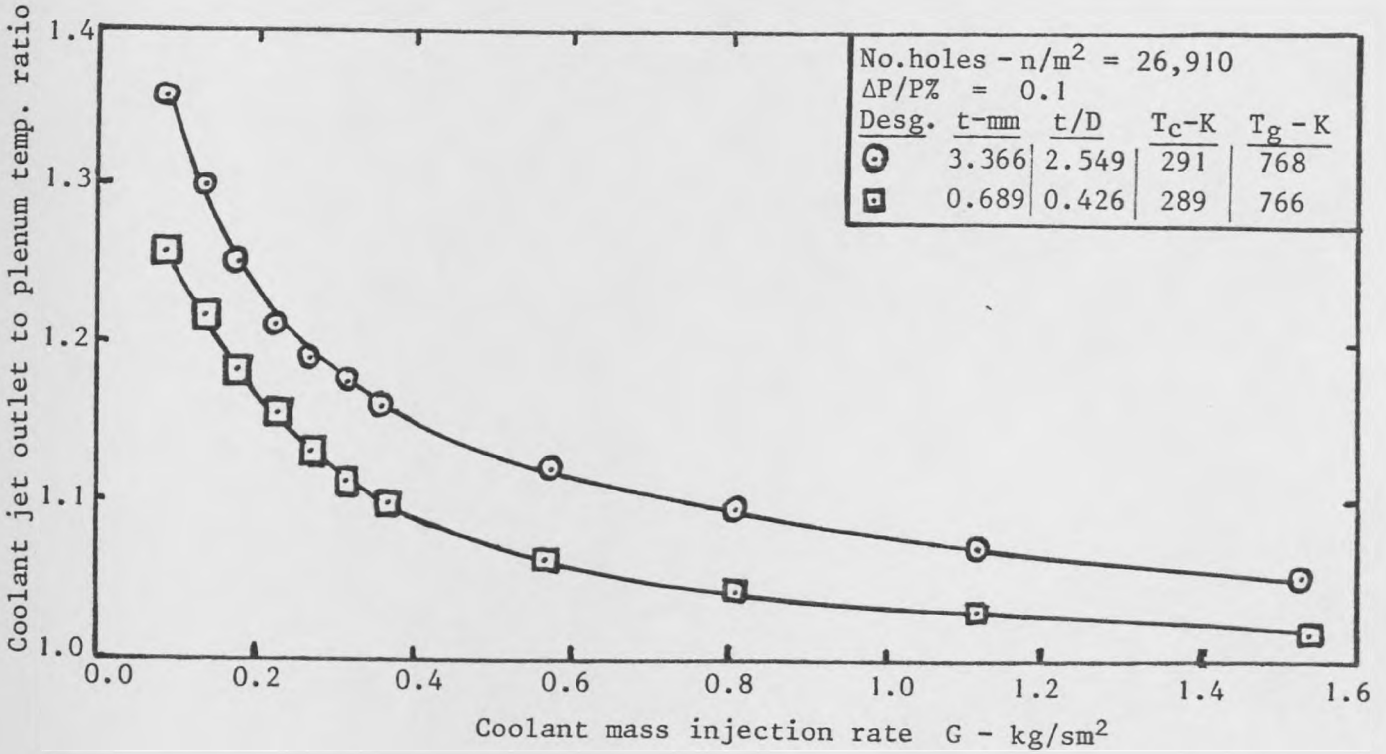

Fig. 6.50: The temperature history of plenum chamber coolant en route to test wall flame-side

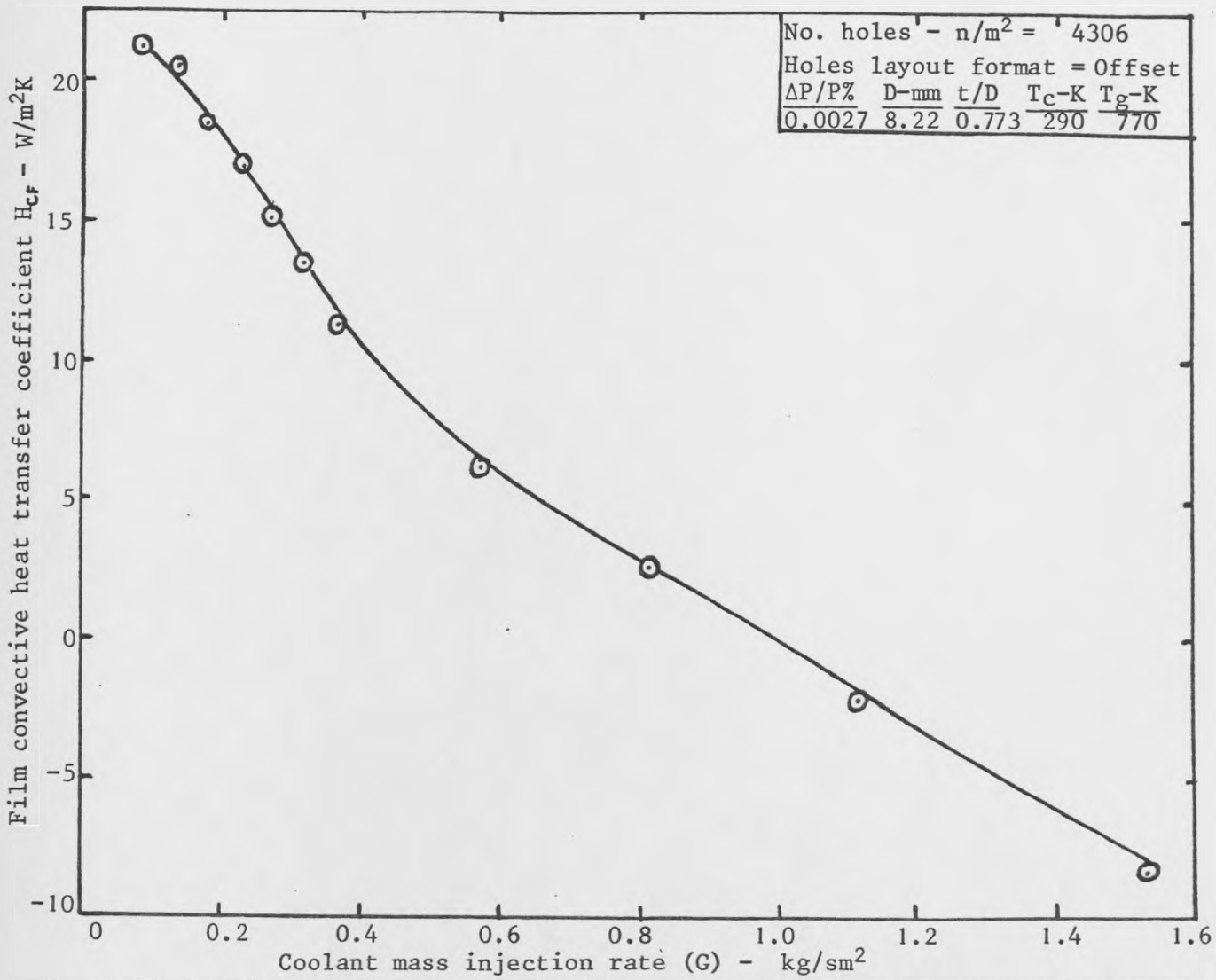

Fig. 6.51: Development of convective heat transfer coefficient with coolant injection at station 5

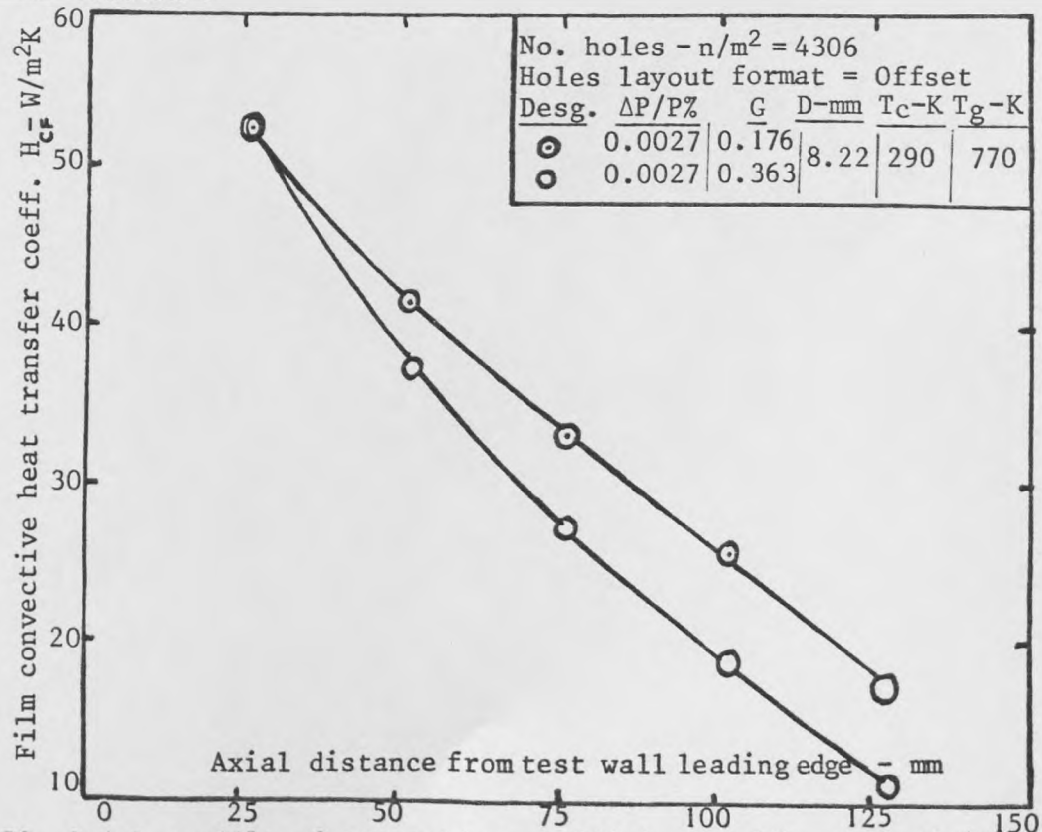

Fig. 6.52: Axial profile of convection coefficient with coolant injection

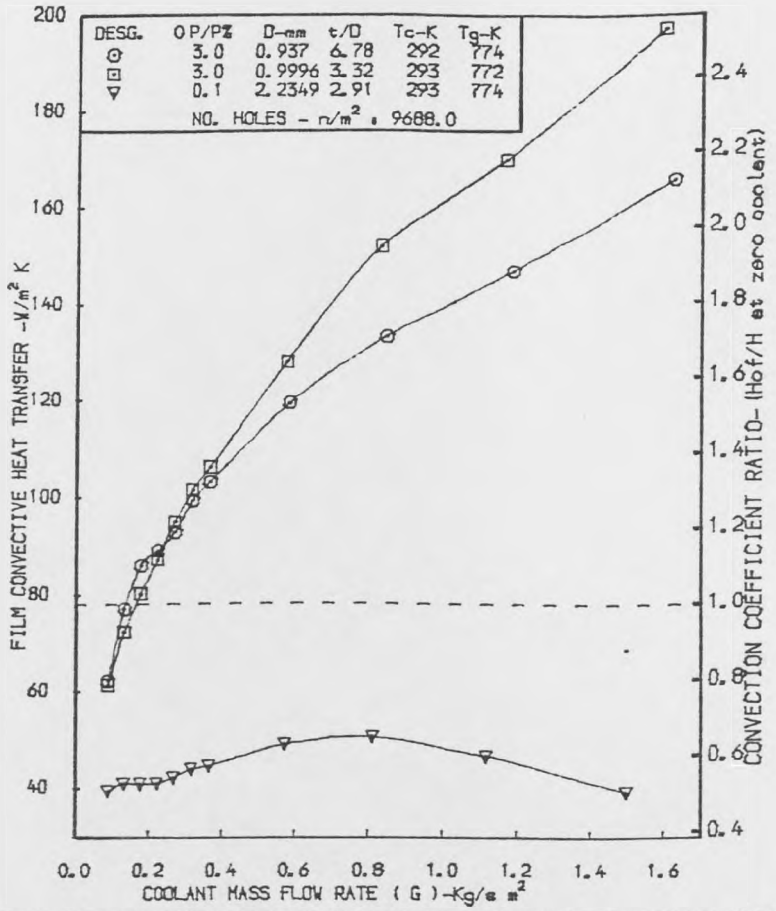

FIG. (6.53) - DEVELOPMENT OF FILM CONVECTIVE HEAT TRANSFER WITH COOLANT INJECTION AT STATION 5

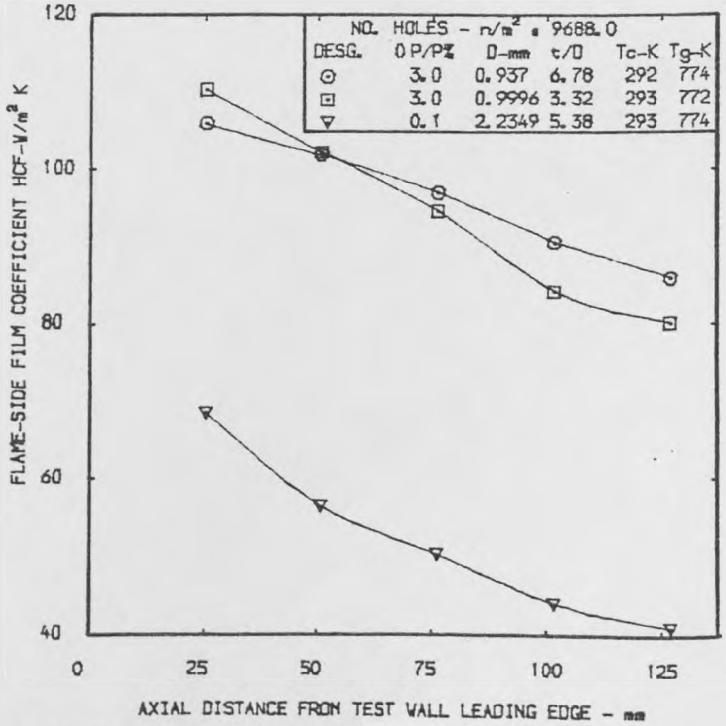

FIG. (6.54) - AXIAL PROFILE OF CONVECTION COEFFICIENT AT COOLANT INJECTION RATE G = 0.2 Kg/sm²

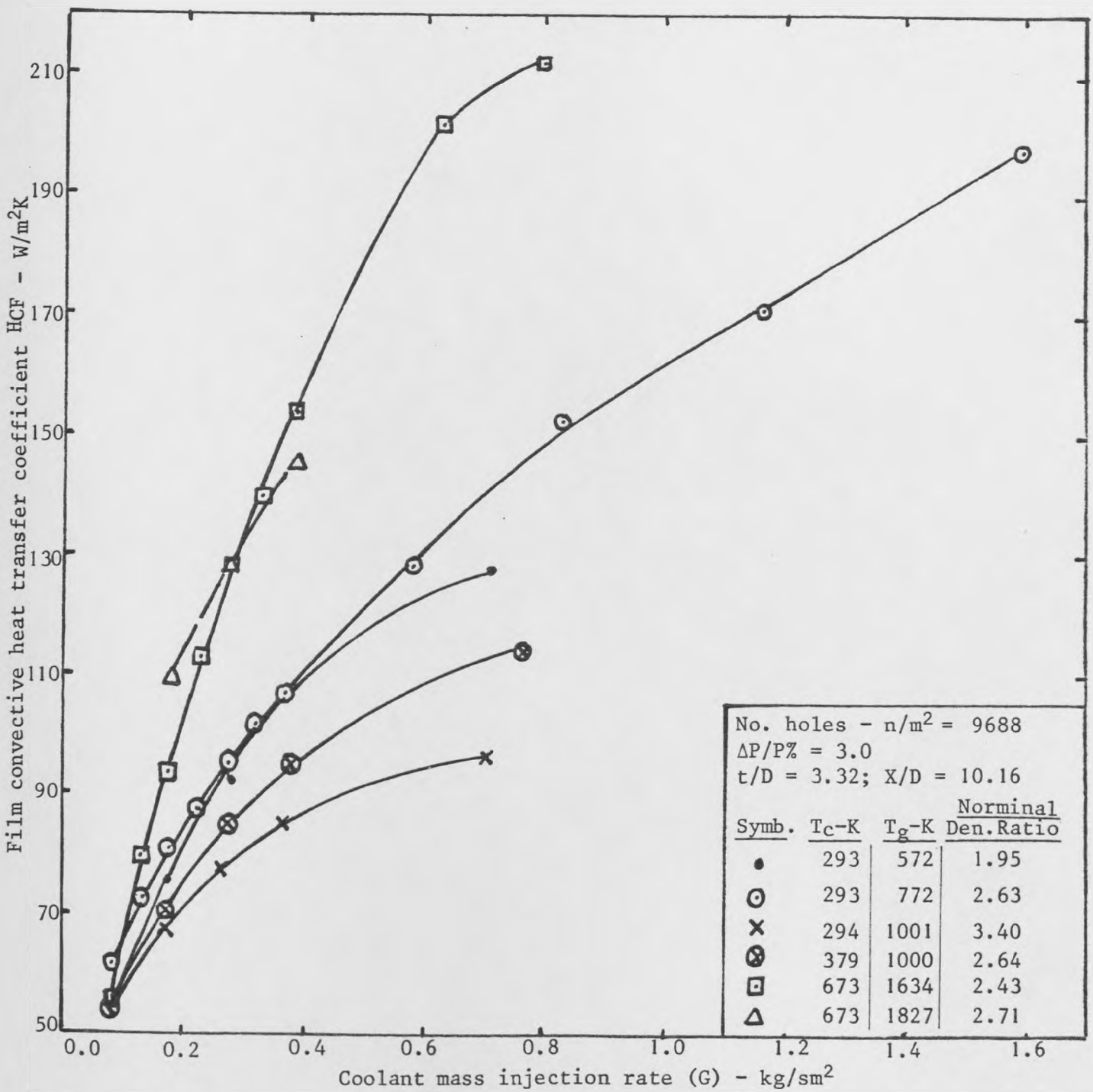

Fig. 6.55: Dependency of film heat transfer coefficient on coolant injection at station 5

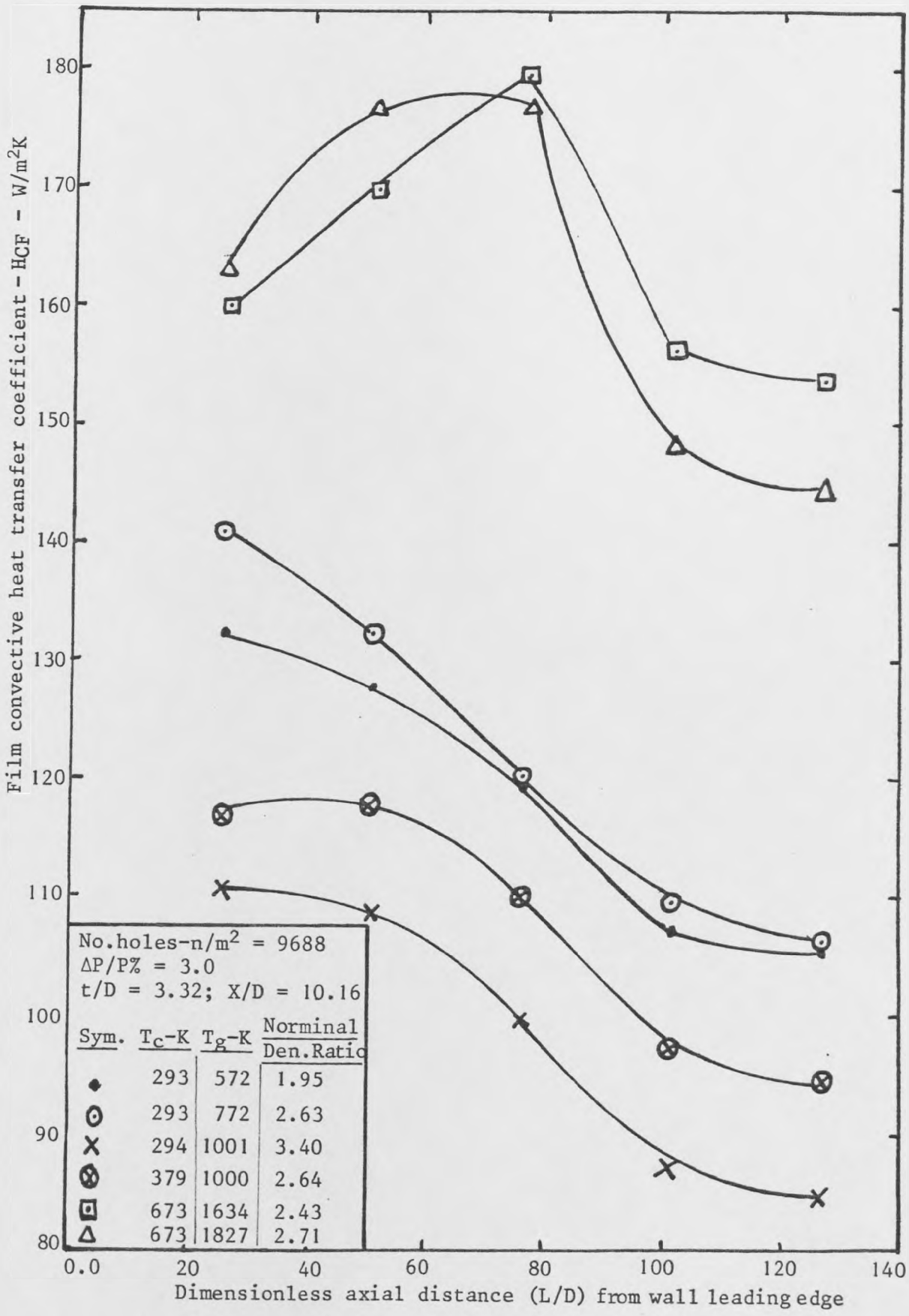

Fig. 6.56: Axial profile of film heat transfer coefficient at $0.36 \leqslant G - kg/sm^2 \leqslant 0.382$

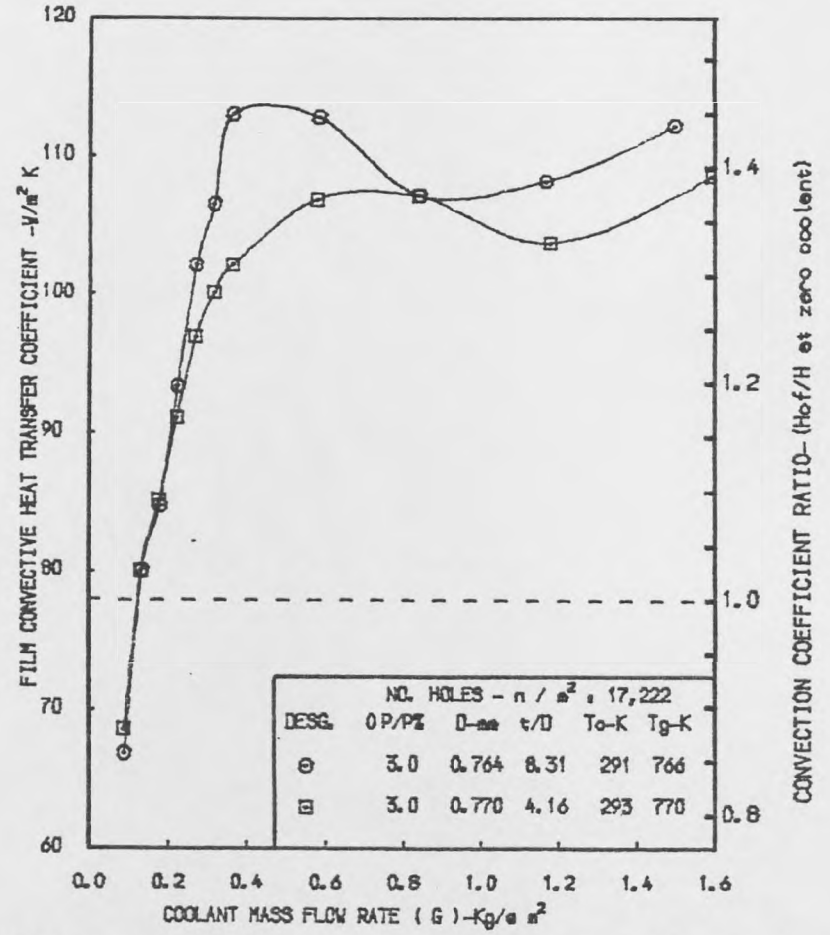

FIG. (6.57) : DEVELOPMENT OF FILM CONVECTIVE HEAT TRANSFER WITH COOLANT INJECTION AT STATION 5

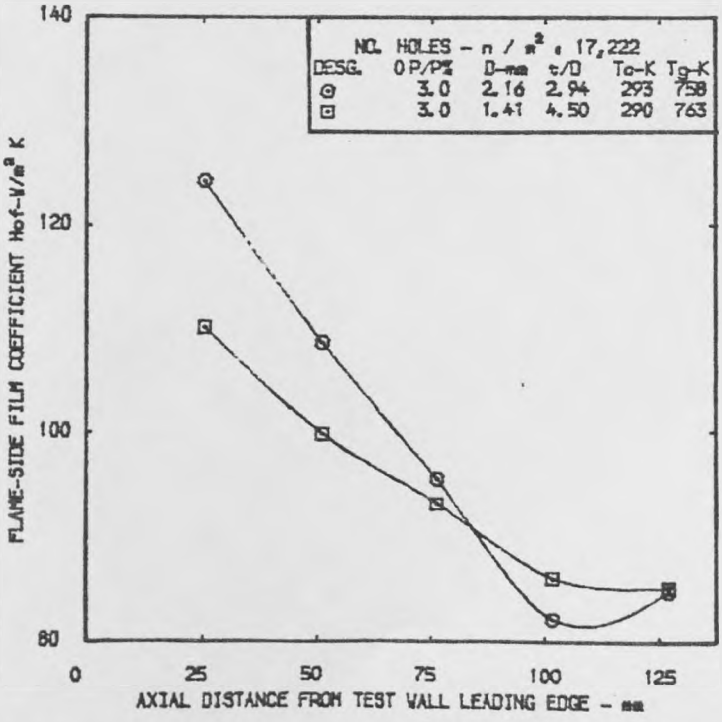

FIG. (6.58) : AXIAL PROFILE OF CONVECTION COEFFICIENT AT COOLANT INJECTION RATE G = 0.2 Kg/sm²

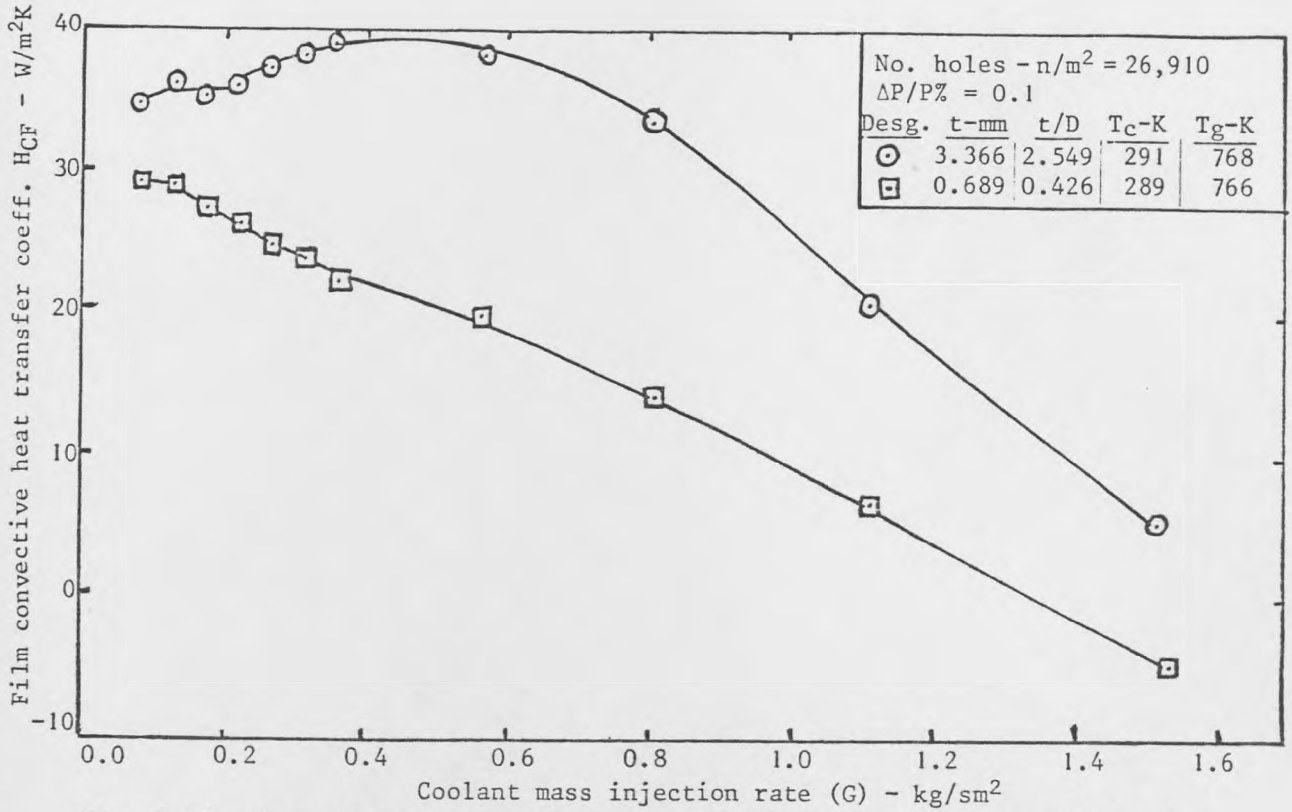

Fig. 6.59: Dependency of film heat transfer coefficient on coolant injection at station 5

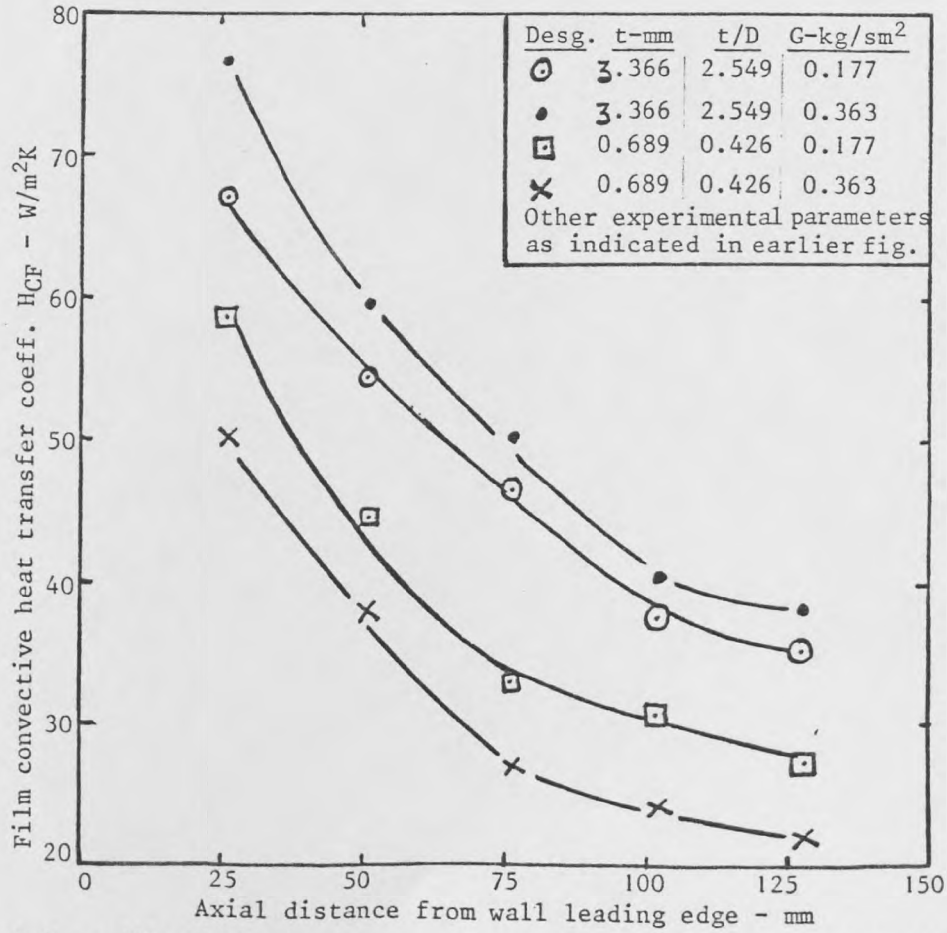

Fig. 6.60: Axial profile of film heat transfer coefficient at constant injection rates

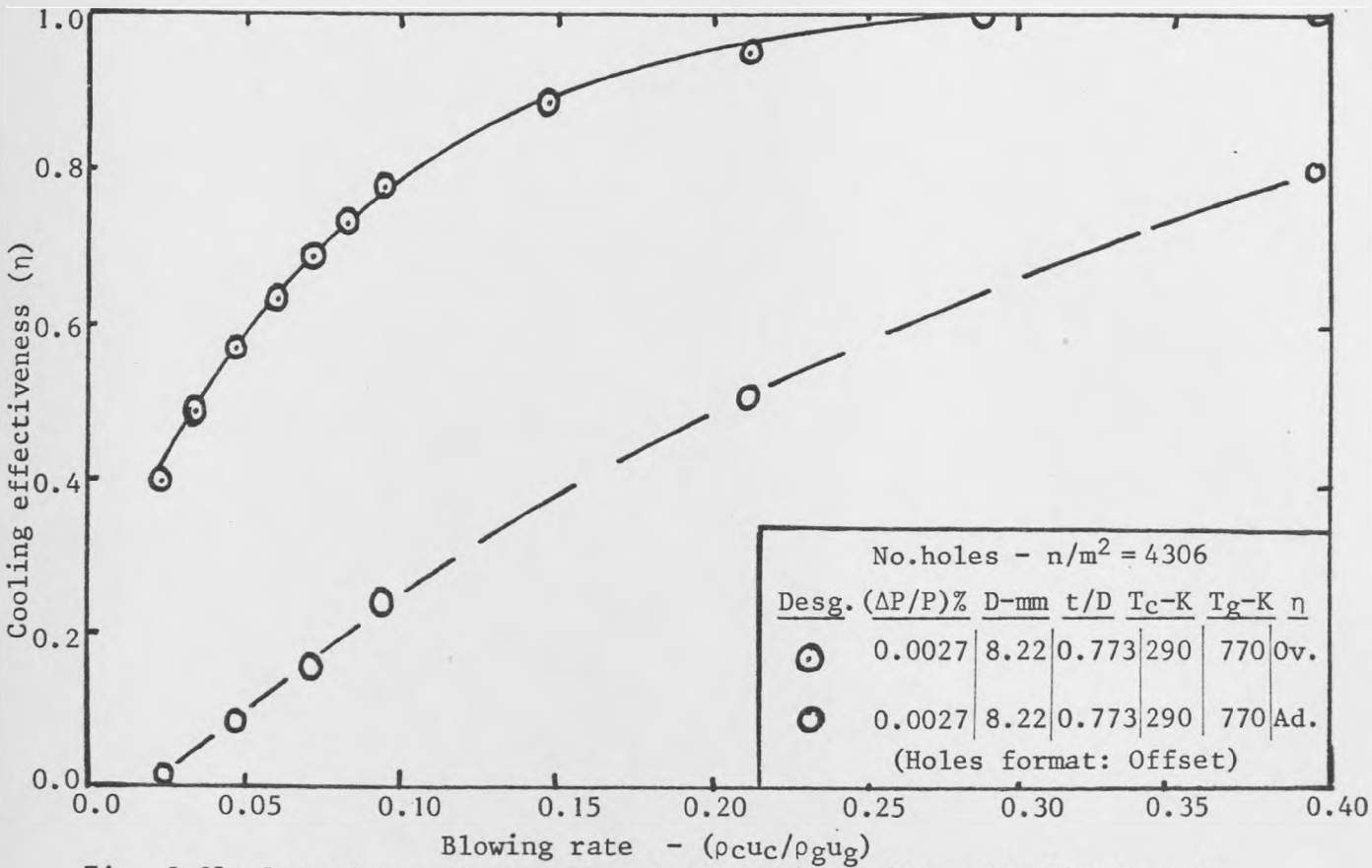

Fig. 6.61: Dependency of overall and adiabatic cooling effectiveness on blowing rate

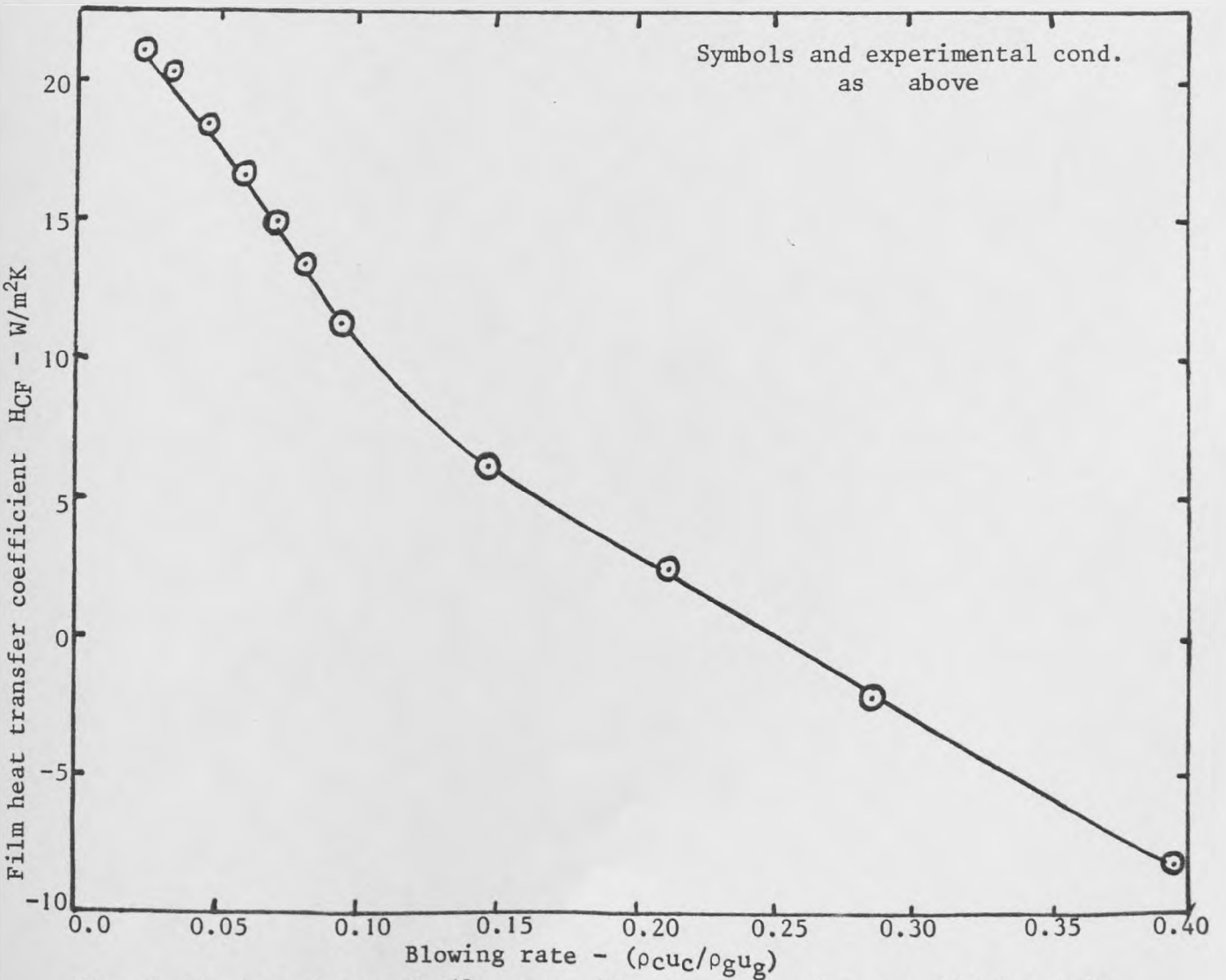

Fig. 6.62: Dependency of film convective heat transfer on blowing rate

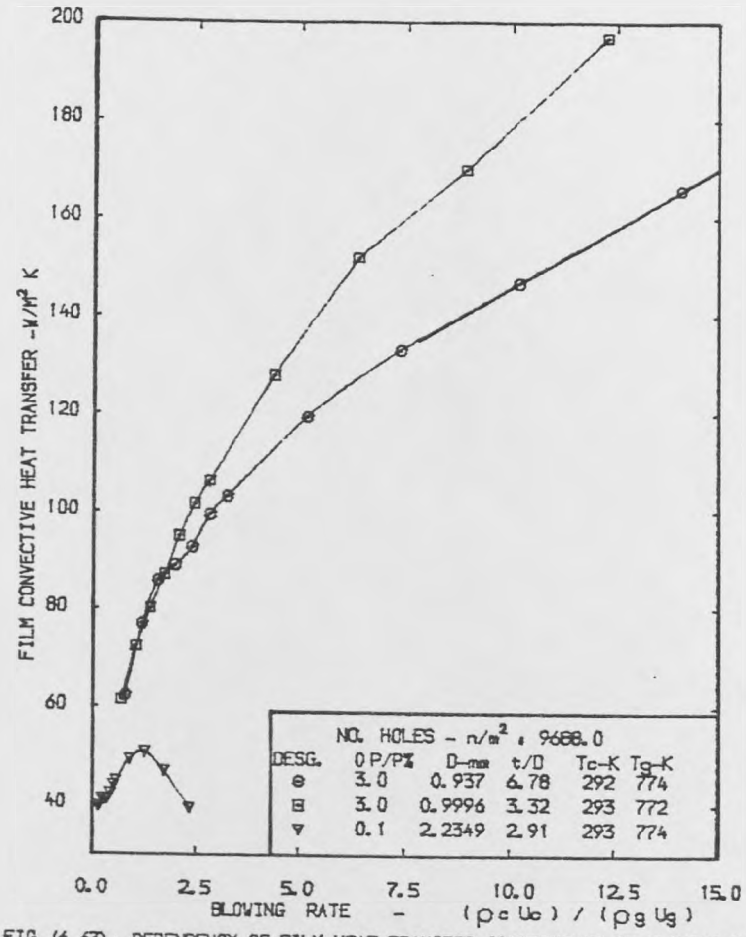

FIG. (6.63) : DEPENDENCY OF FILM HEAT TRANSFER COEFFICIENT ON BLOWING RATE

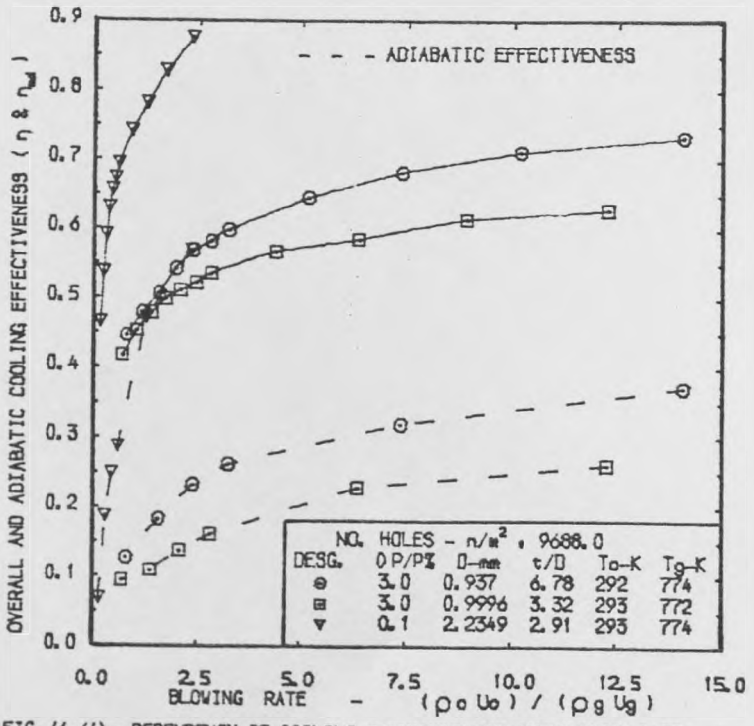

FIG. (6.64) : DEPENDENCY OF COOLING EFFECTIVENESS ON BLOWING RATE

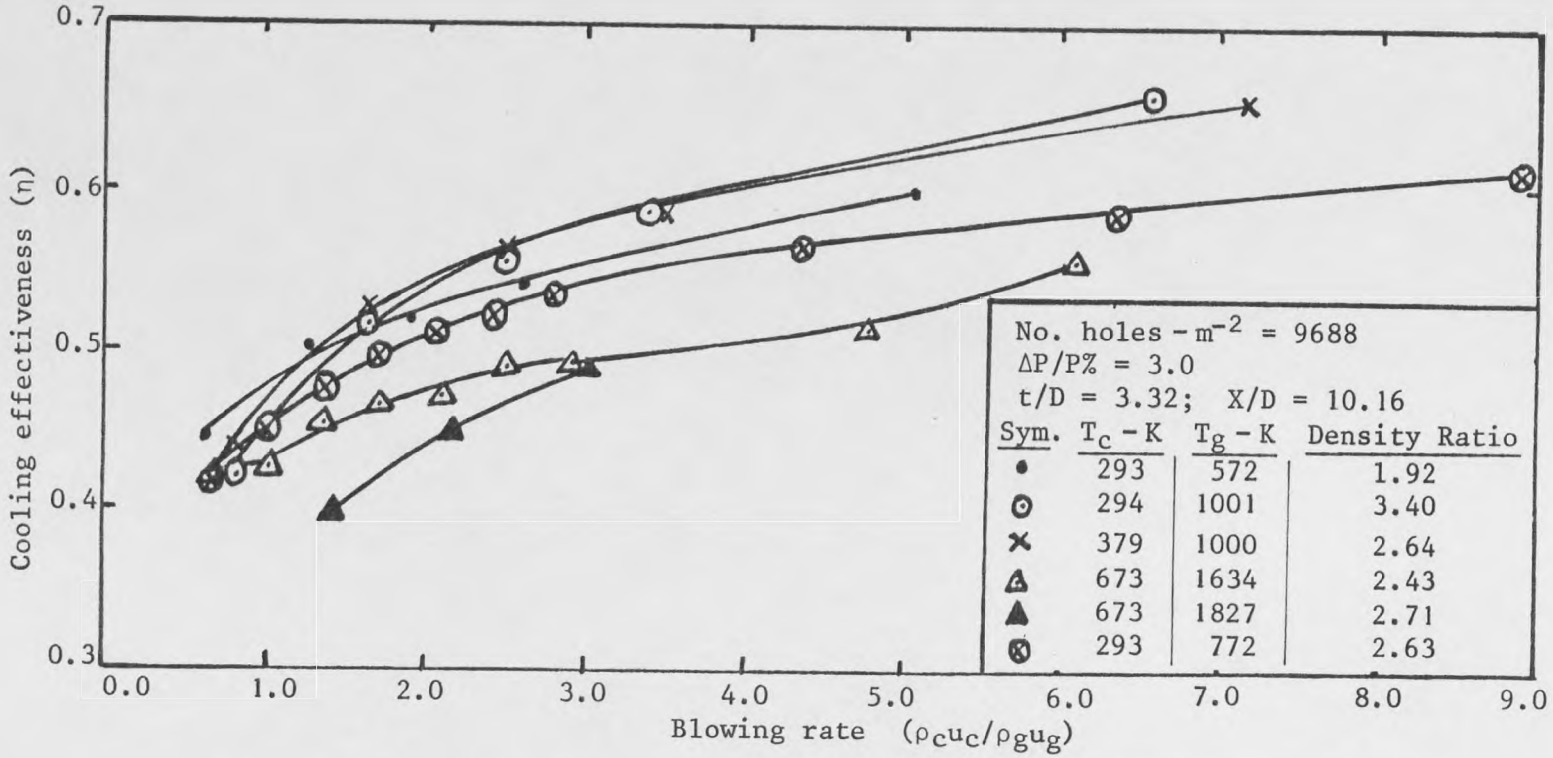

Fig. 6.65: Dependence of cooling effectiveness of a cylindrical combustor for type 9688 m^{-2} holes effusion system on blowing rate

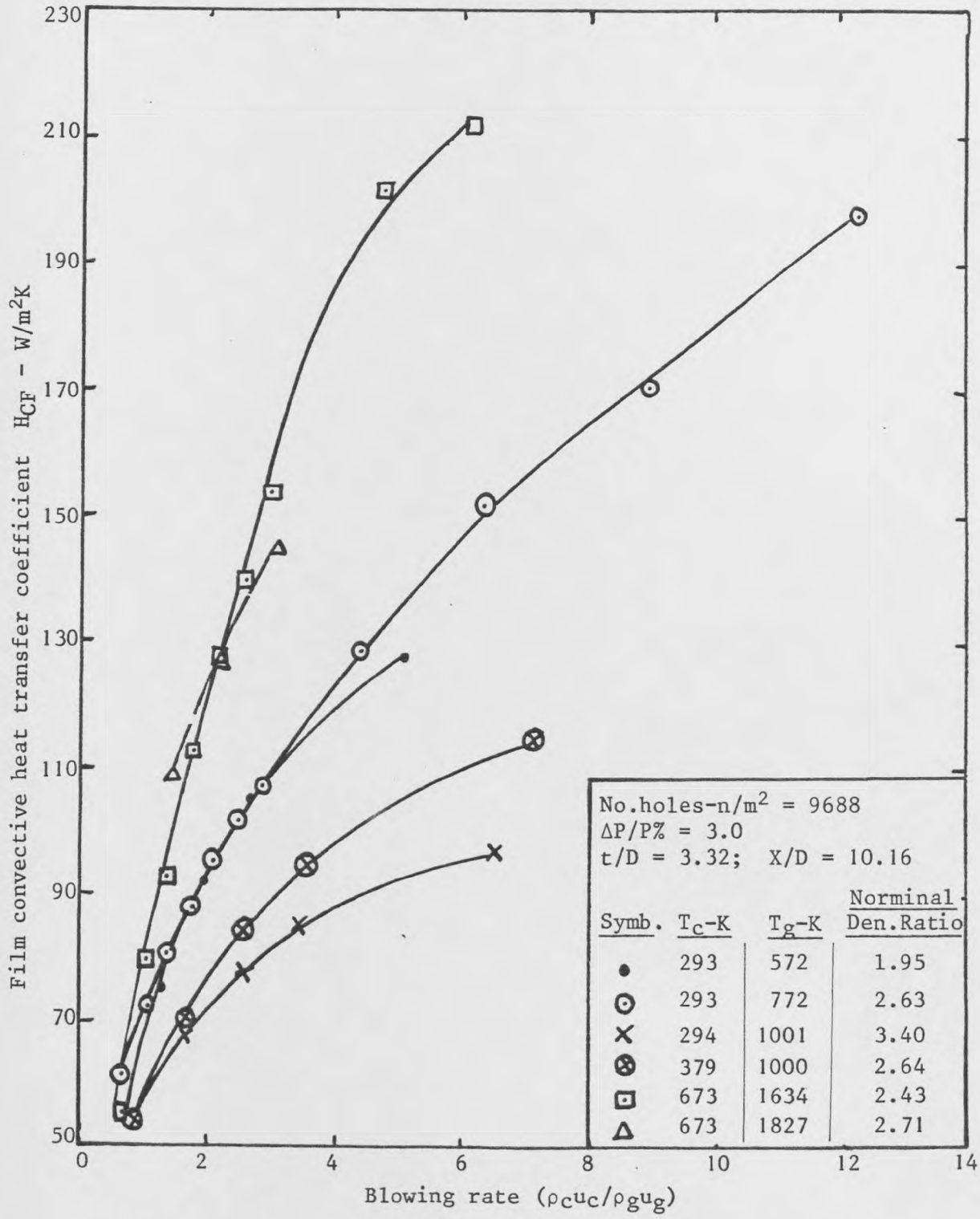

Fig. 6.66: Development of film convective heat transfer coefficient with blowing rate

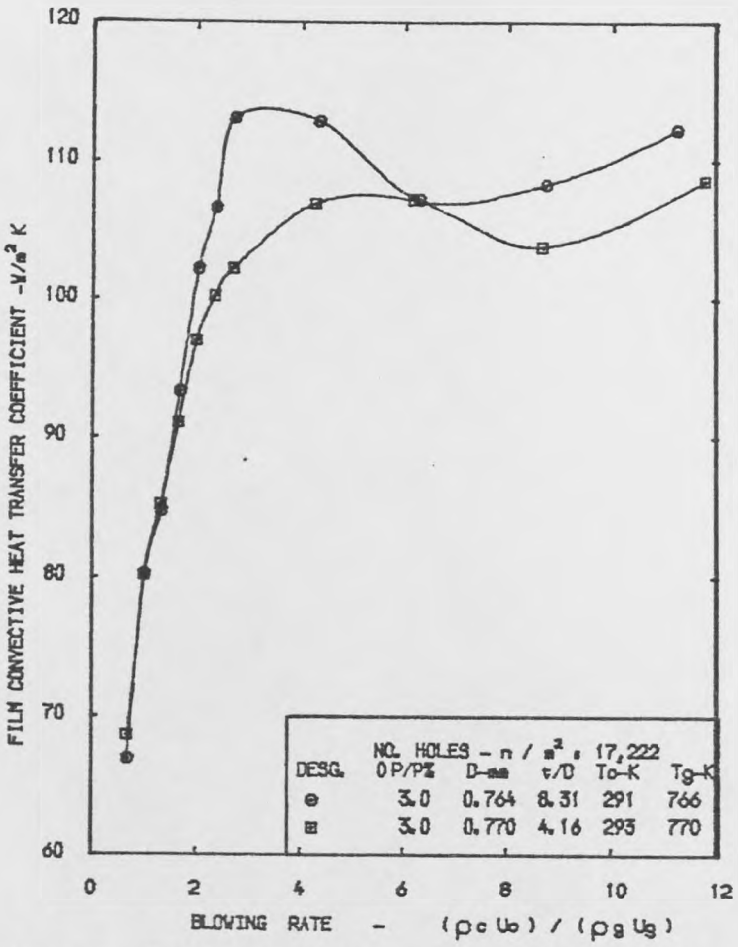

FIG. (6.67) . DEPENDENCY OF FILM HEAT TRANSFER COEFFICIENT ON BLOWING RATE

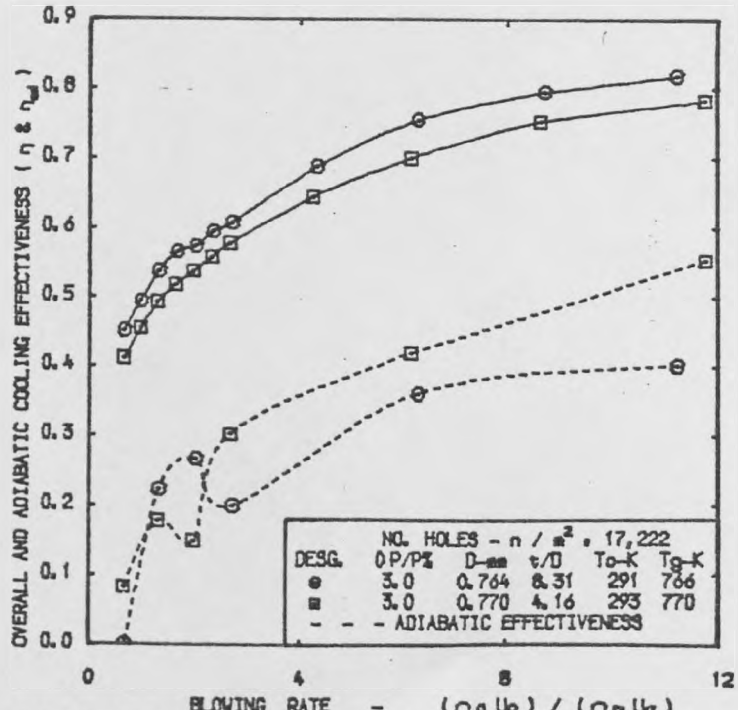

FIG. (6.68) . DEPENDENCY OF COOLING EFFECTIVENESS ON BLOWING RATE

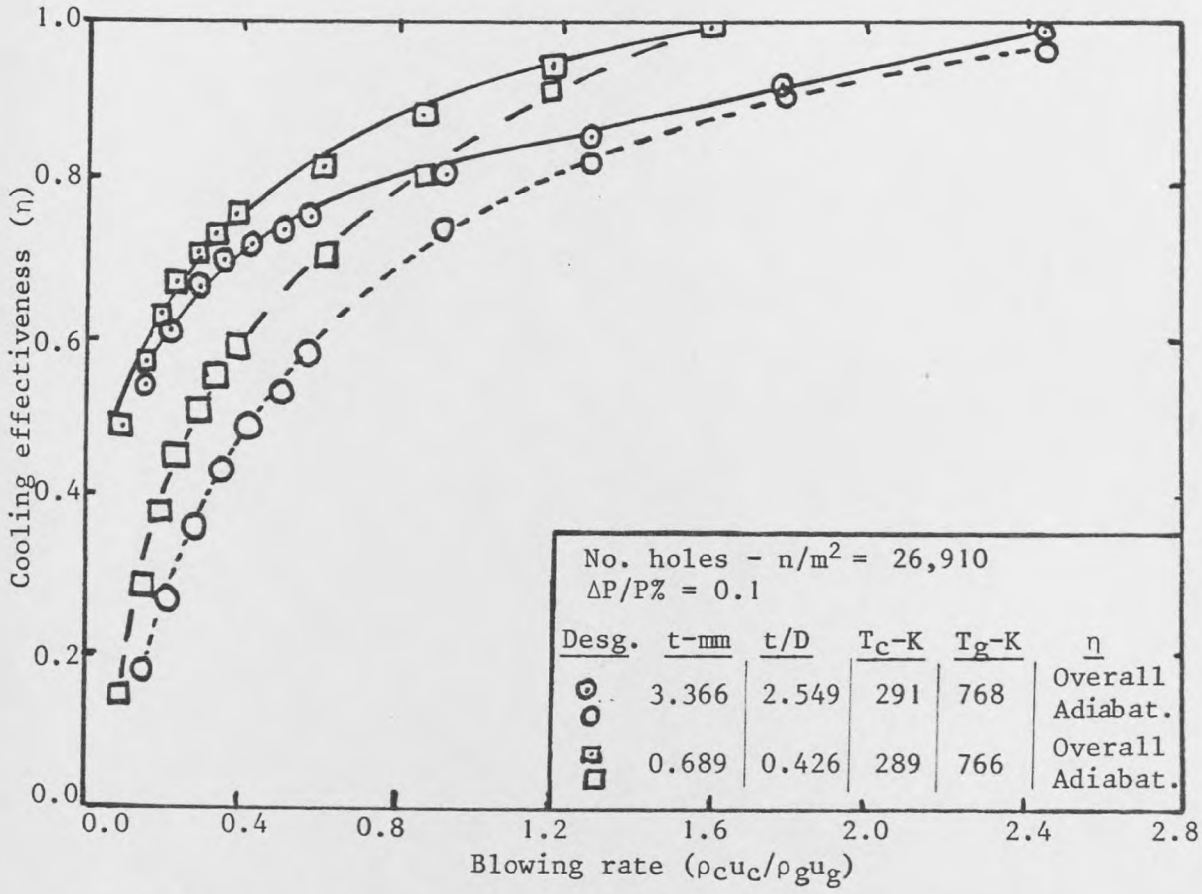

Fig. 6.69: Dependency of overall and adiabatic effectiveness on blowing rate

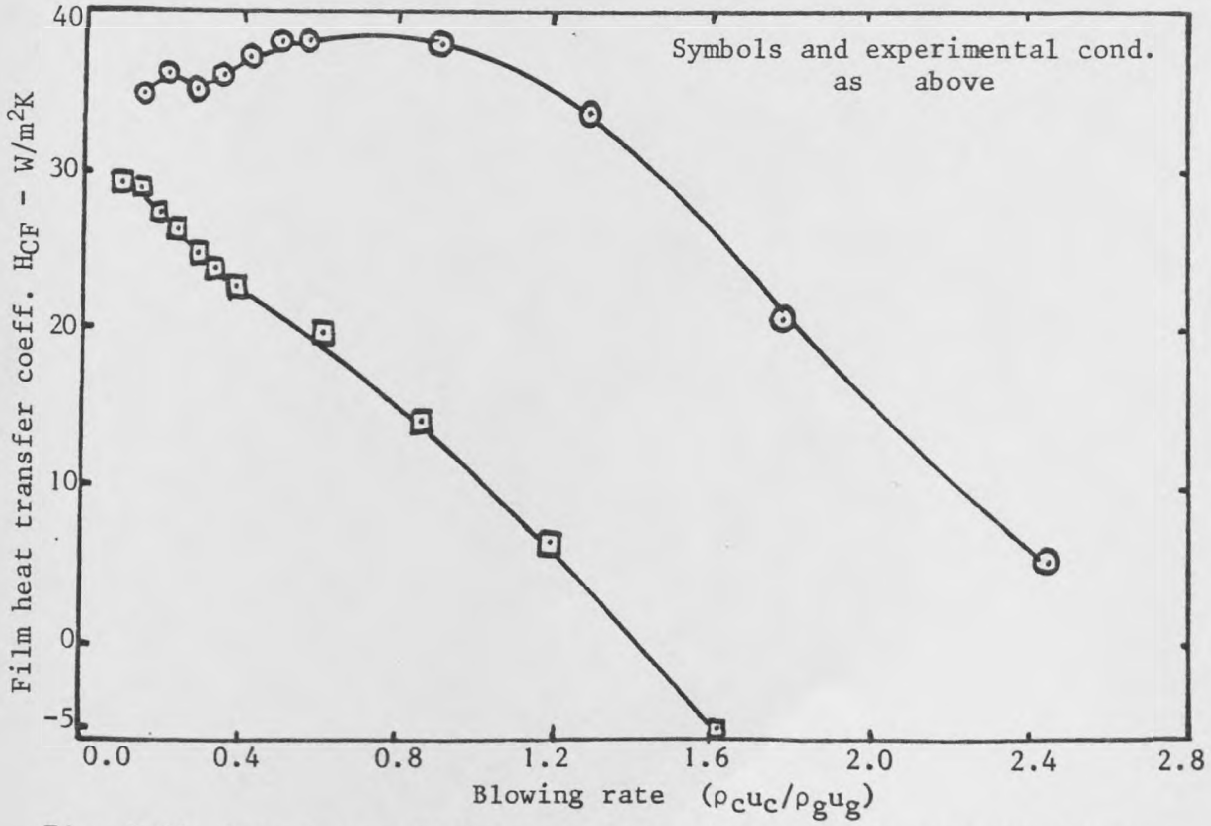

Fig. 6.70: Dependency of film convective heat transfer coefficient on blowing rate

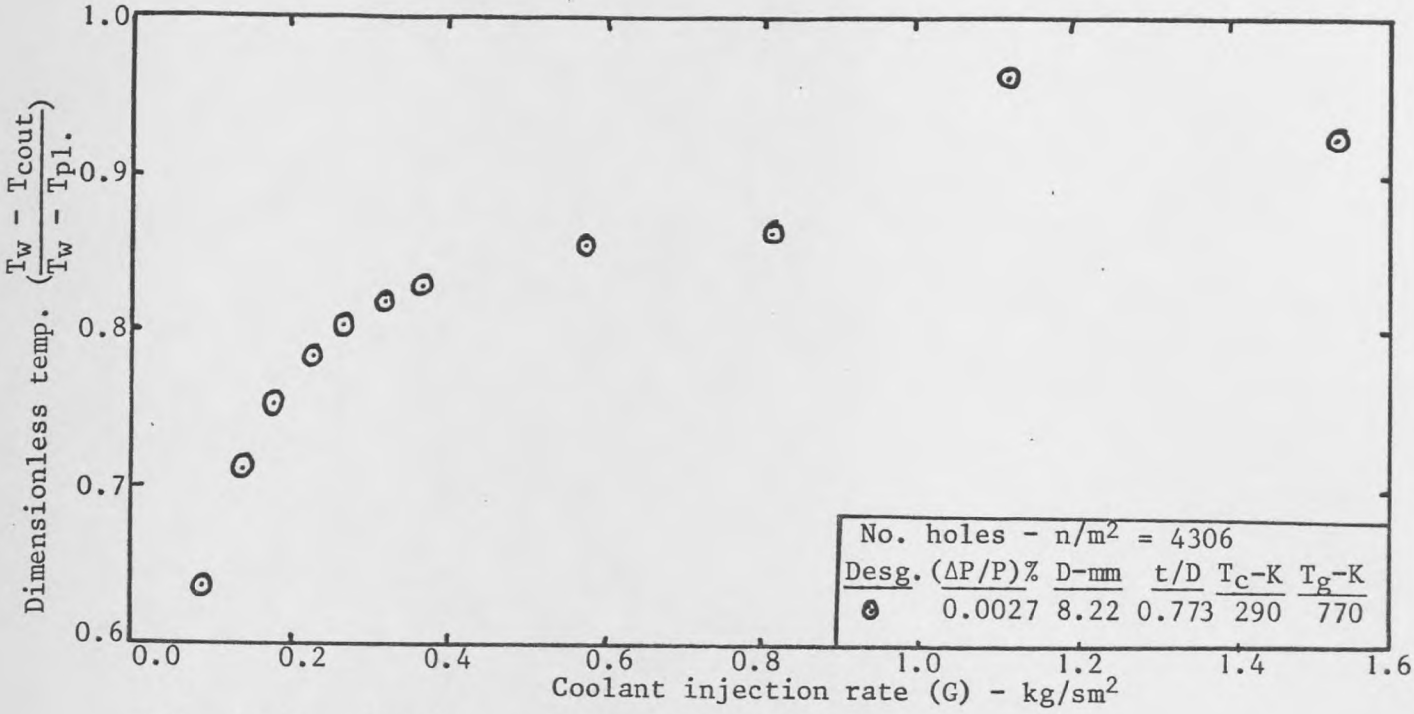

Fig. 6.71: Coolant temperature profile at station 5

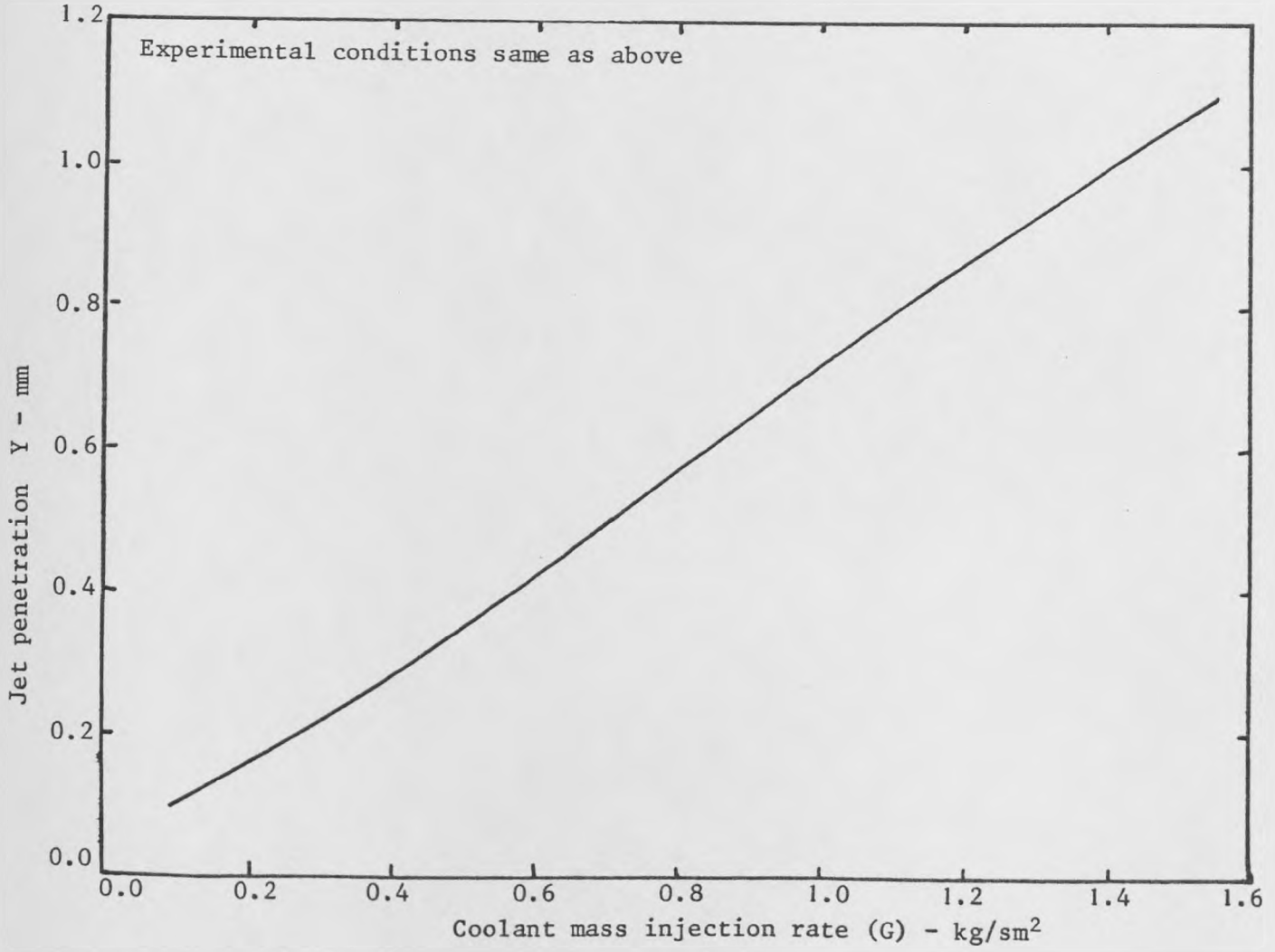

Fig. 6.72: Trajectory of coolant jets into cross-stream

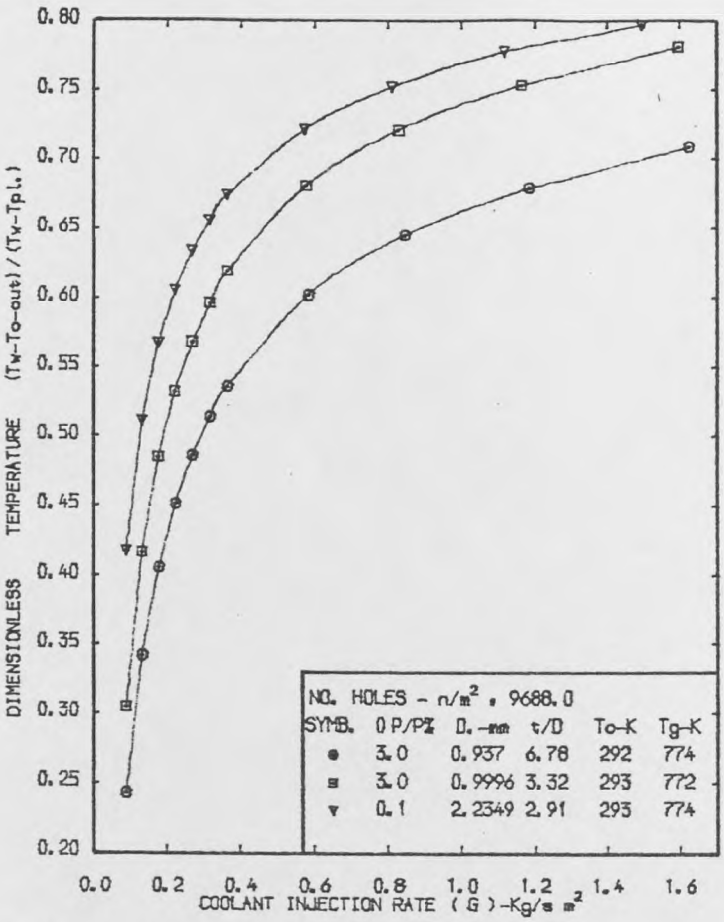

FIG. (6.73) : COOLANT TEMPERATURE PROFILE AT STATION 5

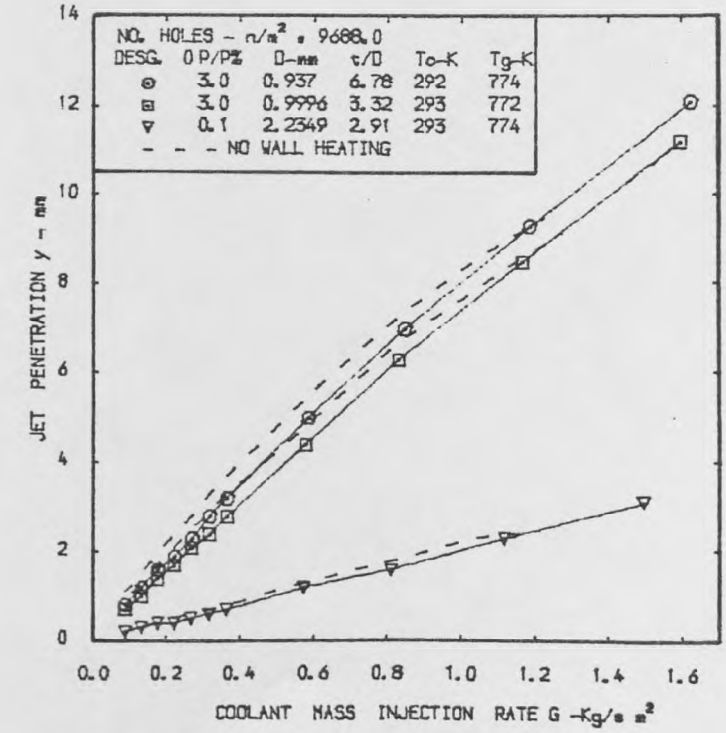

FIG. (6.74) : TRAJECTRY OF COOLANT JETS INTO CROSS-STREAM

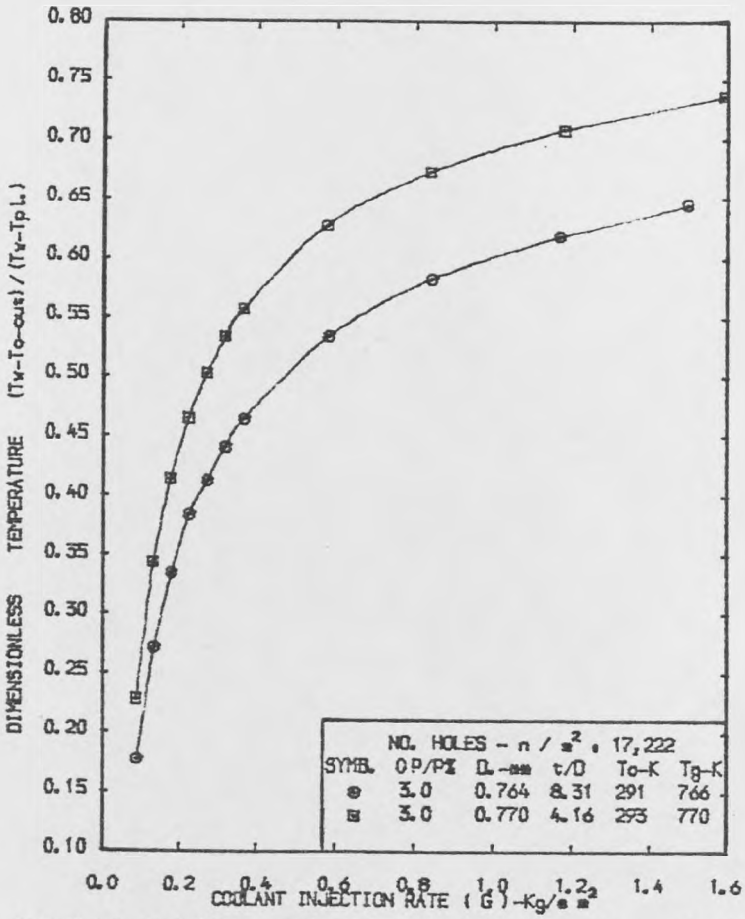

FIG. (6.75) : COOLANT TEMPERATURE PROFILE AT STATION 5

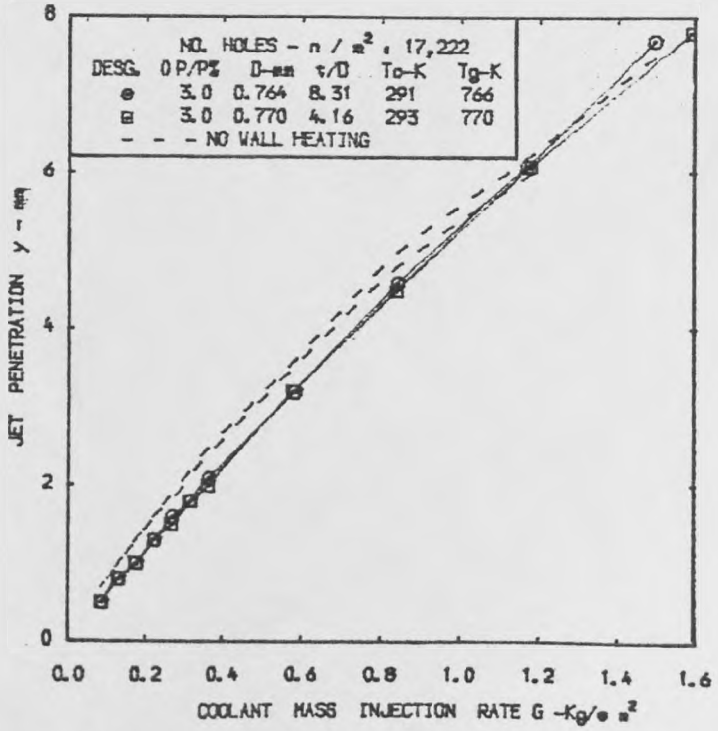

FIG. (6.76) : TRAJECTRY OF COOLANT JETS INTO CROSS-STREAM

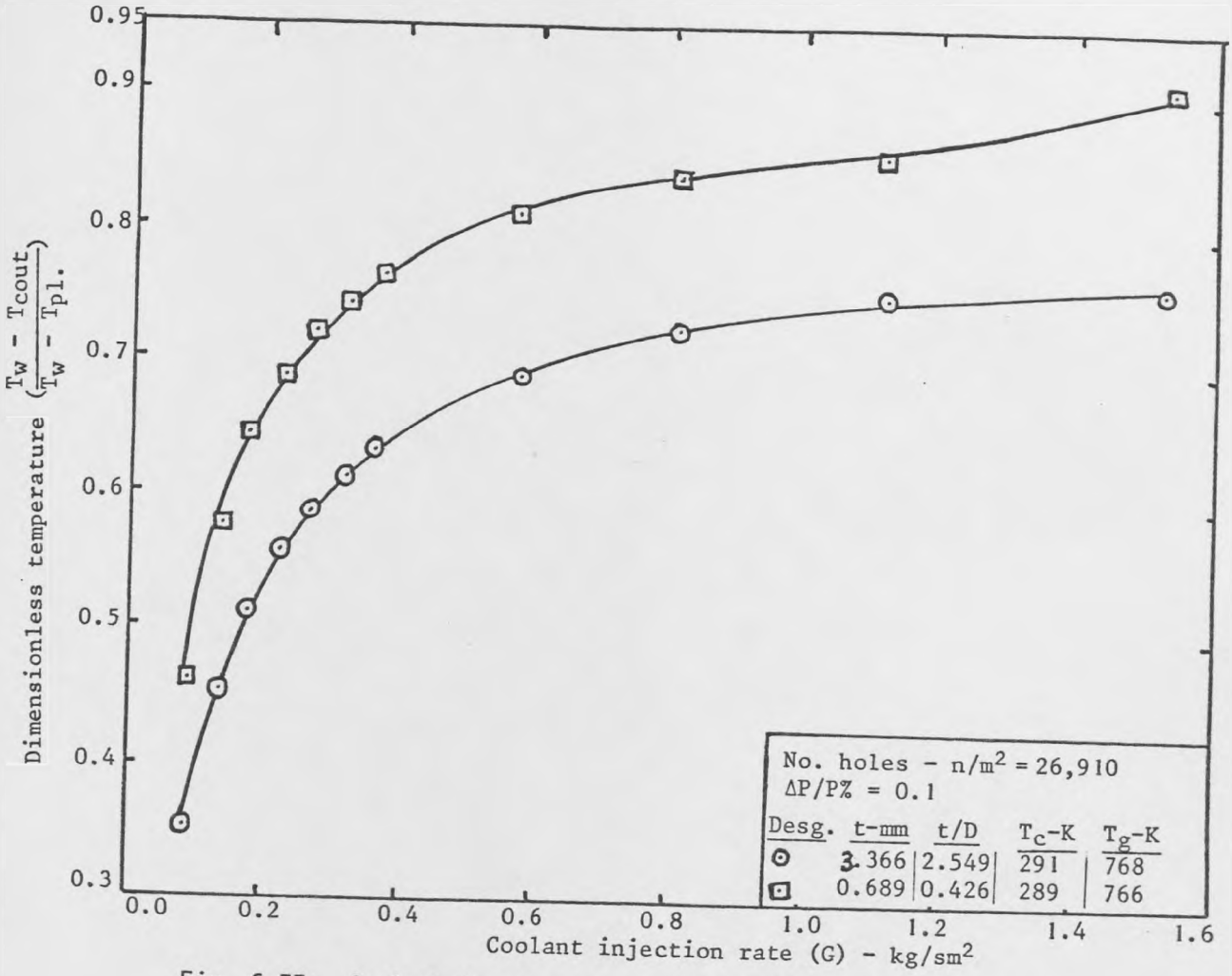

Fig. 6.77: Coolant temperature profile at station 5

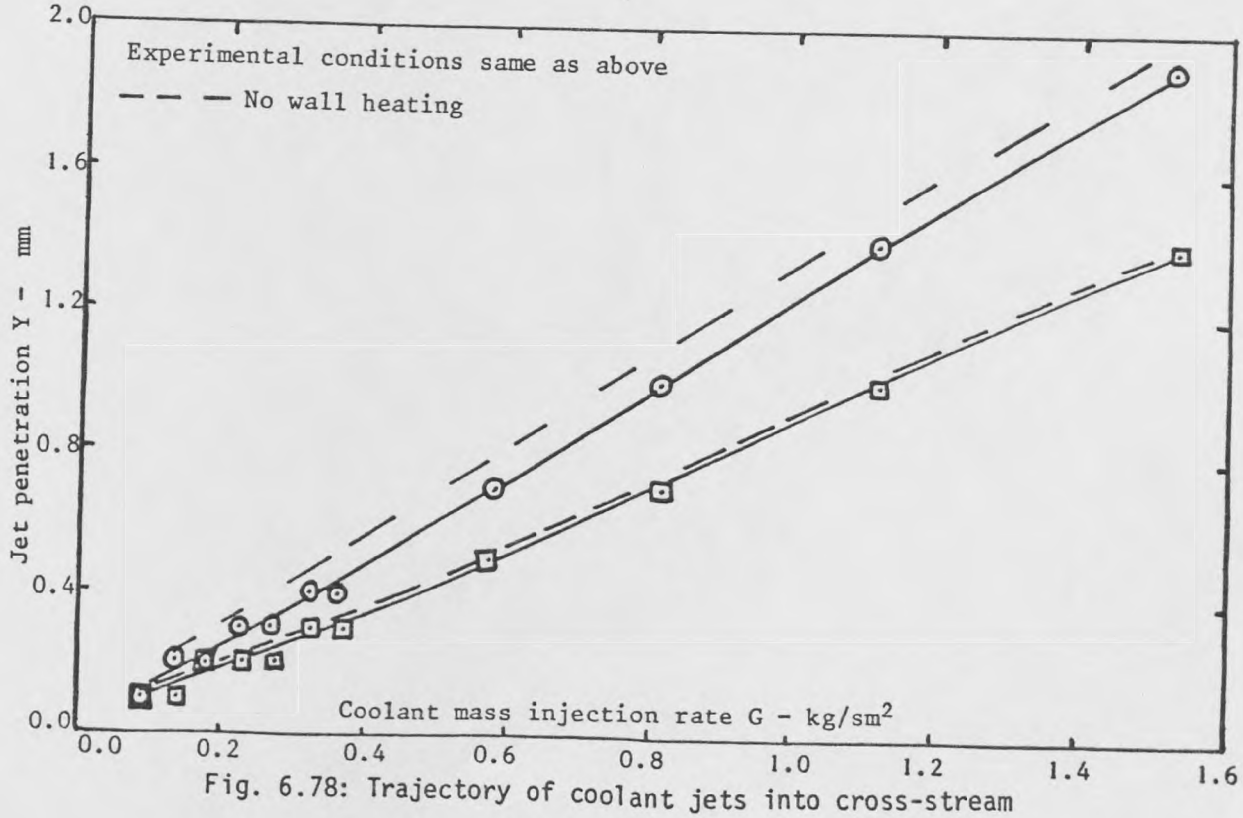

Fig. 6.78: Trajectory of coolant jets into cross-stream

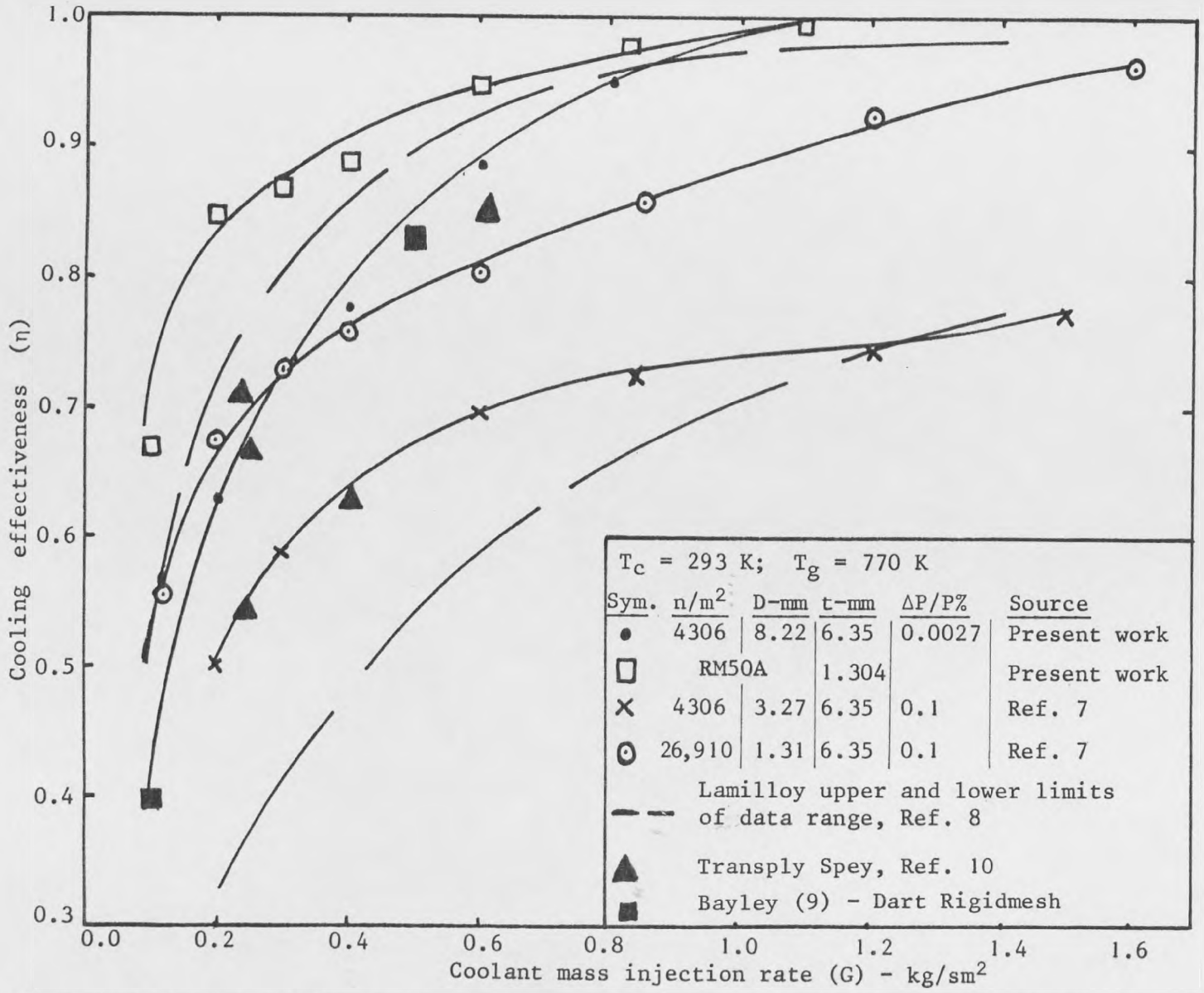

Fig. 6.79: Comparison of the cooling performance of a very low pressure loss wall with that of a low high density holes wall, rigid mesh and surveyed work

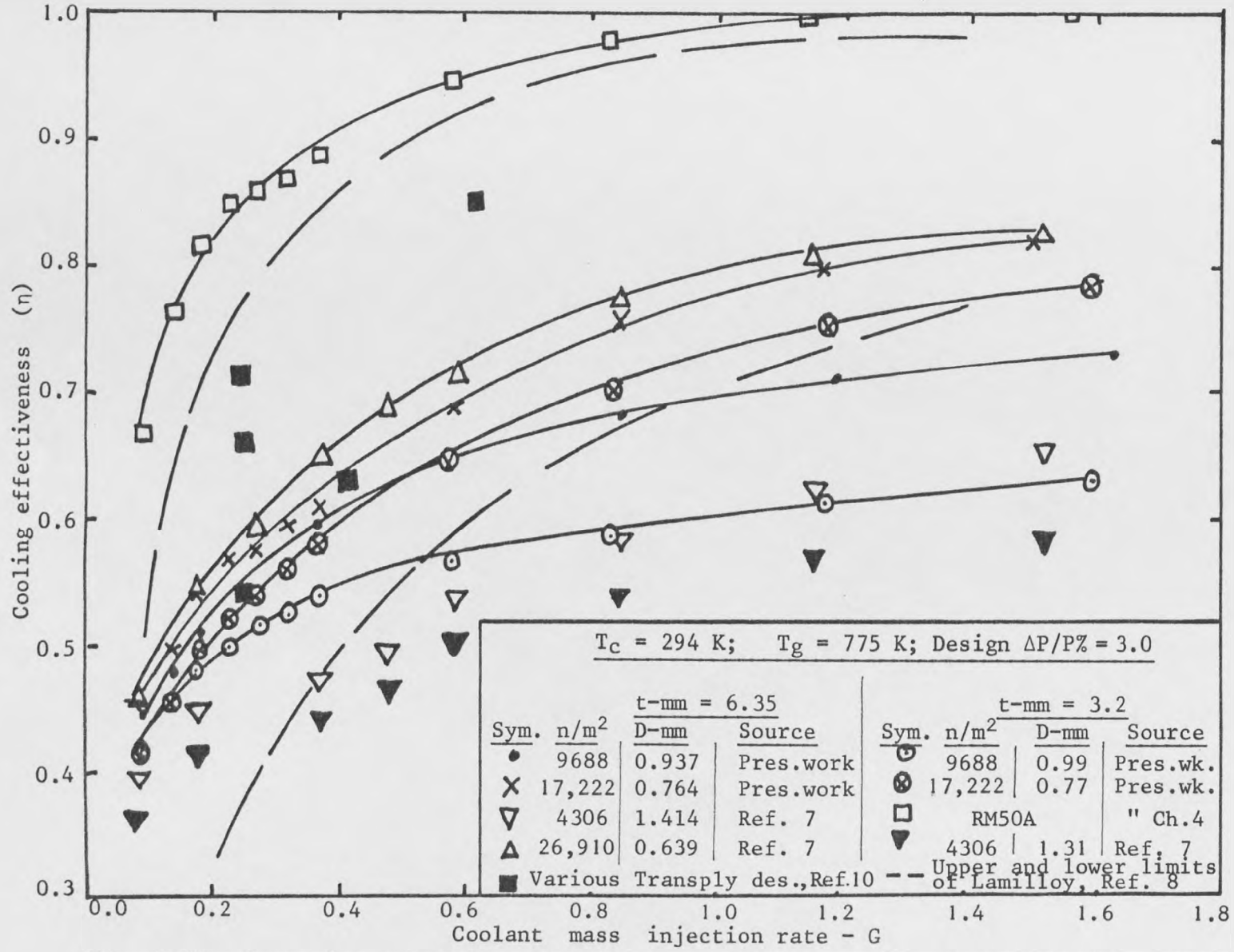

Fig. 6.80: Comparison of cooling effectiveness of different formats of effusion wall of constant design ΔP/P% of 3.0 with surveyed work and tested transpiration wall

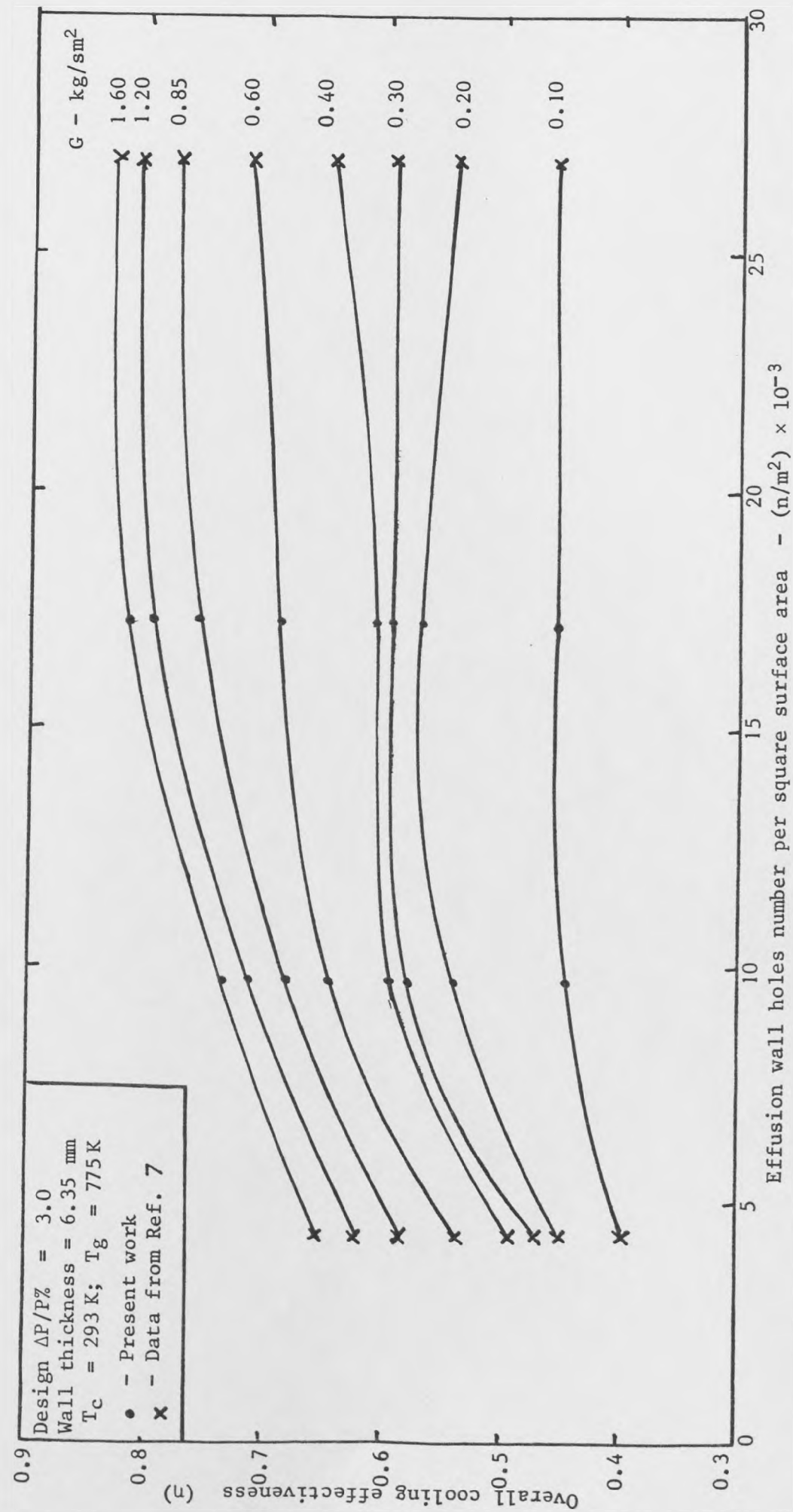

Fig. 6.81: Profile of cooling effectiveness as a function of holes' number for design

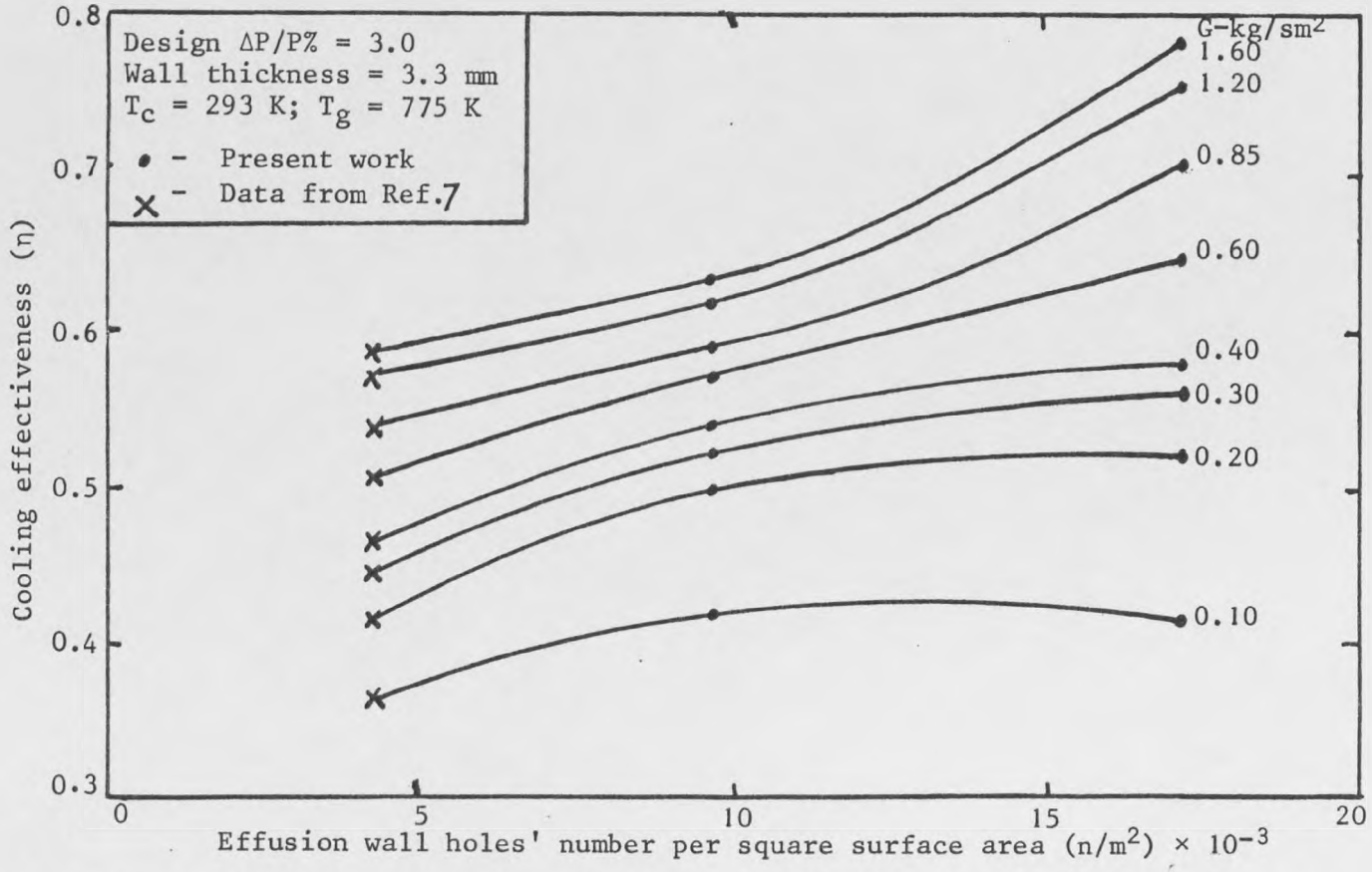

Fig. 6.82: Profile of cooling effectiveness as a function of holes' number for design

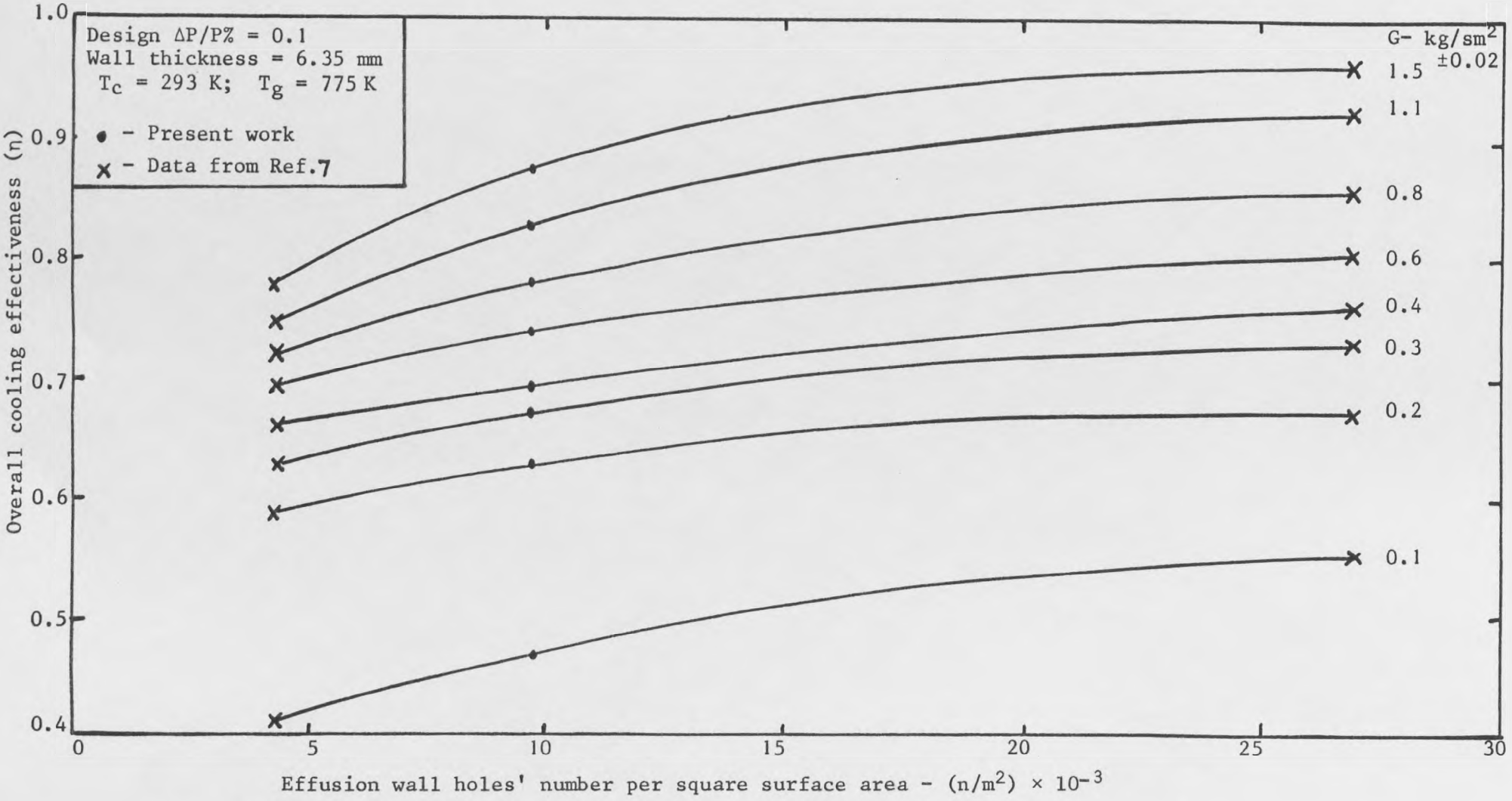

Fig. 6.83: Profile of cooling effectiveness as a function of holes' number for design

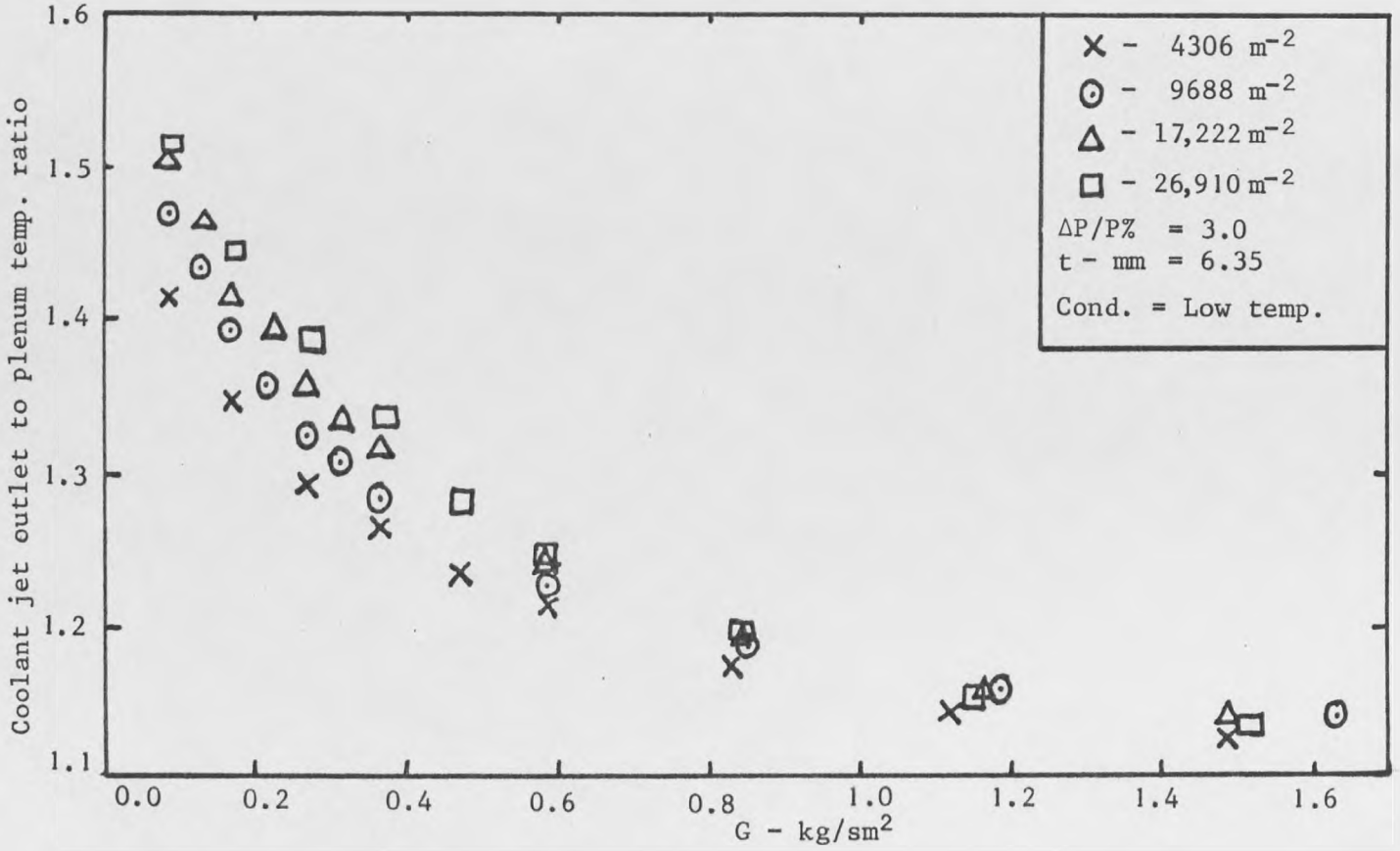

Fig. 6.84: Comparison of coolant temperature rise ratio for various wall holes' density

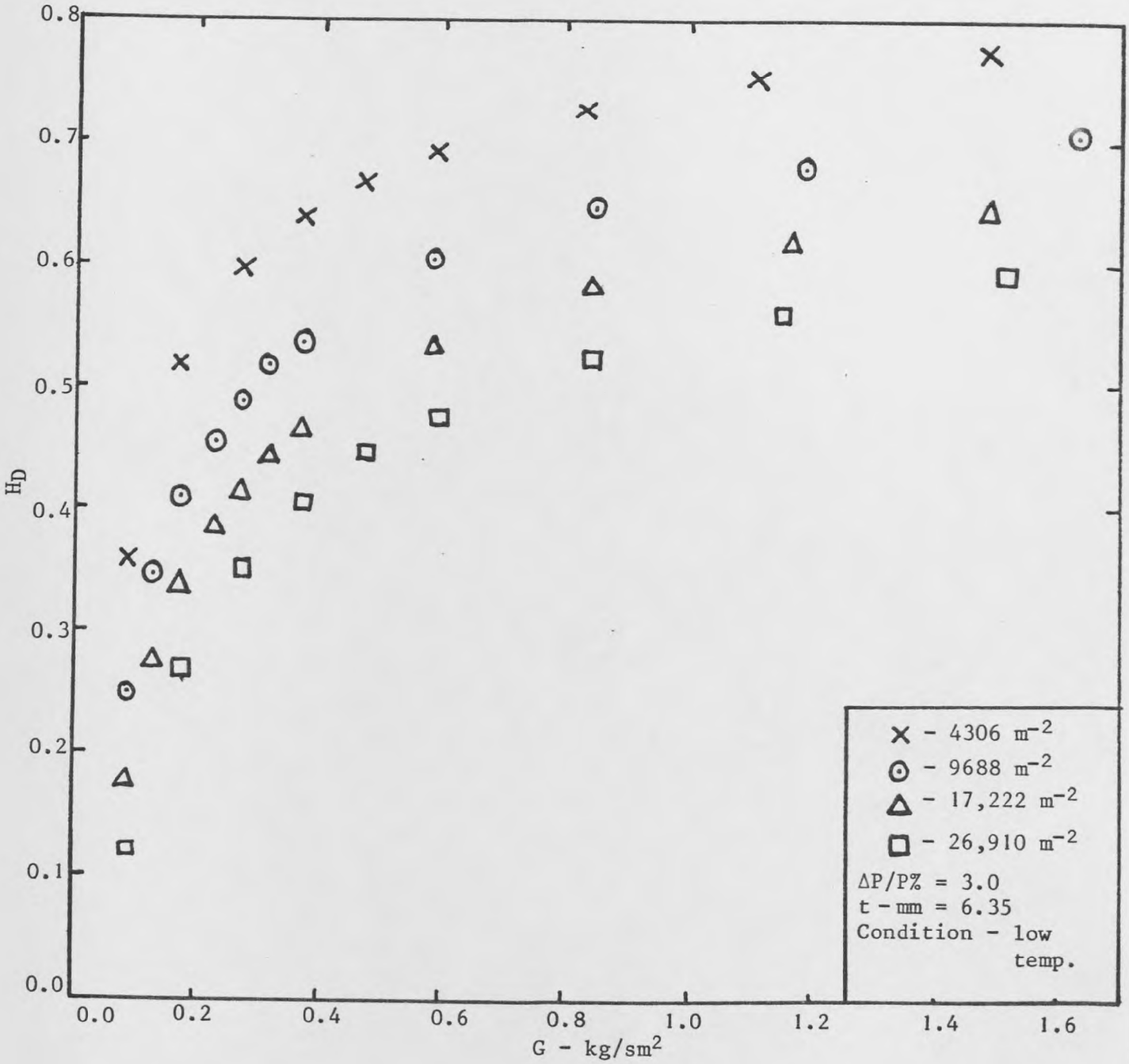

Fig. 6.85: Comparison of dimensionless temperature for various wall holes' density

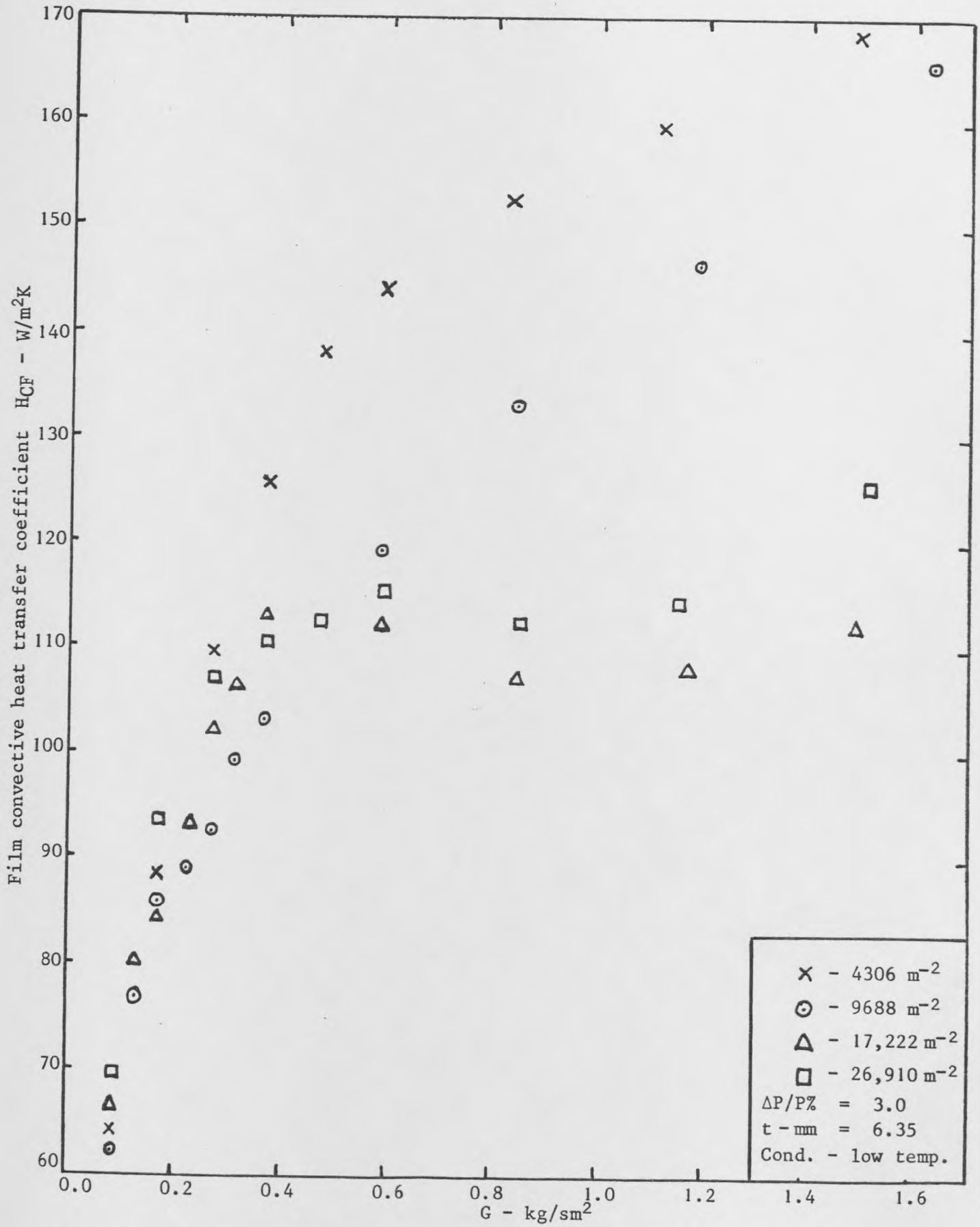

Fig. 6.86: Comparison of film convective heat transfer coefficient for 3% design pressure loss walls

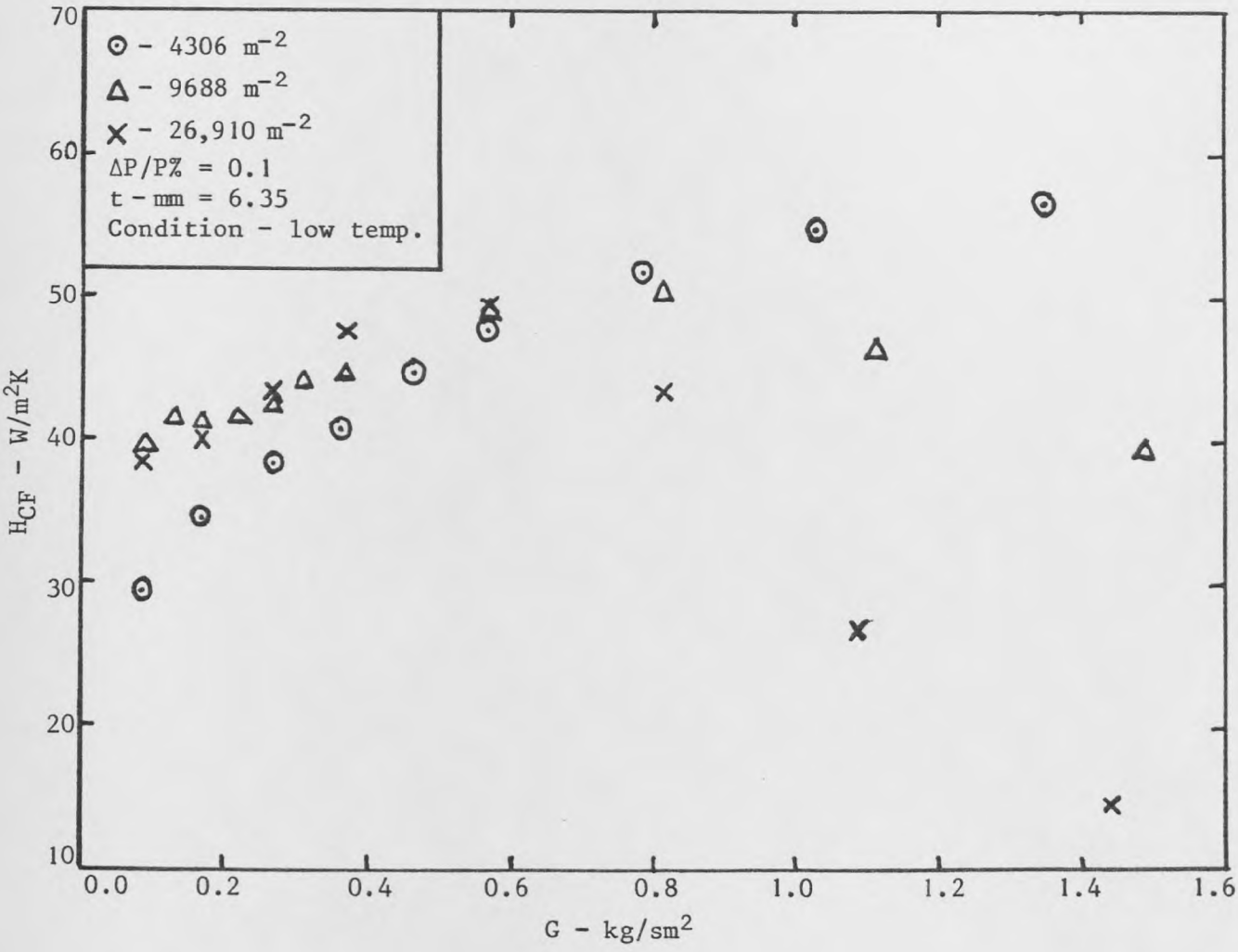

Fig. 6.87: Comparison of film convective heat transfer coefficient for 0.1% design pressure loss walls TH. STATION 5, H5g

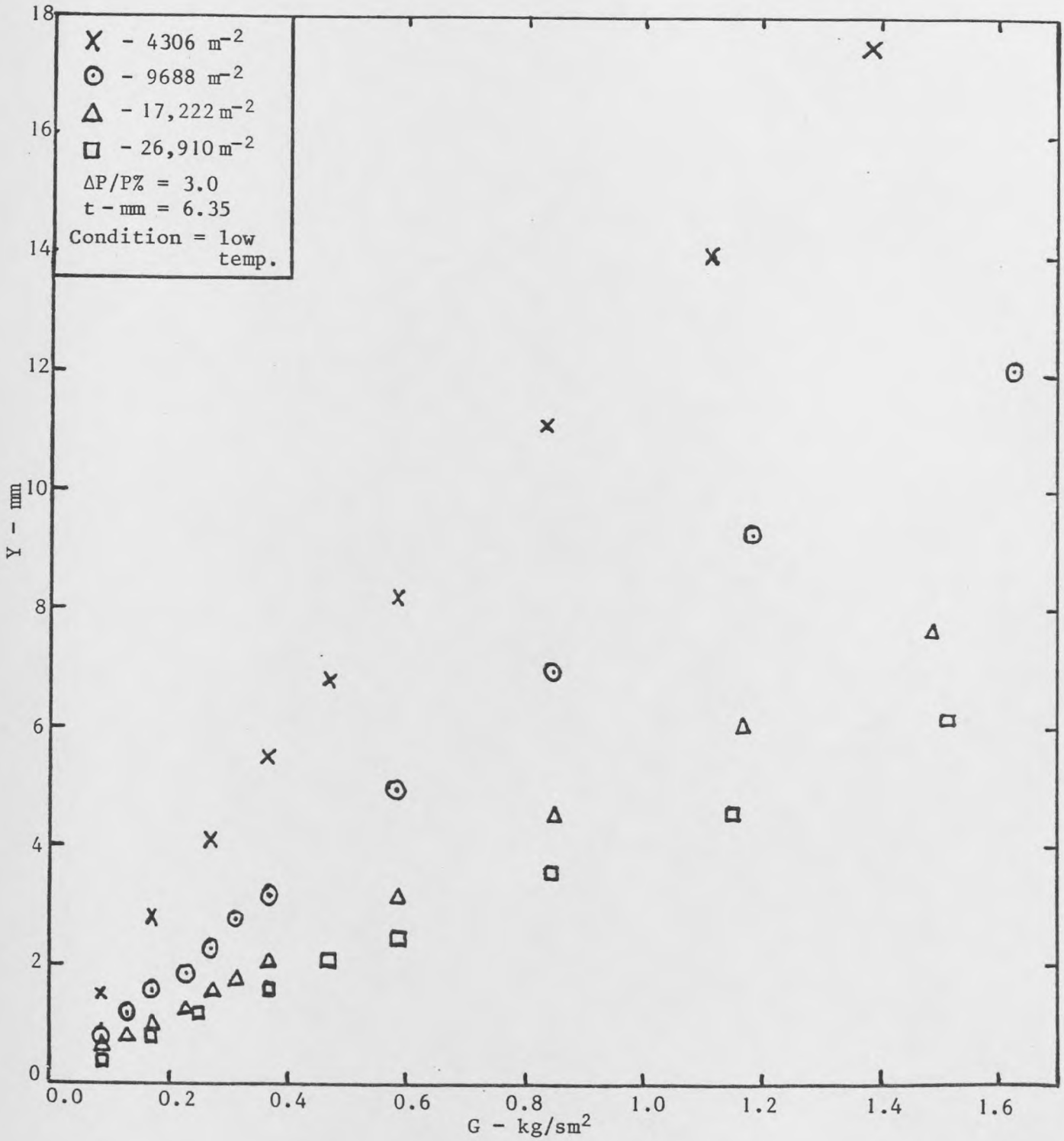

Fig. 6.88: Comparison of coolant jets' penetration into cross-stream for various wall holes' density

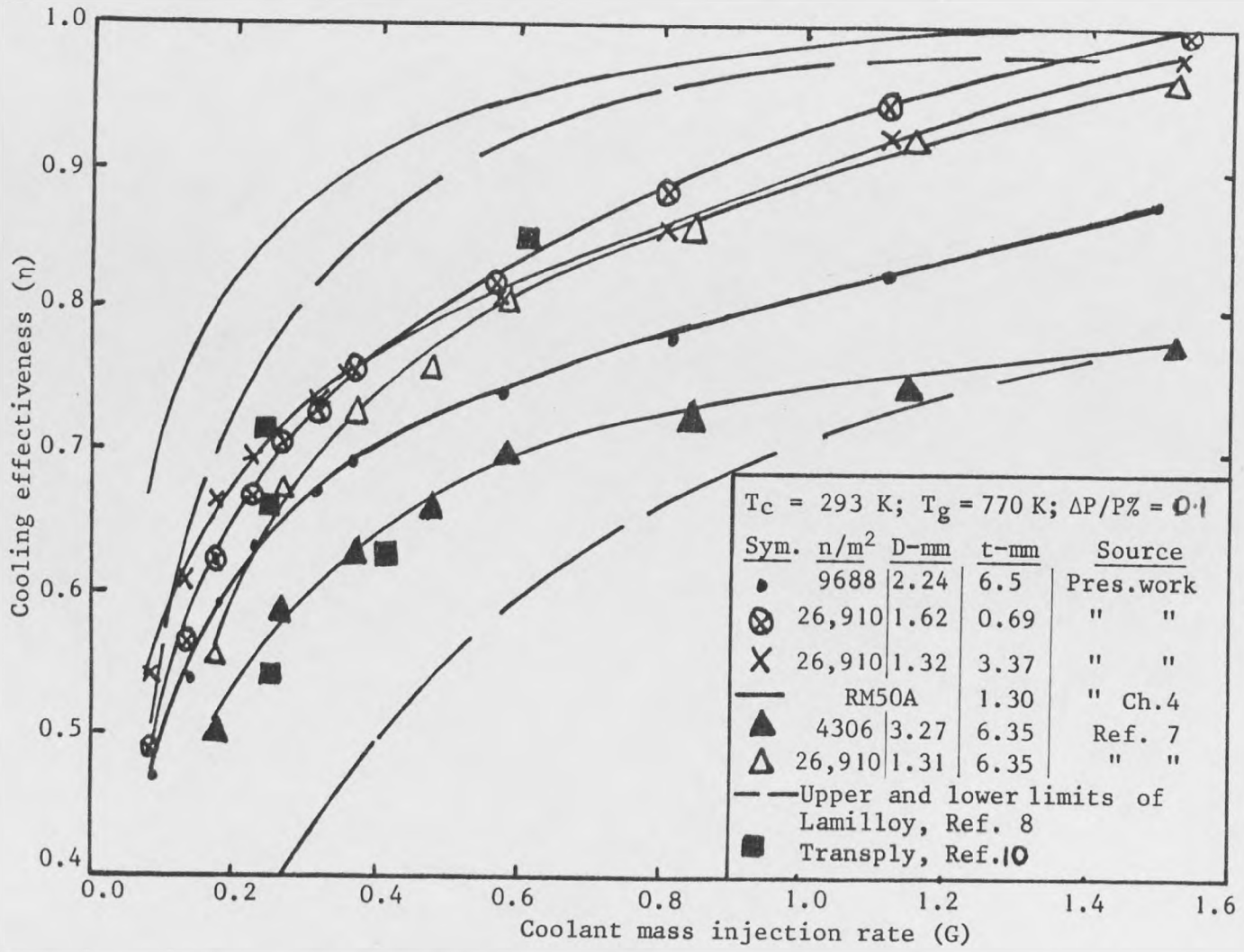

Fig. 6.89: Comparison of overall cooling effectiveness of different format effusion wall of constant design ΔP/P% of 0.1 with surveyed works and tested transpiration wall

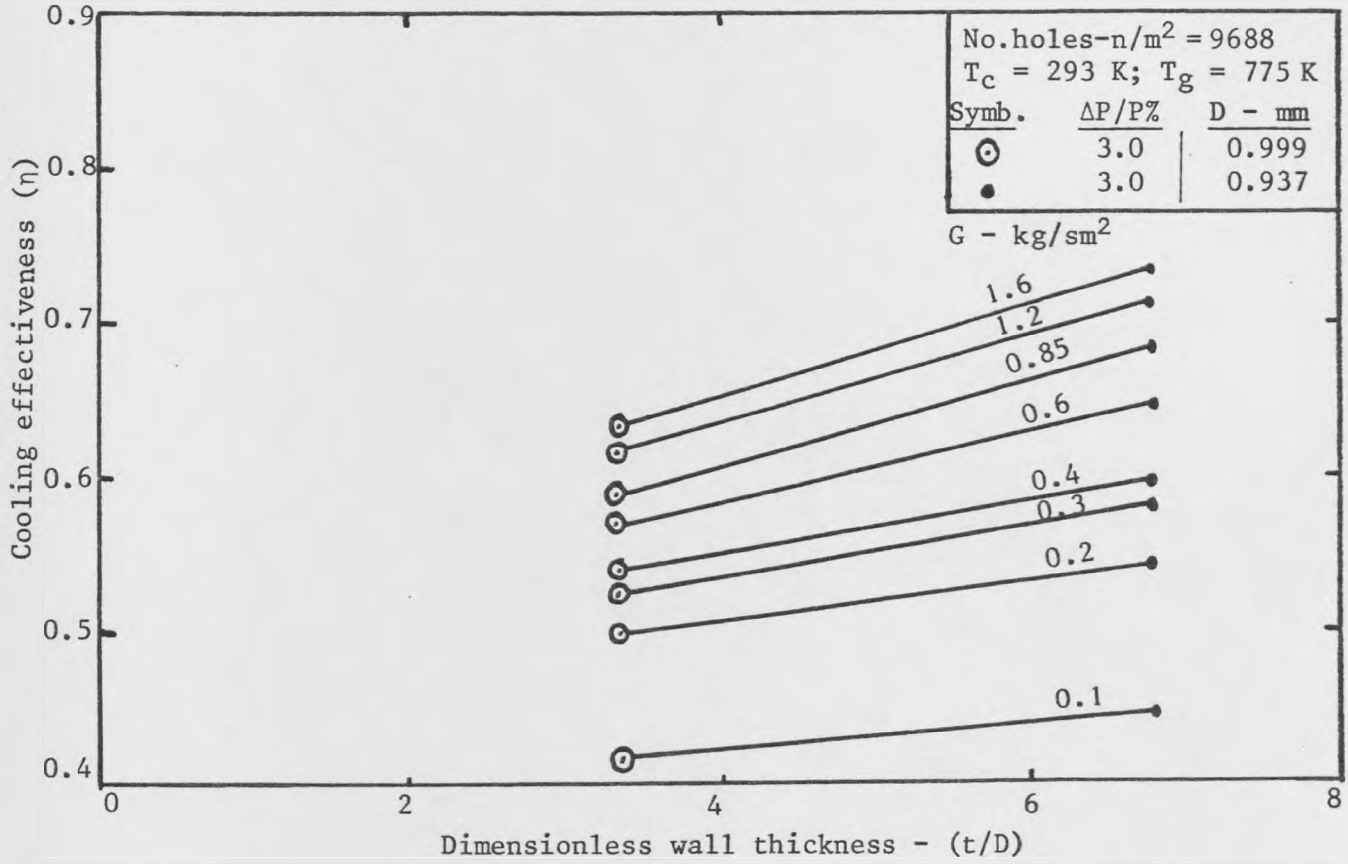

Fig. 6.90: Correlation of 9688 n/m² effusion wall for $\Delta P/P\% = 3.0$

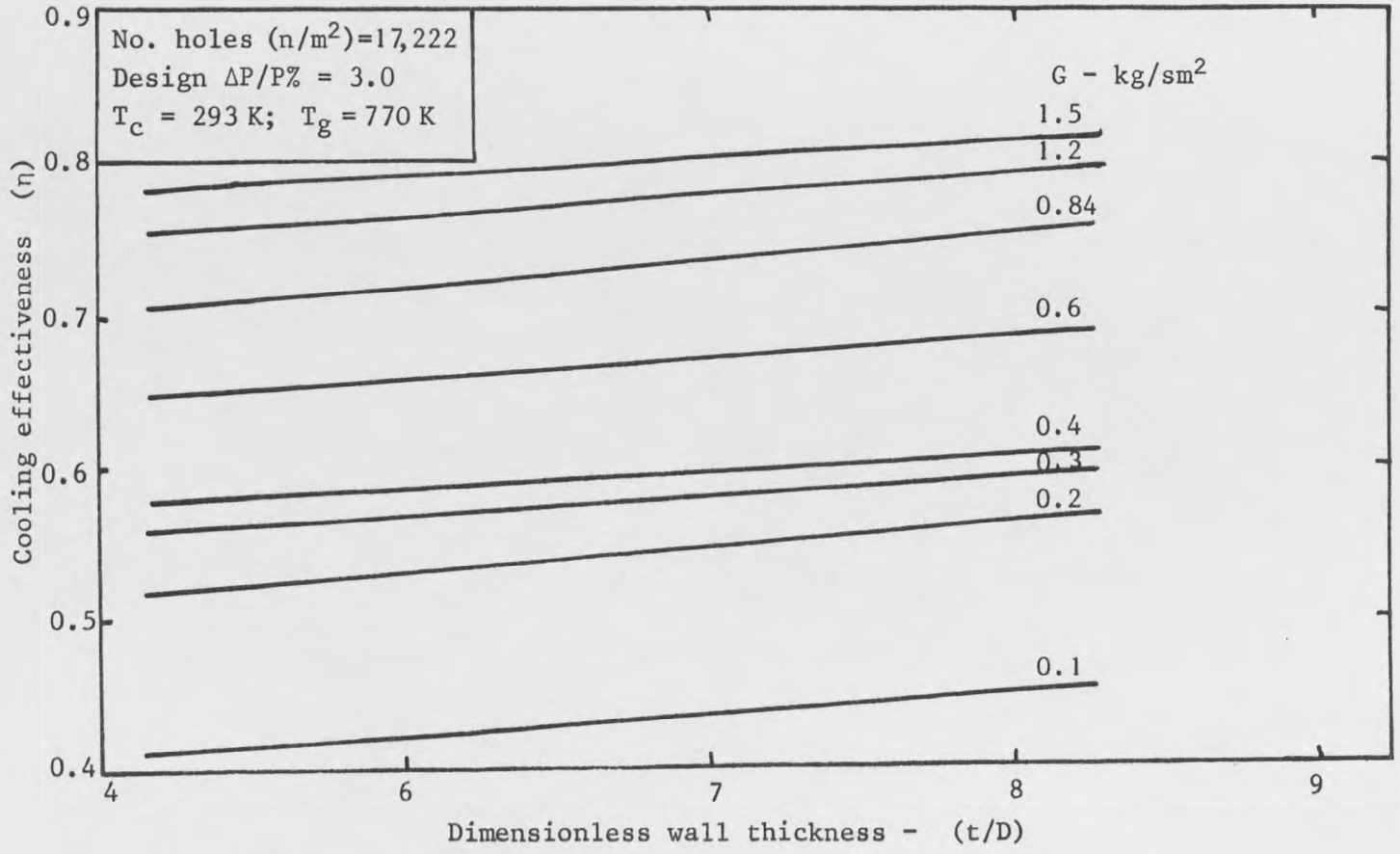

Fig. 6.91: Cooling effectiveness as a function of wall thickness

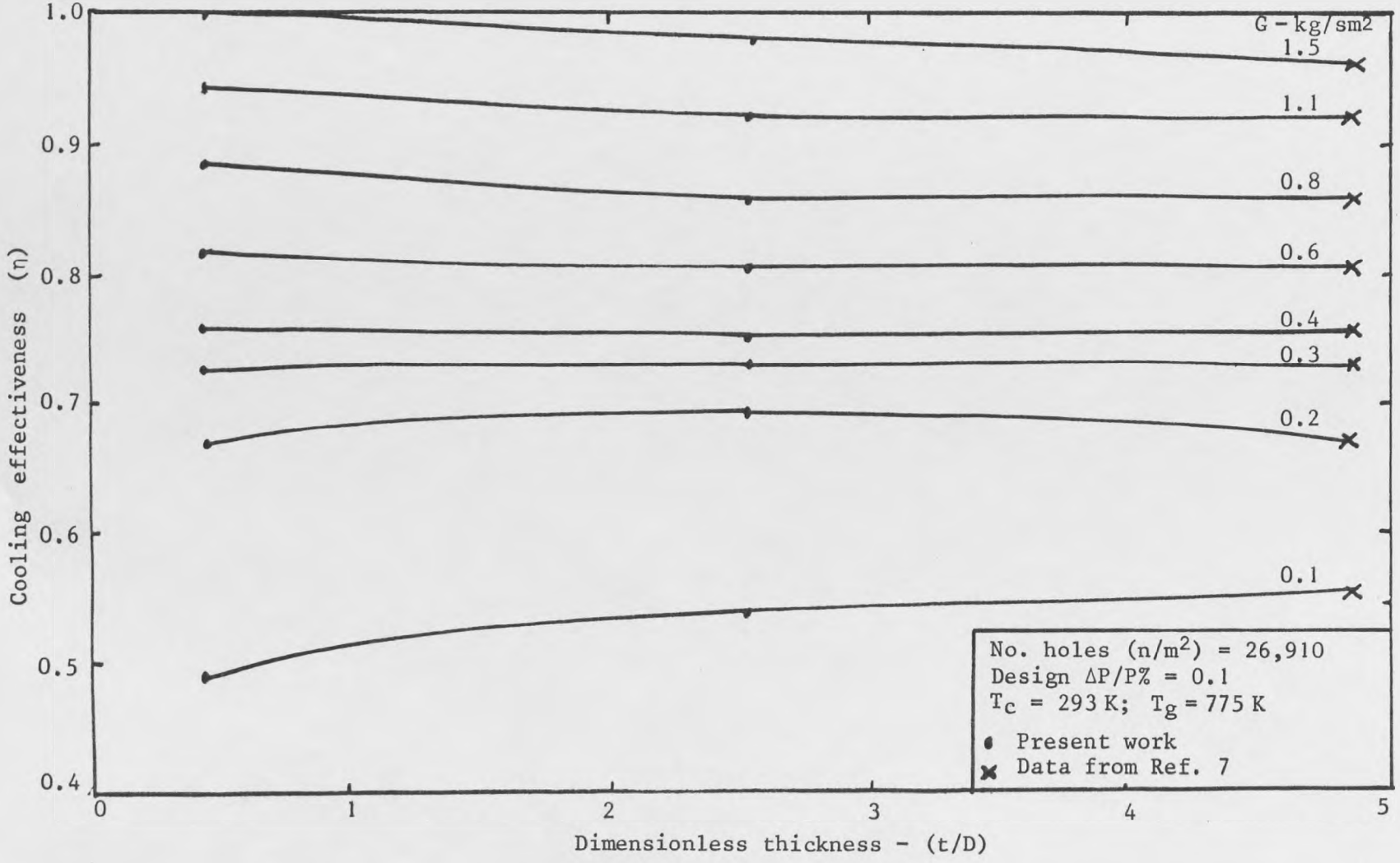

Fig. 6.92: Cooling effectiveness as a function of wall thickness

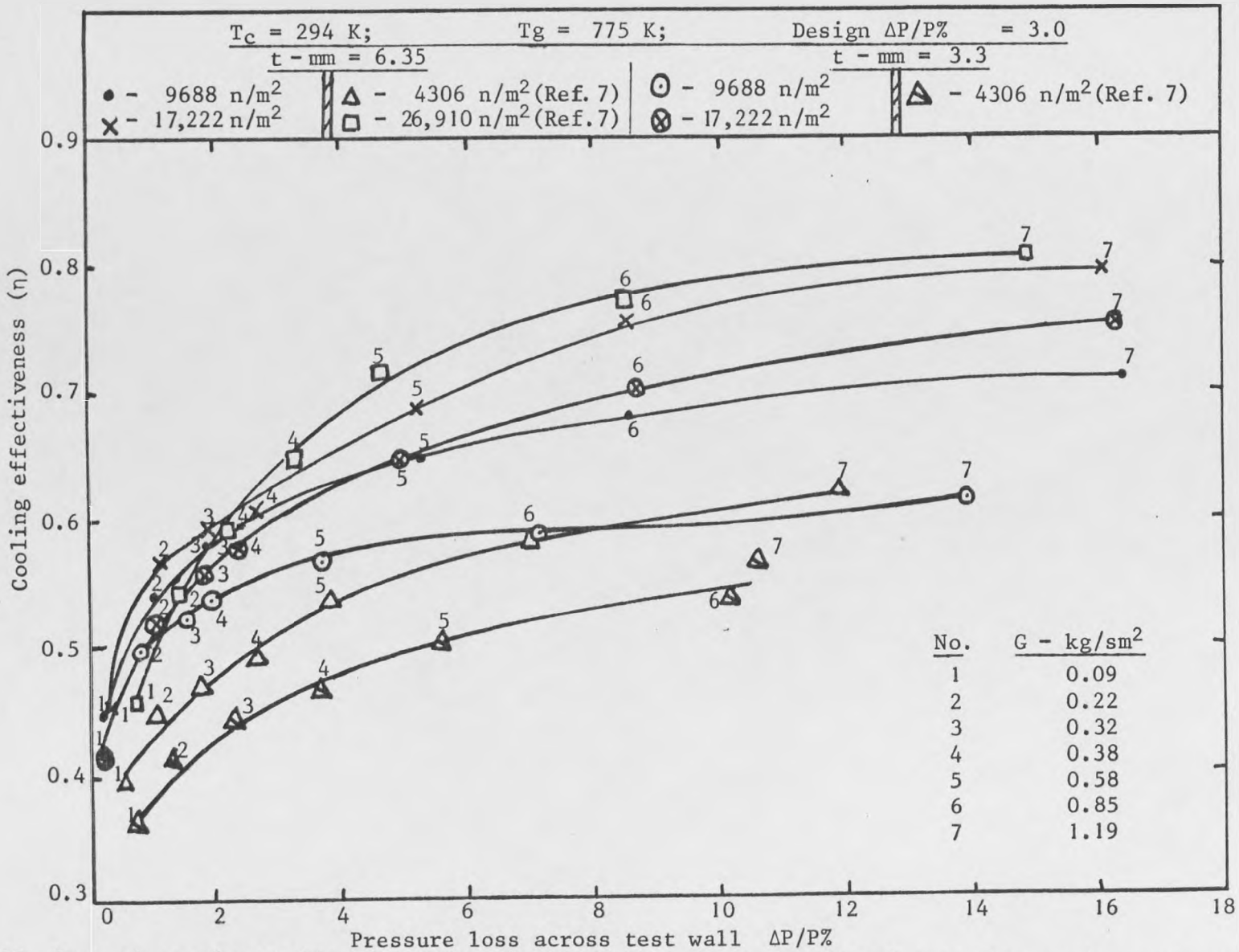

Fig. 6.93: Comparison of operational pressure loss effect on cooling effectiveness for various wall holes' density and thickness (t) at constant design ΔP/P% of 3.0.

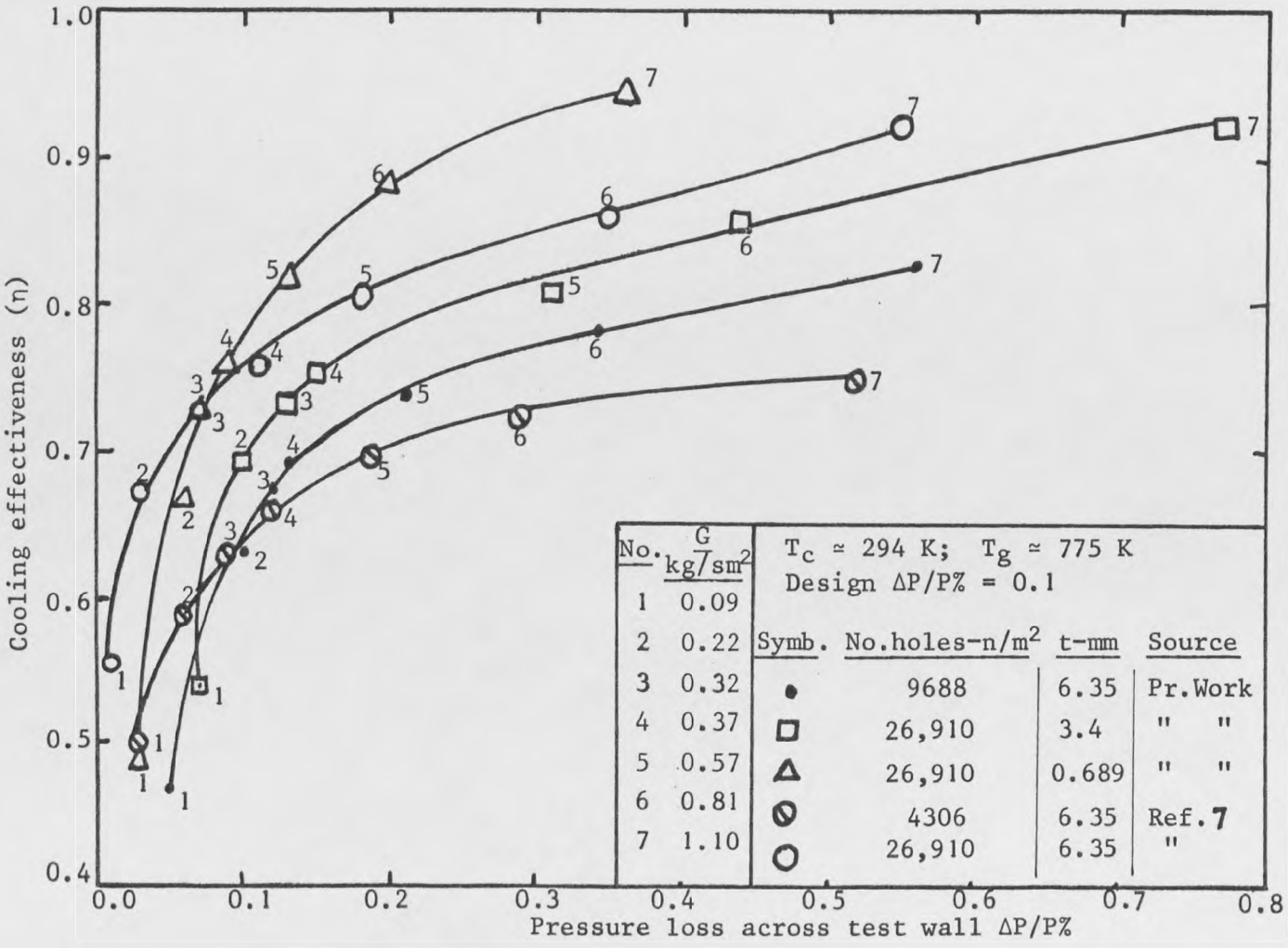

Fig. 6.94: Comparison of operational pressure loss effect on cooling effectiveness for various wall holes' density and thickness (t) at constant design ΔP/P% of 0.1

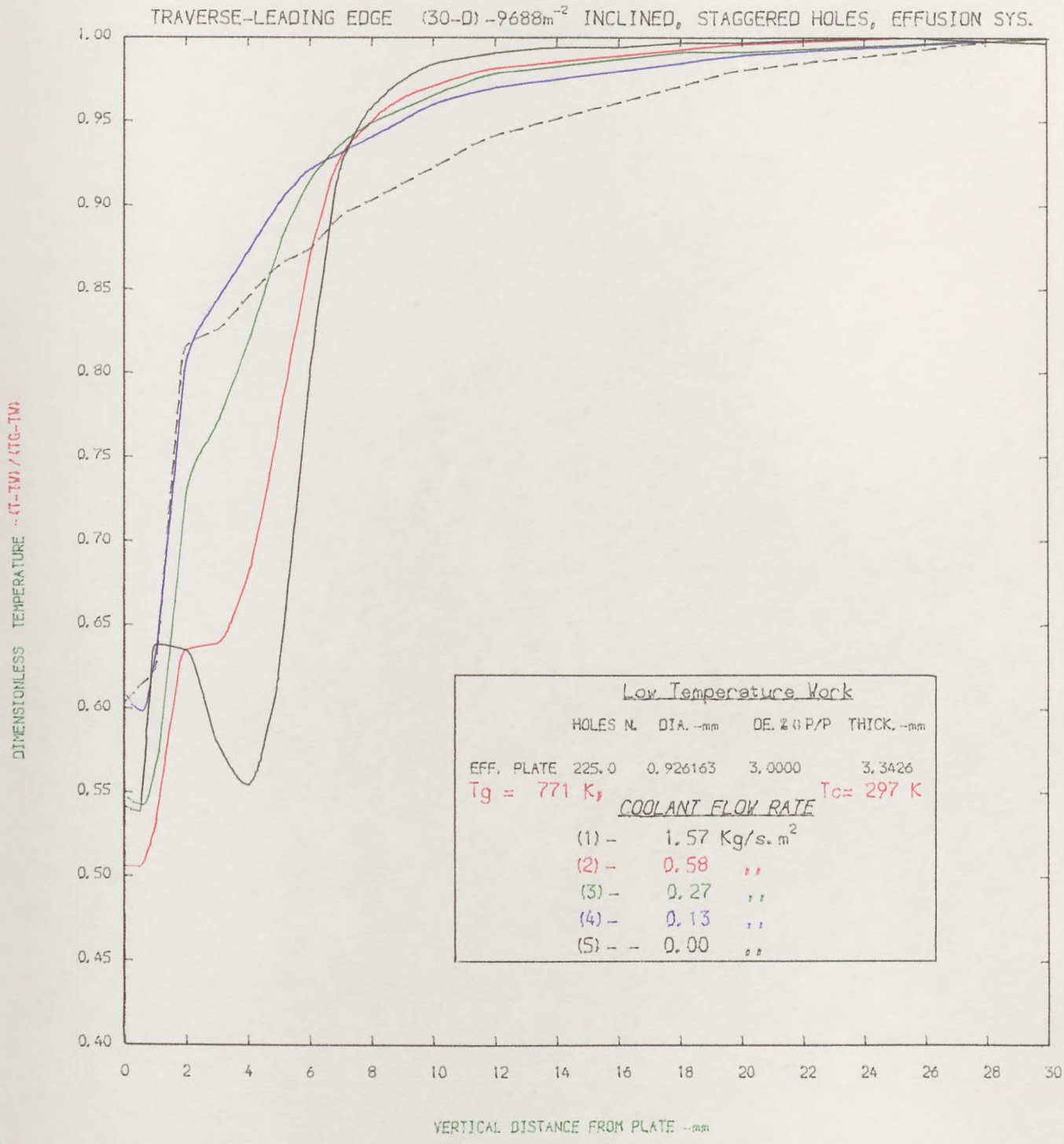

FIG. (6.95) : THERMAL BOUNDARY LAYER DEVELOPMENT NEAR LEADING EDGE OF WALL.

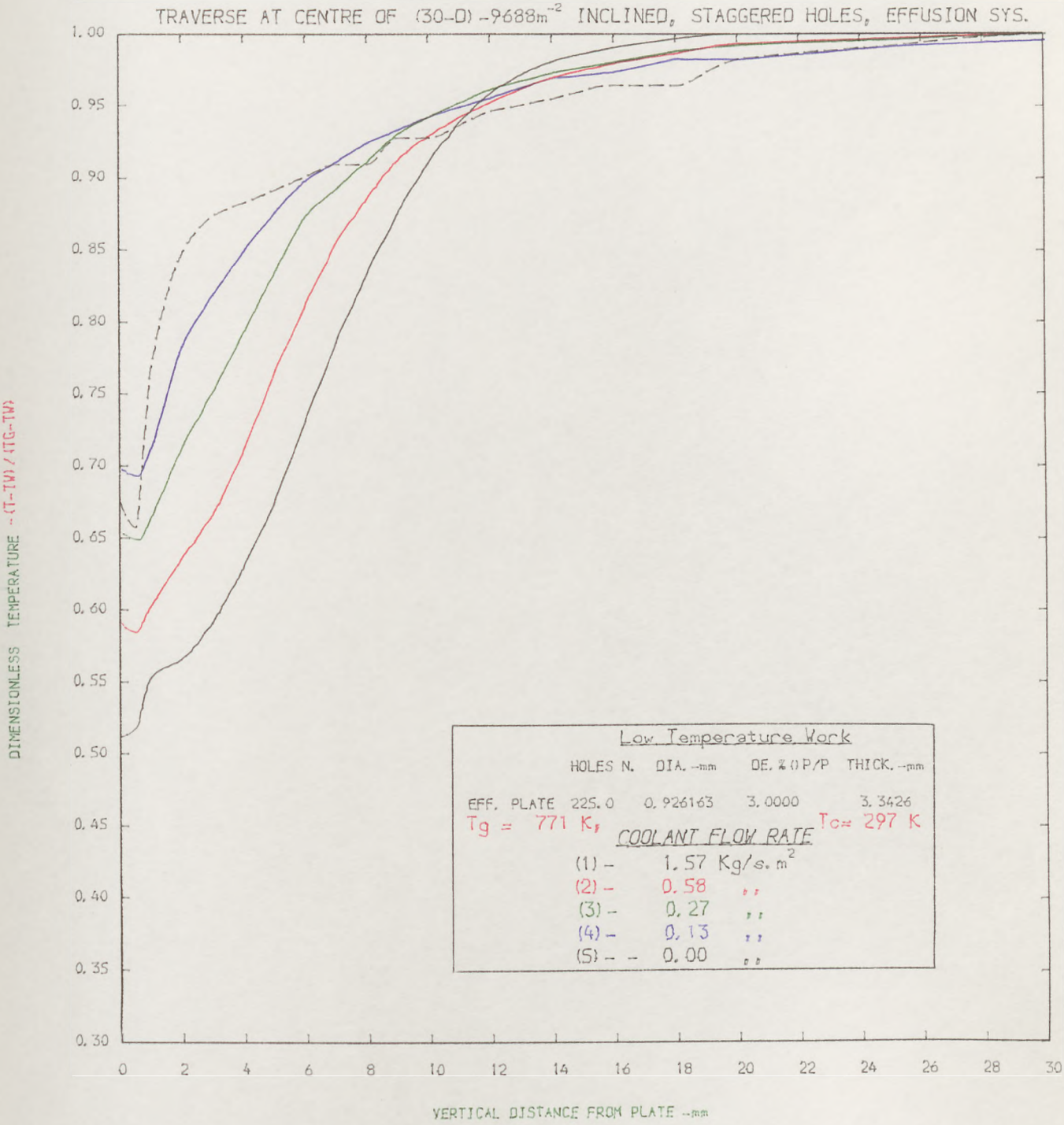

FIG. (6.96) : THERMAL BOUNDARY LAYER DEVELOPMENT AT CENTRAL PLANE OF WALL.

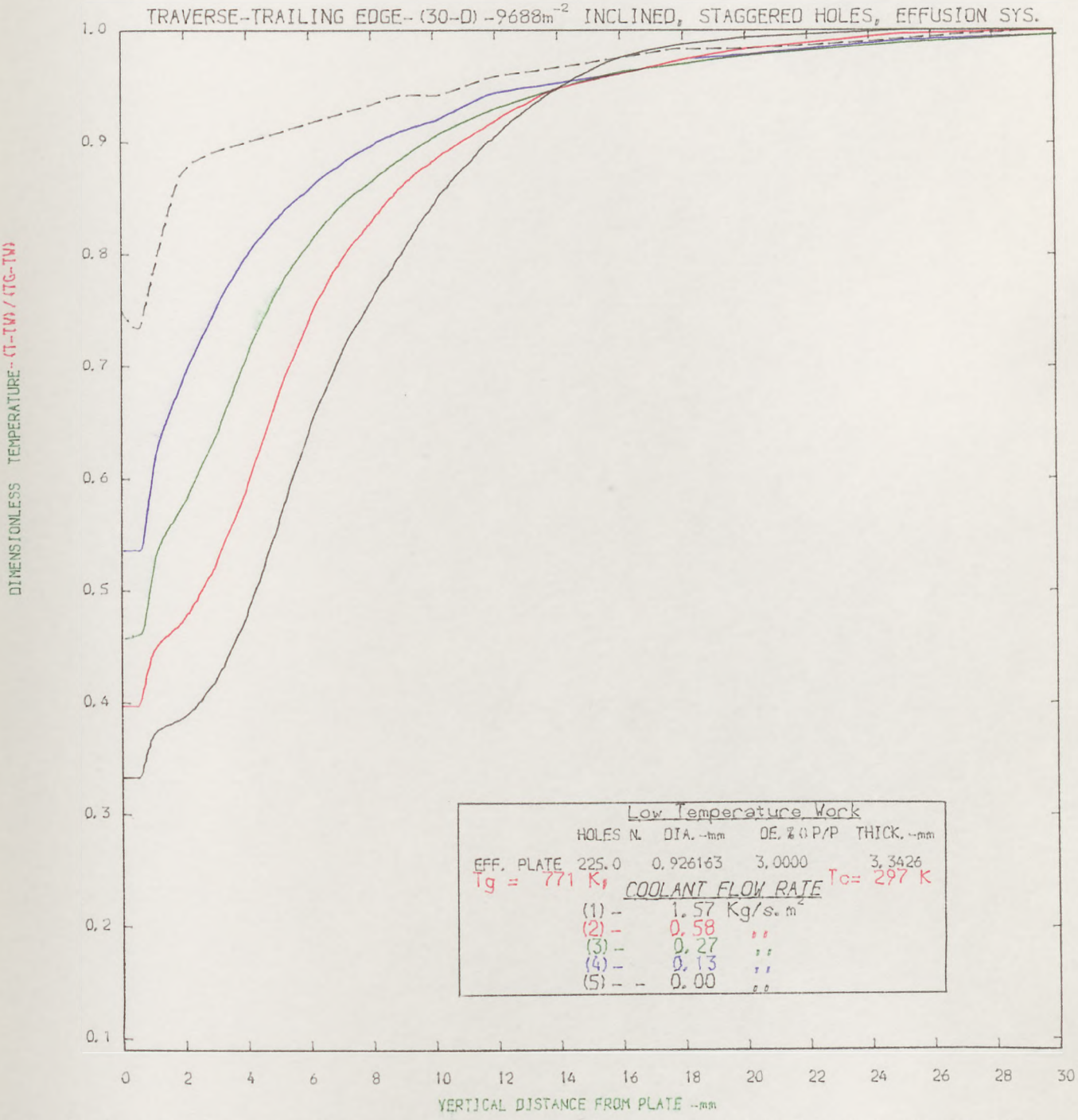

FIG. (6.97) : THERMAL BOUNDARY LAYER DEVELOPMENT NEAR TRAILING EDGE OF WALL

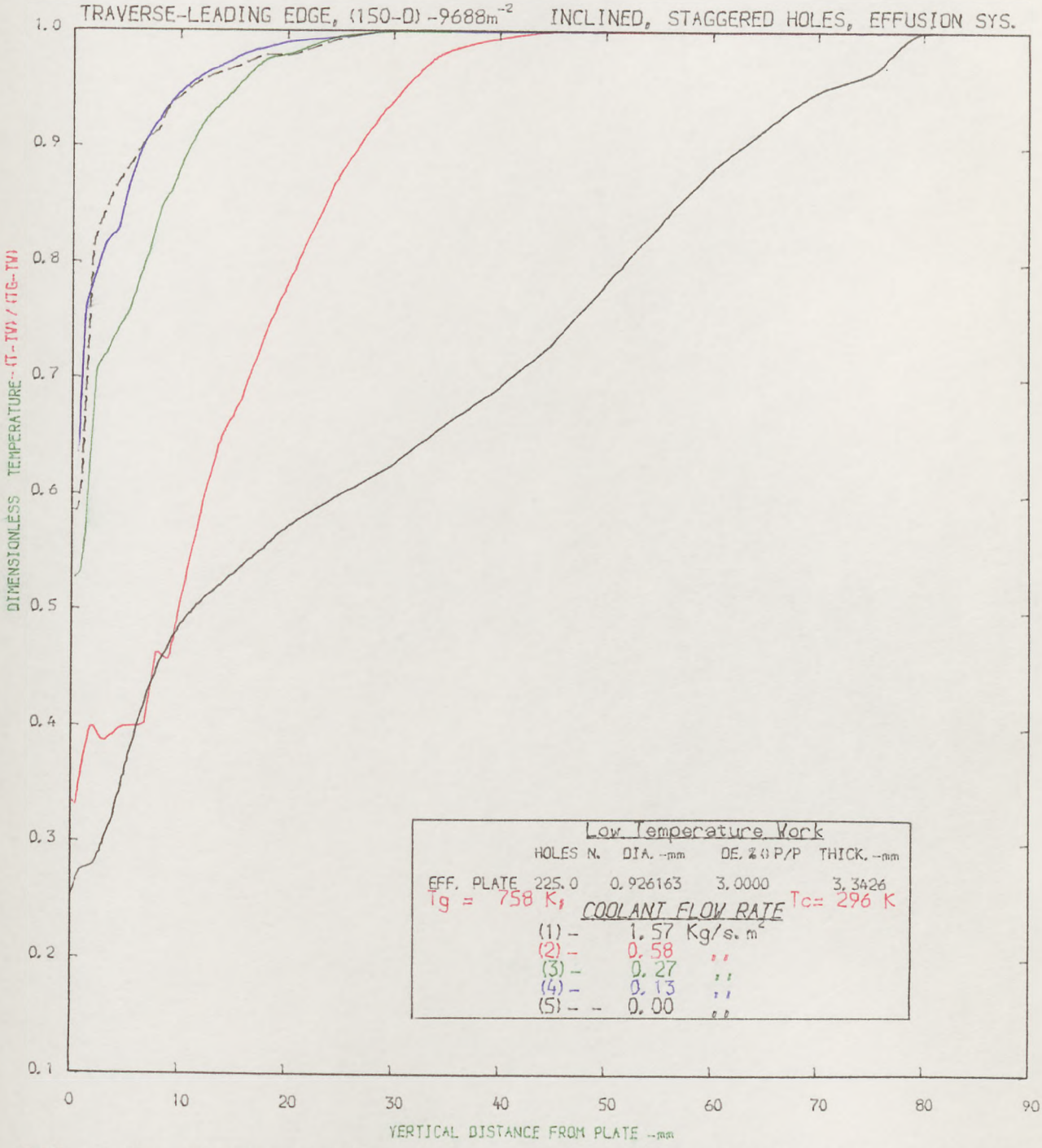

FIG. (6.98) : THERMAL BOUNDARY LAYER DEVELOPMENT NEAR LEADING EDGE OF WALL.

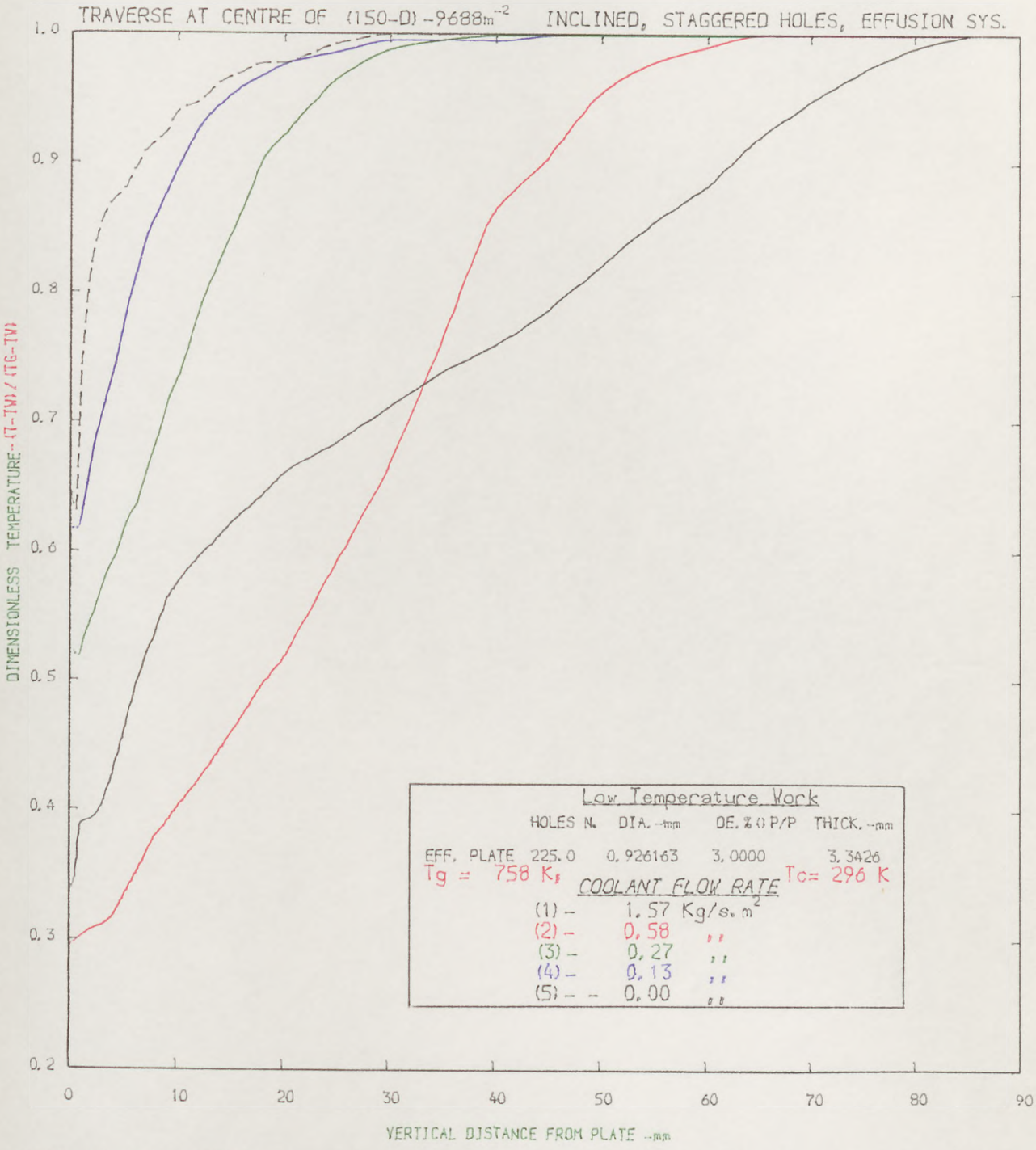

FIG. (6.99) : THERMAL BOUNDARY LAYER DEVELOPMENT AT CENTRAL OF WALL

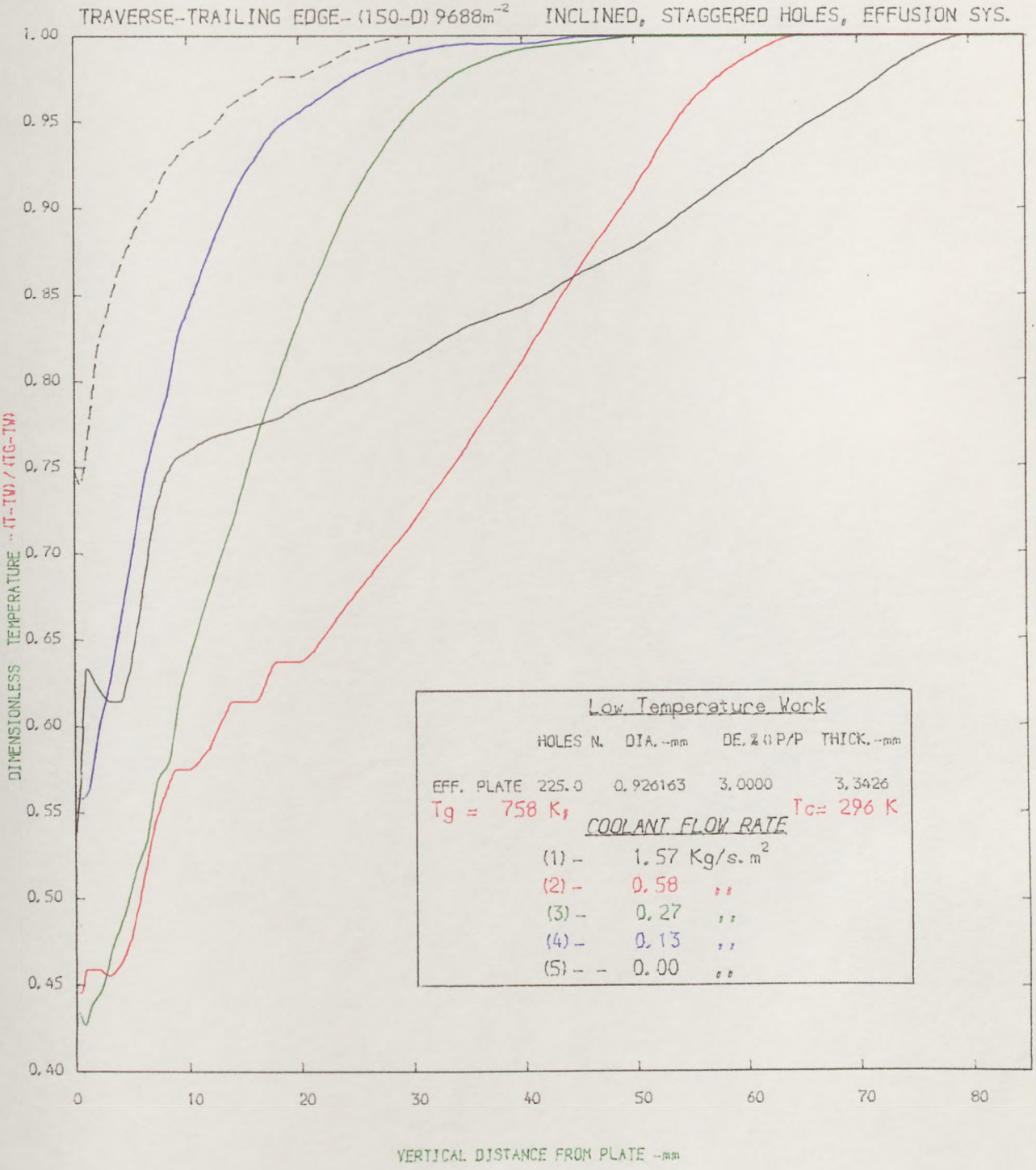

FIG. 6.100 : THERMAL BOUNDARY LAYER DEVELOPMENT NEAR TRAILING EDGE OF WALL

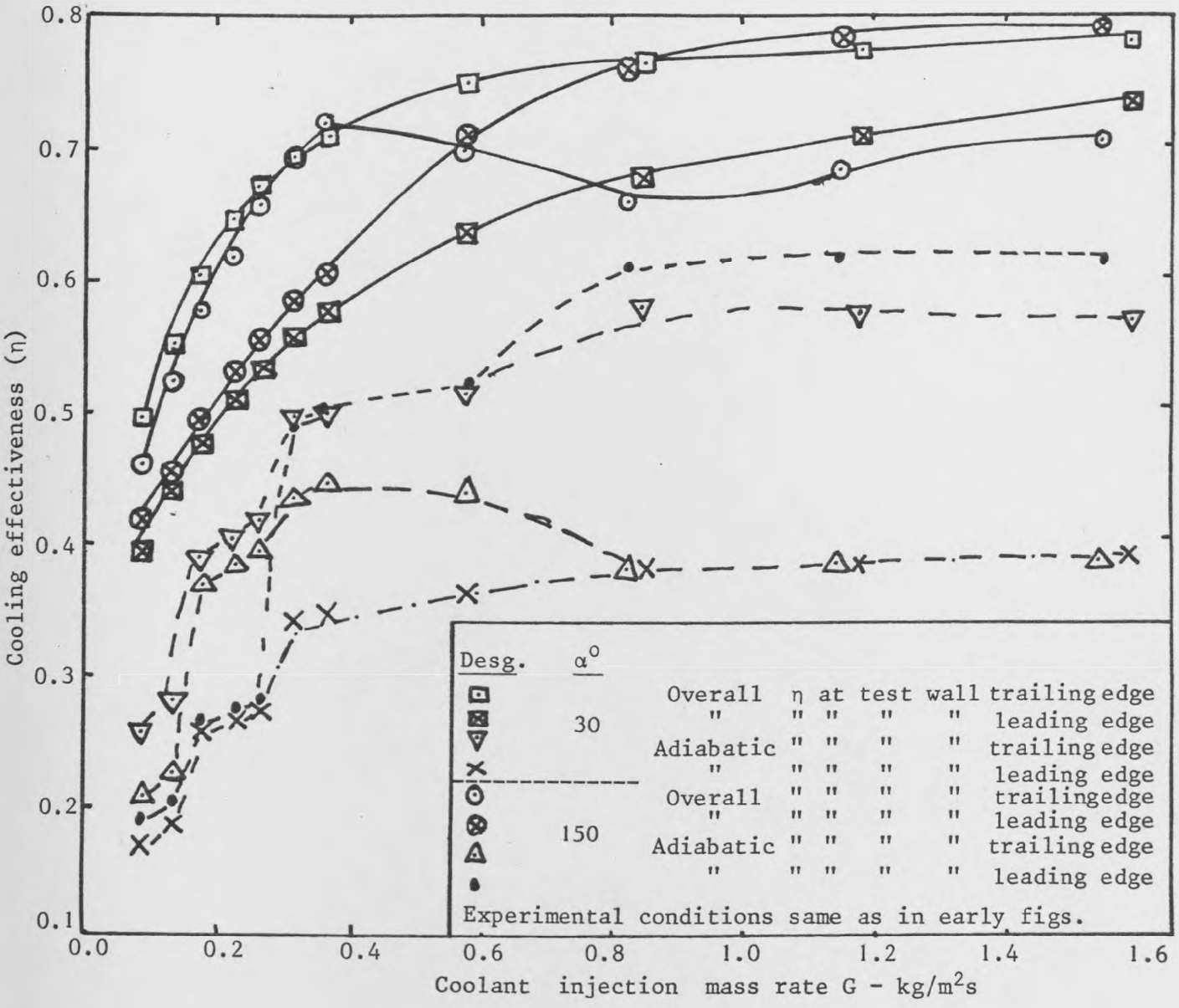

Fig. 6.101: Effect of coolant injection on overall and adiabatic cooling effectiveness at wall's leading and trailing edge

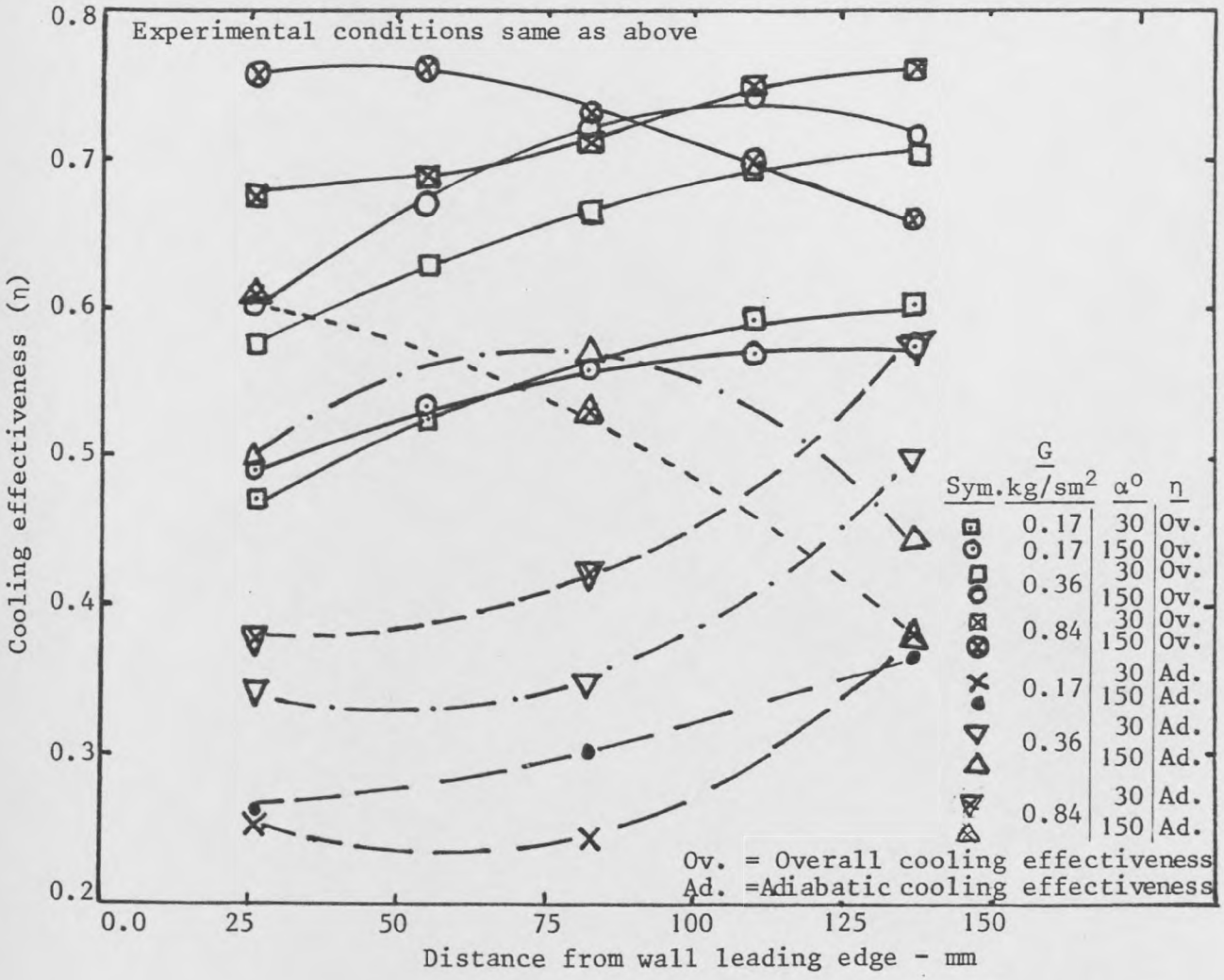

Fig. 6.102: Axial development of both overall and adiabatic cooling effectivenesses at different injection mass rate

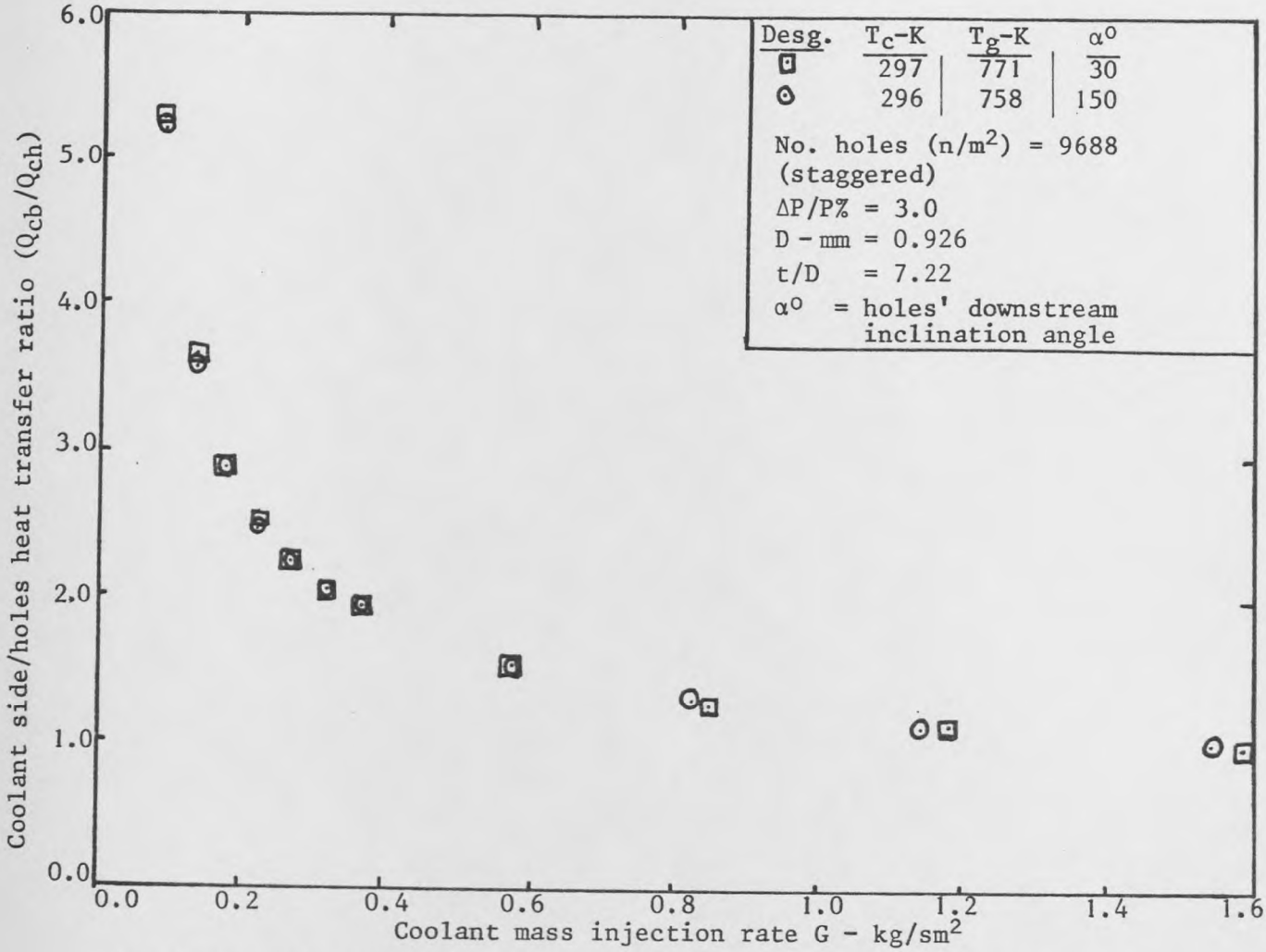

Fig. 6.103: Profile of pre-flame side heat transfer with coolant injection

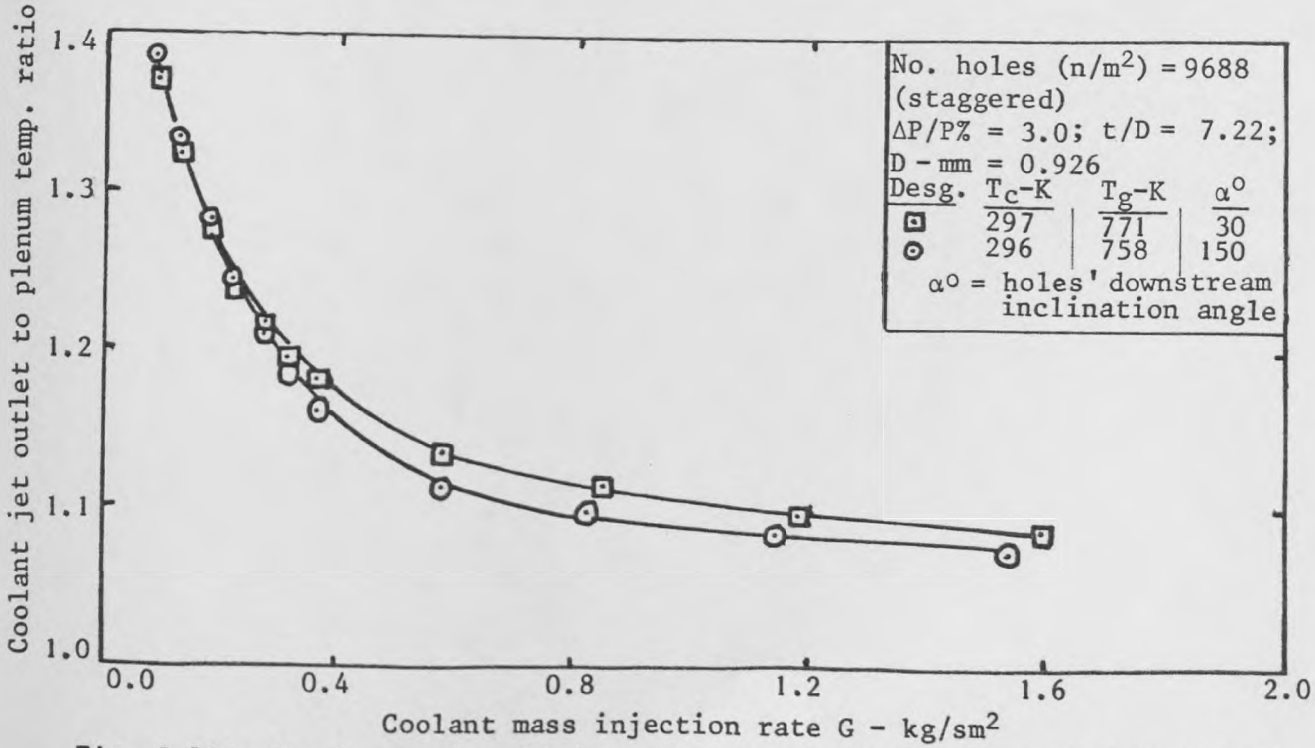

Fig. 6.104: The temperature history of plenum chamber coolant en route to test wall flame-side

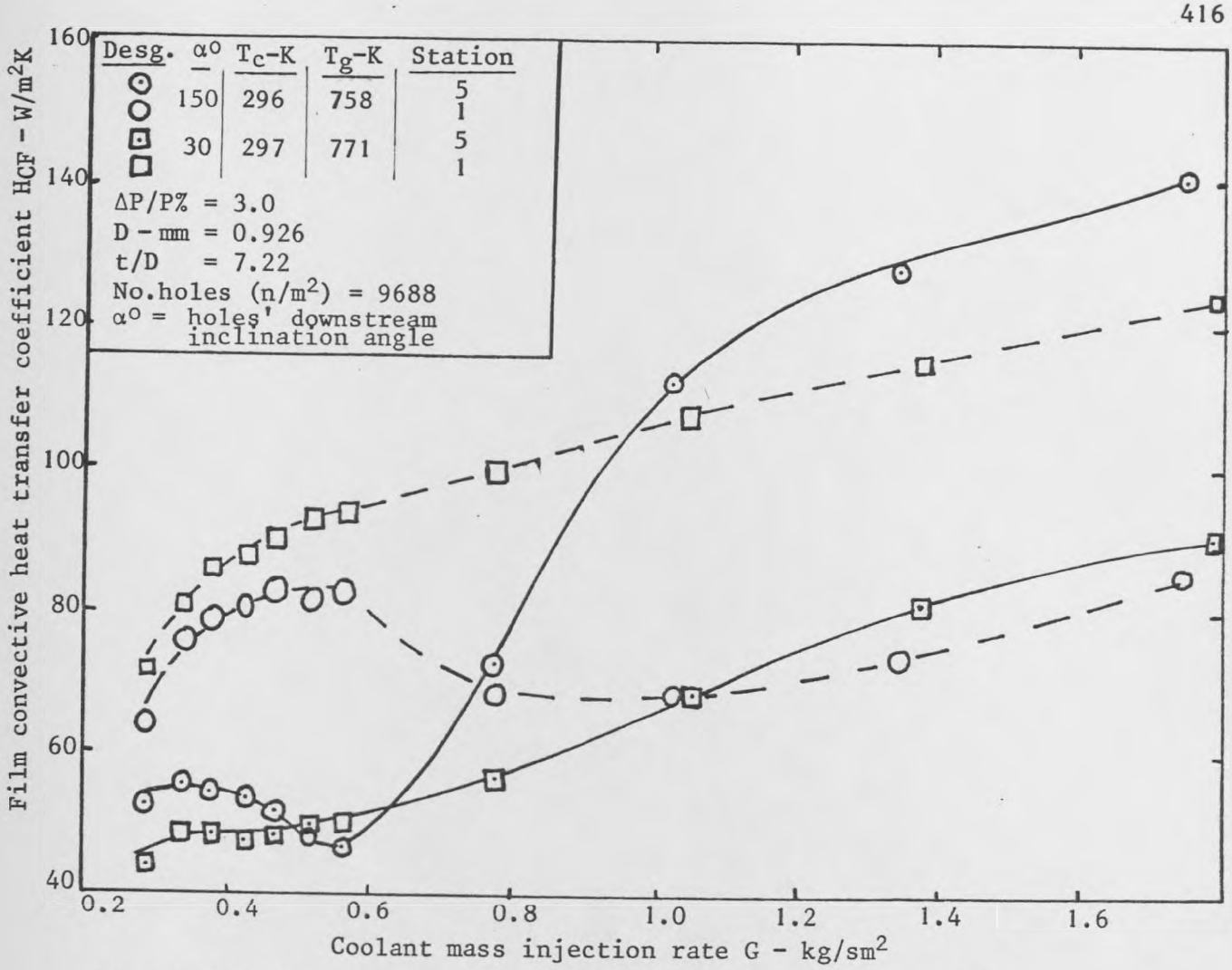

Fig. 6.105: Development of film convective heat transfer with coolant injection

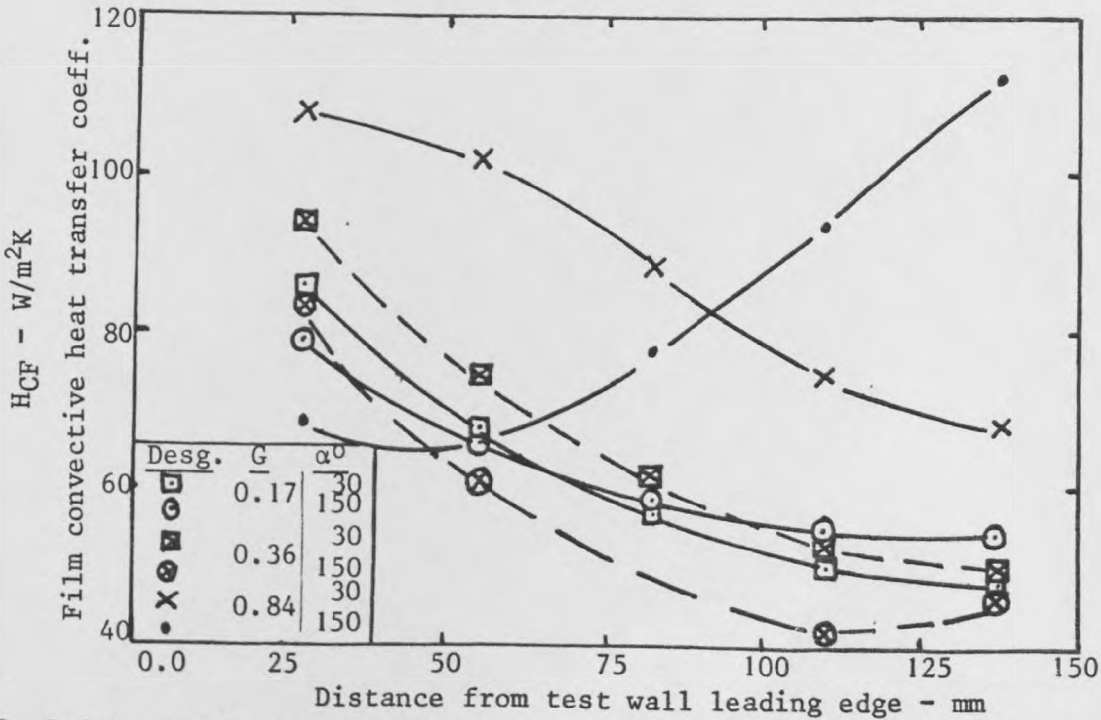

Fig. 6.106: Axial profile of film convective heat transfer coefficient at constant injection rates

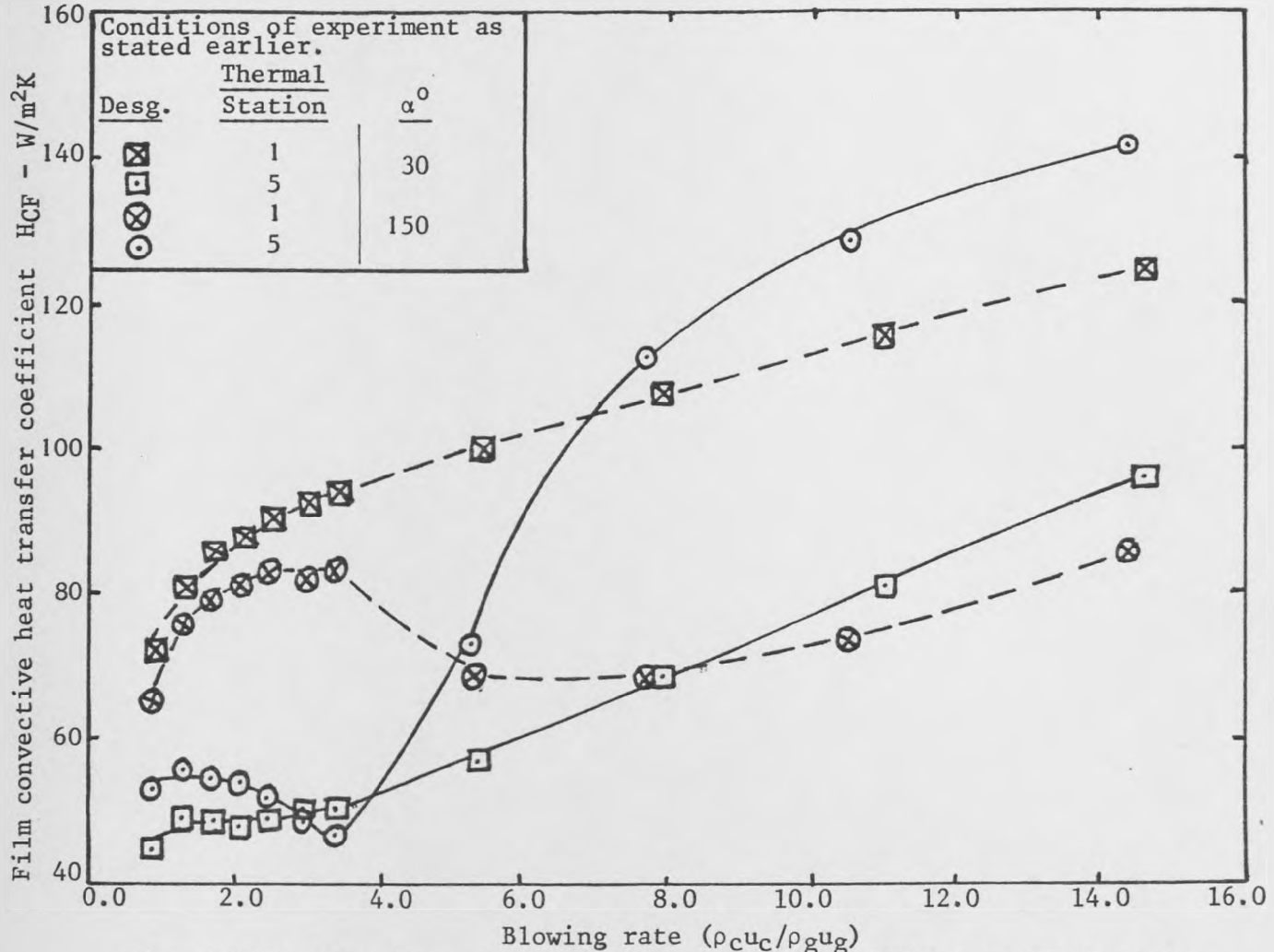

Fig. 6.107: Dependency of film heat transfer coefficient on blowing rate

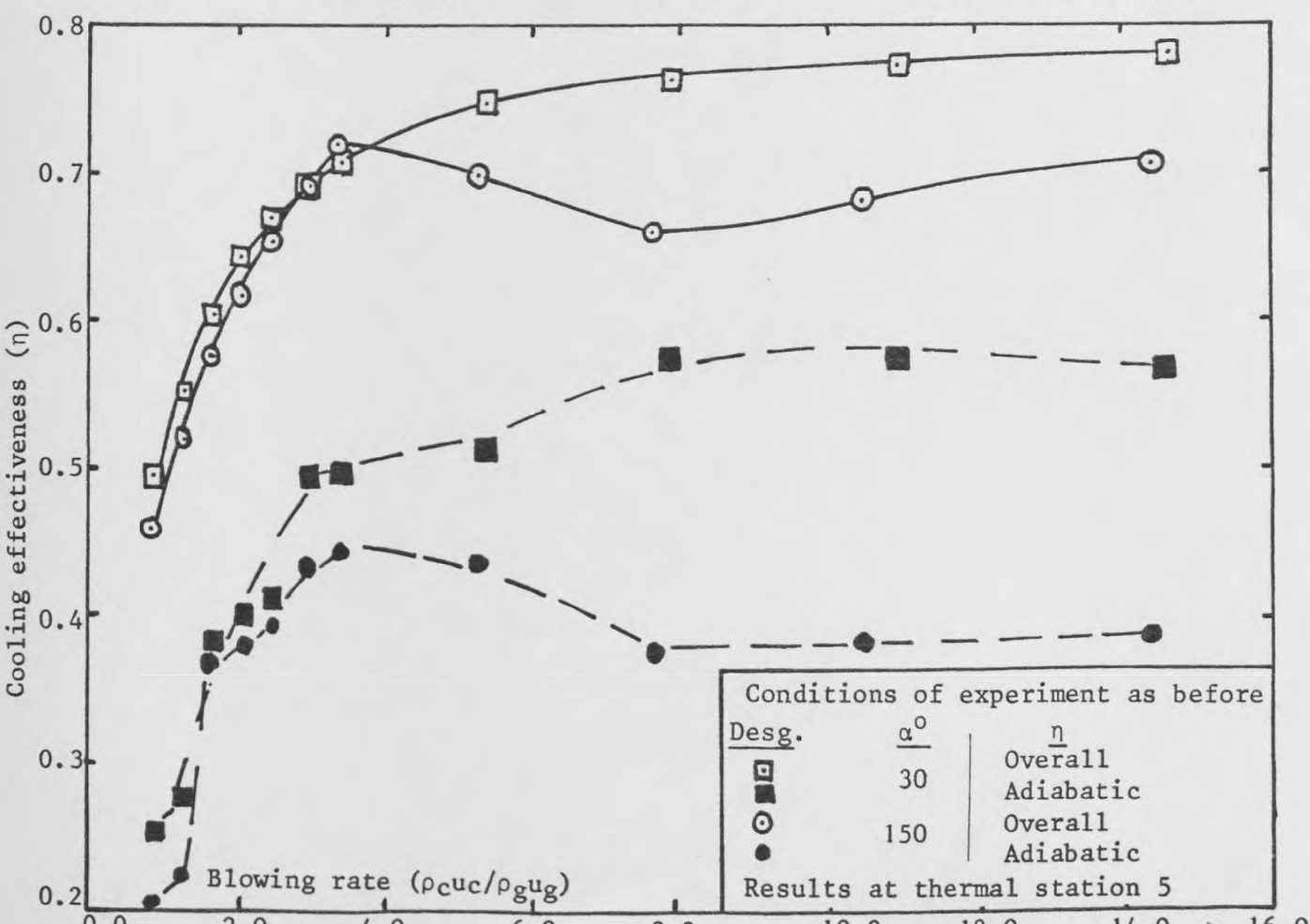

Fig. 6.108: Dependency of overall and adiabatic cooling effectiveness on blowing rate

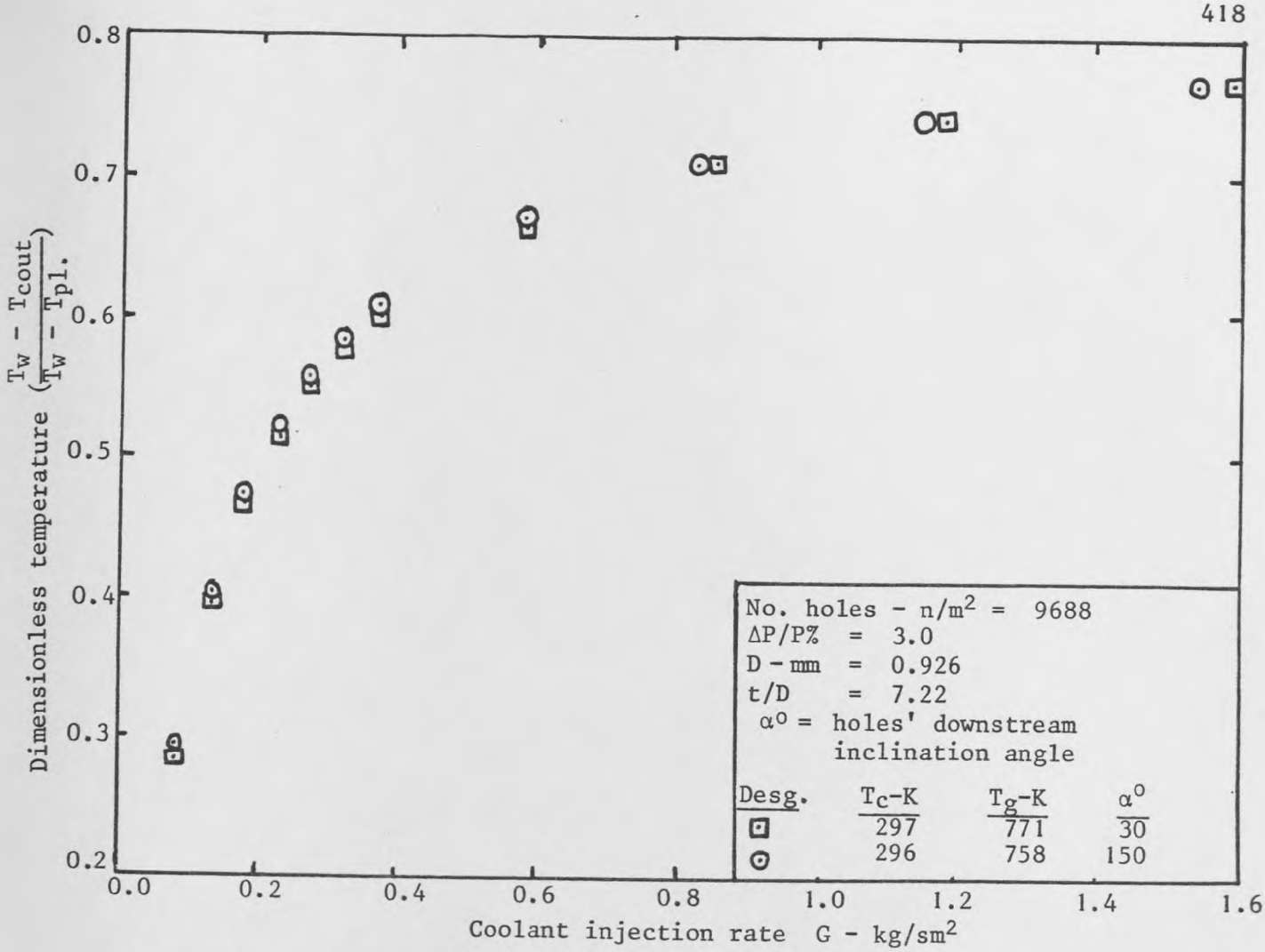

Fig. 6.109: Coolant temperature profile at thermal station 5

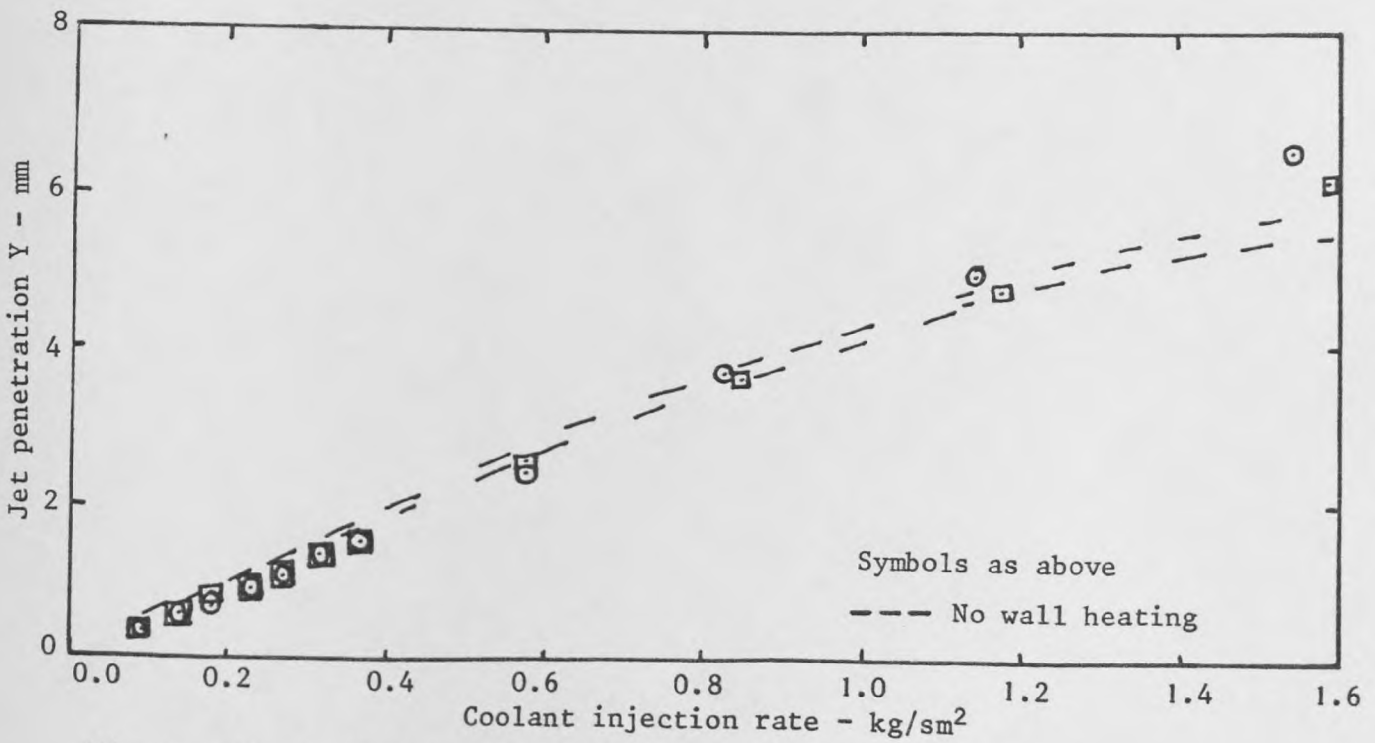

Fig. 6.110: Trajectory of coolant jets into cross-stream

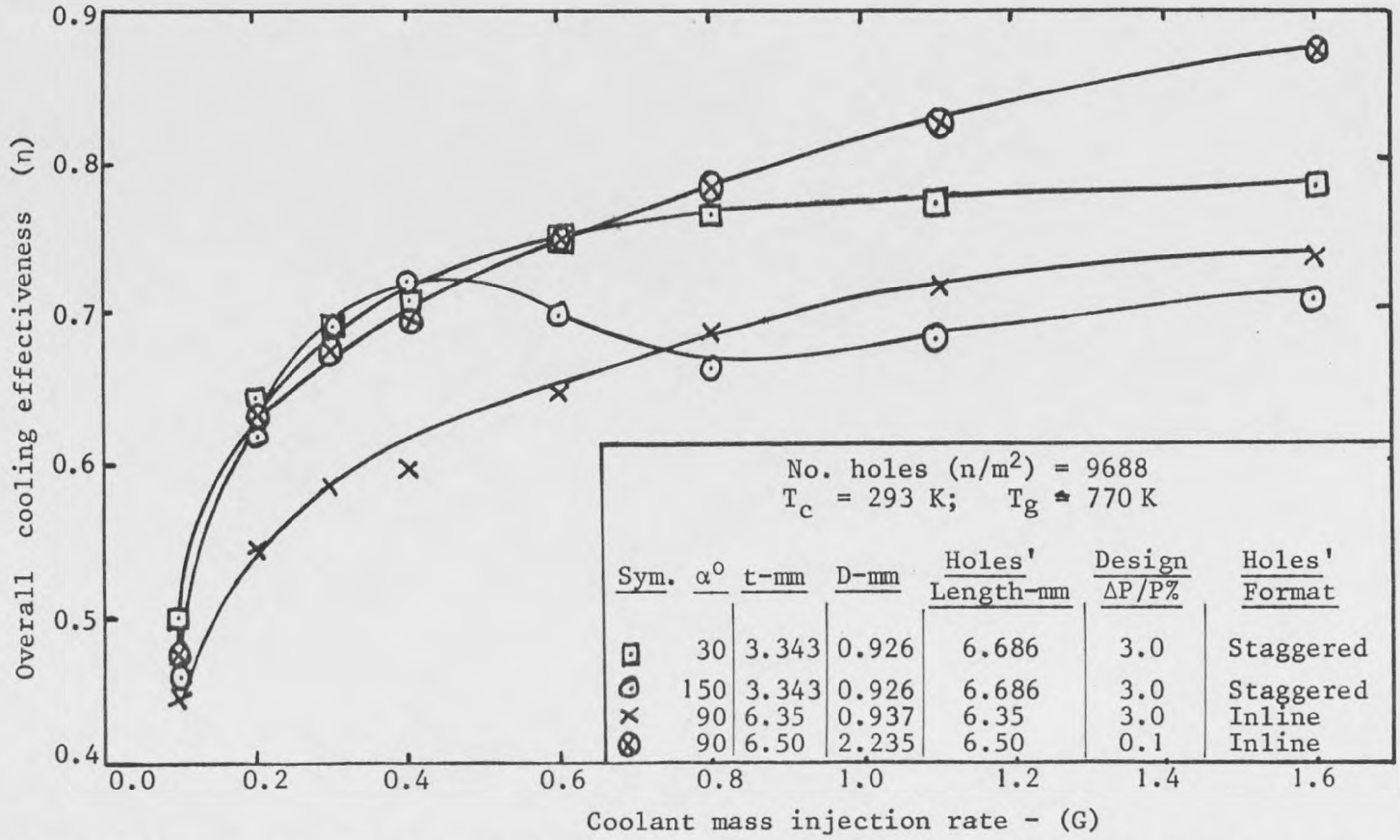

Fig. 6.111: Comparison of overall cooling effectiveness of inclined effusion holes with straight-through holes effusion walls at fifth thermal station

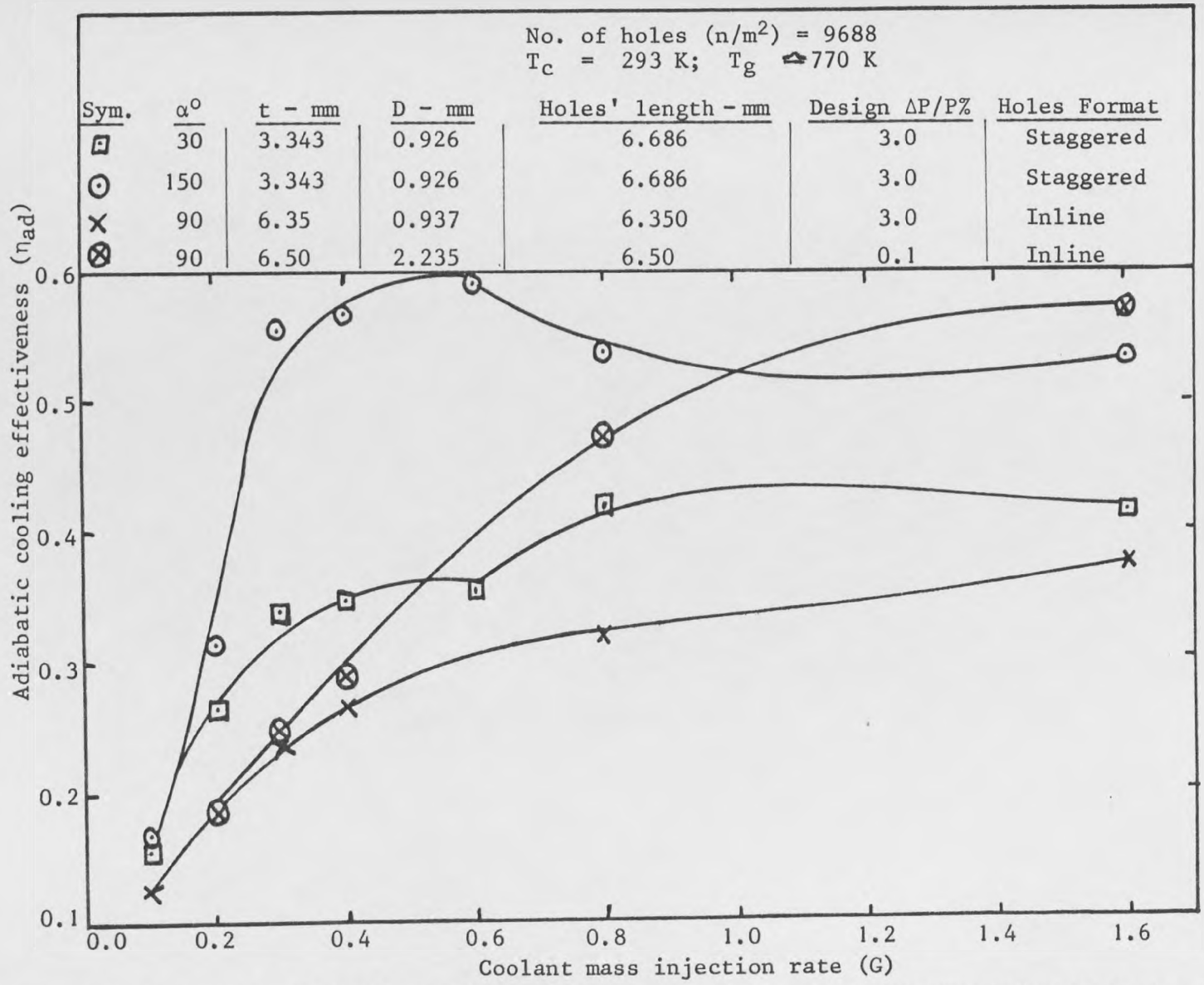

Fig. 6.112: Comparison of adiabatic cooling effectiveness of inclined effusion holes with straight-through holes' effusion walls at third thermal station

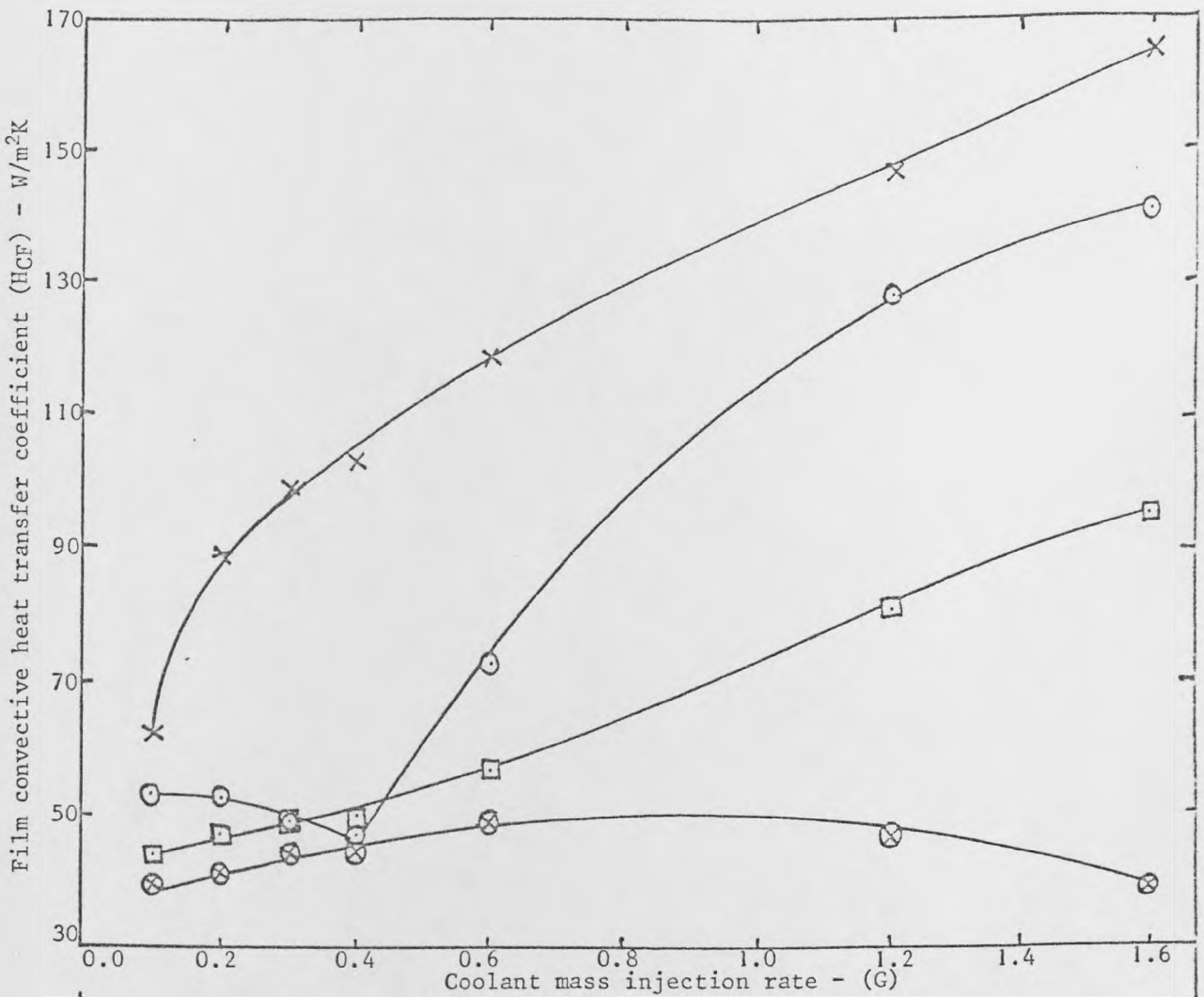

No. of holes - (n/m^2) - 9688
T_c = 293 K; T_g ≃ 770 K

Sym.	α°	t - mm	D - mm	Holes Length - mm	Design ΔP/P%	Holes Format
⊡	30	3.343	0.926	6.686	3.0	Staggered
⊙	150	3.343	0.926	6.686	3.0	Staggered
×	90	6.35	0.937	6.35	3.0	Inline
⊗	90	6.50	2.235	6.50	0.1	Inline

Fig. 6.113: Comparison of film heat transfer coefficient of inclined effusion holes' wall with straight-through effusion holes' wall at the fifth thermal station

CHAPTER 7

Nomenclature

Nu	=	Nusselt number
Re	=	Reynolds number
Pr	=	Prandtl number
Q	=	Heat transfer - W
H	=	Convective heat transfer coefficient - W/m^2K
A	=	Test surface area, or total cross-sectional holes' area - m^2
T	=	Temperature - K
E,ε	=	Emissivity
σ	=	Stefan-Boltzmann constant = 56.7×10^{-9} W/m^2K^4
K_p	=	Thermal conductivity of fluid - W/mK
D	=	Mean holes' diameter - m
R_{NU}	=	Ratio of average Nusselt number to fully developed Nusselt number
R	=	Radiative heat transfer - W
f	=	View factor
$\dot{M}$	=	Coolant mass flow rate - kg/s
C_p	=	Specific heat capacity - J/kgK
X	=	Holes' pitch - m
Z	=	Separating distance between impingement and effusion wall - m

Subscripts:

Nu,CI,r	=	back wall
w	=	wall
c	=	coolant
s,i,pl	=	impingement wall
3	=	plenum wall

H,ch	=	holes
in	=	inlet to holes
CE,W,E,p	=	effusion wall
wc	=	cylindrical combustor
gap	=	separation distance between impingement and effusion wall
t	=	outlet of impingement holes
D	=	nominal diameter
im	=	impinging
c,rf,g,f	=	hot gas or flame
n	=	exchange

CHAPTER 7

HEAT TRANSFER IN FULL COVERAGE DISCRETE HOLE IMPINGEMENT/ EFFUSION COOLING SYSTEM - A THEORETICAL ANALYSIS

7.1 INTRODUCTION

One of the most effective ways of cooling a heated surface is to impinge cool fluid onto the surface in form of jets. Not only are high local heat transfer coefficients attained, but by using a number of jets, the surface heat transfer distribution can be controlled. Round jets impinging on heated surfaces, held normal to the axis of flow, are very attractive in a variety of cooling applications such as for heat treatment of materials in the metal industry, for drying of materials produced in the paper and textile industry, tempering of glass in the glass industry, cooling of electronic components and gas turbine components cooling.

Impingement heat transfer has been extensively investigated using single jets (1-9), single row of jets (10-13) and multiple array of jets (14-25). Livingood and Hrycak (28) and Martin (29) have surveyed and summarized earlier results on heat transfer by impinging jets on a surface. Mikhail et al (30), Sparrow et al (31), Cartwright (32) and Freidman et al (36) have investigated jets impinging on a flat plate using slot nozzles and found that the heat transfer is not as high as in rounded hole jets. Dyban and Mazur (33), Hrycak (23,34,35) and Metzger et al (38) investigated the heat transfer by fluid impinging on a concave cylindrical surface and found that the heat transfer is higher than that of a flat surface.

In most of the analysis reported in the literature, the method of removing the spent jets has been a restriction of the lateral flow of the fluid to one direction or two directions by boxing in three or two of the sides of a rectangular test surface (36), or in general to let the spent fluid escape from all the sides (26). The method of spent fluid removal from the target surface is very important as this will influence the heat transfer from the surface of the target (14,17,26). When one opening is made, the net flow of the spent fluid is not uniform, as the volume of the fluid increases with axial distance, downstream of the first row of the impinging jets. The flow aerodynamics changes and the boundary layer (43) grows downstream. The heat transfer on the surface of the wall will follow the same trend and varies axially as the fluid and temperature fields on the target surface.

Vallis et al (25), working with an axisymmetric jet and electrochemical mass transfer measurement, also found that the heat transfer varies radially on the target surface. Sparrow et al (6), Obot et al (39) and Folayan et al (40) investigated the effect of semi-confinement and non-confinement of the exiting impinging jet on heat transfer. They showed that the effect of partial confinement of the impinging jet was to reduce the heat transfer by the jet which was most significant at nozzle to target spacing of 2 and 8. References 17, 21, 22 and 41 investigated heat transfer to impinging jets, whose spent fluid is constrained to flow in one direction, and found that the heat transfer follows a periodic variation downstream of the first row of jets. These investigations also found that the maxima of heat transfer was downstream of the point of stagnation.

Almost all the investigations on impingement cooling reported to date in the literature on gas turbine wall cooling are mainly for turbine blades application. The target surface in almost all the investigations was a blank solid surface and hence there was cross-flow on this surface with all its drawbacks. The application of impingement cooling to a gas turbine combustor wall is achieved by having a double skin combustor. The outer skin is perforated and serves as the impingement wall, producing impinging coolant jets. The inner skin serves as the target surface and the spent fluid is removed at one end.

Impingement cooling can also be achieved by combining two separately optimized perforated walls together, with a gap in between, to form a double skin combustor. The outer wall serves as the impingement wall and produces the impinging coolant jets. The inner wall, with one of its surfaces in contact with the flame and hot gases, serves as the target wall. The spent impinging fluid accelerates towards nearby holes and effuses straight into the combustor mainstream as cooling jets. The jets are deflected, coalesce and form a cool heat-sink film on this side of the wall. The target wall is called the effusion wall. The coolant fluid serves two major purposes: (a) cooling the inner skin back-side by impingement and (b) protecting the gas side wall surface from mainstream heating by forming a protective heat sink barrier. This hybrid method of cooling is the subject of the present work and it is called Full Coverage Discrete Hole Impingement/Effusion Cooling System, shown in fig. 7.1.

The method of removing spent fluid in this system by effusion prevents unnecessary thickening of the boundary layer, since the

fluid accelerates from the stagnation point to the nearest hole and hence enhances heat transfer. Recirculation of spent fluid is also, for the same reason, reduced. Obot (42) observed an increase in heat transfer at the stagnation region on a permeable surface due to spent fluid suction in comparison with a non-permeable target surface. Hollworth et al (45,46), using a square array of square edge impingement holes combined with a square array of sharp edge round vent holes target flat plate, investigated impingement heat transfer by electrically heating the target wall. They found a significant increase in the impingement heat transfer which was attributed to the suction action of the effusion holes.

Mkpadi (44) and Andrews et al (48-54) investigated the cooling effectiveness of impingement wall cooling under realistic conditions using arrays of sharp edge round impingement holes combined with a flat target surface with sharp edge round vent holes. Andrews et al and Mkpadi carried out their investigation at realistic condition amenable to gas turbine operational condition. The present work is a continuation of that of Andrews and Mkpadi and it is the subject of this chapter to analyse the heat transfer processes in this system.

7.2 IMPINGEMENT/EFFUSION HEAT TRANSFER PROCESS

Impingement/effusion heat transfer has two main components, impingement plate and effusion plate heat transfer, with a third component of inter-plate heat transfer. This latter effect is the heating of the impingement plate based on the effusion plate as a heat source. This has both radiative and convective components which have received no previous investigation.

The cooling of the effusion plate by the impingement jets is

influenced by the presence of the effusion holes. Few studies of this geometry have been undertaken and in the present work no modifications to conventional flat plate impingement heat transfer are made. However, heat transfer at the effusion hole inlet is considered to be additive to that of impingement cooling with no interaction between the two processes.

The present model of the impingement/effusion heat transfer process is shown in figure 7.5. The overall heat balance is summarised by equation 7.1(i).

$$Q_c = (Q_{CI} + Q_H + Q_{im} + Q_{CE} + Q_E + Q_n) - (Q_r + Q_{rf}) \quad \ldots (7.1(i))$$

Each term in this equation will be discussed in detail in the following sections. In principle, the model uses the two main convective heat transfer processes previously discussed for effusion plate cooling. In addition there is the problem of convective and radiative heating of the impingement plate. In this model all the coolant mass flow is assumed to participate in each convective heat transfer process. This may not be valid for convective heating of the impingement plate.

7.3 IMPINGEMENT WALL HEAT TRANSFER

The heat transfer at the impingement wall has not previously been investigated. This is partly due to the fact that many investigations employ nozzles to produce the impinging jets (1-30, 55,56). Where the investigations are for turbine cooling, it is mainly for turbine blade application and all the workers in this area have so far ignored the impingement wall heat transfer.

In both turbine combustor and blade applications, the impingement wall will be heated by convection and radiation. The temperature of this wall will therefore be higher than that of the coolant and hence the coolant will be heated as it passes through the impingement plate.

7.3.1 Back-side of the Impingement Wall Heat Transfer

Two main heat transfer processes will take place on the outer skin of the combustor. These are convective heat transfer and radiative heat transfer. These forms of heat transfer processes have been analysed in Chapter 5, section 5.3.1, and the heat transfer correlations employed for both convection and radiation are restated in equations 7.1 and 7.2 respectively.

For convection, refs. (56,57),

$$Nu = 0.881\ Re^{0.476}\ Pr^{\frac{1}{3}} \qquad \ldots (7.1)$$

$$Q_{CI} = H_{Nu}A(T_w - T_c) \qquad \ldots (7.2)$$

and for radiation,

$$Q_r = \frac{AE_1\sigma}{(1 - E_1)}\left[\frac{(0.952 - 0.953E_1)T_{p1}^4 - (0.952 - 0.952E_1)T_3^4}{(0.952 + 0.047E_1)}\right] \qquad \ldots (7.3)$$

7.3.2 Heat Transfer in the Impingement Wall Holes

The heat transfer to the fluid in the holes is purely convective. The correlation of Mills for a sharp edge 90° inlet has been employed for computing this heat transfer. The processes involved in using the correlation of (61) have been detailed in Chapter 5, section 5.3.2A, and this correlation is restated as in equation 7.4.

$$H_{ch} = 0.023\ Re^{0.8} Pr^{0.33} R_{Nu} K_p / D \qquad \ldots (7.4)$$

$$Q_H = H_{ch} A (T_s - T_{in}) \qquad \ldots (7.5)$$

The parameter R_{Nu} is as defined in equations 5.31 and 5.32.

7.3.3 Gap Impingement Wall Face Heat Transfer

In the conduit of a double wall combustor, the outer wall's surface, on the side of the gap, will receive heat from the back-surface of the inner wall. In the present system of cooling - impingement/effusion cooling system - it follows that not only is the target effusion wall cooled by impinging jets but the impingement wall is heated. In the present work it has been found that the temperature of the impingement plate increases with a decrease in the coolant flow rate. The only investigators who have observed this phenomenon of impingement plate heating are Andrews et al (58). No other investigator of impingement cooling in a gas turbine has reported measurement of the impingement wall or, for that matter, given any information on how such temperature may be predicted. The temperature often used in the impingement correlation is that of the coolant as supplied. As the impingement plate is heated during realistic application, the exit impinging jets attain a temperature higher than that of the coolant as supplied due to heat transfer at the back face and inside of the impingement wall. The implication of the new jet exit temperature is that the impingement heat transfer correlations presently available, when applied, fail to accurately account for the heat transfer at the target wall. It is the objective of this section to analyse the mode of heating processes of the impingement wall and offer a method by which the impingement wall temperature may be predicted and hence the impingement jet outlet temperature.

7.3.3A Heat transfer processes to the impingement wall of impingement/effusion cooling systems

Lefebvre et al (59) and Winter (60) have investigated heat transfer processes to gas turbine double skin flame tube and concluded that the processes by which the outer skin is heated, using conventional cooling methods, are mainly convectional. It was recommended that the radiative process be ignored in the computation of this wall heat transfer. However since there is no net crossflow of coolant in impingement/effusion cooling systems, it may be assumed that there is possibly no heating of the impingement wall. Measurements made of the wall and the fluid in the gap, Z, fig.7.1, in the present work showed that this postulation was wrong.

The heating of the impingement plate is considered to be due to both radiative and convective heat transfer. The radiative heat transfer to the impingement wall can be predicted with accuracy but no information exists for the convective heating of the impingement plate as the phenomenon has not previously been investigated or recognised. As shown in fig.7.3, it is considered that the convective heating is caused by the deflection of impinging jets from the target wall back onto the impingement wall from the point of stagnation. Since the magnitude of the heat transfer at this point has been shown (1,6,12,24,26) to be the maximum and a function of the ratio of the spacing of the jet exit to the target (Z) wall and nozzle diameter, it is strongly considered that heating of the impingement wall is a function of Z.

7.3.3A.1 Radiative heat transfer to the impingement wall

The radiative heat transfer between the target wall and the impingement surface may be treated as radiative heat exchange between two parallel surfaces. Figure 7.4 shows a simple model of the process of radiation between two parallel walls. Considering the walls to be of infinite length (62) compared with the separation between them, Z, the view factor (63) is unity because the wall cannot see itself. The net radiations from surface W, the effusion wall, and surface S, the impingement wall, are respectively given as

$$R_w = \varepsilon_w E_w + (1 - \varepsilon_w) R_s \qquad \ldots (7.6A)$$

$$R_s = \varepsilon_s E_s + (1 - \varepsilon_s) R_w \qquad \ldots (7.7)$$

Substituting for R_w in equation 7.7 and rearranging

$$R_s = \frac{\varepsilon_s E_s + (1 - \varepsilon_s)\varepsilon_w E_w}{[1 - (1 - \varepsilon_s)(1 - \varepsilon_w)]} \qquad \ldots (7.8)$$

Also equation 7.6A may be expressed as

$$R_w = \varepsilon_w E_w + (1 - \varepsilon_w)[\varepsilon_s E_s + (1 - \varepsilon_s) R_w] \qquad \ldots (7.6B)$$

Rearranging,

$$R_w = \frac{\varepsilon_w E_w + (1 - \varepsilon_w)\varepsilon_s E_s}{[1 - (1 - \varepsilon_w)(1 - \varepsilon_s)]} \qquad \ldots (7.9)$$

where R_w = Net radiative heat transfer from the effusion wall - W/m^2

R_s = Net radiative heat transfer from the impingement wall - W/m^2

$\varepsilon_w, \varepsilon_s$ = Emissivity of the surfaces at temperatures T_w and T_s respectively (computed as in Chapter 5)

r_s = Reflectivity from surface S
= $1 - \varepsilon_s$

r_w = Reflectivity from surface W
= $1 - \varepsilon_w$

$$E_w = \sigma T_w^4 \qquad \ldots (7.10)$$

$$E_s = \sigma T_s^4 \qquad \ldots (7.11)$$

where T_w = Temperature of effusion wall - K

T_s = Temperature of impingement wall - K

σ = Stefan-Boltzmann constant = 56.7×10^{-9} W/m^{2}K^4

Combining equations 7.10 and 7.11 with equation 7.9, the net radiative heat transfer to the impingement wall may be expressed in terms of the surfaces' temperatures as in equation 7.12.

$$R_w = A\sigma \left\{ \frac{\varepsilon_w T_w^4 + (1 - \varepsilon_w)\varepsilon_s T_s^4}{[\varepsilon_w + \varepsilon_s(1 - \varepsilon_w)]} \right\} \qquad \ldots (7.12)$$

For industrial and aero gas turbine combustors, the view factor as well as the characteristic dimension separating the two walls may have to be included. However for an annular combustor the view factor is unity because the wall's surface cannot see itself. For a case of a cylindrical combustor, ref. 59 has suggested that the characteristic dimension be represented by the ratio of the outside diameter of the flame tube to the inside diameter of the outer casing. Applying the above parameters and the correlation of (59), the net radiation to the impingement wall becomes

$$R_{wc} = A\sigma f \left[\frac{\varepsilon_w \varepsilon_s}{\varepsilon_w + \varepsilon_s(1 - \varepsilon_w)D_I} \right] (T_w^4 - T_s^4) \qquad \ldots (7.13)$$

where $D_I = \frac{D_w}{D_s} \equiv \frac{\text{outside diameter of effusion wall}}{\text{inside diameter of impingement wall}} \equiv \frac{A_w}{A_s}$

A = Cylindrical inside area of outer casing

f = View factor = 1

For a large cylindrical annular combustor, D_I of equation 7.13 is approximately unity. Furthermore equation 7.13 is only applicable to a turbo-annular combustor, Chapter 1, fig. 1.2. For the annular combustor for which this programme is intended, equation 7.13 will underpredict the radiative heat transfer to the impingement wall. This is underpinned by the following example.

Consider that T_w = 790 K, T_s = 400 K, ε_w = 0.6, ε_s = 0.8. Substituting into equations 7.12 and 7.13, the equations give, for a unit area,

$$R_w = 56.7 \times 10^{-9} \left[\frac{0.6 \times 790^4 + (1 - 0.6) \times 0.8 \times 400^4}{|0.6 + 0.8(1 - 0.6)|} \right] \quad 7.12$$

$$= 1.491 \times 10^4 \text{ W}$$

$$R_{wc} = 56.7 \times 10^{-9} \left[\frac{0.6 \times 0.8}{|0.8 + 0.6(1 - 0.8)|} (790^4 - 400^4) \right] \quad 7.13$$

$$= 1.077 \times 10^4 \text{ W}$$

Equation 7.13 will underpredict the radiation to the impingement wall by up to 28%. Equation 7.12 is employed in the present work

7.3.3A.2 Convective heat transfer to the impingement wall

Since the phenomenon of impingement wall heating has never before been considered, there are neither data nor correlations available to draw on for the prediction of convective heat transfer to the impingement wall. To evaluate this heat transfer to the

wall by the deflected jets a heat balance on the impingement wall is carried out as shown in fig.7.5 and equation 7.14.

$$Q_w + R_w = Q_{CI} + Q_r + Q_H \quad \ldots (7.14)$$

Rearranging, the convective heat transfer, Q_w, to the impingement wall gives

$$Q_w = Q_{CI} + Q_r + Q_H - R_w \quad \ldots (7.15)$$

where Q_w = Convective heat transfer to the wall

Q_{CI} = Convective heat removed by coolant from wall back

Q_r = Radiative heat transfer to plenum from the back wall

Q_H = Convective heat removed by coolant from wall's holes

R_w = Net radiation to the wall from effusion wall

From Q_w the convective heat transfer coefficient and the temperature of fluid in the gap, Z, may be predicted, knowing the outlet temperature of the impinging jets, T_t, predicted from the correlation of (61) as in equation 5.60. With T_t known, the gap temperature is predicted as

$$\dot{M}C_p(T_{gap} - T_t) = Q_w + R_w \quad \ldots (7.16)$$

Rearranging

$$T_{gap} = Q_{wt}(\dot{M}C_p)^{-1} + T_t \quad \ldots (7.17)$$

where T_{gap} = Temperature of fluid in the gap, Z.- K

Q_{wt} = $Q_w + R_w$ --- W

$\dot{M}$ = Coolant mass flow rate - kg/s

C_p = Specific heat capacity computed as in equation 5.10

T_t = Predicted impinging jet outlet temperature

The convective heat transfer coefficient may be predicted as:

$$H_w = \frac{Q_w}{A(T_w - T_t)} \qquad \ldots (7.18)$$

where H_w = Convective heat transfer coefficient - W/m^2K

A = Total surface area of test wall - m^2

T_w = Measured impingement wall temperature - K

Having obtained Q_w and all the parameters of equation 7.15, the temperature of the impingement wall of a cylindrical combustor may be predicted by setting the value of Q_r to zero. A new value of Q_w is obtained and from this T_w is found.

Having obtained the fluid temperature in the gap, the focus of attention will now be on the effusion wall.

7.4 HEAT TRANSFER OF THE EFFUSION WALL IN AN IMPINGEMENT/EFFUSION COOLING SYSTEM

The effusion wall of an impingement/effusion cooling system has a different heat transfer format from that of a single skin effusion combustor. This difference is mainly at the back-side of the wall, where the coolant arrives as jets unlike the uniform flow of coolant in a single wall. This section will therefore commence with the back-side of the effusion wall.

7.4.1A Impinging jet heat transfer at the back-side of the effusion wall

The heat transfer here is accounted for by the impinging jet heat transfer which has been a subject of intensive investigation. The heat transfer on a target surface with spent fluid removal through vent holes has only been reported by Hollworth et al (45-47) and Andrews et al (58). Hollworth et al in the first part of their work investigated the heat transfer coefficient for arrays of

turbulent air jets with jet-to-jet spacing of $10 \leqslant X/D \leqslant 25$ and ratio of jet exit to target wall (Z) to nozzle diameter of $1 \leqslant Z/D \leqslant 15$. They correlated their results as in equation 7.19.

$$Nu_D = 0.435\ Re_D^{0.8}\ Pr^{\frac{1}{3}}\ (X/D)^{-1.4} \qquad \ldots (7.19)$$

where Nu_D = Nusselt number based on perforated wall norminal diameter

Re_D = Reynolds number

Pr = Prandtl number

X = Impingement wall holes' pitch

D = Norminal diameter of jet orifices

The work of (45) shows that X/D was more dominant than Z/D. Many investigators of impingement cooling have correlated their heat transfer data as a function of $(Z/D)^m$ (1-20, 22-26). Andrews et al (26) have estimated the exponent m for Hollworth et al's work to be -0.153. Andrews et al, working with impingement cooling, relevant to the present work at $10 \leqslant X/D \leqslant 13$ and $0.56 \leqslant Z/D \leqslant 14$ correlated their data in terms of Z/D as expressed in equation 7.20.

$$Nu_D = 0.0252\ Re_D^{0.72}\ Pr^{0.33}\ (Z/D)^{-0.14} \qquad \ldots (7.20)$$

In the present work both the ranges of (Z/D) and (X/D) employed by Hollworth et al and Andrews et al are investigated and the above correlations have been applied. The heat transfer according to the above correlations may be expressed as

$$H_{im} = Nu_D \frac{K}{D} \qquad \ldots (7.21)$$

$$Q_{im} = A\, H_{im} (T_E - T_{gap}) \qquad \ldots (7.22)$$

Heat transfer at this back-side also takes place by radiation to

the impingement plate as discussed in 7.2.3A.1. The radiative heat transfer at the back of the effusion wall is given by equation 7.12.

7.4.1B Convective heat transfer at the back-side of the effusion wall, Q_{CE}

As the spent fluid is en route to the effusion wall holes, it scrubs the wall and heat is transferred by convection to the spent fluid from the hot wall. This convective heat transfer has been correlated using the correlations of Sparrow et al. The temperature, T_{on}, of the spent fluid is predicted from the impinging heat transfer, Q_{im}, as stated in section 7.4. The convection at the back of the effusion wall is computed, using the fluid temperature, T_{gap}, equation 7.17, as

$$Q_{CE} = H_{CE} A (T_w - T_{gap}) \quad \ldots (7.23)$$

where Q_{CE} = Effusion back-wall convection - W

H_{CE} = Convective heat transfer coefficient obtained from Sparrow et al's correlation (57)

A = Non-perforated area of the back wall - m^2

T_w = Effusion wall temperature - K

T_{gap} = Predicted fluid temperature (see equation 7.17)

7.4.2 Effusion Wall Holes' Heat Transfer

The heat transfer in the holes of the effusion wall is as detailed in Chapter 5 and the same equation as in section 7.3.2 is employed. This heat transfer is given by equation 7.24.

$$Q_E = H_E A_h (T_w - T_{in}) \quad \ldots (7.24)$$

where Q_E = Mean heat transfer in the holes - W

H_E = Mean heat transfer coefficient in the holes - W/m^2K

A_h = Total cross-sectional area of holes - m^2

T_w = Measured effusion wall temperature - K

T_{in} = Predicted coolant holes inlet temperature - K

7.4.3 Heat Transfer to the Effusion Wall from Mainstream Combustion Gases

The heat transfer processes from the combustor mainstream to the effusion wall have been discussed in detail in Chapter 5, section 5.3.3 and only the relevant mode of heat transfer with relevant correlations will be repeated here. These heat transfer processes are:

(a) Radiation from hot mainstream, Q_{rf},

$$Q_{rf} = A\sigma \frac{(1 + E_p)}{2} E_f T_g^{1.5} (T_g^{2.5} - T_{p1}^{2.5}) \quad \ldots (7.25)$$

(b) Radiative heat exchange, Q_n,

$$Q_n = \frac{AE_p(\sigma T_{p1}^4 Z_5 - Z_3 - Z_4)}{Z_5(1 - E_p)} \quad \ldots (7.26)$$

(c) Convective heat transfer from the hot gas stream Q_c. This heat transfer mode is determined through heat balance as in equation 7.27, fig. 7.5.

$$Q_c + Q_{rf} = Q_{CE} + Q_{im} + Q_E + Q_n + R_w \quad \ldots (7.27)$$

Rearranging,

$$Q_c = Q_{CE} + Q_{im} + Q_E + Q_n + R_w - Q_{rf} \quad \ldots (7.28)$$

Equation 7.28 is similar to equation 5.50 except for Q_{im} which is new and comes from jets' impingement.

With Q_c determined, the film heat transfer coefficient, H_f, is predicted as

$$H_f = \frac{Q_c}{A(T_g - T_w)} \quad \ldots (7.29)$$

For a cylindrical combustor, Q_c is obtained by setting Q_n to zero as discussed in Chapter 5 for modelling.

7.5 FLUID TEMPERATURE HISTORY AND PREDICTIONS

The temperatures of the fluid as it approaches the impingement wall holes change from that at the plenum and continue to do so until it leaves the effusion wall flame side as jets. Figure 7.2 shows the temperature history of the fluid. Temperature T_1 is the plenum temperature. Temperatures T_2 and T_3 are predicted using the correlations of references 57 and 61 respectively, as discussed in Chapter 5 for the single wall. The fluid temperature T_3 was used in computing the impingement heat transfer, Q_{im}.

There are two temperatures in the gap. The first is T_4 and may be computed as in equation 7.30.

$$T_4 = Q_{im}(\dot{M}C_p)^{-1} + T_3 \qquad \ldots (7.30)$$

Temperature T_5 which is regarded as gap temperature is predicted as in equation 7.17 and goes into the computation of convective heat transfer, at the back of the effusion wall, using the correlations of Sparrow et al (57). The fluid's temperatures, T_6 and T_7, on its approach to and exit from the effusion wall holes are predicted using the correlations of refs. 57 and 61 respectively (Chapter 5).

The model of heat transfer processes employed in the gap of the impingement/effusion wall is based on the assumption that the heat transfer processes act separately not interacting with one another. It is on this basis that the temperatures are predicted. Clearly the model predicts a counter-flow region in the gap with a temperature difference between the two and the assumption of no interaction would be unrealistic. Also the assumption that all the

cross-flow participates in the rebound flow is unrealistic. Methods to measure experimentally the overall heat transfer are under development in another project. However in the absence of these data it is considered that the present model is the best approach.

Comparison of the film heat transfer coefficient prediction from the model with those for the effusion plate alone will be made. Although some differences may be expected due to the higher exit velocities and lower coolant densities for the impingement case, large differences would not be expected. If large differences are found from the predictions then this could indicate that the impingement/effusion heat transfer model is inadequate.

7.6 COMPUTER PROGRAM WITH FLOW SHEET

A computer program has been written for the analysis of the above heat transfer as well as the cooling effectiveness offered in the experimental investigation carried out on this system of cooling. The results of the work are reported in Chapter 8.

The flow sheet is similar to that for a single effusion wall detailed in Chapter 5 but with the addition of an impingement wall analysis section. A detailed computer hard copy results output is shown in the appendix.

7.7 CONCLUSIONS

(1) The heat transfer in an impingement wall of a discrete hole full coverage impingement/effusion cooling system, which has never before received treatment from investigators of impingement cooling, has been analysed.

(2) The phenomenon of impingement wall heating, first suggested by Andrews et al (58), has been identified to be caused by both convective and radiative heating from the target wall.

(3) A step-by-step analysis of heat transfer processes of a combined impingement/effusion cooling system has been offered with temperature predictions of fluid in the gap, Z.

(4) A procedure for correction for cylindrical combustors has been suggested, backed up with a computer program.

7.8 REFERENCES

1. Gardon, R., and Cobonpue, J., 'Heat transfer between a flat plate and jets of air impinging on it', Proc. Int. Heat Transfer Conf., Pt. 3, pp. 454-460, 1961.

2. Gardon, R., and Akfirat, J.C., 'The role of turbulence in determining the heat transfer characteristics of impinging jets', Int. J. Heat Mass Transfer, 8, pp. 1261-1272, 1965.

3. Gardon, R., and Akfirat, J.C., 'Heat transfer characteristics of impinging two-dimensional jets', Trans. ASME, Series C, J. Heat Transfer, Vol. 88, pp. 101-107, 1966.

4. den Ouden, C., and Hoogendoorn, C.J., 'Local convective heat transfer coefficients for jets impinging on a flat plate: Experiments using a liquid crystal technique', Proc. 5th Int. Heat Transfer Conf., Tokyo, 1974.

5. Bouchez, J.P., and Goldstein, R.J., 'Impingement cooling from a circular jet in a crossflow', Int. J. Heat Mass Transfer, Vol. 18, pp. 719-730, 1975.

6. Sparrow, E.M., Goldstein, R.J., and Rouf, M.A., 'Effect of nozzle surface separation distance on impingement heat transfer for a jet in a crossflow', ASME - J. Heat Transfer, Vol. 97, pp. 528-533, 1975.

7. Hollworth, B.R., and Bowley, W.W., 'Heat transfer characteristics of an impinging jet in crossflow', ASME Paper 75 - WA/HT-100, 1975.

8. Goldstein, R.J., and Behbahani, A.I., 'Impingement of a circular jet with and without cross flow', Int. J. Heat Mass Transfer, Vol. 25, No. 9, pp. 1377-1382, 1982.

9. Poreh, M., and Cermak, J.E., 'Flow characteristics of a circular submerged jet impinging normally on a smooth boundary', 6th Midwestern Conference, Fluid Mech., University of Texas, Austin, pp. 198-212, 1959.

10. Goldstein, R.J., and Timmer, J.F., 'Visualization of heat transfer from arrays of impinging jets', Int. J. Heat Mass Transfer, Vol. 25, No. 12, pp. 1857-1868, 1982.

11. Ji-Rui, C., and Bao-Guan, W., 'Experimental investigation of heat transfer by a single and a triple row round jets impinging on semi-cylindrical concave surface', Proc. 7th Int. Heat Transfer Conf., 1982.

12. Metzger, D.E., and Korstad, R.J., 'Effect of Crossflow on impingement heat transfer', ASME - J. Eng. Power, Vol. 94, pp. 35-42, 1972.

13. Koopman, R.N., and Sparrow, E.M., 'Local and average transfer coefficients due to an impinging row of jets', Int. J. Heat Mass Transfer, Vol. 19, pp. 673-687, 1976.

14. Florschuetz, L.W., and Isoda, V., 'Flow distributions and discharge coefficient effects for jet array impingement with initial crossflow', J. Eng. Power, Vol. 105, 296-304, April 1983.

15. Kercher, D.M., and Tabakoff, W., 'Heat transfer by a square array of round air jets impinging perpendicular to a flat surface including the effect of spent air', J. Eng. Power, pp. 73-82, 1970.

16. Galant, S., and Martinez, G., 'Cross flow influence upon impingement convective heat transfer in circular arrays of jets: A general correlation', Proc. 7th Int. Heat Transfer Conf., Vol. 3, pp. 343-347, 1982.

17. Florschuetz, L.W., Truman, C.R., and Metzger, D.E., 'Streamwise flow and heat transfer distributions for jet array impingement with crossflow', ASME - J. Heat Transfer Vol. 103, No. 2, pp. 337-342, 1981.

18. Chance, J.L., 'Experimental investigation of air impingement heat transfer under an array of round jets', Tappi Vol. 57, No. 6, pp. 108-112, 1974.

19. Huang, G.C., 'Investigations of heat transfer coefficients for air flow through round jets impinging normal to a heat transfer surface', ASME - J. Heat Transfer, Vol. 85, pp. 237-243, 1963.

20. Metzger, D.E., Florschuetz, L.W., Takeuchi, D.I., Behee, R.D., and Berry, R.A., 'Heat transfer characteristics of inline and staggered arrays of circular jets with crossflow of spent air', ASME - J. Heat Transfer, Vol. 101, pp. 526-531, 1979.

21. Florschuetz, L.W., Berry, R.A., and Metzger, D.E., 'Periodic streamwise variations of heat transfer coefficients for inline and staggered arrays of circular jets with crossflow of spent air', ASME - J. Heat Transf., Vol. 102, No. 1, pp. 132-137, 1980.

22. Florschuetz, L.W., Metzger, D.E., and Su, C.C., 'Heat transfer characteristics for jet array impingement with initial cross-flow', ASME - Paper 83-GT-28.

23. Hrycak, P., 'Heat transfer and flow characteristics of jets impinging on a concave hemishperical plate', Proc. 7th Int. Heat Transf. Conf., Vol. 3, pp. 357-362, 1982.

24. Hrycak, P., 'Heat transfer from round impinging jets to a flat plate', Int. J. Heat Mass Transf., Vol. 26, No. 12, pp. 1857-1865, 1983.

25. Vallis, E.A., Patrick, M.A., and Wragg, A.A., 'Radial distribution of convective heat transfer coefficient between an axisymmetric jet and a flat plate held normal to the flow', Proc. 6th Int. Heat Transfer Conf., Vol. 5, pp. 297-303, Toronto, 1978.

26. Andrews, G.E., and Hussain, C.I., 'Impingement cooling system of gas turbine components', Int. Gas Turbine Congress, Paper 83 - Tokyo - IGTC - 9, 1983.

27. Andrews, G.E., and Hussain, C.I., 'Impingement cooling using arrays of holes', I. Chem. E. Annual Research Meeting, Bath, April 1984.

28. Livingood, J.N.B., and Hrycak, P., 'Impingement heat transfer from turbulent air jets to flat plates - A literature survey', NASA TM X-2778, 1973.

29. Martin, H., 'Heat and mass transfer between impinging gas jets and solid surfaces', Advances in Heat Transfer, Vol. 13, pp. 1-60, Academic Press, New York, 1977.

30. Mikhail, S., Morcos, S.M., Abou-Ellail, M.M.M., and Ghaly, W.S., 'Numerical prediction of flow field and heat transfer from a row of laminar slot jets impinging on a flat plate', Proc. 7th Int. Heat Transf. Conf., Vol. 3, pp. 377-382, 1982.

31. Sparrow, E.M., and Lee, L., 'Analysis of flow field and impingement heat/mass transfer due to a non-uniform slot jet', ASME J. Heat Transf., pp. 191-197, 1975.

32. Cartwright, W.G., and Russell, P.J., 'Characteristics of a turbulent slot jet impinging on a plane surface', Proc. Instn. Mech. Engrs., Vol. 182, Pt. 3H, 1967-68.

33. Dyban, Ye.P., and Mazur, A.I., 'Heat transfer in the vicinity of the stagnation point produced by impingement of a turbulized jet onto a baffle', Heat Transfer - Soviet Res., Vol. 11, No. 1, pp. 52-58, 1979.

34. Hrycak, P., 'Heat transfer from row of impinging jets to concave cylindrical surfaces', Int. J. Heat Mass Transf., Vol. 25, pp. 407-419, 1981.

35. Hrycak, P., 'Heat transfer from a row of jets impinging on a concave semi-cylindrical surface', Proc. 6th Int. Heat Transfer Conf., Vol. 2, pp. 67-72, 1978.

36. Freidman, S.J., and Mueller, A.C., 'Heat transfer to flat surface', Inst. Mech. Eng., ASME - Proc. General Disc. on Heat Transf., pp. 138-142, 11-13 Sept., 1951.

37. Popiel, C.O., and Tass, O., 'The effect of ordered structure of turbulence on momentum, heat and mass transfer of impinging round jets', Proc. 7th Int. Heat Transf. Conf., Vol. 6, pp. 141-146, 1982.

38. Metzger, D.E., Yamashita, T., and Jenkins, C.W., 'Impingement cooling of concave surfaces with lines of circular air jets', J. Eng. Power, Vol. 91, No. 3, July 1969.

39. Obot, N.T., Douglas, W.J.M., and Mujumdar, A.S., 'Effect of semi-confinement on impingement heat transfer', Proc. 7th Int. Heat Transf. Confs., Vol. 3, pp. 395-400, 1982.

40. Folayan, C.O., and Whitelaw, J.H., 'Impingement cooling and its application to combustor design', Joint Gas Turbine Congress, Tokyo, 1977.

41. Behbahani, A.I., and Goldstein, R.J., 'Local heat transfer to staggered arrays of impinging circular air jets', J. Eng. Power, Vol. 105, pp. 354-360, 1983.

42. Obot, N.T., 'Effect of suction on impingement heat transfer', Proc. 7th Int. Heat Transf. Conference, Vol. 3, pp. 389-394, 1982.

43. Schlichting, H., 'Boundary Layer Theory' (Trans. by J. Kestin), 7th edition, McGraw-Hill Book Company, New York, 1979.

44. Mkpadi, M.C., 'Full Coverage Effusion Cooling of Gas Turbine Combustion Chamber', Ph.D. Thesis, Dept. of Fuel and Energy, Univ. of Leeds, 1982.

45. Hollworth, B.R., and Dagan, L., 'Arrays of impinging jets with spent fluid removal through vent holes on the target surface. Part 1: Average heat transfer', J. Eng. Power, Vol. 102, pp. 994-999, Oct. 1980.

46. Hollworth, B.R., Lehmann, G., and Rosiczkowski, J., 'Arrays of impinging jets with spent fluid removal through vent holes on the target surface. Part 2: Local heat transfer', J. Eng. Power, Vol. 105, pp. 393-402, April 1983.

47. Hollworth, B.R., and Berry, R.D., 'Heat transfer from arrays of impinging jets with large jet-to-jet spacing', ASME - J. Heat Transfer, Vol. 100, pp. 352-357, 1978.

48. Andrews, G.E., et al, 'Combustion chamber wall cooling design considerations for low pressure drop drilled plates and for combined impingement and drilled plate systems', Rept. No. GEA/HT/3, Dept. Fuel & Energy, Univ. of Leeds, 1980.

49. Andrews, G.E., Asere, A.A., and Mkpadi, M.C., 'Gas turbine combustor wall cooling', Rept. No. GEA/HT/16, Dept. Fuel & Energy, Univ. of Leeds, 1982.

50. Andrews, G.E., Asere, A.A., and Mkpadi, M.C., 'Gas turbine wall cooling VIII', Rept. No. GEA/HT/17, Dept. Fuel & Energy, Univ. of Leeds, 7.2.83.

51. Andrews, G.E., and Asere, A.A., 'Gas turbine combustor wall cooling IX', Rept. No. GEA/HT/18, Dept. Fuel & Energy, Univ. of Leeds, 15.4.83.

52. Andrews, G.E., and Asere, A.A., 'Gas turbine wall cooling X. Cooling effectiveness and boundary layer temperature profile summary report for three test plate geometries', Rept. No. GEA/HT/19, Dept. Fuel & Energy, Univ. of Leeds, 27.9.83.

53. Andrews, G.E., and Asere, A.A., 'Gas turbine combustor wall cooling XI', Rept. No. GEA/HT/20, Dept. Fuel & Energy, Univ. of Leeds, 2.3.84.

54. Andrews, G.E., and Asere, A.A., 'Gas turbine combustor wall cooling XII. Cooling effectiveness and boundary layer temperature profile measurements for low and high temperature impingement/effusion geometries', Rept. No. GEA/HT/21, Dept. Fuel & Energy, Univ. of Leeds, 7.2.85.

55. Gauntner, J.W., Livingood, J.N.B., and Hrycak, P., 'Survey of literature on flow characteristics of a single turbulent jet impinging on a flat plate', NASA TN D-5652, Feb. 1970.

56. Sparrow, E.M., and Gurdal, U., 'Heat transfer at an upstream-facing surface washed by fluid en route to an aperture in the surface', Int. J. Heat Mass Transfer, Vol. 24, No. 5, pp. 851-857, 1981.

57. Sparrow, E.M., and Ortiz, M.C., 'Heat transfer coefficients for the upstream face of a perforated plate positioned normal to an oncoming flow', Int. J. Heat Mass Transf., Vol. 25, No. 1, pp. 127-135, 1982.

58. Andrews, G.E., Asere, A.A., Hussain, C.I., and Mkpadi, M.C., 'Full coverage impingement heat transfer: The variation in pitch to diameter ratio at a constant gap', AGARD-CPP-390, Heat Transfer and Cooling in Gas Turbines, pp. 26-1-12, 1985.

59. Lefebvre, A.H., and Herbert, M.V., 'Heat transfer processes in gas turbine combustion chambers', Proc. Inst. Mech. Eng., Vol. 174, No. 12, pp. 463-478, 1960.

60. Winter, E.F., 'Heat transfer conditions at the flame tube walls of an aero gas turbine combustion chamber', Fuel - A Quart. J. Fuel Science, Vol. 34, 1955.

61. Mills, A.F., 'Experimental investigation of turbulent heat transfer in the entrance region of a circular conduit', J. Mech. Eng. Science, Vol. 4, No. 1, pp. 63-77, 1962.

62. Siegel, R., and Howell, J.R., 'Thermal Radiation Heat Transfer', 2nd edition, Hemisphere Publ. Corp., Washington, 1981.

63. Gray, W.A., and Müller, R., 'Engineering Calculations in Radiative Heat Transfer', Pergamon Press, 1974.

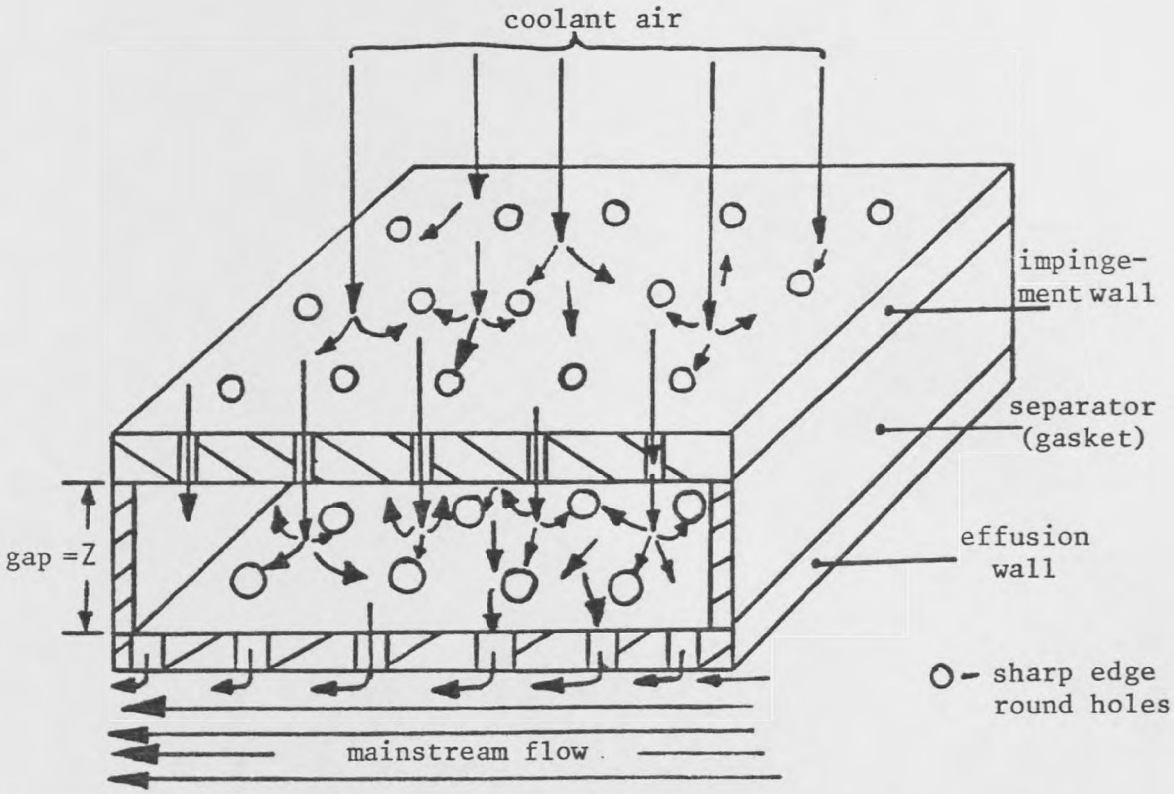

Fig. 7.1: Full coverage discrete hole impingement/effusion cooling system

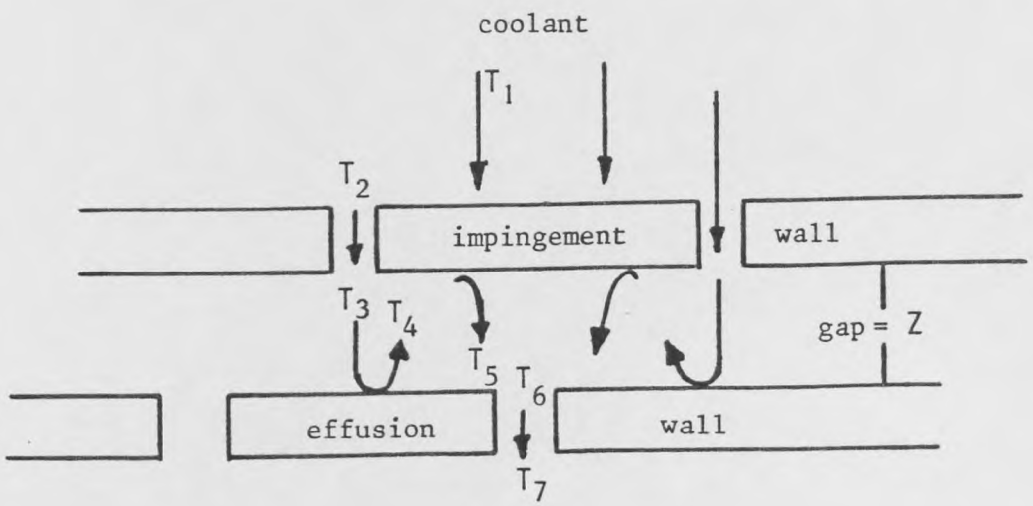

Fig. 7.2: Temperature history of the coolant in impingement/effusion cooling system

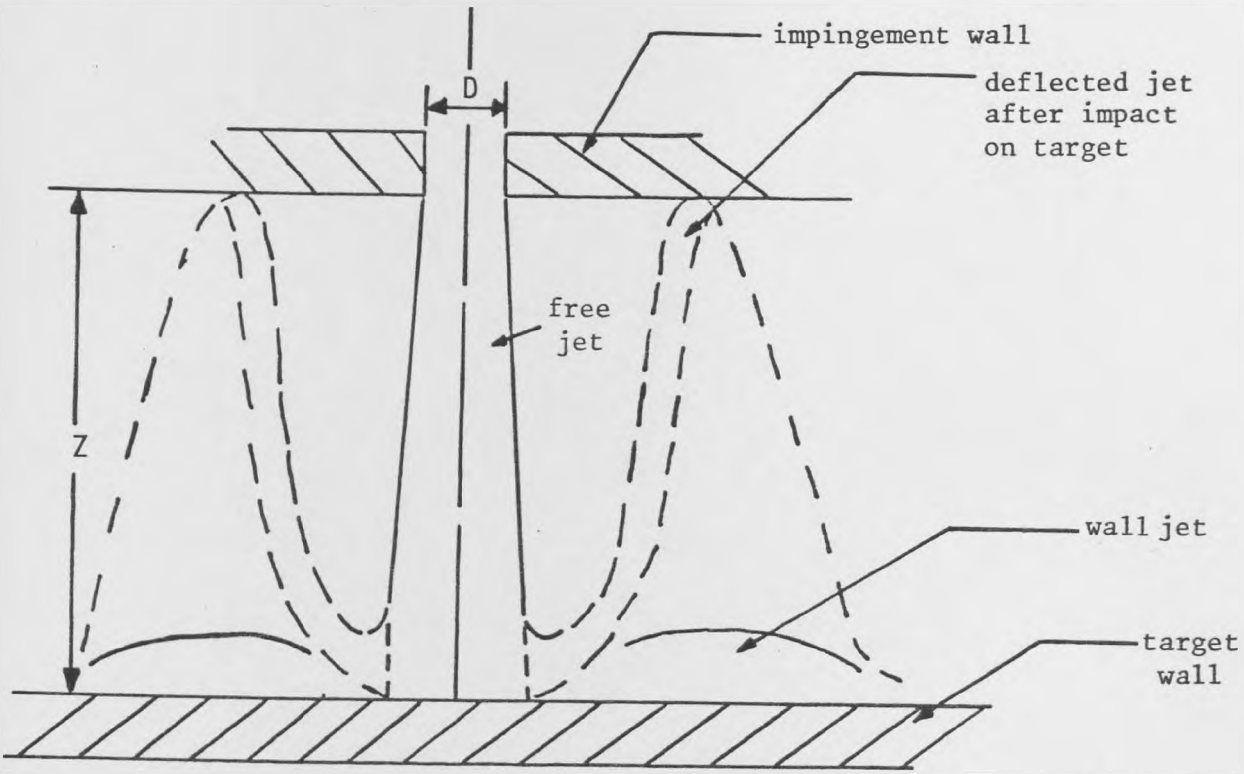

Fig. 7.3: Impinging jet deflection back to the impingement wall after impact on the target wall

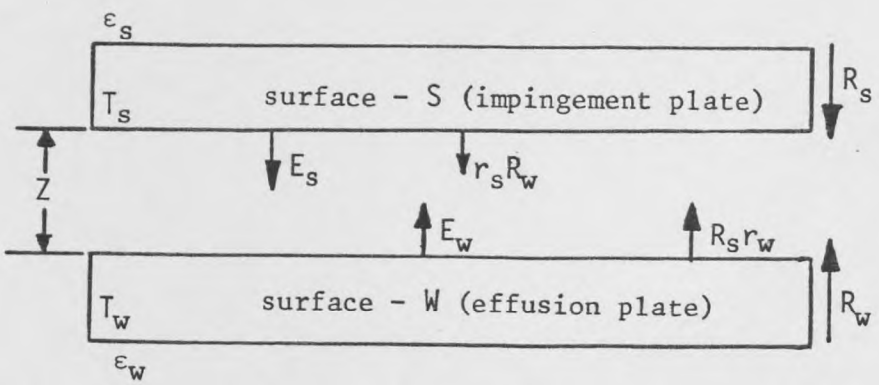

Fig. 7.4: Model of radiative heat transfer between two parallel walls

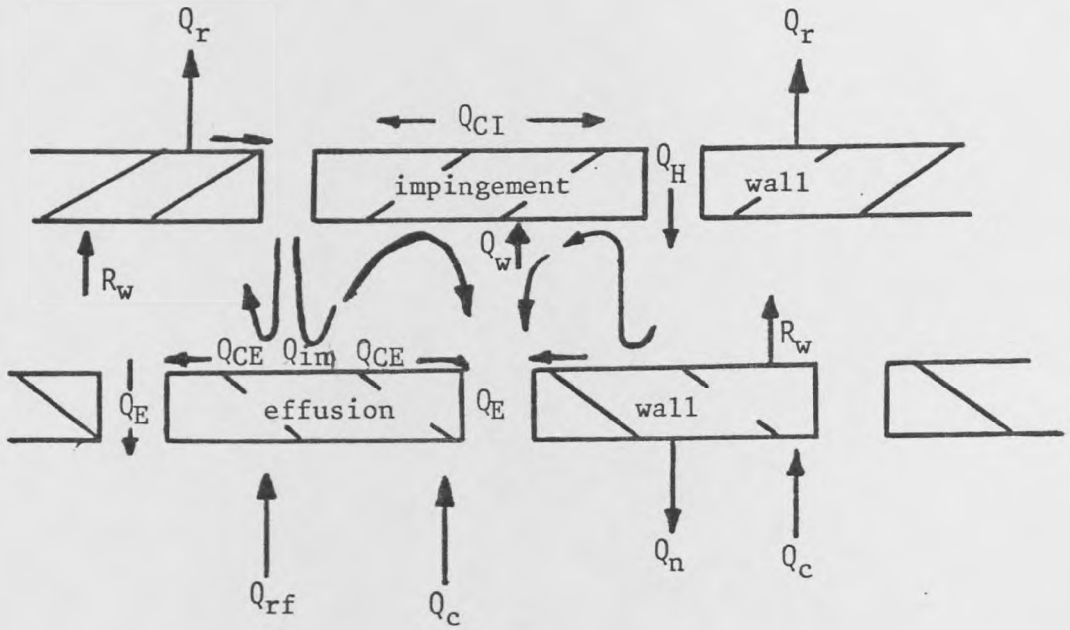

Q_r = Radiative heat transfer at the back of impingement wall

Q_{CI} = Convective heat transfer at the back of impingement wall

Q_H = Convective heat transfer in the holes of the impingement wall

Q_w = Convective heat transfer to the surface of the impingement wall by jets deflected by the effusion wall

R_w = Radiative heat transfer to the surface of the impingement wall and lost from the back of the effusion wall

Q_{im} = Impinging heat transfer from the effusion wall

Q_{CE} = Effusion back-side convection

Q_E = Effusion holes convection

Q_n = Net radiative exchange between effusion wall and duct walls

Q_{rf} = Radiation from hot gases to the effusion wall

Q_c = Convection from hot gases to the effusion wall

Fig. 7.5: Heat transfer processes of impingement/effusion combined cooling system

7.10 APPENDIX

TABLE 7.A1

UNIVERSITY OF LEEDS
DEPARTMENT OF FUEL AND ENERGY
Gas Turbine Combustor Wall Cooling Programme

30- 1 IMPINGEMENT PLATE TEST -(Low_Temp._Work)

PLATE COMBINATION:-IMP.:NO. HOLES: 25.0 HOLES M.DIA.:2.8764009mm PITCH: 30.4799957mm
()P/P: 3.0000% THICK.: 6.350mm FORMAT: offset(drilled) MAT.:nimonic-75
EFFUSION:NO. HOLES:100.0 HOLES M.DIA.:3.2696896mm M. PITCH: 15.2399998mm
()P/P: 0.1000% THICK.: 6.350mm FORMAT: inline(drilled) MAT.: nimonic-75
SEPARATION(Z): 8.0mm Z/D: 2.78125 X/D: 10.597 EXP. DATE:18/ 6/84
ATMOS. PRESS.: 763.80mmHg AT TEMPERATURE: 20.5 Deg.C

FC-COOLANT FLOWRATE AS MEASURED AT ROTAMETER-l/min;PPD-Pa=PLENUM STATIC Gauge PRESS.
TC-K=COOLANT TEMP. AT ROTAMETER;TG(l,c,t)=PLATE LEAD.EDGE,CENTRE & TRAIL.EDGE M.STREAM FLOW TEMP.
CM-Kg/s=COOLANT MASS FLOWRATE, G-Kg/(sm2)=COOLANT MASS FLOW/TEST PLATE AREA
G!=G/(PRESSURE)-Kg/(m2sec.Bar);VI,V&Vm-m/s-ARE VEL. OF COOL. THRO. IMP.&EFF. PL. HOLES, & M.STREAM FLOW
DR & nDr=REAL & NUMINAL DENSITY RATIOS(D.Cool./D.Mainst.);BLR = BLOWING RATE RATIO
REIMP,RE-1&2=REYNOLDS NO. FOR COOLANT THRO. IMP.&EFF. PLATE S & MAINSTREAM FLOW AT TEST PLANE
HIMP,H-1&2=MACH NUMBERS OF BOTH COOLANT & MAINSTREAM AS FOR REYNOLD NO. ABOVE
%Pr & Vrt =(%Press. Loss Across Plate/(Upstream (Plenum) Absolute Press.) & V/Vm

FC-l/min.	PPD-Pa	TC-K	TGl-K	TGc-K	TGt-K	CM-Kg/s	G	G!	VI-m/s	V-m/s	Vm-e/s
1200.0	39098.0	292.66	780.85	781.35	768.56	0.04138	1.781	1.747	152.20	29.45	36.50
1000.0	20666.7	295.36	781.33	781.79	769.00	0.02969	1.278	1.253	127.21	24.61	36.62
800.0	9715.7	296.16	781.28	781.70	768.91	0.02053	0.884	0.867	97.07	18.78	36.75
600.0	4578.4	296.26	780.08	782.78	772.31	0.01384	0.596	0.585	68.93	13.34	36.78
400.0	1941.2	296.46	779.82	782.59	772.10	0.00859	0.370	0.363	44.33	8.58	36.38
350.0	1431.4	296.56	779.49	782.53	771.85	0.00741	0.319	0.313	38.60	7.47	36.40
300.0	1156.9	296.56	780.25	781.97	773.82	0.00629	0.271	0.266	33.00	6.39	36.60
250.0	794.1	296.66	779.61	781.46	773.30	0.00519	0.223	0.219	27.46	5.31	36.49
200.0	500.0	296.46	778.86	780.76	772.60	0.00411	0.177	0.174	21.93	4.24	36.56
150.0	323.5	296.16	781.52	784.66	776.47	0.00306	0.132	0.129	16.52	3.20	36.55
100.0	176.5	295.96	781.38	784.53	776.34	0.00203	0.087	0.086	11.11	2.15	36.56
50.0	88.2	296.36	781.20	784.28	776.09	0.00101	0.044	0.043	5.65	1.09	36.51
25.0	68.6	296.46	781.01	784.07	775.89	0.00051	0.022	0.021	2.91	0.56	36.70
0.0	39.2	296.36	780.95	782.80	775.79	0.00000	0.000	0.000	0.00	0.00	36.63

DR	nDr	BLR	REIMP	HIMP	Re1	H1	Re2	H2	%Pr	Vrt
7.69	2.67	2.97	0.40E+05	0.44E+00	0.89E+04	0.86E-01	0.46E+05	0.63E-01	27.6369	0.8066
5.70	2.65	2.12	0.29E+05	0.37E+00	0.63E+04	0.71E-01	0.46E+05	0.63E-01	16.7658	0.6721
4.26	2.64	1.46	0.20E+05	0.28E+00	0.43E+04	0.54E-01	0.47E+05	0.63E-01	8.6038	0.5111
3.45	2.64	0.99	0.13E+05	0.20E+00	0.29E+04	0.38E-01	0.46E+05	0.64E-01	4.2194	0.3626
2.99	2.64	0.62	0.81E+04	0.13E+00	0.18E+04	0.25E-01	0.46E+05	0.63E-01	1.8043	0.2358
2.90	2.64	0.53	0.70E+04	0.11E+00	0.15E+04	0.21E-01	0.46E+05	0.63E-01	1.3101	0.2052
2.84	2.64	0.45	0.59E+04	0.94E-01	0.13E+04	0.18E-01	0.46E+05	0.63E-01	1.0661	0.1744
2.79	2.63	0.37	0.49E+04	0.78E-01	0.11E+04	0.15E-01	0.46E+05	0.63E-01	0.7164	0.1456
2.73	2.63	0.29	0.38E+04	0.62E-01	0.84E+03	0.12E-01	0.46E+05	0.63E-01	0.4311	0.1160
2.71	2.65	0.22	0.28E+04	0.47E-01	0.62E+03	0.90E-02	0.46E+05	0.63E-01	0.2591	0.0875
2.68	2.65	0.15	0.19E+04	0.31E-01	0.41E+03	0.60E-02	0.46E+05	0.63E-01	0.1249	0.0588
2.67	2.65	0.07	0.92E+03	0.16E-01	0.20E+03	0.30E-02	0.46E+05	0.63E-01	0.0385	0.0300
2.67	2.64	0.04	0.45E+03	0.80E-02	0.98E+02	0.15E-02	0.46E+05	0.63E-01	0.0192	0.0153
2.64	2.64	0.00	0.00E+00	0.00E+00	0.00E+00	0.00E+00	0.46E+05	0.63E-01	0.0289	0.0000

THE PARAMETERS BLOW ARE BASED ON COOLANT GAP-Z TEMP.

TCg=COOLANT TEMP. BETWEEN PLATE GAP-Z; V=VELOCITY OF COOLANT THROUGH EFF. PLATE HOLES
REg & Hg = REYNOIDS & MACH NO. OF COOLANT THRO. EFFUSION PLATE HOLES AT PLANE OF TEST.
Dr=DENSITY RATIO OF COOL. AND MAIN STREAM. Vrt=VELOCITY RATIO OF COOLANT AND MAIN STREAM.

TCg-K	V-m/s	REg	Hg	Dr	Vrt
310.5	31.16	0.85E+04	0.88E-01	3.48	0.8537
318.7	26.40	0.60E+04	0.74E-01	2.95	0.7209
326.7	20.56	0.40E+04	0.57E-01	2.62	0.5594
338.4	15.04	0.26E+04	0.41E-01	2.42	0.4090
352.7	9.98	0.16E+04	0.27E-01	2.26	0.2744
361.5	8.86	0.13E+04	0.23E-01	2.19	0.2435
366.7	7.65	0.11E+04	0.20E-01	2.16	0.2091
377.6	6.52	0.91E+03	0.17E-01	2.08	0.1788
391.4	5.37	0.70E+03	0.14E-01	2.00	0.1469
411.4	4.22	0.51E+03	0.10E-01	1.91	0.1154
436.3	2.97	0.32E+03	0.71E-02	1.80	0.0813
480.2	1.63	0.15E+03	0.37E-02	1.63	0.0447
520.2	0.88	0.71E+02	0.19E-02	1.51	0.0241
566.2	0.00	0.00E+00	0.00E+00	1.38	0.0000

WALL TEMPERATURE & COOLING EFFECTIVENESS

TPH(1 to 5)-K=TEST PLATE FLAMESIDE TEMP. AT INCREASING DISTANCE FROM LEAD. EDGE;
Tc=COOLANT TEMP.; E=COOLING EFFECTIVENESS AT INCREASING DIST. FROM PLATE LEADING EDGE.

		25.4mm		50.8mm		76.2mm		101.6mm		127mm	
Tc-K	G!	TPH1	E	TPH2	E	TPH3	E	TPH4	E	TPH5	E
292.7	1.747	395.7	0.789	379.4	0.823	366.4	0.849	357.4	0.868	352.2	0.878
295.4	1.253	407.1	0.770	388.7	0.808	376.8	0.833	369.7	0.847	366.3	0.854
296.2	0.867	420.0	0.745	399.0	0.788	387.5	0.812	381.4	0.825	379.9	0.828
296.3	0.585	441.8	0.701	417.2	0.752	405.7	0.775	398.5	0.790	398.6	0.790
296.5	0.363	459.5	0.665	436.3	0.712	423.7	0.738	417.5	0.751	418.0	0.750
296.6	0.313	474.2	0.634	448.6	0.687	436.6	0.712	428.2	0.729	429.5	0.726
296.6	0.266	478.2	0.626	452.9	0.678	441.9	0.701	435.0	0.715	435.9	0.713
296.7	0.219	492.2	0.597	469.2	0.644	456.1	0.671	448.5	0.687	449.3	0.685
296.5	0.174	509.2	0.561	487.2	0.606	474.2	0.633	465.6	0.651	466.0	0.650
296.2	0.129	532.2	0.517	511.2	0.560	498.2	0.586	490.2	0.603	489.2	0.605
296.0	0.086	558.2	0.463	540.2	0.500	528.2	0.525	520.2	0.541	519.2	0.543
296.4	0.043	598.2	0.381	586.2	0.406	576.2	0.427	569.2	0.441	566.2	0.447
296.5	0.021	619.2	0.338	612.2	0.353	605.2	0.367	599.2	0.379	594.2	0.389
296.4	0.000	636.2	0.301	633.2	0.308	630.2	0.314	626.2	0.322	620.2	0.334

T(1 TO 4) ARE JET POINT THERMOCOUPLE TEMPERATURES OF EFFUSION PLATE AS PER LOCATION;
Tc=COOLANT TEMP.; E = COOLING EFFECTIVENESS AT THE THERMOCOUPLE LOCATIONS

		107.5mm BY 106.9mm LEAD. EDGE; WALL		122mm BY 106.5mm LEAD. EDGE; WALL		122mm BY 99mm LEAD. EDGE; WALL		122mm BY 91.5mm LEAD. EDGE; WALL	
Tc-K	G	T1-K	E	T2-K	E	T3-K	E	T4-K	E
292.7	1.781	352.9	0.877	342.0	0.899	339.5	0.904	338.1	0.907
295.4	1.278	365.2	0.857	355.5	0.876	352.6	0.882	350.7	0.886
296.2	0.884	377.1	0.833	368.8	0.850	365.5	0.857	363.5	0.861
296.3	0.596	393.5	0.800	386.8	0.814	383.8	0.820	381.7	0.824
296.5	0.370	411.1	0.764	405.6	0.776	403.4	0.780	402.0	0.783
296.6	0.319	422.0	0.742	416.3	0.754	414.1	0.758	412.7	0.761
296.6	0.271	428.0	0.729	423.0	0.740	421.1	0.744	420.0	0.746
296.7	0.223	441.4	0.702	436.4	0.712	434.8	0.715	433.8	0.717
296.5	0.177	458.3	0.666	453.4	0.676	452.3	0.678	451.4	0.680
296.2	0.132	482.2	0.619	477.2	0.629	476.2	0.632	475.2	0.634
296.0	0.087	511.2	0.560	506.2	0.570	506.2	0.570	506.2	0.570
296.4	0.044	539.2	0.461	553.2	0.474	555.2	0.470	556.2	0.468
296.5	0.022	588.2	0.402	582.2	0.414	586.2	0.406	588.2	0.402
296.4	0.000	615.2	0.345	610.2	0.355	615.2	0.345	618.2	0.338

TABLE 7.A2

T(1 TO 4) ARE STAGGERED THERMOCOUPLE TEMPERATURES OF EFF. PLATE AS PER LOCATION SHOWN; Tc=COOLANT TEMP.; E = COOLING EFFECTIVENESS AT THE THERMOCOUPLE LOCATIONS

		16mm BY 15mm LEAD. EDGE; WALL		31mm BY 107.9mm LEAD. EDGE; WALL		108mm BY 136.4mm LEAD. EDGE; WALL		137mm BY 31.5mm LEAD. EDGE; WALL	
Tc-K	G	T1-K	E	T2-K	E	T3-K	E	T4-K	E
292.7	1.781	366.0	0.850	372.7	0.836	352.7	0.877	0.0	0.000
295.4	1.278	387.1	0.811	384.8	0.816	365.7	0.855	0.0	0.000
296.2	0.884	404.5	0.777	397.6	0.791	377.9	0.832	0.0	0.000
296.3	0.596	426.5	0.732	417.4	0.751	393.8	0.800	0.0	0.000
296.5	0.370	446.6	0.691	438.6	0.708	410.1	0.766	0.0	0.000
296.6	0.319	457.5	0.669	449.3	0.686	419.0	0.748	0.0	0.000
296.6	0.271	463.8	0.656	456.6	0.670	425.2	0.735	0.0	0.000
296.7	0.223	477.2	0.628	471.2	0.640	437.0	0.711	0.0	0.000
296.5	0.177	493.2	0.594	489.2	0.602	451.8	0.679	0.0	0.000
296.2	0.132	513.2	0.556	513.2	0.556	472.2	0.640	0.0	0.000
296.0	0.087	532.2	0.517	538.2	0.504	495.2	0.592	0.0	0.000
296.4	0.044	564.2	0.451	579.2	0.420	532.2	0.517	0.0	0.000
296.5	0.022	582.2	0.414	603.2	0.371	556.2	0.467	0.0	0.000
296.4	0.000	595.2	0.386	621.2	0.332	577.2	0.423	0.0	0.000

ADIABATIC COOLING EFFECTIVENESS.

TGc=COMBUSTOR MAINSTREAM TEMP.;G!=G/(PRESSURE)-Kg/(m2sec.bar);Ta(l,c,t)=ADIABATIC WALL TEMP. AT LEADING EDGE, CENTRAL, & TRAILING EDGE ; E=ADIABATIC COOLING EFFECTIVENESS For High Temp. Work Tac=central thermocouple- Only Feature

TGc-K	G!	Tal-K	E	Tac-K	E	Tat-K	E
781.4	1.747	651.2	0.266	543.2	0.487	458.3	0.661
781.8	1.253	651.2	0.269	557.2	0.462	482.2	0.616
781.7	0.867	659.2	0.252	578.2	0.419	512.2	0.555
782.8	0.585	660.2	0.252	592.2	0.392	530.2	0.519
782.6	0.363	669.2	0.233	619.2	0.336	559.2	0.460
782.3	0.313	669.2	0.233	626.2	0.321	569.2	0.439
782.0	0.266	676.2	0.218	634.2	0.305	580.2	0.416
781.5	0.219	675.2	0.219	646.2	0.279	596.2	0.382
780.8	0.174	681.2	0.206	659.2	0.251	615.2	0.342
784.7	0.129	686.2	0.202	669.2	0.236	647.2	0.281
784.5	0.086	704.2	0.164	685.2	0.203	672.2	0.230
784.3	0.043	706.2	0.160	702.2	0.168	692.2	0.189
784.1	0.021	710.2	0.152	708.2	0.156	703.2	0.166
782.8	0.000	715.2	0.139	715.2	0.139	711.2	0.147

PREDICTED TEMPERATURE AND COOLING EFFECTIVENESS FOR CYLINDRICAL COMBUSTOR

T(1 TO 5)p-K = PREDICTED TEST WALL TEMPERATURE -BASED ON WALL THERMAL STATIONS.
F = CORRESPONDING WALL COOLING EFFECTIVENESS; G!=COOLANT MASS FLOW(Kg/(s.m2.bar))

	25.4mm		50.8mm		76.2mm		101.6mm		127mm	
G!	T1p-K	E	T2p-K	E	T3p-K	E	T4p-K	E	T5p-K	E
1.747	392.4	0.796	374.6	0.832	359.9	0.862	349.5	0.884	343.3	0.896
1.253	404.6	0.775	384.5	0.817	371.1	0.844	362.9	0.861	358.9	0.869
0.867	418.0	0.749	394.7	0.797	381.6	0.824	374.5	0.839	372.7	0.842
0.585	441.3	0.702	413.9	0.758	400.7	0.785	392.2	0.803	392.4	0.802
0.363	460.2	0.663	433.5	0.718	418.6	0.749	411.1	0.764	411.7	0.763
0.313	476.2	0.630	446.8	0.691	432.6	0.720	422.4	0.741	424.0	0.738
0.266	480.3	0.622	450.7	0.683	437.3	0.710	428.7	0.728	429.9	0.725
0.219	495.1	0.591	467.8	0.647	451.7	0.680	442.1	0.700	443.2	0.698
0.174	513.7	0.552	487.3	0.606	471.0	0.640	460.0	0.662	460.5	0.661
0.129	539.5	0.502	513.9	0.554	497.4	0.588	486.9	0.609	485.6	0.612
0.086	572.8	0.433	551.4	0.477	536.4	0.508	526.1	0.529	524.8	0.532
0.043	625.9	0.325	612.7	0.352	601.2	0.375	593.1	0.392	589.5	0.399
0.021	657.6	0.259	650.6	0.274	643.4	0.288	637.2	0.301	631.9	0.312

PREDICTED IMPINGING-GAP COOLANT TEMPERATURE

T(1-5)K = OUTLET COOLANT TEMPERATURE FROM IMPINGING WALL; TKK IS THE MEAN; T6P-K=MEASURED.
T(1-5)R & TP(1-5) ARE GAP TEMPERATURE RATIOS FROM PREDICTIONAND MEASURED GAP TEMPERATURE
T(1-5)-K = IMPINGING PLATE TEMPERATURE AS MEASURED.

T1K	T2K	T3K	T4K	T5K	TK	T6P	T1I	T2I	T3I	T4I	T5I
348.8	336.3	328.2	322.8	317.7	330.7	310.5	315.3	308.7	305.6	303.8	300.7
362.7	347.2	336.0	334.2	330.0	342.6	318.7	323.6	315.2	311.9	310.1	307.3
379.3	360.1	350.9	346.3	343.0	355.9	326.7	332.1	321.9	317.8	316.1	313.3
406.4	382.0	370.7	365.0	362.4	377.3	338.4	345.3	332.4	326.7	324.7	321.8
434.2	408.1	394.2	388.1	386.2	402.2	352.7	358.9	345.0	338.1	335.6	333.1
453.1	424.2	409.4	401.3	400.1	417.6	361.5	367.6	352.8	344.8	341.8	339.4
463.3	433.5	418.7	411.2	409.9	427.3	366.7	373.7	358.7	350.2	347.2	344.9
483.5	454.5	437.2	428.5	427.2	446.2	377.6	382.3	367.3	358.3	354.8	352.5
511.6	481.9	463.3	453.0	451.6	472.3	391.4	395.1	379.6	369.6	365.7	363.6
550.1	520.4	500.7	489.9	487.3	509.7	411.4	411.0	395.9	385.5	381.2	379.0
599.7	573.0	553.9	542.9	540.8	562.1	436.3	427.6	413.8	403.5	399.5	398.0
685.3	666.8	650.9	641.0	636.7	656.2	480.2	451.1	439.8	430.3	426.4	424.8
742.8	733.0	723.2	715.3	708.6	724.6	520.2	472.2	463.0	455.0	451.8	449.3

G	T1R	T2R	T3R	T4R	T5R	TRM	TP1	TP2	TP3	TP4	TP5
1.781	0.4344	0.4186	0.4163	0.4173	0.4001	0.7064	-0.0422	0.0273	0.0901	0.1466	0.2301
1.278	0.4832	0.4619	0.4583	0.4571	0.4413	0.6851	-0.0604	0.0505	0.1149	0.1629	0.2208
0.884	0.5494	0.5252	0.5186	0.5183	0.5001	0.7174	-0.0628	0.0659	0.1395	0.1815	0.2254
0.596	0.6364	0.6087	0.5949	0.5968	0.5754	0.7803	-0.0718	0.0736	0.1581	0.2028	0.2351
0.370	0.7439	0.7125	0.6969	0.6952	0.6753	0.8781	-0.0612	0.0869	0.1812	0.2264	0.2491
0.319	0.7876	0.7595	0.7367	0.7382	0.7172	0.9247	-0.0561	0.0925	0.1902	0.2444	0.2611
0.271	0.8404	0.8140	0.7860	0.7851	0.7647	0.9695	-0.0657	0.0870	0.1893	0.2390	0.2563
0.223	0.8972	0.8671	0.8446	0.8437	0.8236	1.0329	-0.0417	0.1024	0.2065	0.2610	0.2767
0.177	0.9824	0.9502	0.9235	0.9253	0.9078	1.1209	-0.0312	0.1096	0.2148	0.2724	0.2867
0.132	1.0828	1.0546	1.0289	1.0280	1.0155	1.2254	0.0031	0.1313	0.2313	0.2855	0.3037
0.087	1.1950	1.1572	1.1316	1.1322	1.1259	1.2934	0.0599	0.1635	0.2467	0.2905	0.3019
0.044	1.3399	1.3131	1.2907	1.2875	1.2866	1.4046	0.1665	0.2336	0.2918	0.3227	0.3363
0.022	1.4594	1.4390	1.4250	1.4210	1.4199	1.5074	0.2588	0.3048	0.3459	0.3688	0.3882

CONVECTION TO THE SURFACE OF IMPINGING PLATE FROM JET BOUNCE-BACK THEORY.

Q(1 TO 5)C= CONVECTION BASED ON THERMAL STATIONS IN WATTS; H(1-5)E = COEFFICIENT OF CONVECTIVE HEAT TRANSFER IN W/M.K

H1E	Q1C	H2E	Q2C	H3E	Q3C	H4E	Q4C	H5E	Q5C
117.2	87.9	95.7	57.9	88.3	44.7	87.3	37.3	58.4	22.3
93.1	81.7	72.2	51.8	67.4	41.0	64.9	35.1	47.5	24.2
73.2	77.3	58.9	50.4	54.2	40.1	53.3	36.1	41.1	27.4
54.5	74.5	45.7	50.7	40.5	39.9	41.0	37.0	32.6	29.7
33.8	57.0	28.9	40.8	26.0	32.7	25.7	30.2	21.3	25.4
27.6	52.9	24.8	39.7	21.5	31.1	21.9	29.2	18.2	24.7
23.9	47.9	22.2	37.2	18.9	29.0	19.0	27.2	16.1	23.4
17.0	38.6	15.8	30.8	14.2	25.0	14.4	23.8	12.1	20.3
10.7	28.0	10.2	23.5	9.1	19.1	9.8	19.1	8.3	16.4
2.7	8.5	3.3	9.1	3.0	7.8	3.6	8.7	3.0	7.2

TABLE 7.A3

IMPINGING WALL TEMPERATURE PREDICTION

T(1 TO 5)E=EXPERIMENTALLY MEASURED TEMPERATURE, T(1-5)P = PREDICTED

T1E	T1P	T2E	T2P	T3E	T3P	T4E	T4P	T5E	T5P
315.3	297.2	308.7	303.2	305.6	308.1	303.8	311.7	300.7	313.7
325.6	303.5	315.2	310.6	311.9	315.5	310.1	318.5	307.3	319.8
332.1	308.7	321.9	317.7	317.8	322.8	316.1	325.6	313.3	326.2
345.3	316.2	332.4	327.7	325.7	333.3	324.7	337.0	321.8	336.7
358.9	326.8	345.0	339.0	338.1	346.0	335.6	349.6	333.1	349.0
367.6	332.0	352.8	346.2	344.8	352.9	341.8	358.1	339.4	356.9
373.7	337.7	358.7	352.4	350.2	358.8	347.2	363.3	344.9	362.3
382.3	344.9	367.5	359.0	358.3	367.2	354.8	372.4	352.5	371.4
395.1	355.8	379.6	369.9	369.6	378.5	365.7	385.0	363.6	384.2
411.0	370.5	395.9	385.1	385.5	394.5	381.2	400.9	379.0	401.3
427.6	389.9	413.8	402.8	403.5	411.6	399.5	418.6	398.0	419.2
451.1	421.9	439.8	429.1	430.3	435.5	426.4	441.5	424.8	444.2
472.2	453.9	463.0	454.5	455.0	456.4	451.8	461.1	449.3	465.2

CYLINDRICAL COMBUSTOR IMPINGING HEAT TRANSFER FROM PREDICTION

THIS HEAT TRANSFER IS BASED ON BOTH HOLLWORTH & ANDREWS ET AL: Ho-W/M*2.K & Q(1-5)i-WATT =HEAT TRANSFER COEFFICIENT & IMPINGING HEAT TRANSFER ALL BASED ON HOLLWORTH. Ha-W/M*2.K & Q(1-5)a-WATT =IMPINGING HEAT TRANSFER ALL BASED ON ANDREWS ET AL. (1-5) =THERMAL STATIONS ON EFFUSION PLATE: Ns & Na ARE NUSSELT NUMBERS OF THE CORRELATIONS

Ho	Q1i	Q2i	Q3i	Q4i	Q5i	Ns#
646.2	1393.1	1147.2	941.1	792.7	708.6	68.7
502.7	1168.9	955.2	809.5	720.0	679.7	52.2
381.2	974.3	789.5	683.0	624.5	613.5	38.7
285.6	850.5	690.2	612.5	560.8	565.2	28.1
200.7	651.2	545.3	485.0	453.7	459.0	19.1
181.4	637.5	532.1	481.8	443.2	452.0	16.9
160.6	566.9	473.7	433.2	405.1	411.3	14.8
140.7	528.5	455.2	412.0	384.7	389.9	12.6
119.9	482.1	423.3	387.6	361.0	364.0	10.4
98.2	429.8	384.4	355.5	335.5	334.2	8.2
73.6	353.0	326.4	308.2	293.8	292.6	5.9
45.0	240.3	232.8	226.1	219.9	217.1	3.3
27.1	139.6	139.1	138.1	135.6	133.4	1.9

Ha	Q1a	Q2a	Q3a	Q4a	Q5a
378.8	816.6	672.5	551.6	464.7	415.4
302.8	704.2	575.4	487.7	433.7	409.5
236.6	604.7	490.0	423.9	387.6	380.7
183.0	545.0	442.3	392.5	359.4	362.2
133.7	433.8	363.2	323.1	302.2	305.8
122.3	429.9	358.8	324.9	298.8	304.8
109.7	387.4	323.7	296.0	276.8	281.1
97.6	366.9	316.0	286.0	267.0	270.7
84.8	341.0	299.5	274.2	255.4	257.6
71.2	311.4	278.5	257.6	243.2	242.2
55.2	264.6	244.6	231.0	220.2	219.3
35.7	190.6	184.7	179.4	174.4	172.2
22.7	117.3	116.9	116.0	113.9	112.1

CYLINDRICAL COMBUSTOR EFFUSION BACK WALL CONVECTIVE HEAT TRANSFER - IMPINGING-SYSTEM.

Q(1-5)E-WATT =CONVECTIVE HEAT TRANSFER - BASED ON WALL THERMOCOUPLE STATIONS, WHILE QE IS THE MEAN AT THE BACK OF TEST WALL; QHCE-W/M*2.K = CONVECTIVE HEAT TRANSFER COEFFICIENT; BNE=NUSSELT NUMBER

Q1E	Q2E	Q3E	Q4E	Q5E	QHCE	QE	BNE
148.4	122.2	100.3	84.5	75.5	105.5	106.2	9.38
131.7	107.7	91.2	81.1	76.6	90.9	97.7	7.83
115.2	93.4	80.8	73.9	72.6	76.8	87.2	6.52
103.6	84.0	74.6	68.3	68.8	64.2	79.9	5.26
80.9	67.7	60.2	56.4	57.0	51.8	64.5	3.97
78.0	65.1	59.0	54.2	55.3	48.6	62.3	3.61
69.1	57.7	52.8	49.4	50.1	45.1	55.8	3.27
62.3	53.7	48.6	45.4	46.0	41.5	51.2	2.87
53.5	47.0	43.1	40.1	40.4	37.5	44.8	2.41
42.4	37.9	35.1	33.1	33.0	33.0	36.3	1.87
27.1	25.0	23.6	22.5	22.4	27.6	24.1	1.18
3.4	3.3	3.2	3.1	3.0	20.4	3.2	0.37
12.1	12.1	12.0	11.8	11.6	15.0	11.9	0.04

HOLES INLET TEMPERATURE PREDICTION

T(1-5)e = PREDICTED COOLANT INLET TEMPERATURE INTO EFFUSION HOLES; =Tin= MEAN &, pTz = PREDICTED COOLANT TEMPERATURE IN THE GAP.

T1e-K	T2e-K	T3e-K	T4e-K	T5e-K	=Tin-K	pTz-K
333.1	325.8	319.9	315.7	313.1	321.5	323.9
344.3	335.2	329.3	325.7	323.8	331.7	333.9
356.5	344.9	338.5	335.1	334.0	341.8	344.2
376.7	361.4	354.1	349.6	349.4	358.3	360.4
399.7	382.9	373.6	369.0	369.1	378.9	381.2
414.9	395.6	386.2	379.7	380.5	391.4	393.2
422.7	402.6	393.3	387.6	388.2	398.9	401.0
439.9	420.3	408.7	401.9	402.4	414.6	416.7
462.7	442.5	430.1	421.8	422.1	435.8	437.2
495.8	474.8	461.3	452.8	451.6	467.3	466.9
542.1	523.0	509.6	500.6	499.4	514.9	507.1
621.7	608.7	597.3	589.3	585.7	600.6	575.7
670.5	663.4	656.2	649.7	644.2	656.8	597.6

CYLINDRICAL COMBUSTOR EFFUSION HOLE"S CONVECTION TO COOLANT-BASED ON PREDICTED WALL TEMP. IMPINGING - SYSTEM

HCi-W/=M*2.K = CONVECTIVE HEAT TRANSFER COEFFICIENTQ(1-5)Hi-WATT = CONVECTION IN THE HOLES BASED ON WALL THERMOCOUPLE STATIONS ON WALL"S THERMOCOUPLE STATIONS; QH-W =MEAN HOLE CONVECTION; NUS.#= HOLE"S NUSSELT NO. BASED ON WALL"S THICKNESS

Hc	Q1h	Q2h	Q3h	Q4h	Q5h	Qh	Nus.#
564.15	218.03	179.55	147.29	124.07	110.90	155.97	128.35
435.54	171.35	140.03	118.67	105.55	99.64	127.05	96.45
326.48	130.88	106.05	91.75	83.89	82.41	98.99	70.43
240.63	101.41	82.39	73.03	66.87	67.59	78.20	49.84
166.43	65.63	54.96	48.88	45.73	46.26	52.29	32.87
148.88	59.55	49.70	45.01	41.40	42.22	47.58	28.60
131.18	49.24	41.14	37.63	35.19	35.72	39.79	24.80
113.47	40.67	35.20	31.86	29.75	30.15	33.56	20.77
95.26	31.67	27.81	25.46	23.71	23.92	26.51	16.73
76.58	21.84	19.53	18.06	17.05	16.98	18.69	12.71
58.43	11.31	10.45	9.87	9.41	9.37	10.08	8.66
33.54	0.91	0.88	0.85	0.83	0.82	0.86	4.57
19.69	1.63	1.63	1.63	1.60	1.58	1.62	2.50

TABLE 7.A4

CYLINDRICAL COMBUSTOR CONVECTION FROM COMBUSTION GAS TO TEST WALL -Based On Predicted Wall Temperature.

W(1-5)ct & Qct-WATT=CONVECTION FROM GAS STREAM TO TEST WALL --BASED ON WALL THERMOCOUPLE STATIONS - Qct IS MEAN;
H(1-5)g & HMg-W/M2.K =ARE BOTH CONVECTIVE HEAT TRANSFER COEFFICIENT -BASED ON WALL THERMOCOUPLES- & HMg IS MEAN.
Nu.t=NUSSELT NO. BASED ON TEST WALL LENGTH

H1g	Q1ct	H2g	Q2ct	H3g	Q3ct	H4g	Q4ct	H5g	W5ct	HMg	Qct	Nu.t
196.5	1775.4	154.6	1460.5	122.3	1197.1	100.5	1007.8	88.5	900.4	132.5	1268.3	723.4
170.2	1491.3	131.9	1216.8	108.0	1030.3	94.1	915.8	88.0	864.3	118.4	1103.7	629.5
147.3	1244.0	111.9	1005.6	93.5	868.9	83.9	794.0	82.1	779.7	103.7	938.5	537.0
137.1	1067.2	102.6	878.8	87.7	778.5	78.5	712.1	79.1	717.5	97.0	834.8	482.2
111.8	837.2	86.0	697.0	73.1	618.1	66.9	577.5	67.8	584.1	81.1	662.8	384.5
115.6	821.9	87.4	681.0	75.6	614.5	67.5	564.1	69.1	575.3	83.0	651.4	382.9
104.8	734.2	79.1	608.4	69.2	554.3	63.1	517.3	64.2	525.0	76.1	587.9	345.2
103.5	668.2	80.6	587.2	69.0	528.7	62.5	492.3	63.5	498.8	75.8	559.0	333.1
102.5	634.4	80.8	550.7	69.6	500.8	62.4	464.7	63.0	468.4	75.6	523.8	318.7
101.4	577.5	81.0	509.0	69.9	466.4	63.4	438.1	62.8	435.8	75.7	485.4	301.4
101.6	499.5	83.7	453.4	73.4	422.7	66.7	400.3	66.0	398.0	78.3	434.8	288.3
108.9	400.7	95.2	379.5	85.1	361.7	78.4	348.0	75.6	342.1	88.6	386.4	289.6
108.2	317.6	99.5	308.4	91.5	298.9	85.0	289.9	79.9	282.3	92.8	299.4	283.3

PREDICTED COOLANT'S HOLES OUTLET TEMPERATURE AND TEMPERATURE PROFILES-Based On Predicted Wall Temp.

T-(1 TO 5)o=OUTLET TEMPERATURE BASED ON HEAT TRANSFER FROM THERMAL LOCATIONS 1 TO 5 OF TEST WALL.
=To = MEAN OUTLET TEMPERATURE; T(1 to 5)r = OUTLET TO PLENUM COOLANT TEMP. RATIO

T1o-K	T2o-K	T3o-K	T4o-K	T5o-K	=To-K	T1r	T2r	T3r	T4r	T5r
338.4	350.1	323.5	318.7	315.8	325.3	0.54173	0.54317	0.54252	0.54154	0.54323
350.1	359.9	333.3	329.2	327.2	335.9	0.49971	0.50077	0.49957	0.49837	0.49992
362.9	350.0	342.9	339.1	338.0	346.6	0.45289	0.45371	0.45289	0.45182	0.45393
384.0	367.3	359.4	354.4	354.3	363.9	0.39597	0.39636	0.39625	0.39481	0.39726
407.2	389.2	379.2	374.3	374.5	384.9	0.32419	0.32423	0.32370	0.32271	0.32468
422.8	402.2	392.2	385.3	386.1	397.7	0.29835	0.29781	0.29797	0.29640	0.29844
430.4	409.0	399.2	393.1	393.8	405.1	0.27259	0.27167	0.27212	0.27101	0.27275
447.6	426.9	414.7	407.6	408.2	421.0	0.24082	0.24057	0.24046	0.23943	0.24093
470.2	449.1	436.2	427.5	427.8	442.2	0.20181	0.20187	0.20212	0.20107	0.20212
502.7	481.0	467.0	458.3	457.1	473.2	0.15343	0.15348	0.15374	0.15319	0.15366
547.5	527.9	514.3	505.1	503.8	519.7	0.09400	0.09435	0.09474	0.09444	0.09469
622.6	609.5	598.1	590.1	586.5	601.4	0.01065	0.01077	0.01087	0.01088	0.01088
667.4	660.4	653.1	646.7	641.3	653.8	.03172	.03234	.03286	.03295	.03302

COOLANT JET OUTLET VELOCITY AND JET VELOCITY TO MAINSTREAM VELOCITY RATIOS

-Based On Wall temperature Prediction

V0(1 TO 5)-M/S = COOLANT JET OUTLET VELOCITY-BASED ON WALL THERMAL STATIONS
V(1 TO 5)R = COOLANT JET OUTLET VELOCITY TO MAINSTREAM VELOCITY RATIOS
Vrt = VELOCITY RATIO AS ABOVE

V01	V1R	V02	V2R	V03	V3R	V04	V4R	V05	V5R	Vrt
33.96	0.930	33.13	0.908	32.47	0.889	31.99	0.876	31.70	0.868	0.80
29.00	0.792	28.16	0.769	27.61	0.754	27.28	0.745	27.10	0.740	0.67
22.83	0.621	22.03	0.599	21.58	0.587	21.34	0.581	21.27	0.579	0.51
17.07	0.466	16.33	0.444	15.98	0.434	15.76	0.428	15.75	0.428	0.36
11.53	0.317	11.02	0.303	10.75	0.295	10.59	0.291	10.60	0.291	0.23
10.37	0.285	9.86	0.271	9.62	0.264	9.45	0.260	9.47	0.260	0.20
8.98	0.245	8.54	0.233	8.33	0.228	8.21	0.224	8.22	0.225	0.17
7.73	0.212	7.38	0.202	7.17	0.196	7.04	0.193	7.05	0.193	0.14
6.45	0.177	6.17	0.169	5.99	0.164	5.87	0.160	5.87	0.161	0.11
5.15	0.141	4.93	0.135	4.79	0.131	4.70	0.129	4.69	0.128	0.08
3.73	0.102	3.60	0.098	3.50	0.096	3.44	0.094	3.43	0.094	0.06
2.12	0.058	2.07	0.057	2.03	0.056	2.01	0.055	1.99	0.055	0.03
1.13	0.031	1.12	0.031	1.11	0.030	1.10	0.030	1.09	0.030	0.02

JET OUTLET DENSITY TO FLAME DENSITY RATIOS-Based On Wall Temp. Prediction

D1OF(1 TO 5) = RATIOS OF OUTLET COOLANT JET DESITY TO THAT OF MAINSTREAM-BASED ON WALL THERMAL STATIONS ;nDr = NORMINAL DENSITY RATIO

D1of	D2of	D3of	D4of	D5of	nDr
3.19	3.27	3.34	3.39	3.42	7.69
2.68	2.76	2.82	2.85	2.87	5.70
2.36	2.44	2.49	2.52	2.53	4.26
2.13	2.22	2.27	2.31	2.31	3.45
1.96	2.05	2.10	2.13	2.13	2.99
1.87	1.97	2.02	2.06	2.05	2.90
1.84	1.93	1.98	2.01	2.01	2.84
1.76	1.84	1.90	1.93	1.93	2.79
1.67	1.75	1.80	1.83	1.83	2.73
1.56	1.66	1.68	1.72	1.72	2.71
1.43	1.49	1.53	1.56	1.56	2.68
1.26	1.29	1.31	1.33	1.34	2.67
1.17	1.19	1.20	1.21	1.22	2.67

COOLANT JETS OUTLET TO MAINSTREAM TEMPERATURE RATIOS AND JET PENETRATIONS

-Based On Wall Temperature Prediction

T(1 TO 5)r = COOLANT JET OUTLET TO MAINSTREAM TEMPERATURE RATIOS
Y(1 TO 5)p = MAINSTREAM PENETRATION BY JET-mm;-BASED ON WALL THERMAL STATIONS
nYp=Normimal Jet Penetration-mm

T1r	Y1p	T2r	Y2p	T3r	Y3p	T4r	Y4p	T5r	Y5p	nYp
0.433	5.2	0.422	5.2	0.414	5.1	0.408	5.1	0.404	5.1	8.0
0.448	4.0	0.435	4.0	0.426	3.9	0.421	3.9	0.418	3.9	5.7
0.464	2.9	0.448	2.8	0.439	2.8	0.434	2.8	0.432	2.8	3.7
0.491	2.0	0.469	1.9	0.459	1.9	0.453	1.9	0.453	1.9	2.4
0.520	1.3	0.497	1.2	0.485	1.2	0.478	1.2	0.478	1.2	1.5
0.540	1.1	0.514	1.1	0.501	1.1	0.492	1.0	0.494	1.0	1.3
0.550	0.9	0.523	0.9	0.511	0.9	0.503	0.9	0.504	0.9	1.1
0.573	0.8	0.546	0.7	0.531	0.7	0.522	0.7	0.522	0.7	0.9
0.602	0.6	0.575	0.6	0.559	0.6	0.548	0.6	0.548	0.6	0.7
0.641	0.5	0.613	0.5	0.595	0.4	0.584	0.4	0.582	0.4	0.6
0.698	0.3	0.673	0.3	0.656	0.3	0.644	0.3	0.642	0.3	0.4
0.794	0.2	0.777	0.2	0.763	0.2	0.752	0.2	0.748	0.2	0.2
0.851	0.1	0.842	0.1	0.833	0.1	0.825	0.1	0.818	0.1	0.1

FLUX-METER HEAT TRANSFER

Tg=COMBUSTOR GAS TEMP.;T-(in,ot,pl)=COOLANT INLET,OUTLET &PLATE TEMP.
Cpf=SP. HEAT CAPACITY(J/KgK); FMM=COOL. MASS FLUWRATE(Kg/sec.)
Hav=AVERAGE CONV. HEAT TRANSFER COEFF.(W/m2K); Q=HEAT TRANSFER-(W)

Tg-K	Tin-K	Tot-K	Tpl-K	Cpf	FMM	Hav	Q
781.4	301.8	375.3	406.7	0.101E+04	0.346E-02	70.7	256.38
781.8	306.5	388.4	420.2	0.101E+04	0.297E-02	70.0	245.11
781.7	307.7	395.9	427.6	0.101E+04	0.257E-02	66.7	228.64
782.8	309.2	405.0	436.5	0.101E+04	0.231E-02	66.6	223.15
782.6	311.0	409.4	440.1	0.101E+04	0.215E-02	64.5	213.68
782.3	311.4	411.8	442.3	0.101E+04	0.212E-02	65.2	214.71
782.0	311.4	411.3	442.1	0.101E+04	0.210E-02	64.4	211.74
781.5	312.7	416.5	447.0	0.101E+04	0.208E-02	67.2	217.58
780.8	313.3	419.5	449.9	0.101E+04	0.206E-02	68.9	220.57
784.7	314.3	425.4	456.2	0.101E+04	0.204E-02	72.2	229.36
784.5	314.4	424.1	455.1	0.101E+04	0.203E-02	70.6	225.17
784.3	315.4	428.0	459.1	0.101E+04	0.203E-02	73.2	230.51
784.1	315.1	425.1	456.7	0.101E+04	0.203E-02	71.1	225.15
782.8	315.4	426.4	458.3	0.101E+04	0.203E-02	72.2	226.86

CHAPTER 8

Nomenclature

T_c = Coolant temperature - K

T_g = Mainstream temperature - K

$T_{z'}$ = Impingement wall inner surface heating parameter as defined in equation 8.1

T_z = Predicted gap temperature - K

T_{im} = Impingement wall temperature - K

T_{pl} = Effusion wall temperature - K

z = Gap or separating distance between the impingement wall and effusion in combined system - mm

D = Impingement holes mean diameter unless otherwise stated - mm

G = Coolant mass injection rate - kg/sm^2

η_{ov} = Overall cooling effectiveness

η_a = Adiabatic cooling effectiveness

H_f = Film convective heat transfer coefficient - W/m^2K

T_{1-4e} = Staggered effusion wall temperature - K

T_{1-4J} = Stagnation and wall jets path effusion wall temperature - K

T_{1-4b} = Effusion wall back side temperature - K

T_{1-5} = Effusion wall centre line temperature - K

$\Delta P/P\%$ = Wall's design pressure loss

η = Cooling effectiveness

IMP = Impingement wall

EFF = Effusion wall

M = Mean

DESG. PRESS. = $\Delta P/P\%$

SYM = Symbol

H_w = Convective heat transfer coefficient to the impingement wall inner surface from bounce back theory - W/m^2K

X = Hole pitch - mm

CHAPTER 8

FULL COVERAGE DISCRETE HOLE IMPINGEMENT/EFFUSION SYSTEM - EXPERIMENTAL WORK RESULTS

8.1 INTRODUCTION

Work on full coverage discrete hole impingement/effusion hybrid cooling system of the present design was first proposed by Andrews et al (1) and investigated by Mkpadi (2). Mkpadi investigated the cooling performance of two geometries with different hole densities at one gap, Z, of 6.35 mm and for one geometry at a Z of 3.2 mm. The thickness of both the impingement and effusion walls in Mkpadi's investigations was 6.35 mm. In the present work, the influence of impingement wall holes' concentration, walls' thickness, dimensionless gap, Z/D (D = impingement holes' mean diameter) and coolant to mainstream density ratio on cooling performance and film heat transfer of the hybrid wall were investigated.

Two similar rigs were used in the investigation, Mk III and Mk IV, as discussed in Chapter 6. The test geometries were bolted to the plenum as discussed in Chapter 2, using high temperature autostick cement and separating gaskets, through which a thermocouple for measuring gap fluid temperature was inserted. After the cement had set, the plenum was placed on the combustion duct for testing. The data obtained were analysed for the cooling performance of the double wall and its heat transfer processes using the computer program of the heat transfer model developed and discussed in Chapter 7.

In this presentation, the number of wall's holes has been expressed as the numbers per square metre of plate surface. The design pressure loss of the impingement wall to that of the effusion

wall has been expressed as a ratio and designates the title of the figures' tables. An example of this is a hybrid wall of a 3.0% design pressure loss impingement wall and 0.1% design pressure loss effusion wall is referenced as a 30:1 impingement/effusion cooling system. This ratio is also equal to the square of the hole area ratio. All the experimental parameters are presented on the figures as easy-to-read tables. The results are based on the final wall temperature unless otherwise stated. This final temperature may also be stated as thermal station 5. Work at a mainstream temperature, T_g, less than 900 K is referenced as Low Temperature while at $T_g > 900$ K it is referenced as High Temperature Work, and uses the kerosine fuelled flame stabiliser.

The cooling effectiveness, both overall, η_{ov}, and adiabatic, η_a, are as defined previously in Chapter 6.

The heating of the impingement wall, as discussed in Chapter 7, is illustrated by plotting T_z' as a function of coolant injection. T_z' is defined as

$$T_z' = \frac{T_z - T_{im}}{T_{pl} - T_{im}} \qquad \ldots (8.1)$$

where T_z = Predicted gap temperature - K

T_{im} = Impingement wall temperature - K

T_{pl} = Effusion wall temperature - K

All the results reported here are 'corrected' for a cylindrical combustor based on the model developed in Chapter 7.

8.2 THE INFLUENCE OF THE NUMBER OF IMPINGEMENT HOLES COMBINATION WITH 4306 m^{-2} HOLES, 0.1% DESIGN PRESSURE LOSS EFFUSION WALL

The advantage in reducing the number of holes in the impingement

wall compared with equal number of impingement and effusion holes as primarily used (2), is the saving in mechanical manufacturing time, cost and simplicity. The results of the work reported here are those of 269, 1076, and 4306 m^{-2} impingement holes combined with the 4306 m^{-2} holes effusion wall at a constant Z of approximately 8 mm giving Z/D of 1.4, 2.5, 2.8 and 4.2. These three impingement geometries have the same hole area and X/D but have X in the ratio 1:0.5:0.25 respectively. The present results with 269 and 1076 m^{-2} impingement holes are compared with the previous result (2) for 4306 m^{-2} with all three sets of data processed by the computer program described in Chapter 7.

8.2.1 Temperature Distribution on the Effusion Wall

Figures 8.1 and 8.2 show the effusion wall temperature distribution at two test conditions, low and high temperatures, and at coolant flow rates (G) of 0.363 and 0.386 kg/sm^2 respectively, for the 269 m^{-2} impingement/ 4306 m^{-2} effusion holes combination. Thermocouples T_{1b}, T_{2b}, T_{3b} and T_{4b} give the measured temperature on the impingement side of the effusion wall (back side). Other thermocouples measure the flame side effusion wall temperature but the centre line ones, T_{1-5}, are used as a datum. The thermocouple T_{4e} was faulty in this particular experiment. T_{2j} is the thermocouple in line with the impinging jet while T_{1j}, T_{3j} and T_{4j} are in the path of the wall jets. At both conditions of tests, T_{2j} indicates the least temperature, confirming its jet stagnation point location. The maximum temperature difference between any two points on the effusion wall surface between the stagnation points and the wall jet path are summarized in table 8.1.

TABLE 8.1

Wall combination	269/4306		1076/4306	
T_g - K	759	1859	783	1762
G - kg/sm^2	0.363	0.386	0.370	0.384
Surface - K	29	64	16	42
Thickness - K	24	42	15	37
T_{pl} - K	429	982	418	990

At the high temperature, the differences for this combination are probably too high from thermal stress point of view and hence for an adequate life cycle of the combustor particularly for the 269/4306 combination. The differences for the 269/4306 wall are significantly higher than those for the 1076/4306 m^{-2} holes combination. However at high temperature, temperature difference is only 4% of the wall temperature. Using 'thermal paint', the temperature changes at both effusion wall back side and impingement wall inner surface at high temperature were investigated. The impingement and effusion wall thermal paint change are shown in plates 8.1 and 8.2 respectively.

As the wall was investigated for a range of G values in an experimental time lasting seven hours, too much may not be read into this result since colour change is both temperature and time dependent. However the plates indicate the worst temperature change at the minimum test coolant injection. On the effusion wall, the marked impinging jets' stagnation points, as well as the path of the wall jets, indicate a possible colour and hence temperature change from under the impingement jets to the region between jets. This has also been found in tests at GEC Gas Turbines. Figure 8.5 (3) shows

that a colour change from red to yellow involves a temperature change of 313-323 K, which is comparable with the measured high temperature figures in table 8.1.

The impingement wall inner surface, plate 8.1, shows a uniform temperature of 823 K maximum, confirming the conclusion that impingement wall heating is significant which has up till now been overlooked (4).

Figures 8.3 and 8.4 show the temperature distribution on the effusion wall for the 1076 m^{-2} impingement/4306 m^{-2} effusion combination for two test temperature conditions, at G values of 0.363 and 0.384 kg/sm^2 respectively. The maximum temperature difference between any two points on the effusion wall surface between the stagnation points and the wall jet paths are shown in table 8.1. The differences are low and pose no thermal stress problem even at high temperature. The differences are significantly lower than for the 269 impingement wall holes but for every impinging jet there are 4 effusion suction holes while there are 16 suction holes for the 269 impingement wall. Effusion hole air feed and impingement jet surface coverage are likely to be better for the 1076 m^{-2} impingement system,although the influence of number of holes on temperature gradients is clearly not excessively large.

8.2.2 Low Temperature Cooling Effectiveness

Figure 8.6 shows the final cooling effectiveness, η_{ov}, of the 269, 1076, 4306 m^{-2} holes impingement wall combined with a 4306 m^{-2} holes effusion wall as well as the single 4306 m^{-2} effusion wall on its own, as a function of coolant mass injection, G. All the results of the hybrid walls were superior to the single effusion wall at all G values greater than 0.1 kg/sm^2. The performance of

the 4306/4306 m^{-2} wall was superior at all G values greater than 0.1 kg/sm^2. This was 6% better than those of 1076/4306 m^{-2}; 11% better than 269/4306 m^{-2} and 16% better than the single wall at $G \geqslant 0.2$ kg/sm^2. Although these differences are small in relation to the great improvements in the impingement geometry manufacturing costs, they are nevertheless significant in terms of reduced flame tube life.

The performance of the 1076/4306 at the three ranges of Z/D investigated can be represented by a single line and hence display a lack of sensitivity to $2.5 \leqslant Z/D \leqslant 4.2$. This insensitivity of impingement heat transfer to Z/D in this region has also been found by Andrews and Hussain (12) for impingement heat transfer.

Figure 8.7 shows the cooling effectiveness as a function of axial distance downstream of the wall leading edge. The axial profiles of the cooling effectiveness indicate that there is little to be gained by using the 4306/4306 m^{-2} holes combination instead of the 1076/4306 m^{-2}. The figure reinforces the conclusion above that the 1076/4306 m^{-2} is insensitive to gap variation in the range of Z/D investigated. The axial performance of the double walls are superior to that of the single wall.

The results of the adiabatic effectiveness, η_a, of the 269, 1076 - m^{-2} combination and the single wall are shown in figure 8.8. The results indicate that 1076/4306 η_a are superior to those of 269/4306 and the single wall. The single wall and the 269/4306 m^{-2} double wall have almost the same η_a at all values of G suggesting that the film heat transfer to the surface of the walls were similar.

8.2.3 Low Temperature Heat Transfer

The results of the film heat transfer coefficient to the surface of the test walls from hot gases are shown in fig. 8.9 as a function of coolant mass injection rate G at the final thermal station. There are considerable variations as the impingement geometries are used, even though there is a constant effusion geometry. The film cooling will be dominated by the effusion plate geometry and the only influence of the impingement geometry should be on the effusion hole outlet temperature arising from the difference in impingement heat transfer. This will cause small changes in film cooling due to the density ratio change. However, the large difference in fig. 8.9 would not be expected.

It is considered that the large differences in film heat transfer coefficient shown in fig. 8.9 are due to the inadequacies of a single impingement correlation for all the impingement geometries. Work is in progress on a separate test facility to determine the combined impingement/effusion heat transfer coefficient. Until this information is available, the present predictions for H_f are uncertain.

Figure 8.10 shows the axial profiles of the film heat transfer to the effusion wall surface for both the double and single walls. Again the profiles are apparently dependent on the number of impingement wall holes, with smallest number of impingement holes giving the highest value of H_f on an axial basis.

8.2.4 Impingement Wall Convective Heat Transfer

Figure 8.11 presents the results of the impingement wall heating by the impinging jet as it is deflected back, by its impact on the back side of the effusion wall, to the impingement wall.

The model's prediction breaks down at low G value as values of T_z' greater than unity are predicted which is impossible.

This high value of T_z' results from the heating of the impingement plate being dominated by radiative heat transfer from the effusion plate at very low coolant flow rates. This results in an impingement wall temperature nearly equal to the effusion wall temperature. When this happens the denominator in equation 8.1 becomes very small. Values of T_z' greater than unity at this condition are clearly unrealistic and result from error in the impingement heat transfer correlations in the heat balance programme. These errors are magnified when T_z is close to T_{pl}. Direct measurement of impingement heat transfer correlations for every test geometry are currently in progress to improve these predictions.

The convective heat transfer to the impingment wall from the bounce-back theory is shown in fig. 8.12 as a function of G. The results confirm high convective heating of the wall for the 4306/4306 double wall while the least heating is indicated for the 269/4306. At low G values less than 0.18 kg/sm^2 the results converge towards a low value of the convective heat transfer and the high values of T_z' in Fig. 8.11 are due to radiative exchange. The analysis of an impingement wall convective heating until now has never been undertaken and so there are no comparable results.

The results clearly show that the heating of the impingement wall is a function of the impingement holes number, the gap, Z/D, and the coolant mass injection, G. The higher the number of impingement holes, the higher the convective heating of this wall. The explanation for this is that for every impingement hole, for the present work, in the 4306/4306 m^{-2} wall, there is one effusion

suction hole while there are four for the 1076/4306 m^{-2} wall and sixteen effusion suction holes for the 269/4306 m^{-2} wall. The effect of the suction holes is to reduce the energy by which the jet is able to bounce back to the impingement wall simply by sucking away the wall jets and exerting a pulling effect on the jets, as the latter journey back to the impingement wall surface. The more suction holes there are relative to the impinging jets, the less the bounce back of the jet at impact on the target wall and the less the heating of the impingement wall will occur by convection. The above discussion supports the results in figures 8.11 and 8.12 in which least heating is indicated by the 269/4306 wall while the impingement wall of the 4306/4306 is the most heated. Except for Andrews et al (4,5), this phenomenon has not been previously recognized by any investigator.

8.2.5 High Temperature Cooling Effectiveness

Figure 8.13 shows the final results of the wall cooling performance as a function of G for the high temperature work. The results indicate that for the lower number of impingement holes, double walls have superior cooling effectiveness to the large impingement holes one. It is considered that this reversal of the trends at low temperature may be due to problems in establishing a uniform value of T_g across the duct. The η results of 1076/4306 m^{-2} at Z/D of 4.2 and mainstream temperature, T_g, of 1550 K were exceptionally poor. The cause of the reduction in the performance was uncertain. It was considered that the factor that may be held responsible was a crosswise mainstream maldistribution of kerosine fuel at this high testing temperature with a probable hot spot in the central region. After this particular test a new three swirler

combustor was commissioned and traversed to check for flame bias at high temperature as detailed in Chapter 6. The repeat test did not confirm the initial results and hence flame bias may be assumed to be the reason for the low η. Except for this wall, all the double wall's cooling performance results are better than those of the effusion single wall, with values ranging from 21% to 30% at G value of 0.2 kg/sm^2 to 29% to 37% at G = 0.6 kg/sm^2.

All the cooling effectiveness results are also shown with hot stream gas radiation set to zero in the heat balance. Despite this, they all show a lower cooling effectiveness in comparison with their low temperature cooling effectiveness, fig. 8.6, by almost 0.12, with that of the 4306/4306 system giving a decrease of up to 0.2 at all $G \geq 0.2$ kg/sm^2. The explanation for this may be the higher velocity of the coolant jets from the effusion wall at the higher coolant temperatures, which will result in a high constant pressure loss for the same G and in enhanced boundary layer 'jet stirring' and hence reduced film cooling effectiveness. The higher coolant temperature also reduces the hole Reynolds number for the same G due to the strong increase in viscosity with temperature. This will reduce the internal wall convective heat transfer for the same G. Both these factors contribute to the inferior cooling effectiveness value at high temperature compared with the low temperature results.

Figure 8.14 shows the axial profiles of the cooling effectiveness at $0.382 \leq G \leq 0.394$. The axial results confirm the superiority of the lower numbers of impingement holes over those of the 4306/4306 system. As mentioned previously, this is the opposite trend to the low temperature results and may simply reflect the difficulty of establishing a reliable T_g at high temperature. The measured values

of T_g are particularly suspect in Ref. 2 as a home-made thermocouple was used, not the present mineral insulated type. The axial profiles are mainly flat, indicating a uniform film protection. This was also found at low temperature as shown in fig. 8.7.

The adiabatic effectiveness, η_a, of the wall at 76.2 mm from the leading edge is shown in fig. 8.15, as a function of G. These results contrast with the overall cooling effectiveness as the 1076/4306 system, at Z/D of 4.2, shows a better η_a than the rest and agree with the low temperature results in fig. 8.8. The trends of the 1076/4306 system, at Z/D of 2.8, and 269/4306 system are inconsistent with their overall cooling effectiveness. The reasons for this are associated with the difficulty in obtaining reliable values of η_a due to the variation of T_{gw} between the holes. For consistent results, T_{gw} would need to be in precisely the same position in each test and this is difficult to achieve of the test rig.

8.2.6 High Temperature Heat Transfer

The results of the film heat transfer to the wall, as a function of G, are shown in fig. 8.16, and as a function of axial distance in fig. 8.17. The values are much higher than for the low temperature test and show an apparent greater influence of impingement geometry. As discussed in relation to the low temperature tests, the values rely entirely on the accuracy of the wall heat transfer model and the apparent differences in the film heat transfer coefficient may possibly reflect an inadequacy in the impingement model to account for the influence of the impingement geometry.

Figure 8.18 shows the heating of the impingement wall by convection by the jets which are deflected by their impact on the

target wall. The profiles are similar to the low temperature work except for that of 4306/4306 combined system at $G \leqslant 0.46$ kg/sm^2. The results also confirm the dependence of $T_{z'}$ on the number of impingement holes for this effusion geometry.

8.3 INFLUENCE OF WALL THICKNESS

To cut costs in double skin combustor manufacture, a reduction in the wall thickness is an attractive one. For aero-engines, a reduction in combustor wall thickness is essential. The work reported here was carried out using a double skin impingement/effusion system, each of a 3.3 mm thickness as contrasted with the standard wall thickness of 6.35 mm each, normally employed in this programme. The results of the cooling performance of these thin walls in comparison with the 6.35 mm thickness are the focus of presentation in the following sections. The thin impingement/effusion system design parameters are shown in table 8.2.

TABLE 8.2

	No. Holes m^{-2}	Design Pressure Loss %	Thick. mm	Diameter mm	Hole Pitch / Diameter
IMPINGEMENT	1076	3.0	3.34	2.86	30.48
EFFUSION	4306	0.1	3.35	3.24	15.24

The combination has a gap of Z/D = 2.8 where Z is 8.0 mm.

8.3.1 Cooling Effectiveness

The cooling performance of the thin wall impingement/effusion system is compared with the 6.35 mm wall thickness results in fig. 8.19

as a function of coolant mass injection, G, for both low and high temperature conditions. The thin wall's performance at a low mainstream temperature, T_g, of 755 K was very similar to that of the thick walls, with slightly higher value of η for G values greater than 0.4 kg/sm^2 but slightly lower value of cooling performance for $G \leqslant 0.4$ kg/sm^2. At a higher T_g of 1391 K, the thin wall's performance, below G of 0.3 kg/sm^2, was superior to all the rest and equal to the performance of the thick wall at T_g of 783 K, for all $G \geqslant$ 0.3 kg/sm^2. The reason for this high cooling effectiveness is associated with the influence of density ratio as discussed in the next section. At the highest testing temperature of $T_g \geqslant 1730$ K, the overall cooling performance of both walls thicknesses are very similar but are lower by 0.11 than the lower temperature conditions. For this high temperature ($T_g \geqslant 1730$ K) the overall cooling performance of the walls are the same for all $G \geqslant 0.4$ kg/sm^2 with the thicker walls being slightly better, 2%, at $G > 0.7$ kg/sm^2. With the hot gas stream radiative heat transfer set to zero, the difference between the walls' high temperature performance and that at lower temperature is 0.06.

The adiabatic cooling effectiveness of both systems of walls is similar for all values of G investigated except for the thin wall at T_g of 1738 K, which is lower.

Figure 8.20 shows the axial profiles of the cooling performance of these walls at $0.365 \leqslant G \leqslant 0.387$ for all the conditions of test. The profiles are similar indicating similar axial developments of the film cooling.

8.3.2 Heat Transfer

Figure 8.21 shows the convective heat transfer to the surface of the effusion wall of the test systems from the hot mainstream, as a function of coolant injection at the 127 mm axial position. There is very little influence of the wall thickness, which is only a reflection of the similar wall temperature which are the input to the prediction procedure for the film heat transfer coefficient. The strong influence of T_g on the results indicates a related influence on the film mixing as previously discussed.

The values of H_f for the thin wall , at T_g of 1391 K, are higher than for the lower temperature conditions and hence suggest a lower cooling effectiveness but this has been seen not to be the case. The reason for this is the dominance of heat removal at the back of the thin wall rather than inside the wall, a case which was highlighted in Chapter 6.

The axial profiles of the film heat transfer are shown in fig. 8.22 at $0.365 \leqslant G \leqslant 0.387$. Again the trend is that of decreasing values of H_f downstream of the wall's leading edge and little influence of the wall thickness.

The impingement wall surface heating by deflected jets is presented in figure 8.23 as a function of coolant mass injection. The results indicate a slightly higher heating of the impingement surface at a low temperature test condition than is the case at high temperatures. There is, again, little influence of the wall thickness.

8.4 EFFECT OF DENSITY RATIO ON COOLING PERFORMANCE OF AN IMPINGEMENT/EFFUSION SYSTEM

Density ratio effects reported in the literature are for single wall cooling geometries and often these are for a single hole, single row or double rows of holes (6-9). Except for Ref. 8, all make use of foreign gases in their investigations to simulate the effect of density ratio. The use of foreign gases has drawbacks (10).

A real practical means of investigating density ratio effect of any wall cooling system, is to vary both coolant and mainstream temperatures as close to a practical turbine operating conditions as possible. This is what has been accomplished in the work reported here. Coolant temperature was varied from 293 K to 677 K, representing turbine compressor delivery air, while the mainstream temperature was varied from 755 K to 1738 K by using an electrical heating element and firing propane/kerosine respectively. The test condition of T_g = 750 K and T_c = 293 K has a density ratio of 2.5 and the objective was to investigate different values. The above temperatures are equal and above the working temperature of most of the common gas turbine engines presently in service. The results of this investigation on double wall 1076/4306 - m^{-2} holes impingement/effusion system is the subject of the subsections below. The design parameters of this cooling wall geometry are as detailed in table 8.2.

8.4.1 Cooling Effectiveness

Figure 8.24 shows the cooling effectiveness results as a function of coolant mass injection, G, for coolant to mainstream density ratios of 1.4 to 2.6. The results show that the cooling performance is dependent on fluid density ratio, increasing in

superiority with decreasing density ratio. The lowest density ratio of 1.4 shows a cooling performance 10% better than those of density ratios 2.07 to 2.58 and 19% better than that of density ratio of 2.61, for all $G \leqslant 0.4$ kg/sm^2. At all $G \geqslant 0.4$ kg/sm^2, it is 4, 5 and 13% better than those of density ratios of 2.07 (at T_g = 967 K), 2.07 - 2.58 and 2.61 respectively. At low G values less than 0.4 kg/sm^2 the two 2.07 density ratios investigated, by using different coolant and mainstream temperatures, give almost the same result and are only slightly better than the low temperature work of T_g = 755 K. These however are 19% better than the performance of density ratio of 2.61 at G equal to 0.2 kg/sm^2 but only 9% better at all $G \geqslant 0.3$ kg/sm^2. The adiabatic cooling effectiveness reflects the same trends but not as prevailing as in the overall cooling effectiveness due to the difficulty of traversing at precisely the same position relative to the holes.

The axial profiles of the wall cooling performance for the various density ratios investigated are presented in fig. 8.25 at $0.365 \leqslant G \leqslant 0.387$. Again the superiority of 1.4 density ratio cooling performance is dominant and the axial trends as observed in fig. 8.24 are maintained, though the performance of the 2.58 and 2.07 density ratios for T_g at 967 K are inseparable.

The explanation for the trends of the results is that the lower the density ratio of the fluid the easier it is for the mainstream to deflect the coolant jets towards the effusion wall preventing high penetration and entrainment of the mainstream to the proximity of the test wall. Also the boundary layer on the wall will be thin resulting in effective film protection on the wall.

8.4.2 Heat Transfer

Figure 8.26 shows the film heat transfer to the surface of the test wall for all the density ratios investigated, as a function of G. These results do not follow the same trend as that of the wall's cooling performance; rather it seems to be dependent on coolant delivery temperature. For all the density ratios there is a sharp reduction of H_f at all G values less than 0.25 kg/sm^2. This is an indication of improvement in film protection, absence of jet penetration, entrainment or recirculation at the wall, and a thin boundary layer, as the coolant injection increases from 0.088 kg/sm^2 up to the G value of 0.25 kg/sm^2. The net effect of this is a rapid increase in the cooling effectiveness at low G. With further coolant injection beyond a G value of 0.4 kg/sm^2 most of the density ratios work show a gradual rise in H_f, a process that continues for most of the G values investigated. This phenomenon is associated with jet penetration into and entrainment of the hot gas mainstream. The effect of this on cooling effectiveness is a reduction in its growth, followed by levelling off.

Figure 8.27 shows the axial profiles of the film heat transfer coefficient at $0.365 \leqslant G \leqslant 0.387$. Again, the profile does not follow the norm displayed by the cooling effectiveness but shows a similarity with the profiles in fig. 8.26, with the high density ratio showing the highest convective heat transfer to the surface while the 2.58 density ratio shows the least. A decreasing trend in H_f downstream of the leading edge of the test wall is common to all the density ratios, and lends support to the findings in figure 8.25.

Figure 8.28 shows the impingement plate heating to be apparently dependent on density ratio for a coolant temperature of 670 K. However, this is surely a reflection of the higher value of T_{im} and hence T_z as T_g increases. At lower coolant temperature there is more heat transfer due to the higher Reynolds number for the same G.

8.5 THE 4306 m^{-2} HOLE, 0.0027% DESIGN PRESSURE LOSS WALL PERFORMANCE IN IMPINGEMENT/EFFUSION SYSTEMS

The 0.0027% design pressure loss, 4306 m^{-2} hole effusion wall is a highly optimized single skin cooling wall. In Chapter 6, it was shown that its performance was close to that of the transpiration cooling system at high coolant injection rates. The results for this effusion wall in combination with impingement walls of various hole densities and at various operating temperature conditions are presented in the following subsections.

8.5A The Influence of Impingement Holes' Number

The performance of this low pressure loss wall was investigated in its combination with two holes density, 1076 m^{-2} and 4306 m^{-2}, impingement walls. Both the impingement and the effusion walls were of the standard 6.35 mm.

8.5A.1 Cooling effectiveness

The results of the cooling performance of the 1076/4306 4306/4306 - m^{-2} of the 0.0027% design pressure loss systems, are presented and compared with the performance of the 4306/4306, of the 0.1% effusion system, as well as the low pressure loss single wall, in fig. 8.29 as a function of G. The results show that at all G values greater than 0.18 kg/sm^2, except for the single wall, the

4306/4306 - 0.0027% system has a performance far superior to the rest and behaves, at high G values, as a transpiration system. In this region of coolant injection rate, it is better than the 4306/4306 - 0.1% and the 1076/4306 - 0.0027% system by 9% and 15%, on average, respectively.

At all G values below 0.2 kg/sm^2 it has a slightly poorer cooling performance than the other combined system but better than the single wall. This may be due to axial pressure gradients at low G leading to non-uniform coolant distribution.

The 1076/4306 has the poorest performance at all G values greater than 0.36 kg/sm^2, but equals the performance of the 4306/4306 - 0.1% system at all values of G below 0.2 kg/sm^2. Hence a reduced number of impingement holes is not viable in this situation.

The single wall's performance is better than those of the 4306/4306 - 0.1%, and 1076/4306 - 0.0027% systems at all G values greater than 0.4 kg/sm^2. The improvement due to impingement cooling is relatively small and is most significant in the low G region, $G < 0.6$.

The adiabatic effectiveness of the 4306/4306 - 0.0027% and 1076/4306 - 0.0027% system results indicate the same order of magnitude at low values of G less than 0.3 kg/sm^2 but the 4306/4306 performs better at all G values greater than 0.3 kg/sm^2.

The main lesson of the results is that there appears to be little to be gained from a combined system whose effusion wall has been adequately optimized and in fact a loss of performance may occur if such a wall is used in combination with insufficient numbers of impingement holes.

Figure 8.30 shows the axial profiles of the results at $0.363 \leqslant G \leqslant 0.368$. These indicate that the 4306/4306 - 0.0027% is

superior in cooling effectiveness to the rest, while the 1076/4306 - 0.0027% is the worst of the combined systems.

The single effusion wall shows a much steeper axial dependence of η, although the final values are similar. It is considered that this is due to the influence of axial pressure gradients which create a higher static pressure loss across the trailing edge compared with the leading edge. This creates a flow maldistribution with more air in the trailing edge region and thus a higher cooling effectiveness. With a 3% pressure loss impingement wall these axial static pressure gradients are too small to create any flow maldistribution unless this occurs within the gap, which may be unlikely. The reason for the large deterioration in the cooling effectiveness with a reduced number of impingement holes is difficult to explain. It may be associated with a reduction in the 'suction' enhancement of the impingement heat transfer.

8.5A.2 Heat transfer

The results of the film heat transfer coefficient to the effusion walls are shown in figure 8.31 as a function of G. The trends of H_f in this work are split into two types: those of the 1076/4306 - 0.0027% and 4306/4306 - 0.1% systems which are of upward trends and those of the 4306/4306 - 0.0027% system and single wall which are of decreasing trends.

The difference in the effusion results and the 4306/4306 impingement/effusion results may positively be associated with the flow maldistribution problem discussed above and positively due to the neglect of any 'suction' influence on the impingement heat transfer in the internal wall cooling computations.

The continuous decrease in H_f as G is increased is a characteristic of transpiration cooling systems. The results for the 1076/4306 system are possibly due to the inadequacies of the impingement heat transfer correlation used. It is difficult to explain why such large changes in H_f should occur when there had been minimal change in the film aerodynamics.

Figure 8.32 shows the axial profiles of the wall's H_f at $0.363 \leqslant G \leqslant 0.368$. For this coolant injection, the trends are that of a continuous reduction in convective heat transfer to the wall downstream of the leading edge, indicating a growth in the thermal boundary layer film protection.

The heating of the impingement wall by deflected jets is presented in fig. 8.33 as a function of G. The least heated is the impingement wall of the 4306/4306 - 0.0027% system, reflecting the lower values of T_{im} and hence T_z.

Figure 8.34 shows the results of the convective heat transfer coefficient to the inner surface of the impingement wall from the bounce back theory. The results indicate that the 4306/4306 - 0.0027% system is the highest, followed by the 4306/4306 - 0.1% system, while the 1076/4306 - 0.0027% system is the least. These profiles are the order of cooling performance of the three systems of walls.

These results in fig. 8.34 may explain the inferior performance of the 1076/4306 system. The results indicate that the heat transfer by reflected jets is much reduced if the number of jets is reduced. This in turn will reduce the overall wall internal heat transfer and these effects are not taken into account in the heat transfer model. Clearly further work in this area is required to directly measure the reflected jets' heat transfer coefficient.

8.5B The 1076/4306 - 0.0027% System Performance at Z/D = 2.8

This wall system, with a gap Z/D of 2.8, has been investigated at two temperatures, low and high, in comparison with the 1076/4306 - 0.1% system at the same Z/D, with both walls having the same holes pitch to diameter ratios. The outcome of this investigation is discussed in the following sections.

8.5B.1 Cooling effectiveness

The results of the final overall cooling effectiveness of the 1076/4306 - 0.0027% design pressure loss system at two coolant and mainstream temperatures are presented in fig. 8.35 and compared with the 1076/4306 - 0.1% system and the 4306 - 0.0027% single wall. At low G values less than 0.3 kg/sm^2, the 1076/4306 - 0.0027% system at both T_g of 777 K and 1457 K is virtually the same in cooling performance, which is superior to that of the single wall and the 1076/4306 - 0.1% system (at T_g = 1762 K).

For G values greater than 0.3 kg/sm^2, the effusion single wall results are superior to the combined impingement/effusion results. This is in strong contrast to the results with equal number of holes shown in fig. 8.29, where there was no significant deterioration in the cooling effectiveness with impingement. Also the 0.1% effusion results did not show the same magnitude of deterioration of cooling effectiveness when the impingement holes were reduced from 4306 to 1076 per m^2. It is clear that the reduced number of holes cannot be tolerated with the very low pressure loss effusion wall. The reason for this may be the reduced 'suction' effect of the effusion holes on the impingement heat transfer. However the most likely reason for the fall in cooling effectiveness is the elimination of the flow maldistribution in the

effusion test. This is reflected in flatter axial variations of cooling effectiveness, as shown in fig. 8.36.

Figure 8.37 shows the adiabatic effectiveness at axial distance 76.2 mm downstream of the walls' leading edge. For all G values the results indicate a better adiabatic effectiveness for 1076/4306 - 0.0027% at T_g of 777 K over the rest, except for the single wall at G greater than 0.65 kg/sm^2. The adiabatic at 1457 K compares favourably with the rest. In general, these results are clear indication of effective film protection and that the reduced number of impingement holes has not similarly deteriorated the film protection. The change from the effusion only result is likely to be influenced by the coolant flow maldistribution.

8.5B.2 Heat transfer

The results of the film heat transfer coefficient to the surface of the walls from the mainstream are shown as a function of G in fig. 8.38. The results are strongly influenced by the use of a single impingement correlation in the model, which ignores any influence of the effusion holes on the impingement heat transfer. Thus the similar results for the 0.1 and 0.0027% effusion walls may not be valid if, as has been argued, the impingement heat transfer is reduced for the 0.0027% situation. The abnormally low results for the effusion plate alone are due to the coolant flow maldistribution already referred to.

Figure 8.39 shows the axial profiles of the film convective heat transfer coefficient at $0.363 \leqslant G \leqslant 0.4$. The trends, for all the walls, are similar. The higher results for the impingement/effusion wall compared with the effusion are likely to be associated with the inadequacies of the heat transfer model, as previously discussed.

Figure 8.40 shows the heating effect of deflected jets on the impingement wall. Low heating is indicated for the high temperature conditions possibly due to lower jet Reynolds numbers for the same G. The similarity in the results for the two different diffusion geometries is somewhat surprising as an enhanced jet deflection, due to a reduced 'suction' effect from the effusion holes, had been expected. However, the calculation of T_z, does rely on the assumption of an impingement heat transfer correlation not influenced by the effusion geometry and hence may not reveal the true situation. It is clear that detailed impingement/effusion heat transfer correlations are required if the present results are to be correctly analysed.

8.6 THE 1076/26910 m^{-2} HOLES, IMPINGEMENT/EFFUSION SYSTEM

The earlier work (2) on 26910 m^{-2} holes, standard thickness (6.35 mm), 0.1% design pressure loss, single effusion wall and 26910/26910 m^{-2} holes combined impingement/effusion system showed very encouraging results. This stimulated interest in further investigation on a double wall system but with a reduced number of impingement wall holes, as the 26910 holes per m^2 is expensive to manufacture. A 1076 m^{-2} holes impingement wall of 3.0% design pressure loss was chosen for direct comparison with the equivalent system, 1076/4306. This is a 96% reduction in the number of impingement wall holes employed in Ref. 2. The results of the work carried out on a 1076/26910 m^{-2} holes hybrid wall are the focus of presentation in the following subsections.

8.6.1 Cooling Effectiveness

Figure 8.41 shows the results of the cooling performance of

the 1076/26910 m^{-2} holes combined system in comparison with those of the 26910/26910 m^{-2} combined system and the single 26910 effusion wall as a function of coolant mass injection. The results show that for all G values less than 0.4 kg/sm^2 the 26910/26910 system is superior to the 1076/26910 system by just 1.6% and at higher values of G the 1076/26910 is slightly superior. In general the reduction in the number of impingement holes has only a small effect on the cooling effectiveness. Both combined system geometries have a cooling performance better than the single wall by 4% at G equal to 0.3 kg/sm^2, while the magnitude is 8% at all G values greater than 0.55 kg/sm^2.

The reason for the good performance of the 1076/26910 m^{-2} holes system in comparison with the poorer performance of the 1076/4306 system is probably the suction effect of the 25 effusion holes per impingement hole compared with only 5 per impingement hole in the 1076/4306 system. The 25 effusion holes exert a suction force on the jet reducing its degree of freedom to bounce back to the impingement wall surface. The effect of this is good scrubbing of the back side of the effusion wall and enhanced effusion back side convective heat removal by the coolant.

The influence of impingement cooling is only a small increase in the effusion only cooling effectiveness. This is indicative of the good internal wall cooling of the effusion system. However this may be partially due to t/D of 10 with the 6.35 mm thick wall. With impingement, the wall thickness could be considerably reduced.

Figure 8.42 shows the axial profiles of the 1076/26910 m^{-2} system in comparison with the 26910/26910 m^{-2} system and the single effusion wall. The profiles are similar with the double walls being

superior to the single wall. The axial variations of cooling effectiveness are similar and there is no evidence of the flow maldistribution creating steeper axial gradients for the effusion only situation as discussed for the very low pressure loss 4306 m^{-2} system.

8.6.2 Heat Transfer

The convective heat transfer coefficients of the film for the three walls are presented in fig. 8.43, as a function of coolant mass injection rate G. The profiles indicate a trend of decreasing magnitude of H_f which is particularly sharp at all values of G greater than 0.4 kg/sm^2. All the walls display an initial increase in H_f but a special feature of this result is that the 26910/26910 m^{-2} system has nearly the same magnitude of H_f as those of the single wall at all G values greater than 0.1 kg/sm^2, while the 1076/26910 m^{-2} system is better by having less at all G values greater than 0.5 kg/sm^2. This shows that for this geometry the present impingement/effusion heat transfer model of Chapter 7 is reliable. The decreasing H_f as G is increased is a feature of transpiration cooling and this indicates that the 26910 m^{-2} effusion system is close to the ideal. The 1076/26910 m^{-2} system is therefore the optimum impingement/effusion wall cooling geometry.

Figure 8.44 shows the axial variation of H_f for $0.363 \leqslant G \leqslant 0.373$. The trend is that of a sharp decrease in the magnitude of H_f up to a distance of 100 mm from the leading edge for both the 26910/26910 system and the single effusion wall, while it is 70 mm in the case of the 1076/26910 m^{-2} system. For the rest of the axial distance the convective heat transfer coefficient tends to level off. These support the results of fig. 8.42 where the gradual rise in axial

effectiveness ceased at approximately 100 mm axial distance downstream of the leading edge and was at equilibrium state for the rest of the axial distance.

8.7 THE 9688/9688 m^{-2} HOLES IMPINGEMENT/EFFUSION SYSTEM

Though the performance of the 26910/26910 m^{-2} holes combined system is very high, its large concentration of holes means high manufacturing cost and though the 4306/4306 m^{-2} holes combined system will cost much less to manufacture, its performance is not as good. If a one to one ratio of the impingement/effusion holes system is required, the minimum number of holes that will achieve a performance close to that of the 26910 system is required. It was shown in Chapter 6 that for an effusion wall, the 9688 m^{-2} option had the optimum number of holes. It is the objective of this section to investigate whether this conclusion would also hold for the impingement/effusion system.

8.7.1 Cooling Effectiveness

The cooling effectiveness results of the 9688/9688 m^{-2} holes system are presented in fig. 8.45 as a function of the coolant mass injection rate, G, and compared with those of the 26910/26910-m^{-2}, 4306/4306-m^{-2} and the single 9688-m^{-2} effusion wall system. At low coolant injection rates of interest in the present work, up to a G value of 0.4 kg/sm^2, the cooling performance of both the 9688/9688 m^{-2} and 26910/26910 m^{-2} systems are similar. At G values up to 0.6 kg/sm^2, the 26910/26910 system is better in performance by only 1.5% than the 9688/9688 system but at high G values this magnitude is up to an average value of 2.1%. For all G values, the cooling performance of the 9688/9688 m^{-2} wall is superior to both the 4306/4306 m^{-2}

system and the single wall by 5% ($G \geq 0.26$) and 14% respectively. It is clear that this 9688 m^{-2} impingement/effusion system has achieved the desired aims of a performance similar to the 26910 m^{-2} system.

Figure 8.46 shows the axial profiles of the cooling performance of the four walls at $0.365 \leq G \leq 0.372$. The inferior performance of the 4306 m^{-2} system is clearly due to the lack of continuous axial development of the cooling effectiveness. Up to 76 mm, all three designs have a similar performance, although the cooling effectiveness does increase with the number of holes.

8.7.2 Heat Transfer

Figure 8.47 shows the film heat transfer results for the three double walls and the single effusion wall, as a function of coolant mass injection rate, G. As shown previously in section 8.6 for the 26910 m^{-2} system, the 9688 m^{-2} system shows similar film convective heat transfer results as the effusion holes. This indicates that the impingement/effusion heat transfer model described in Chapter 7 is reasonably reliable for this geometry. The reason why the model was less successful for the 4306-m^{-2} geometry needs to be investigated. It is clear from fig. 8.47 that at low G values ($G < 0.4$), all three impingement/effusion designs have a similar film cooling effectiveness and hence the difference in the overall cooling effectiveness must be due to internal wall cooling differences. At high G values there are large differences in the film cooling effectiveness which are likely to be the cause of the large differences in the overall cooling effectiveness in fig. 8.46.

Figure 8.48 shows the axial profiles of the film heat transfer coefficient at $0.365 \leq G \leq 0.372$. The profiles are those of

continuous decrease in H_f for the whole length of the test wall for the 26910 and 9688 m^{-2} system and a fairly constant value for the 4306 m^{-2} system beyond 76 mm.

The impingement wall surface heating by deflected jets is shown in fig. 8.49 as a function of G. The effect is clearly significant at all values of G and not strongly influenced by the number of holes.

Figure 8.50 shows the computed convective heat transfer coefficient to the impingement wall inner surface from the deflected jets after impinging on the target effusion wall. At low G there is little influence of the number of holes, but there are large differences at high G. The 9688 m^{-2} system has the lowest result and the reason for this needs to be investigated.

8.8 REFERENCES

1. Andrews, G.E., Gupta, M.L., and Mkpadi, M.C., 'Combustion chamber wall cooling design considerations for low pressure drop drilled plates and for combined impingement and drilled plate systems', Report No. GEA/HT/3, Dept. of Fuel and Energy, University of Leeds, 1980.

2. Mkpadi, M.C., 'Full Coverage Effusion Cooling of Gas Turbine Combustion Chamber', Ph.D. Thesis, Dept. of Fuel and Energy, University of Leeds, 1982.

3. Cannon, M.F., G.E.C. Industrial Gas Turbine, Communication, May 1985.

4. Andrews, G.E., Asere, A.A., Hussain, C.I., and Mkpadi, M.C., 'Full coverage impingement heat transfer: The variation in pitch to diameter ratio at a constant gap', AGARD Meeting, 'Heat Transfer and Cooling in Gas Turbines', Paper 26, Bergen, Norway, May 1985.

5. Andrews, G.E., Asere, A.A., Hussain, C.I., and Mkpadi, M.C., 'Transpiration and impingement/effusion cooling of gas turbine combustion chambers', 7th Int. Symposium on Air Breathing Engines, Peking, 1985.

6. Pedersen, D.R., Eckert, E.R.G., and Goldstein, R.J., 'Film cooling with large density differences between the mainstream and the secondary fluid measured by the heat-mass transfer analogy', ASME - J. Heat Transf., Vol. 99, pp. 620-627, Nov. 1977.

7. Foster, N.W., and Lampard, D., 'Effect of density and velocity ratio on discrete hole film cooling', AIAA J., Vol. 13, pp. 298-304, 1975.

8. Afejuku, W.O., Hay, N., and Lampard, D., 'Measured coolant distributions downstream of single and double rows of film cooling holes', ASME - J. Eng. Power, Vol. 105, pp. 172-177, 1983.

9. Forth, C.J.P., Loftus, P.J., and Jones, T.V., 'The effect of density ratio on the film-cooling of a flat plate', AGARD Meeting 'Heat Transfer and Cooling in Gas Turbines', Paper 10, Bergen, Norway, May 1985.

10. Andrews, G.E., Discussion on Ref. 8, ASME - J. Eng. Power, Vol. 105, 1983.

11. Tirmahi, A., 'Gas Turbine Combustion Chamber Wall Cooling: Full-coverage Discrete Hole Wall Cooling', M.Sc. Dissertation, Dept. of Fuel and Energy, University of Leeds, Leeds, Sept. 1985.

12. Andrews, G.E., and Hussain, C.I., 'Impingement cooling of gas turbine components', Int. Gas Turbine Congress, Tokyo, Paper 9, 1983.

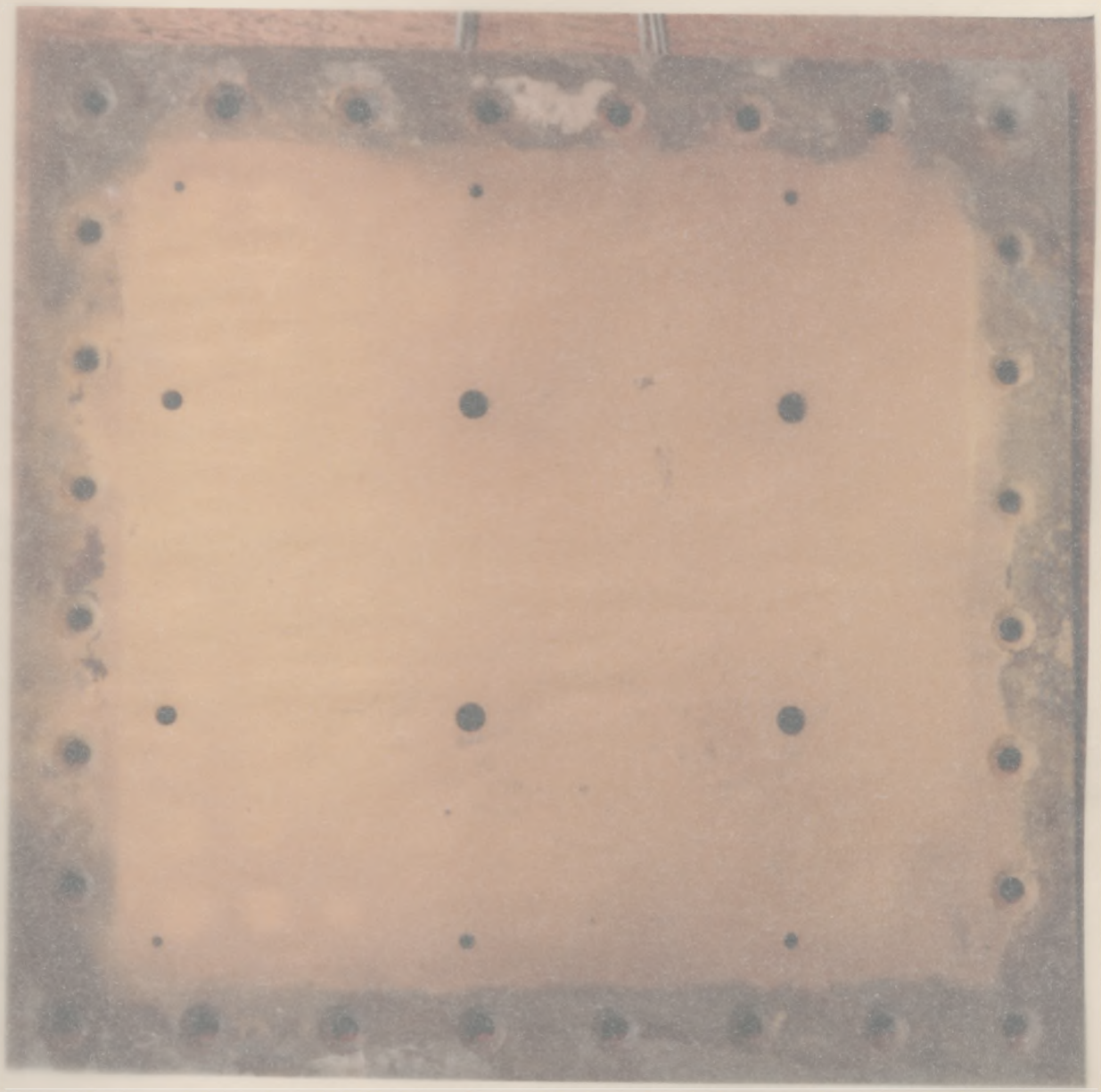

Plate (8.1): The 269 m^{-2} holes, 3.0% $\Delta P/P$, impingement wall - thermal paint colour change at T_c = 673 K and T_g = 1859 K.

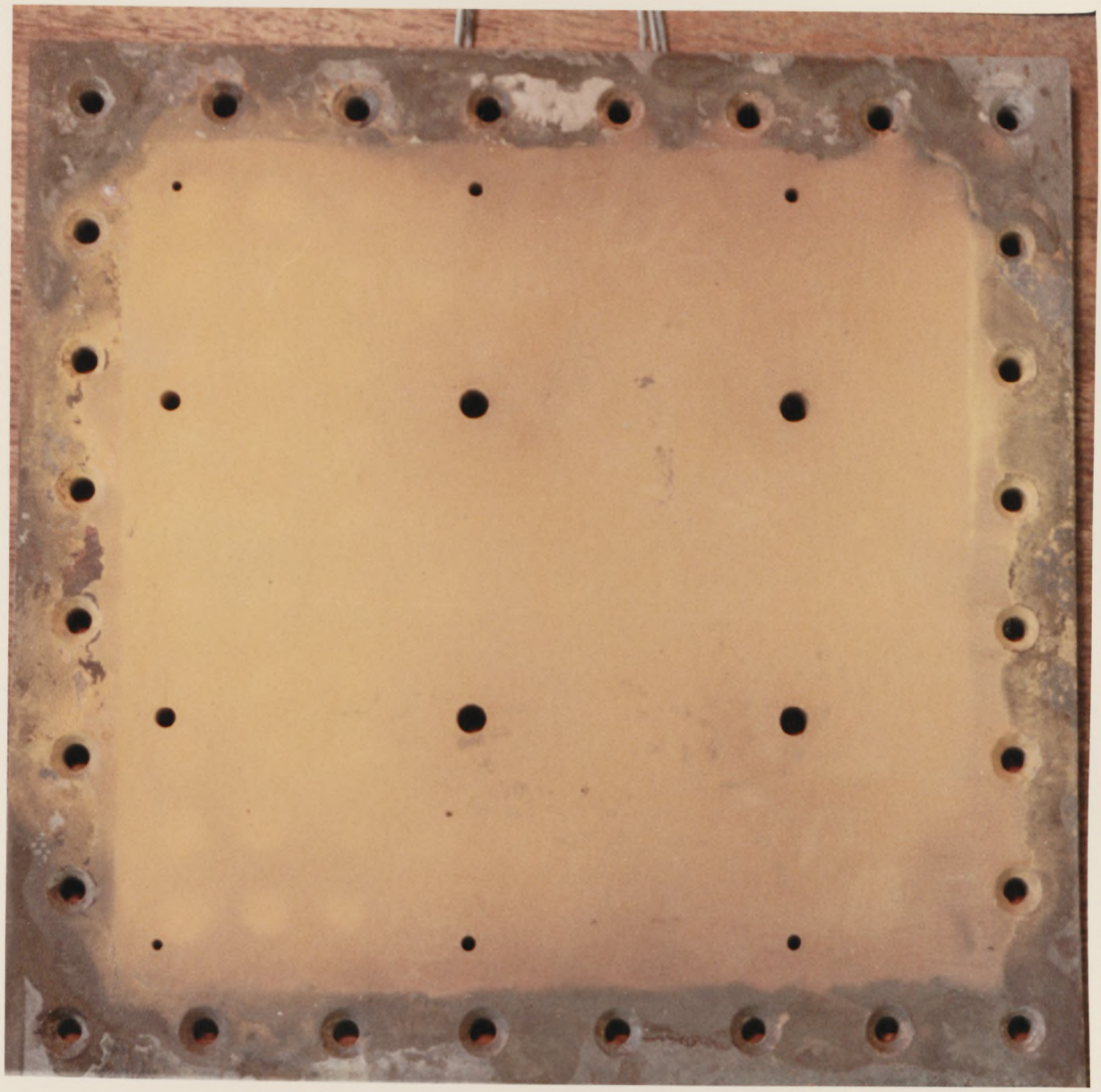

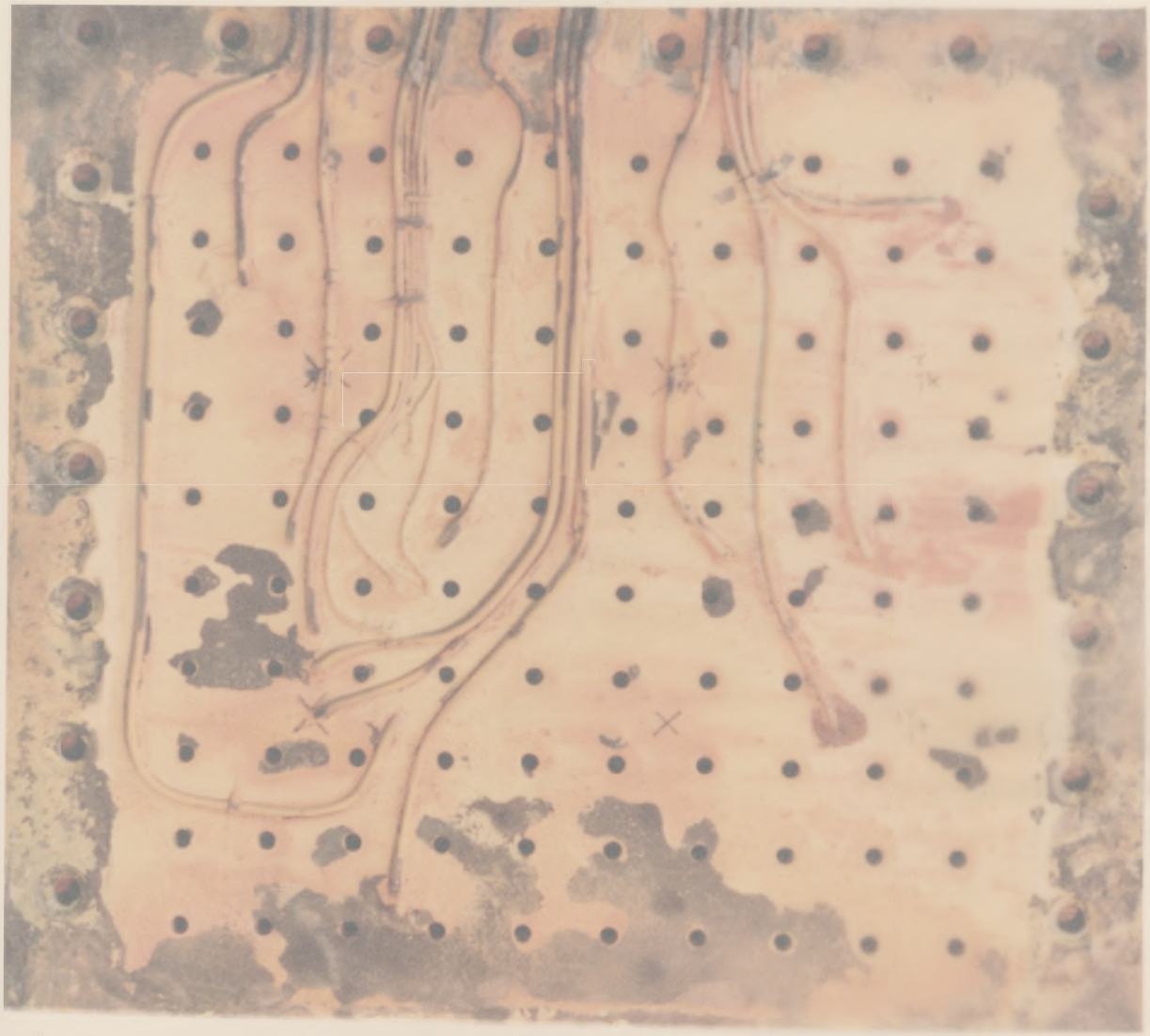

Plate (8.2): The 4306 m^{-2} holes, 0.1% $\Delta P/P$, effusion wall - thermal paint colour change at T_c = 673 K and T_g = 1859 K.

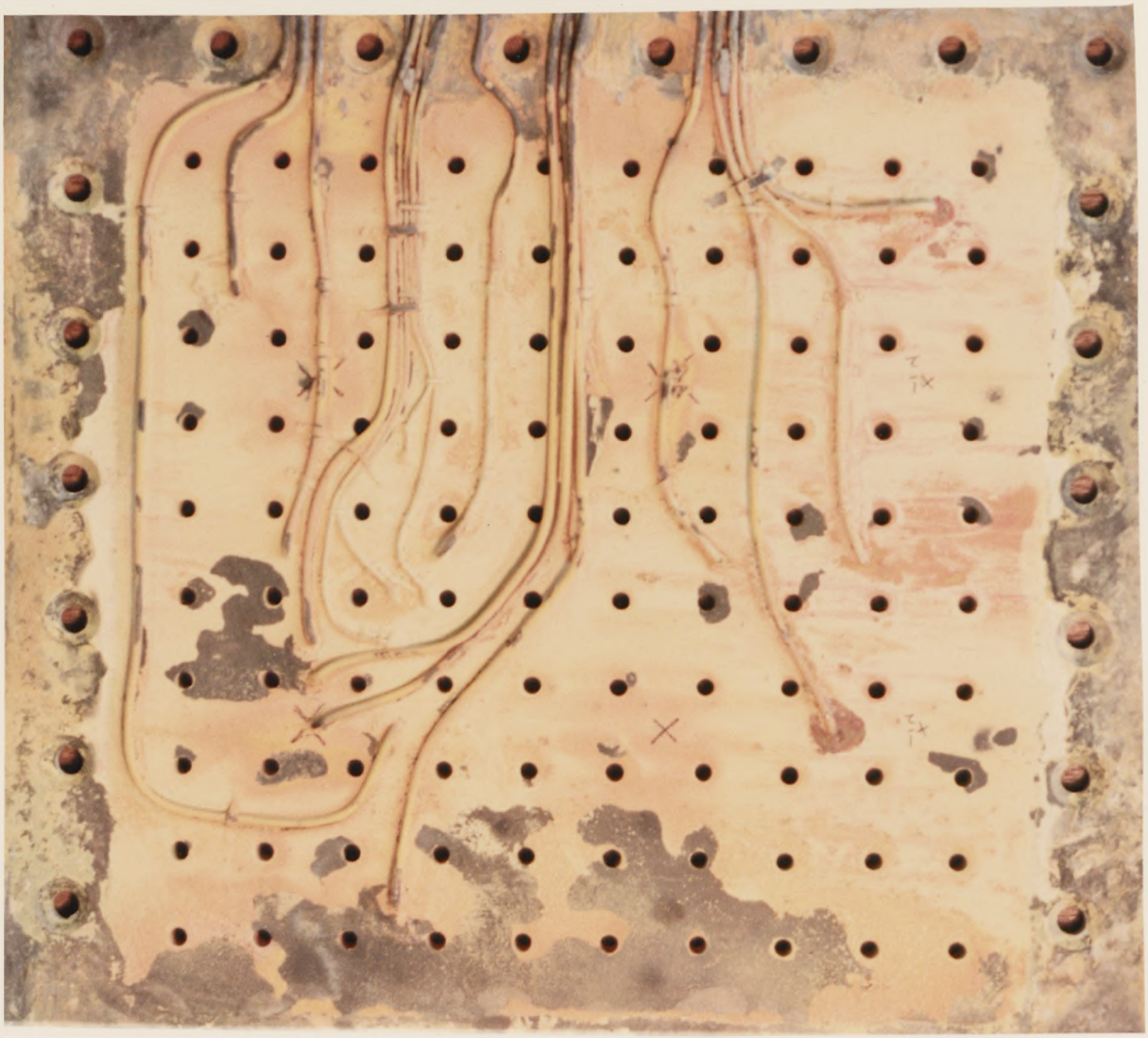

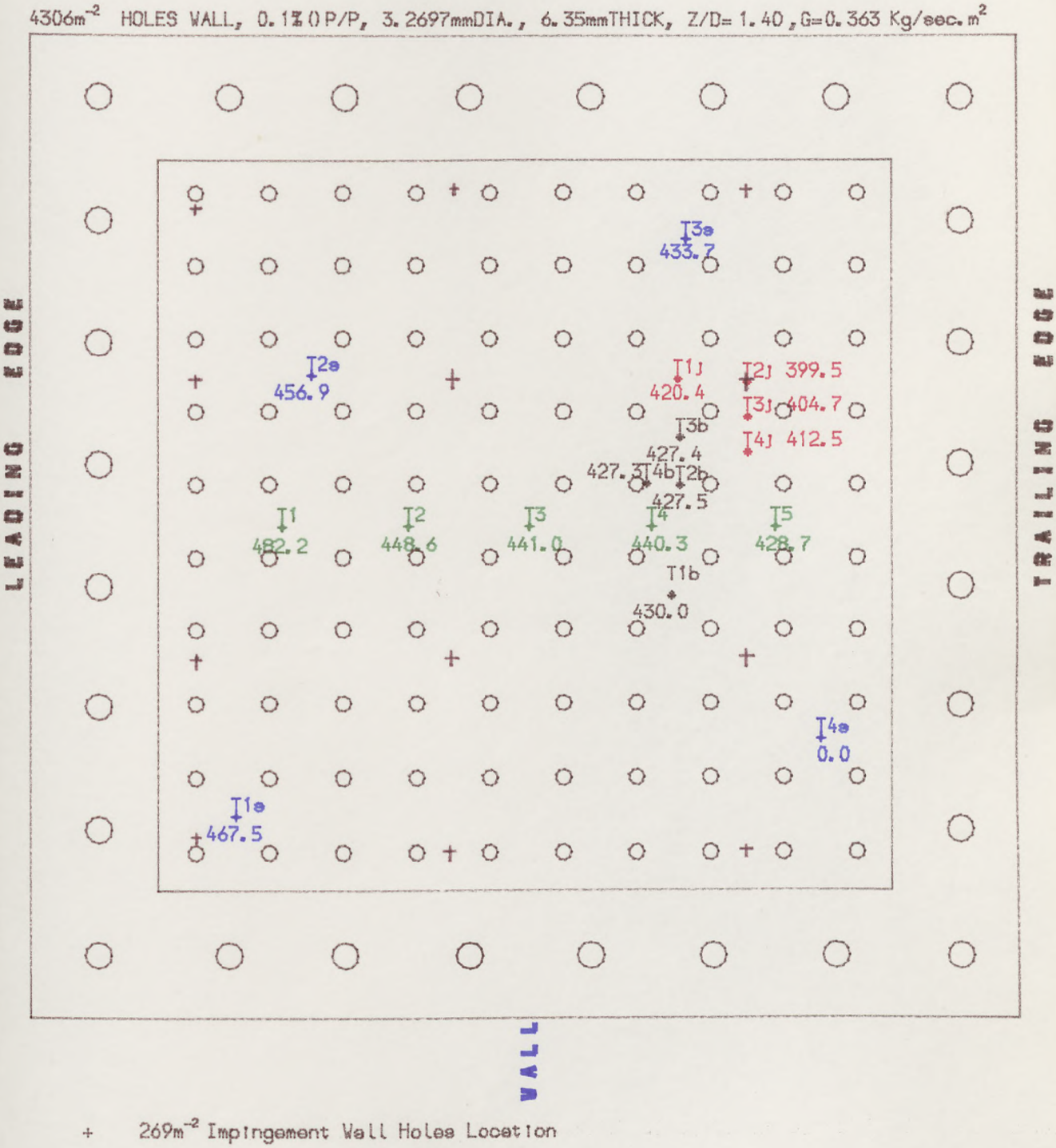

FIG. 8.1 ,30,1 IMP. WALL TEMP. DISTRIBUTION-(Z=8.0mm, Tc=293K, Tg=759K).
(269/4306-0.1% Impingement/Effusion system)

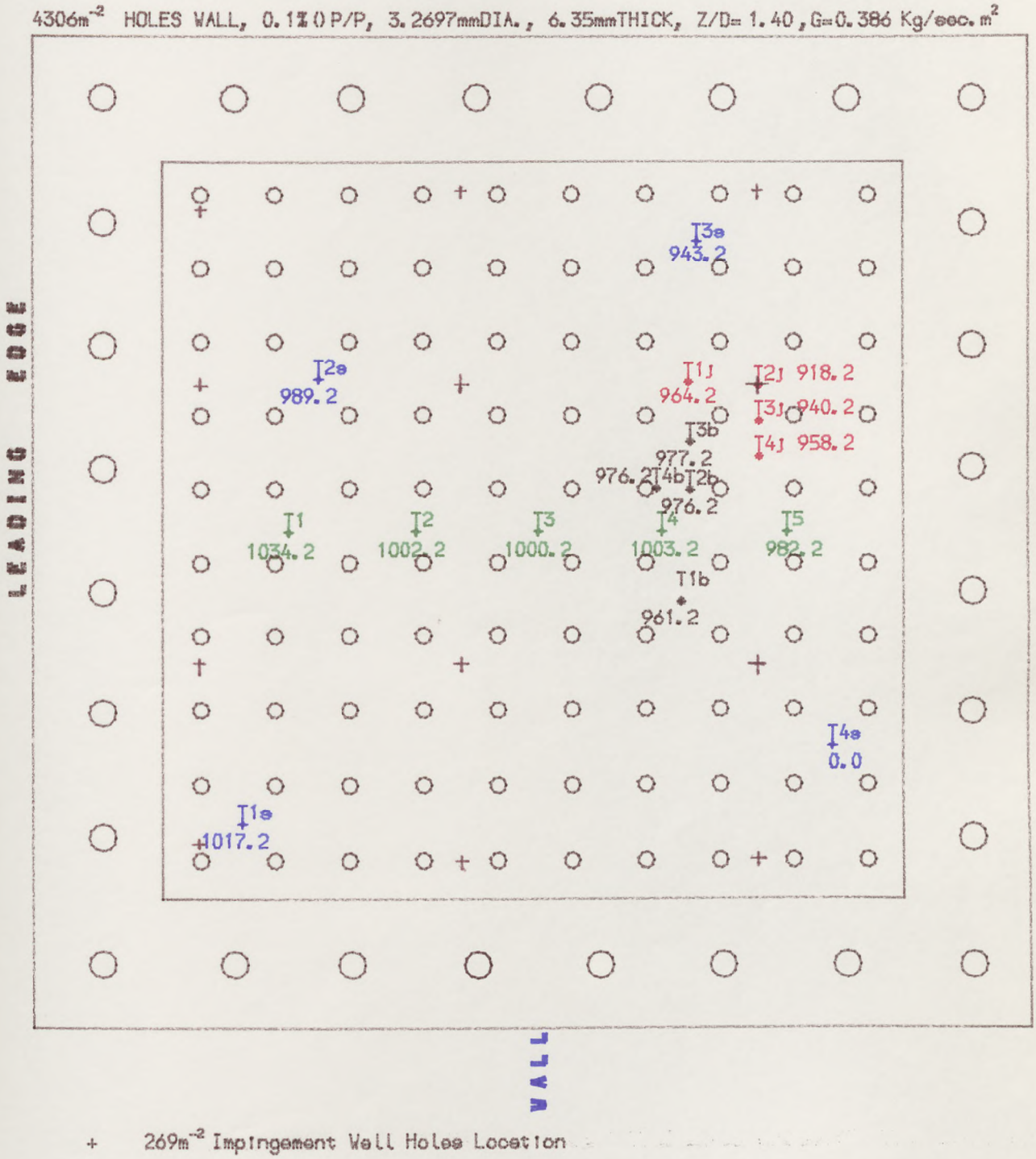

FIG. 8.2 ,30,1 IMP. WALL TEMP. DISTRIBUTION- (Z=8.0mm, Tc=673K, Tg=1859K)
(269/4306-0.1% Impingement/Effusion system)

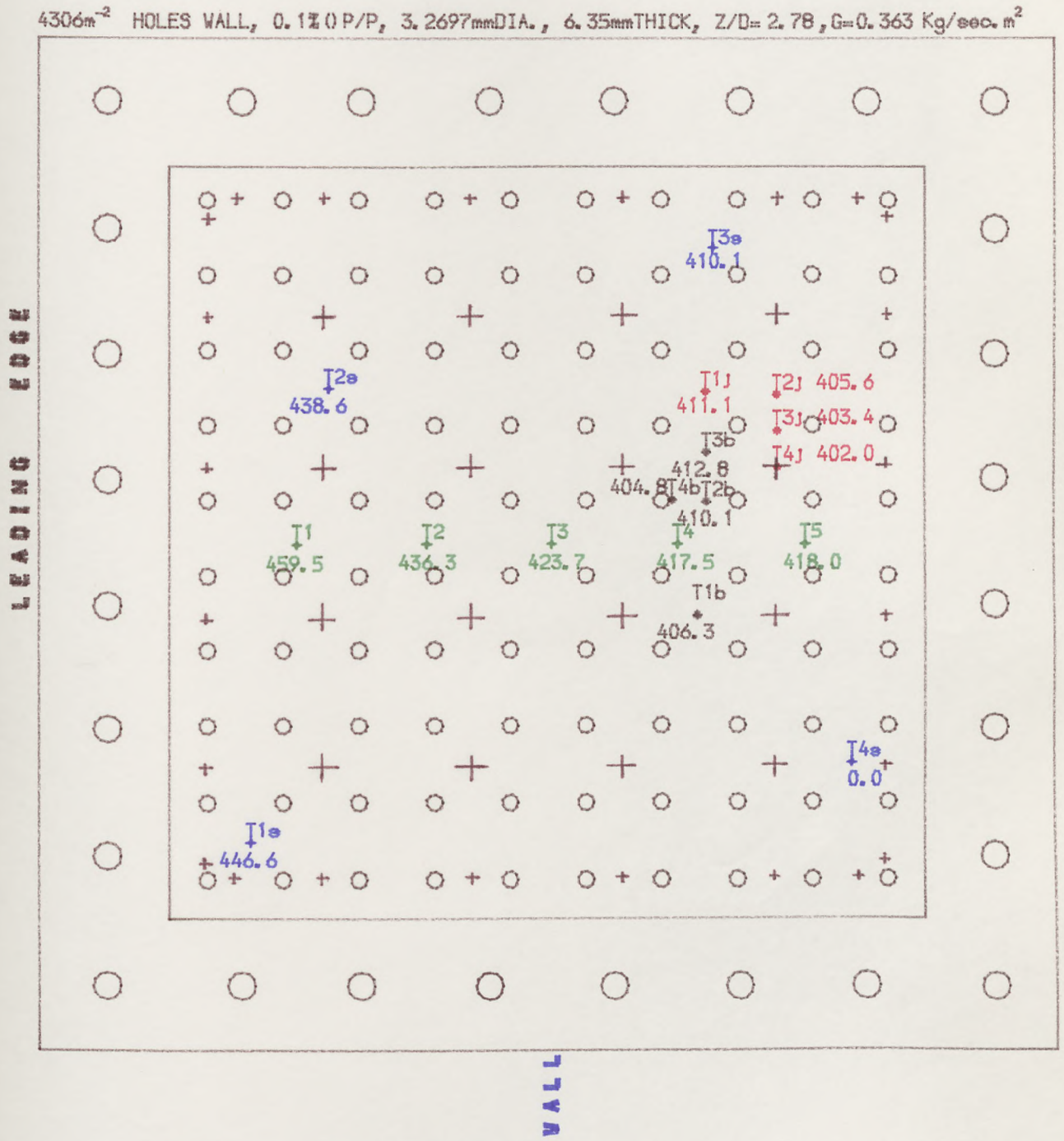

FIG. 8.3 ,30,1 IMP. WALL TEMP. DISTRIBUTION-(Z=8.0mm, Tc=296K, Tg=783K).
(1076/4306-0.1% Impingement/Effusion system)

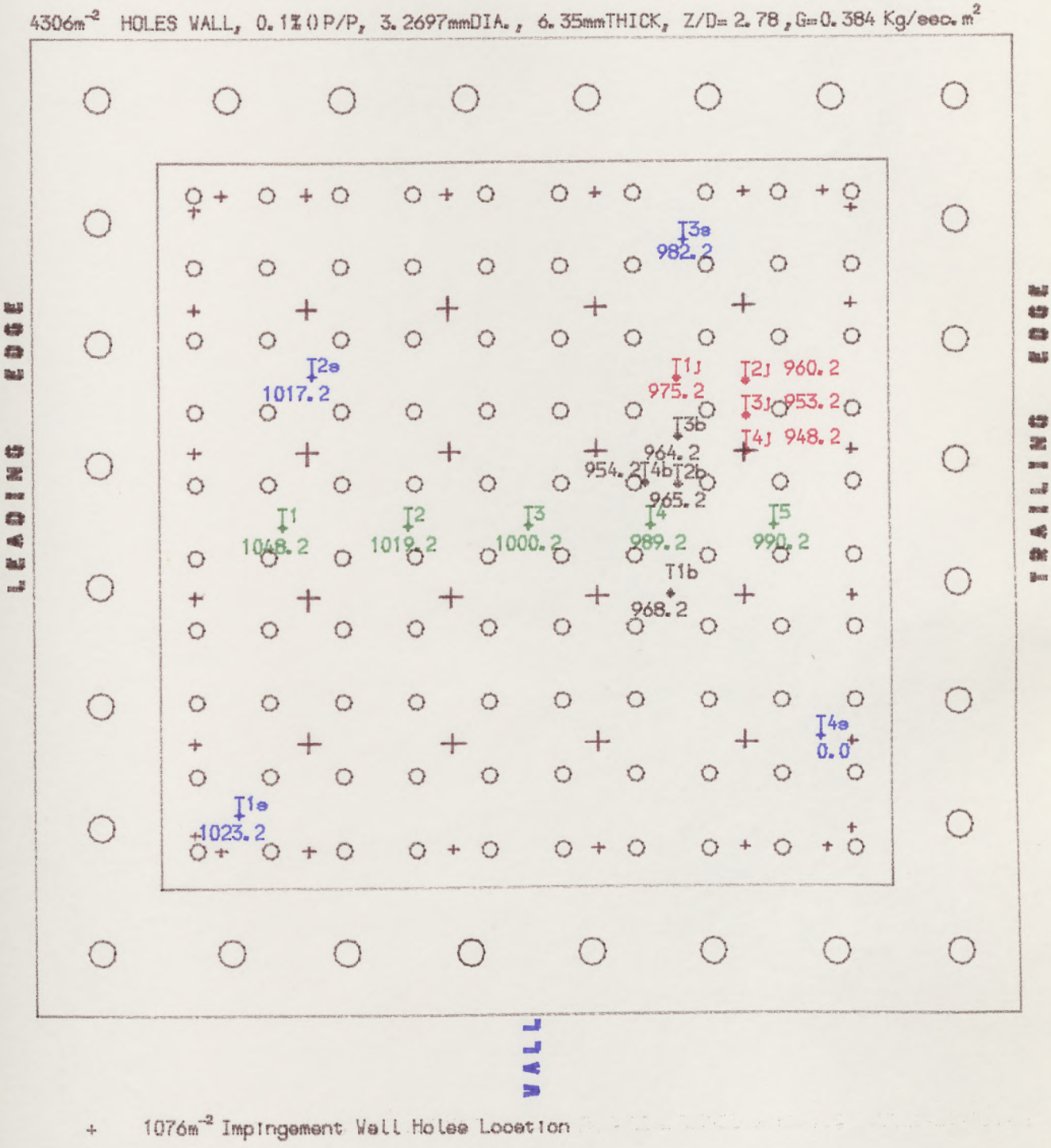

FIG. 8.4 ,30,1 IMP. WALL TEMP. DISTRIBUTION-(Z=8.0mm, Tc=643K, Tg=1762K)
(1076/4306-0.1% Impingement/Effusion system)

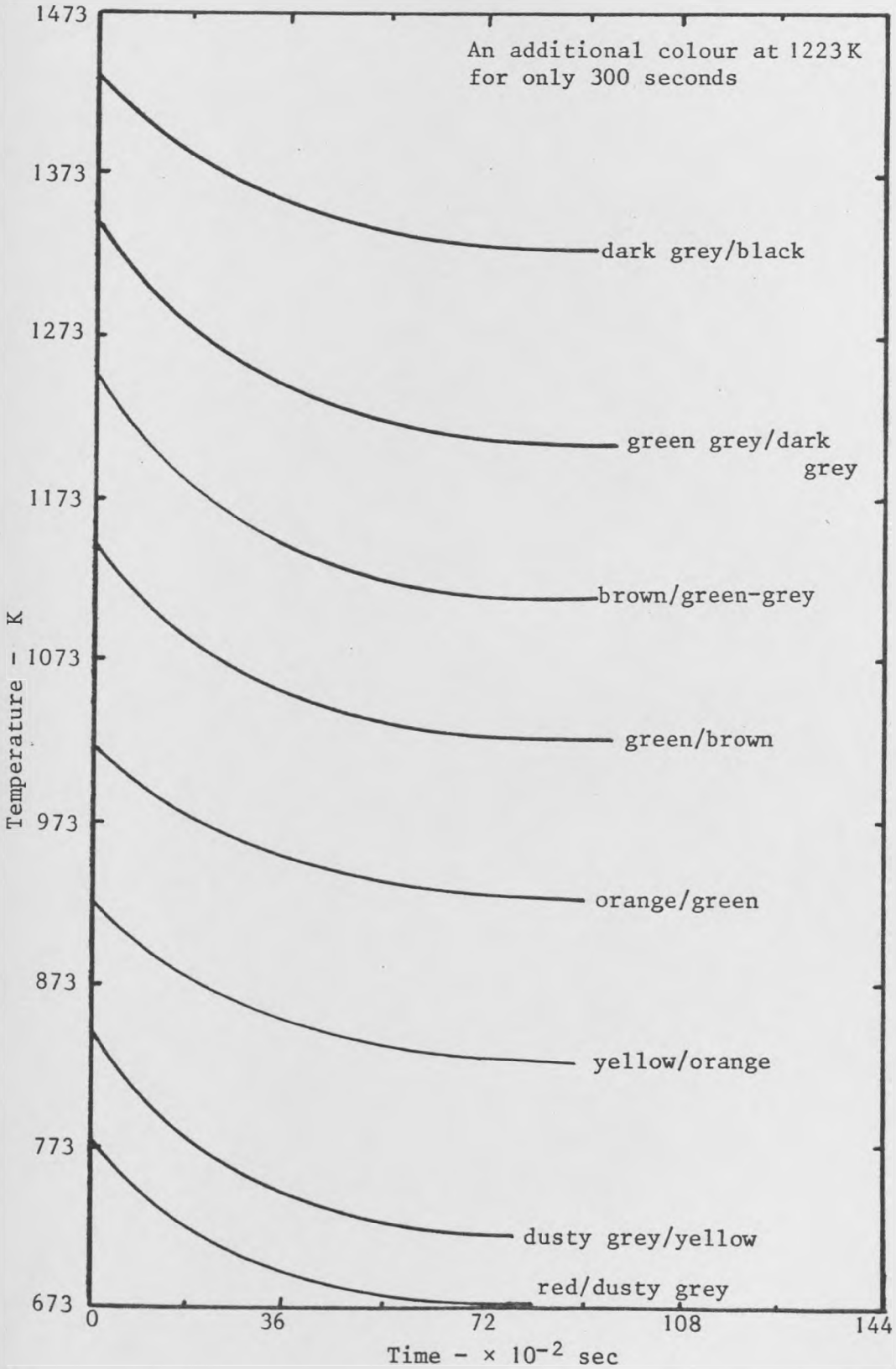

Fig. 8.5: Thermal paint temperature change chart (after Ref. 3)

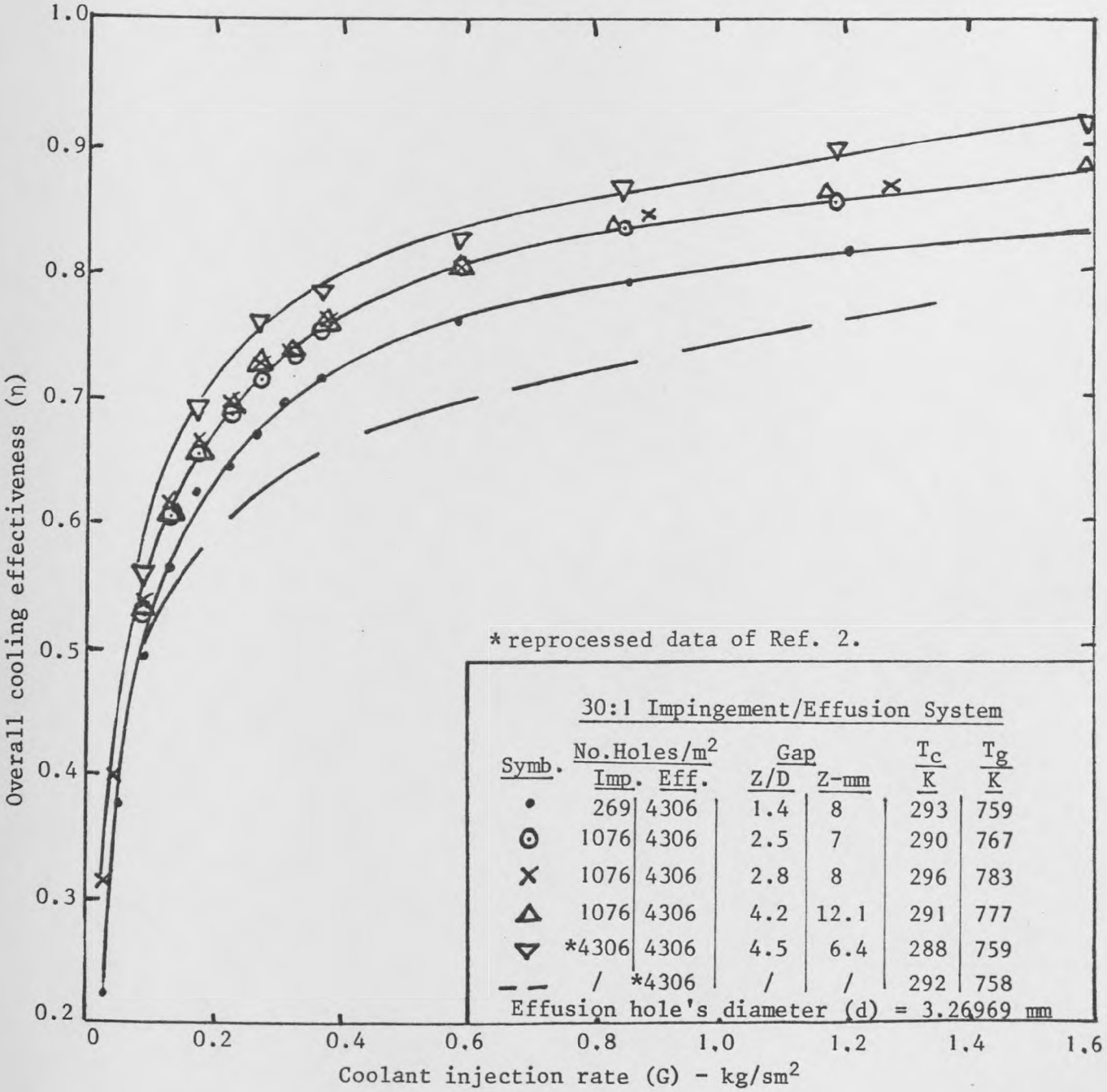

Symb.	No.Holes/m² Imp.	No.Holes/m² Eff.	Gap Z/D	Gap Z-mm	T_c K	T_g K
•	269	4306	1.4	8	293	759
⊙	1076	4306	2.5	7	290	767
×	1076	4306	2.8	8	296	783
△	1076	4306	4.2	12.1	291	777
▽	*4306	4306	4.5	6.4	288	759
– –	/	*4306	/	/	292	758

Fig. 8.6: Development of overall cooling effectiveness with coolant mass injection at station 5.

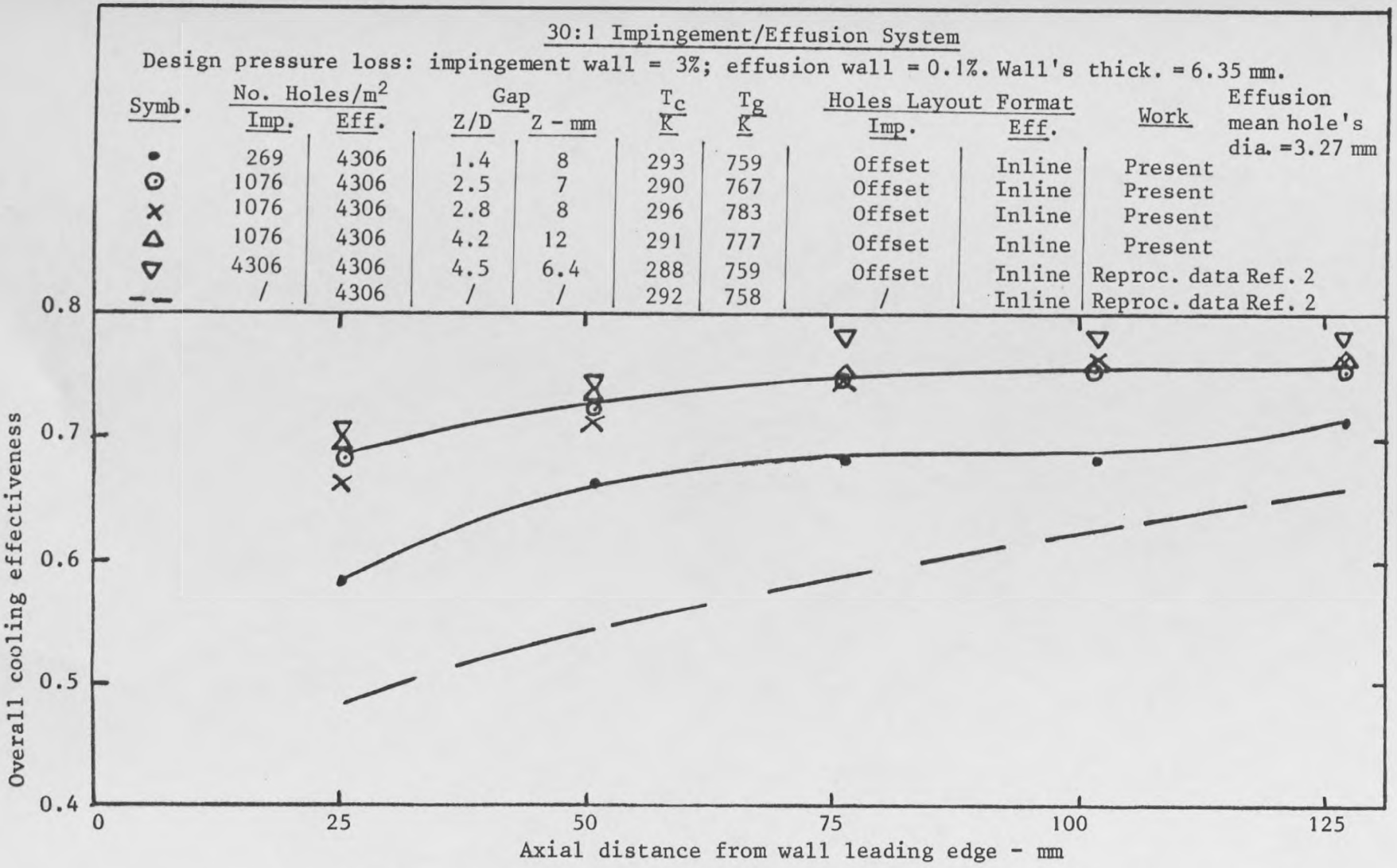

Symb.	No. Holes/m² Imp.	No. Holes/m² Eff.	Gap Z/D	Gap Z - mm	T_c K	T_g K	Holes Layout Format Imp.	Holes Layout Format Eff.	Work
•	269	4306	1.4	8	293	759	Offset	Inline	Present
⊙	1076	4306	2.5	7	290	767	Offset	Inline	Present
×	1076	4306	2.8	8	296	783	Offset	Inline	Present
△	1076	4306	4.2	12	291	777	Offset	Inline	Present
▽	4306	4306	4.5	6.4	288	759	Offset	Inline	Reproc. data Ref. 2
— —	/	4306	/	/	292	758	/	Inline	Reproc. data Ref. 2

Fig. 8.7: Axial profile of overall cooling effectiveness at coolant mass flow injection of $0.32 \leqslant G \leqslant 0.39$

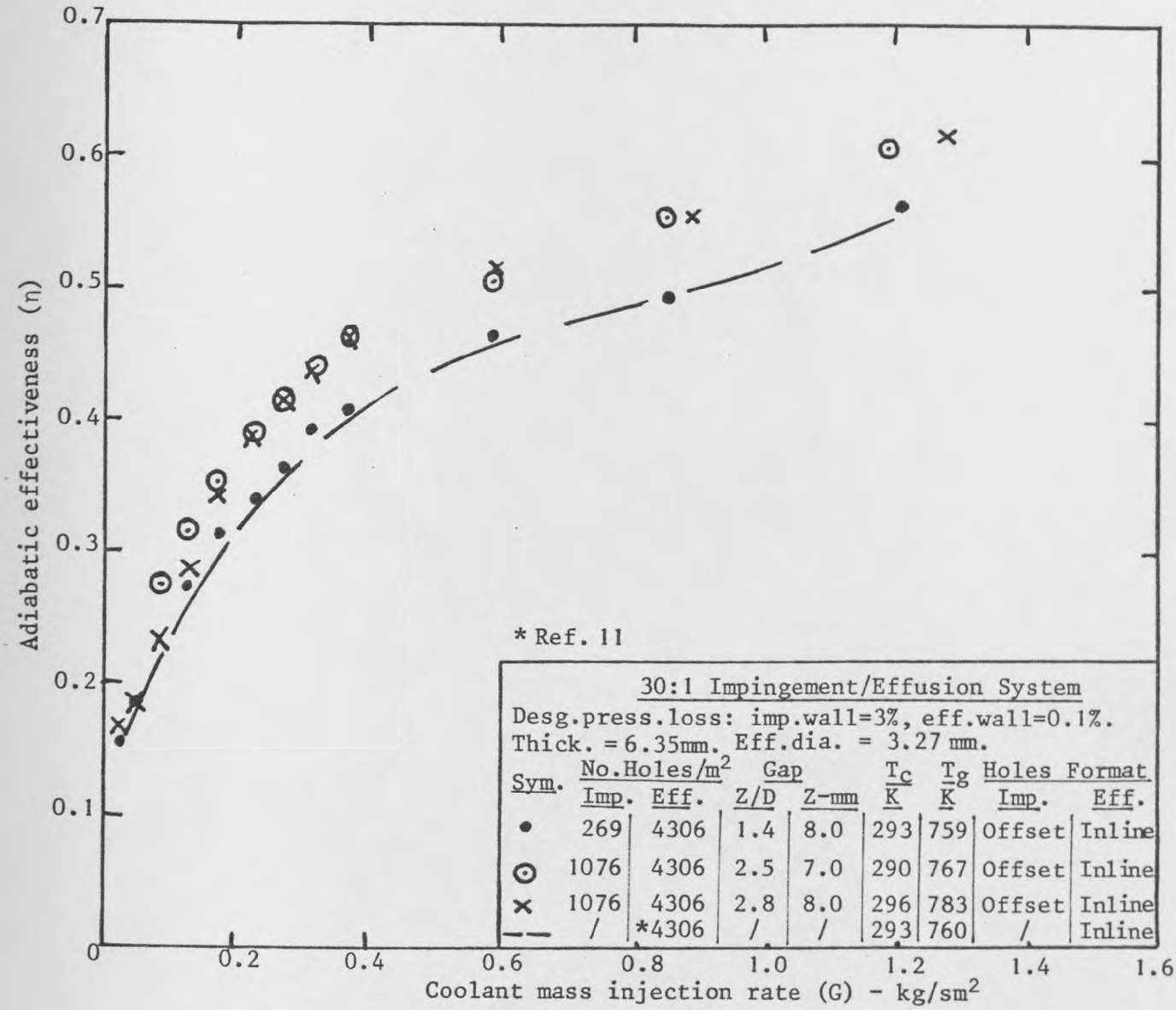

Fig. 8.8: Development of adiabatic cooling effectiveness with coolant injection at thermal station 5

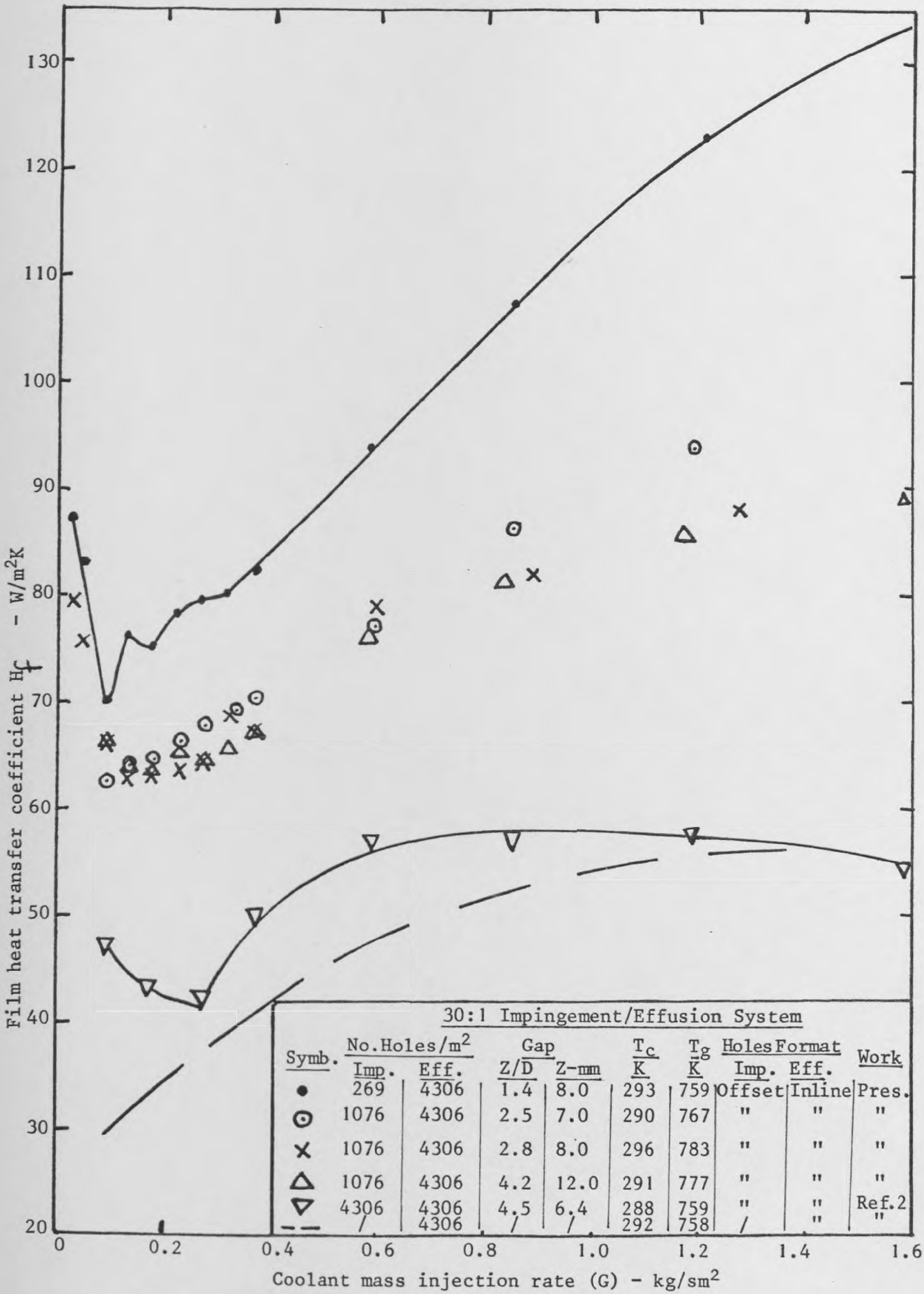

Fig. 8.9: Development of film heat transfer coefficient with coolant injection at thermal station 5

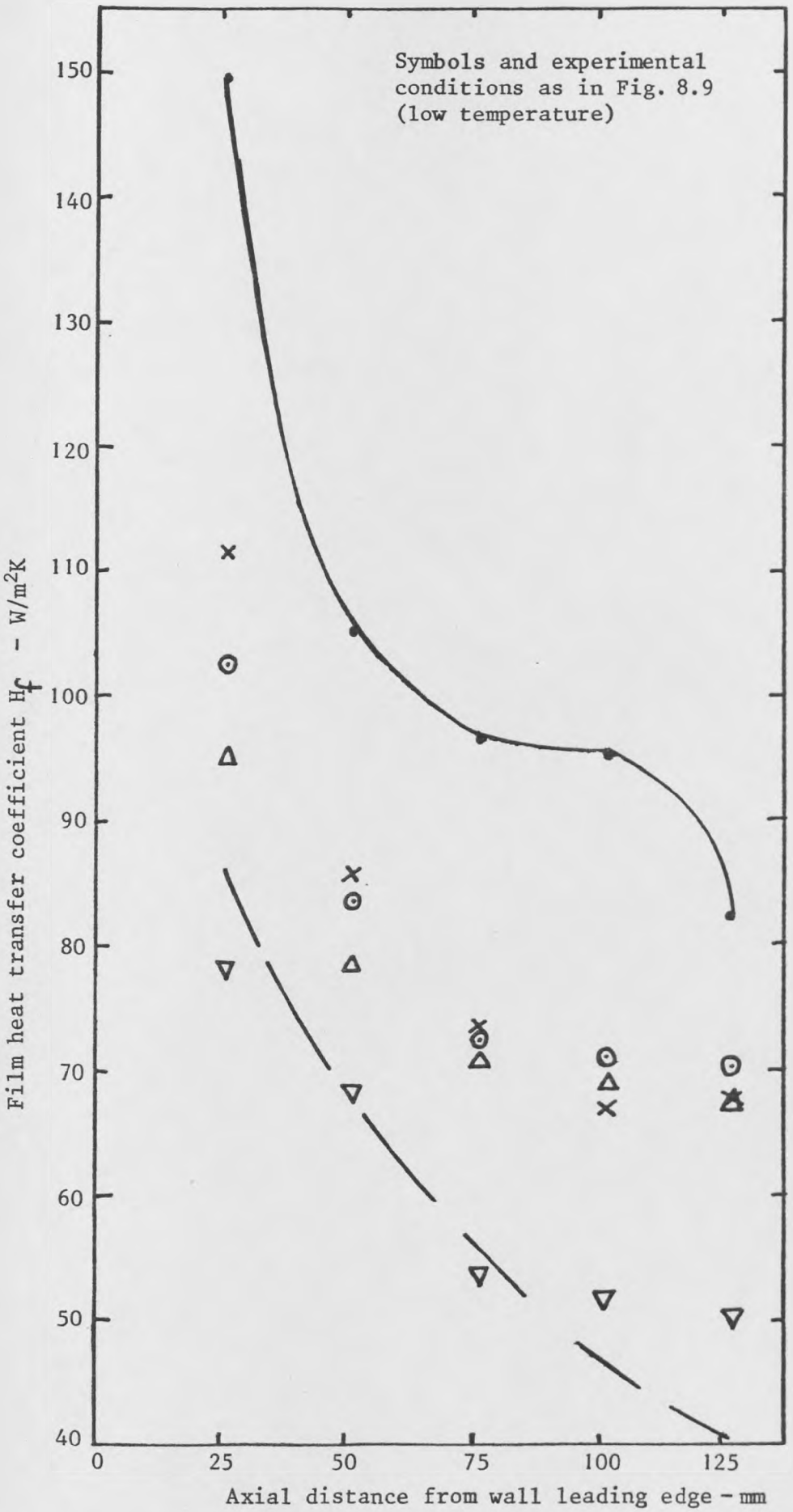

Fig. 8.10: Axial profile of film heat transfer coefficient at coolant mass injection of $0.32 \leqslant G \leqslant 0.39$

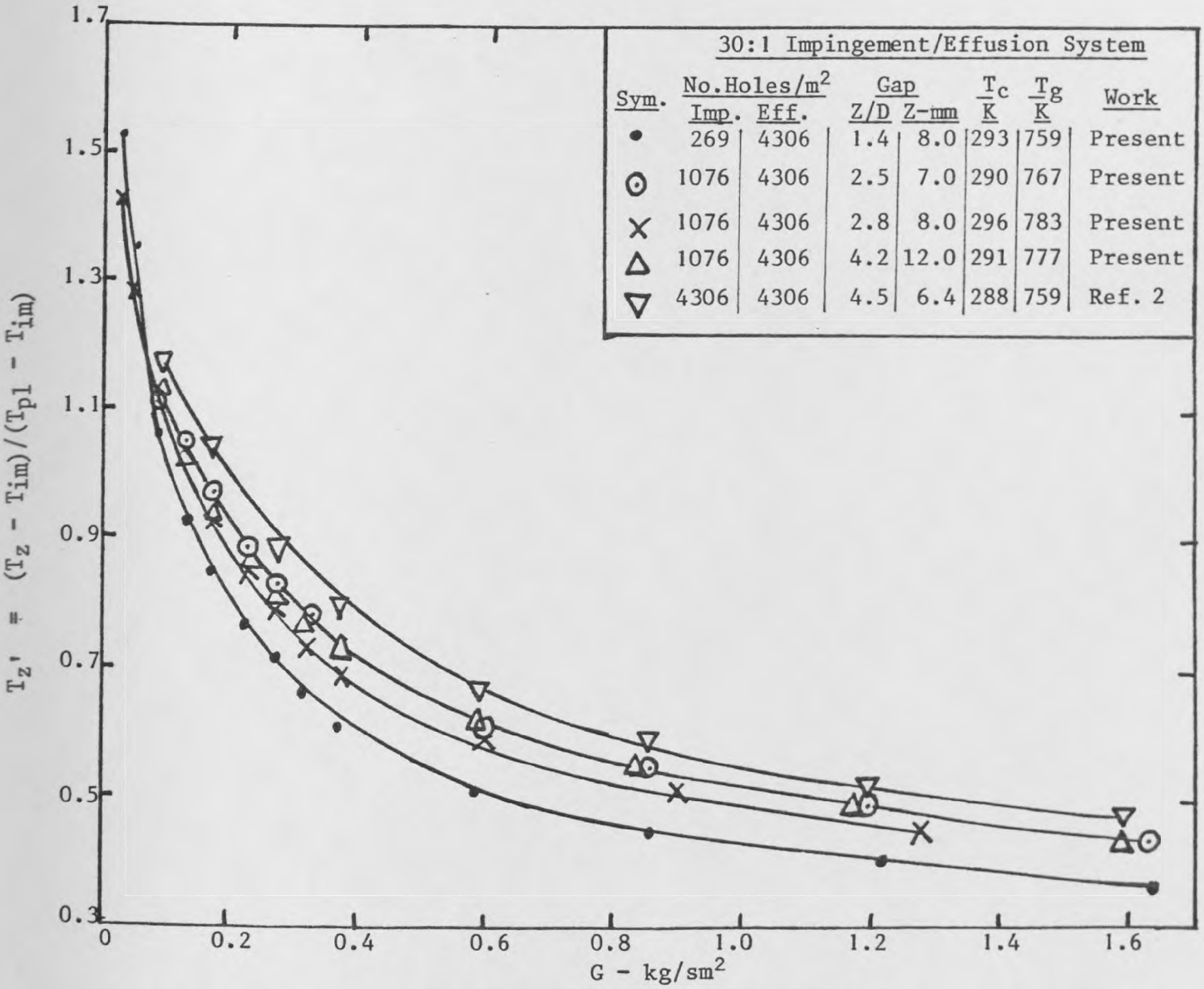

Fig. 8.11: Impingement wall heating as a function of coolant mass injection

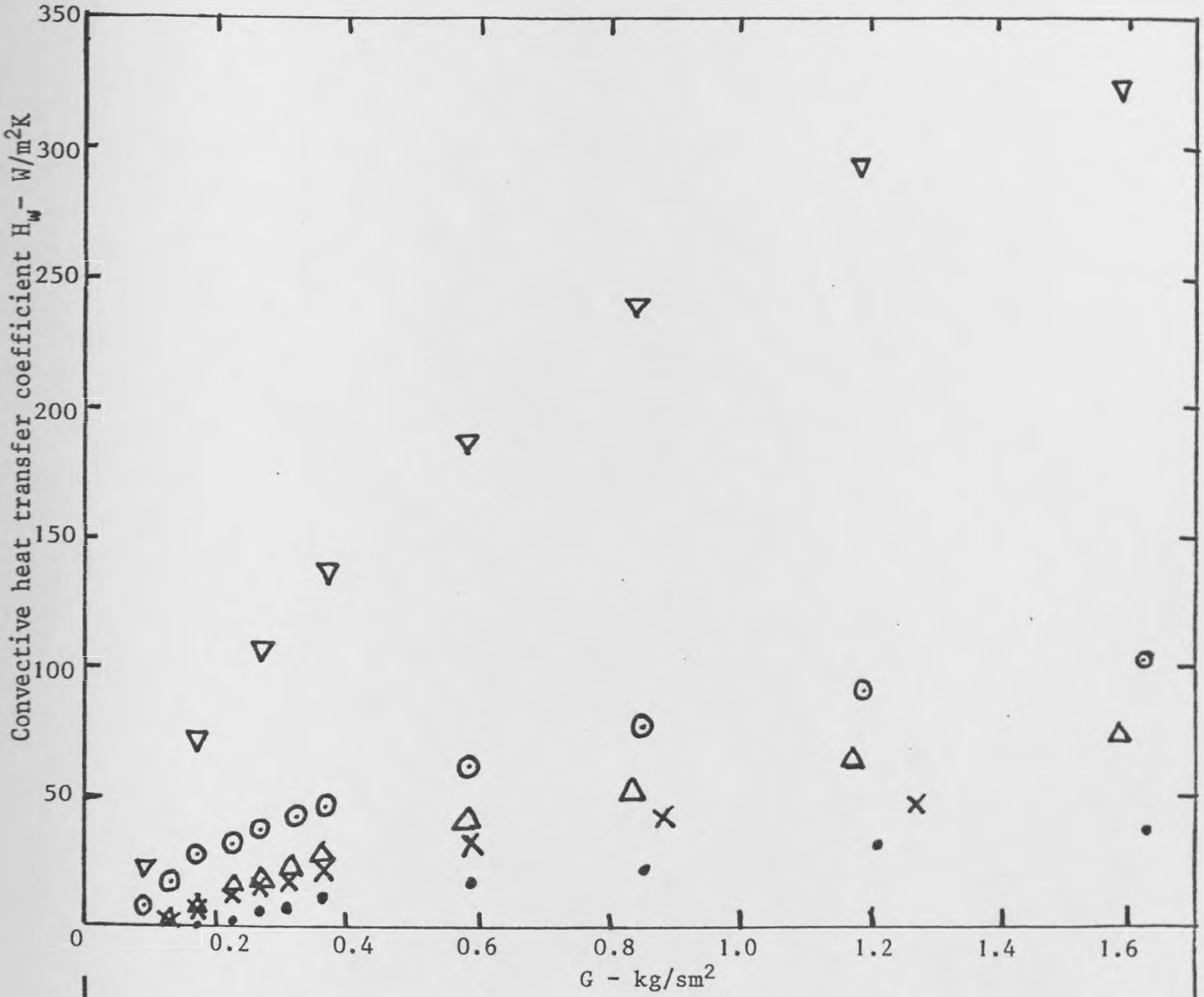

30:1 Impingement/Effusion System

Design pressure loss: impingement = 3.0%, effusion = 0.1%; thick. = 6.35 mm; effusion mean holes dia. = 3.27 mm.

Sym.	No.Holes/m^2 Imp.	No.Holes/m^2 Eff.	Gap Z/D	Gap Z-mm	T_c K	T_g K	Holes Layout Format Imp.	Holes Layout Format Eff.	Work
•	269	4306	1.4	8.0	293	759	Offset	Inline	Present
⊙	1076	4306	2.5	7.0	290	767	Offset	Inline	Present
×	1076	4306	2.8	8.0	296	783	Offset	Inline	Present
△	1076	4306	4.2	12.0	291	777	Offset	Inline	Present
▽	4306	4306	4.5	6.4	288	759	Offset	Inline	Reprocessed data Ref. 2

Fig. 8.12: Convective heat transfer coefficient at the inner surface of impingement wall as a function of coolant mass injection

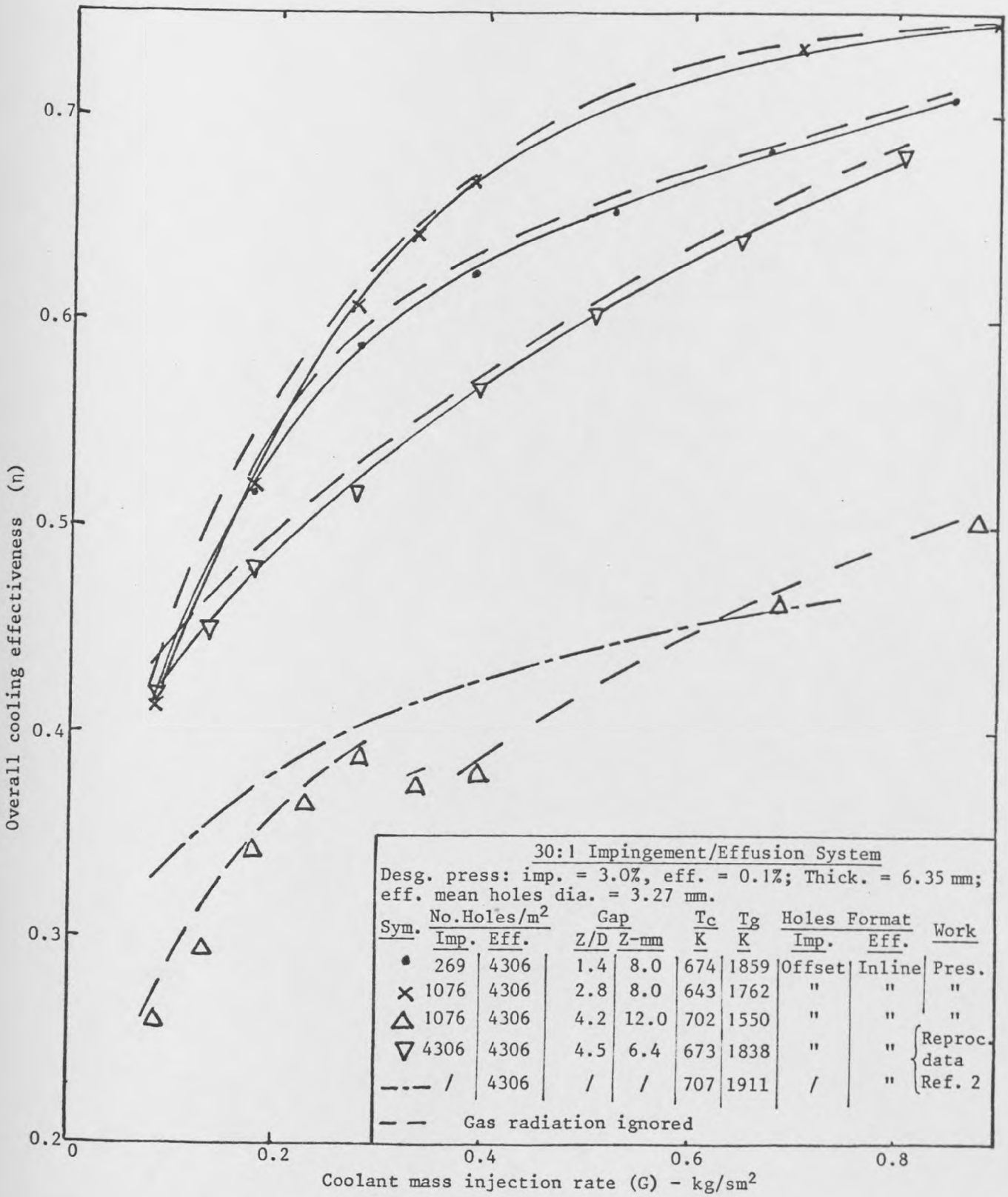

Fig. 8.13: Development of overall cooling effectiveness with coolant injection at thermal station 5

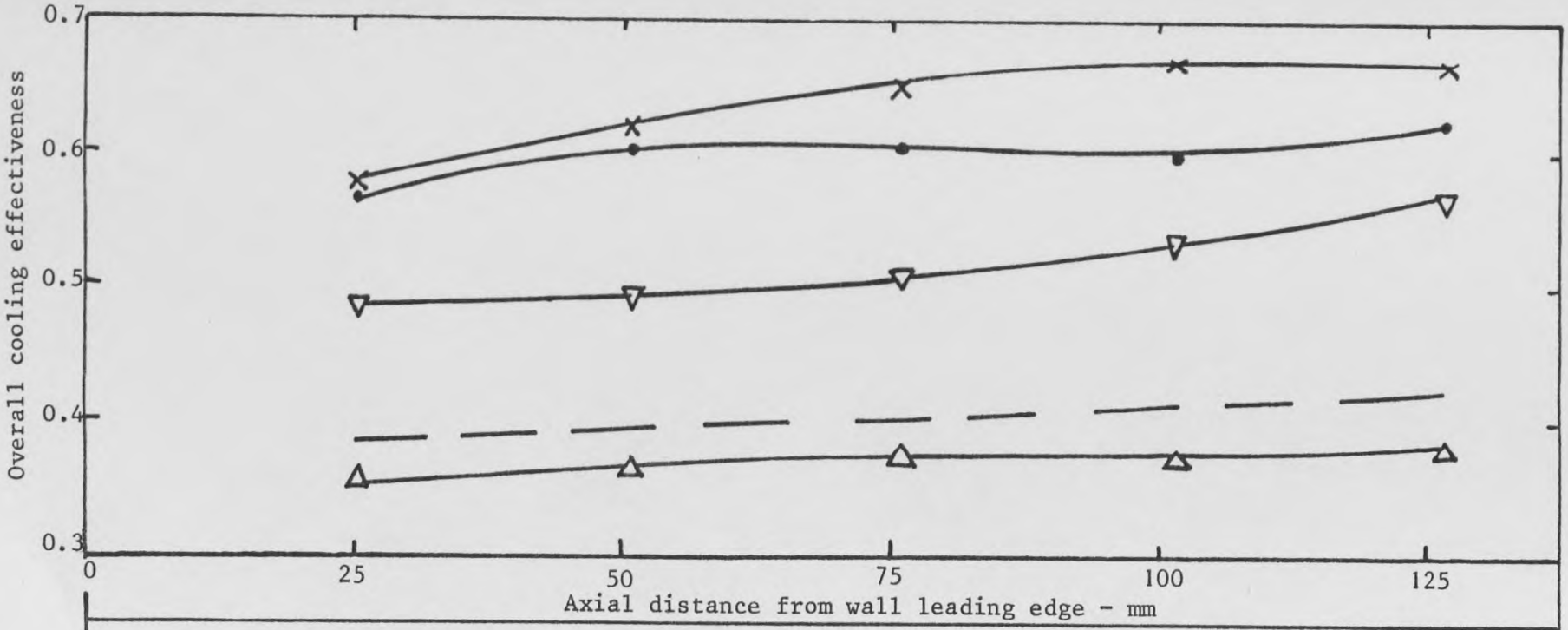

30:1 Impingement/Effusion System

Design pressure loss: imp. = 3.0%, eff. = 0.1%; wall thickness = 6.35 mm; eff. mean holes dia. = 3.27 mm.

Sym.	No.Holes/m^2 Imp.	No.Holes/m^2 Eff.	Gap Z/D	Gap Z-mm	T_c K	T_g K	Holes Format Imp.	Holes Format Eff.	Work Origin
●	269	4306	1.4	8.0	674	1859	Offset	Inline	Present
×	1076	4306	2.8	8.0	643	1762	Offset	Inline	Present
△	1076	4306	4.2	12.0	702	1550	Offset	Inline	Present
▽	4306	4306	4.5	6.4	673	1838	Offset	Inline	Reprocessed data Ref. 2
– –	/	4306	/	/	707	1911	/	Inline	Reprocessed data Ref. 2

Fig. 8.14: Axial profile of overall cooling effectiveness at $0.382 \leqslant G \leqslant 0.394$

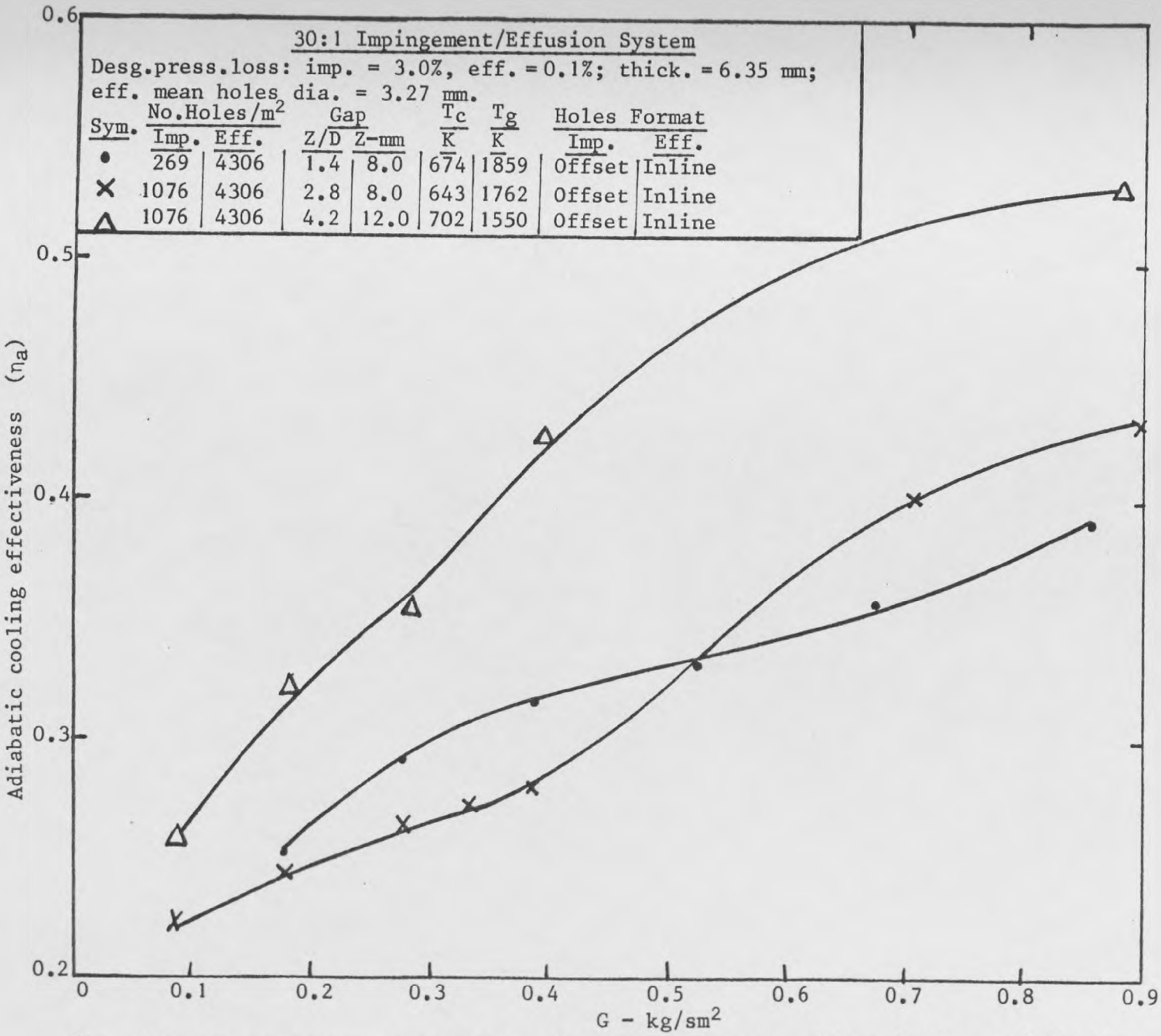

Fig. 8.15: Development of adiabatic cooling effectiveness with coolant mass injection

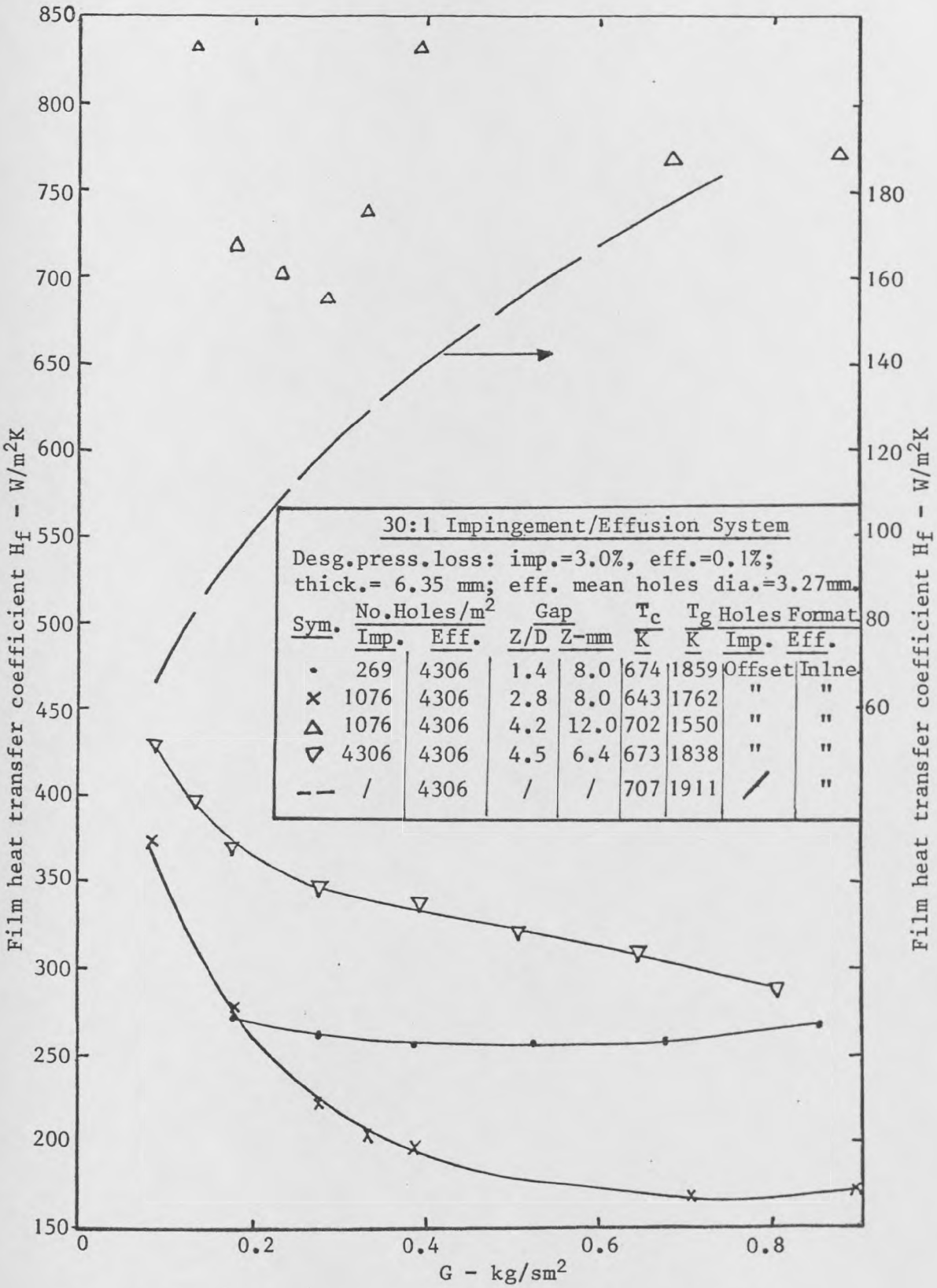

Sym.	No.Holes/m^2 Imp.	Eff.	Gap Z/D	Z-mm	T_c K	T_g K	Holes Format Imp.	Eff.
•	269	4306	1.4	8.0	674	1859	Offset	Inlne.
×	1076	4306	2.8	8.0	643	1762	"	"
△	1076	4306	4.2	12.0	702	1550	"	"
▽	4306	4306	4.5	6.4	673	1838	"	"
— —	/	4306	/	/	707	1911	/	"

Fig. 8.16: Dependency of film heat transfer coefficient on G

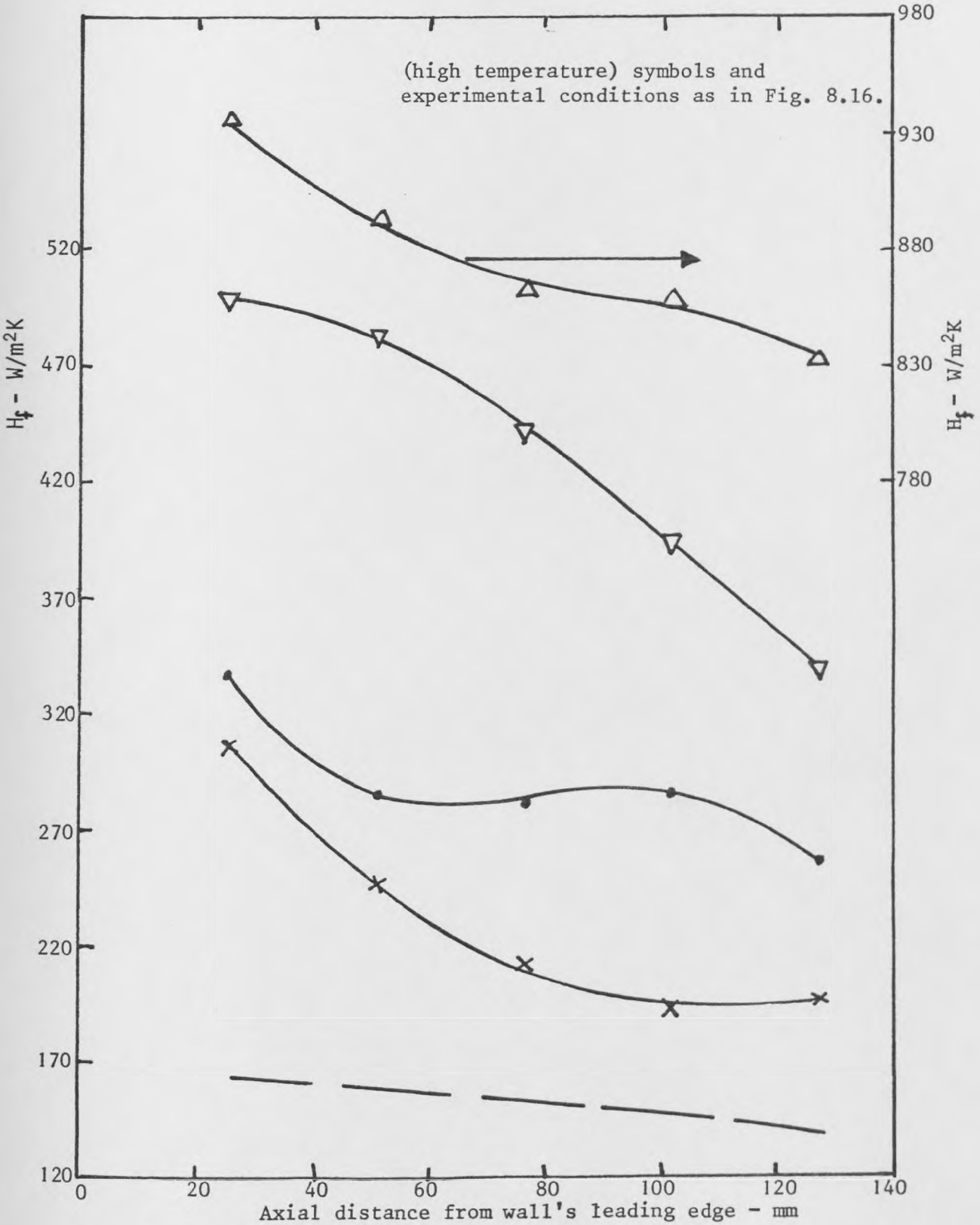

Fig. 8.17: Film heat transfer coefficient axial profiles at $0.382 \leqslant G$ - kg/sm^2 $\leqslant 0.394$

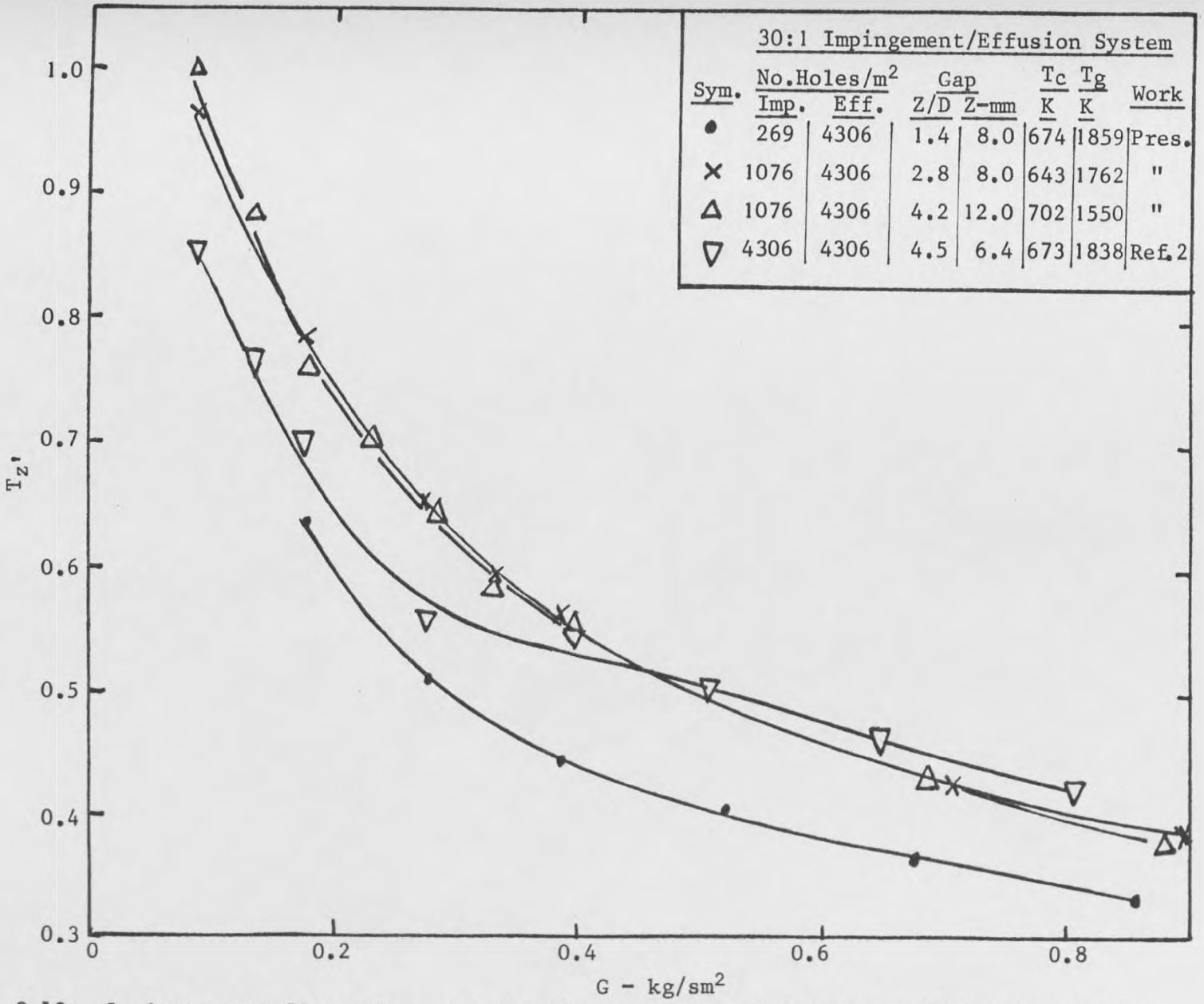

Fig. 8.18: Impingement wall heating as a function of coolant injection at high temperature.

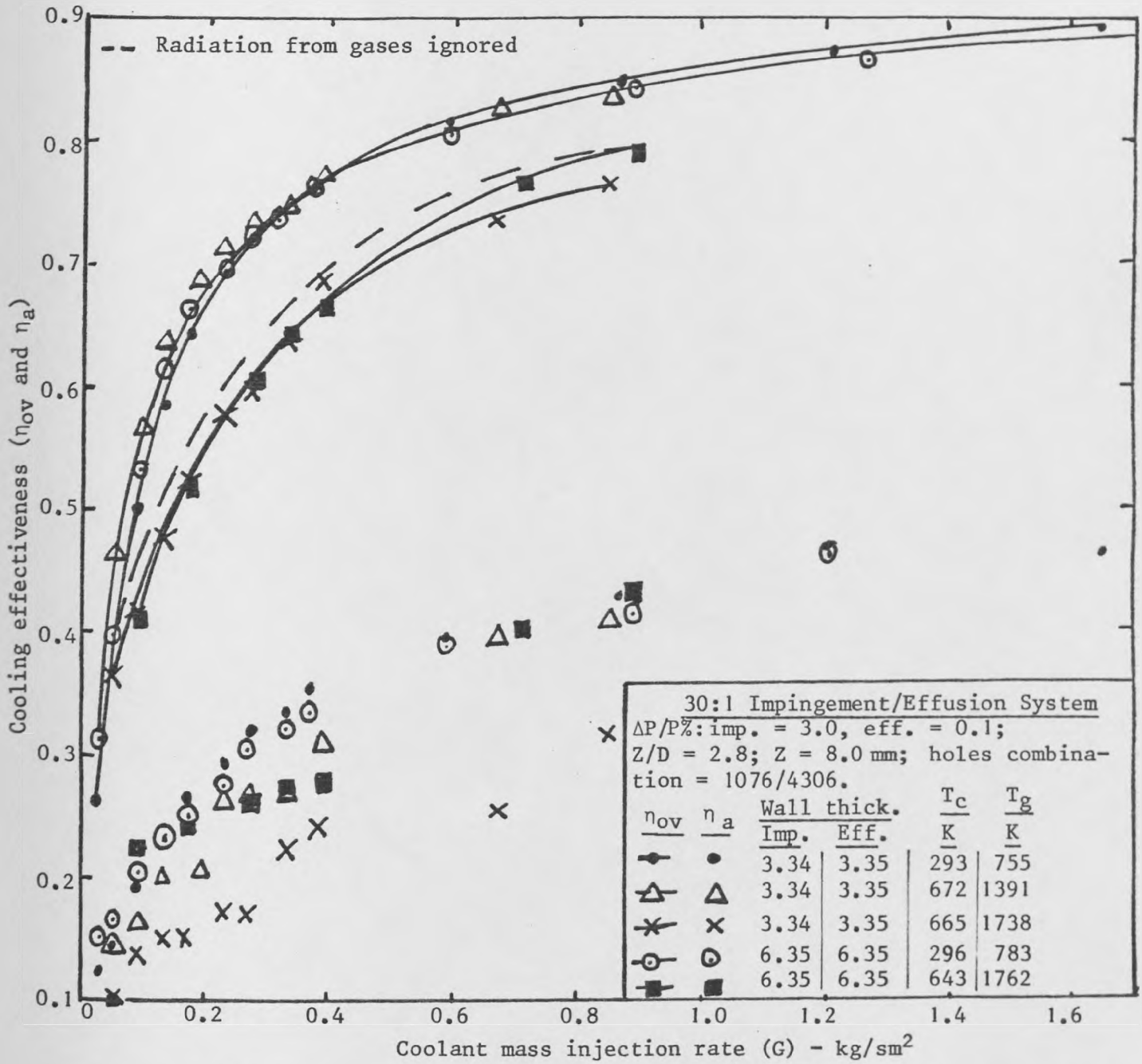

Fig. 8.19: Dependency of cooling effectiveness on coolant mass injection (G)

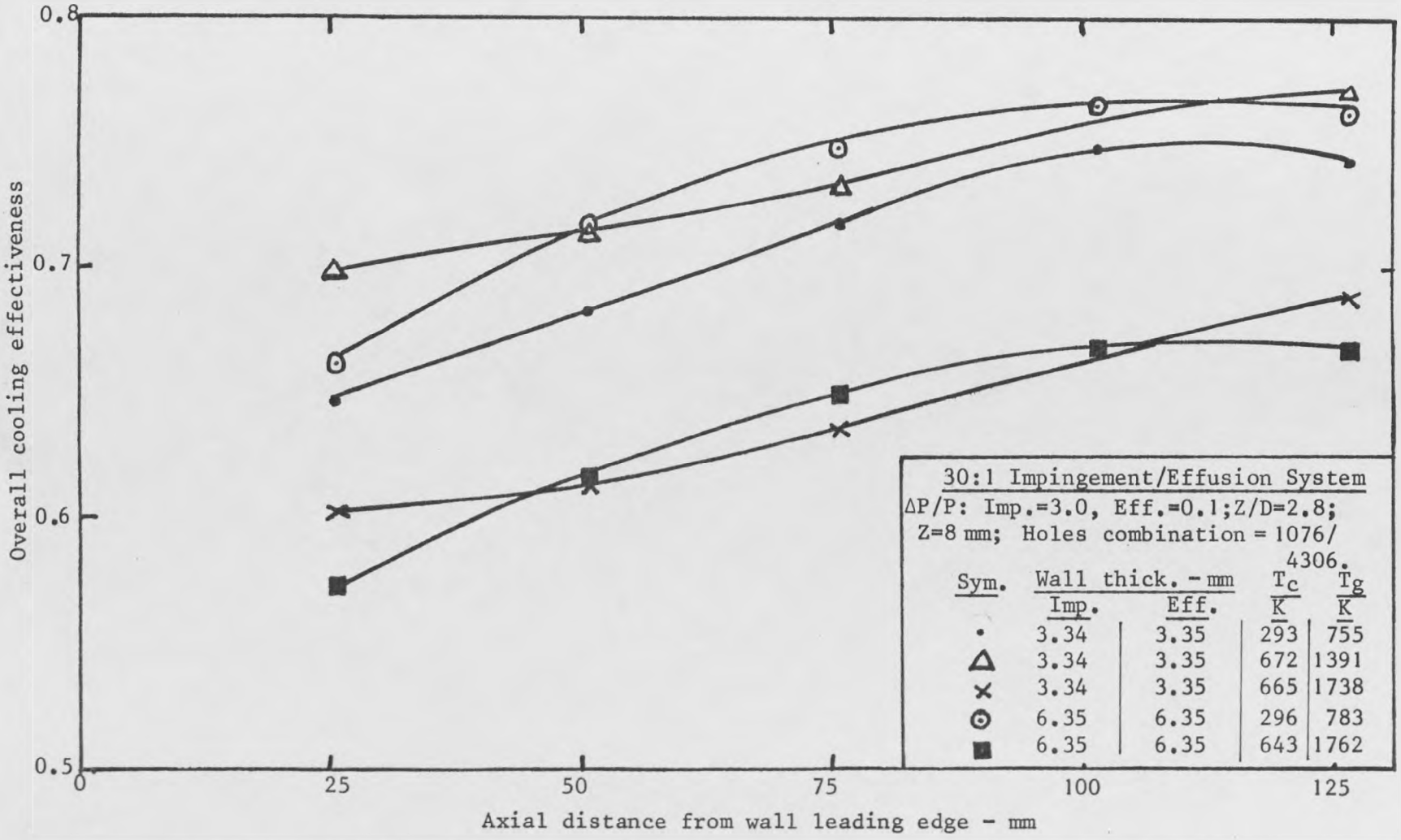

Fig. 8.20: Axial profile of overall cooling effectiveness at $0.365 \leqslant G \leqslant 0.387$

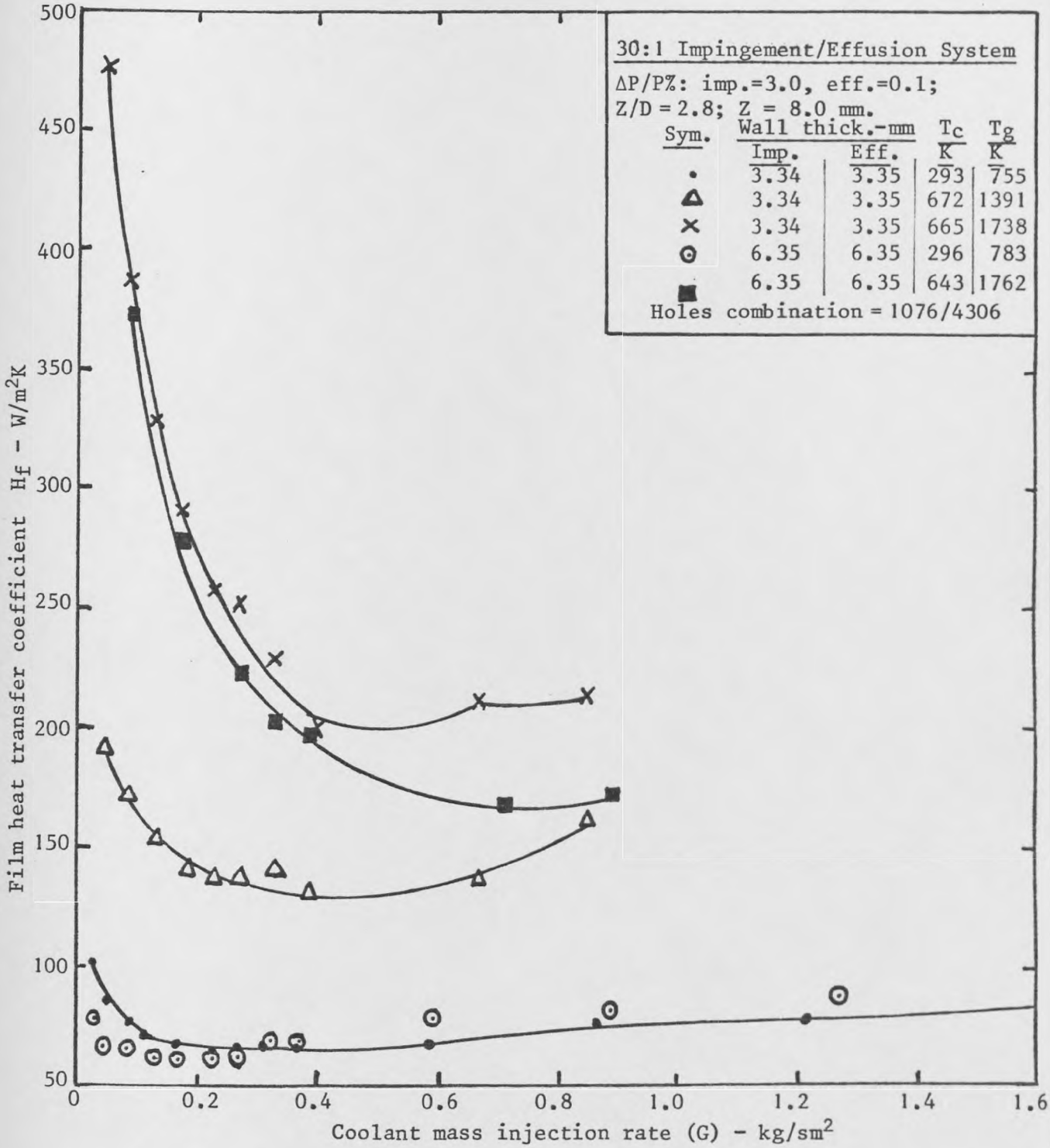

Fig. 8.21: Development of film heat transfer coefficient with coolant injection (G)

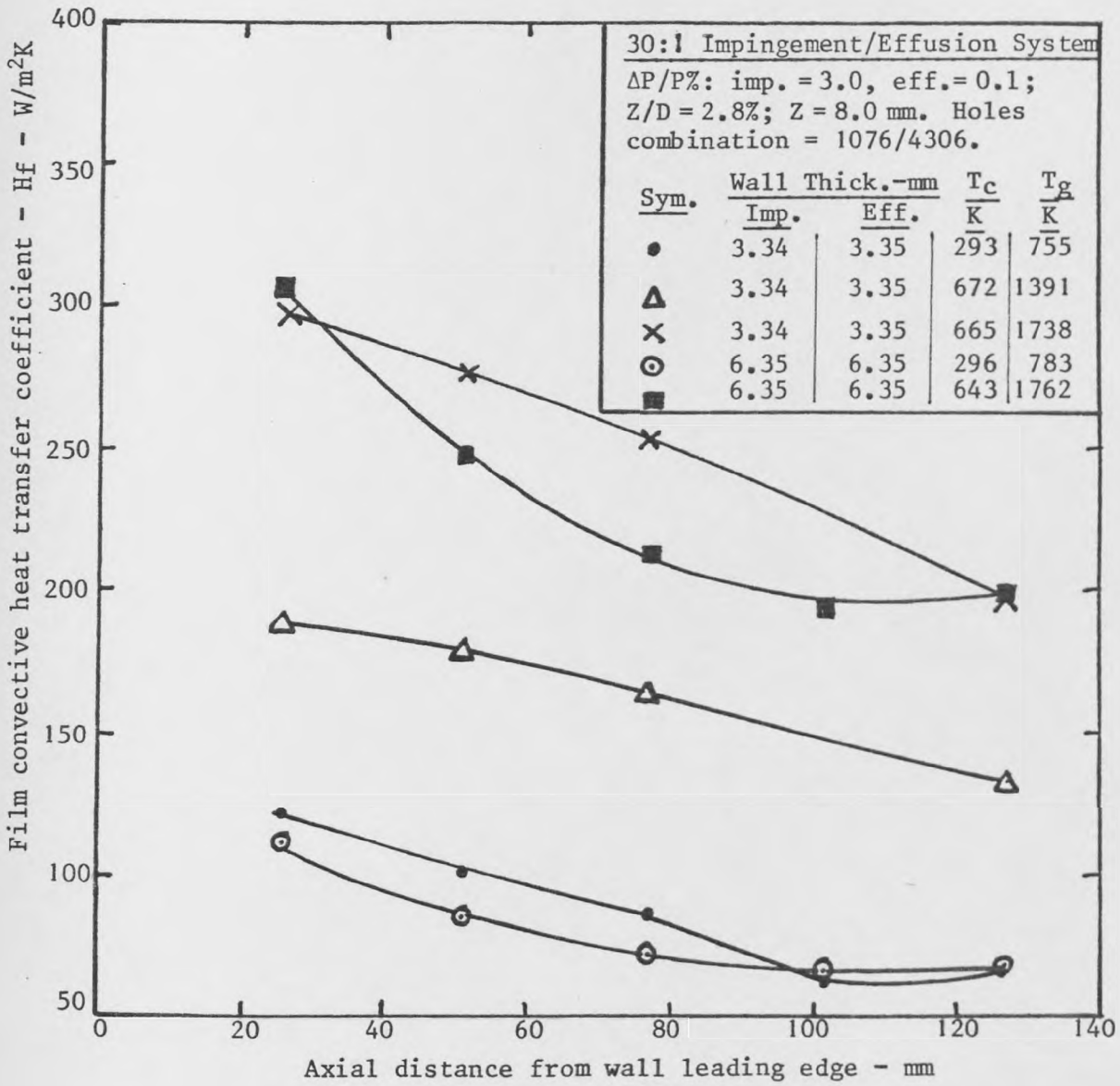

Fig. 8.22: Axial profile of film convective heat transfer coefficient at $0.365 \leq G \leq 0.387$

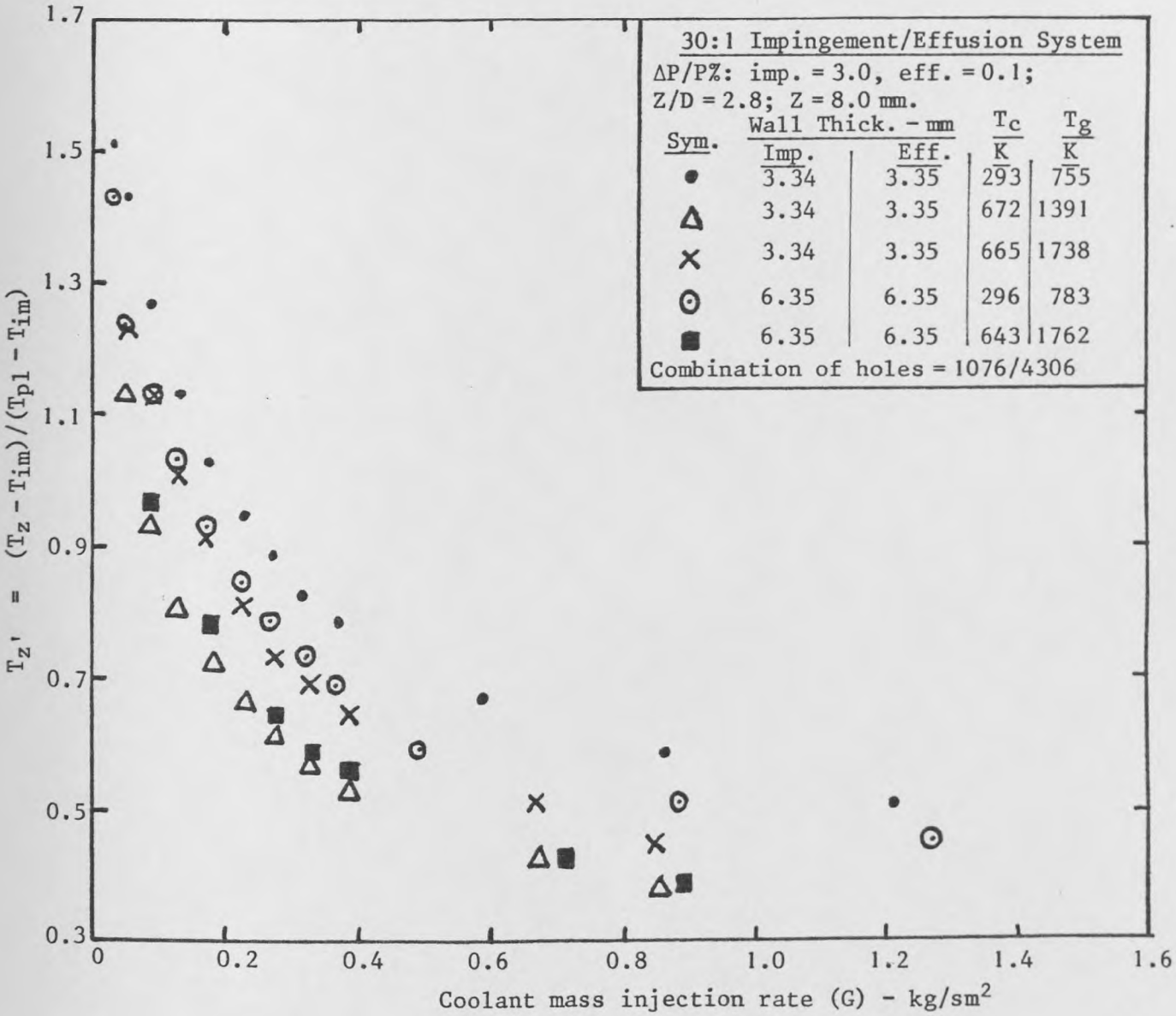

Fig. 8.23: Impingement wall heating profile

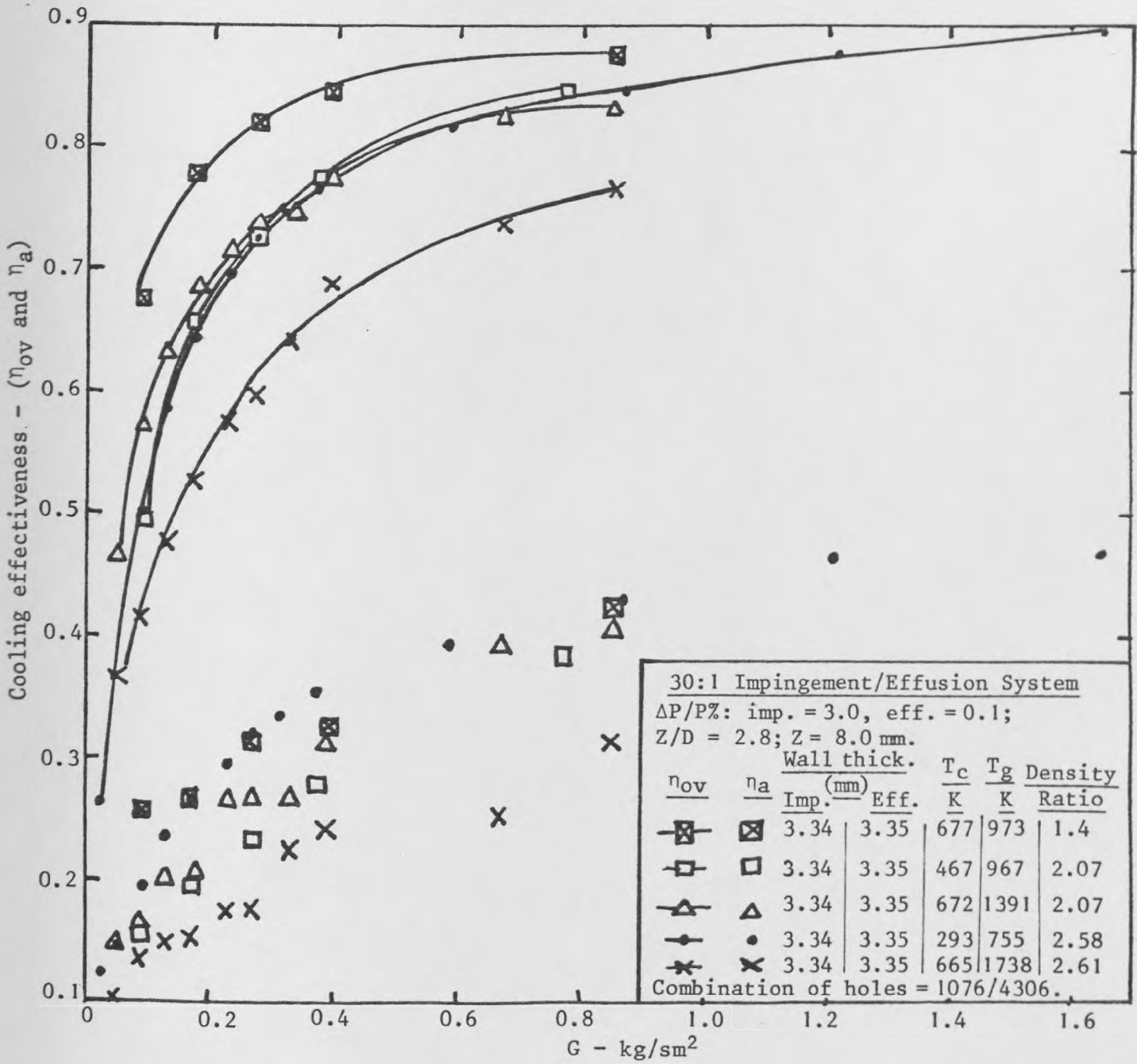

Fig. 8.24: Coolant to mainstream density ratio effect on cooling effectiveness

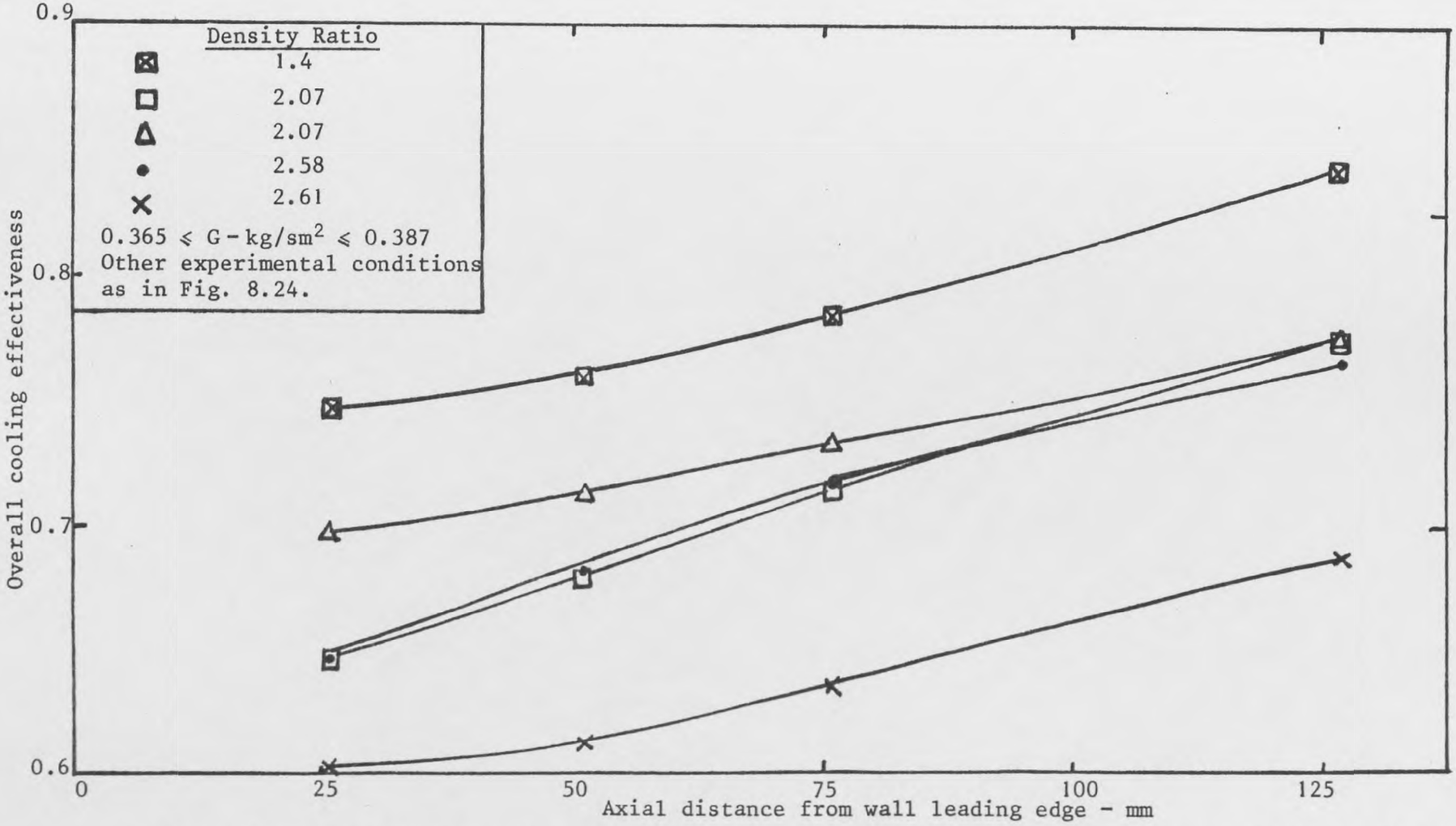

Fig. 8.25: Fluid density ratio effect on axial profile of cooling effectiveness at $0.365 \leqslant G \leqslant 0.387$

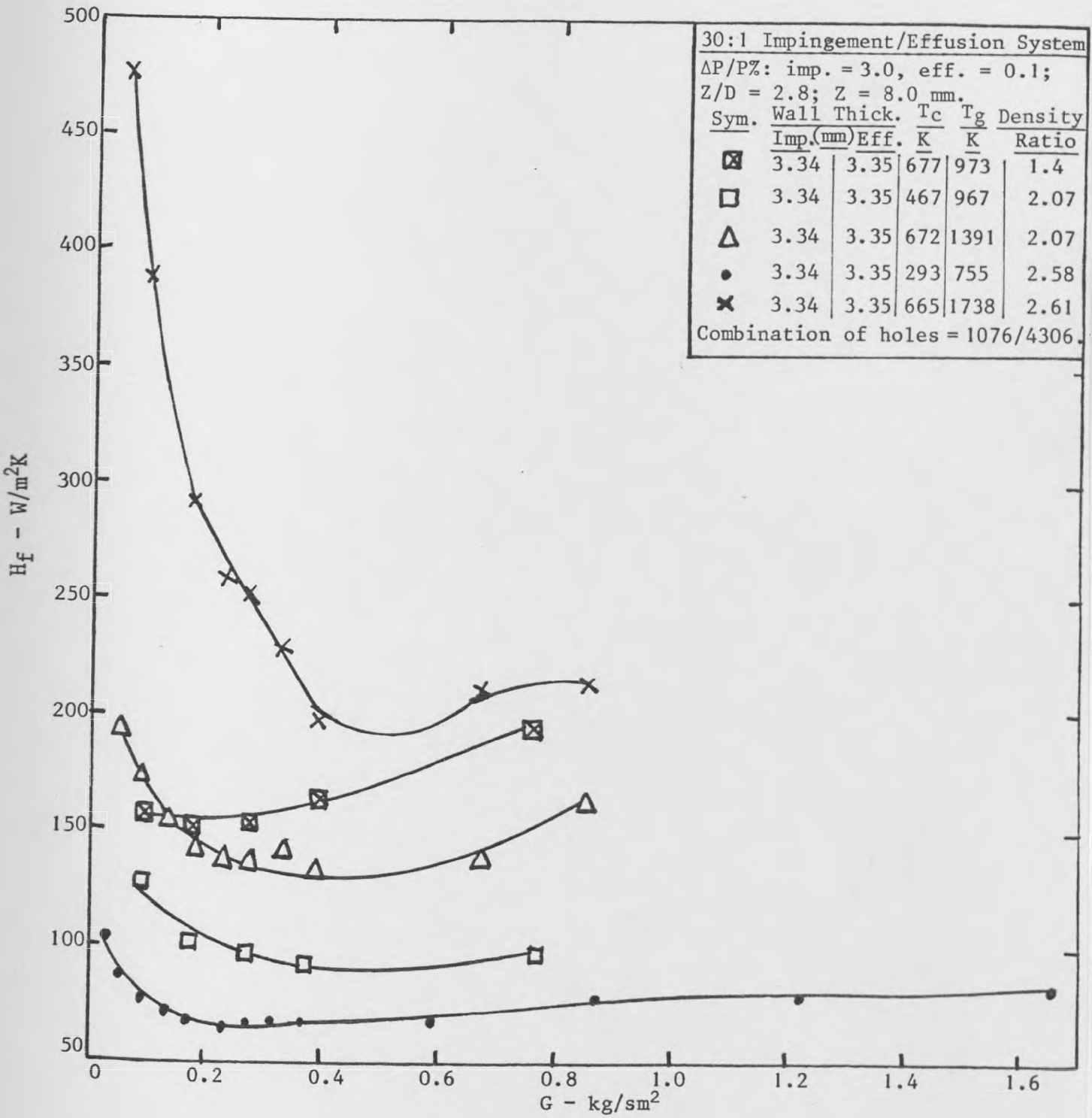

Fig. 8.26: Effect of fluid density ratio on H_f

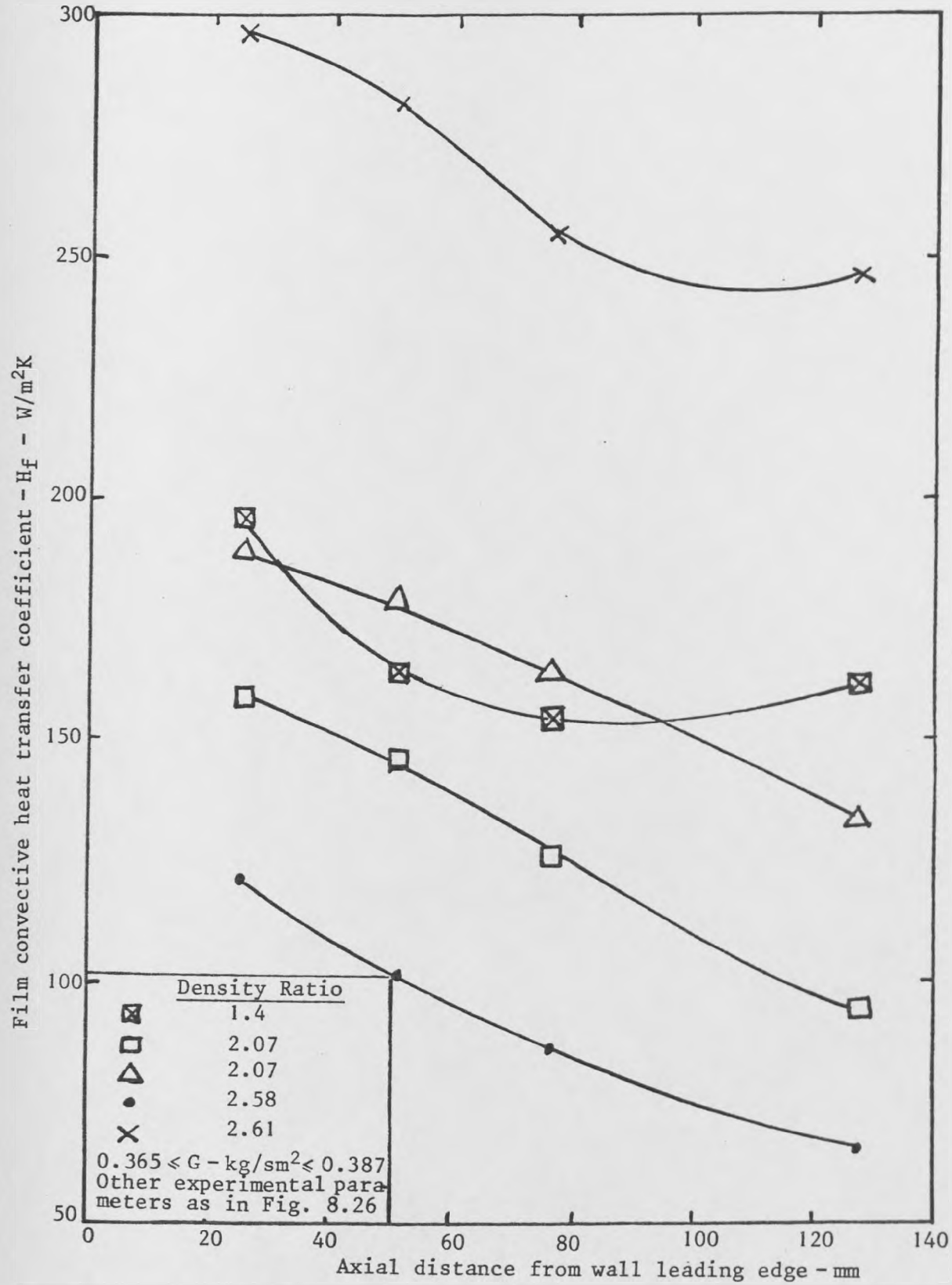

Fig. 8.27: Axial film heat coefficient profile dependence on fluid density ratio

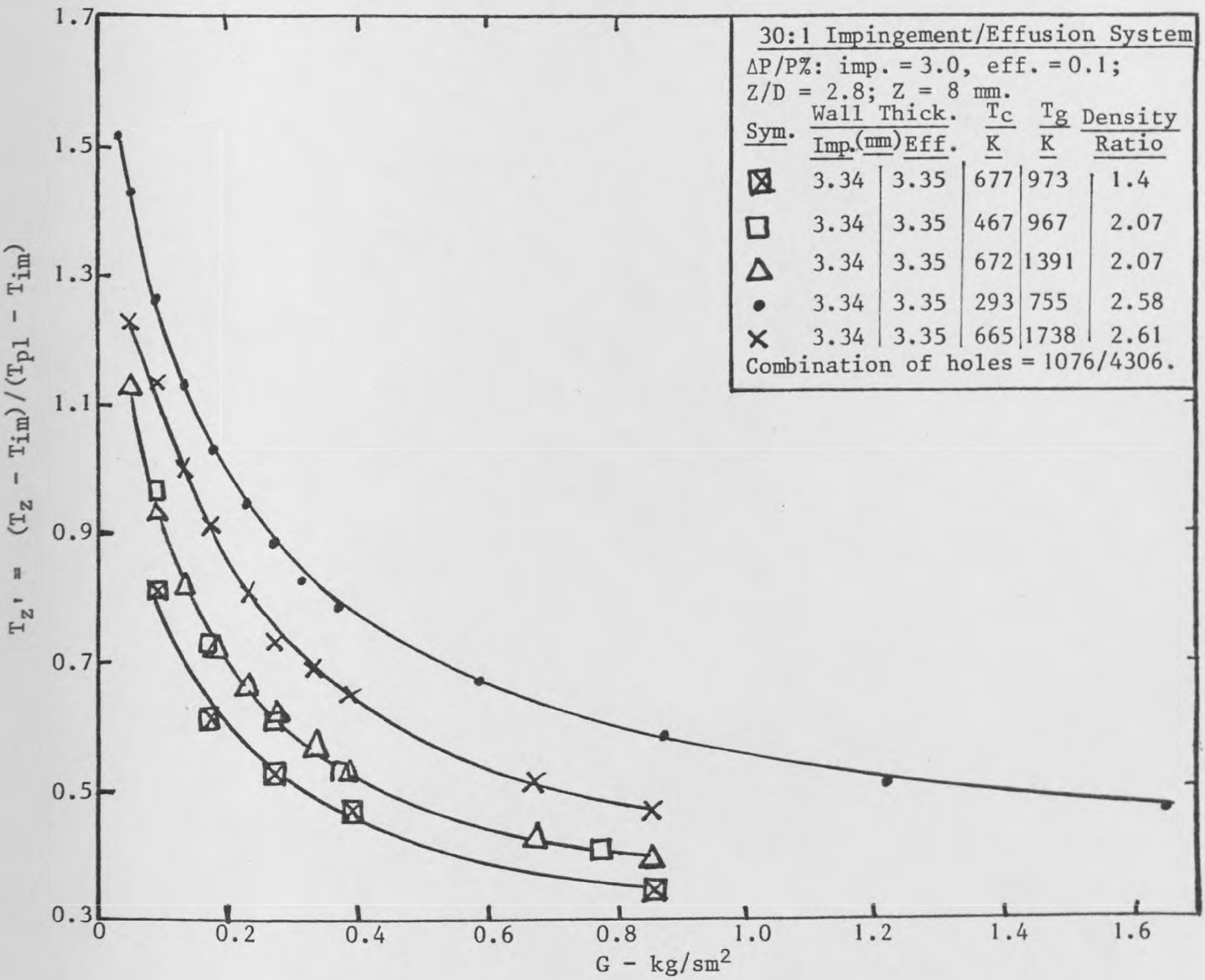

Fig. 8.28: Dependency of impingement wall heating on fluid density ratio

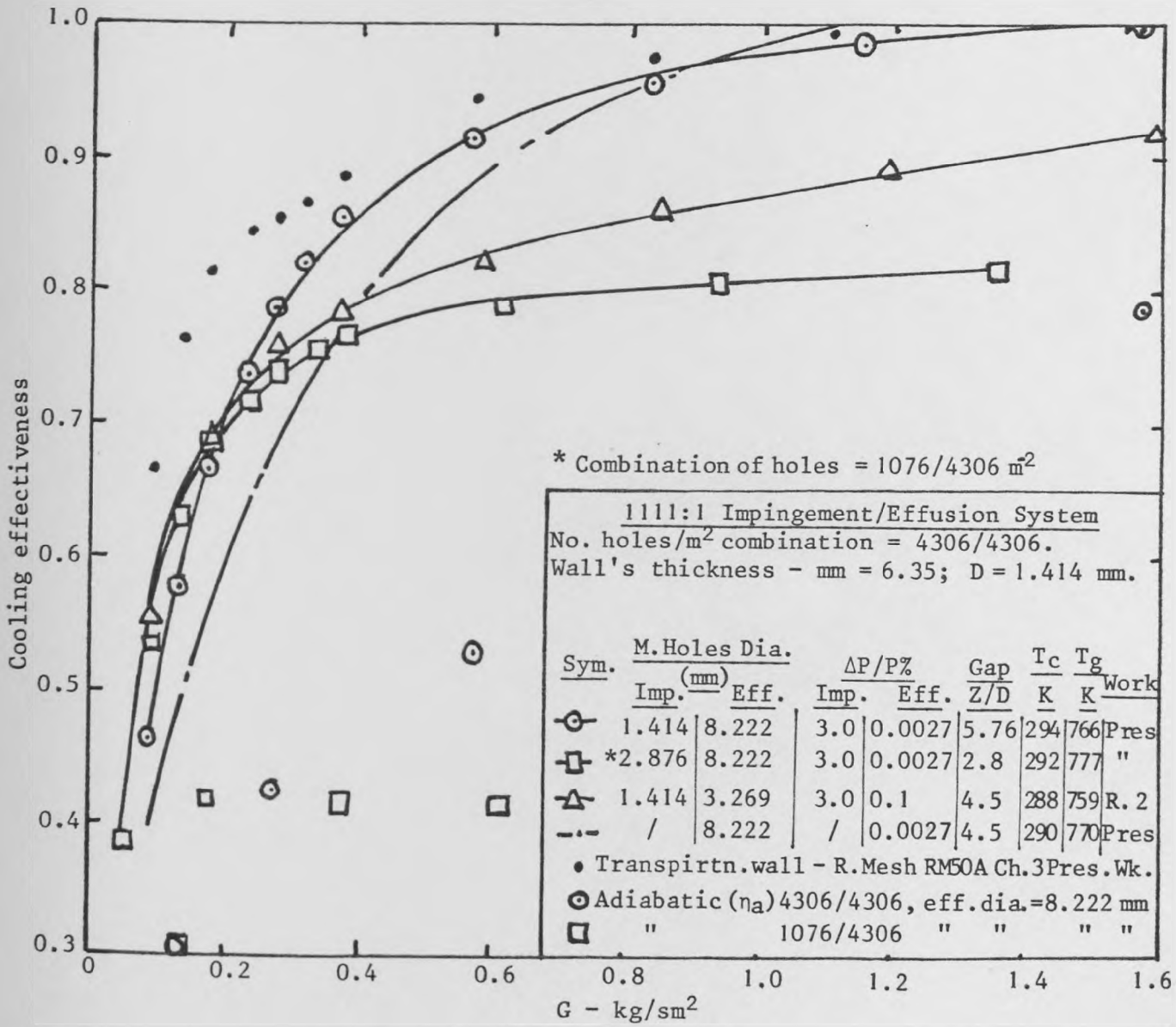

Fig. 8.29: Cooling effectiveness as a function of G

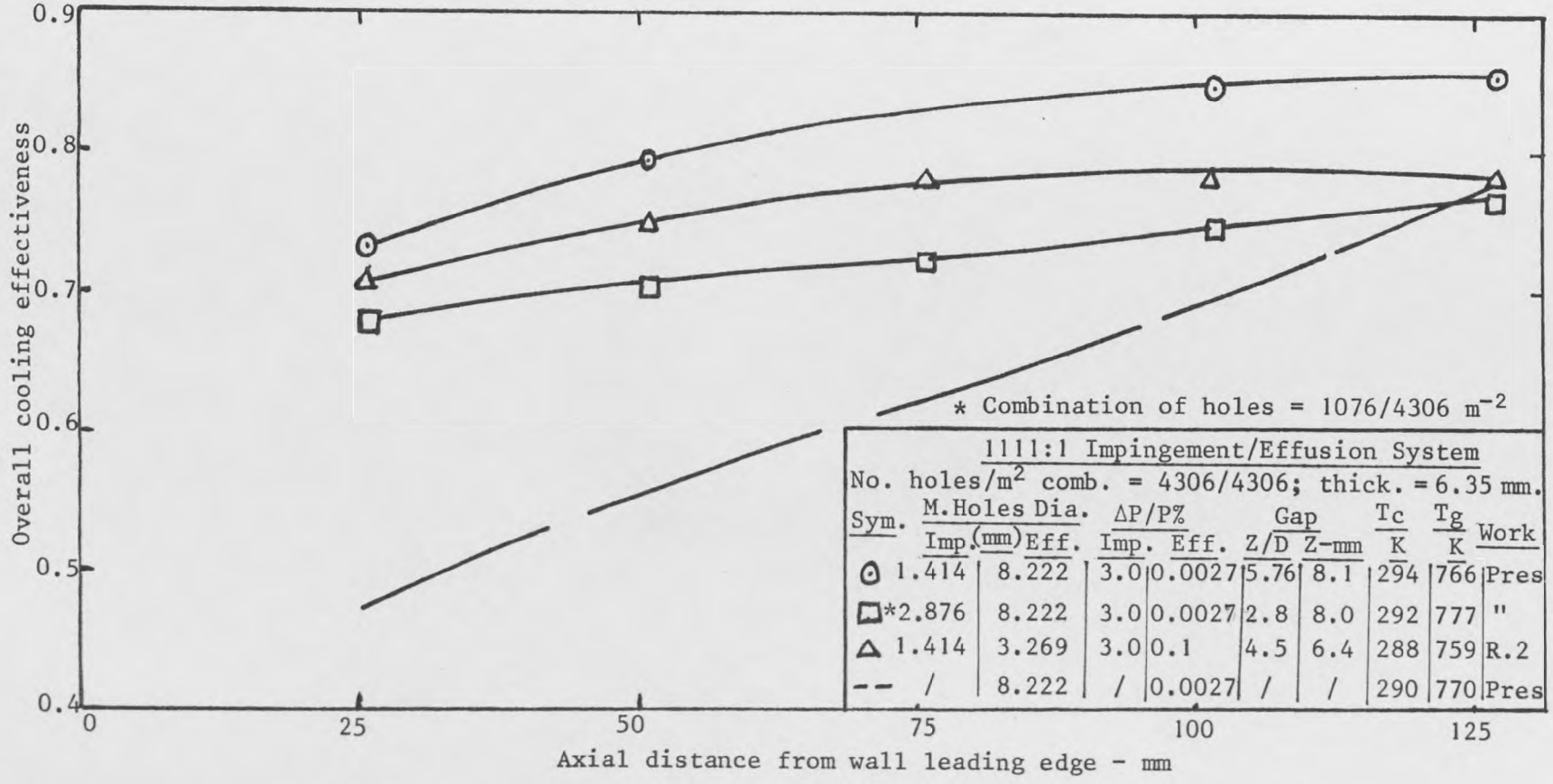

Fig. 8.30: Axial profile of cooling effectiveness at $0.363 \leqslant G \leqslant 0.368$

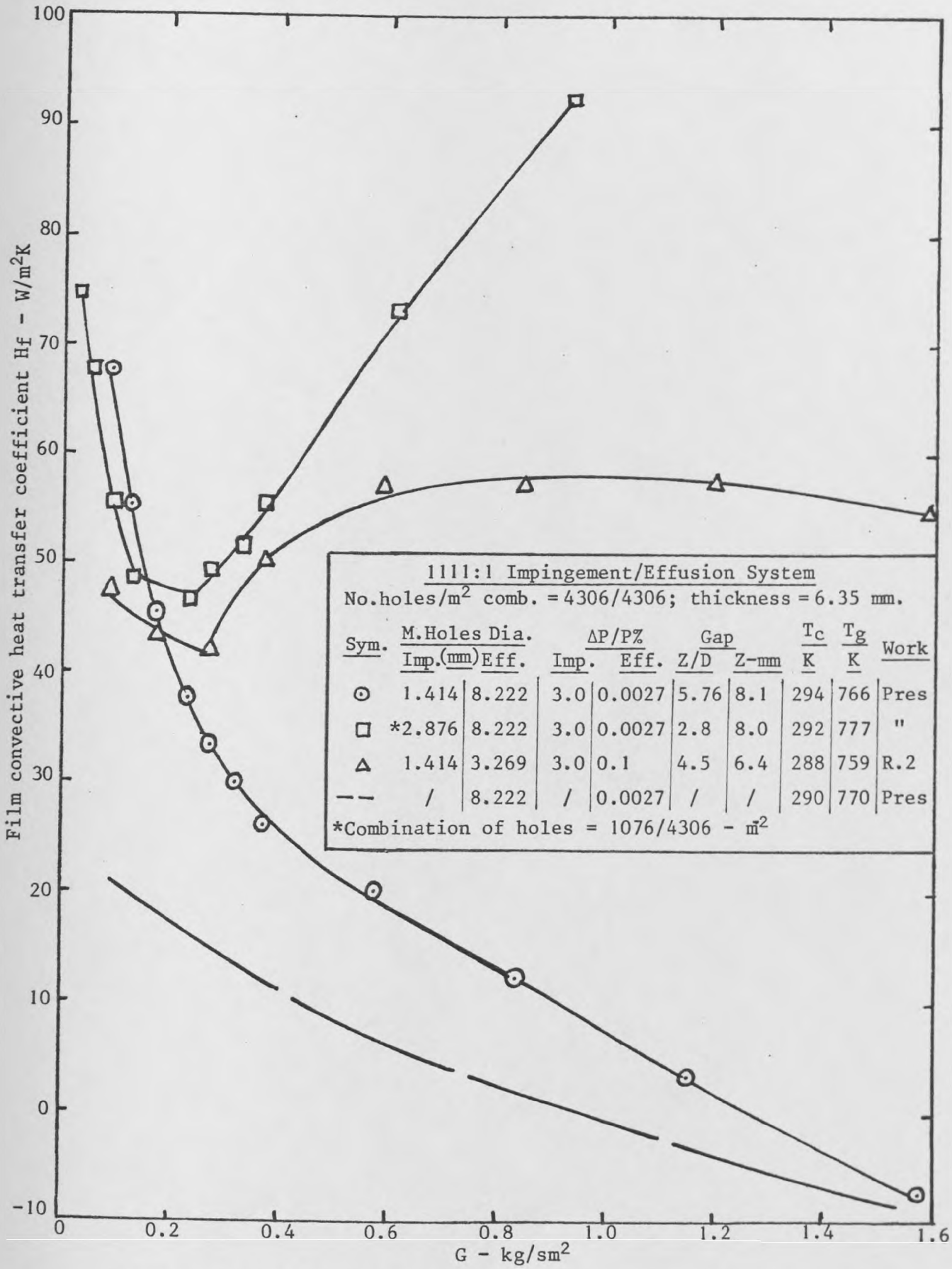

Fig. 8.31: Film heat transfer coefficient dependence on coolant mass injection

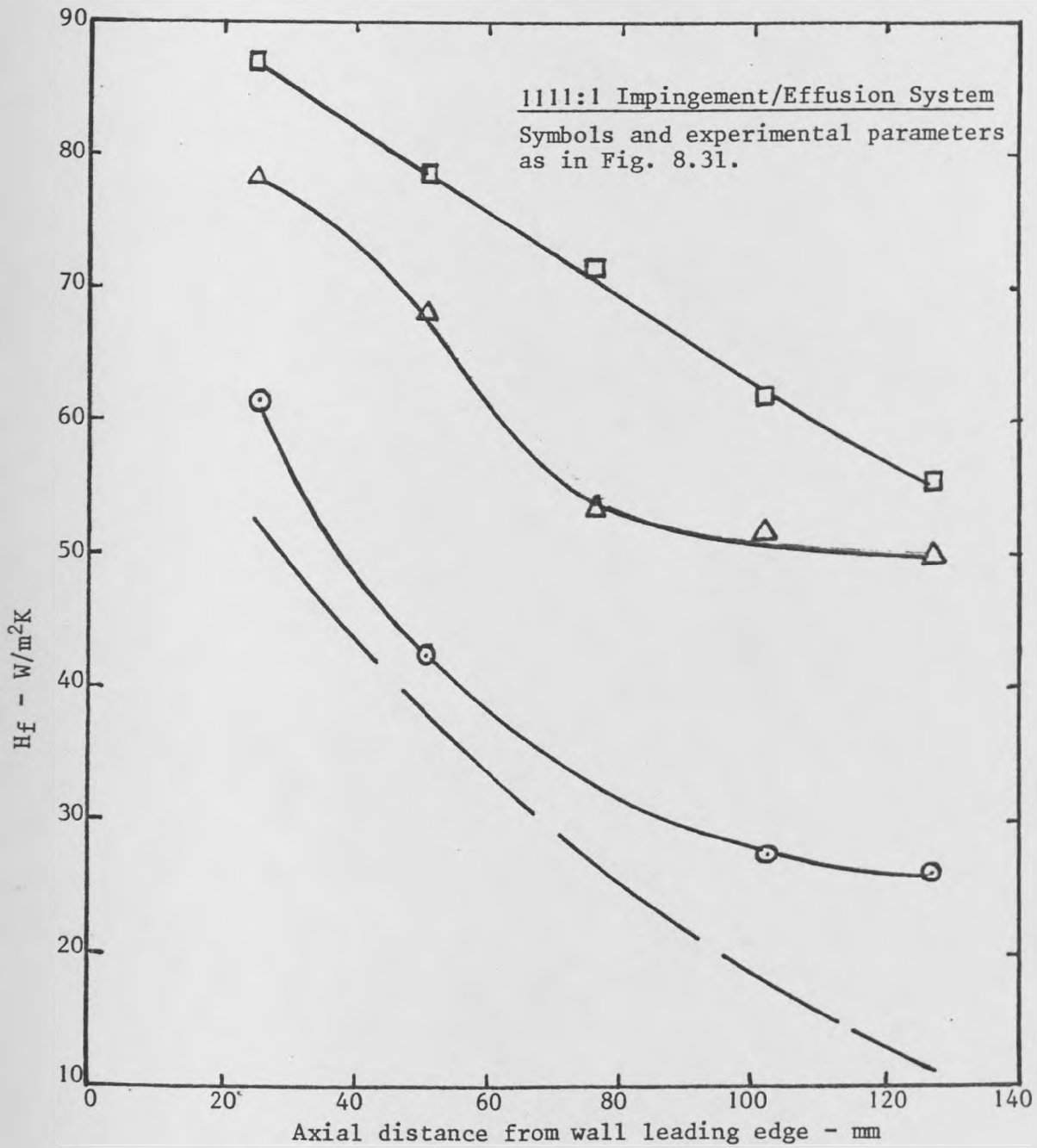

Fig. 8.32: Axial profile of film heat transfer coefficient at $0.363 \leqslant G \leqslant 0.368$.

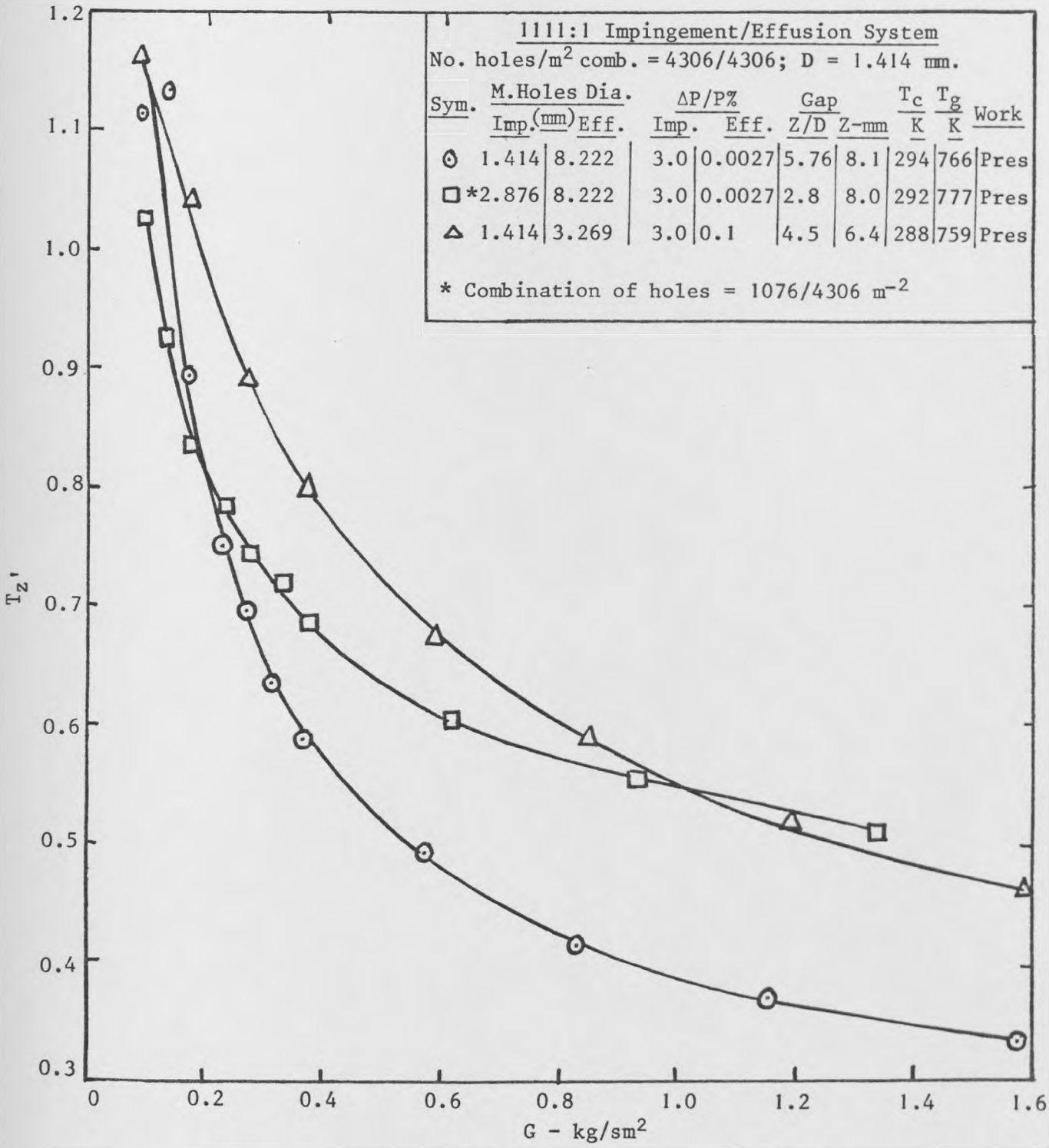

Fig. 8.33: Impingement wall heating as a function of coolant mass injection

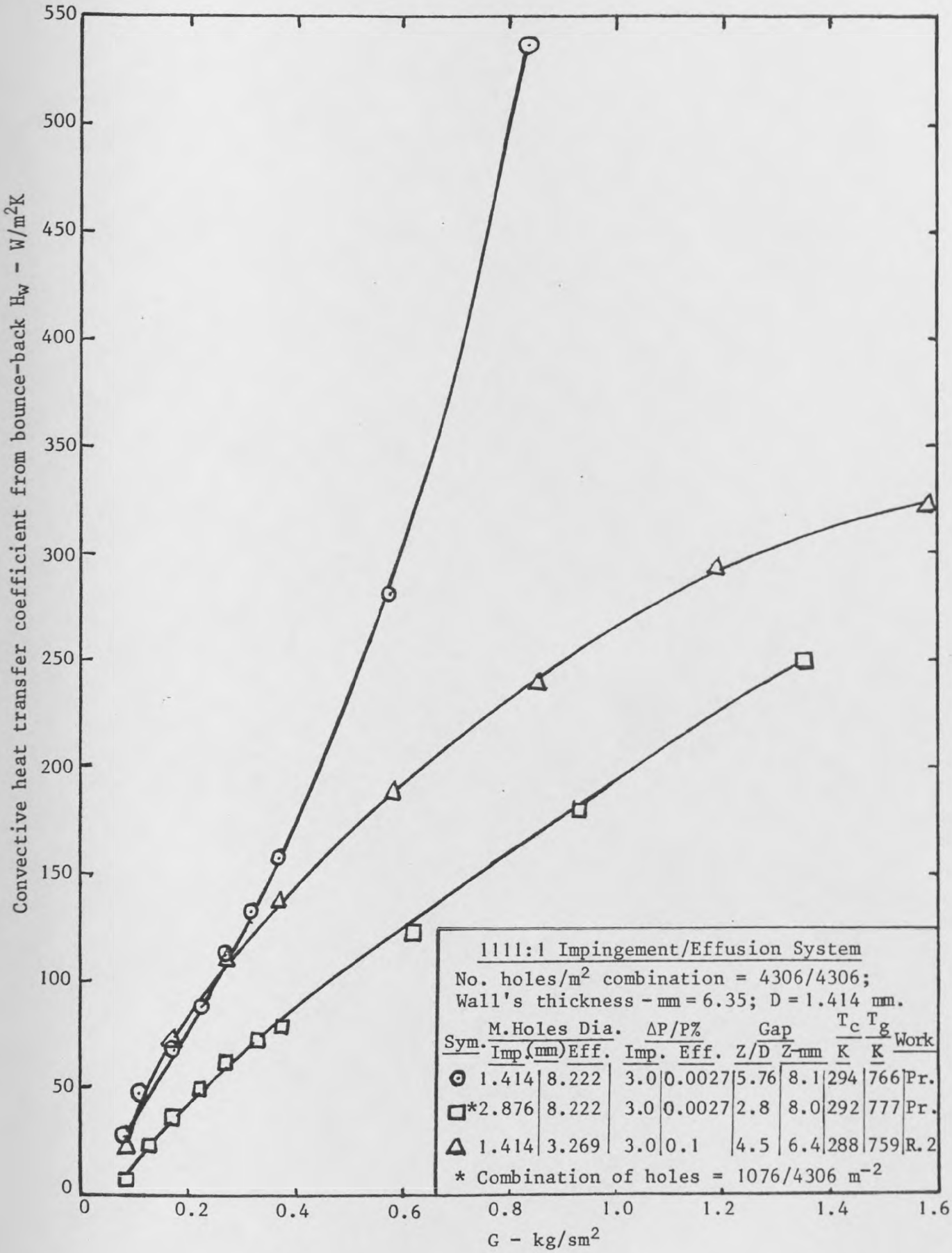

Fig. 8.34: Impingement inner surface wall convective heat transfer coefficient from bounce-back theory as a function of coolant mass injection.

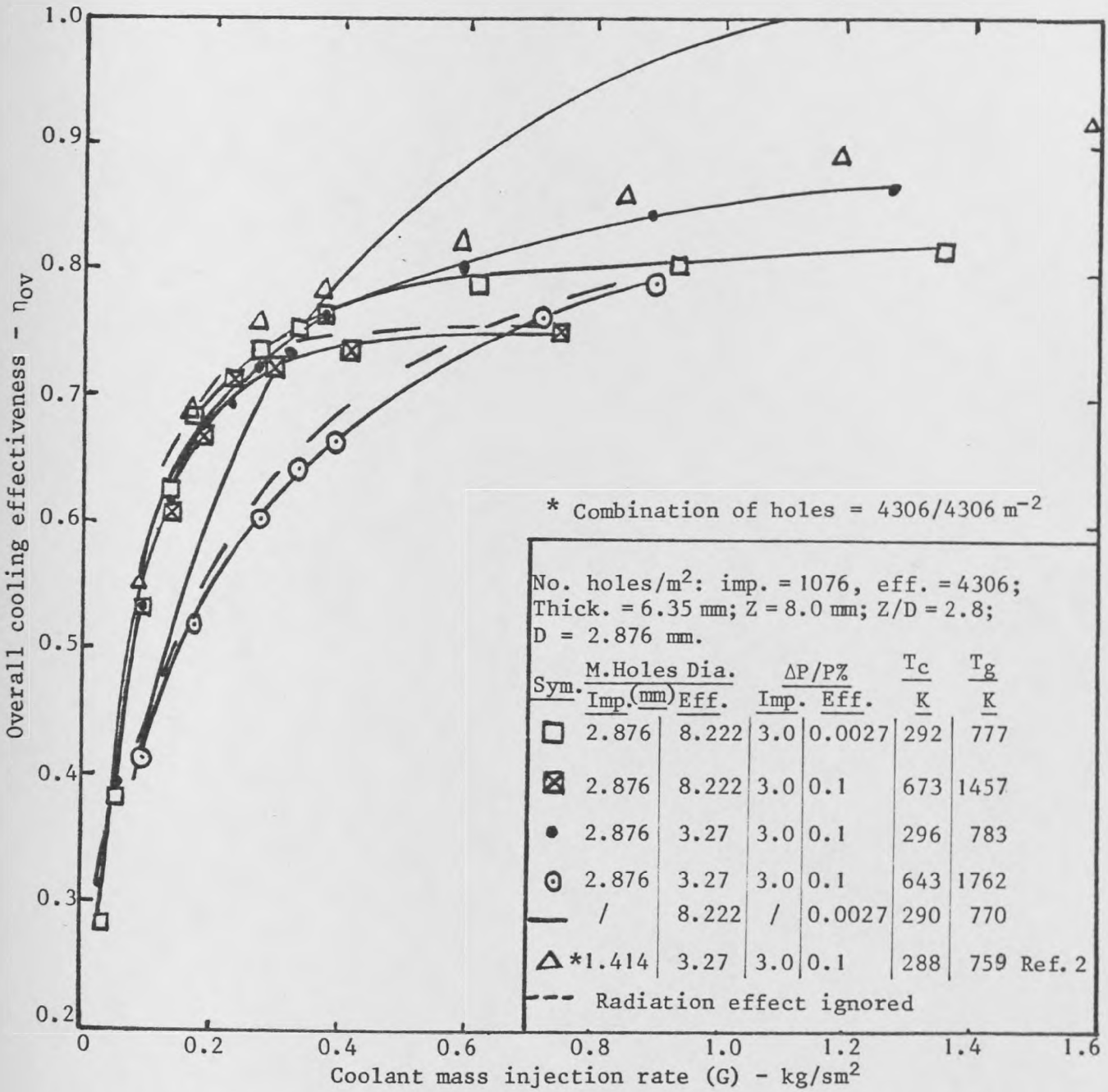

Fig. 8.35: Development of overall cooling effectiveness as a function of G

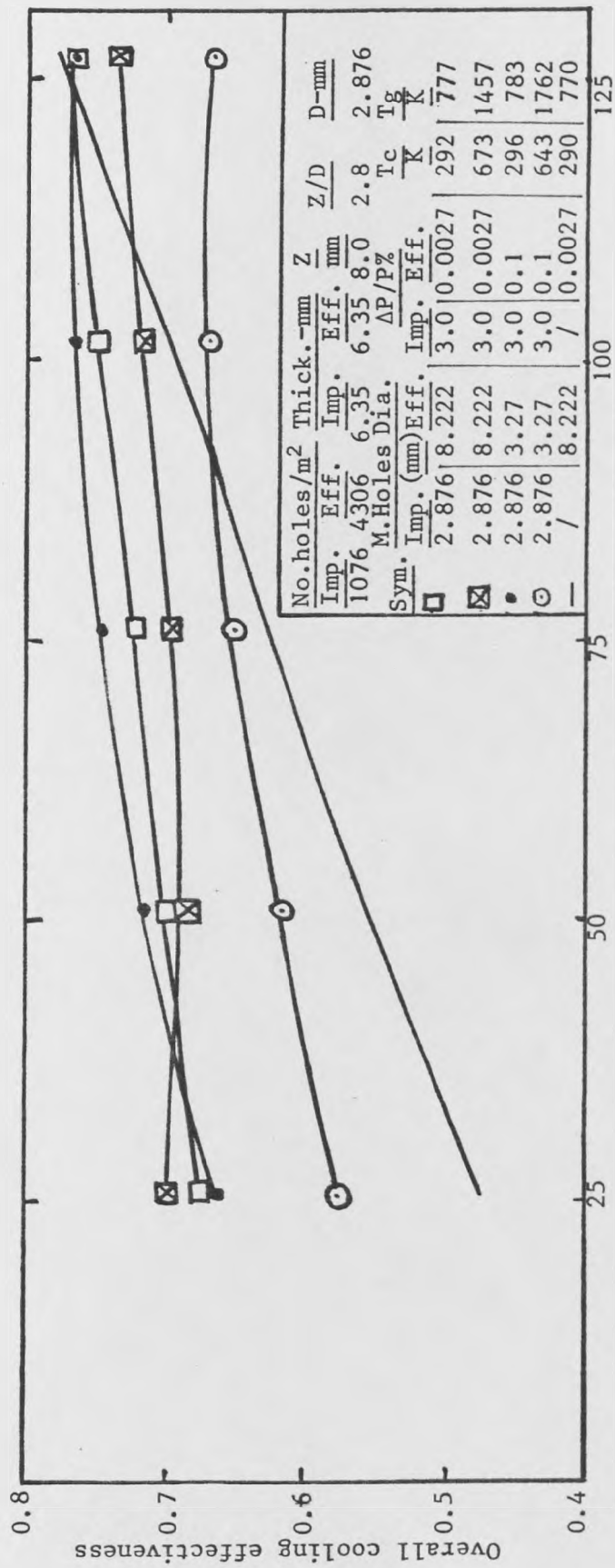

Fig. 8.36: Axial profile of overall cooling effectiveness at $0.363 \leq G \leq 0.4$

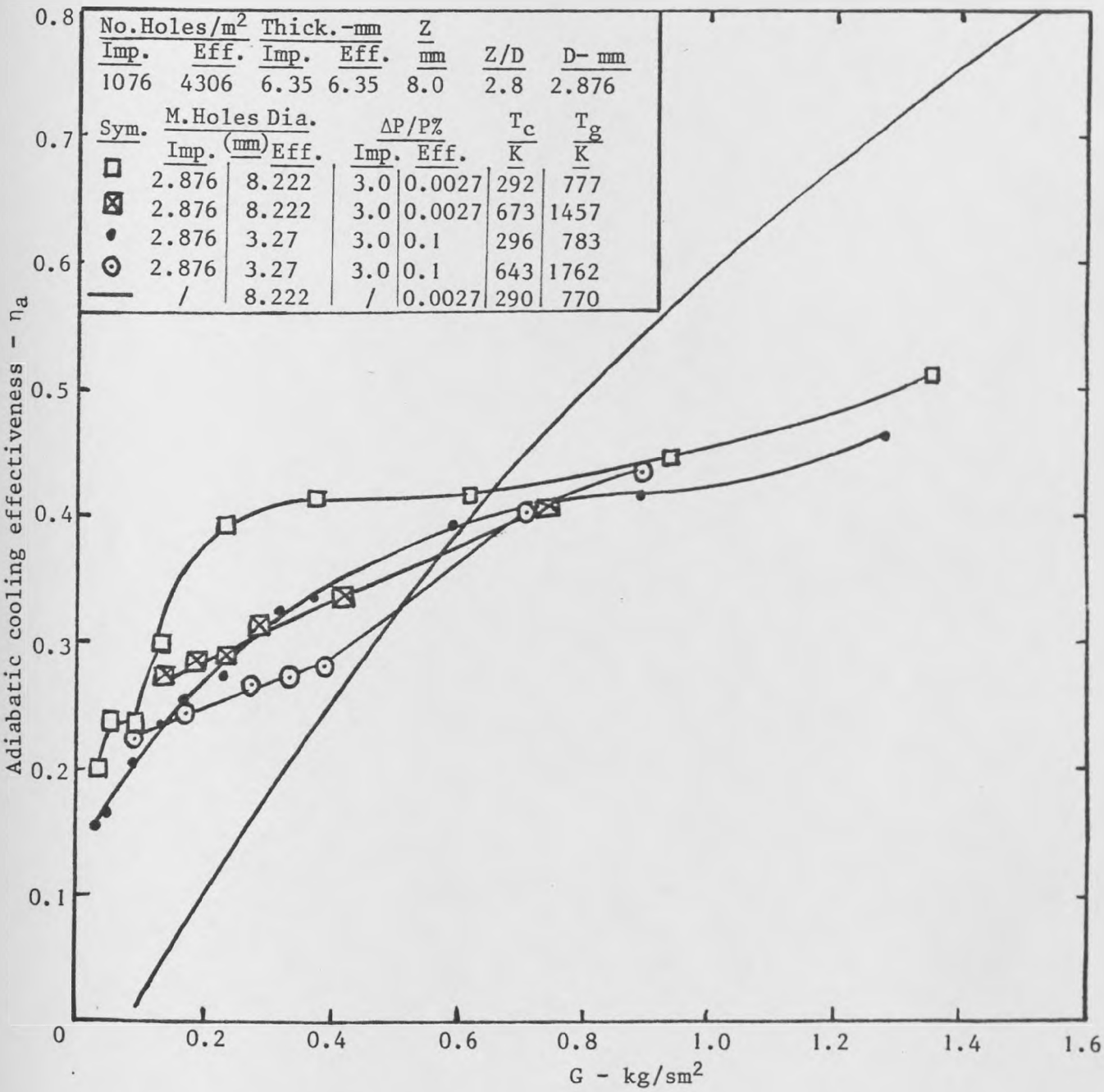

Fig. 8.37: Development of adiabatic cooling effectiveness with coolant injection

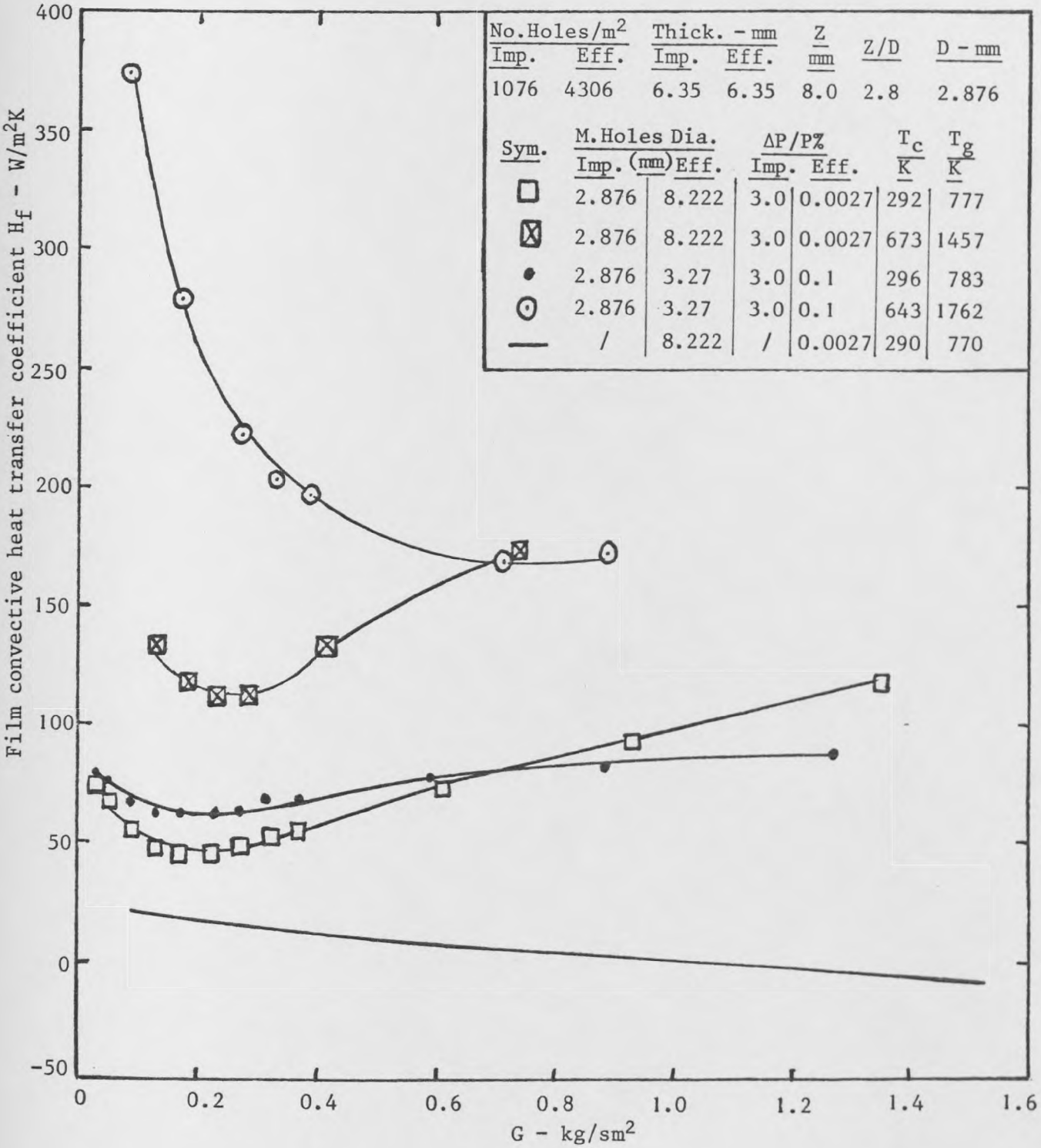

Fig. 8.38: Film convective heat transfer coefficient dependence on coolant mass injection rate

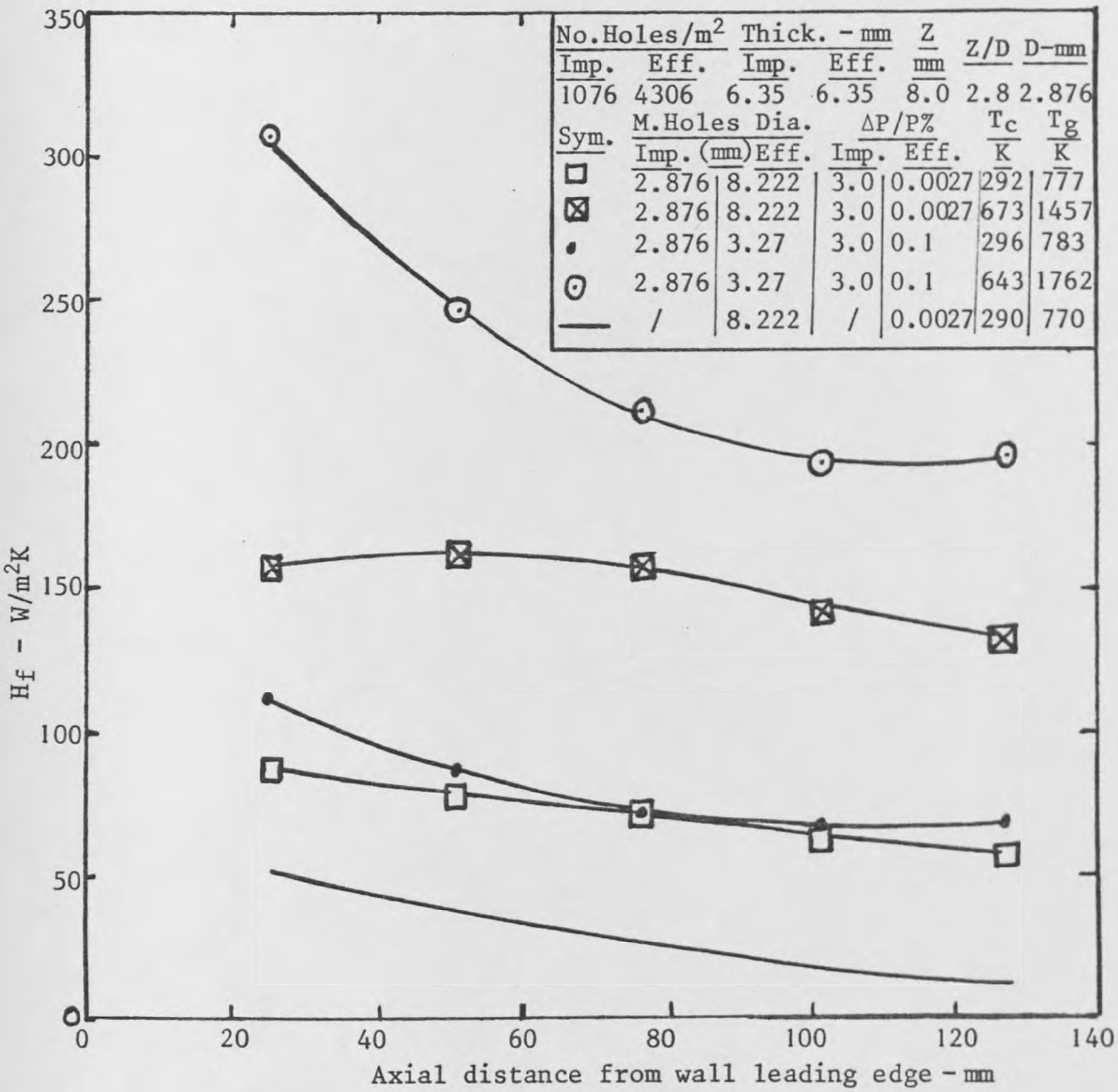

Fig. 8.39: Axial profile of film convective heat transfer coefficient at $0.363 \leqslant G \leqslant 0.4$

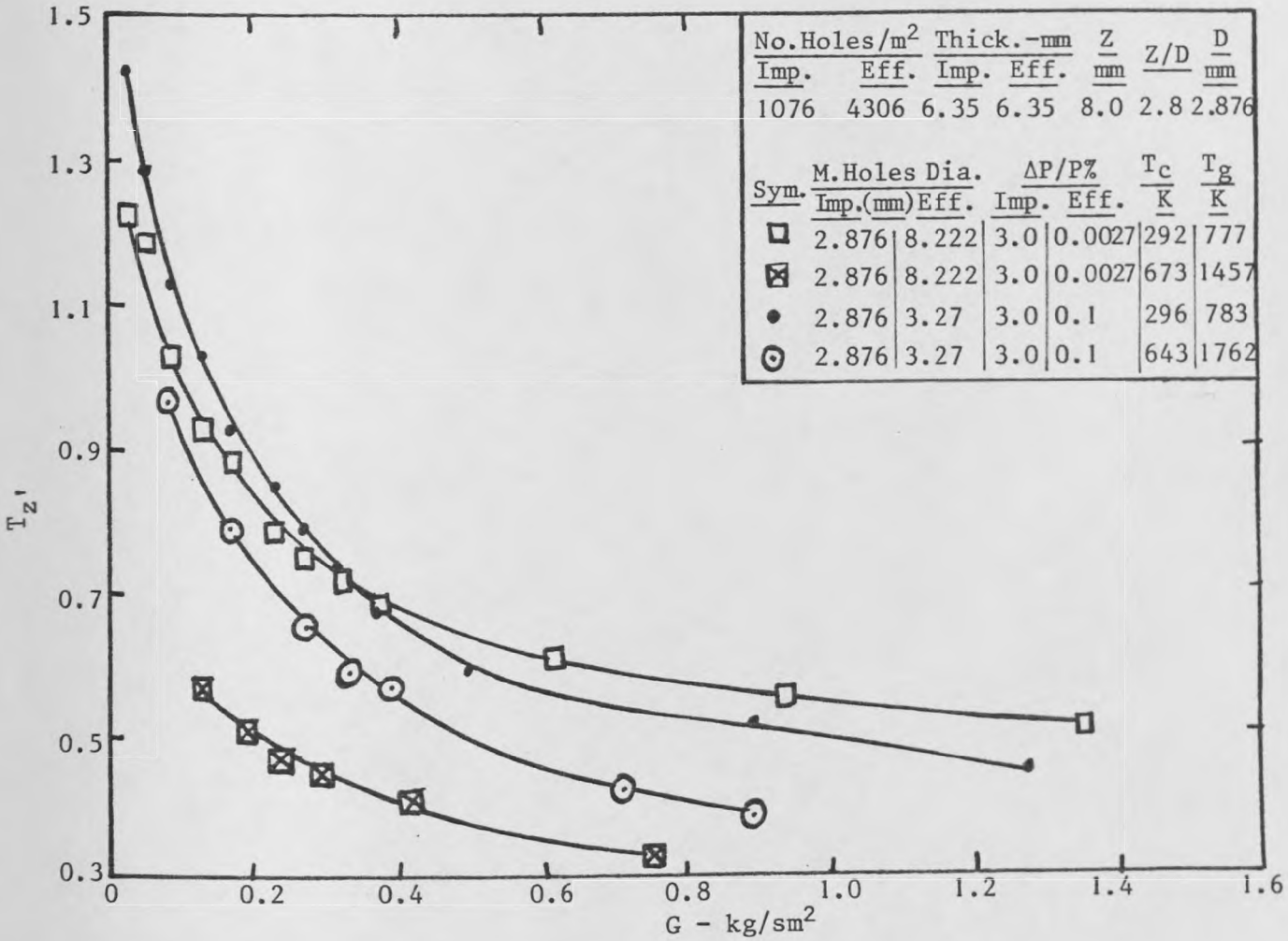

Fig. 8.40: Impingement wall heating as a function of G

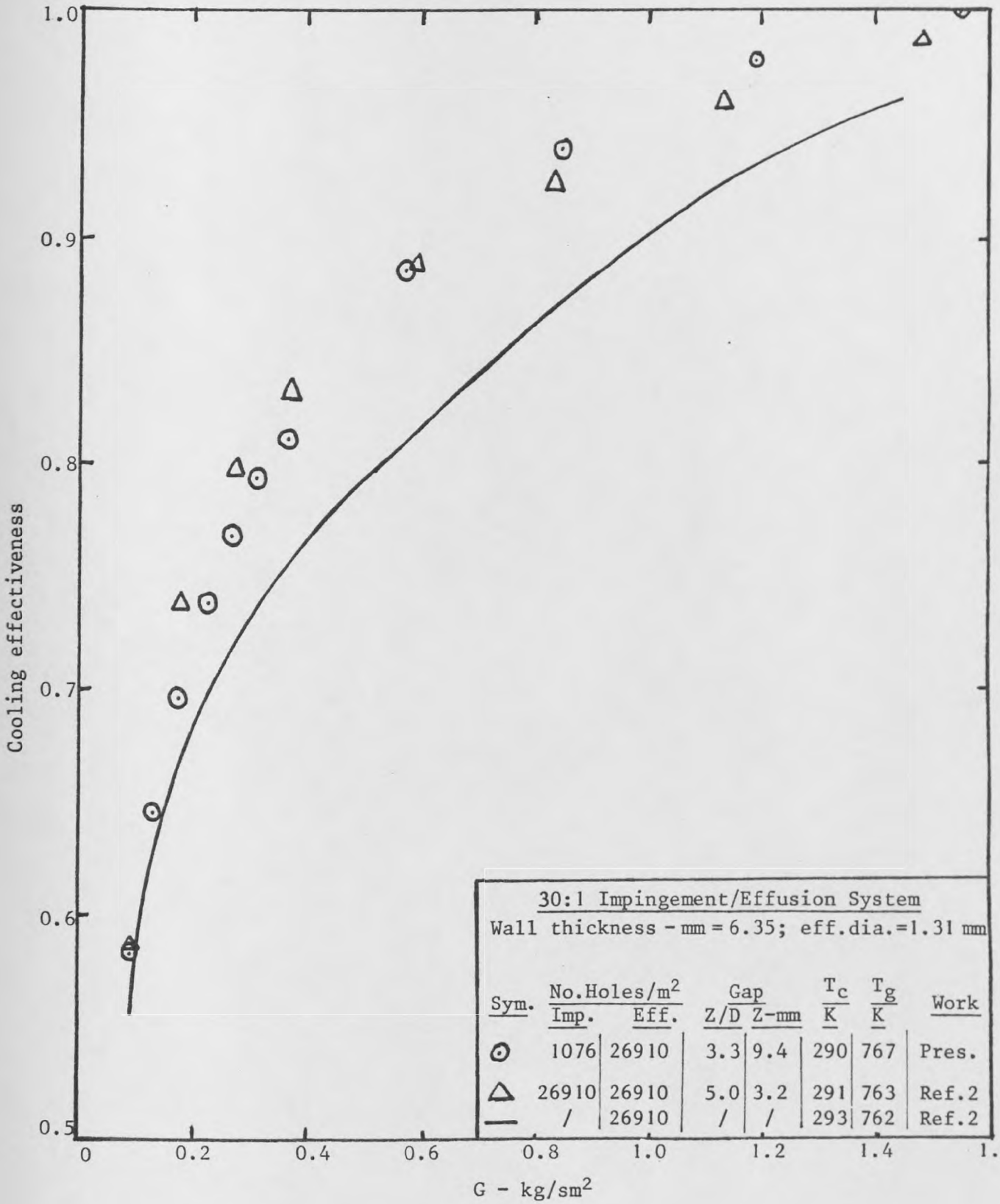

Fig. 8.41: Cooling effectiveness as a function of coolant mass injection

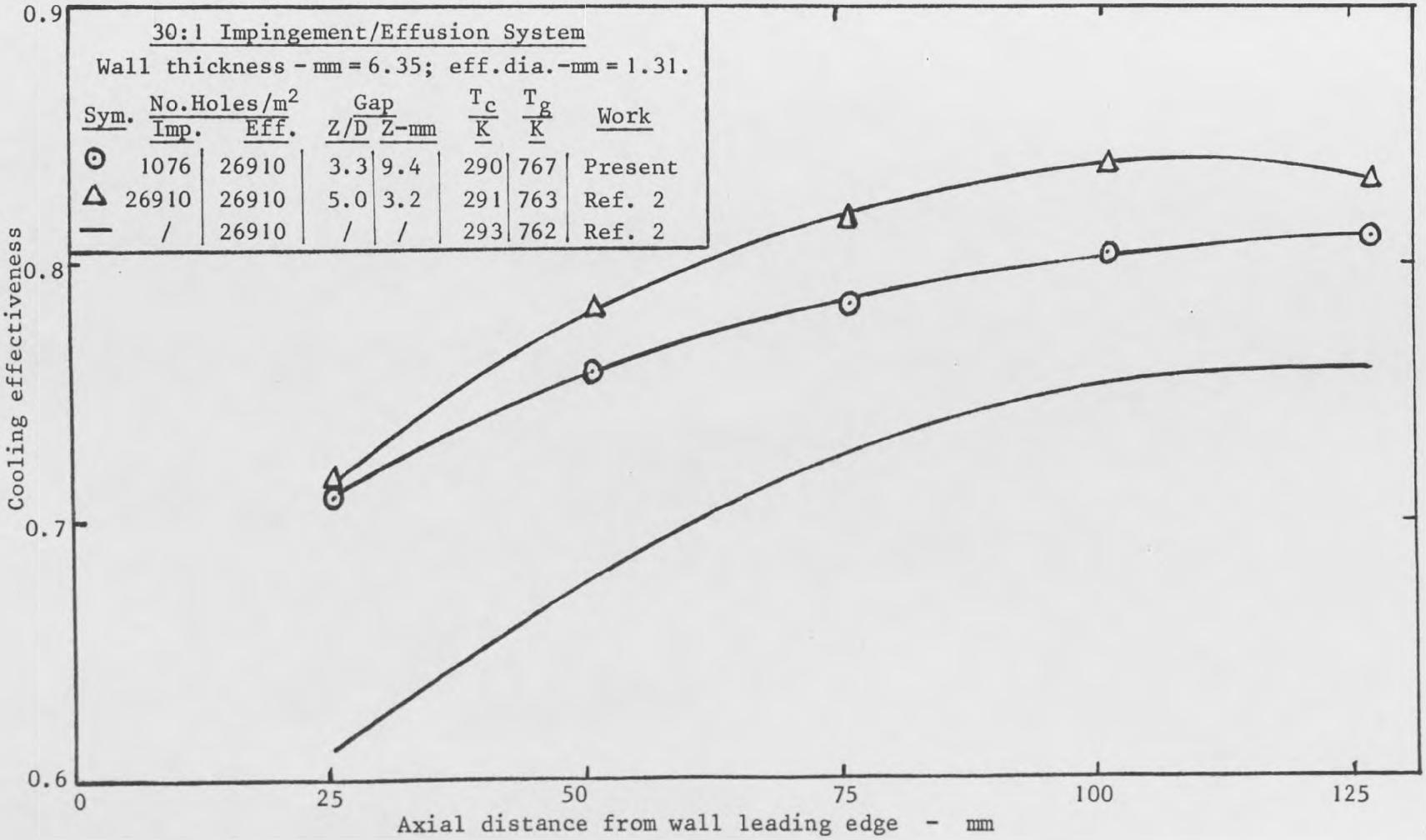

Fig. 8.42: Axial profile of overall cooling effectiveness at $0.363 \leqslant G \leqslant 0.372$

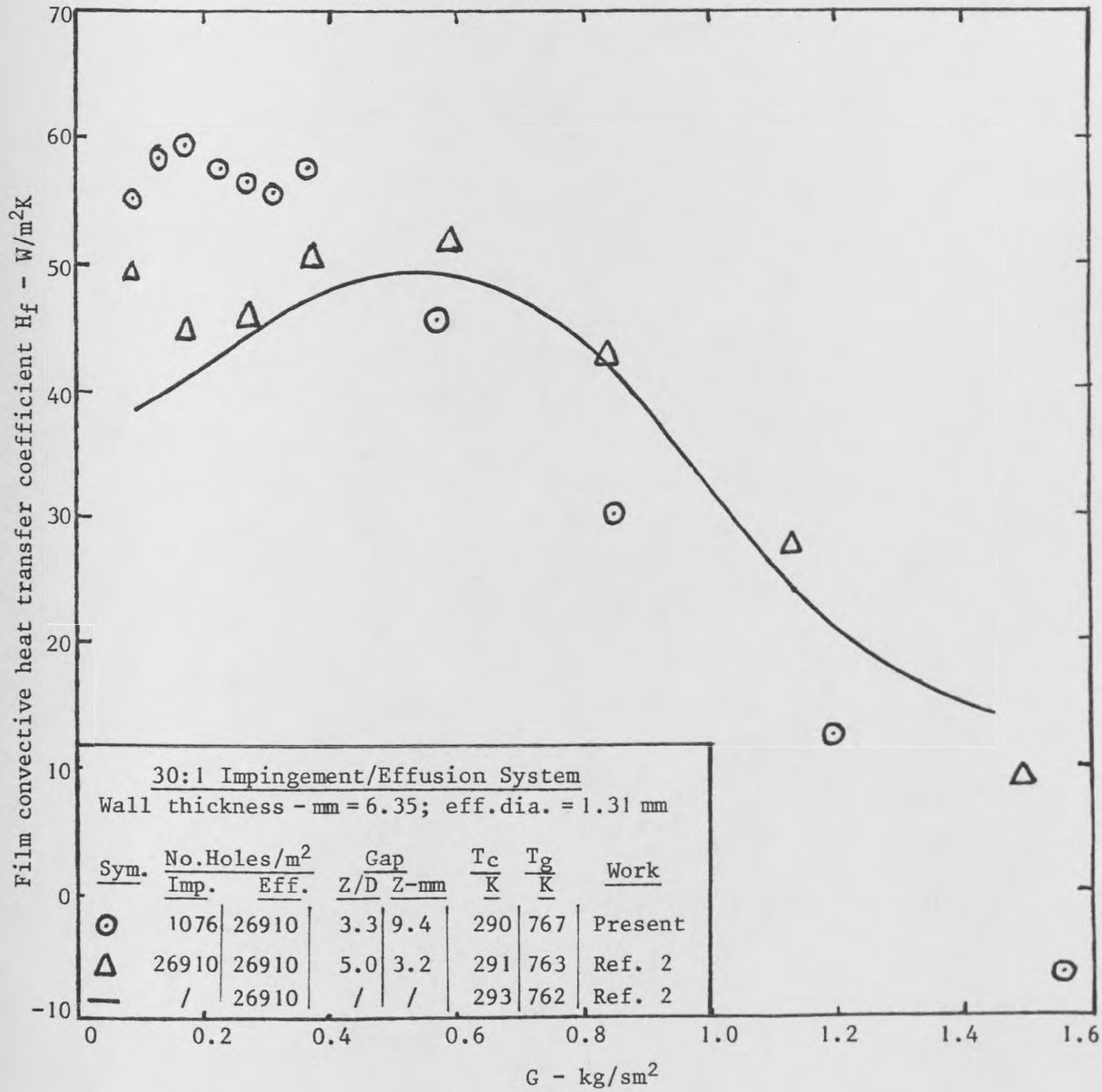

Fig. 8.43: Profile of film convective heat transfer coefficient with coolant mass injection

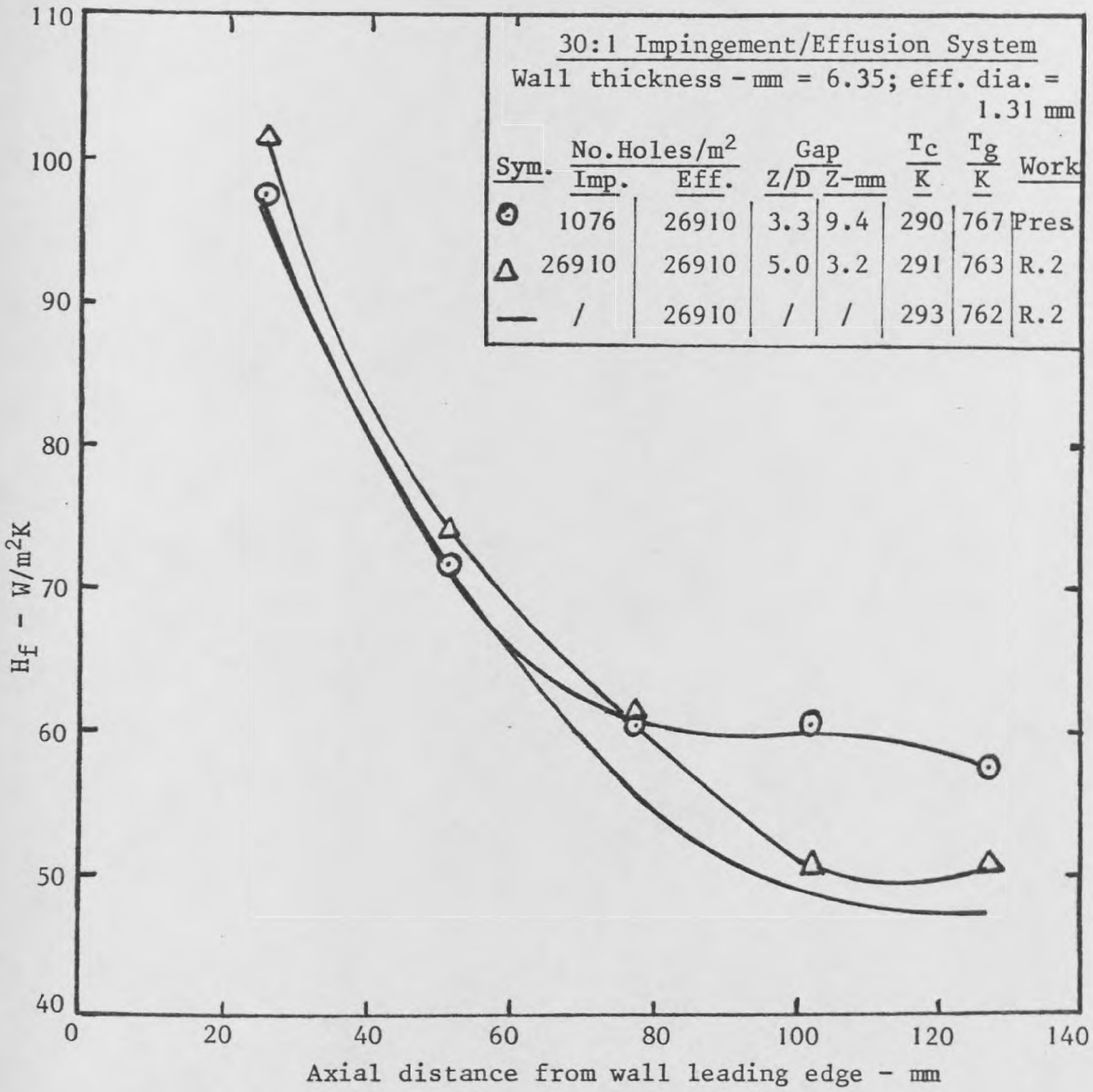

Fig. 8.44: Axial profile of film convective heat transfer coefficient at $0.363 \leqslant G \leqslant 0.372$.

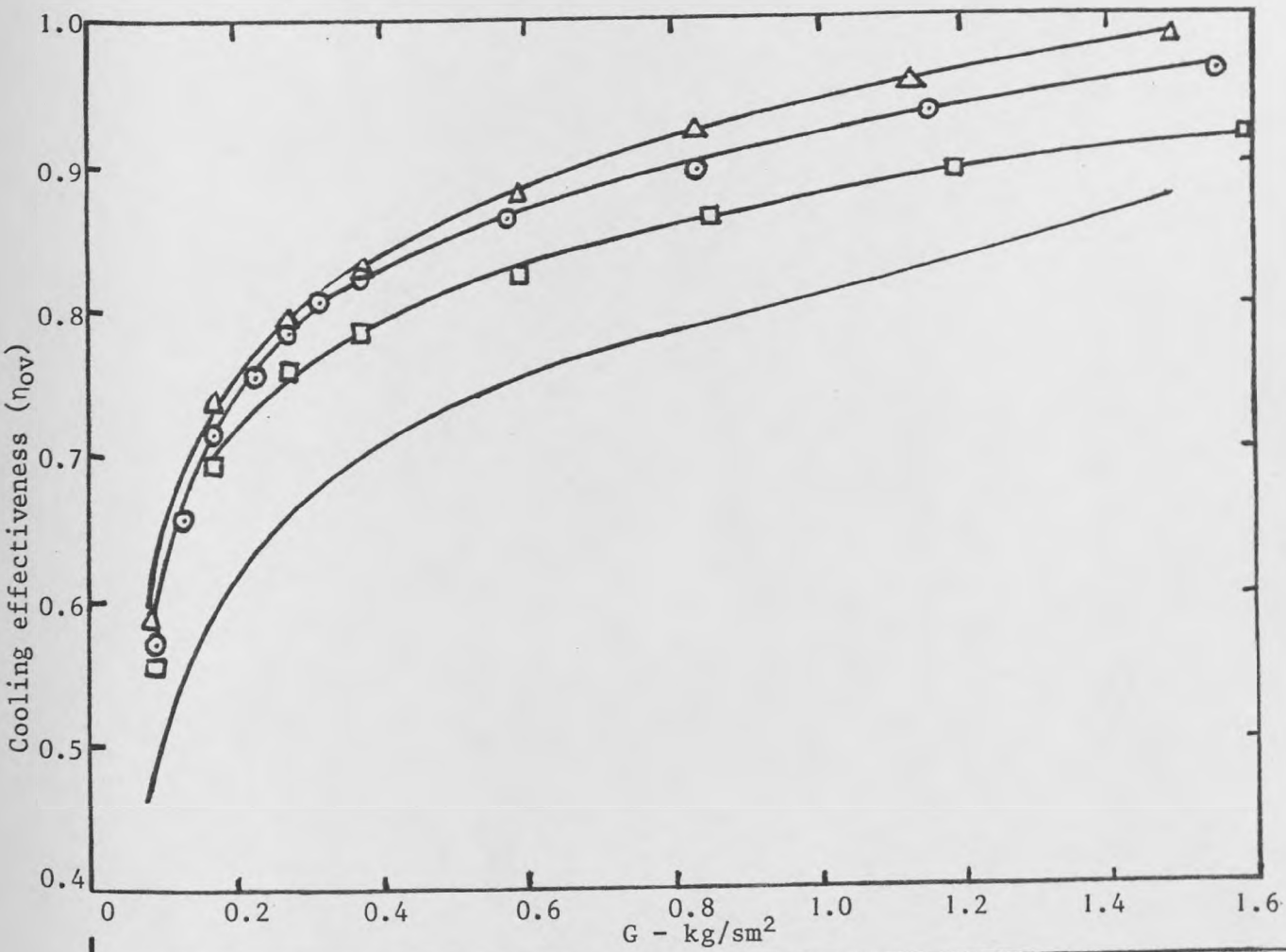

30:1 Impingement/Effusion System

Design pressure loss: imp. = 3%, eff. = 0.1%.

Sym.	No.Holes/m^2 Imp.	No.Holes/m^2 Eff.	M.Holes Dia. Imp.(mm)	M.Holes Dia. Eff.	Wall Thick. Imp.(mm)	Wall Thick. Eff.	Gap Z/D	Gap Z-mm	X/D	T_c K	T_g K	Holes Format Imp.	Holes Format Eff.	Work
⊙	9688	9688	0.999	2.235	3.321	6.5	4.5	4.5	10.16	294	777	Inl.	Offs.	Pres
—	/	9688	/	2.235	/	6.5	/	/	/	293	774	/	"	"
△	26910	26910	0.639	1.307	6.35	6.35	5.0	3.2	9.6	291	763	Offs.	Inl.	R.2
□	4306	4306	1.414	3.27	6.35	6.35	4.5	6.4	10.78	288	759	"	"	"

Fig. 8.45: Development of cooling effectiveness with coolant mass injection

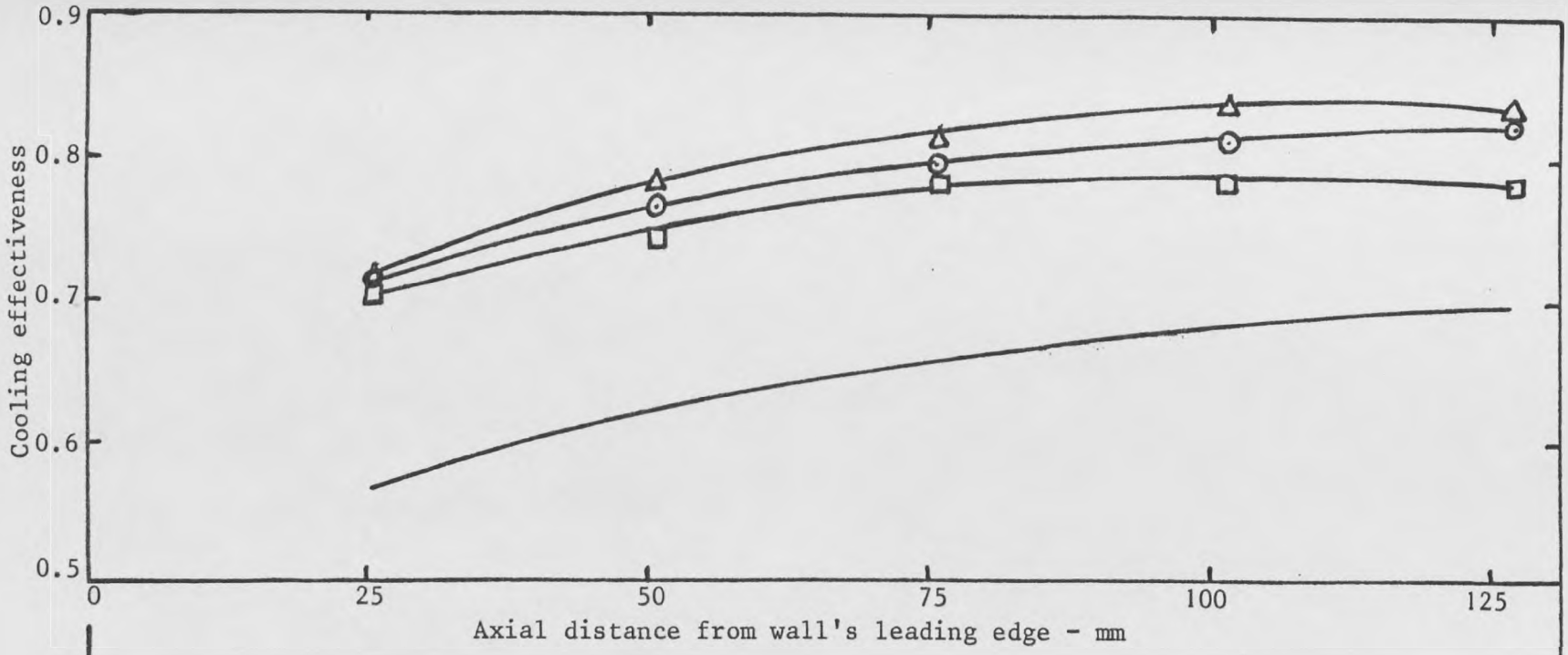

30:1 Impingement/Effusion System

Design pressure loss: impingement wall = 3.0%, effusion wall = 0.1%.

Sym.	No.Holes/m^2 Imp.	No.Holes/m^2 Eff.	Holes Dia.-mm Imp.	Holes Dia.-mm Eff.	Wall Thick. Imp. (mm)	Wall Thick. Eff.	Gap Z/D	Gap Z-mm	X/D	T_c K	T_g K	Holes Format Imp.	Holes Format Eff.	Work
⊙	9688	9688	0.999	2.235	3.321	6.5	4.5	4.5	10.16	294	777	Inline	Offset	Present
——	/	9688	/	2.235	/	6.5	/	/	/	293	774	/	Offset	Present
△	26910	26910	0.639	1.307	6.35	6.35	5.0	3.2	9.6	291	763	Offset	Inline	Ref. 2
□	4306	4306	1.414	3.27	6.35	6.35	4.5	6.4	10.78	288	759	Offset	Inline	Ref. 2

Fig. 8.46: Axial profile of overall cooling effectiveness at $0.365 \leqslant G \leqslant 0.372$

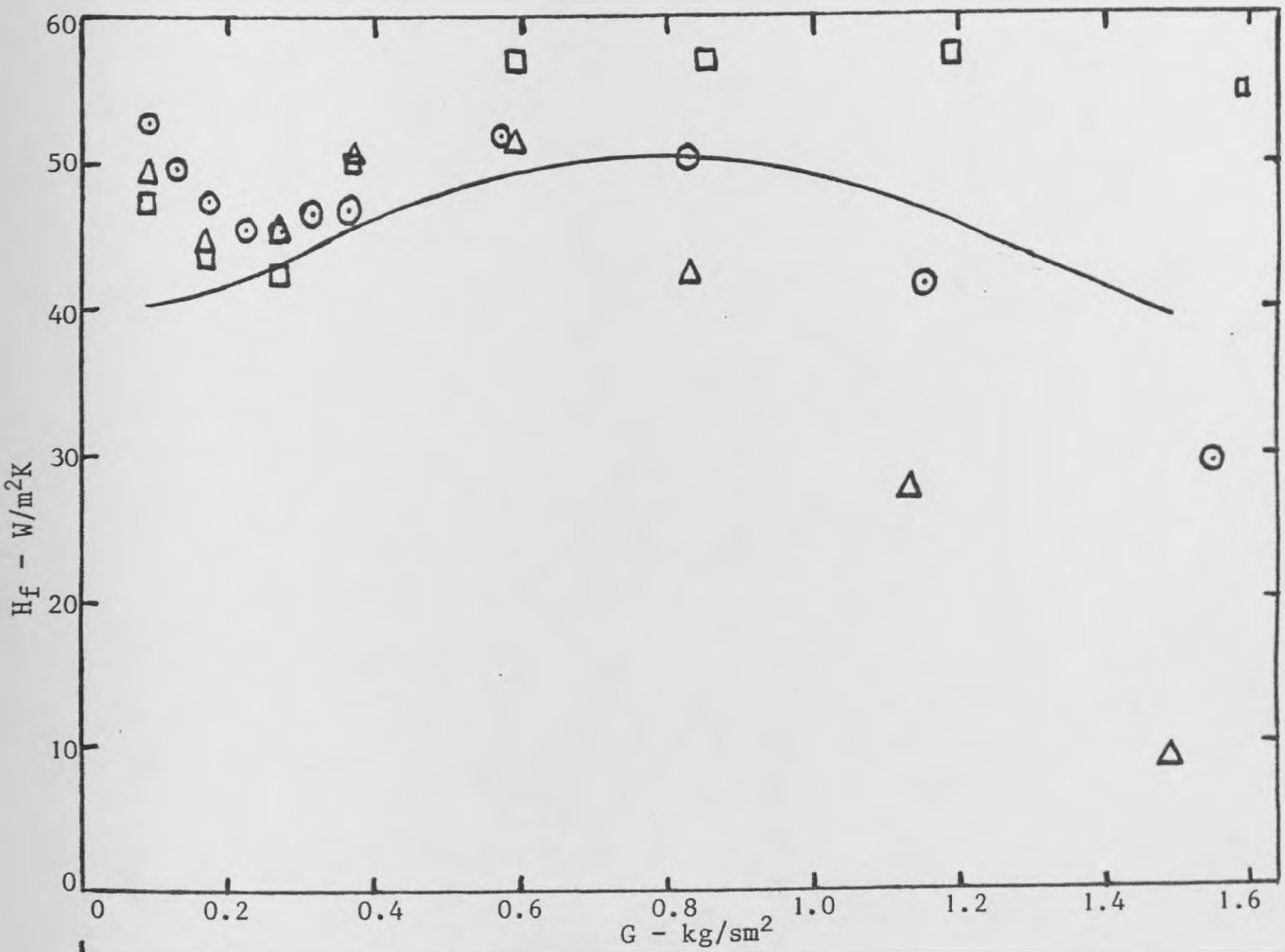

30:1 Impingement/Effusion System

Design pressure loss: impingement = 3.0%, effusion = 0.1%.

Sym.	No.Holes/m^2 Imp.	Eff.	M.Holes Dia. Imp. (mm)	Eff.	Wall Thick. Imp. (mm)	Eff.	Gap Z/D	Z-mm	X/D	T_c K	T_g K	Hole Format Imp.	Eff.	Work
⊙	9688	9688	0.999	2.235	3.321	6.5	4.5	4.5	10.16	294	777	Inline	Offs.	Pres
—	/	9688	/	2.235	/	6.5	/	/	/	293	774	/	Offs.	"
△	26910	26910	0.639	1.307	6.35	6.35	5.0	3.2	9.6	291	763	Offset	Inl.	R.2
□	4306	4306	1.414	3.27	6.35	6.35	4.5	6.4	10.78	288	759	Offset	Inl.	"

Fig. 8.47: Film convective heat transfer coefficient development with coolant injection

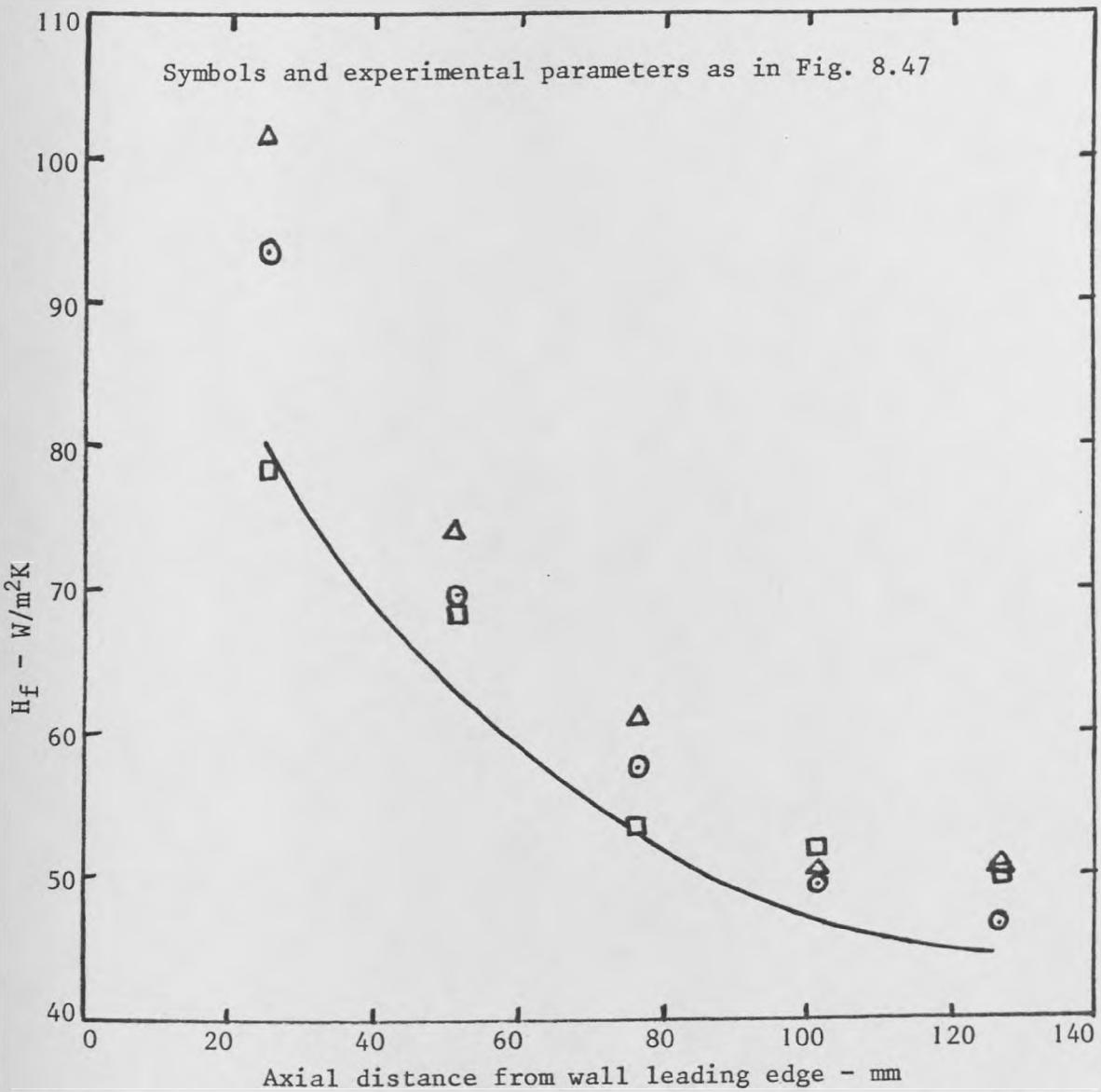

Fig. 8.48: Axial profile of film convective heat transfer coefficient at $0.365 \leqslant G \leqslant 0.372$

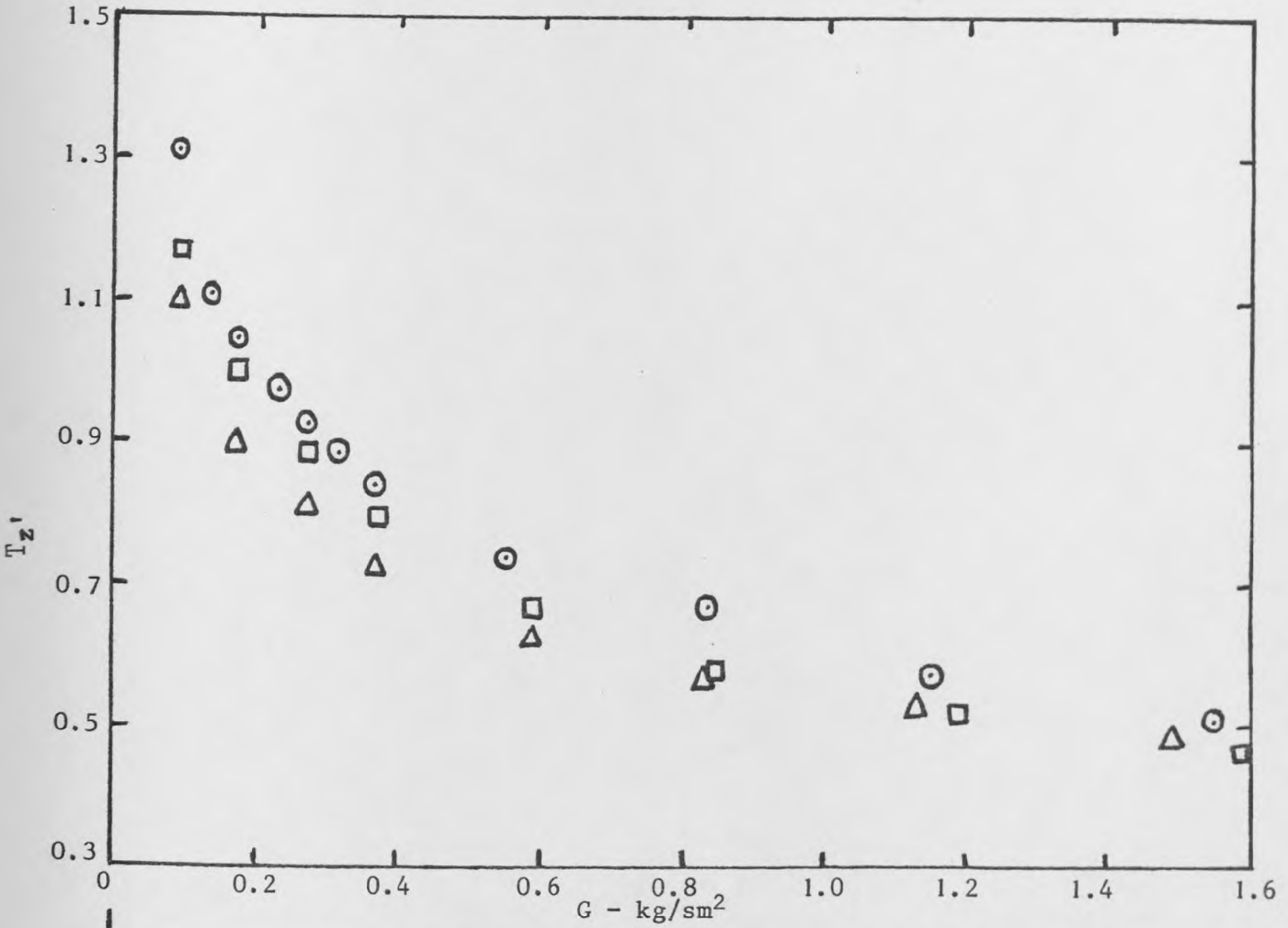

30:1 Impingement/Effusion Cooling System

Design pressure loss: impingement = 3.0%, effusion = 0.1%.

Sym.	No.Holes/m^2 Imp.	Eff.	M.Holes Dia. Imp. (mm)	Eff.	Wall Thick. Imp. (mm)	Eff.	Gap Z/D	Z-mm	X/D	T_c K	T_g K	Holes Form. Imp.	Eff.	Work
⊙	9688	9688	0.999	2.235	3.321	6.5	4.5	4.5	10.16	294	777	Inl.	Offs.	Pres
△	26910	26910	0.639	1.307	6.35	6.35	5.0	3.2	9.6	291	763	Offs.	Inl.	R.2
□	4306	4306	1.414	3.27	6.35	6.35	4.5	6.4	10.78	288	759	Offs.	Inl.	"

Fig. 8.49: Impingement wall heating as a function of coolant mass injection

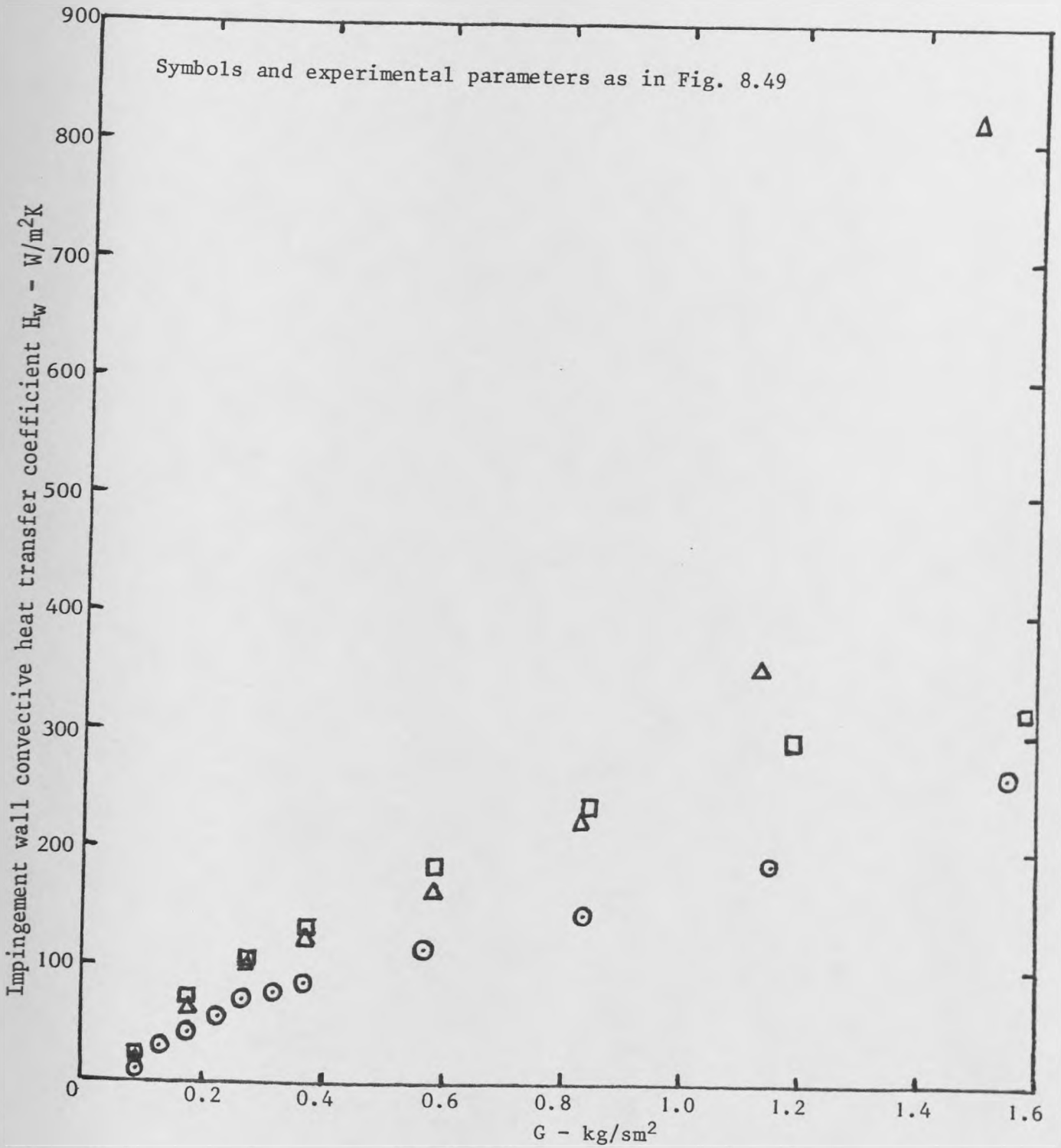

Fig. 8.50: Dependence of impingement heat transfer coefficient on G from bounce-back impinging jets

CHAPTER 9

CHAPTER 9

RECOMMENDATIONS FOR FUTURE INVESTIGATION AND CONCLUSIONS

9.1 RECOMMENDATIONS FOR FUTURE INVESTIGATION

9.1.1 The effect of impingement holes and Z/D on the discharge coefficient of the effusion holes of a combined impingement/effusion hybrid system is recommended for future work.

9.1.2 The direct measurement of the interstitial heat transfer coefficient of a Rigid Mesh is recommended for future work, to enable the best correlation to be developed and hence enhance the modelling of a flat plate work for a cylindrical combustor.

9.1.3 Coolant to mainstream density ratio effect on effusion wall needs further investigation to enable a general prediction procedure to be developed.

9.1.4 Heat transfer coefficient to the gap surface of an impingement wall, in an impingement/effusion system, requires further work for a general correlation to be developed for the prediction of the impingement wall temperature.

9.1.5 The temperature changes of the jet in the gap of the impingement/effusion system demand further investigation.

9.1.6 The present impingement heat transfer correlation requires modification to account for suction effect.

9.1.7 Different impingement hole geometries in combination with 9688, 17222 and 26910 m^{-2} holes, low design pressure losses, effusion wall,

both walls having reduced wall thickness, must be the focus of future work in this area.

9.1.8 Impingement/effusion global heat transfer coefficient evaluation is recommended for future work. This may be determined by direct measurement of the film heat transfer coefficient of the impingement/effusion wall using transient response techniques.

9.1.9 Further work is recommended using staggered arrays of holes at various design pressure losses and thicknesses.

9.1.10 Further work using inclined holes at various angles, holes concentration, design pressure losses and thicknesses is recommended.

9.1.11 The design of various pressure loss walls and thicknesses in the 9688, 17222 m^{-2} effusion walls, as well as testing their performance, is called for.

9.2 CONCLUSIONS

9.2.1 For multiple holes of a single wall, the high Reynolds number discharge coefficient is not strongly affected by the cross stream, although the effect is significant for some designs.

9.2.2 The C_d of impingement holes has a weak dependence on hole concentration but is more strongly affected by the effusion holes' diameter. The larger the effusion holes' diameter, the poorer the value of the impingement holes' C_d.

9.2.3 For all geometries of holes investigated, apart from the 26910 m^{-2} holes, compressibility effect is significant at the region where C_d is independent of Reynolds number, i.e. $Re \geqslant 10^4$.

9.2.4 Transpiration cooling results in a thermal boundary layer whose thickness increases with axial distance and no steady state thickness was found within the present 127 mm limit.

9.2.5 The cooling effectiveness of transpiration walls is a function of the wall permeability, the higher this parameter the better the wall cooling effectiveness. Film cooling is a major proportion of the overall cooling effectiveness at all coolant injection rates and is the dominant process at $G \geqslant 0.8$ kg/sm^2.

9.2.6 Heat removal in transpiration walls is an important contributor to high overall cooling effectiveness at low G values.

9.2.7 Empirical correlating equations for coolant flow through the transpiration walls and the pressure loss across them have been deduced.

9.2.8 Heat transfer at the back and inside the wall of full coverage discrete hole film cooling systems which have not been previously analysed have been treated and shown to be significant in the wall cooling performance.

9.2.9 A method of computing the total heat transfer in a full coverage discrete hole film cooling system and the use of this method in modelling the cooling performance of a cylindrical full coverage discrete hole film cooling system has been presented.

9.2.10 Wall thickness in effusion cooling is a significant parameter in the design of this system. It has a strong influence on the cooling performance for the holes geometries investigated; below a hole concentration $\leqslant$ 17222 m^{-2}, the thicker the wall the better the performance but for n > 17222 m^{-2} the dependence of cooling performance on thickness is weak.

9.2.11 The 9688 m^{-2} holes geometry is the optimum hole geometry in terms of saving on hole manufacture and cooling performance.

9.2.12 The larger the effusion hole diameter the better the cooling performance of the full coverage discrete hole film cooling system. At this large hole diameter, the cooling performance, shown by the present work, compares very well with that of the transpiration system, Lamilloy upper limit, and is better than most of the Transply design results.

9.2.13 The higher the holes' density, the better the cooling performance provided the walls are of the same design pressure loss.

9.2.14 The heat transfer of an impingement wall in an impingement/effusion cooling hybrid system has been analysed. The heating of the surface of this wall by jets deflected by the target wall, a phenomenon that has not been recognized before, is a function of Z/D.

9.2.15 Theoretical and experimental analyses of the heat transfer in an impingement/effusion system have been presented and a model for a cylindrical combustor has been proposed.

9.2.16 Theoretical predictions, backed up by experiment, of the various temperatures of the fluid in the impingement/effusion gap have been presented. At low coolant flow rate experiment shows the predictions to be susceptible to global errors of the correlating equations employed.

9.2.17 The heat transfer coefficient to the gap face of the impingement wall, which has never been treated before, from jets reflected back to their source by the target wall, has been presented and has a strong dependence on Z/D, impingement holes to effusion holes ratio, and on effusion holes' diameter.

9.2.18 The cooling performance of the impingement/effusion hybrid cooling system is weakly dependent on wall thickness. Reducing both the thicknesses of the impingement and effusion walls of the hybrid system by 50% alters the cooling performance of the system by a mere 1%.

9.2.19 The benefit of combining an impingement wall with an effusion wall of which the optimum cooling performance has been maximized is not significant, and much fewer impingement holes numbers in comparison with those of the wall may result in poor cooling performance.

9.2.20 The 9688 m^{-2} holes impingement in combination with 9688 m^{-2} holes effusion, has a cooling performance superior by only 5% to

that of the 4306/4306 holes system. In terms of saving in holes drilling cost, the 9688/9688 m^{-2} is the most attractive for the impingement/effusion hybrid system.

9.2.21 The cooling performance of fewer impingement holes numbers in combination with 0.1% design pressure loss effusion wall of various holes density is better, when saving in holes drilling cost is taken into account, than that of equal numbers of holes for both impingement and effusion wall of the hybrid system.

9.2.22 The experimental results of the film heat transfer coefficient of the impingement/effusion cooling system appear to be in error relative to the equivalent effusion wall only data and more work on the impingement heat transfer of the target wall with suction holes is called for.

9.2.23 The cooling performance of the impingement/effusion hybrid system is superior to that of a single effusion wall.

9.2.24 Density ratio has an influence on the film heat transfer coefficient and cooling performance of a single effusion wall but low temperature results do not show any consistent influence. Further work is clearly required before a general prediction procedure can be devised.

9.2.25 The influence of density ratio, using realistic practical temperature on the impingement/effusion system cooling performance and film heat transfer, is quite strong. The lower the density ratio, the better the wall cooling performance.

9.2.26 For both single and combined systems investigated, the pseudo-adiabatic film cooling effectiveness is high and in some cases accounts for about 50% of the overall cooling effectiveness.

9.2.27 The cooling effectiveness of all the cooling systems increases with increase in coolant mass injection rate, G. A cooling effectiveness of 0.7 has been demonstrated at G = 0.2 kg s^{-1} m^{-2} which is a superior performance to that of current wall cooling systems and as good as the best Transply and Lamilloy designs, and close to the ideal transpiration cooling.